

**Scientific Cruise Report of the  
Arctic Expedition ARK-XI/1 of RV "Polarstern" in 1995**

**(German-Russian Project LADI:  
Laptev Sea - Arctic Deep Basin Interrelations)**

**Wissenschaftlicher Fahrtbericht über die  
Arktis-Expedition ARK-XI/1 von 1995  
mit FS "Polarstern"**

---

**Edited by Eike Rachor  
with contributions of the participants**

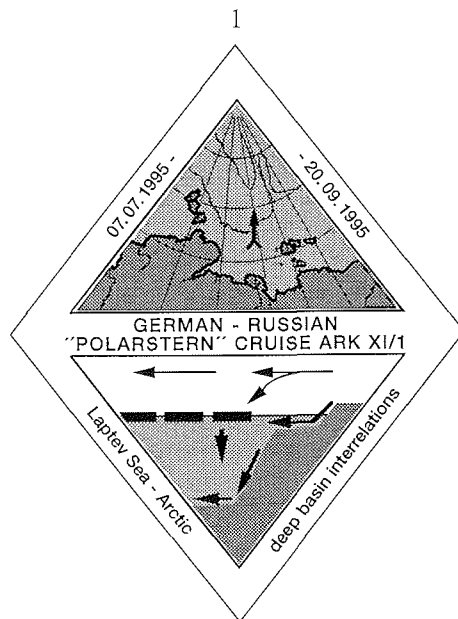
**Ber. Polarforsch. 226 (1997)  
ISSN 0176 - 5027**



## Cruise Report ARK XI/1, Contents

	Page
1. INTRODUCTION .....	1
2.1 ITINERARY (Cruise Summary) .....	2
2.2 Maps and Transect Profiles .....	8
3. WEATHER AND GENERAL ICE CONDITIONS (U. Bergholter) .....	12
4. PHYSICAL AND CHEMICAL OCEANOGRAPHY (B. Rudels, C. Darnall, J. Gunn, E. Zakharchuck; F. Haubrich, F. Légeleux, J. Lobbes, Y. Nalbandov, S. Searson & W. Stein) .....	17
4.1 PHYSICAL Oceanography:	
4.1.1 CTD observations (B. Rudels et al.) .....	22
4.1.2 Acoustic Doppler Current Profiler observations (J. Gunn) .....	25
4.1.3 Mooring Deployments (C. Darnall & B. Rudels) .....	26
4.1.4 Observations of internal waves (E. Zakharchuck) .....	28
4.2 CHEMICAL Oceanography:	
4.2.1 Inorganic nutrients etc. (Y. Nalbandov) .....	31
4.2.2 Barium and total inorganic carbon (B. Rudels) .....	32
4.2.3 Dissolved organic matter (J. Lobbes & F. Haubrich) .....	36
4.2.4 Tritium, <sup>3</sup> He and <sup>18</sup> O (W. Stein) .....	37
4.2.5 Freons and Krypton (S. Searson) .....	38
4.2.6 Natural radionuclides (F. Légeleux) .....	39
5. SEA ICE PHYSICS AND REMOTE SENSING (H. Eicken, A. Darovskikh, K.-U. Evers, J. Freitag, C. Haas, P. Jochmann, J. Kolatschek, S. Syrtsov, F. Valero Delgado & A. Zatchek) .....	40
5.1 Sea-ice conditions in the Laptev Sea (H. Eicken et al.) .....	40
5.2 Acquisition of satellite data (J. Kolatschek) .....	43
5.3 Radar overflights and video recordings (A. Darovskikh et al.) .....	44
5.4 Thermal conditions of melt puddles (A. Zatchek & A. Darovskikh) ....	47
5.5 Morphology of ice pressure ridges (K.-U. Evers & P. Jochmann) .....	49
5.6 Thickness and roughness of the ice cover (C. Haas) .....	55
5.7 Properties, microstructure of sea ice (H. Eicken & F. Valero Delgado)...	61
5.8 Conductivity of the ice cover, hydrological tracer studies (J. Freitag) ...	64
5.9 Drifting buoys with ice-freeboard pressure sensors (H. Eicken et al.) ....	67
5.10 Distribution and redistribution of sediments within the sea-ice cover (H. Eicken, J. Freitag, J. Kolatschek, F. Lindemann) .....	68
5.11 Spectral and integral albedo of sea ice (J. Kolatschek & A. Zatchek) .....	70
6. SEA ICE BIOLOGY AND SEDIMENTOLOGY (M. Gleitz, S. Grossmann, C. Krembs, F. Lindemann & I. Werner) .....	73
6.1 Productivity in ice-associated habitats (S. Grossmann & M. Gleitz) .....	73
6.2 Small scale distribution of sympagic organisms and the coupling to hydrodynamic factors within and below sea ice (C. Krembs) .....	79
6.3 Under one roof - the under-ice community (I. Werner) .....	83
6.4 Sediment at the under-ice surface (F. Lindemann & I. Werner) .....	85

6.4	Sediment at the under-ice surface (F. Lindemann & I. Werner) .....	85
6.5	Sediments in sea ice (F. Lindemann) .....	86
6.6	Export of particulate material from sea ice (M. Gleitz et al.) .....	88
7.	<b>MARINE BIOLOGY</b> (S. Grossmann, N. Anisimova, A. Bartel, H. Deubel, M. Gleitz, K. Kosobokova, V. Potin, E. Rachor, T. Scherzinger & S. Timofeev) .....	89
7.1	Phyto- and protozooplankton and vertical particle flux (A. Bartel) .....	89
7.2	Phytoplankton and bacterial production (M. Gleitz & S. Grossmann) ..	92
7.3	Zooplankton (K. Kosobokova et al.) .....	94
7.3.1	Copepod ecology (K. Kosobokova & T. Scherzinger) .....	94
7.3.2	Chaetognaths: Population biology (S. F. Timofeev) .....	99
7.3.4	Euphausiids: Distribution and population biology (S. F. Timofeev) ...	100
7.3.5	Planktic foraminifers (R. Spielhagen) .....	102
7.4	Zoobenthos (N. Anisimova et al.) .....	103
8.	<b>BENTHIC BIO-GEOCHEMISTRY</b> (E. Damm, C. Grahl & G. Hulthe) .....	111
8.1	Sediment sampling and measurements .....	111
8.2	Preliminary results:	
8.2.1	Benthic microbiology (C. Grahl) .....	112
8.2.2	Oxygen concentration profiles (E. Damm) .....	114
8.2.3	Benthic carbon fluxes and relation to oxygen fluxes (G. Hulthe et al.)..	115
9.	<b>MARINE GEOLOGICAL INVESTIGATIONS</b> (R. Stein, M. Behrends, M. Bourtman, K. Fahl, M. Mitjajev, E. Musatov, F. Niessen, N. Nørgaard-Petersen, V. Shevchenko & R. Spielhagen) .....	117
9.1	Sediment PARASOUND echosounding (F. Niessen & E. Musatov) ....	118
9.2	Geological sampling, description, and methods applied aboard .....	128
9.2.1	Aerosol sampling, size-distribution measurements (V. Shevchenko)..	129
9.2.2	Sampling in the water column (K. Fahl & V. Shevchenko) .....	130
9.2.3	Sea floor sediment sampling and description (M. Behrends et al.) .....	133
9.3	Physical properties in marine sediments (F. Niessen et al.) .....	134
9.3.1	Core logging of density, P-wave velocity and magnetic susceptibility ...	139
9.3.2	Shear strength and density determination of discrete samples .....	143
9.4	Lithostratigraphy and sediment characteristics (R. Stein et al.) .....	143
9.4.1	Sediment surfaces .....	143
9.4.2	Long sediment cores .....	146
9.5.	Aerosols (V. Shevchenko) .....	153
10.	<b>REFERENCES</b> .....	155
11.	<b>ANNEXES:</b>	
11.1	Station List .....	A2
11.2	Weather data .....	A18
11.3	Hydrochemistry data .....	A28
11.4	Geological tables and core descriptions.....	A39
11.5	Guidelines .....	A158
11.6	Participants .....	A171



## 1 INTRODUCTION

The first leg of the eleventh Arctic expedition from 7 July to 20 September 1995, was RV POLARSTERN's second cruise to Siberian waters following ARK IX/4 in 1993. At the same time it was a further successful contribution to the German-Russian co-operation in Arctic research and especially to the LAPTEV SEA SYSTEM project.

The expedition focussed on the Laptev Sea - Arctic Deep-Basins Interrelations (LADI). Accordingly, the main objectives of the multi-disciplinary program were to study the material fluxes and the ecological relationships between the Siberian shelf seas, the northern Laptev Sea as well as the northeastern Kara Sea and the northwestern East Siberian Sea, and the adjoining Arctic Deep Basins. In addition, the large-scale water circulation, ice drift and related transport processes were also investigated.

After the cruise, several teams were able to continue their studies during the third German-Russian TRANSDRIFT expedition (LAPTEV SEA SYSTEM project) with the Russian icebreaker "Kapitan Dranitsyn" in the Laptev Sea during early autumn.

This report describes the work done during the expedition and provides station and sample data as well as preliminary results. In the Annex, guidelines for the evaluation and publication procedures, as agreed upon during the cruise, are also indicated.

### *Acknowledgements*

The editor of this report (and chief scientist on board), expresses his gratitude to the Russian authorities and institutions who supported the expedition so fruitfully. Thanks are also due to the ship's master, Kapitän Heinz Jonas, and his crew for their extraordinary contribution to the success of our work. The major components of this report were written by the participants.

## 2.1 ITINERARY (Cruise Summary)

### POLARSTERN - Expedition ARK XI/1

Bremerhaven - (Murmansk) - LAPTEV SEA - (Murmansk) - Tromsø  
7. July - 20. September 1995

The first leg of the XI. Arctic expedition of the German RV POLARSTERN started in Bremerhaven on the 7th of July, with the ship heading to Murmansk for embarkation of the Russian participants for a cooperative German-Russian research program in Siberian shelf and adjacent Arctic deep sea waters (LADI - Laptev Sea - Arctic Deep Basin Interrelations). The expedition is regarded a major contribution to the project "(Ecological-climatological) System of the Laptev Sea" of the Agreement about Cooperation in Marine and Polar Research between the Russian Federation and Germany from 10. February 1995.

A group of science administrators (from the European Commission, ESF, AOSB, Germany) used the opportunity to inform themselves about Arctic research activities and to discuss common problems during the part leg Bremerhaven - Murmansk. Prof. Max Tilzer, director of AWI, chaired several information and discussion meetings and acted as chief scientist during this time. Along the route, on the 11th of July, sampling was initiated at an extra station in the *Norwegian Sea*. This allowed to give some practical information, to test some new instruments and to obtain a sediment core for Norwegian institutes.

POLARSTERN arrived at *Murmansk* in the morning of the 13th of July and left it on the 14th in the early afternoon. Eike Rachor took over as chief scientist. From Murmansk, POLARSTERN headed to the Kara Strait and sailed up to the western entrance of *Vilkitsky Strait*, before sampling was started again (Stations 2 and 2a, on July 19).

According to the available satellite information on the sea ice distribution it was decided to steam to the easternmost of the planned transects ("A", in the transition area to the East Siberian Sea) and to initiate the main sampling program there. POLARSTERN passed Vilkitsky Strait independently, but joined a small convoy of the Northeastern Sea Route, guided by the nuclear-power-fueled icebreaker "Sovietsky Sojus", east of the Strait to pass an ice barrier on her way to the central northern *Laptev Sea*. Thereafter, open water allowed good progress without support.

On her route to the east POLARSTERN again steamed into the ice to re-sample a station at 2000 m depth on the continental margin near its junction to the Gakkel Ridge, where remainders of a hydrothermal vent fauna had been detected in a trawl catch during the 1993 cruise. Comparable mollusc shells were again found in a deep layer of a gravity corer obtained by the geologists.

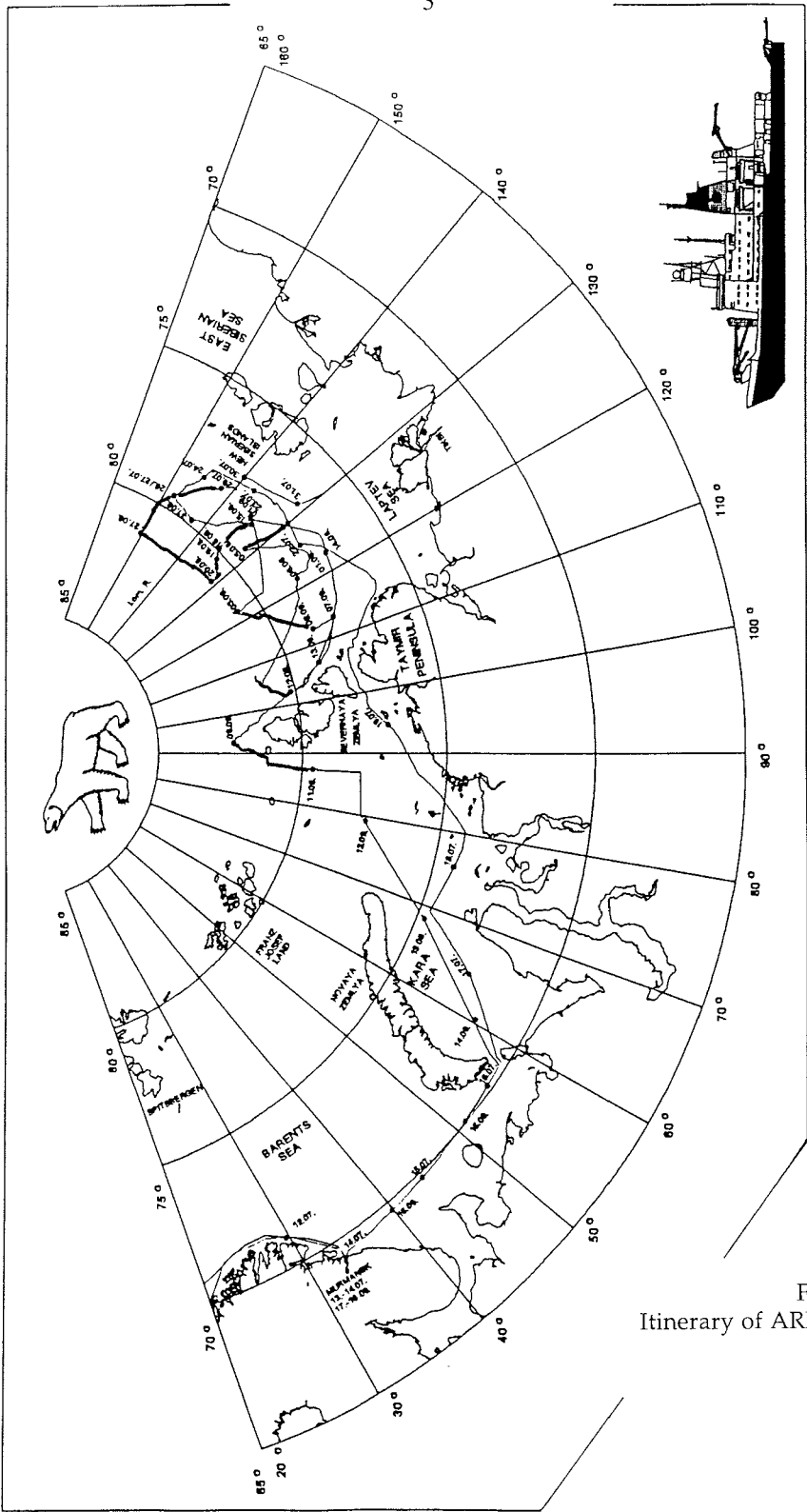


Fig. 2-1:  
Itinerary of ARK XI/1

Since this station (no. 3) was in the pack ice, the majority of all work planned for future "main stations" was initiated: Ice sampling and surveying by helicopter; physical and chemical oceanography by CTD/Rosette-sampling; sampling of suspended matter by a deep-water pumping device; stratified plankton collected with a closing multi-net and, in addition, by a bongo-net; zoobenthos and surface sediments for geology with a large box sampler (Großkastengreifer); and deeper sediments by a long gravity corer. Aerosols were also collected using a pump installed on the uppermost deck of the vessel.

Thereafter, POLARSTERN continued her way to the east and started sampling of transect A on the 24th of July (station no. 4). In addition to the sampling gear mentioned already, an Agassiz trawl for collecting larger epifauna from the sea floor was used. Soon after the first station, POLARSTERN came into very resistant (and sediment-laden) pack ice allowing only slow progress towards greater water depths in the North. At station no. 7, on the 26th of July, it was decided not to continue to try to go northward, but, to steam back to the south and thereafter to the central Laptev Sea to work under more favourable conditions and to resume work on transect A on a later stage of the expedition.

Accordingly, all shallow shelf stations in the open waters of a part of the *East Siberian Sea* and the *northeastern Laptev Sea* were successfully sampled passing then into transect C which again led to the North and allowed ice research. Its northernmost station (no. 24, at a depth of almost 3200 m) was finished on the 5th of August.

As the satellite ice images showed persistent favourable ice conditions in the *northwestern Laptev Sea* (east of Severnaya Zemlya, where normally the so-called Taymir ice massif prevents any ship-borne research), we steamed to the Northwest to perform a northwardly shifted transect E across the continental slope east of the islands. All kinds of sampling could be done there from depths of more than 3300 m to as shallow as 100 m between the 7th and the 13th of August. The glaciologists used the opportunity to study surface features, origin and drift of icebergs released from the large glaciers of *Severnaya Zemlya*. Scouring and stranding features on the sea floor were analysed by Parasound echograph surveying.

Then it was time to resume research in the eastern working area. Accordingly, POLARSTERN steamed again eastward, performing on her way some oceanographic measurements near the upper edge of the continental slope, where bottom depressions (small trough-like structures, Pleistocene channels) may allow intrusion of Atlantic water onto the shelf.

POLARSTERN went directly to the location of the westernmost of the planned long-term oceanographic moorings. These moorings are intended to study the circulation in the whole water column at a water depth of 1700 m, mainly to understand the Atlantic water mass exchange between the Amundsen and Makarov Basins at the Lomonosov Ridge. Ice thickness and movements will be measured by upward looking sonars. Recovery is planned during the joint



expedition of POLARSTERN and the Swedish RV ODEN in 1996, as part of the Arctic Climate System Study (ACSYS).

As the first mooring station (no. 40) was located in the marginal ice zone, the full scope of research could again be carried out along the transect B, bringing us northward and to deeper waters. After extensive work at a 3300 m deep sea station (no. 45) on the 18th/19th of August, we deviated from our northerly course to try and sample in shallower waters above seamount-like elevations, indicated in the available sea floor maps (GEBCO). Despite Parasound echograph surveys in the areas indicated, we did not find any of such morphological features, but met the greatest depths of the whole cruise (station no. 47, water depth more than 3900 m, 20th/21st of August). Meanwhile it was apparent that the decision to come back to this part of the research area at a later time was right: POLARSTERN was not faced by any problems within the pack ice and proceeded without delay.

After the 21st, sampling began along a West-to-East transect ("F"), crossing the *Lomonosov Ridge* and allowing comparison of the environment on either slopes, up from the *Amundsen Basin*, and down into the *Makarov Basin*. The second oceanographic mooring, additionally equipped with two sediment traps for the biologists, was successfully deployed on the western side of the Ridge (station no. 51, 1700 m deep, 23rd of August).

The Ridge proved to be double-crested. Therefore, both elevations were sampled (stations nos. 52 and 53), especially to obtain gravity cores in locations of meagre sedimentation, allowing insights into several glacial/interglacial cycles. Gravity corer sampling proved to be very successful. Not regarding the ice, several Agassiz trawls could be taken. Altogether, they brought about very few animals, indicating that the zoobenthos in the Lomonosov Ridge and adjacent slope areas is very much impoverished compared with the benthos on the Laptev Sea continental slope.

The deepest location in the Makarov Basin of transect F was sampled on the 27th of August (station no. 57, 2600 m). This was the northeasternmost point of the whole expedition (ca. 81°11.5' N and 150°30' E); and from there POLARSTERN headed southward to sample the continental slope stations of transect A. At station no. 60, the third mooring was deployed. On the 30th of August, transect A was finished at station 65, at about the location of station 7, where the transect had been interrupted on the 26th of July.

Then we went back close to the location of the first mooring and worked up the shallow stations of transect B, which were finished with no. 73 on the 2nd of September.

The very favourable ice conditions in the west of the Laptev Sea and even north of Severnaya Zemlya enabled us to fully complete our program in the Laptev Sea and adjacent deep basins (transect D) and even sample along an extended transect G on the continental slope of the northeasternmost Kara Sea.

The northernmost station of transect D was situated in the ice close to the Gakkel Ridge and provided samples from the deep Amundsen Basin. Geological gravity

coring was then performed on the *Gakkel Ridge*; and thereafter a set of stations from the *Nansen Basin* up to shallow waters off the Taymir Peninsula were sampled. This work was finished at a water depth of 100 m (station no. 84) on the 7th of September.

On our way to the *North of Severnaya Zemlya* we obtained some additional geological cores and repeated the station no. 33 of transect E (no. 87), where we had encountered a phytoplankton bloom during the first visit.

After a CTD cast north of the archipelago, we ran a transect from ice-covered deep waters (2700 m) - the northernmost station of the whole cruise (82°21'N) - to the shallow shelf of the *Kara Sea* (station no. 94, 100 m). Two deeper locations in the *Voronin Trough* were additionally chosen for oceanographic, biological and geological sampling. South of a sill in the Trough, at 79°33'N, the last station work of the expedition was performed in the evening of the 11th of September (no. 96). The soft sediments in a depression of the Trough floor enabled us to obtain a long gravity core from this very specific environment, which is normally badly accessible.

POLARSTERN then continued southward, later heading southwest towards the Kara Strait, which was passed on the 15th of September. *Murmansk* was reached two days later. After disembarkation of the Russian cruise participants and handing over of equipment for the next German-Russian Laptev Sea expedition (with the icebreaker *KAPITAN DRANITSYN* in October), POLARSTERN steamed towards *Tromsø*, where the expedition ended on the 20th of September.

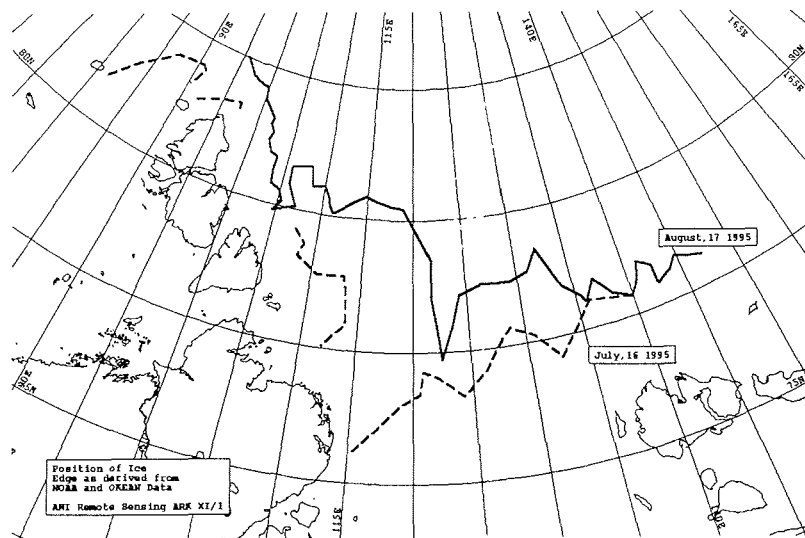


Fig. 2-2: Locations of the ice edges in the Laptev Sea at about July 16 and August 17, derived from satellite images and ship-borne observations. The ice-edges of August 17 roughly correspond to the minimum ice extent found during 1995.

## CONCLUSIONS:

Altogether, the second POLARSTERN expedition to Siberian waters again proved to be very successful. Due to the very favourable ice conditions, large ice-free areas or such with well transgressable ice, all planned transects could be sampled even to greater depth than anticipated. The unique conditions around Severnaya Zemlya, in addition, enabled us to sample in the normally almost inaccessible waters on the continental slope between the Kara and the Laptev Seas.

It has to be regarded a promising signal also for future Russian-German cooperation in the Arctic that both sides benefitted again from their joint efforts and that the Russian Ministry of Research extended the research permission to the waters north of Severnaya Zemlya during the expedition. As in 1993, an agreement for the continuation of work after the expedition was drafted on board by the participants (Guidelines, s. 11.5 Annex).

Though it is too early to draw definite conclusions about new findings obtained during the expedition ARK XI/1, we can state that we obtained valuable *oceanographic data* for a better understanding of the circulation and water exchange processes especially across and along the Lomonosov Ridge, but also along the continental slope from the Kara Sea along the Laptev up into the the East Siberian Seas.

*Nutrient and tracer chemistry* analyses will be completed in the home laboratories; but, the samples available from ARK XI/1 are regarded a unique material to further our understanding of water exchange and advective processes between the shelf and deep basin areas sampled, as well as to support biological productivity studies.

*Sea-ice research* brought out the strong contrasts in morphology and properties of ice of different regional origin and formation modes. The very thick ice found at the boundary between the Laptev and the East Siberian Seas was heavily sediment-laden, well shown by satellite imagery. A comprehensive data set could be obtained on the importance of summer melting processes for the evolution of multi-year ice. Transport and freezing processes in the ice have been analysed in detail and shown the importance of horizontal infiltration and internal freezing e.g. for lateral, respectively vertical transport processes in the ice.

The *biologists* on board obtained samples from all important compartments of the ecosystem (ice - water - sea floor) and will be able to contribute to the understanding of the formation, transformation and sediment burial of organic matter in the system. By the analysis of bottom communities with respect to the dominance of feeding guilds, areas of advective food input could be identified (predominance of suspension feeders, e.g. east of Severnaya Zemlya and on the slopes of the Lomonosov Ridge).

The large ice-free areas, which are normally ice-covered, may even enable us to elaborate scenarios about ecosystem changes following global warming, as primary production and the organic matter fluxes in the food web are very different in open and ice covered waters (as again shown during the cruise).

Sedimentary processes were studied by micro-biologists and *bio-geochemists*. They are intended to better describe transformations and release of C-compounds and nutrients at the sea floor, and - together with the quantitative zoobenthos work - to allow budgetting of biological carbon use.

On another time-scale, the *geologists* are now in a position to trace the sedimentation regimes under very different climatological conditions. The (gravity and box) cores taken from the Laptev Sea and East Siberian shelves, will allow to reconstruct the postglacial regional development, while the long cores obtained on the Lomonosov and Gakkel Ridges may help to reconstruct the conditions since several glacial cycles. Surface sediment properties will be compared with seston properties, as obtained from in-situ filtration and sediment traps (in cooperation with the biologists).

Data and samples obtained are challenging for all participants and their home partners. New insights into the environment of the Eurasian part of the Arctic Ocean and its sensitivity to climatic changes as well as a great amount of regional details may be produced.

Some station and sampling statistics are presented in the following tabulation:

*Table: Sampling statistics of ARK XI/1*

Number of ship stations	96
CTD/Rosette casts (including hand-CTD)	123
In-situ-pumping	25
Multinet plankton hauls	96
Bongonet plankton hauls	80
Large box samplers (GKG)	177
Multicorers	106
Gravity corers: - (Schwerelote)	47
- (Kastenlote)	8
Agassiz trawls (no. of stations)	23
Ice stations (from ship)	22
Helicopter surveys:	on 46 days,
with 71 operation hours (including additional ice stations)	

## 2.2 MAPS AND TRANSECT PROFILES

Fig. 2-3: Locations of stations

Figs. 2-3a-g: Transect sections (A = East Siberian, B = Eastern Laptev Sea, C = Central Laptev Sea, D = Western Laptev Sea, E = Severnaya Zemlya, F = transect across the Lomonossov Ridge, G = Kara Sea transect)

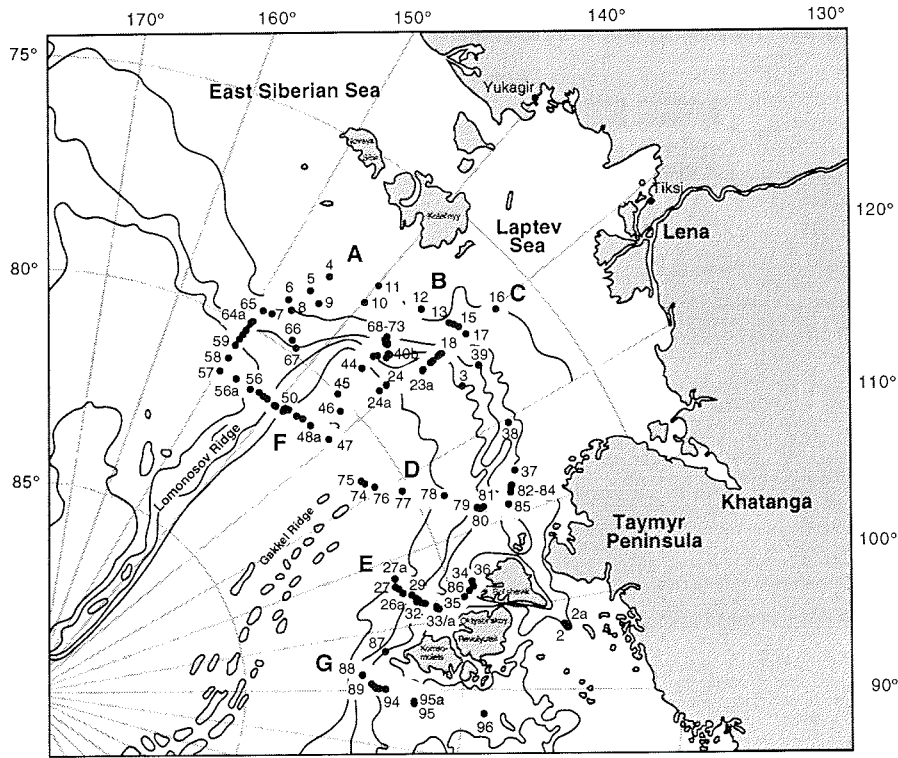


Fig. 2-3: Locations of stations 2 to 96, 19 July to 11 September, 1995

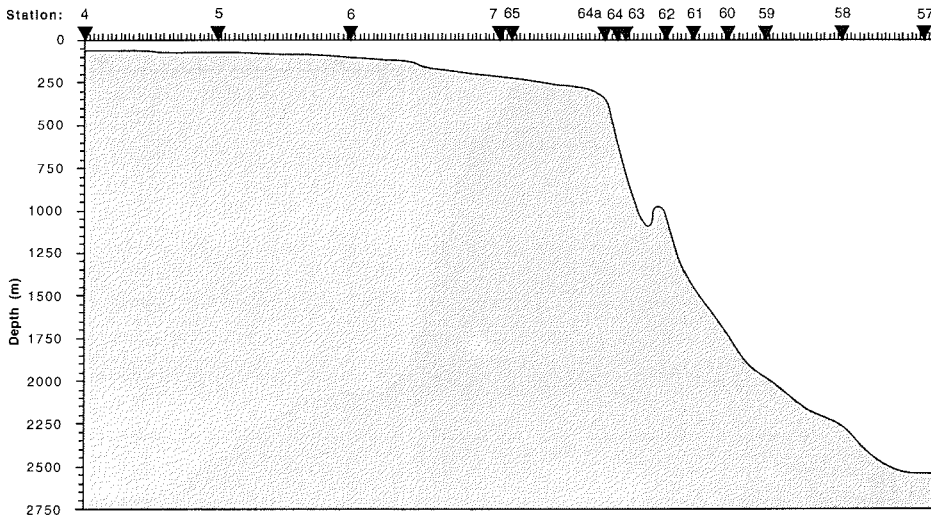


Fig. 2-3a: Section of transect A (24-26 July and 26-30 August; total distance 257 nm)

Fig. 3b : Transect B, July 31th, September 1st to 2nd and August 15th to 21th, 1995

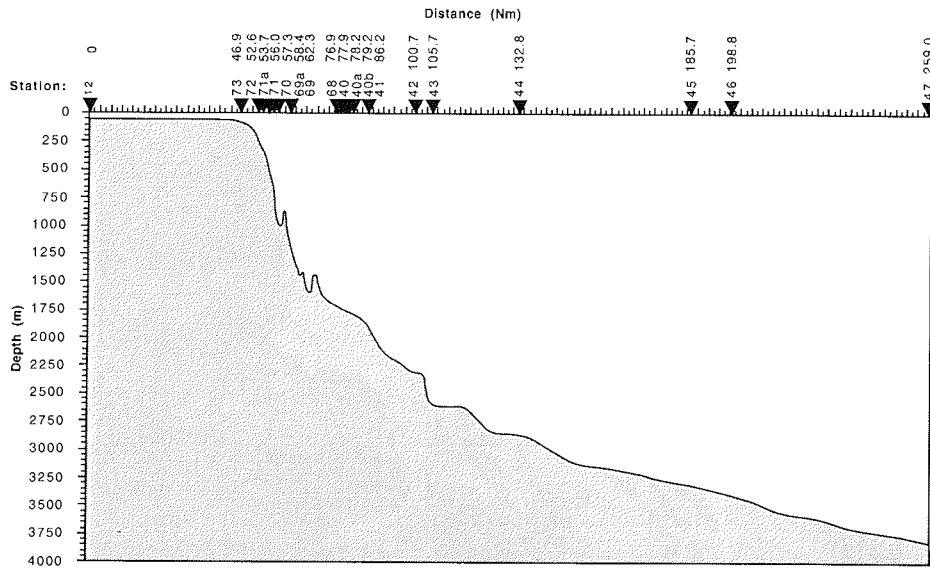


Fig. 3c : Transect C, July 31th to August 5th, 1995

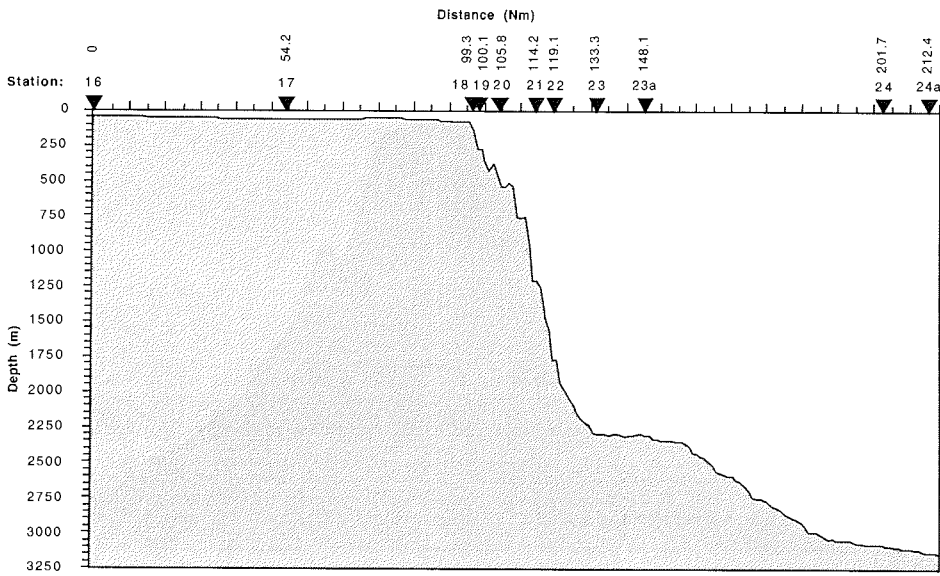


Fig. 3d : Transect D, September 3rd to 7th, 1995

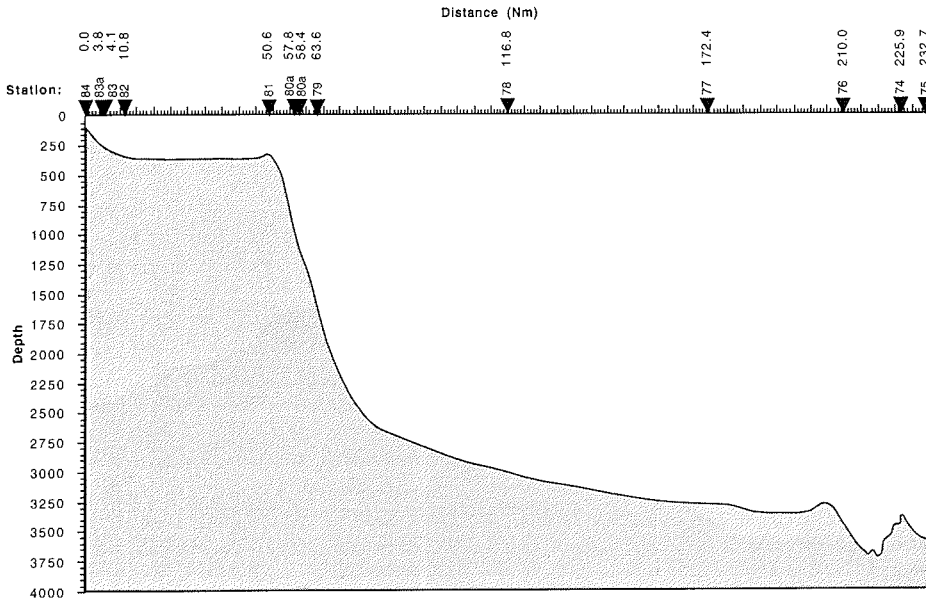


Fig. 3e : Transect E, August 7th to 13th and September 9th, 1995

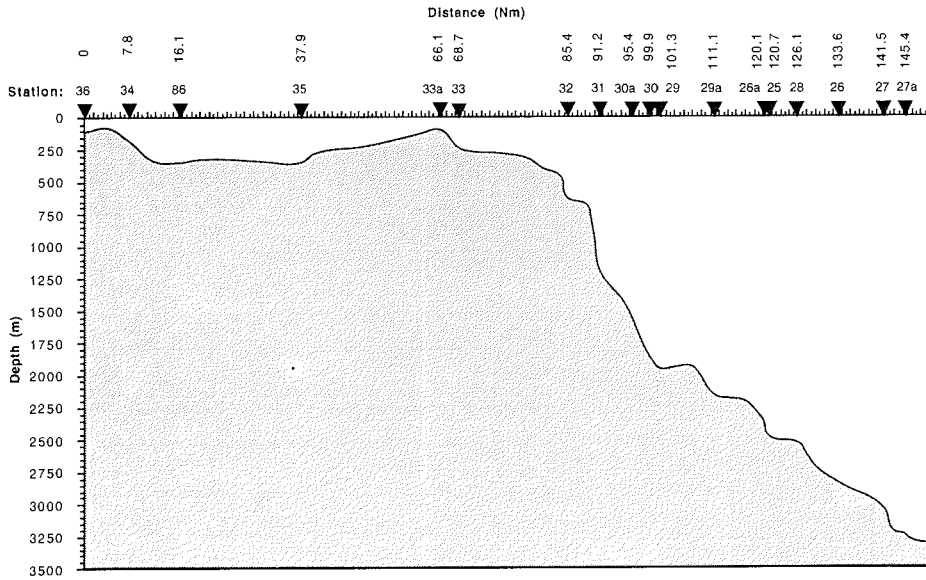


Fig. 3f : Transect F, August 20th to 27th, 1995

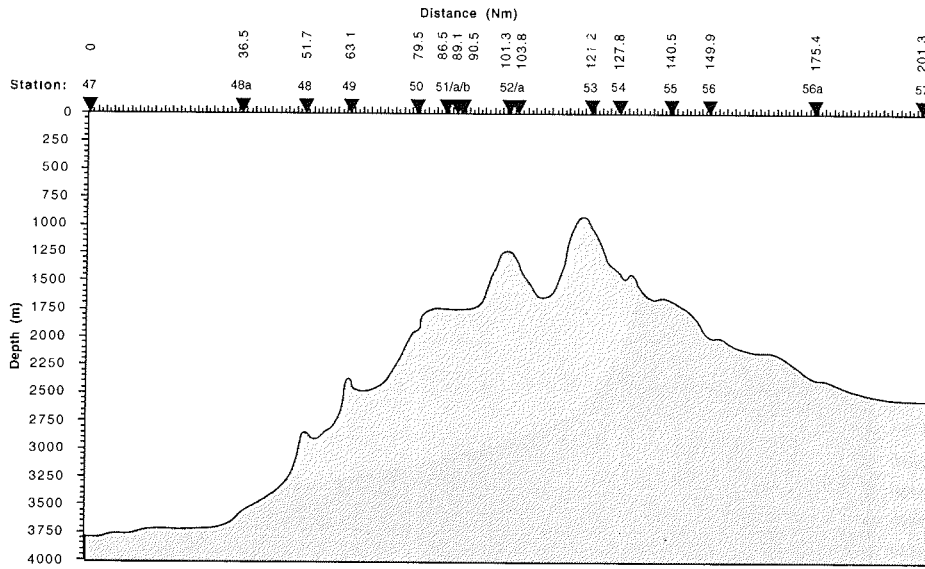
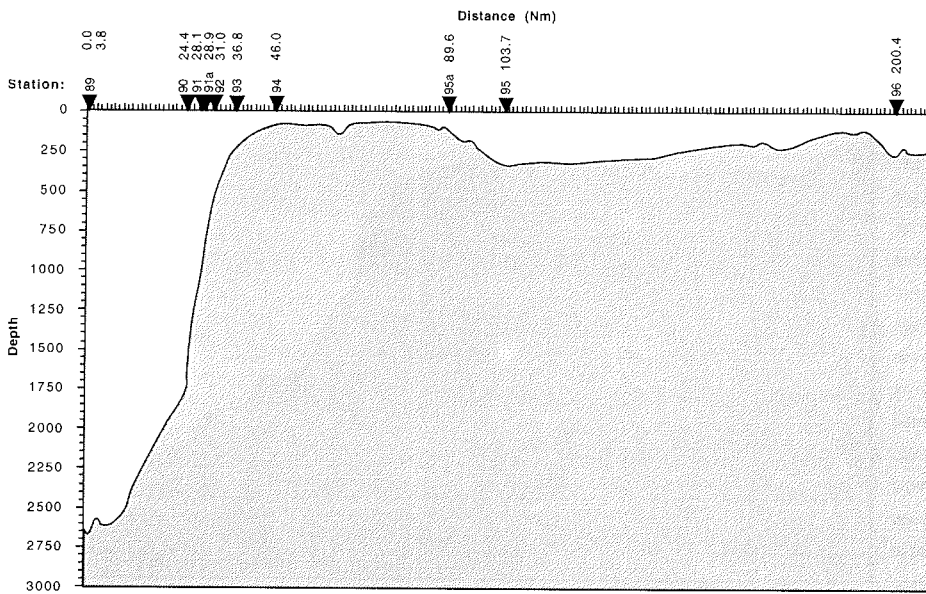


Fig. 3g : Transect G, September 9th to 11th, 1995





### 3 WEATHER and general ice conditions during ARK XI/1

(U. Bergholter)

Weather and ice conditions have generally been favourable for navigation and research work. Weather conditions may be called typical for the season, but were better than expected.

Weather:

During the first weeks of the cruise advection of mild airmasses over the cold ocean was dominant over the Laptev Sea. A very striking example can be seen from the radiosonde ascent of July 21st, when we sailed under a strong southerly flow close to the Taimyr Peninsula. The air temperature in 500m was almost 20 degrees higher than at the surface, where the air was only a little warmer than the water (Fig. 3-1).

The weekly average air temperature was at first higher than, later approximately equal to the melting temperature of sea ice (-1.6 °C). The cold spells at the end of August and after the 8th of September rendered weekly averages of -2.2 and -4.4 °C. The overall average was -1.6 °C, the lowest recorded single value being -11.9 °C. A diagram is attached showing the course of air and water temperatures during the cruise, starting with warm North Sea waters (Fig. 3-2). The constant level sections of water temperature show clearly the presence of sea ice, keeping the temperature at the melting point. These sections were interrupted when we steamed in open water, sometimes in the vicinity of large river estuaries as for example at the end of July (off Lena). While the air temperature never can rise very much over the surface temperature, during cold spells it was well below, especially on September 10th, when we had entered the ice for the last time.

After the mid of August, when the very dry and warm summer weather in central Europe ended, there was a change of weather over Siberia as well. Formerly a persistent area of low pressure had been located over the northern Ural mountains and south of the Kara Sea as well as over the Taimyr Peninsula, leading to cold advection over the Barents Sea deep into Russia. Later migrating lows and highs caused temporary progress of polar air into our area, but, only by the 8th of September a major outbreak of cold air happened and caused colder weather which lasted for the rest of the cruise.

As expected from climatological data, summer cloudiness was very high over the eastern Arctic Ocean. Persisting temperature inversions brought about the formation of mostly overcast skies with a rather low cloud base. Visibility was good quite often, and fog was observed within only 23% of the time, which is less than anticipated from statistical data. Fog conditions occurred mainly within the warmer spells at the end of July, in the beginning and in the second half of August. With about 15% of the observations we had rain or snowfall, which was mostly light except for very few cases when newly developed frontal systems crossed the area.

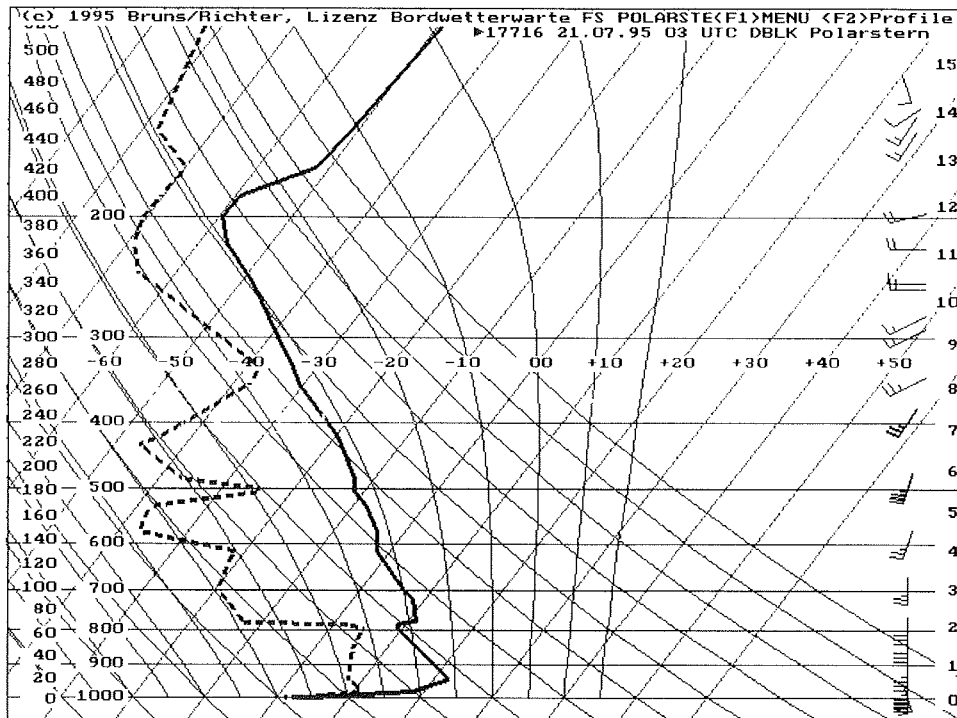


Fig. 3-1: Radiosonde diagram of 21.07.95 / 03 UTC

The frequency distribution of wind directions (see diagram Fig. 3-3) shows maxima for southeasterly to easterly and also for northwesterly to westerly winds, whereas northeasterlies and southwesterlies were less frequent. The distribution of wind speed has a similar, but less pronounced structure, showing higher speed of northwesterly and southeasterly winds. The overall average wind speed was 16.1 knots (5 Bft), the highest single value being 9 Bft. Southeasterly winds were mostly related to stationary low pressure systems over the Taimyr Peninsula or the region south of the Kara Sea and high pressure towards north or northeast. The northwesterlies were caused by transient lows east of the operational area, bringing close colder air.

Detailed list of weather observations, see Annex 11.2.

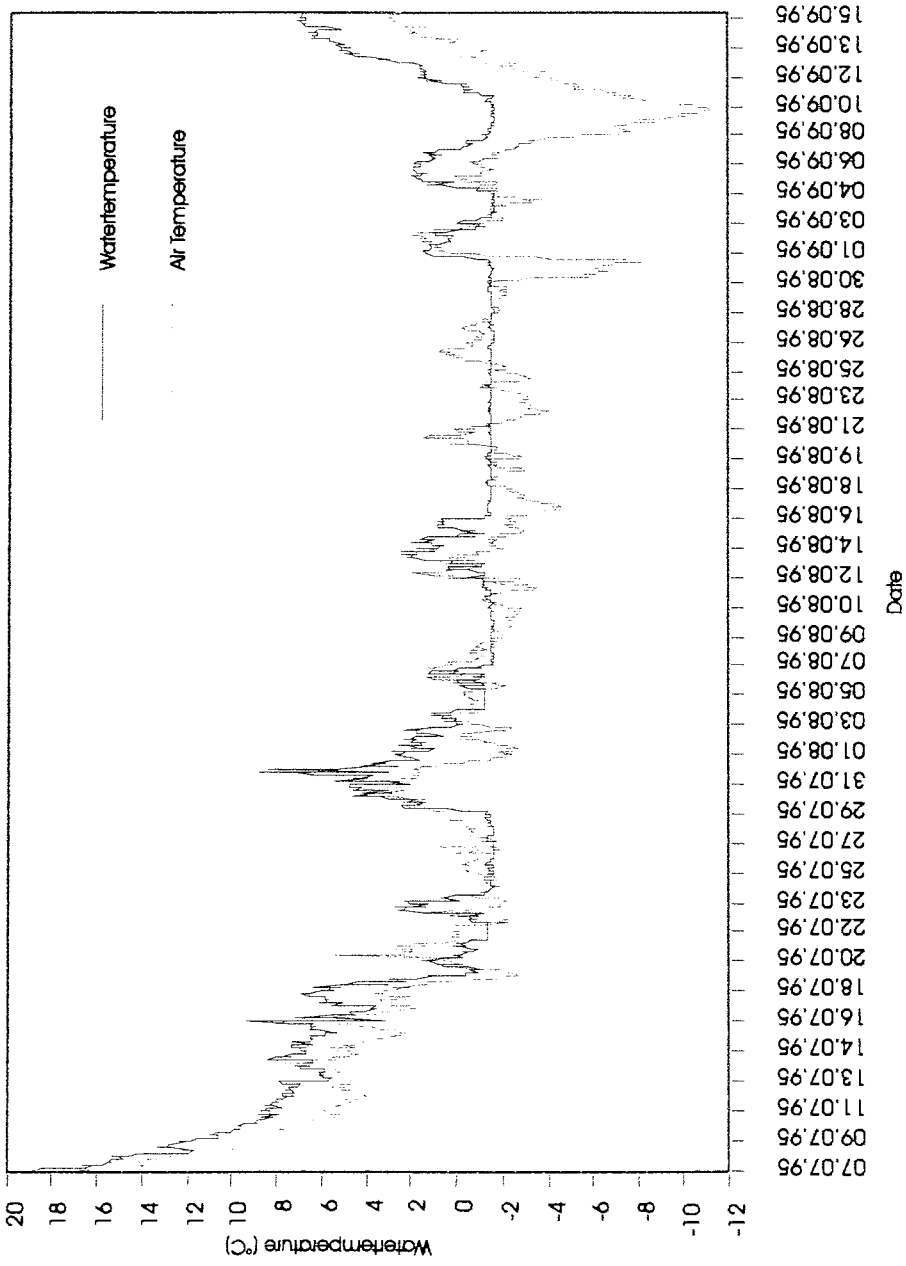


Fig. 3-2: Air/water temperature diagram

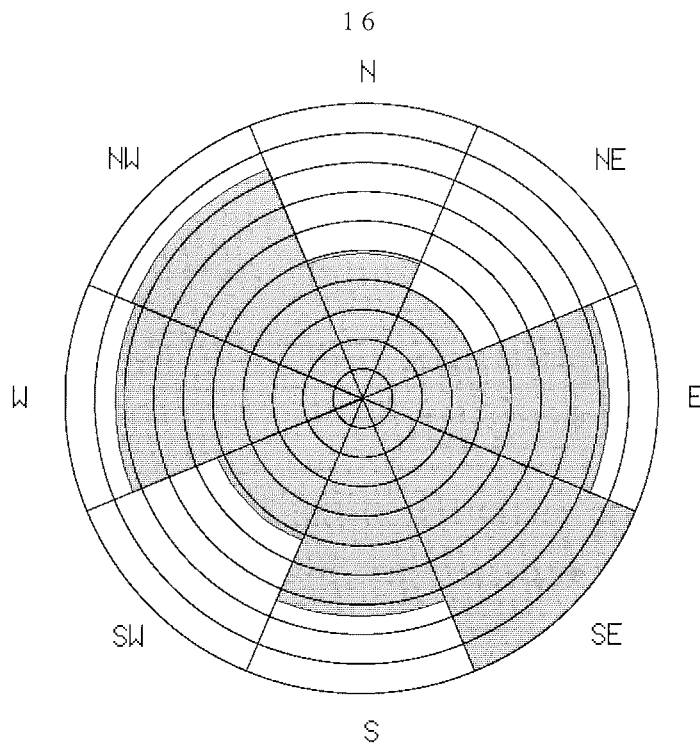


Fig. 3-3: Frequency distribution of wind directions

Ice conditions:

Already at the end of June and in the beginning of July, several strong and lasting warm spells over the Arctic Ocean were observed, which may have contributed to the rather light ice conditions we met on arrival in the western Laptew Sea. The pack ice had been forced back noticeably to the north by persisting southeasterly wind, easing very much our way into the operational area. In the east, however, the ice was under pressure, so that after a first futile attempt to reach latitudes north of 80°N a more southwesterly location was chosen to continue research work.

During the following weeks weather and wind development caused significant melting and changes of ice movement, making possible the access to any of the planned transects without great difficulty. Even the area north of Severnaya Semlya, normally covered with pack ice, was mostly ice free and well navigable, thus giving a rare occasion for research investigations otherwise not possible. During the last days of research work the formation of new ice could be observed in cold weather. It was interesting to observe that under an overcast sky with low clouds ice formation ceased when the wind was low, as a combined effect of thermal radiation and low turbulent heat flux.

## 4. PHYSICAL AND CHEMICAL OCEANOGRAPHY

### 4.1 Physical Oceanography.

(B. Rudels, C. Darnall, J. Gunn, E. Zakharchuck)

#### Introduction

The physical oceanography of the Eurasian Basin of the Arctic Ocean is dominated by interactions, forced by freezing, cooling and melting, between inflowing Atlantic water from the Norwegian Sea, river runoff and sea ice. The Atlantic water enters via two paths, through Fram Strait (Fram Strait branch) and over the Barents Sea (Barent Sea branch). These two inflows meet and merge north of the Kara Sea.

The Atlantic inflow is a heat source for the Arctic and is especially important for the extent of the ice cover in the Arctic Ocean. However, mixing with sea ice melt and river run off create less dense water masses, which act as an insulating lid between the Atlantic water and the surface. Further interactions occur between the Atlantic layer and waters from the shelves, which have become dense through ice formation and brine release. These waters sink down the continental slope, entraining intermediate waters until they reach a density level corresponding to their own, where they then penetrate into the water column. This leads to further cooling of the Atlantic layer and to a vertical transfer of heat downwards, to the deeper layers.

The *water masses* encountered in the Eurasian Basin of the Arctic Ocean, from the surface downward, are:

- SURFACE WATER - The approximately 20 m thick low salinity surface layer, which in the interior of the basin is mainly caused by seasonal ice melt and in the shelf areas by summer river runoff as well as by ice melt.
- THE POLAR MIXED LAYER - The layer which is homogenized by local, haline convection each winter. The PML extends to the surface in winter, and its depth varies between 30 and 100 m depending upon the location.
- THE HALOCLINE - A layer between the PML and the Atlantic Water, where the temperature remains low, but the salinity increases dramatically. The halocline is formed either by an injection of water of intermediate density from the shelves, which penetrates between the PML and the Atlantic Layer or by the outflow of low salinity surface water from the shelves, which reduces the depth of the local convection. The deeper part of the PML will then no longer be ventilated, and a cold halocline is formed.
- THE ATLANTIC LAYER - The Atlantic Layer is created by the inflows from the Norwegian Sea and is historically defined as having temperatures above zero. In the Eurasian Basin it consists of the thermocline with increasing salinity and temperature, the temperature maximum associated mainly with the Fram Strait branch, and the salinity minimum created by the Barents Sea branch.

- DEEP WATERS -

Below the Atlantic Layer four different deep waters can be distinguished:

UPPER POLAR DEEP WATER, characterized by a temperature decreasing and a salinity increasing with depth.

CANADIAN BASIN DEEP WATER, is recognized, in the Eurasian Basin, by a salinity maximum at about 1800 m. The Canadian Basin Deep Waters is generally warmer and more saline than the Eurasian Basin Deep Waters.

EURASIAN BASIN DEEP WATER, characterized by a temperature decreasing with depth and a constant or slightly increasing salinity.

EURASIAN BASIN BOTTOM WATER, having both temperature and salinity increasing with depth.

Table 4-1 shows the depth, potential temperature and salinity of the water column at a few levels for each station: at 15 m indicating the seasonal Surface Layer; at the temperature minimum representing the Polar Mixed Layer; at the temperature maximum and the intermediate salinity minimum which describe the two Atlantic inflows; and at the deepest record indicating the nature of the bottom water. For stations shallower than 150 m only the 15 m values, the temperature minimum and the deep record are given.

#### The Program

The oceanography program during the ARK XI/1 cruise studies the merging of the two branches of Atlantic Water entering from the Norwegian Sea, and how the interactions between the Atlantic Water and the upper layers are affected by the freezing and melting of sea ice and by the large injection of low salinity shelf water from the Laptev Sea.

It consisted of four parts: CTD measurements and water sampling; ADCP observations; observations of internal wave motions and mooring deployments. These different parts are described separately below.

Next pages:

*Table 4-1: The depth and the characteristics of the 15 m level, the temperature minimum, the temperature maximum, the intermediate salinity minimum and the bottom value. For depths less than 250 m only levels 1, 2 and 5 are given.*

Layer:	Surface			Temp. min.			Temp. max.			Sal. min.			Bottom		
Stat.	press.	theta	sal.	press.	theta	sal.	press.	theta	sal.	press.	theta	sal.	press.	theta	sal.
2	15	-1.71	33.11	28	-1.76	33.40	**	**	**	**	**	**	138	-1.29	34.25
3	15	-1.48	30.43	52	-1.79	33.70	242	2.09	34.89	673	0.28	34.87	1938	-0.89	34.92
4	15	-1.75	33.06	15	-1.75	33.06	**	**	**	**	**	**	44	-1.75	33.07
6	15	-1.80	33.47	51	-1.81	33.55	**	**	**	**	**	**	86	-1.46	33.80
7	15	-1.76	33.23	46	-1.79	33.41	**	**	**	**	**	**	202	0.83	34.75
8	15	-1.78	33.41	54	-1.80	33.47	**	**	**	**	**	**	89	-1.54	33.72
9	15	-1.75	33.25	15	-1.75	33.25	**	**	**	**	**	**	66	-1.80	33.44
10	15	-0.38	32.66	15	-0.38	32.66	**	**	**	**	**	**	44	-1.67	33.08
11	15	0.46	32.92	15	0.46	32.92	**	**	**	**	**	**	31	0.29	32.96
12	15	-0.87	31.96	15	-0.87	31.96	**	**	**	**	**	**	37	-1.69	32.76
13	15	-0.10	31.29	15	-0.10	31.29	**	**	**	**	**	**	41	-1.42	33.59
14	15	0.32	31.46	15	0.32	31.46	**	**	**	**	**	**	45	-1.32	33.76
15	15	1.78	29.55	15	1.78	29.55	**	**	**	**	**	**	53	-1.06	33.99
16	15	-0.63	30.24	16	-0.66	30.46	**	**	**	**	**	**	43	-1.37	33.66
17	15	-1.12	30.62	40	-1.55	33.55	**	**	**	**	**	**	56	-0.83	34.16
18	15	-1.06	30.36	43	-1.62	33.79	**	**	**	**	**	**	88	-0.93	34.20
19	15	-1.32	30.50	39	-1.62	33.70	**	**	**	**	**	**	237	-0.83	34.35
20	15	-0.60	30.17	38	-1.63	33.10	287	1.83	34.86	288	1.83	34.86	464	1.41	34.88
21	15	-0.44	31.46	61	-1.70	33.84	240	1.57	34.82	241	1.57	34.82	1153	-0.16	34.88
22	15	-0.63	30.14	54	-1.83	33.71	219	1.91	34.85	674	-0.07	34.82	1769	-0.72	34.91
23	15	-0.85	29.95	69	-1.85	33.72	270	1.98	34.90	699	0.05	34.87	2323	-0.91	34.93
24	15	-1.47	30.50	46	-1.80	33.27	249	1.87	34.88	744	-0.15	34.86	3121	-0.93	34.94
25	15	-1.73	33.44	90	-1.82	34.44	262	2.64	34.96	563	0.57	34.87	2544	-0.93	34.93
26	15	-1.74	33.38	21	-1.76	34.11	265	2.72	34.96	1015	-0.26	34.91	2926	-0.93	34.94
27	15	-1.71	34.06	85	-1.84	34.43	299	2.68	34.96	1077	-0.36	34.91	3130	-0.93	34.94
29	15	-1.73	33.15	44	-1.83	34.34	203	1.93	34.87	337	0.13	34.78	2042	-0.90	34.92
30	15	-1.68	32.37	40	-1.82	34.28	220	2.02	34.91	498	-0.51	34.80	1849	-0.82	34.91
31	15	-1.62	32.51	44	-1.77	34.08	296	0.96	34.84	363	-0.29	34.76	1187	-0.61	34.82
32	15	-1.69	33.75	22	-1.72	33.92	132	0.81	34.67	142	0.08	34.62	564	-0.43	34.74
33	15	-1.34	33.13	40	-1.60	34.42	107	0.69	34.77	144	-0.65	34.69	236	-0.33	34.75

35	15	-0.11	32.88	44	-1.77	34.43	307	0.04	34.79	307	0.04	34.79	318	0.01	34.80
36	15	-1.30	32.31	15	-1.30	32.31	**	**	**	**	**	**	84	-1.47	34.32
37	15	-1.47	33.04	64	-1.54	33.69	**	**	**	**	**	**	177	-0.67	34.48
38	15	-0.39	31.73	38	-1.51	33.60	**	***	**	**	**	**	250	-0.07	34.64
39	15	0.01	30.06	15	0.01	30.06	**	**	**	**	**	**	244	-0.70	34.45
40	15	-0.30	29.37	61	-1.83	33.67	277	1.86	34.88	586	0.37	34.85	1758	-0.71	34.91
41	15	-1.35	29.36	56	-1.80	33.48	267	1.99	34.89	756	0.01	34.86	1946	-0.80	34.91
42	15	-1.58	30.31	67	-1.82	33.71	235	1.91	34.88	661	0.10	34.86	2106	-0.85	34.90
43	15	-1.56	29.99	74	-1.79	33.83	233	1.89	34.88	674	0.04	34.86	2518	-0.92	34.93
44	15	-1.61	30.86	58	-1.81	33.41	246	1.86	34.88	497	0.64	34.86	2863	-0.92	34.93
45	15	-1.60	30.40	55	-1.79	33.30	255	1.79	34.87	270	1.75	34.87	3408	-0.93	34.94
46	15	-1.74	32.55	132	-1.84	33.98	282	1.75	34.87	666	0.08	34.86	3549	-0.94	34.94
47	15	-1.65	31.20	50	-1.81	33.52	247	1.75	34.87	259	1.72	34.87	3912	-0.94	34.94
48	15	-1.59	30.71	46	-1.80	33.35	256	1.78	34.87	713	-0.05	34.86	2896	-0.92	34.93
49	15	-1.59	30.50	67	-1.81	33.52	253	1.80	34.87	652	0.08	34.85	2379	-0.91	34.92
50	15	-1.65	30.98	49	-1.78	33.27	256	1.79	34.87	622	0.21	34.85	2010	-0.86	34.92
51	15	-1.65	31.35	48	-1.79	33.24	236	1.75	34.86	676	0.16	34.85	1723	-0.84	34.92
52	15	-1.66	31.25	47	-1.79	33.30	247	1.80	34.87	661	0.09	34.86	1218	-0.47	34.89
53	15	-1.65	31.04	38	-1.78	33.15	259	1.60	34.86	276	1.54	34.85	928	-0.23	34.87
54	15	-1.66	31.48	45	-1.78	33.17	248	1.64	34.85	248	1.64	34.85	1379	-0.52	34.91
55	15	-1.66	31.12	52	-1.79	33.26	237	1.43	34.84	237	1.43	34.84	1669	-0.51	34.94
56	15	-1.66	31.48	45	-1.79	33.10	247	1.51	34.84	256	1.46	34.84	2020	-0.51	34.95
57	15	-1.73	32.31	61	-1.79	33.53	265	1.45	34.85	284	1.35	34.84	2607	-0.51	34.95
58	15	-1.73	32.19	52	-1.76	33.14	236	1.42	34.84	254	1.33	34.84	2315	-0.51	34.95
59	15	-1.72	32.15	46	-1.76	33.02	267	1.57	34.86	675	0.14	34.85	2022	-0.50	34.95
60	15	-1.72	32.19	47	-1.76	33.02	273	1.58	34.85	293	1.48	34.85	1743	-0.51	34.94
61	15	-1.69	32.11	40	-1.76	33.05	261	1.55	34.85	673	0.06	34.85	1458	-0.61	34.90
62	15	-1.70	32.34	46	-1.76	33.05	238	1.60	34.84	469	0.49	34.84	1047	-0.23	34.88
63	15	-1.60	31.94	27	-1.73	33.12	351	1.25	34.86	470	0.54	34.83	728	0.12	34.85
64	15	-1.63	32.02	27	-1.74	33.09	305	1.49	34.85	320	1.36	34.83	512	0.57	34.84
65	15	-1.70	32.09	58	-1.79	33.54	**	**	**	**	**	**	226	1.07	34.75
66	15	-1.70	32.27	63	-1.80	33.58	261	1.67	34.85	551	0.56	34.85	565	0.53	34.85
67	15	-1.71	32.36	56	-1.79	33.56	257	1.49	34.83	274	1.39	34.83	981	-0.20	34.86
68	15	1.31	29.05	83	-1.85	33.83	275	2.00	34.89	736	0.10	34.86	1696	-0.75	34.91



Layer: Stat.	Surface		Temp. min.		Temp. max.		Sal. min.		Bottom	
	press.	theta	press.	theta	press.	theta	press.	theta	press.	theta
69	15	0.74	63	-1.78	300	1.84	626	0.38	1175	-0.19
70	15	0.53	49	-1.72	291	1.76	291	1.76	790	0.18
71	15	-0.42	64	-1.71	270	1.82	584	0.61	584	0.61
72	15	-1.22	29	-1.56	**	**	**	**	234	-0.75
73	15	-1.04	15	-1.04	**	**	**	**	90	-1.30
75	15	-1.73	49	-1.80	230	1.96	281	1.50	3592	-0.94
77	15	-1.62	73	-1.84	265	2.24	877	-0.17	3356	-0.93
78	15	0.82	43	-1.64	256	1.95	646	0.15	3084	-0.93
79	15	-1.14	32	-1.63	213	1.22	257	0.61	1637	-0.70
80	15	1.00	41	-1.61	246	2.34	783	-0.46	1099	-0.43
81	15	0.18	45	-1.53	288	0.78	353	0.10	521	0.04
83	15	-0.72	43	-1.54	**	**	**	**	225	-0.42
84	15	-0.26	15	-0.26	**	**	**	**	88	-1.37
87	15	-0.77	39	-1.38	**	**	**	**	**	-0.26
88	15	-1.45	34	-1.61	194	2.01	219	1.44	1693	-0.73
89	15	-1.68	35	-1.70	254	2.64	918	-0.69	2729	-0.92
90	15	-1.59	45	-1.73	258	2.54	531	0.10	1739	-0.78
91	15	-1.63	48	-1.65	212	1.34	223	1.02	1002	-0.66
92	15	-1.59	51	-1.66	183	0.68	183	0.68	519	-0.72
93	15	-1.42	39	-1.54	87	1.53	213	-0.93	227	-0.93
94	15	-1.66	15	-1.66	**	**	**	**	78	-1.36
95	15	-0.75	51	-1.75	134	0.37	190	-0.66	309	-1.02
96	15	0.12	15	0.12	**	**	**	**	245	-1.25

#### 4.1.1 CTD observations (B. Rudels, C. Darnell, J. Gunn, E. Zakharchuck)

The CTD work consisted of CTD casts and water sampling. A total of 87 CTD stations were obtained in the area and, in addition to the primary measurements of temperature, conductivity and pressure, water samples were taken at all stations and analysed for oxygen, nutrients, alkalinity and pH. Samples, to be analysed ashore, were taken for CFCs, Helium-3, Tritium, Oxygen-18, dissolved organic matter, Barium and total inorganic carbon. Moreover, large volume samples were collected from the rosette for Radium, Krypton and for biological studies. On several stations this resulted in multiple casts, and, thus, a total of 122 CTD casts were taken.

A Seabird SBE-11 plus CTD and a Seabird Carousel rosette equipped with 12.5 l Niskin bottles were used. The system worked smoothly during the entire cruise. To keep track of the CTD sensors at least one salinity sample was taken at each station and was measured on board using a Guildline 800 autosal. Two protected and one unprotected thermometers (Gohla) were attached to four of the Niskin bottles.

A CTD thermistor broke in the middle of the cruise (station 34) and had to be replaced. This led to a jump in the salinity (the difference between the CTD and the measured bottle salinities were around -0.003 before the exchange and about -0.009 after). Apart from this jump the sensors appear (at this stage) to have been very stable.

Six transects from the deep basin across the continental slope onto the shelf were obtained: in the East Siberian Sea (a), in the eastern (b), central (c) and western (d) Laptev Sea, toward Severnaya Zemlya (e) and into the Kara Sea (g). One section was also taken from the Amundsen Basin across the Lomonosov Ridge into the Makarov Basin.

On the Kara and Severnaya Zemlya sections a rather narrow frontal zone was observed, separating almost undiluted Fram Strait branch water from the colder and fresher Barents Sea branch on the continental slope (Fig. 4-1). The frontal area was characterized by strong lateral mixing, and several inversions in temperature and salinity were found. Further to the east this mixing region was broader and the inversions smaller, but more regular having up to 20 interleaving layers with almost the same thickness.

In the area enclosed by the western Laptev Sea and the Lomonosov Ridge transects (Fig. 4-2) the intermediate waters are colder and have a lower salinity, which indicate that the part of the boundary current that reaches so far consists primarily of water entering over the Barents and Kara Seas. The Barents Sea branch is identified as a salinity minimum (Fig. 4-2) which is seen to follow the slope and then turn to flow along the Amundsen Basin side of the Lomonosov Ridge implying that part of the boundary current turns northward and flows toward Fram Strait within the Amundsen Basin. The Fram Strait branch is strongest on the western Laptev Sea section. Its salinity is, however, clearly lower than on the Severnaya Zemlya section, and its warmest part appears to recirculate

toward the west in the Nansen Basin, before it enters the area enclosed by the two transects.

On the East Siberian Sea transect in the Makarov Basin (Fig. 4-3) the salinity maximum of the Atlantic Layer is weaker but still detectable. The temperature is, however, almost as high in the Makarov Basin as in the Amundsen Basin and much higher than what is normally reported for the Canadian Basin. The salinity minimum of the Barents Sea branch is still observed, and the water column down to more than 1600 m is dominated by the relatively low salinity water of the Amundsen Basin. This indicates that the sill depth of the Lomonosov Ridge close to the continental slope is about 1700 m, deeper than the minimum depth (<1000 m) found where we crossed the ridge. This implies that pulses of low salinity, cold, intermediate water may enter the Makarov Basin and show up as colder intrusions deep in the Makarov Basin water column.

At station 51 on the Amundsen Basin side of the ridge a thin layer of warmer, higher salinity water was observed at 1650 m, 50 m above the bottom. The presence of this water, with Canadian Basin Deep Water characteristics confirms a sill depth of 1700 m close to this part of the Lomonosov Ridge. It also indicates that Canadian Basin Deep Water, at least intermittently, crosses the Lomonosov Ridge at other locations than north of Greenland.

The difference between the the water columns of the two basins is clearly seen below the sill depth, the deep water of the Makarov Basin being warmer and more saline than that of the Amundsen Basin. Such differences are not found higher up in the water column. In particular the sharp front over the Lomonosov Ridge, which was observed on the ODEN-91 crossing further to the north, is not to be seen. This implies that the stations obtained during the ARK XI/1 cruise were all taken in a region dominated by the eastward moving boundary current along the continental slope.

The upper parts of the water column, the Surface Water and the Polar Mixed Layer, are more saline in the west than in the east. North of the Kara Sea the temperature minimum is shallow and considerably above freezing, and no underlying isothermal halocline is present (Table 4-1). This allows for a strong heat transfer from the Atlantic Layer directly to the Mixed Layer, which by convection during winter will reach the sea surface and the atmosphere. The depth of the temperature minimum varies strongly, however, and often several minima are seen. Especially at some of the western stations further into the basin the temperature minimum is found much deeper and its temperature is lower.

The high salinity of the Mixed Layer in the west and the absence of a Halocline suggest that the mixed layer there is created primarily out of sea ice melt and Atlantic water. The influence from the river runoff becomes strong only further to the east where the salinity of the Mixed Layer is lower. The depth of the local winter convection then decreases and an intermediate, cold Halocline is developed from the layers of water no longer ventilated by the convection. The Halocline acts as a barrier for the heat transfer between the Atlantic Layer and the Surface Water, and the vertical heat flux from the Atlantic Layer is reduced.

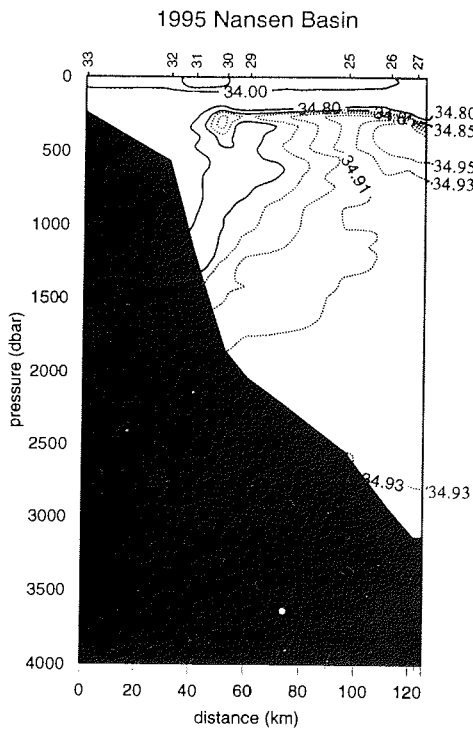


Fig. 4-1: The salinity distribution on the Severnaya Zemlya transect.

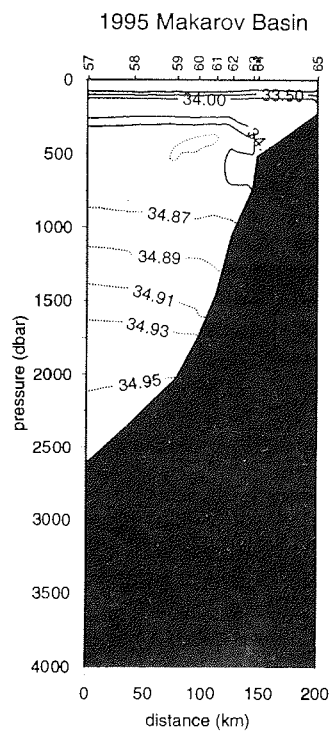


Fig. 4-3: The salinity distribution on the East Siberian Sea transect.

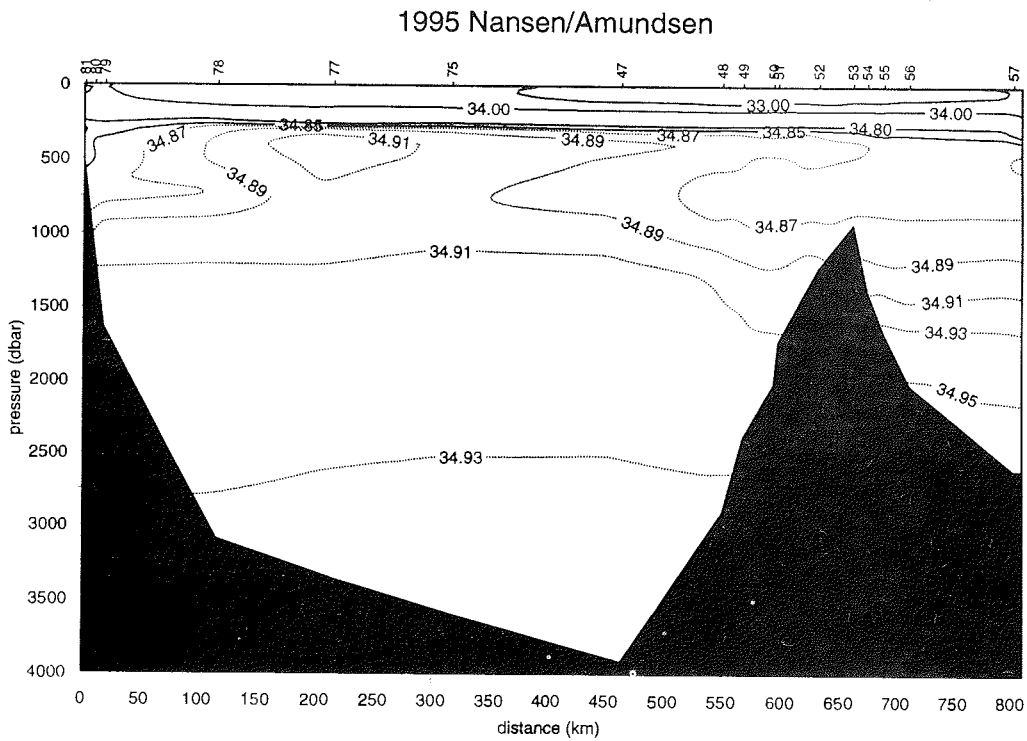


Fig. 4-2: The salinity distribution on a combined section consisting of the Western Laptev Sea and the Lomonosov Ridge Sea transects.

Further sources for Halocline water are to be found on the shelves, where brine released during freezing may lead to the formation of water dense enough to be injected between the Polar Mixed Layer and the Atlantic Layer. At some stations the Halocline has fairly high temperatures and salinities, which suggests that the convection on the shelves could penetrate into and further cool an already diluted layer of Atlantic water, which then enters the basin supplying one of the layers of the Halocline.

The observations obtained during the ARK XI/1 then support the idea of two separate inflows from the Norwegian Sea, which come together and interact north of the Kara Sea. The high temperatures observed in both the Amundsen and the Makarov Basin are also in accordance with recent observations in the Canadian Basin that an influx of warmer Atlantic water across the Lomonosov Ridge is taking place. The lower salinity of the Polar Mixed Layer to the east suggests that most of the river run-off from the Ob and the Yenisei as well as from the Lena enters the Eurasian Basin over the Laptev Sea.

#### 4.1.2 Acoustic Doppler Current Profiler Observations (J. Gunn)

The upper layers of the water column were sampled during the ARK XI/1 cruise using the hull-mounted Acoustic Doppler Current Profiler (*ADCP*). This instrument uses four orthogonal beams of high frequency sound (150 kHz) angled 30 degrees from the vertical to measure water currents beneath the ship to a depth of 350 m, or the bottom, whichever is shallower. The *ADCP* measures currents by sensing the Doppler shift of the returned echo as it passes through the water column and converting this into a profile of current velocity.

The *ADCP* was used in either one of two modes during the cruise. The first mode, bottom tracking, measured the currents as well as the ship's velocity while underway. In this mode the absolute currents on the shallow shelf could be measured as the ship transited an area. In the second mode, drifting, the ocean bottom was beyond the range of the *ADCP*, and direct measurement of the bottom velocity was not possible. In this mode the ship's position as recorded by the ship's GPS navigation system was used to estimate ship velocity. This mode was used while the ship was drifting on station and during slow speed maneuvers. The second mode was used the majority of the time.

The sampling interval in the *ADCP* is selectable by the user and was generally set at one minute in order to optimize the maximum measurement accuracy and resolve the desired frequencies in the currents. A sampling time of five minutes was used during bottom tracking mode in order to minimize the higher signal noise levels occurring during underway data collection.

The *ADCP* current measurement program had two primary goals. The first goal was to obtain time averaged estimates of the vertical shear of horizontal currents, so these could be related to the temperature and salinity distribution as measured by the concurrent CTD program. The warm, saline core of Atlantic water, at depths of 300 to 350 meters falls within the profiling range of the *ADCP*. Preliminary review of the data showed significant vertical shear associated with

the presence of the Halocline at the upper boundary of this water mass as well as with other weaker features above it.

The second goal of the program was the detection of internal waves as present in the upper ocean to assist in the evaluation of their influence in mixing and the observed distributions of temperature and salinity. Previous observations in the Laptev Sea during ARK IX/1 in 1993 revealed internal waves increasing towards the shelf break; and combination of the two data sets may provide an excellent opportunity for detailed spectral analysis.

Data were collected during most stations and at several transits along the shelf. In total over 650 hours of ADCP data were collected at 78 locations. At approximately one fourth of the stations, data were collected continuously for periods in excess of 12 hours. The resulting time series of currents will allow evaluation of vertical shear in the horizontal currents which can be important to upper level oceanographic processes such as internal waves and other parameters important to ocean mixing processes.

The ADCP was not used during transit through pack ice due to the interference to quality of data collection caused by ice and bubbles in the path of the acoustic signal. Interruption of the acoustic path in this manner produces spurious signals in the data which prevent reasonable data analysis. Experience has shown this to be a common problem with ADCPs used in sea ice. Other than this, the system performed very well with no problems apparent at this time, given the preliminary level of analysis of data.

#### 4.1.3 Mooring Deployments (C. Darnall & B. Rudels)

During the cruise three moorings were deployed at the continental slope and at the Lomonosov Ridge. The moorings were located at the 1700 m isobath, one north of the Laptev Sea, one north of the East Siberian Sea and one on the Eurasian side of the Lomonosov Ridge. The positions are shown on the cruise map (Fig. 3), and the general design of the moorings is indicated in Fig. 4-4. The objectives of the deployment are to determine the strength of the boundary current and to study the inferred splitting of the current at the Lomonosov Ridge.

The moorings were equipped with 5 current meters placed at 100, 270, 700, 1100 m and 20 m above the bottom. The two uppermost and the deepest current meters were combined with Seacats to more accurately measure the conductivity and temperature. The chosen depths should allow for a monitoring of the Halocline (100), the warm Atlantic core (270), the Barents Sea inflow (700 and 1100 m) and also determine if any dense water leaves the shelves in this area. This would presumably show up as a velocity increase close to the bottom.

Two of the moorings had upperward looking sonars for the study of ice motions and the one at the Lomonosov Ridge was also equipped with two sediment traps.

After initial heavy ice conditions to the east the mooring were deployed during the middle and later parts of the cruise. The deployments were all anchor first. The first deployment was at the ice edge, and the wind was occasionally fairly

strong causing a large angle on the mooring line. The other two deployments were made within the ice cover and under ideal conditions. The moorings were all put at their planned depths.

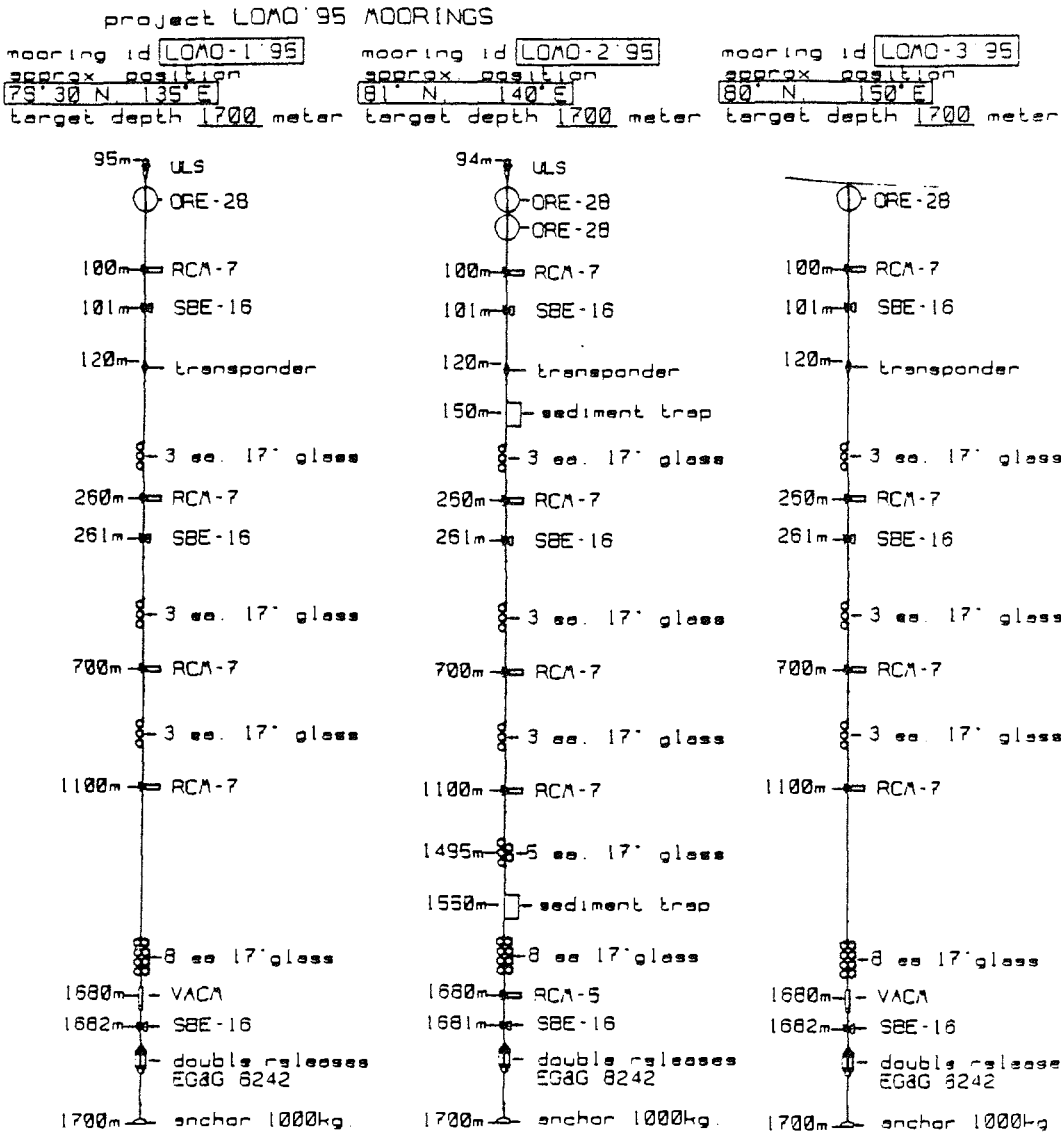


Fig. 4-4: The design and the planned positions of the three moorings.

The mooring deployment involves the effort of several institutions, (APL Seattle, AWI Bremerhaven, University of Göteborg, IfM Hamburg, SAIC Seattle)

and can be considered a part of the Arctic Climate System Study program initiated by WMO. They are to be recovered by ODEN and POLARSTERN during the planned ACSYS cruise in 1996.

*(Note by the editor: All the moorings were successfully recovered during the ACSYS cruise of POLARSTERN in summer 1996.)*

#### 4.1.4 Observations of internal waves in the Laptev Sea continental shelf and slope area (E. Zakharchuk)

To study internal waves in the Laptev Sea, observations of small-scale fluctuations in temperature and salinity were carried out on several stations. Measurements were made with a Seabird SBE-19 profiler from the drifting ship at fixed depths in the seasonal pycnocline. The observations lasted for about 1 hour, and measurements were recorded every 10 seconds. As the phase velocity of internal gravity waves is one order of magnitude higher than the drift velocity of the ship, the obtained data can be regarded as representative for the estimation of parameters of internal waves.

Analysis of the obtained data shows that in the sub-surface layer of the Laptev Sea the fluctuations of temperature and salinity have periods from 2 to 13 minutes (Fig. 4-5). Maximum fluctuations of temperature and salinity were 0.2-1.6 °C and 0.3-1.5 PSU respectively. These fluctuations appear to be connected with high-frequency internal gravity waves with frequencies close to the Brunt-Väisälä frequency. The most interesting observation was made at station 80, where a packet consisting of 9 waves with 5 minute period and one solitary wave with 9 minute period were recorded (Fig. 4-5).

Theoretical studies show that in a two-layers ocean the largest velocities of the lower modes internal waves are registered in surface and near bottom layers. Therefore, current measurements were carried out at station 42 from a drifting ice-floe. The measurements were made at a fixed depth (10 m) with an Aanderaa current meter for a duration of 10 hours with 30 second time interval. The results are shown in Fig. 4-6. Intensive, high-frequency fluctuations of the relative current velocity (maximum 13 cm/s) are clearly seen. The period of the current fluctuations varied from 2 to 15 minutes, the same as period of the temperature and salinity fluctuations.

Since tidal motions are present in the Laptev Sea motions, one possible mechanism for the generation of small-scale internal waves and fine structures in temperature and salinity can be proposed:

When an internal, tidal wave arrives at the slope it is destroyed, and small-scale internal waves are generated. Instability of the internal waves intensifies mixing in the continental slope-shelf zone, which leads to the generation of fine structure. This mechanism could explain the wide spreading of fine structures observed at northeast of Severnaya Zemlya. It is also possible that destruction of small-scale internal waves promotes the heat flux from deeper horizons to the sea surface.



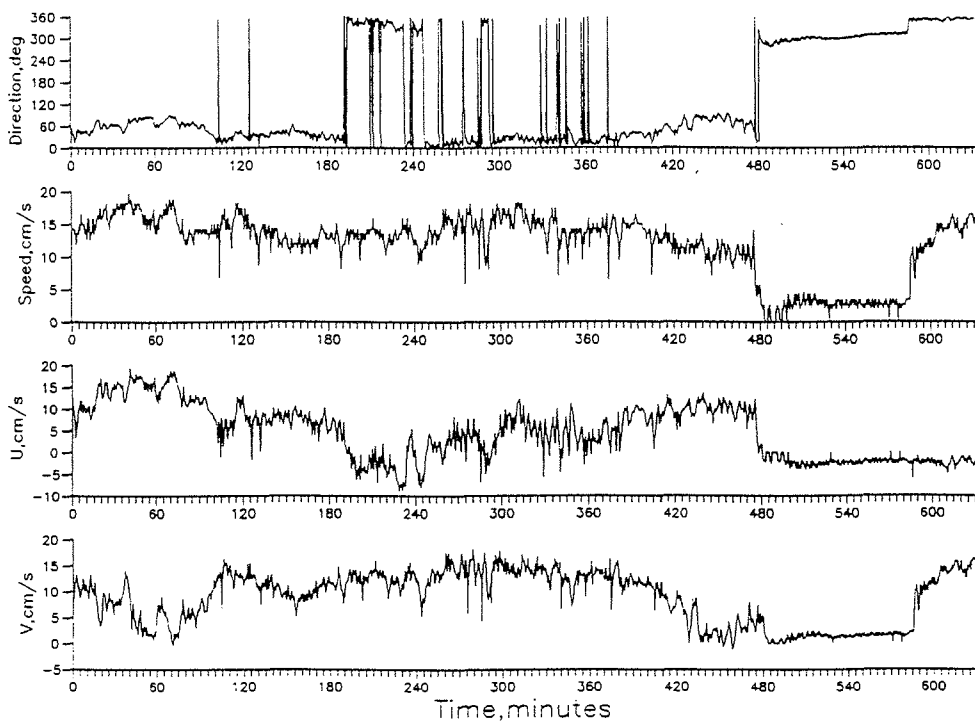


Fig. 4-5: Small-scale fluctuations of temperature and salinity in the seasonal pycnocline at different stations of Laptev Sea.

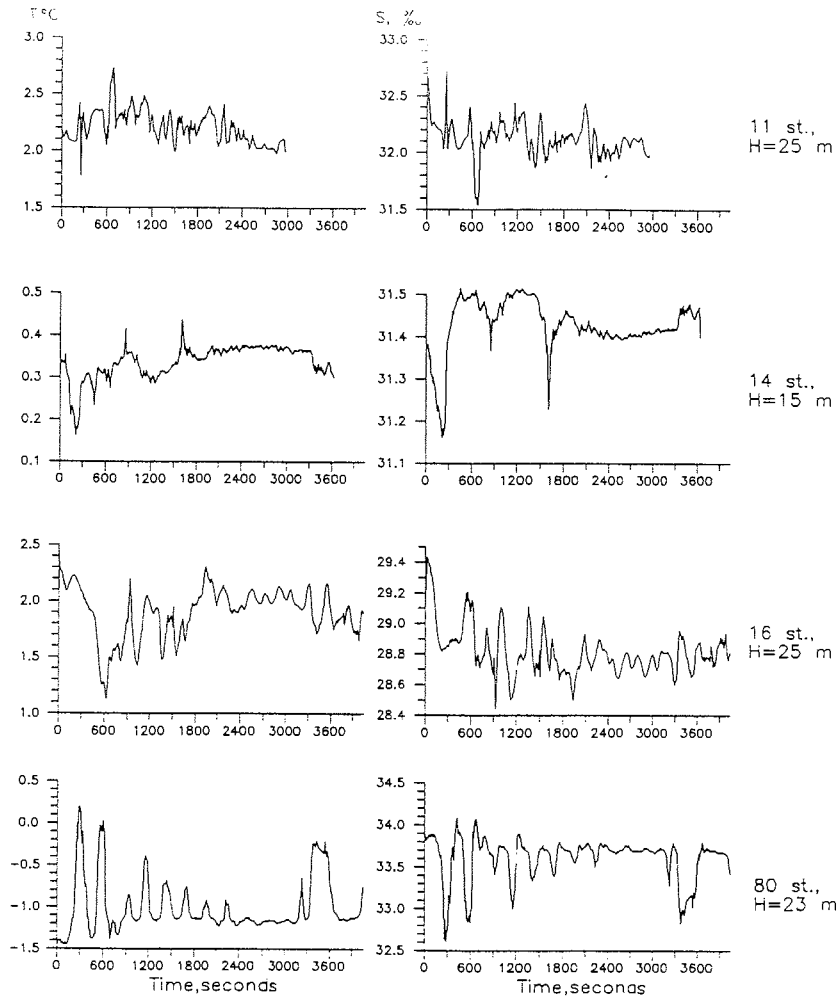


Fig. 4-6: High-frequency fluctuations of relative current velocity at 10 m depth, measured at Station 42 from a drifting ice-floe.

## 4.2 Chemical Oceanography

### 4.2.1 Inorganic nutrients, dissolved oxygen, pH and alkalinity (Y. Nalbandov)

Interest in oceanography of the Arctic Ocean has increased in recent years, in part because of the recognition that this region may respond dramatically to global change. For example, "greenhouse warming" of the troposphere should be most pronounced at high northern latitudes, and global warming may increase primary productivity in the Arctic.

Although polar regions have always fascinated oceanographers, knowledge of nutrient cycling and primary productivity in this region can still be considerably improved.

The Arctic Ocean proper receives about 10% of the world-wide runoff, even though it comprises only 2-3% of the total oceanic area. It also receives low salinity waters via the Bering Strait. These factors contribute to the existence of a strong halocline and shallow mixed layers throughout most of the Arctic Ocean proper. Some investigators suggest that winter convection in the Eurasian Basin is generally limited to depth of less than 50 m. During summer, mixed surface layers throughout the Arctic Ocean are typically a few meters or less, but brines that penetrate to depths of at least a few hundred meters appear to be formed over portions of the shelves during ice-formation.

Studies of dissolved oxygen, elements of the carbonate system and nutrients carried out during the 1995 expedition on "Polarstern" can help us to understand the nature of the processes in the water column as well as in the upper "biologically active" layer as in the deep waters.

Dissolved oxygen, pH and nutrient data are useful to investigate the primary production rates in the upper layers. Total alkalinity and pH measurements will give us the possibility to calculate the carbon dioxide exchange between water and atmosphere in the sub-surface layer. The alkalinity/salinity ratio shows the traces of waters from the rivers or from melted ice. Nutrient measurements in the layers below the halocline help us to find out the Atlantic waters.

#### Methods:

Dissolved oxygen - Winkler method with special bottle capacity of ~100 ml (normality of the titrant solution was tested before each set of samples).

pH - pH-meter/millivoltmeter "pH-121" (calibration of the pH-meter was tested by standard buffer solutions 6.86 and 9.18 before and after each set of samples)

Total alkalinity - automatic titration with 0.015N HCl (25 ml aliquote; normality of the titrant solution was tested before each set of samples)

Phosphates - "Technicon" AutoAnalyzer AA II (according to manuals)  
 Nitrates (3 standard solutions was measured before and after each set of  
 Silicates samples; baseline and drift of each line were taken into account)  
 Nitrites - Bernshnider/Robinson's method with UV-Vis Spectrophotometer  
 (543.0 nm; calibration was tested weekly)

#### Samples:

During the expedition in the Laptev Sea 996 samples were analysed from the Rosette bottles (68 hydrological stations). Dissolved oxygen, pH, total alkalinity were measured directly after recovering during 3-4 hours. Most nutrients were analyzed during 1-5 days after freezing at a temperature of -18 °C.

Additional samples (melted ice, porous water, incubation samples) were measured after freezing at the same temperature. The total number of these samples was 586.

#### Results:

The preliminary results are summarized in the tables of the Annex 11.3.

General pictures of the nutrient distributions in the surface and bottom waters are presented in Figs. 4-7a-f. They indicate reductions in the surface waters especially of the northeastern Laptev Sea and near the marginal ice zones, which may be related to increased primary production.

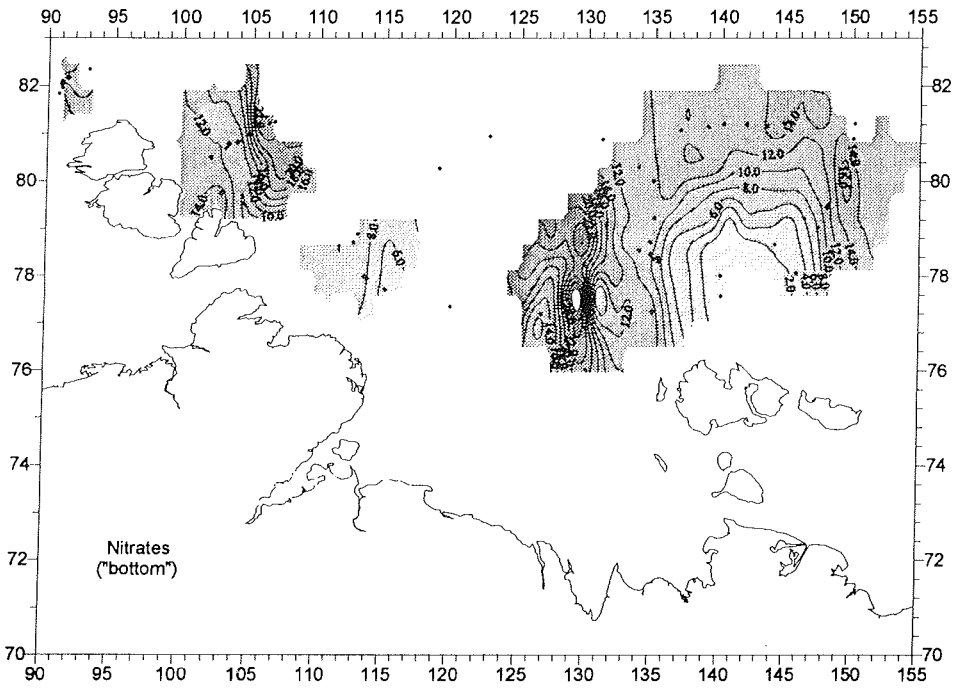
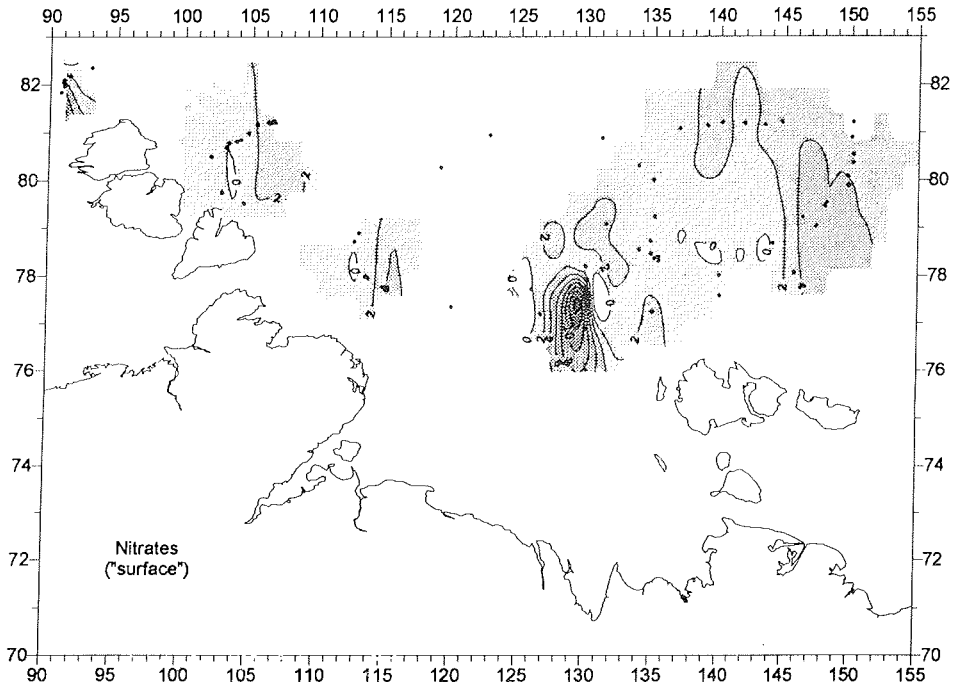
#### 4.2.2 Sampling for Barium and total inorganic carbon analyses (B. Rudels)

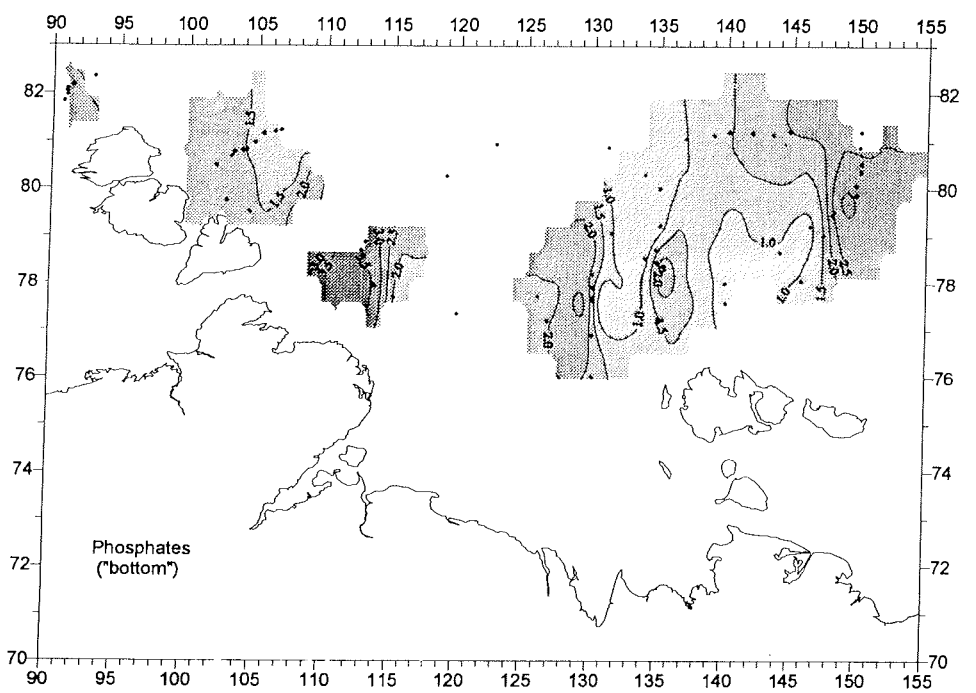
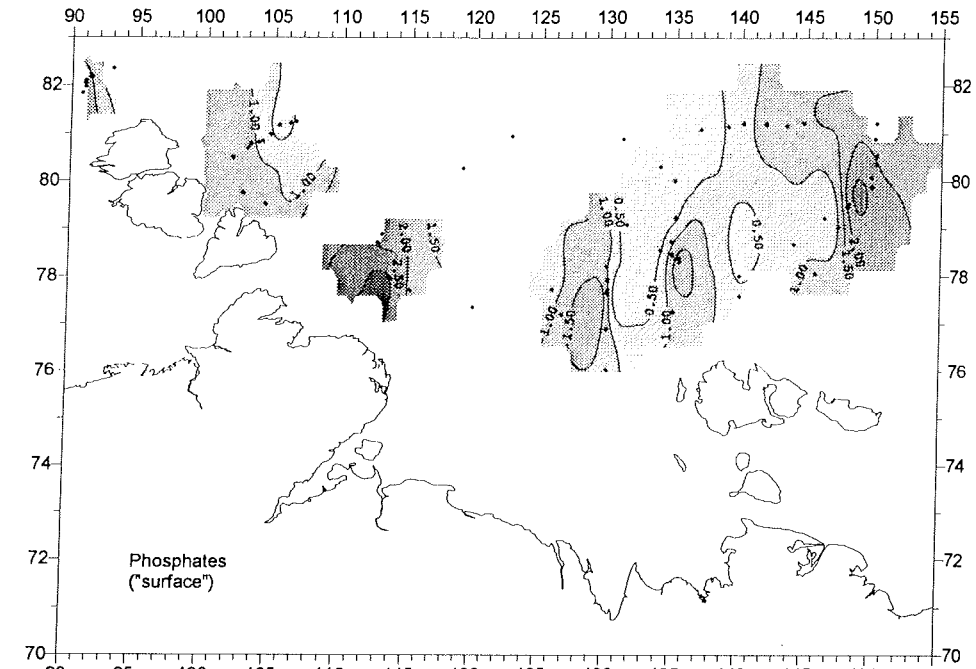
Almost 1000 water samples were obtained for the analysis of Barium content. The samples were taken from the rosette at all depths on most of the stations. They were obtained at the request of and were provided to Dr. K. K. Falkner, Oregon State University, USA, who will carry out the analysis.

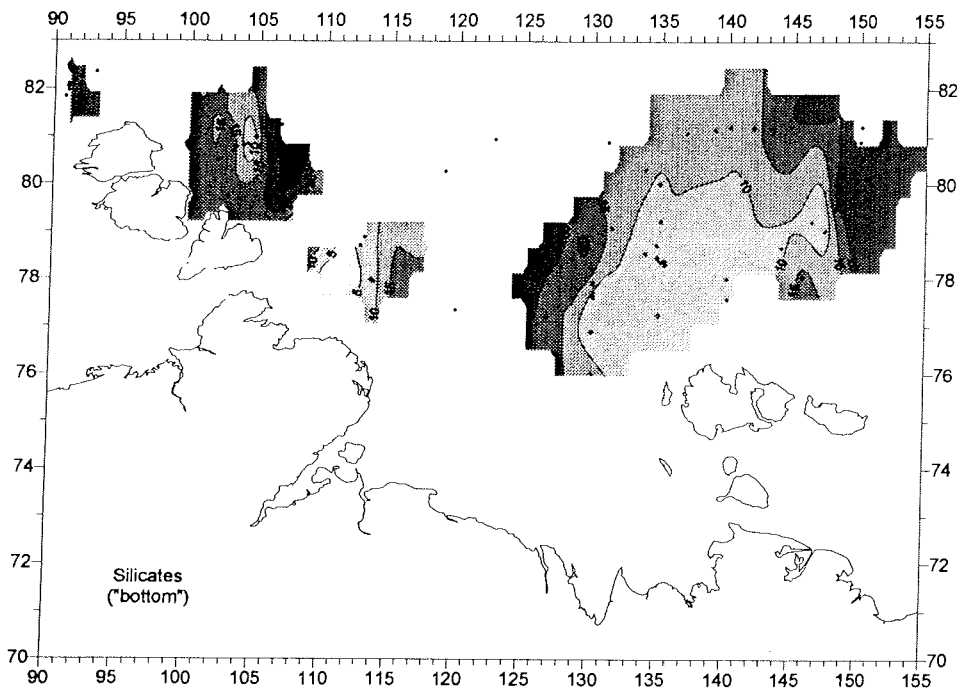
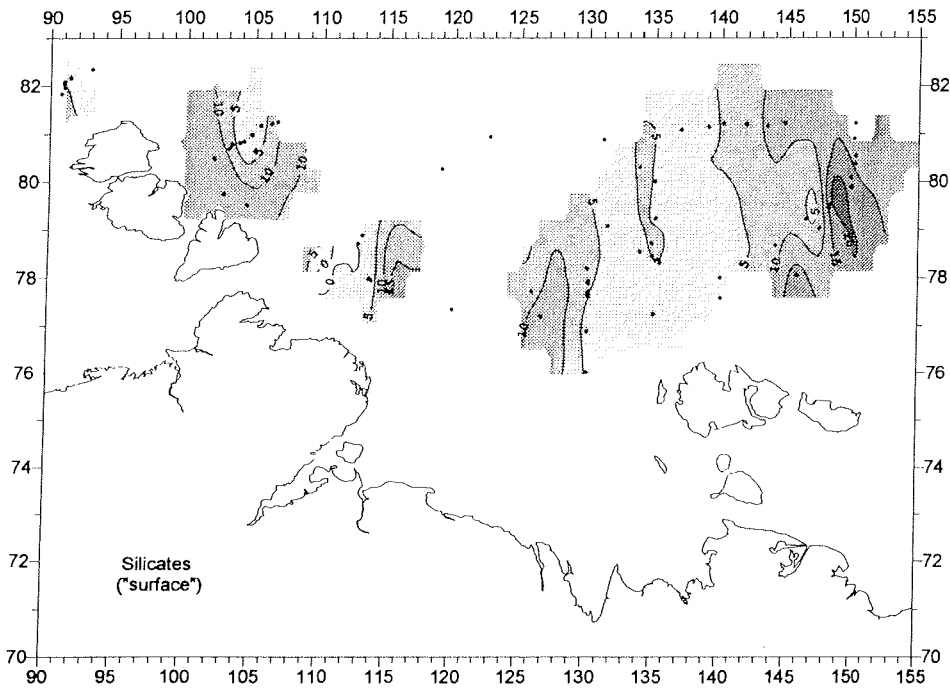
More than 900 water samples were obtained for on-shore analysis of total inorganic carbon. The samples were obtained at the request of and were provided to Prof. L. G. Anderson at the University of Göteborg, who will perform the analysis.

#### Next pages:

*Figs. 4-7 a-f: Maps of spatial distributions of inorganic nutrients in the north of the Laptev Sea (ARK XI/1, summer 1995).*  
*a. Nitrates in surface waters, b. in near-bottom waters*  
*c. Phoshates in surface waters, d. in near-bottom waters*  
*e. Silicates in surface waters, f. in near-bottom waters*







#### 4.2.3 Dissolved organic matter (J. Lobbes & F. Haubrich)

The role of dissolved organic matter (DOM) in marine systems is critical for the understanding of the global carbon and nitrogen cycles. DOM in the ocean contains approximately the same amount of carbon as the atmosphere. Also, the greatest part of nitrogen of the surface water in the oceans is bound as DOM.

It is a very interesting fact that the structure of some organic substances can change to very stable humic compounds, so that these compounds can abandon the active cycles for long periods of time. The humic substances are quite resistant to microbial attack; accordingly, they can represent a sink for (atmospheric) CO<sub>2</sub>.

A significant portion of the DOM in the Arctic Ocean has its origin in the high loads of the Siberian rivers. A part of this terrigenous DOM is transported with the transpolar drift through the Arctic Ocean towards the Fram Strait and the North Atlantic. Organic substances are transported in the form of particulate and dissolved matter in the water masses or included in ice matrices.

*Sampling, work on board, and further treatment of samples in our home laboratories in Bremerhaven:*

During the cruise we sampled water from the CTD and the sea water pump system of *Polarstern*, drilled ice cores and stored surface sediment samples from the MUC. Gelbstoff-fluorescence was measured *in situ* with a fluorescence sensor coupled to the CTD-system. In special water layers and transects general fluorescence was measured with a luminescence spectrometer Perkin Elmer LS 50 B.

A. For extraction of humic substances and other organic substances from sea water specially cleaned XAD-resins were used. 20 ml of resins XAD 2, XAD 4 and XAD 7 were packed in a liquid chromatography column. Before extraction, sea water samples were filtered through glass-fibre filters (GF/C, Whatman). 20 l were acidified to pH 2 with HCl (Merck, Suprapure) and passed through the XAD-column (at a flow rate of 1 l/h). The resins with the adsorbed substances were stored frozen (-18°C) in polyethylene bottles, and also the filters in Petri-dishes.

Back in Bremerhaven the adsorbed substances will be eluted first with 0.2 N NaOH (hydrophobic acid fraction) and second with Methanol (hydrophobic neutral fraction). Several analyses will be carried out on these samples: Primarily we are interested in the contribution of lignin monomers as tracers of terrestrial input to DOM and the time dependent development of their chemical structures. Furthermore in the amino acid distribution, amino acid epimerization and racemization; molecular size and charge variation, <sup>12</sup>C/<sup>13</sup>C ratio, elemental compositions and optical characteristics. The elemental composition of DOM will be compared with the elemental composition of POM (see B.). The particulate material on the filters will be investigated with special interest to the lignin monomers. Altogether, 123 resin samples were obtained.

B. We stored samples for free and combined amino acids, dissolved organic carbon (DOC) and carbohydrate analyses in pre-heated glass-ampoules (5h at 550°C). Samples for dissolved organic nitrogen (DON) analyses were stored in PE-



bottles. All these water samples were filtered through glass-fibre filters (GF/F, Whatman, 5h, 450°C). The water samples and filters were stored at -18°C.

After preparation of the sample materials, amino acids will be analysed by HPLC, DOC by HTCO (high temperature catalytic oxidation). DON will be measured as the difference between dissolved inorganic nitrogen (DIN) before and after wet oxidation. The GFF-filters will be used for analysing carbon content and C/H/N-ratios.

In addition we filtered sea water through 0.4 µm polycarbonate filters for a further chemical characterisation of the inorganic compounds of suspended particulate matter.

Altogether 4 x 528 ampuls, 528 PE-bottles, and 528 GFF-filters are available for these analyses.

C. The organic matter from drilled ice cores of one- and multi-year ice flows will be analysed to estimate the role of sea ice in the transport, transformation and bioavailability especially of humic substances. 24 ice cores samples of 95-204 cm lengths were obtained.

D. In surface sediment cores (20 MUC samples from different water depths, cores up to 30 cm long) we shall analyse the contribution and distribution of lignin monomers to obtain information about the origin and age of the organic matter. In addition, it is planned to make similar measurements with material from deeper sediments (in cooperation with the geologists) and to compare the results with related parameters.

#### 4.2.4 Tritium, $^3\text{He}$ and $^{18}\text{O}$ (W. Stein)

Anthropogenic Tritium was mainly released to the atmosphere by the nuclear weapon testing during the 1950's and 1960's. In the troposphere, Tritium is incorporated in the water molecule and takes part in the natural water cycle. Through river-runoff, precipitation and water vapor exchange it enters the ocean surface waters. Due to its radioactive decay ( $T_{1/2} = 12.43$  y), it can, together with its daughter product  $^3\text{He}$ , be used for the dating of water masses. At the ocean surface  $^3\text{He}$  is in equilibrium with the atmosphere. Once the water parcel leaves the surface, Tritium decay leads to enrichment of  $^3\text{He}$ . The combined measurements of Tritium and Helium allow the calculation of a formal Tritium/ $^3\text{He}$ -age. When no mixing occurs, the formal age is identical to the time since the water parcel has left the surface.

$^{18}\text{O}$  is a stable isotope of oxygen and is as Tritium incorporated in the water molecule. These water molecules are heavier compared to the normal water molecules containing the  $^{16}\text{O}$  and take part in the natural water cycle. The different physical properties cause the water to be enriched or depleted in  $^{18}\text{O}$  each time it undergoes a phase change. Continental rain is depleted in  $^{18}\text{O}$  and river-runoff is marked by low  $^{18}\text{O}/^{16}\text{O}$ -ratios.

The Tritium and  $^{18}\text{O}$  samples taken from the rosette Niskin bottles were stored in 1 litre glass bottles. The samples for Helium analyses were stored in copper

tubes that were closed at both ends with stainless steel clamps while flowing sample water through.

Further processing and measurement of the samples will be done in Heidelberg at the Institute for Environmental Physics. Prior to the measurement, the Helium samples are degassed in a special vacuum extraction system. Helium is then measured by mass spectrometry from the extracted gas.

Tritium analyses will be done using the  $^3\text{He}$  ingrowth method. The water sample is degassed and stored in a sealed glass bulb. During the storage time (usually six months),  $^3\text{He}$  will accumulate from Tritium decay. The measurement of this small gas amount is then also done by mass spectrometry.

For the  $^{18}\text{O}$  analyses an aliquot of water is set in isotopic equilibrium with  $\text{CO}_2$ -gas. The  $^{18}\text{O}/^{16}\text{O}$  ratio of the equilibrated  $\text{CO}_2$  gas is then determined by a special mass spectrometer.

During the cruise about 500 samples were collected for Tritium and Helium analyses and about 750 for  $^{18}\text{O}$  analyses. The stations where samples for Tritium, He and  $^{18}\text{O}$  were taken are: 2, 3, 6, 7, 10, 17, 18, 19, 21, 22, 23, 24, 25, 26, 27, 29, 29a, 30, 31, 32, 33, 35, 36, 40a, 41, 42, 43, 44, 45, 46, 47, 48, 49, 50, 51, 51a, 52, 52a, 53, 55, 56, 56a, 57, 58, 59, 60a, 62, 64, 71, 73, 75, 89, 92. Additional stations were sampled only for  $^{18}\text{O}$ : 4, 9, 11, 12, 14, 16, 37, 38, 39, 65, 66, 67, 77, 78, 80, 81, 84, 90, 91, 93, 94, 95, 96.

#### 4.2.5 Freons and Krypton (S. Searson)

Chlorofluorocarbons (CFC's, "Freons") are a group of man-made compounds that are widely used in refrigerants, aerosol propellants, plastic foam and solvents; most eventually they enter the atmosphere. Atmospheric concentrations have been increasing since their introduction in the 1930's. At equilibrium, the concentration of dissolved compounds in surface waters of the oceans is a function of the atmospheric concentration and the temperature and salinity of the water. Therefore, measurements in the water column and the known historical atmospheric record are used to estimate the age of the water since it was at the surface. Hence, the pathways can be mapped, along which newly formed sub-surface water enters into the interior regions of the Arctic Ocean.

CFC samples were drawn from 12 litre Niskin bottles into 200cc glass syringes fitted with metal caps. Samples were transferred into 60cc glass ampules and then flame sealed. Analysis will be done back at Lamont-Doherty Earth Observatory, using gas chromatography.

Approximately 1000 samples were taken at the majority of all the stations (at about 90 locations; see Fig. 3).

$^{85}\text{Krypton}$  is a radioactive inert gas with a half-life of 10.8 years. It forms when uranium and plutonium undergo fission. The main sources of  $^{85}\text{Krypton}$  to the atmosphere are nuclear weapons testing and nuclear reactors. The specific activity of this radionuclide in the atmosphere, which has been steadily increasing, is well known. Coupled with its inertness, this makes it an ideal tracer of water masses as they become isolated from the surface. It can also be used to

determine if radioactivity from non-atmospheric sources is entering the Arctic Ocean.

Each sample was collected using six Niskin bottles, tripped at the same sampling depth. The water from the Niskin bottles was transferred into three 20 litre pre-evacuated flint glass bottles. A vacuum system was used to de-gas the sample. Approximately one litre of gases were extracted and then stored in pre-evacuated steel tanks. The samples will be analysed at Lamont-Doherty Earth Observatory by low level gas proportional counting.

Nine samples were taken over four stations of transect "E" and eight samples over five stations of transect "G" in order to provide a composite vertical profile for each transect. In addition, there were two samples at deep water stations (greater than 3000m) in the basins north of the central Laptev Sea and one sample in the Barents/Kara Sea outflow observed at station 22.

The tracer data will be interpreted within the framework of the hydrographic data and in collaboration with the other tracer and physical oceanography investigators including R. Bayer, P. Schlosser, B. Rudels, U. Schauer, and R. Muench.

#### 4.2.6 Natural radionuclides (F. Légeleux)

Naturally occurring radionuclides are powerful tools for studying oceanic processes, such as particle dynamics and water mass circulation. During the cruise ARK XI/1, two natural radionuclides have been investigated: Thorium and Radium.

##### *A. Natural radionuclide as tracer for particle fluxes: $^{234}\text{Th}$*

Highly particle-reactive radionuclides, such as Thorium, produced in the water column by decay of their relative soluble Uranium parent, are suitable tracers for studying particle dynamics in the ocean. During ARK XI/1,  $^{234}\text{Th}$  ( $T_{1/2} = 24.1$  d) was measured in order to study particle fluxes related to biological production in the surface ocean and transport and resuspension of particles in the bottom nepheloid layer. Both studies have required the determination of  $^{234}\text{Th}$  activities in the dissolved and particulate forms.

Seawater samples were obtained with the 24 x 12 l Rosette sampler at 16 stations along the East Siberian, the eastern Laptev Sea, the central Laptev Sea and the Severnaya Zemlya transects. For some surface samples, the ship's water supply was used. All samples were filtered over 1 mm Nucleopore filters. Filters were then drained by suction, air dried and carefully folded. Dissolved  $^{234}\text{Th}$  was determined using the following method: addition of a  $^{230}\text{Th}$  spike, co-precipitation of Thorium with  $\text{Fe}(\text{OH})_3$ , ion exchange separation and purification, and plating of Th on silver plate. Because of the very short half-life of this radionuclide (24.1 d), both dissolved and particulate  $^{234}\text{Th}$  activities were measured on board by beta spectrometry. Alpha counting of  $^{230}\text{Th}$  to estimate the efficiency of the chemistry will follow in Bremerhaven.

First definitive results obtained for the particulate phase display at some stations (e.g. 7, 19, 60 and 65) a net increase of the particulate  $^{234}\text{Th}$  content near the bottom, with activities as high as 0.65 dpm/l, suggesting a possible particle resuspension. Final results for the dissolved phase will allow us further conclusions.

Besides, sediment cores were collected with the multi-corer at 4 stations (19, 31, 33 and 65) in order to complete the study of particle transport and resuspension in the bottom nepheloid layer. Indeed, in case of particle resuspension, we should expect a deficit of Thorium relative to Uranium in the bottom nepheloid layer, that may lead to an excess of  $^{234}\text{Th}$  in the surface sediments. Sediment cores were sliced every 0.25 cm, and a known volume of each subsample was filtered. Filters were air dried, carefully folded and counted in beta counter. However, this first counting does not allow us to distinguish  $^{234}\text{Th}$  in excess from that in equilibrium with U in the sedimentary column. This will be possible only after a second counting that will be done in Bremerhaven, when  $^{234}\text{Th}$  in excess will have decreased by radioactive decay.

*B. Natural radionuclides as tracers of the water mass circulation:  
Radium isotopes ( $^{226}\text{Ra}$  and  $^{228}\text{Ra}$ )*

Apart from Thorium, two Radium isotopes were investigated:  $^{226}\text{Ra}$  ( $T_{1/2} = 1602$  y) and  $^{228}\text{Ra}$  ( $T_{1/2} = 5.75$  y). Both are supplied to the ocean from deep-sea and continental shelf sediments. Thus, a water mass in contact with the sea floor is enriched with Ra diffusing out of the sediments. However, since both isotopes have very different half-lives, a high  $^{228}\text{Ra}/^{226}\text{Ra}$  activity ratio in the water column will give evidence of a recent contact with slope and shelf sediments. Our purpose in the context of ARK XI/1 is to try to specify, from the  $^{228}\text{Ra}/^{226}\text{Ra}$  activity ratio distributions in surface and deep waters, the origin and transport rates of shelf waters in the Arctic basin.

Because of the very low  $^{228}\text{Ra}$  activities in seawater, particularly in intermediate and deep waters, seawater samples of about 40 l were collected at 37 stations with the 24 x 12 l Rosette sampler. After filtration, a solution of barium chloride was added to the samples, and Ra co-precipitated with  $\text{BaSO}_4$ . For the stations where  $^{234}\text{Th}$  was also measured, the  $\text{BaSO}_4$  precipitation was done on the same seawater samples, just after the  $\text{Fe}(\text{OH})_3$  precipitation. Then, the  $\text{BaSO}_4$  precipitates were dried and put in small tubes. Radium activities will be determined by gamma spectrometry at the AWI. For the intermediate waters, where  $^{228}\text{Ra}$  contents may be very low, Ra activities will be measured at the *Laboratoire Souterrain de Modane* in France (in collaboration with the *Centre des Faibles Radioactivités*, France, CNRS-CEA), where it is possible to use gamma detectors of high efficiency and very low background.

Furthermore, during ARK XI/1, some sediment cores were collected for radionuclide measurements. These measurements will be done in AWI and in partner laboratories (e.g. IPSN, France).

## 5 SEA ICE PHYSICS AND REMOTE SENSING

### 5.1 Observations on sea-ice conditions in the Laptev Sea during the cruise (H. Eicken, J. Kolatschek, K.-U. Evers, P. Jochmann)

While the ship was moving through the ice, observations on the ice conditions were carried out from the bridge at hourly intervals by a team of observers consisting of A. Darovskikh, H. Eicken, K.-U. Evers, J. Freitag, C. Haas, P. Jochmann, J. Kolatschek, F. Lindemann and A. Zachek. The observations were conducted according to the protocol employed by G. Liljeström et al. during the ARCTIC 91 expedition, with some modifications regarding observations of sediment-laden ice. Data will be compiled and edited by K.-U. Evers and P. Jochmann, who also collected corresponding technical data of ship's performance.

Although these observations are obviously hampered to some degree by bias towards open water with respect to routing of the ship, errors with respect to quantitative estimates of ice concentrations, ice thickness and other parameters as well as intercomparability between different observers, they may nevertheless provide useful information in combination with more objective estimates based on satellite data and radar/video-camera overflights (Sections 5.2 and 5.3). Below, a short overview of ice conditions during the cruise will be given.

During the peak of the melt season in July, the ice margin had retreated to north of 76° N in the Laptev Sea, excepting the region to the Northeast of the Taimyr Peninsula (see satellite image shown in Fig. 5-1). South of 80° N, the ice cover was mostly loose with ice concentrations less than 80 %. East of Vilkitskii Strait, scattered small floes and ice cakes abounded (mostly <10 % ice cover). Some of this ice was highly ridged, with level ice thickness not exceeding 1 to 1.5 m. A portion of this ice had been advected through Vilkitskii Strait from the Kara Sea under prevailing southeasterly wind directions. The fast ice belts lining Bolshevik Island, the Taimyr Peninsula and Maly Taimyr and Starokadomskiy Islands had almost completely decayed by the end of July with some remnants left along the northeastern margin of the Taimyr Peninsula and the eastern coast of Komsomolets Island, where the fast ice was stabilised by large numbers of grounded icebergs (see Fig. 5-1).

Travelling along the ill-defined edge of the loose ice field covering the southern Laptev Sea, "Polarstern" headed for the area north of the New Siberian Islands, where a compact ice edge was met at roughly 78° 05' N and 145° E. Ice concentrations increased to close to 100 % within less than 15 km into the ice. The ice cover was soiled by large amounts of ice sediments found throughout the ice cover. Melt puddle coverage in dirty ice spots was mostly 50 % or larger, with puddle bottoms often covered by a layer of pure sediment. While classic, linear pressure ridges were mostly absent, individual floes consisted of highly rubbled, rough ice devoid of level or flat areas. Due to the compactness of the ice and its thickness which exceeded 2 to 3 m in many areas, the ship did not penetrate far into the pack and traversed into the western Laptev Sea during the first week of August.

After a longer period of persistent strong westerly and southwesterly winds, the ice had started to withdraw from the coast of Severnaya Zemlya during the last week of July and the beginning of August. By mid-August, the waters north of Severnaya Zemlya were ice-free up to a latitude of  $82^{\circ} 30'N$  (see Fig. 5-2; the withdrawal of the ice edge as derived from satellite data shown schematically in Fig. 2-2, see Itinerary), a rather unusual situation compared to the typical ice situation with heavy ice (the so-called Taimyr ice massif) in the western Laptev Sea. This year, a passage past the northernmost cape of Severnaya Zemlya was possible without encountering any ice at all. The ice edge to the East of Severnaya Zemlya was fairly well defined, with bands of ice brash grading into floes of more than 8/10 concentration over a distance of few tens of kilometers at most. The radar satellite scene shown in Fig. 5-2 also shows a prominent band of ice compacted along its windward edge at the extending from the southern reaches of the Laptev Sea pack.

As a result of strong winds and associated swell, ice floes were of comparatively small sizes in the western Laptev Sea, ranging mostly only few hundred meters in diameter with a large fraction of the ice cover composed of small floes and ice cakes. Highly rubbled ice (accounting for more than 50 % of the total ice area and rising up to several meters above the surface) was found at roughly  $81^{\circ} N$  and  $105^{\circ} E$ , these possibly being the remnants of a former shear zone from the East of Severnaya Zemlya. While in the area, satellite data and in-situ observations showed a large piece ( $>20$  km diameter) of former fast ice to detach from the coast of Komsomolets Island and drift eastward. The fast ice cover, sampled at Maly Taimyr and Starokadomskiy Islands when "Polarstern" entered the Laptev Sea, had almost completely vanished.

Helicopter overflights and ship-based observations revealed a large number of icebergs near the source areas of Matussevich Fiord and in particular the outlet glaciers of the northeastern coast of Komsomolets Island. Correlation of altitude measurements and frequency with water depth as derived from the ship's bottom profiling system showed that most of these bergs were grounded on the seafloor. Only few icebergs were sighted within the pack ice of the central and eastern Laptev Sea.

Along the transect towards the Lomonosov Ridge in the East, "Polarstern" passed through a rather homogeneous area of first-year ice extending from about  $135$  to  $150^{\circ} E$  along  $81^{\circ} N$  latitude (see also Section 5.3.4). Floe sizes were mostly in the range of few hundred meters, the thickness of level ice amounted to between 1 and 1.5 meters, with linear ridges mostly less than 1.5 m high occurring within and at the margins of floes. Up to 50 % of the ice was covered by melt puddles which began to freeze over during mid-August. In the East this stretch of homogeneous ice bordered on the rubbled, heavily sediment-laden ice area sampled during the early part of the cruise. This region was revisited in late August, when the degree of compactness of the ice cover had decreased significantly, as also evident when comparing the sharply defined ice edge shown in Fig. 5-1 with the ragged, drawn-out margin in Fig. 5-2.

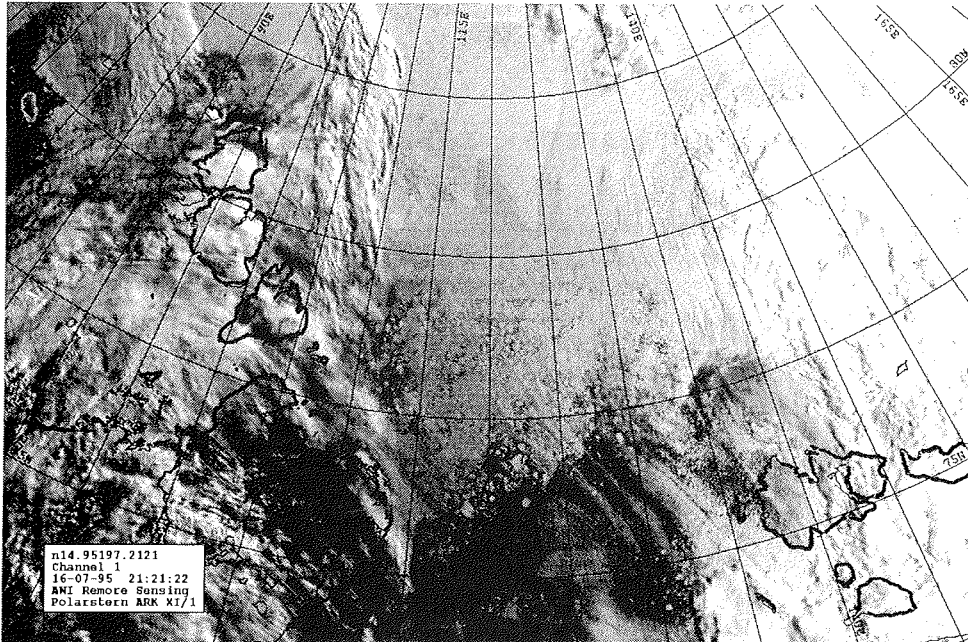


Fig. 5-1: Satellite image for July 16, 1995, from the Advanced Very High Resolution Radiometer (AVHRR) onboard NOAA Satellite 14 (channel 1) showing the ice conditions during the early part of the cruise in the Laptev Sea.

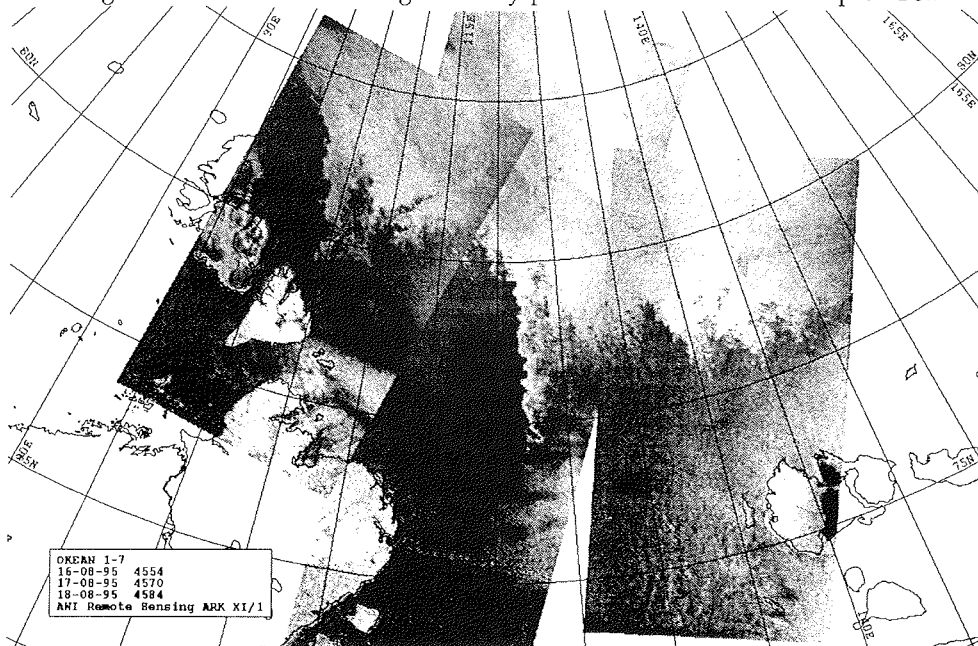


Fig. 5-2: Ice conditions during the second half of the cruise as evident from a composite satellite image based on overflights during August 16 to 18, 1995, from the real-aperture radar flown onboard the Okean satellite.

## Remote Sensing of Sea Ice

### 5.2 Acquisition of satellite data (J. Kolatschek)

#### NOAA - AVHRR data

With a ship mounted receiving system for the AVHRR (Advanced Very High Resolution Radiometer) 180 images transmitted from the NOAA-12 and NOAA-14 satellites were recorded on board "Polarstern" during the cruise ARK XI/1. All the digital data have been archived on magnetic tape.

The AVHRR data consists of five channels, two in the visible part of the spectrum, one in the near infrared and two in the thermal infrared. The swathwidth of the radiometer is 2800 km.

The resolution ranges from 1.2 km in the subsatellite point to 4 km at the edges.

From the top-of-atmosphere albedo values measured with this instrument, ground albedo will be calculated with the help of atmosphere correction algorithms. This should provide important information on the change of albedo of sea ice induced by sediments on the surface.

#### NOAA - DCS data

On September 27, 1995, an ARGOS buoy (number: 9360) was deployed by a helicopter in an area with high sediment concentration on the ice (79° 14.42' N, 152° 04.45' E, see also section 5.3.6). With the Data Collection System (DCS) on board of the NOAA satellites it was possible to track the position of the buoy for some weeks directly from the ship. In this time, the buoy travelled a distance of approximately 160 km from the point of deployment with an average velocity of 4 cm/s (Fig. 5-3).

#### OKEAN - RLSBO data

In cooperation with NPO Planeta and the DLR Neustrelitz it was possible to receive side looking radar data from the RLSBO sensor on board of the Russian OKEAN 1-7 satellite. The information was transmitted in the 137 MHz APT telemetry mode and has a ground resolution of 2.5 km and a swath width of 475 km. The data are also recorded on board of the satellite and downlinked in the 466 MHz mode with a slightly higher resolution to the ground receiving station in Obninsk, when the satellite is in the range of this station.

The data proved to be of high value as an important information source on the condition of the sea ice, especially in times when the working area was covered by clouds and the images of the NOAA satellites were of little value. It was also possible to geocode the received images on board, so that ice charts could be produced with information on the ice extent in the Laptev Sea and as an aid to ship navigation.

Data were received from the beginning of August until the middle of September with on average one complete coverage of the Laptev Sea (three images) per week. It has to be mentioned that, because of the comparatively high meltwater content of the sea ice at the beginning of August which reduced the backscattered



signal significantly, the first images are of lower quality than those which were received later.

A mosaic of three radar images is shown in Fig. 5-2 in section 5.1. The extent of the ice cover is clearly visible. The high backscatter from some areas of open water is caused by waves.

Through the combination of data from the NOAA AVHRR, buoy drift and radar data it is planned to gain information about the ice drift regime in the Laptev Sea and its importance for transport of ice-rafted sediments.

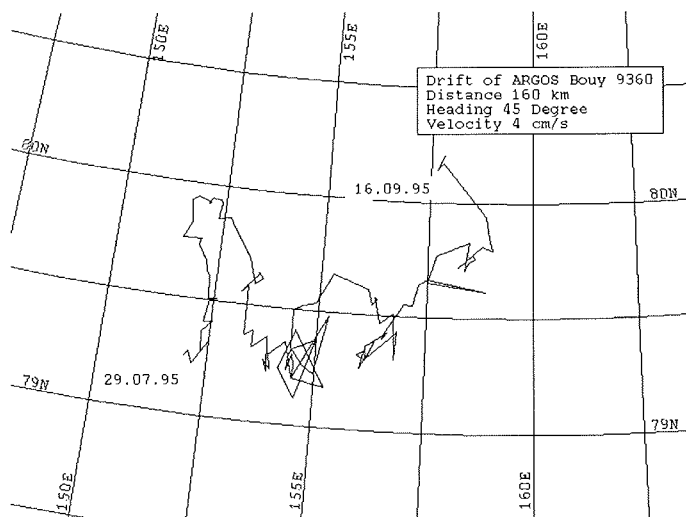


Fig. 5-3: Drift of ARGOS buoy 9360 during the course of the expedition.

### 5.3 Side-looking radar overflights and aerial video recordings

(A. Darovskikh, S. Syrtsov, H. Eicken)

During the ARK-XI/1 cruise, radar investigations of sea ice were carried out with a helicopter-borne side-looking radar. The aims of this investigation are:

- (1) calculation of backscattering coefficients of different ice surfaces and ice types;
- (2) measurements of sizes and shapes of ice floes;
- (3) statistical properties of radar images;
- (4) calculations of ice drift using radar images;
- (5) comparison of side-looking radar images from helicopter with that of radar images from satellites.

The radar data were evaluated and analysed with the help of programs developed by the INTAARI company, St. Petersburg.

The radar looked to the right side along the flight direction. The technical specifications of the system are shown in Table 1.

Table 1: Technical specifications of radar system

Frequency	9.4 GHz
Peak power	3 kW
Pulse duration	100 ns
Pulse repetition frequency	1 kHz
Flight altitude	250 - 1500 m
Swathwidth	( 6 - 10 ) * flight altitude
Horizontal beamwidth	0.5 deg.
Transmitted polarization	Hor.
ADC digitation rate	20 MHz
Range sampling	7.5 m
Weight	85 kg
Used power	9 A, 27 V

For comparison with the radar data and for the determination of ice characteristics (floe sizes, melt puddle coverage, etc.), radar measurements were carried out in conjunction with side-looking and nadir-viewing video recordings (SLVR and NVR ). Table 2 gives an overview of all radar flights.

Table 2: Overview of radar and video flights completed during ARK XI/1 (NVR - Nadir-viewing video recording, SLVR - side looking video recording)

No.	Date	Flight time h:min	NVR time h:min:sec	SLVR time h:min:sec	Starting location deg. min. (decimals)	
1	22-07	1:15	0:20:18	-	77 57.140 N	125 44.52 E
3	24-07	1:30	0:25:18	-	78 03.963 N	144 34.025 E
4	26-07	1:00	0:23:36	-	79 16.802 N	147 32.587 E
5	26-07	0:35	0:09:08	-	79 26.950 N	148 05.539 E
6	29-07	1:05	0:22:32	-	78 34.547 N	144 08.567 E
7	07-08	1:12	0:01:02	-	81 05.919 N	105 20.977 E
8	08-08	0:38	0:05:38	-	81 09.852 N	106 14.878 E
9	09-08	2:00	0:06:14	0:06:43	81 12.339 N	106 55.773 E
10	11-08	0:30	0:10:52	0:24:20	78 40 N	135 00 E
11	11-08	2:00	0:47:21	1:00:37	78 43.527 N	135 00.229 E
12	18-08	0:25	0:03:17	0:02:17	79 09.005 N	135 04.404 E
13	20-08	1:45	0:50:31	0:43:30	80 53.801 N	131 03.809 E
14	22-08	1:00	-	-	81 03.728 N	136 35.244 E
15	22-08	0:55	0:00:33	0:01:38	81 03.792 N	136 19.219 E
16	25-08	1:50	0:47:49	0:41:56	81 10.813 N	143 22.290 E
17	26-08	2:10	0:58:03	0:58:24	81 16.257 N	147 02.971 E
18	30-08	0:50	0:21:15	0:18:00	79 52.387 N	149 48.490 E
19	09-09	2:00	-	-	82 23.236 N	091 32.056 E

Mostly, the length of profiles flown amounted to 60 nm, with a constant speed of 80 knots (above ground) and an altitude of 300 m. Geopositioning of radar data was achieved by GPS receiver (50 m accuracy), logged continuously during each flight. At several locations absolute radar calibration flights were performed. Trihedral corner reflectors (100 m\*m backscattering cross-section) were deployed on the ice and radar overflights carried out at different angles of incidence and altitudes.

Almost the entire study period in the Laptev Sea was characterized by typical summer conditions of melting ice with wet firm and a high amount melt puddles covering the ice surface. The radar backscattering signals of these surfaces are weak, and hence the images exhibit small contrast. Fig. 5-4 shows an example of such type of image. The later flight missions took place under changed conditions. Due to the decreasing surface temperatures melt processes were terminated and the signature of the ice types changed. A typical radar image under these conditions is shown in Fig. 5-5. The contrast in this image is much higher compared with Fig. 5-4, and the texture of the sea-ice radar image can be determined.

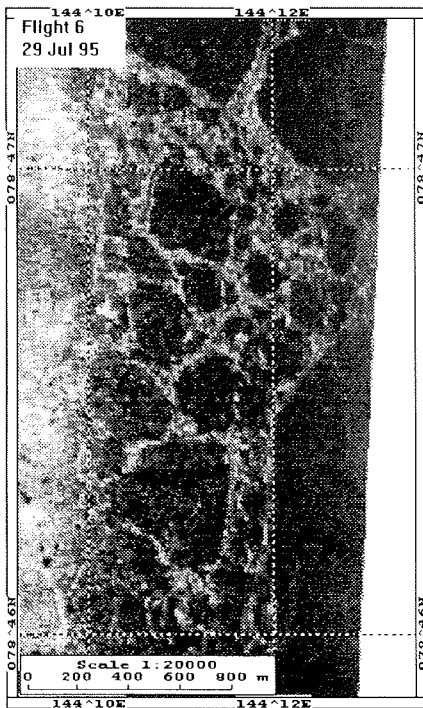


Fig. 5-4: Scene from radar flight 6 (July 29), at 250 m altitude.



Fig. 5-5: Scene from radar flight 16 (August 25), at 500 m altitude.

#### 5.4 Thermal conditions of open and frozen melt puddles

(A. Zatchek, A. Darovskikh)

The processes of destruction and formation of the sea ice cover in summer are determined to a great degree by the intense melting of ridges and the development and freezing of melt puddles and leads. This investigation focusses on physical processes in selected structural units of the sea ice cover, including convective mixing, and on heat budgeting of melt puddles. In this paper we present preliminary results of our measurements.

##### Instrumentation and methods

The following components for estimating the heat energy budget of the surface were measured and calculated:

- global radiation (Q)
- reflected solar radiation (Rk)
- net long-wave radiation (Bl)
- turbulent flux of sensible heat (H)
- thermal profiles in open and frozen melt puddles including
- salinity distribution
- ice core temperature profiles (from puddle bottom)
- puddle ice cover temperatures

Additionally, extensive weather and ice observation were carried out. Short-wave radiation was measured using two pyranometers:

- PP-1 with spectral range of 0.39-0.78 microns
- CM11-from RV "Polarstern"

Long-wave radiation was measured by one pyrgeometer (P2-30) with a spectral range of 2-30 microns. Albedo was measured with a hand-held albedometer mounted on a special cardanic system. Temperature profiles in puddles, in ice and in the air were measured by semiconductor thermistors, data registered on a Laptop PC with time resolution 1 s. The absolute error of the mean temperature is less than 0.02 °C.

Turbulent fluxes: While the ship was in stations the turbulent fluxes were estimated by the most commonly used parametrization:

$$H = C * f * U * (T_a - T_o)$$

where H - sensible heat flux, C - bulk transfer coefficient for sensible heat, U - the wind speed at reference level; T<sub>a</sub> - temperature on the same level, T<sub>o</sub> - temperature of the surface, f - temperature coefficient. Salinity in puddles was measured using a microprocessor salinometer.

##### Data and preliminary results

During the ARK XI/1 expedition, from 05.08. to 04.09.95, on 12 ice stations data of the heat and radiation budget above and within some parts of sea ice cover were obtained. During this period the transition from the melting to the freezing regime occurred in the northern part of the Laptev Sea. Air temperature varied

from +1 to -8 °C (aver. -1.8). Our estimations of components of the heat budget have shown the following results :

incoming SW radiation	+56 W/m <sup>2</sup>
integral albedo of ice cover	52 %
net LW radiation	-9 W/m <sup>2</sup>
sensible heat flux	-24 W/m <sup>2</sup>
latent flux (rough estimation)	-10 W/m <sup>2</sup>
<hr/>	
heat budget	-13 W/m <sup>2</sup>

It is necessary to pay attention to the fact that during the regarded period the air temperature in the near-surface layer (h = 5 cm) in all cases was higher than measured onboard. All of this shows that in August and the beginning of September loss of heat took place. This heat was stored in the ice cover during the period of intensive melting in June - July. Thus, successive measurements of the thermal condition of melting puddles and the proper ice cover show the tendency and cooling rate of ice and freezing of puddles. We would like to point out the role of thermal and density stratification for the processes of heat exchange in puddles with different salinity. As an example, measurements carried out in a melt puddle are presented in the Table 1 below.

Table 1: Temperature conditions of open and frozen melt puddles

STATION NUMBER: (238, Julian day) and PUDDLE NUMBER: 238-1  
 DATE: 27.08 TIME: 7:38  
 POSITION: LATITUDE 81°12' N, LONGITUDE 150°18' E  
 PUDDLE SIZE (m): 4\*30  
 DEPTH (m): 0.25  
 COLOURS: blue  
 ICE COVER THICKNESS: 0.06 m  
 TEMPERATURE IN ICE COVER (°C): -0,06  
 AIR TEMPERATURE (°C): 0.05m above puddle: 0.40  
 29.00m POLARSTERN sens: -0.20  
 WIND on board RV "POLARSTERN" (h = 37 m): 8 (m/s)  
 ALBEDO (%): 24, RADIATION BUDGET (W/M2): 38

TEMPERATURE and SALINITY distribution within the puddle:

depth (m)	temperature (°C)	salinity (ppt)
0.00	-0.03	
0.05	0.19	0.2
0.10	0.29	
0.15	0.34	0.8
0.20	0.25	
0.25	0.12	1.4

## ICE CORE TEMPERATURE DATA (core from puddle bottom)

depth (m)	temperature (°C)
0.05	-0.12
0.10	-0.11
0.20	-0.14
0.30	-0.16
0.35	-0.13

Thus, a good data base for detailed calculations of the mass - and heat - budgets of ice cover was obtained.

### 5.5 Sub-surface and surface morphology of ice pressure ridges (K.-U. Evers & P. Jochmann)

At 14 ice stations along the transects in the Laptev Sea, sub-surface profiling of ice pressure ridges was carried out by application of the sonar technique while the surface morphology was determined by the laser levelling method. The investigated ridges were in general embedded in rubble ice fields. In most cases the ridge sails were weathered, and a significant snow cover was missing.

In general at each pressure ridge 5 surface profiles were measured perpendicular to the ridge sail. In addition to the center profile, 4 parallel lines, two to the left and two to the right side of the center-profile, were drawn in a distance of  $\pm 4$  m respectively  $\pm 8$  m. The elevation of the ridge crest was determined in a range of  $\pm 15$  m, to the left and to the right side of the point where the center-profile line crosses the ridge crest line, in steps of 1 m in order to use the same amount of data for the sail elevation as for the keel depth while computing the  $H_K/H_S$ -ratio.

The location of the sonar head depended on the surrounding ice thickness of the ridge. A hole of 150 mm diameter for sinking the sonar head was drilled at a minimum distance from the ridge sail on the main profile line in the area where no ridge material was expected. A second hole located on the same profile line was drilled in a distance of about 10 m for submerging the sonar reflector.

The sonar head was submerged to a depth of about 16.5 m and adjusted in such a way that the sonar beam was perpendicular to the crest-line of the ridge. For this procedure, the sonar reflector was submerged in the second hole in order to verify the correct direction of the sonar beam on the monitor.

After finishing the scanning of the main subsurface profile, the sonar head was turned stepwise by  $5^\circ$  in a  $100^\circ$  sector, heading from  $310^\circ$  to  $50^\circ$  to describe the spatial elongation of the ridge keel area. The raw data were sampled and stored in ASCII files on a portable PC. The standard software package *Plotit for Windows* was used to process grid files from the raw data to achieve 3-D-images showing the variability of the ridge keel. An example is presented in Fig. 5-6. The same software was employed to plot the sub-surface data together with the surface elevations as 2-dimensional cross sections. Fig. 5-7 shows an example of such 2-D-profile-illustration.

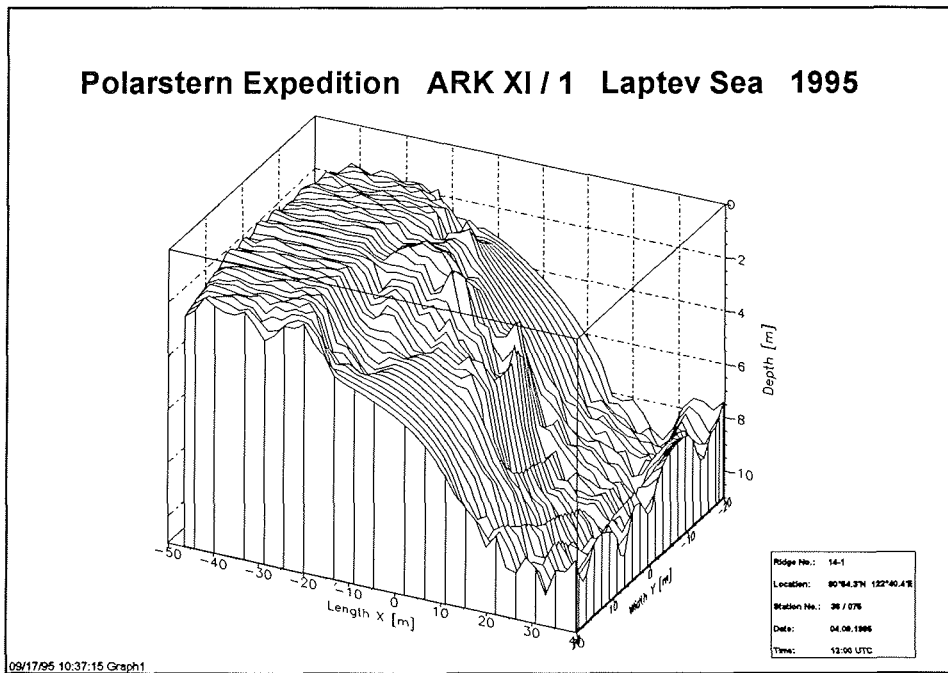


Fig. 5-6: Example of the morphology of a ridge keel (station 75)

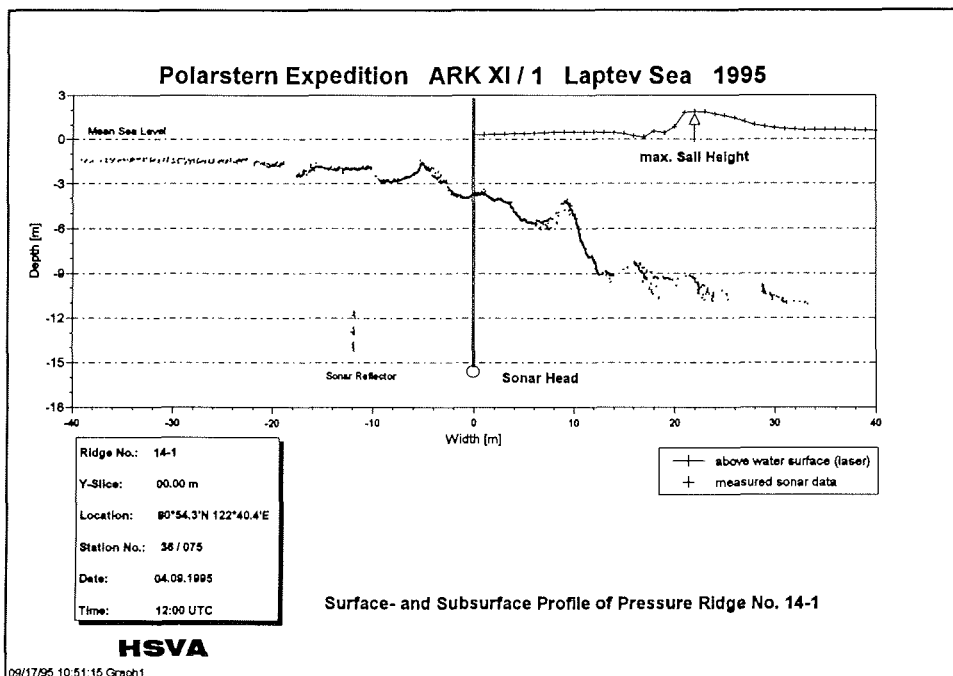


Fig. 5-7: 2-D-profile illustration of the ridge shown in Fig. 5-6

The calculation of characteristic pressure ridge parameters was carried out by use of *MS Excel*. Parameters such as

- sail height and width
- keel depth and width
- sail and keel angle
- $H_K / H_S$  - ratio

are summarized for each individual investigated pressure ridge in form of tables. An example is shown in the subsequent *Table 1*:

Y-Slice	Keel Depth	Sail Height	Ratio	Keel Width	Sail Width	Keel Angle	Sail Angle
	$H_K$	$H_S$	$H_K / H_S$	$K_W$	$S_W$	$\alpha_1$	$\alpha_1$
[m]	[m]	[m]		[m]	[m]	[°]	[°]
-15.0	-9.6	0.7	13.9				
-14.0	-9.7	0.9	11.1				
-13.0	-10.0	1.1	8.9				
-12.0	-9.7	1.4	6.8				
-11.0	-10.4	1.5	6.9				
-10.0	-10.0	1.4	7.3				
-9.0	-10.2	1.4	7.1				
-8.0	-10.6	1.6	6.7	41.6	9.4	12	9
-7.0	-10.5	2.1	5.1				
-6.0	-10.9	1.8	6.1				
-5.0	-10.3	1.9	5.5				
-4.0	-10.3	1.8	5.9	41.6	9.4	12	9
-3.0	-10.8	1.9	5.8				
-2.0	-10.5	1.8	5.7				
-1.0	-10.4	1.8	5.7				
0.0	-10.7	2.0	5.3	43.8	8.3	11	22
1.0	-10.6	2.0	5.3				
2.0	-10.6	2.0	5.5				
3.0	-10.7	1.6	6.8				
4.0	-10.3	1.7	6.1	46.2	7.5	10	10
5.0	-10.4	1.5	6.8				
6.0	-10.7	1.8	6.1				
7.0	-10.3	1.3	7.7				
8.0	-10.7	1.0	10.7	44.0	6.2	9	14
9.0	-10.4	1.5	6.9				
10.0	-10.8	1.6	6.6				
11.0	-10.5	1.6	6.6				
12.0	-10.4	1.6	6.6				
13.0	-10.2	1.5	6.8				
14.0	-10.8	1.4	8.0				
15.0	-9.6	1.4	7.0				
mean	-10.4	1.6	7.0	43.5	8.2	10.7	12.8
std dev	0.4	0.3	1.9	1.7	1.2	1.2	4.9



The mean values and standard deviations of the characteristic parameters of each individual pressure ridge were computed and listed in the Table 2 below. The numbers for the keel and sail angle indicate that all investigated ridges were first-year ridges because the angles of multi-year ridges are steeper. The results of keel width and sail width (half profile) as well as sail height and keel depth are in good agreement with results given in the literature for other Arctic regions (e.g. Beaufort Sea).

Table 2

Station No.	Ridge No.	Keel Depth		Sail Height		Ratio		Keel Width		Sail Width		Keel Angle		Sail Angle	
		$H_K$ [m]	std dev	$H_S$ [m]	std dev	$H_K / H_S$	std dev	$K_W$ [m]	std dev	$S_W$ [m]	std dev	$\alpha_1$ [°]	std dev	$n_1$ [°]	std dev
36/007	1	-9.2		2.1		4.4		7.5		4.1		36.5		30.0	
36/024	2	-18.6	2.2					42.5	2.8			20.9	3.1		
36/027	3	-9.6	0.5	1.1		9.5		20.4	3.6	3.2		17.8	1.6	12.5	
36/042	4	-9.8	0.3	1.4	0.2	7.2	1.3	23.4	3.9	4.8	1.3	30.7	16.5	11.1	6.5
36/044	5	-10.6	0.3	1.3	0.5	9.5	3.1	33.9	5.8	6.0	1.7	11.8	3.0	12.7	7.4
36/045	6	-6.1	0.3	1.0	0.4	6.7	1.8								
36/047	7	-19.0	1.7	4.7	0.4	4.1	0.5	34.4		10.4		18.6		24.9	
36/049	8	-5.5	0.3	1.3	0.2	4.2	0.7	25.1	6.1	5.7	0.5	8.5	1.2	14.8	0.5
36/051A	9	-6.3	0.5	1.3	0.2	5.2	1.1	14.6	1.2	3.2	0.9	10.5	1.0	19.4	8.3
36/055	10	-9.4	0.5	1.5	0.2	6.4	1.4	26.3	4.5	6.0	1.9	12.2	2.5	13.1	5.6
36/057	11	-12.2	0.7	1.8	0.3	6.9	1.3	28.2	3.2	6.0	2.1	18.8	1.3	20.0	6.5
36/062	12	-12.0	1.0	1.4	0.3	8.9	2.5	25.7	5.4	10.9	1.3	23.3	5.6	11.3	3.4
36/074	13	-9.7	0.9	1.9	0.6	5.9	2.4	28.2	3.4	7.1	1.4	19.3	2.9	12.5	5.4
36/075	14	-10.4	0.4	1.6	0.3	7.0	1.9	43.5	1.7	8.2	1.2	10.7	1.2	12.8	4.9
mean		-10.6		1.7		6.6		27.2		6.3		18.4		16.3	
std dev		3.9		0.9		1.8		9.7		2.4		7.9		5.8	

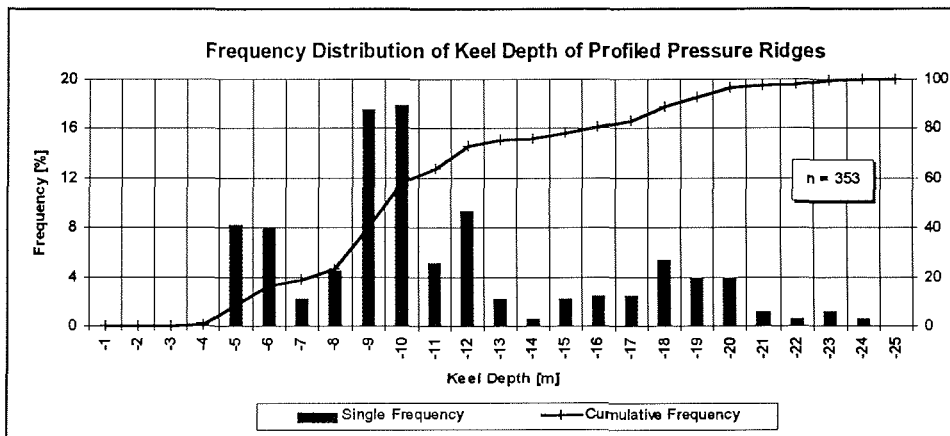
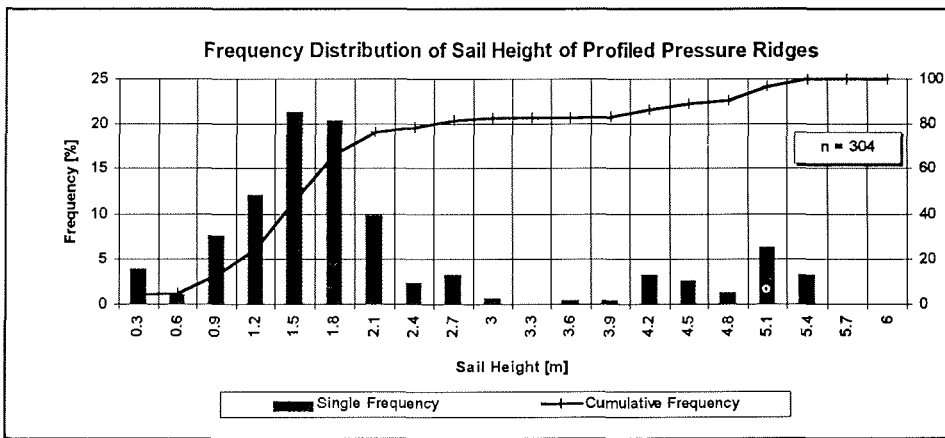
Due to the fact that the mean  $H_K/H_S$  - ratio of  $6.6 \pm 1.8$  is significantly higher than those reported in the literature, detailed analysis was carried out. Looking at the characteristic parameters as they turned out choosing only those data values, where the ridge sail height was found to be a maximum, leads to results as listed in the following Table 3:

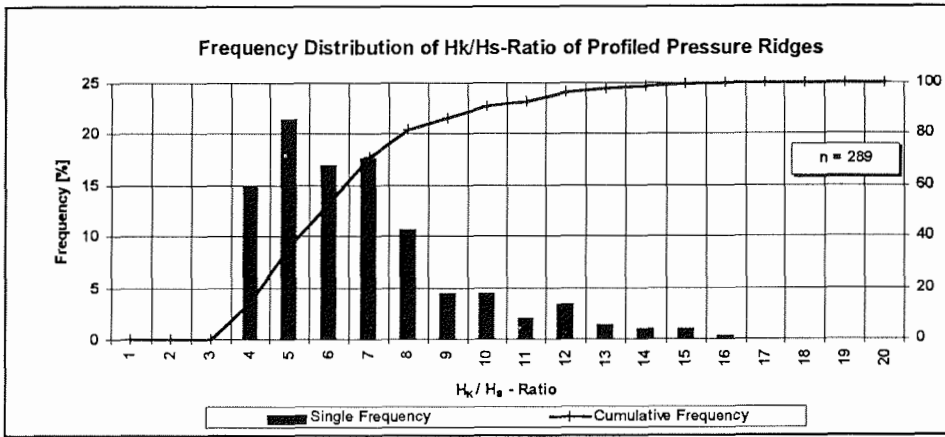
Station No.	Ridge No.	Keel Depth $H_K$ [m]	Sail Height $H_S$ [m]	Ratio $H_K / H_S$	Keel Width $K_W$ [m]	Sail Width $S_W$ [m]	Keel Angle $\alpha_1$ [°]	Sail Angle $n_1$ [°]
36/007	1	-9.2	2.1	4.4	7.5	4.1	36.5	30.0
36/024	2							
36/027	3	-10.2	1.1	9.5	23.1	3.2	17.2	12.5
36/042	4	-9.4	1.5	6.4	17.0	5.9	46.1	10.8
36/044	5	-11.1	2.2	4.9	42.7	4.3	7.3	23.1
36/045	6	-6.1	1.6	3.8				
36/047	7	-18.1	5.0	3.6	34.4	10.4	18.6	24.9
36/049	8	-5.3	1.6	3.4	17.2	6.4	10.0	14.1
36/051A	9	-6.6	1.8	3.7	16.3	2.1	9.5	31.1
36/055	10	-8.3	1.8	4.6				
36/057	11	-12.0	2.6	4.6				
36/062	12	-12.6	2.0	6.4				
36/074	13	-10.3	2.7	3.8	23.4	5.4	21.1	18.2
36/075	14	-10.7	2.0	5.3	43.8	8.3	11.0	22.0
mean		-10.0	2.2	5.0	25.0	5.6	19.7	20.7
std dev		3.2	0.9	1.6	11.9	2.4	12.5	6.9

Subsequently, the  $H_K/H_S$  - ratio turns out to be  $5.0 \pm 1.6$  as a mean for all ridges. Neglecting the value of ridge no. 3, which is with a  $H_K/H_S$  - ratio of 9.5 essentially higher than those of all other investigated ridges, our  $H_K/H_S$  - ratio drops down to a mean of  $4.6 \pm 1$ , which is in good agreement with results reported in the literature.

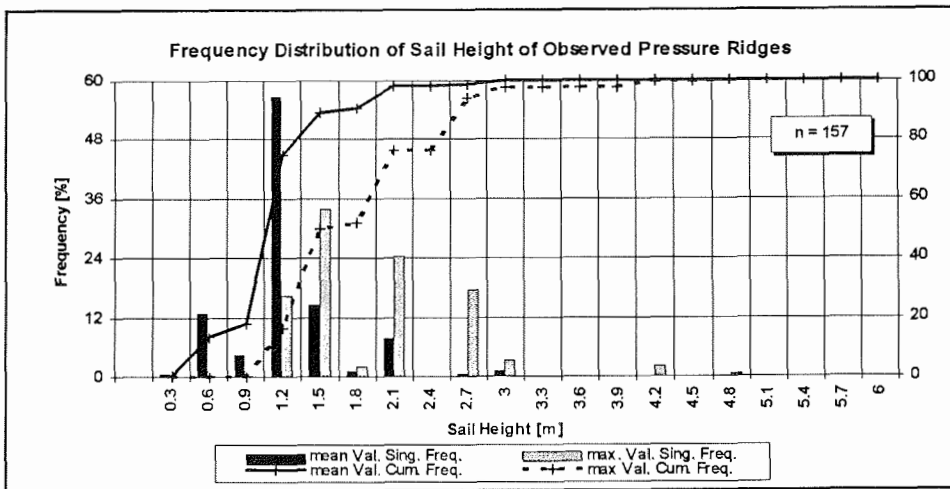
Frequency distributions were computed for the keel depth, the sail height and the  $H_K/H_S$  - ratio obtained from all investigated ridges. The following Figs. 5-6 a-c show the results as histograms of single, respectively cumulative frequencies:

Figs. 5-6 a-c: (see text)





During the hourly ice watch from the bridge of RV POLARSTERN, ice pressure ridges were observed, and their average and maximum values were classified. Data available from 157 records of these visual observations have been analysed and are presented in the following histogram as single, respectively cumulative, frequencies (Fig. 5-7):



The most frequently observed mean value of the ridge sail height is about  $H_S = 1.2$  m, which is insignificantly smaller than the most frequently profiled mean value  $H_S = 1.5$  m. This difference may be caused by the fact that for profiling purposes only ridges with significant sail height were selected.

## 5.6 Thickness and roughness of the ice cover (C. Haas)

### *Laser altimetry*

#### *Sea ice roughness*

With a vertically downward-looking laser altimeter mounted on a helicopter, flights were performed to measure sea-ice roughness, an important parameter for estimating ice-atmosphere interaction, and a major input variable for sea-ice models. The instrument used was an IBEO PS100E (wavelength 905 nm), measuring the instrument height above the ice surface and a relative echo amplitude with a frequency of 2 kHz. With a speed of almost 60 knots above ground at a height of 30 to 40 m above sea level, this resulted in a measurement point spacing of 0.013 m. Most flights were divided into three legs forming a triangle with sides of equal length. In total, 14 flights of 30 to 80 nautical miles in length were undertaken, together resulting in 710 nautical miles of surface profiles. As can be seen in Fig. 5-8, the flights provide a good coverage of the working area; and in particular data from both the homogenous 'clean' ice (Sector II in Fig. 5-8) and the heavily deformed sediment-laden ice (Sector III) were gathered (see section 5.7 for a description of these two regions). Laser data also exist in the vicinity of all three upward looking sonar moorings (Fig. 5-8 "Lomo", see also section 4.1.3 Darnall/Rudels).

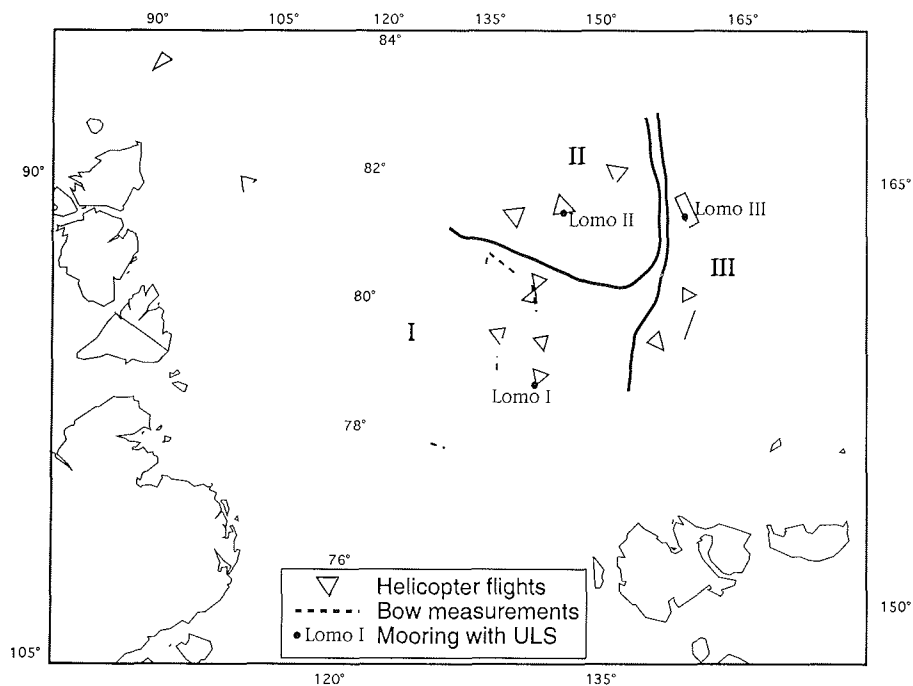


Fig. 5-8: Map showing positions of helicopter laser-altimeter profiles and EM thickness profiles from the ship's bow. Also shown are three sectors of different ice conditions (see section 5.7) and the positions of the moored upward looking sonars, "Lomo I-III".

After data processing, mainly removal of the helicopter motion, ridge statistic estimates like the distributions of ridge height, spacing and shape will be worked out, and aerodynamic drag coefficients will be calculated. Work will then focus on comparison of the different regions outlined above (Fig. 5-8), in particular whether sectors II and III can also be distinguished with regard to their surface roughness structures.

Further, the results of the laser measurements will serve as ground proof for satellite radar-altimeter data (e.g. from ERS-1 and 2), which will be tested for their suitability in monitoring sea-ice roughness in the near future.

Due to the season and region of investigation, two main problems occurred with the laser measurements: First, over melt ponds, which covered 30 to 40 % of the ice surface, as over open water the laser does not get echoes, resulting in many data gaps. Since thus the puddle surface cannot be measured, it is impossible to distinguish between open water and melt ponds (i.e. floe sizes cannot be estimated); and it is more difficult to reconstruct the surface of level ice, which is necessary for the helicopter-motion removal. Second, floe sizes were rather small (mostly less than some 100 m), with a lot of brash covering the narrow leads and wakes in between. Thus, the largest roughness features were often located at the margins of floes, consisting of ice pile-ups or pointed, upright floe segments rather than true pressure ridges. This has to be considered when comparing the results with standard ridge models. A raw-data example is presented in Fig. 5-9, where, coming from a puddled floe, a small standing floe at the floe edge (at 40 m) was profiled, before flying over open water with some brash (40-60 m). Note that the echo amplitude drops to zero over water.

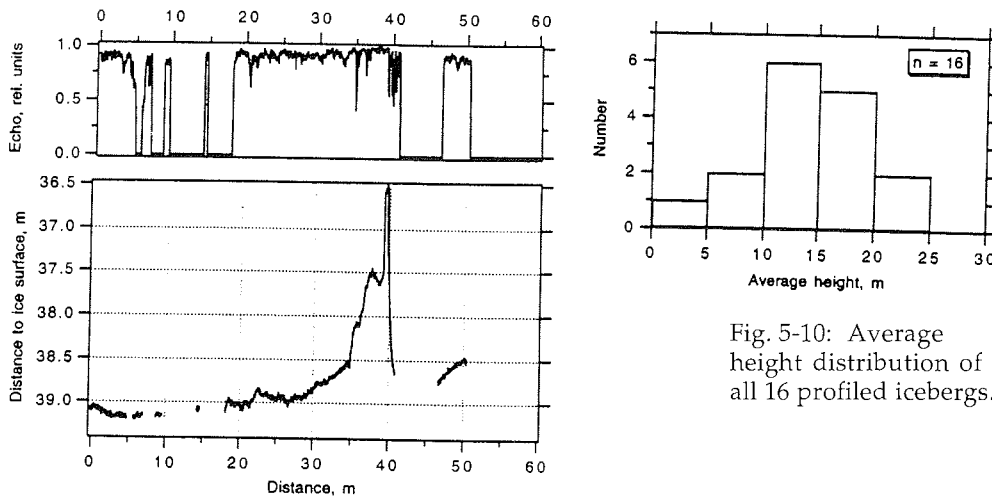


Fig. 5-9: Laser raw-data example showing a short section across a puddled floe (0-40 m) with a small standing floe on its edge (at 40 m). 40 to 60 m is over open water with some brash.

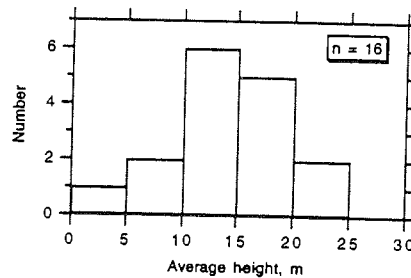


Fig. 5-10: Average height distribution of all 16 profiled icebergs.

*Profiling of icebergs east off Severnaya Zemlya*

One laser flight was undertaken to profile icebergs close to Matussevich Fiord on October Revolution Island and an ice tongue north of it, which are believed to be the major sources for the production of icebergs in the Laptev Sea. In total, 16 mostly tabular bergs were overflown. The main characteristic of these bergs was their undulating pinnacled surface, extending some meters above the mean height in many places. Sometimes, depressions were filled with meltwater. Fig. 5-10 presents the average height distribution of all 16 bergs, having a maximum between 10 and 15 m. Although the number of observations is rather small, it can be assumed that the largest bergs expected to occur will not be much higher than 30 m. This is of importance with regard to iceberg draft, which for the tabular bergs probably will not exceed 250 to 300 m. Thus, the laser measurements complement PARASOUND observations of ice gouges (see section 9.1), which were found in water depths even below 250 to 300 m. These gouges must therefore mark former events, when glaciation was at a higher stage than today.

*Ice thickness and morphology profiling*

During all ice stations, a total of about 4.5 km of ice thickness and surface morphology data were acquired along profiles 100 to 400 m long, representative for the respective floes. Ice thickness was measured indirectly with an electromagnetic (EM) active-induction device (Geonics EM31: frequency 9.8 kHz, coil spacing 3.66 m) in horizontal dipole mode with a point spacing of 5 m. For better progress, to shelter the instrument, and to make measurements on melt puddles easier, the EM31 was mounted into a kayak which thus served as an amphibic sledge. In addition, a total of 382 drill-hole measurements of ice thickness with variable spacing between 5 and 25 m were performed along the profiles. Surface elevation was surveyed with a laser-levelling instrument at a point spacing of mostly 1 m, which also applies for measurements of melt-puddle depth performed with a ruler stick. A typical example for a 300 m long profile (Station 235 in Sector II) is shown in Fig. 5-11.

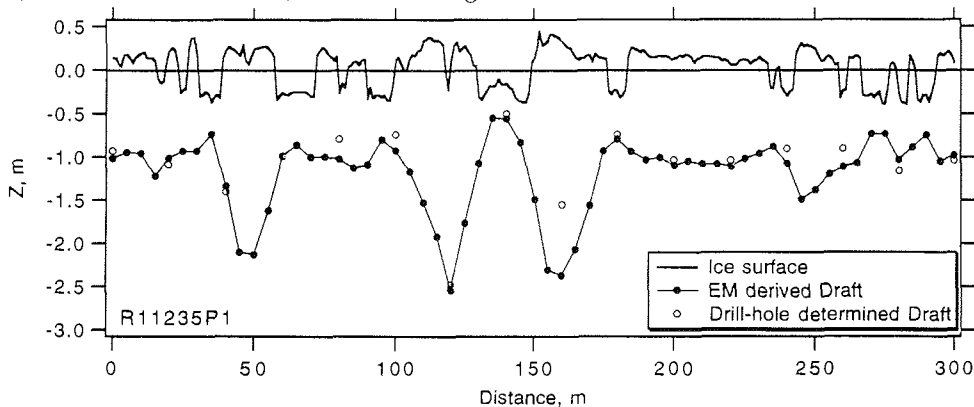


Fig. 5-11: Cross profile through an ice floe comprising surface elevation data from laser-levelling and drill-hole and electromagnetic (EM) thickness measurements.

As in most floes in this region, the surface was covered by a large number of melt puddles, which form the major roughness features over longer distances. Apart from the puddles, the surface appears rather level, although some small ice keels exist at the ice underside. Note that the thinnest ice almost occurs below melt puddles, which thus form weak points in the case of floe break-off.

For profiles like that of Fig. 5-11, the agreement between EM derived and drill-hole determined draft is very satisfactory.

Total ice thickness (ice plus surface layer or ice plus melt-puddle depth, respectively) was calculated from the EM signal (a measure of underground apparent electrical conductivity) using an empirical transformation equation derived from comparison of EM and drill-hole measurements during ARK IX/4 in 1993. Probability density functions (PDFs) of total ice thickness as derived from all EM and drill-hole measurements are presented in Fig. 5-12 (bin width 0.1 m). The maximum for both types of data is between 1.0 and 1.5 m and represents the thickness of virtually undeformed, level ice mainly originating from congelation ice growth. The large thicknesses in the PDFs mainly comprise the heavily rafted and rubbled ice from Sectors I and III, and they may not be representative for the complete area of investigation. These thicknesses are under-represented in the EM data, because here the assumption of 1-dimensional layering as used for the thickness calculations is not any more fulfilled. Additionally, rafting was always associated with water-filled gaps within the ice, leading to too small thickness estimates. Fig. 5-12 also shows that EM measurements (in particular with the instrument parameters used here) are very well suited for deriving the thickness distribution of level and moderately deformed first-year sea-ice.

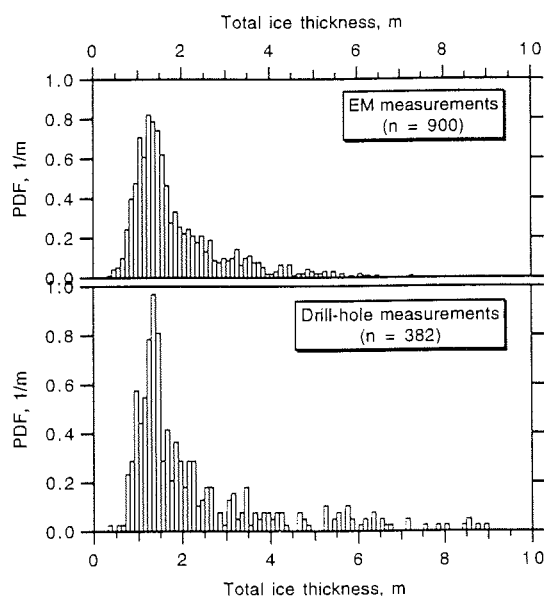


Fig. 5-12: Probability density functions (PDFs) of total ice thickness as derived from the complete drill-hole and EM data set.

In Fig. 5-13, the EM-measured apparent conductivity is compared with drill-hole determined total ice thickness at coincident sites, showing the expected negative-exponential relationship. Fitting an exponential function to the data results in

apparent conductivity =  $80.3 + 1004.1 \cdot \exp(-0.838 \cdot \text{total thickness})$ ,

explaining 94 % of the total variance. Compared with results from measurements during ARK IX/4, the scatter in the present data set is rather high. This is obvious not only at larger ice thicknesses, but also below 4 m. May-be, this scatter is an indication for a relatively rough ice underside, as mentioned already with regard to Fig. 5-11.

Further data analysis will mainly focus on the discription of interrelations between level and deformed ice portions.

The average of all surface elevation measurements was 0.29 m ( $\pm 0.31$  m), compared to 0.1 m, the maximum of the PDF. The distribution of puddle depths shows a broad maximum with a bi-sectioned peak at 0.1 and 0.25 m, with an average of 0.27 m ( $\pm 0.15$  m).

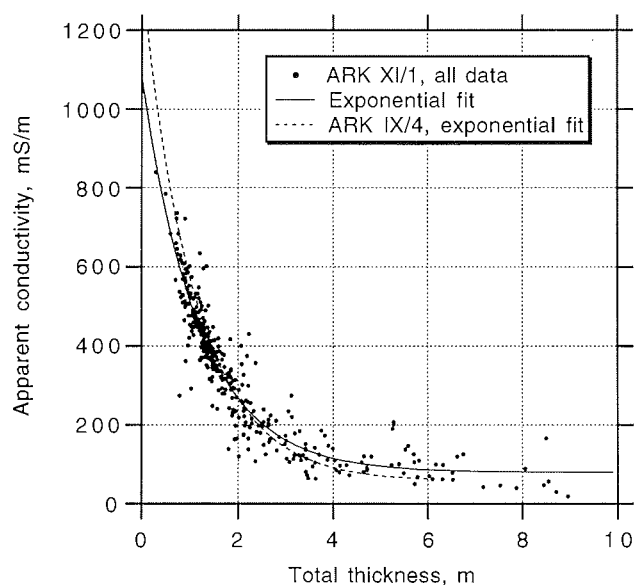


Fig. 5-13: EM signal (apparent conductivity) vs. drill-hole determined total ice thickness for all 365 coincident EM and drill-hole measurement sites. Exponential fits to the present data set and data from ARK IX/4 in 1993 are also shown.

#### *Continuous thickness profiling from the ship's bow*

During some short transects (Fig. 5-8) when the ship was ice-breaking, continuous thickness measurements were performed with the EM31 along with a vertically downward looking laser altimeter (see above), suspended below the



ship's bow crane. For these measurements, the EM31 was operated in vertical dipole mode to increase the effective penetration depth. While the EM31 measures the distance to the ice underside or water surface, respectively, the laser determines the distance to the ice surface. Subtracting the latter distance from the former yields the thickness of the ice below the instruments.

For calibration, the instruments were raised over ice free water from shortly above the surface to a height of 9 m, and the EM31 output (apparent conductivity) was measured along with the instrument height (Fig. 5-14). The measured relation excellently fits with a model curve, calculated for a seawater conductivity of 2.6 S/m and a distance of 0.5 m between laser and EM31.

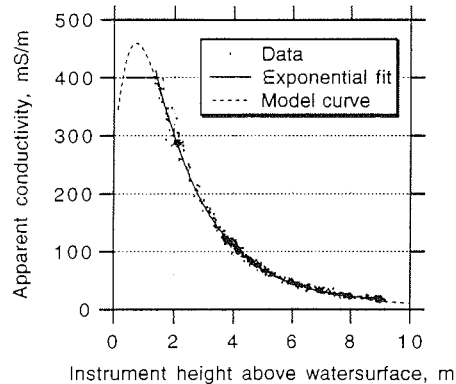


Fig. 5-14: Apparent conductivity vs. instrument height above water surface, as determined during a calibration measurement (see text). An exponential fit to the data and a model curve are also shown.

An exponential fit yields

$$\text{Apparent conductivity} = 11.1 + 839.9 * \exp(-0.533 * \text{Height}).$$

Assuming the electrical conductivity of sea ice to be zero, this equation can also over ice serve directly to transform apparent conductivity into height above the water surface, thus enabling calculation of the distance to the ice underside or ice thickness, respectively.

Fig. 5-15 presents a short section of laser and EM data (as calculated from the above equation), when the ship passed through a bigger and two smaller floes. Sampling frequency was 20 Hz, resulting in 1000 datapoints representing about 250 m with a ships speed of 10 knots. No major data processing has been applied.

Over open water (e.g. between points 2000 and 2800), EM and laser distances are equal, representing zero ice thickness, while when crossing any ice the EM measures the ice draft. The ship's pitch generally is comprised in the data, which is most obvious when ice breaking. Then the laser-determined ice surface can be below the equilibrium distance to the water level (Fig. 5-15, dashed line), as is the case e.g. between points 1200 and 1500. When subtracting laser distance from EM distance to derive ice thickness, the pitching comprised in each data set cancels out, so that no care has to be taken.

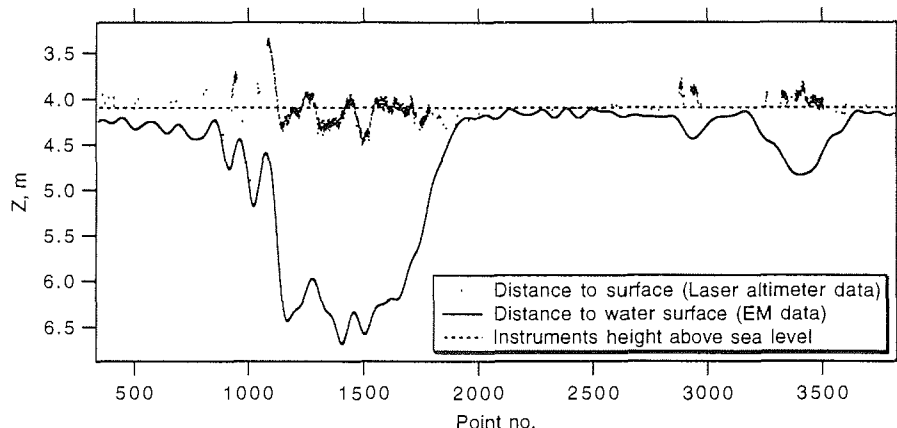


Fig. 5-15: Raw data example of EM and laser data when passing with the ship through a bigger and two smaller floes. The dashed line represents the average location of the water level relative to the instruments.

### 5.7 Properties and microstructure of sea ice (H. Eicken, F. Valero Delgado)

The ice-core sampling program during the expedition had three main aims:

- (1) to study the importance of dynamic growth processes for the formation and thickening of level ice over the shelf areas and in the transition to the multi-year ice of the Transpolar Drift,
- (2) to assess the importance of ablation processes for the evolution of second- and multi-year ice in the Arctic Basin, and
- (3) to provide a linkage between entrainment and transport of sediments in sea ice and glaciological processes. While the latter program is described in more detail in Section 5.5.1, the former two topics will be outlined below.

#### Material and methods:

At a total of 34 stations (8 reached by helicopter) ice cores were collected (see Fig. 5-16 for sampling locations). Except for 5 helicopter stations, cores were drilled through the entire thickness of the floe at all these main sites. Mostly, three full cores were taken (9.1 cm core diameter, drilled with a titanium barrel, CRREL-type corer powered with a 2-stroke engine). The main core was processed in a glaciological laboratory (-25 to -30 °C) aboard ship. A second core was inserted into an insulated core tube immediately after drilling, and ice temperatures in its interior were measured at 5 to 10 cm intervals. The core was retained for archiving purposes and transferred for storage at -30 °C aboard ship. A third core was obtained for biochemical studies (F. Haubrich, R. Lara, AWI; we are grateful for the excellent support provided by Frank Haubrich in the field), also stored at -30 °C.

Thick sections were produced along the entire length of the master core, upon which a textural stratigraphy of the core was based (for details see Eicken et al., in press). At selected depths within cores, horizontal and vertical thin sections will

be produced. Based on the stratigraphy, the core was sectioned into 5 to 15 cm segments. At each depth, a third of the core was retained for stable-isotope measurements in the home laboratory. After melting at 4 °C in the dark, salinity was measured with a conductimetric sonde (WTW 191), and the water filtrated for measurements of chlorophyll-a (carried out by A. Bartel, see section 7.1 on water column biology). A small volume was used for measurements of inorganic nutrient concentrations (performed by Y. Nalbandov).

A further, important component of the ice-core program consisted of density measurements on 10 cm core sections, which were sawed and whose dimensions were measured on the ice, with later weighing for volumetric determination of density. Furthermore, the same or parallel cores were processed for micro-structural analysis of the pore space. For this purpose, the samples were kept isothermal in insulated boxes, with the liquid phase removed by centrifuging at in-situ temperatures aboard ship (technique of brine removal described by WEISSENBERGER et al., 1992). The volume and salinity of the brine were determined and the samples stored in tight glass bottles at 4 °C for stable-isotope measurements. Based on the temperature, salinity and density measurements of bulk cores and the volume determinations of the extracted liquid, the relative fractions of liquid, solid and gas can be derived. The size, shape and connectivity of pores will be determined on the remaining ice matrix at the Alfred-Wegener-Institut. Samples for density and pore studies were obtained in locations of level ice as well as from ridges and bottoms of melt puddles.

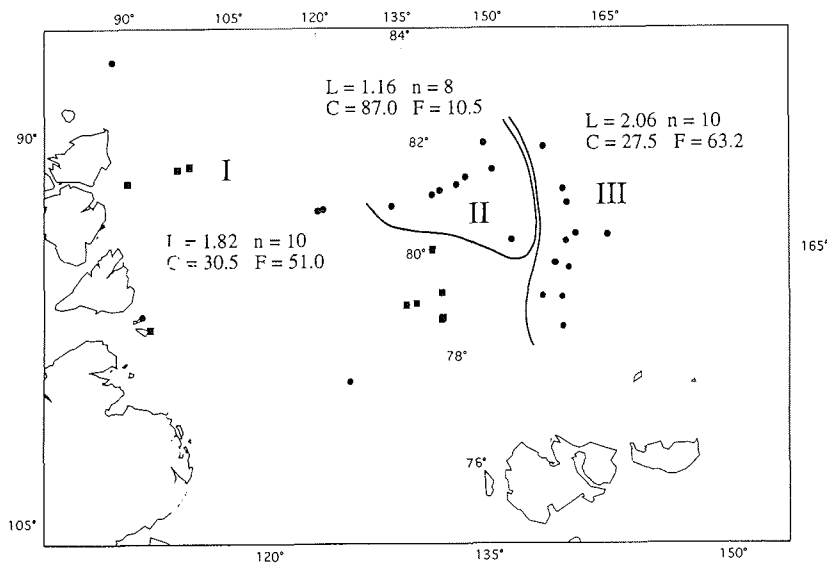


Fig. 5-16: Map showing sea-ice sampling stations (shaded dots: July 22 to 28, squares: August 4 to 19, solid dots: August 20 to September 9). Roman numerals indicate different ice regimes (for details see text; parameters shown are average core length  $L$ , number of cores drilled through entire floe thickness  $n$ , fractions of undeformed congelation ice,  $C$ , and frazil ice,  $F$ , of total core length).

## Preliminary results:

Based on the stratigraphic studies, three major ice regimes could be identified as shown in Fig. 5-16. While the sample spacing in area I is not sufficient to warrant definite conclusions, analysis of satellite imagery and field observations indicate that most of this ice originates from the Laptev Sea, with possibly some ice advected through Vilkitsky Strait from the Kara Sea. Based on a first, preliminary evaluation of the data, no indications for multi-year ice were found in the entire study area. At the locations to the North and Northeast of Severnaya Zemlya, the ice had been advected from the southwestern Laptev Sea during the course of the expedition (see section 5.1 for details). As indicated in Fig. 5-16, a large fraction of the ice was of dynamic growth origin (51 % frazil), accounting for an average level ice core length of 1.82 m. In contrast, area II was highly homogeneous on a large scale, with mostly flat ice devoid of major ridges, displaying a high areal coverage by melt puddles (see also section 5.6). The vast majority of this ice was formed through quiet congelation of sea water at the base of the ice cover (almost 90 %), indicating an origin from a divergent or stagnant growth regime in the absence of major storm events. Ice thickness based on cores was slightly less than that based on thickness drilling which included deformed areas (1.16 m as compared to 1.44 m). In contrast with areas I and II, area III was characterized by highly deformed ice of dynamic growth origin, both on a large scale (see section 5.1) as well as from a micro-structural point of view. More than 60 % of the ice cover consisted of frazil (excluding 4 enclosed level ice floes, this value rises to >80 %), sometimes accumulating to >3 m thickness in unridged areas. The average ice thickness including deformed ice amounted to 2.45 m (>3 m without 4 level ice floes). Furthermore, region III was characterised by extremely high loads of sediments within the ice cover (see section 5.10 for details).

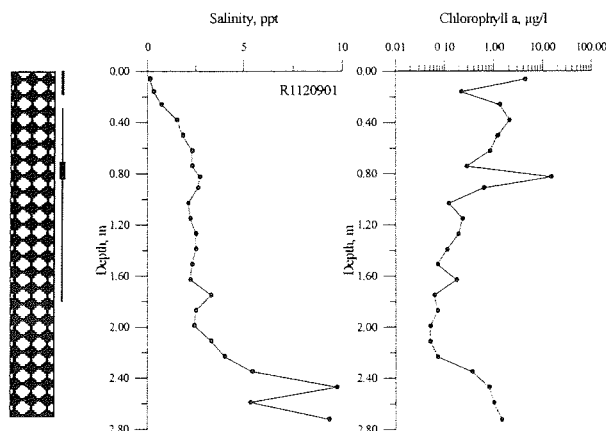


Fig. 5-17: Textural stratigraphy (shown at left, core entirely composed of granular ice; bars of different thickness denote visually identified sediment inclusions in low, medium and high concentrations within the core), salinity (middle) and chlorophyll-*a* concentrations (right) of core R1120901 sampled in the center of area III shown in Fig. 5-16.

An exemplary core from region III is shown in Fig. 5-17. Throughout its entire thickness the floe consisted of granular ice, formed from accumulation of frazil ice grown in the upper meters of the water column. Analysis of thick sections also indicates that a significant fraction of the non-ridged ice contained fragments of deformed ice with tilted grains and brine channels, requiring further study of thin sections and stable-isotopes throughout the core. Visually, accumulations of sediment could be recognized within the upper two thirds of the core, with layers of higher sediment concentration at the surface and at roughly 0.8 m depth. As indicated by the salinity profile, downward freshwater flux due to surface melting of ice and snow has resulted in lower salinities in the upper decimeters of the core. Nevertheless, compared with profiles of multi-year ice (Doronin and Kheisin, 1977, Eicken et al., in press) the salinity values are still fairly high, suggesting an age of less than two years.

The vertical distribution of chlorophyll-*a* as a measure of microalgal biomass exhibits two characteristic features. First, a distinct maximum at the bottom of the ice, which was found in the vast majority of cores, indicates the dominance of so-called bottom communities (cf. sections 6.2 and 6.3), which are typical of Arctic sea ice in general. Second, the two maxima at the top and 0.85 m depth as well as elevated levels throughout the upper half of the core coincide with visually identifiable sediment inclusions in the ice. Further work will have to establish whether this biomass represents detrital material entrained with sediments during ice growth or whether it originates from in-situ production, enhanced by remineralisation and release of nutrients from sediment-rich layers.

As outlined above, work will be continued on the collected material to establish the linkage between ice pore microstructure and summer ablation processes, and between the microstructure and the physical properties of the ice, including transport of dissolved and particulate substances through the ice matrix.

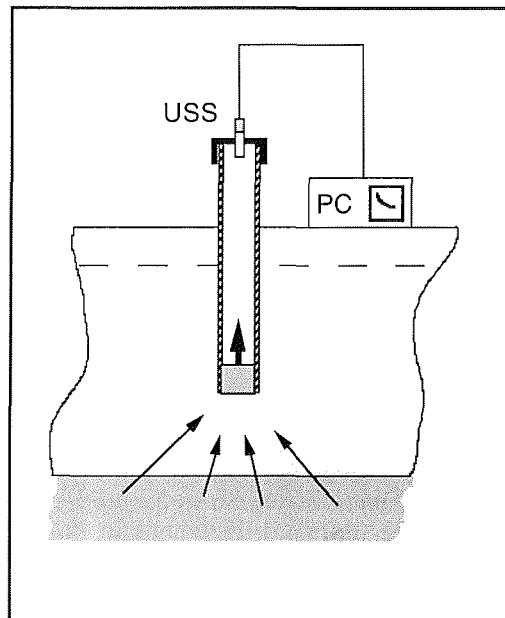
## 5.8 Hydraulic conductivity of the ice cover and hydrological tracer studies (J. Freitag)

During the summer months extensive surface melting of Arctic sea ice occurs. Separation by melting decreases the ice thickness by about 1 m. The meltwater can transport heat and occasionally incorporated matter. To assess whether and to what extent this transport contributes significantly to the overall redistribution of sediment within the ice, two hydrological investigations were carried out along two lines: I. *In situ* measurements of hydraulic conductivity of sea ice, II. Measurements of the melt water flow through sea ice with the aid of hydrological tracers.

### I. *In situ* measurements of the hydraulic conductivity of sea ice:

At 15 different stations measurements in level ice, deformed ice and sediment-laden ice were performed. The conductivity was derived from time-series measurements of the water-level adjustment within sack holes. Fig. 5-18 shows a sketch of the experimental set up. Sack holes were sealed lengthwise by an aluminium tube, which froze to the ice. The water level was measured with an

Fig. 5-18: Experimental set-up of the *in situ* measurements of sea ice permeability



ultrasonic sensor mounted on top of the tube (resolution:  $\pm 0.5$  mm) with a maximum frequency of 20 Hz. Prior to every measurement, water in the sack holes was removed with valve bail. The measured water level curves demonstrated a good fit of the exponential dependence over time. From the exponents and the geometrical parameters the permeability can be derived.

An interesting aspect was the change of pore space structure as a result of melt- or sea-water percolation. This could be seen by the change in permeability during repeated measurements at the same site. Salinity-dependent melting or refreezing processes associated with water percolation may affect the hydraulic conductivity. Therefore, salinity of percolated water was also noted. To detect significant changes in pore space structure, repeated measurements had to be performed in ice that had exhibited a varying increase of salinity of percolated water over time.

## II. Measurements of melt water flow in sea ice:

To initiate flow in a porous medium a driving force is required. The driving force of meltwater percolation in sea ice can be the hydraulic pressure of melt ponds laying above sea level (and meltwater in regions of pressure ridges), the wind stress on open water surfaces and the pressure variations due to the interaction of the under ice flow field with the ice floe topography. During this cruise flow field investigations on 6 locations were performed, taking these

different driving forces into account. To visualize the melt water flow, a tracer technique was applied. The velocity of flow was estimated from the shift of the tracer concentration maximum with time. As tracers the fluorescent dyes Sulfo-Rhodamine and Uranine were used. In an experimental sea ice area transects of about 4-5 sack holes were drilled with depths of approximately 60 cm and diameters of 5 cm. Either the center hole or a melt pond located in the center were colored by a defined amount of dye (30-200 mg). For the duration of the experiment (approximately 6-20 h) the pore water of sack holes were sampled in time intervals of 3 h - 6 h. On board, the tracer concentrations were measured with a fluorometer at 491nm/512nm wave lengths (Uranine) and 565nm/590nm (Sulfo-Rhodamine). The detection limit for Uranine was  $10^{-6}$  mg/l (Rhodamine:  $10^{-5}$  mg/l) with a saturation concentration of about 2 mg/l. Both tracers could be used simultaneously since fluorescence spectra do not overlap. The effect of different salinities of pore water on the calibration curves was taken into consideration. Furthermore, control experiments of the adsorption of both dyes in sea ice were carried out.

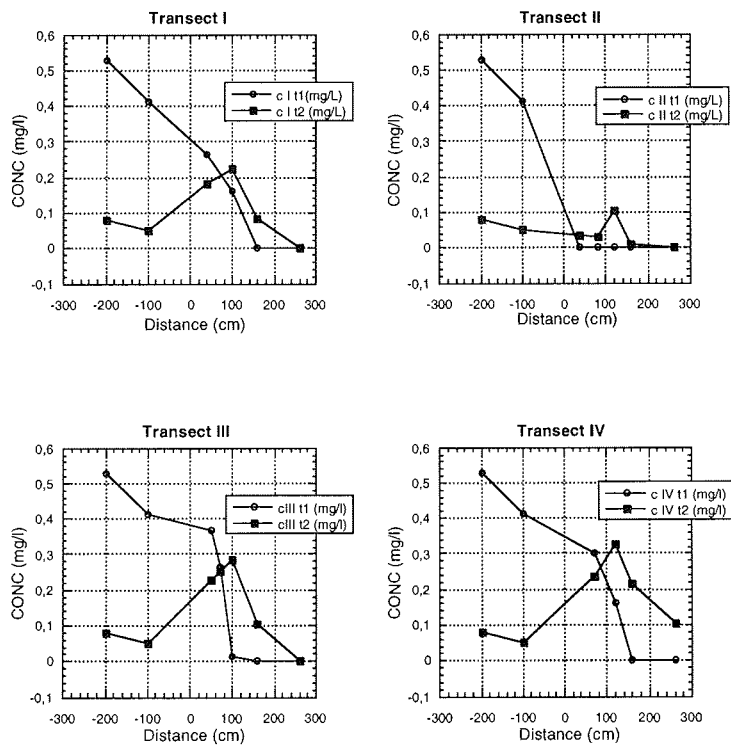


Fig. 5-19: Migration curves of Uranin at different time steps after injection ( $t_1 = 4$ ,  $t_2 = 14$  hours). Range of melt-pond: -200 cm to 0 cm; of sea ice: 0 cm to 300 cm.

In Fig. 5-19 an example of the migration of Uranine in sea ice forced by a hydraulic pressure gradient is shown. A melt pond with a water level 50 cm above sea level in a rubble ice field was selected. Four transects with sack holes originating in the melt pond and deviating by  $120^\circ$  were drilled at a distance of 50 cm to each other. After 16 hours the peak of the Uranine concentration shifted about 1 m into the ice. The resulting lateral flow velocity was  $2 \cdot 10^{-5}$  m/s. This corresponds to a horizontal permeability of about  $2 \cdot 10^{-10}$  m<sup>2</sup>.

Summary and preliminary conclusions:

The measured vertical conductivities of Arctic summer sea ice lay in the range between  $10^{-5}$  m<sup>2</sup> and  $10^{-9}$  m<sup>2</sup>. The permeability of sea ice is highly heterogeneous vertically as well as horizontally. Extremely impermeable layers were observed in some cases at the bottom of drilled cores close to melt ponds.

In areas of pressure ridges and under strong wind stress exerted onto open melt pond surfaces, lateral melt water flow could be measured. The characteristic length and time scales are about 1 m per day. These findings emphasize the effect of meltwater on the heat and mass balance of sea ice in these areas. Therefore, the potential for lateral sediment redistribution seems comparatively high.

#### 5.9 Deployment of drifting buoys equipped with ice-freeboard pressure sensors (H. Eicken, with C. Kottmeier and H. Tüg, AWI Bremerhaven)

To further understand the ice drift in an area that so far lacks coverage by drifting buoys in comparison with the Arctic Basin, three Argos buoys were deployed in the eastern Laptev Sea (for details see Table 1). Buoy 9360 was positioned near the center of the heavily sediment-laden area studied along the two easternmost transects (see also section 5.10). Buoys 9363 and 9364 were furthermore equipped with GPS positioning systems and a screened temperature sensor mounted at their tops. Both buoys were positioned along the northernmost transect in the northeast of the Laptev Sea.

In addition, the latter two buoys were connected to two highly sensitive pressure gauges each, allowing for measurements of ice freeboard at two sites in the immediate vicinity of each buoy. The freeboard sensors were developed by the Alfred-Wegener-Institute's electronics laboratory and consist of a highly sensitive pressure gauge suspended in a casing at a fixed depth within the upper ice layer. The relative position of the sensor with respect to sea level and its change in time can then be deduced from differential measurements between hydrostatic and air pressures. Thus, changes in the freeboard of the floe unit affecting the sensors, such as accretion of ice from below during winter, snow-fall events and surface melting during summer will be recorded. At the installation sites and their vicinity, detailed measurements of ice thickness and general ice characteristics were carried out. Since a revisit is planned during a later expedition, one of the locations was also fitted with a radio-transmitter (buoy 9363, fitted with Telonics TMB-500 radio-transmitter, transmitting a signal once every second at 163.020 MHz with a projected operating life-time of two years).



At the two buoy locations 9363 and 9364, experimental sites to study small-scale distribution of different types of natural and artificial sediments were laid out for later sampling (for details see section 5.10).

Table 1. Deployment sites and specifications of Argos buoys  
(P - air pressure, T - air temperature, F - freeboard pressure gauge)

<i>Buoy ident. code</i>		<i>Deployment</i>		<i>Parameter</i>
<i>Argos</i>	<i>WMO</i>	<i>Date, Time (UTC)</i>	<i>Location</i>	
6360	63662	26.7.95, 17:00	79°14.4'N 152°04.4'E	P
6363	25573	25.8.95, 19:35	81°12.1'N 143°24.3'E	P, T, F
6364	25574	20.8.95, 12:00	80°54.0'N 131°05.2'E	P, T, F

#### 5.10 Large- and small-scale distribution and redistribution of sediments within the sea-ice cover (H. Eicken, J. Freitag, J. Kolatschek, F. Lindemann)

Despite the importance of sea-ice rafting of sediments, data from direct observations of entrainment of particulate matter into growing sea ice are extremely sparse, with no published data from the Eurasian Arctic available. This is in part due to the inaccessibility of the study areas and harsh environmental conditions during freeze-up. A major aim of the work carried out during the expedition was to attempt to deduce information about entrainment mechanisms and the distribution and redistribution of ice-rafted sediments from ice-core studies, ground measurements and remote sensing.

First, it needs to be established to what extent the large scale distribution of dirty ice can be determined and mapped from satellite remote sensing. The pilot study of Reimnitz et al. (1993) in the Beaufort Sea demonstrated that dirty ice may be recognized in Landsat images. Yet, no detailed analysis of satellite data in conjunction with ground measurements was carried out. While data from the Advanced Very High Resolution Radiometer (AVHRR) flown onboard NOAA satellites and received onboard "Polarstern" during the cruise cover the entire Laptev Sea and adjacent areas, analysis of the images will focus on an area of highly sediment-laden ice found in the eastern Laptev Sea in the transition to the East Siberian Sea (area III as outlined in sampling map in section 5.7, Fig. 5-16). In this area, detailed ground sampling, helicopter overflights with a video camera system and measurements of spectral albedo (see sections 5.3 and 5.11) provided sufficient ground truth to compare direct and indirect observations of sediment distribution. To complement this analysis, SPOT satellite data (with three channels in the visible range) which may provide more detailed spectral information, have been ordered for the study area.

Detailed analysis of sea-ice cores may provide information about the origin of the sediment-laden ice and in particular about entrainment mechanisms. In order to assess the suitability of ice-core studies, a set of cores (mostly between 0.8 and 1.5m in length) has been obtained from 22 locations (5 of which coincided with the main sampling stations, cf. section 5.7) for detailed stratigraphic analysis. This comprises visual inspection of thick sections over the entire length of cores,

augmented by thin-section analysis to quantify ice texture, in particular grain-size distributions. From this data, growth and entrainment mechanisms will be deduced. A first, preliminary indication of entrainment could be obtained from a total of 17 cores. Except for one station, all visually identifiable sediment inclusions occurred as mm- to sub-mm inclusions in granular and mixed columnar/granular ice, mostly formed through compaction of frazil crystals grown in the water column and congealing at the water surface.

In several cases these stratigraphic units of granular ice extended over much of the entire thickness of an ice cover, as can also be seen in Fig. 5-17, section 5.7, showing layers with variable, visually identifiable enrichment of sediments. The thickness of such sediment layers ranged between 0.01 and 2.93 m (median value of 0.08 m,  $n = 24$ ), the latter value representing also the maximum depth at which sediment could be identified within cores. Further, combined glaciological and sedimentological analysis in the home laboratories will have to establish whether these inclusions are the result of one or several entrainment events, possibly taking place over a longer duration.

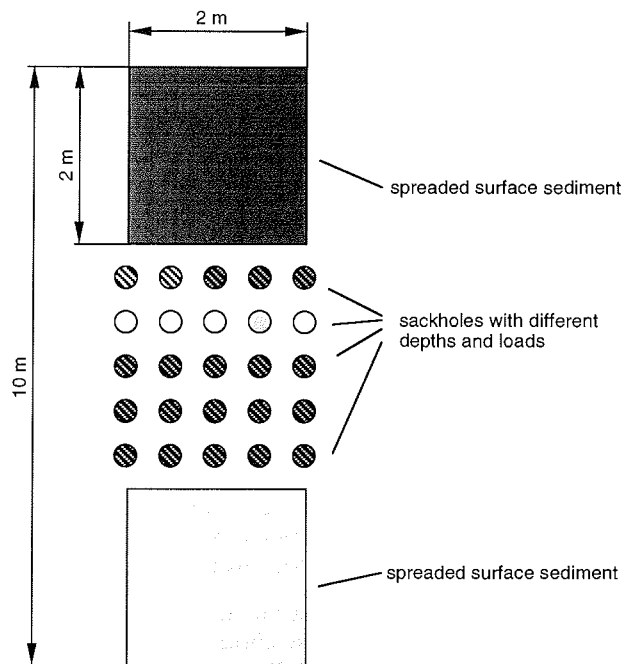


Fig. 5-20: Arrangement and size of experimental field comprising surface sediments and cryoconite holes.

Since the detectability of sea-ice sediments through remote-sensing and the climatological importance of highly absorbing particulate material entrained in sea ice depend strongly on the small-scale (in particular vertical) distribution, the ice core data are of further interest in this context. To learn more about the temporal evolution of sediment distribution within the ice as a function of sediment type and concentration as well as ablation rates, two test fields were set up in the vicinity of drifting buoys deployed during the expedition (Fig. 5-20). As pictured, two large sites with homogeneously dispersed surface sediments bound an area of artificial cryoconite holes ranging between roughly 0.1 and 0.6 m in depth. These holes contain defined amounts of different sediment types including carbonaceous sand and silt as well as fluorescent sediment particles.

#### **5.11 Spectral and integral Albedo of sea ice** (J. Kolatschek, A. Zatchek)

The inclusion of sediments in sea ice over wide areas as observed during the cruise ARK XI/1 of the RV "Polarstern" can induce significant changes in the amount of short-wave solar radiation which is absorbed by the sea ice. This may lead to an increased melting at the ice surface in the summer months. To estimate this influence of the sediments, measurements of spectral and integral albedo of sea ice surfaces of different kind and different sediment load have been performed.

The albedo measurements serve also as important ground truth data for the evaluation of high and medium resolution satellite images of the same area. From these data it should be possible to estimate the large scale albedo change induced by sediments on the surface of the sea ice and in melt puddles.

The spectral albedo was measured using a Spectron Engineering SE590 spectroradiometer with a hemispherical diffusor. To obtain the albedo, two measurements had to be made: One of the incoming solar radiation with the instrument looking upward and one of the radiation reflected by the surface with the instrument turned by hand and pointing downward. As the time between the two measurements is only a few seconds, the intensity of the incoming solar radiation does not change significantly under appropriate cloud conditions. The albedo is then calculated as the ratio of these two spectra. No radiometric calibration of the instrument is needed.

In order to reduce the effect of direct solar radiation, the measurements were most of the time performed when the sky was covered completely with clouds or high fog, leading to a nearly ideal diffuse radiation environment. Due to the low sensitivity of the silicon CCD detector of the instrument to wave-lengths shorter than 410 nm and longer than 1050 nm only the data between these two points are used.

An example for the strong influence of different sediment loads especially on the short-wave part of the spectral albedo of the sea ice is given in Fig. 5-21.

From these spectral albedo measurements integral albedos have been calculated and compared to measurements of the same surface made with a hand-held pyranometer. Although the wave-length range of these two measurements is slightly different, there is a good agreement of the results, also with the measure-

ments carried out by B. Ivanov and V. Alexandrov during the cruise ARK IX/4 of RV "Polarstern" (Table 1).

Table 1: Integral albedo values of sea ice with different sediment load

Year	bare ice	low sediment	medium sediment	high sediment
1995 (spectrorad.)		0.59±0.05	0.28±0.05	0.10±0.05
1995 (pyranometer)	0.67±0.06	0.58±0.05	0.36±0.06	0.13±0.05
1993	0.64±0.03	0.55±0.06	0.34±0.09	0.14±0.06

To estimate the amount of radiation which is absorbed in melt puddles, measurements of the albedo of puddles of different depth and sediment content were made (Table 2).

Table 2: Integral albedo of melt puddles of different depth and sediment load

puddle depth	no sediment	low sediment
0.10 cm	0.54±0.04	0.25±0.03
0.20 cm	0.34±0.03	0.19±0.04
0.30 cm	0.30±0.05	0.14±0.03
0.40 cm	0.25±0.05	0.12±0.04

By application of absorption data for melt ponds from Kraus et. al., the albedo of melt puddle bottoms has been calculated. It was found that there is a difference in albedo for shallow and deep melt puddles: melt puddles with a depth less than 10 cm have an albedo of 64±4% and those with a depth larger than 10 cm of 55±6%.

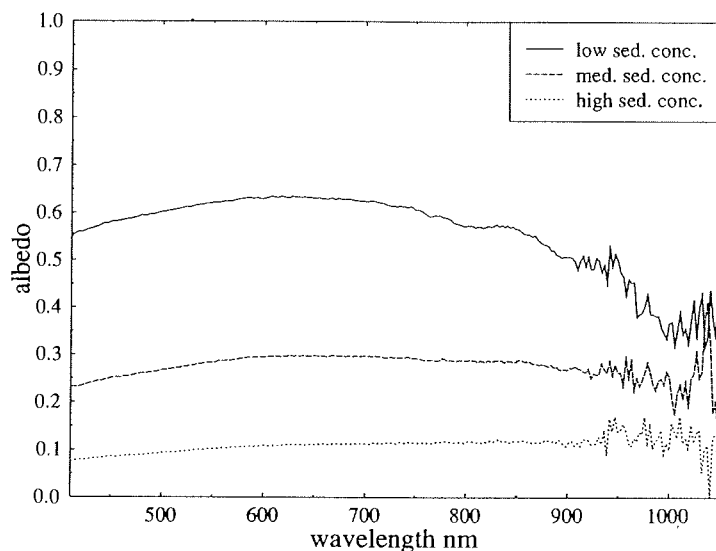


Fig. 5-21: Influences of different sediment loads on sea ice albedo

## 6 SEA ICE BIOLOGY AND SEDIMENTOLOGY

### 6.1 Primary and micro-heterotrophic productivity within ice-associated habitats (S. Grossmann & M. Gleitz)

#### Objectives

In order to get a complete picture of the pelagic regime of the Laptev Sea, the distribution and productivity of organisms in and under sea ice must be taken into consideration. Biological processes mediated by sea-ice associated organisms are major determinants of turnover and fluxes of organic material within the ice environment and between ice and the underlying water column. The aim of this study is to estimate autotrophic production and heterotrophic consumption of organic matter within ice-related microbial food webs. Primary build-up of biomass was traced by determinations of ice algal standing stock and productivity, and was compared with that of phytoplankton assemblages in the water column beneath the sea ice cover. Heterotrophic bacterial utilization of organic matter was estimated by measurements of biomass and productivity of bacteria in ice and under-ice water. In order to achieve information about the fate of algal and bacterial cells, grazing experiments were carried out. Comparison of algal primary production, bacterial secondary production, and protozoan grazing pressure on the algae and bacteria within sea ice habitats and in underlying waters in the North of the Laptev Sea will help to quantify fluxes of energy and organic carbon within and/or among microbial food webs of these compartments, and will give indications on ecological couplings between the sea ice and the pelagic environment of this Arctic area.

#### Work at sea

Sea ice samples were obtained by coring. Under-ice water (from a depth of 20-40 cm beneath the sub-surface of the ice) was sampled through core holes using a hand-operated vacuum pump connected to a silicon tube. Ice samples were melted. In order to minimize osmotic stress, salinity was held at 20-25 ‰ by adding artificial sea water salt during the melting process.

Subsamples of melted ice and under-ice water were filtered onto glass-fibre filters for Chl-*a* analysis and onto precombusted glass-fibre filters for POC/PON determinations which are to be conducted at AWI. Additional samples for microscopical analyses were preserved with formaldehyde.

Photosynthetic activity was measured by adding  $\text{NaH}^{14}\text{CO}_3$  to 40 ml subsamples of melted ice and under-ice water. These were exposed for 3 to 5 hrs to irradiances of 1 to 110  $\mu\text{mol photons m}^{-2} \text{s}^{-1}$  at  $-1^\circ\text{C}$  using a light incubator, subsequently filtered, and the radioactivity retained on the filters measured by liquid scintillation counting. Carbon assimilation rates were calculated based on sample specific radioactivity and DIC concentration.

In order to relate carbon assimilation measured by  $^{14}\text{C}$  incubations to *in situ* light availability, a spherical PAR sensor (400-700 nm) was lowered through the core

hole, and the photosynthetically active radiation (PAR) was recorded at the ice/water interface for time periods of up to 23 hours. Additionally, an under-ice light profile was obtained by measuring PAR in intervals of 1 m down to a depth of 18 m. In order to estimate light attenuation by ice cover, downwelling PAR was recorded by means of a hemispherical sensor mounted 40 cm above the ice surface.

Bacterial and protozoan cell numbers and biomasses are to be determined by direct epifluorescence microscopy at the AWI. For this purpose, subsamples were fixed with formaldehyde (0.8 % final conc., unbuffered, for preservation of bacteria; 0.5 % final conc., buffered with hexamine, for preservation of protozoa) and stored at 1-4°C.

Bacterial growth was measured by incorporation of [<sup>3</sup>H]thymidine into DNA. Triplicate samples of 20 ml were incubated with 10 nM of [*methyl*-<sup>3</sup>H]thymidine (diluted with cold thymidine to a specific activity of 40.5 Ci mmol<sup>-1</sup>) for 90 min at -1°C. After termination of incubations with formaldehyde (0.4 % final conc.), samples were filtered onto 0.2 µm Nuclepore filters, extracted 5 min with 5 % ice-cold trichloroacetic acid, and radioassayed in a liquid scintillation counter. Three formaldehyde pre-killed samples were treated in the same manner and used as blanks. Conversion factors for estimation of bacterial biomass production in terms of organic carbon from incorporation rates of thymidine will be obtained from calibration experiments (to be evaluated at AWI), in which bacterial growth is followed directly by microscopy parallel to measurement of thymidine incorporation.

For estimation of protozoan grazing pressure on algae and bacteria, dilution experiments were conducted according to the method of Landry and Hassett (1982, *Mar. Biol.* 67, 283-288). In this method, the potential algal or bacterial growth rate ( $\mu$ ) and the protozoan grazing rate ( $g$ ) are decoupled by serial dilution of the original sample. Since  $g$  is a function of the encounter rate between algal/bacterial cells and protozoans, it is proportionally reduced by increasing dilution, while  $\mu$  remains unaffected. Four dilution steps (1.0, 0.7, 0.4, and 0.2), made with original sample and 0.2 µm pre-filtered sample water (3 replicates each), were incubated at 0°C under constant light of 20 µmol photons m<sup>-2</sup> s<sup>-1</sup>. After 48-72 hours, subsamples were taken for determination of chlorophyll-*a* concentration and bacterial and protozoan biomasses. Plotting the apparent algal or bacterial growth rate (obtained from the exponential growth model,  $\int \mu - g$ ) at the 4 dilution steps against the dilution factor,  $\mu$  and  $g$  are represented by the Y-axis intersection and the slope of the regression line, respectively.

#### Preliminary results and discussion

Chl-*a* concentrations ranged from 0.3 to about 50 µg l<sup>-1</sup> in melted bottom ice, and from 0.2 to 1.4 in under-ice water (Fig. 6-1). Median values were 5.5 and 0.5 µg Chl-*a* l<sup>-1</sup> for ice and under-ice water samples, respectively. Carbon assimilation rates were generally higher by one order of magnitude for ice samples, and hence, roughly followed algal pigment concentrations (Fig. 6-2).

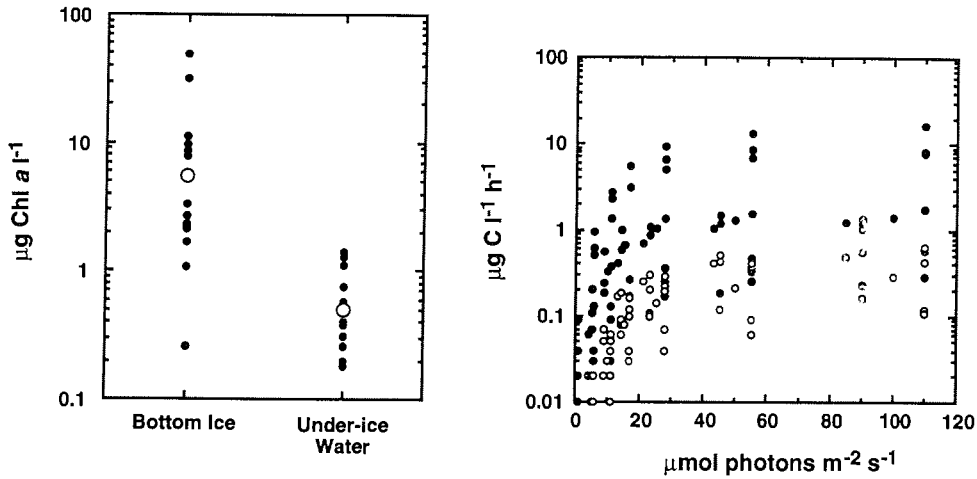


Fig. 6-1 (left): Concentrations of Chl-*a* ( $\mu\text{g l}^{-1}$ ) in melted bottom ice and under-ice water samples. Filled dots: data points, open dots: median values.

Fig. 6-2 (right): Photosynthetic carbon assimilation ( $\mu\text{g C l}^{-1} \text{ h}^{-1}$ ) in melted bottom ice and under-ice water samples as a function of light intensity as recorded in the incubation experiments.

Duplicate samples were exposed to quantum fluxes of 1 to 110  $\mu\text{mol m}^{-2} \text{ s}^{-1}$  for 3 to 5 hours at a constant temperature of  $-1^\circ\text{C}$ . Filled dots: ice samples, open dots: under-ice water samples.

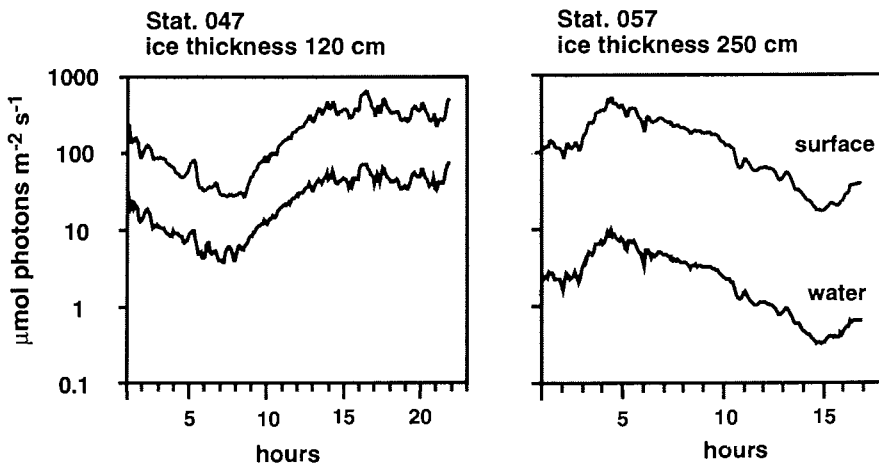


Fig. 6-3: Photosynthetically active radiation ( $\mu\text{mol photons m}^{-2} \text{ s}^{-1}$ ) at stations 47 (ice thickness 120 cm) and 57 (ice thickness 250 cm).

Radiation was measured with a hemispherical sensor 40 cm above the ice surface (upper curve) and with a spherical sensor at the ice/water interface (lower curve) for time periods of 16 to 23 hours.

Maximum rates recorded for ice samples mostly ranged between 1 and 10  $\mu\text{g C l}^{-1} \text{ h}^{-1}$ , whereas photosynthetic rates did not exceed 1  $\mu\text{g C l}^{-1} \text{ h}^{-1}$  in under-ice water samples.

Light data were analysed for station 47 (ice thickness 120 cm) and for station 57 (ice thickness 250 cm, Fig. 6-3). Ambient PAR at the ice/water interface was about one order of magnitude lower than downwelling PAR at stat. 47, whereas at stat. 57, PAR was attenuated by almost 2 orders of magnitude. Mean daily quantum flux allowed photosynthesis up to a depth of 14 m beneath the ice at stat. 47, whereas this depth was reduced to only 0.5 m at stat. 57. Mean daily insolation at these two stations was related to carbon assimilation rates measured in the incubator in order to estimate *in situ* primary production. These calculations revealed that the primary production associated with bottom ice was of the order of 0.2 to 0.3  $\text{mg C m}^{-2} \text{ d}^{-1}$ , suggesting that algal productivity was negligible in the lowermost section of sea ice. Total production under one square meter of sea ice was estimated to amount to 20  $\text{mg C d}^{-1}$  at stat. 47, and to 0.4  $\text{mg C d}^{-1}$  at location 57, indicating that light transmittance through the ice cover and hence, depth of the under-ice euphotic zone, largely controlled total production. For the sake of comparison, open water production was calculated for stat. 12 (with typical Chl-*a* concentrations). It amounted to 338  $\text{mg C m}^{-2} \text{ d}^{-1}$ , suggesting that the bulk of the seasonal production in the investigation area may not be related to sea ice, but to areas of open water.

In contrast to these observations, dense algal blooms were observed at stations 74, 75, 89 at disintegrating, overhanging ice floe edges and in melt puddles with contact to the underlying seawater. Chl-*a* concentrations at an overhanging ice floe edge (stat. 75) and in a melt puddle (stat. 89) amounted to 6 to 7  $\text{mg m}^{-2}$  (Fig. 6-4).

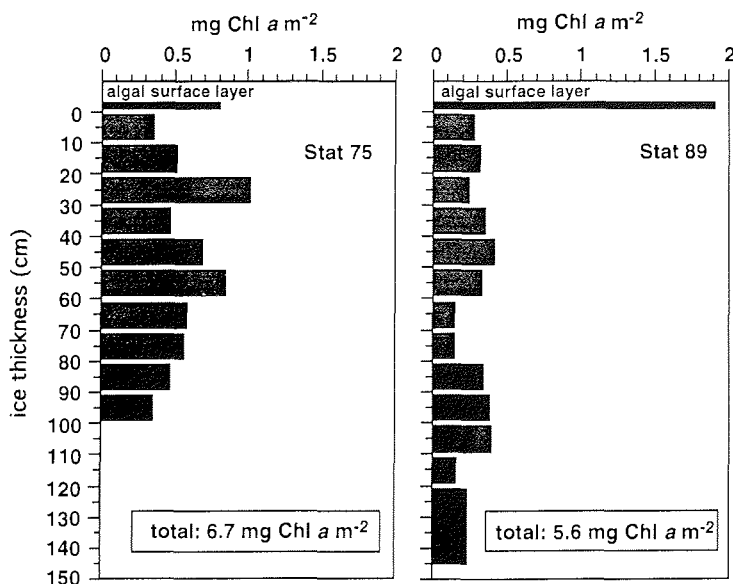


Fig. 6-4: Areal concentrations of Chl-*a* (at ice surface and in 10 cm core segments)



About 10 to 30 % of Chl-*a* was found in a thin layer on the ice surface, which was carefully removed by means of a 100 ml syringe before core drilling commenced. The primary production associated with these blooms was estimated for station 75 to amount to about 150 mg C m<sup>-2</sup>d<sup>-1</sup>. This figure is comparable to open water production, and consequently, these blooms may significantly enhance the amount of ice-related primary production available to sympagic and pelagic consumers, provided widespread areal coverage.

First results of heterotrophic bacterial productivity in the ice and in under-ice water sampled directly below the floes are summarized in Fig. 6-5. Since the conversion factors for calculation of bacterial biomass production in units of carbon have to be evaluated by microscopy at the AWI, relative rates of bacterial activity are shown, given as picomoles thymidine incorporated per liter and day. Comparison of data reveals that the ice stations can be divided into two groups. In the first group, bacterial productivity (on a per volume base) was clearly higher in the ice than in the water below. As indicated by chlorophyll concentrations, activity rates of bacteria here are strongly correlated with chl-*a* biomass. This can be considered as the "normal case".

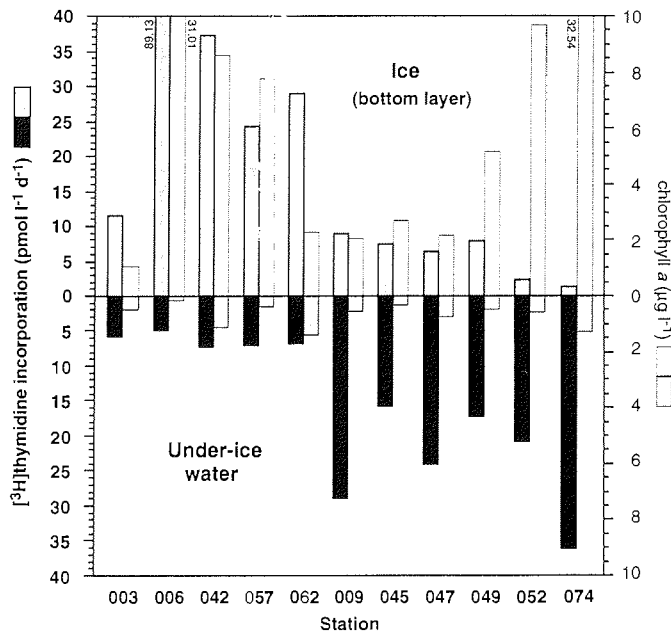


Fig. 6-5: Incorporation rates of thymidine (left bars) as a measure for bacterial productivity, and chlorophyll concentrations (right bars) as a measure for algal biomass in the bottom layer of sea ice and in under-ice water.

In Arctic as well as in Antarctic sea ice, bacteria are usually closely coupled with ice algae, and productivity rates are often higher in the bottom layer of sea ice than in a equivalent cube of under-ice water (e.g. KOTTMEIER & SULLIVAN, 1990). In the second group of samples, concentrations of chl-*a* were also clearly higher in the ice than in the water below. Rates of bacterial productivity, however, were very low in the ice, but were enhanced in the under-ice water at these sites. In order to fully understand this reversed pattern of bacterial productivity rates, the whole data set has to be evaluated, particularly the microcopic analyses for biomass determinations. Possibly, establishment of bacteria was impeded at certain sites in the ice and, at the same time, was favoured in the under-ice water.

In the same manner as given above for primary production of microalgae, bacterial productivity rates were calculated per square meter of sampling area (Table 1). For comparison of data, this has been done for the euphotic zone estimated from the light measurements at these stations. On an areal base, bacterial productivity was low in the ice and was substantially higher in under-ice and/or open water. In order to estimate the relative contribution of bacteria to cycles and fluxes of organic carbon within these habitats, production rates will be calculated in units of carbon using the conversion factors to be determined by microscopy. In this context, the unusual activity patterns in ice and under-ice water, as shown above (Fig. 6-5), suggest that bacteria-mediated food webs are restrained and/or favoured under certain circumstances, which is of special interest for budget calculations.

Table 1: Incorporation rates of thymidine at stations 47 and 57 in ice, under-ice water, and open water, given per m<sup>2</sup> of sampling area. In the water column, productivity rates were calculated for the depth of the euphotic zone estimated from light measurements.

	Ice stations		Open water
	Stat. 47	Stat. 57	Stat. 12
<i>depths of the euphotic zone (m)</i>	14	0.5	45
bottom ice production (nmol thy m <sup>-2</sup> d <sup>-1</sup> )	0.4	2.3	--
water production (nmol thy m <sup>-2</sup> d <sup>-1</sup> )	336.3	3.5	1031.8

A first result of studies on heterotrophic processes other than those mediated by bacteria is given in Fig. 6-6. Shown are results of a dilution experiment conducted for estimation of protozoan grazing pressure within sea ice. As indicated by the regression line, there was a clear dilution effect on algal net growth in this sample. This leads to the conclusion that grazing by protozoa takes place within the ice habitat, and may be a significant component of ice-related food webs. In

order to obtain a full picture, all parameters have to be compared, especially the numbers and biomasses of these potential consumers of ice algae and bacteria.

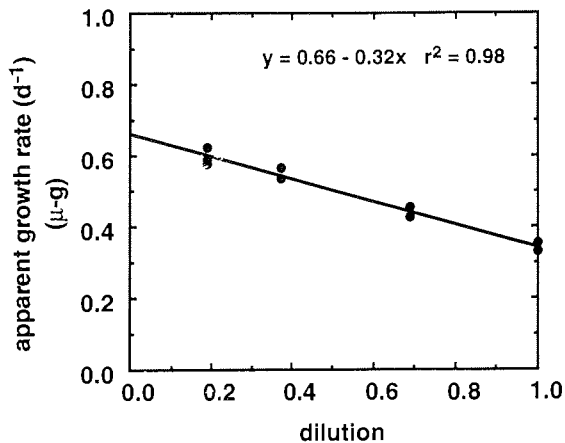


Fig. 6-6: Results of a serial dilution experiment conducted with bottom sea ice (stat. 52). Dependence of apparent algal growth rate ( $\mu\text{-g}$ ) on dilution.

## 6.2 Small scale distribution of sympagic organisms and the degree of coupling to hydrodynamic factors within and below Arctic sea ice (C. Krembs)

Sea ice of the Arctic constitutes a unique habitat for a specialized, sympagic community. Organisms inside the ice inhabit a diverse 3-dimensional network of brine channels ranging from several  $\mu\text{m}$  to several cm in diameter. Processes in the ice and at the ice-water interface influence the pattern of colonization, the food web structure and eventually the degree of export of organic matter to deeper water strata.

### Methods:

During ARK XI/1 melt-ponds and deteriorated melt-ponds that lacked a bottom contributed a significant fraction to the ice floe's overall appearances (approximately 3-5/10). Investigation sites on the ice floes for ice material and experiments were selected within 2 m of the nearest melt-pond, where ice undersides were flat and ice thickness was less variable.

Holes (10 cm in diameter) were drilled through the ice for the deployment of a current meter underneath the ice, which allowed to determine current profiles and current direction at each station. The lowest 10 cm of the ice cores from these sites were cut longitudinally into two equivalent parts and processed for further analysis of the abundance of sympagic organism and their spatial distribution within the ice on scales of 10 cm to  $1\mu\text{m}$ . Some samples were further processed on board, melted in sea water at 4 °C and filtered onto nucleopore filters. Spatial

distributions on scales from 10 cm to 1 $\mu$ m will be analyzed with a new cryogenic substitution technique (SIP-method) in the home laboratory.

An under-ice floe tank used for dye tracer experiments was successfully deployed at the ice-water interface on selected ice floes. A dye tracer with high adsorbance (Rhodamin chloride) was used to determine the degree of spatial variability of water exchange across the ice-water interface and the degree of coupling to algal biomass (Chl-a) to this variability along 1 m transects (interval approx. 25 cm). The floe tank allowed to simulate in-situ flow conditions under the ice by maintaining a defined parcel of water adjacent to the ice-water interface with a steady flow. After incubation for 2-3 hours, cores were drilled along the transect and sectioned in 10 cm intervals. Sections were melted and measured fluorometrically and spectro-fluorometrically to determine dye, Chl-a and Phaeophytin contents together with salinity of the melted ice.

Under-ice water samples were taken with a syringe connected to a tube adjacent to the current meter. Abundances of the planktonic organisms will be compared with that of the ice using the standard filtration method, with DAPI stained samples and epifluorescent microscopy.

#### First results:

Preliminary results indicate that there is a tight coupling between the abundance of algae not only at the ice-water interface but also deeper in the ice. Advection of water through the ice primarily seems responsible for this distribution. Dye concentrations in the ice sometimes were higher than at the ice-water interface (Fig. 6-7). Concentrations of Chl-a were also higher at these sites. Chl-a concentrations showed to be variable vertically and horizontally on scales below 1 m. Fig. 6-8 shows the location of the transect to the ice floes' topology. Elevated concentrations of the tracer closer to the thawhole and 80 cm in the ice hint to an interaction of the oscillation of the pycnocline with the exchange mechanisms within the ice. Chl-a distributions were sometimes strongly affected locally by the distribution of sediments in the ice (not shown).

To determine the potential for active water exchange mechanisms across the ice-water interface that might explain the variable, high algal biomass in the ice, pressure oscillations and oscillations of the pycnoclines under the ice and inside melt-puddles were continuously recorded. Periods ranged from 10 sec to 5 min. Pycnoclines in the melt-ponds were visible by drifting naturally buoyant bleached algae aggregates. Whether oscillations constitute an active pumping mechanism for nutrients across the interface and may aid algae to prosper more vigorously in deeper layers of the ice still needs to be tested experimentally.

Current profiles (0-180 cm) under the ice (sensitivity >6 cm/sec) and direction showed a clear decrease and occasional straying of current direction towards the ice water interface. Velocities ranged from < 6 cm to approx. 25 cm sec. when wind stress was high (approx. 17 m/sec). When boulders under the ice were present, interpretation of the current profile was difficult. The contribution of water current velocity for the spatial variability of water exchange will be further analyzed.

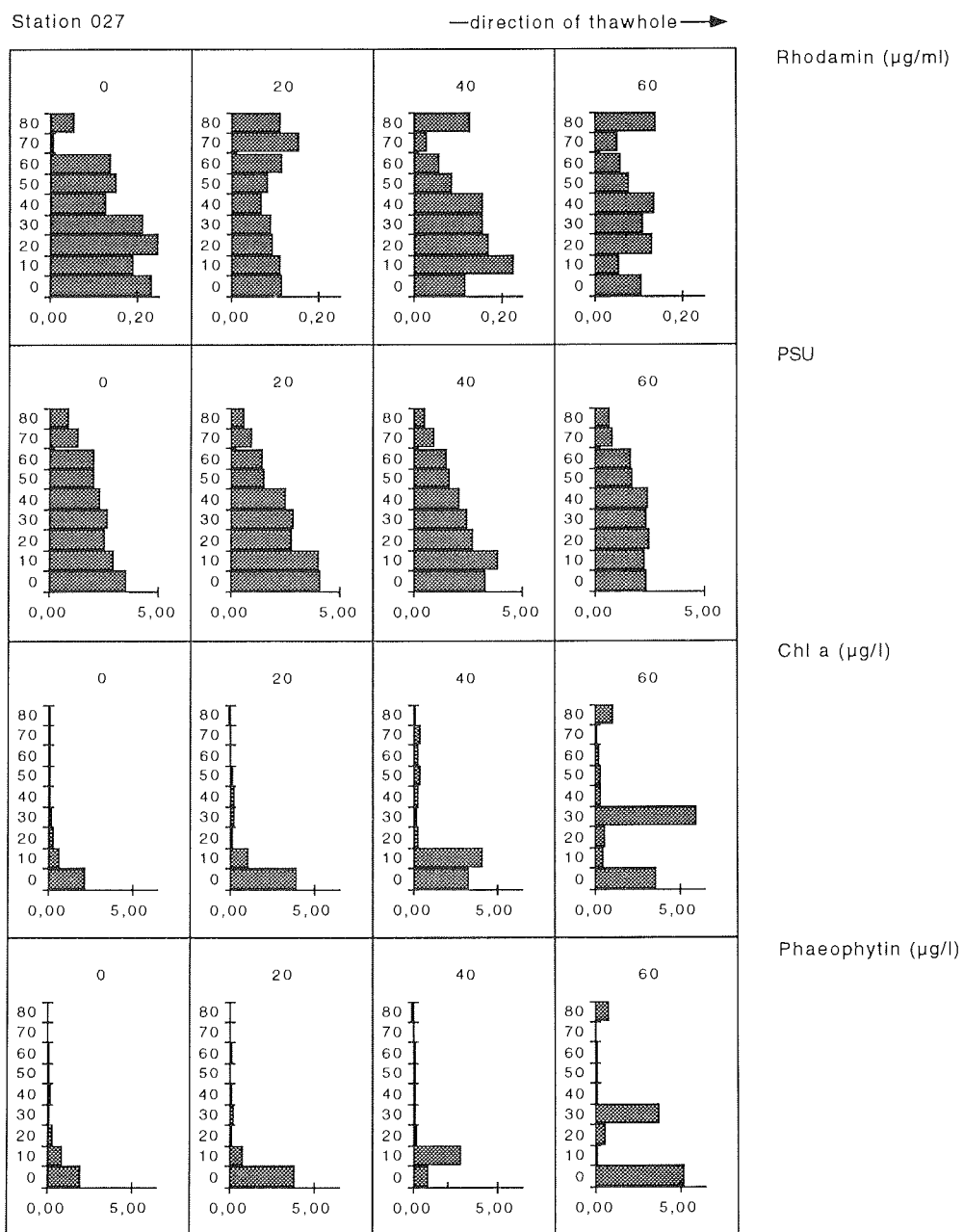


Fig. 6-7: Distribution of Rhodamin ( $\mu\text{g}/\text{ml}$ ; upper file), salinity (PSU; second file), Chl.-a ( $\mu\text{g}/\text{l}$ ; third file) and Phaeophytin ( $\mu\text{g}/\text{l}$ ; lowest file) in the ice thickness (ordinate, 0-80 cm) at stat. 27. (For more details, see Fig. 6-8.)

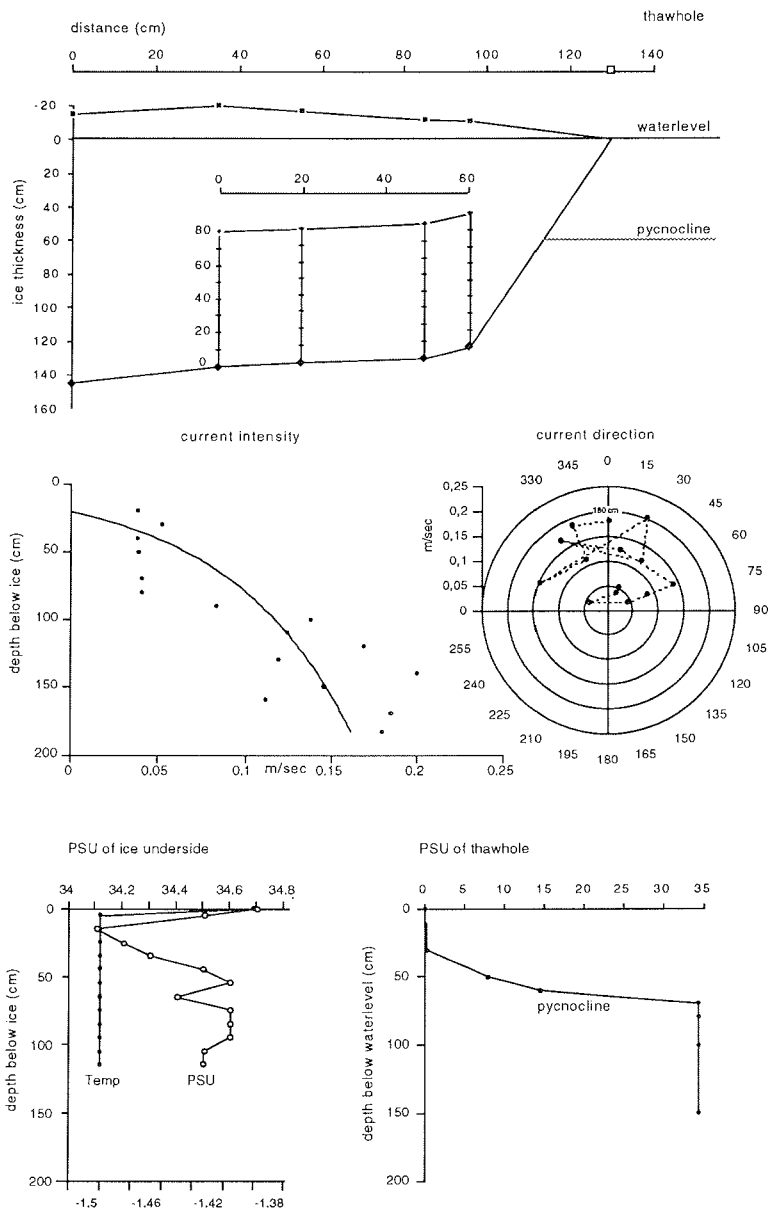


Fig. 6-8: Location of the transect at station 27 in relation to the ice floes' topology and some results of measurements (see text).

First observations of ice cores from the transect indicated a very heterogeneous vertical porosity distribution with a pronounced porous layer within the interior of the ice (max. observed diameter approx. 1.5 cm), whereas the lower 5-30 cm consisted of solid, rather impermeable ice with only sporadic, but big pores (approx. 4 cm). On other stations the ice had very abundant and big pores (approx. 4 cm). The increase of substrate area was measured using a controlled freeze-adsorption-dye technique which allowed to assess the porous surface area (resolution porous >1 mm) of big ice pieces spectro-fluorometrically. Dye content was prior calibrated against ice pieces of known size. Substrate surfaces and biomass of algae were enhanced by a factor of approx. 50 per square meter.

Latticed crystal were observed at inside the bottom-less meltponds located at the depths of the pycnocline. A crystal layer separated the puddle into two distinct zones. Above the layer the ice appeared barren of algae, whereas below thick mats of ice algae coated the ice which correlated with the steep salinity gradient (Fig 6-8). Meltponds that froze shut and had no pycnoclines, possessed algal mats which coated a very porous ice matrix. Algal mats thereby extended up to the already frozen new ice cover with occasional inclusions in the newly formed ice. Besides algal mats vigorous life of fish and crustaceans could be observed in these puddles. Porous layers extended several meters into the ice floe, and there was vigorous life also in the interior of the floe. Ice cores from the porous layer rendered up to five (max.) amphipods per drilled ice core (90 cm), even though the bottom layer of the ice was nearly impermeable. However, yields declined rapidly over time probably due to the escape behavior of these organisms. This allows to conclude that pores must have ended with adequate diameters into the open water column. Occasional openings of several cm (approx. 4 cm) in diameter confirmed this hypothesis.

Whether algae grow along such channels in the ice and depend on water advection mechanisms will be determined from collected ice samples in the home laboratory.

### 6.3 Under one roof - the under-ice community (I. Werner)

The world under an ice-floe is a habitat with special and variable conditions. The underside of the ice is not an even and homogenous surface, it is rather characterized by a variety of cracks and crevices, protrusions or rafted pieces of other floes. Even whole floes can underly each other, thus building a complex under-ice landscape. This is the environment for a specialized under-ice community.

During ARK XI/1, a total of 16 ice stations were used for investigations on the under-ice community. Temperature and salinity profiles were recorded over the upper 5 metres of the water column under the ice. The underside of the ice was sampled for measurements of chlorophyll-*a* and the C/N-ratio; a video camera was deployed under the ice to gather information on the morphology and structure of the habitat as well as on abundance and distribution of under-ice amphipods; and a pumping system delivered quantitative samples of the sub-ice

fauna, caught from the water layer directly under the ice. On board POLARSTERN, experiments with under-ice amphipods were carried out to gain insights into their feeding ecology and fecal pellet production.

Regarding the temperature/salinity regime, two different scenarios were found. At 7 of the stations, a thin (10-20 cm) pycnocline could be recorded directly under the ice (Fig. 6-9a), probably due to melting processes. At the other 9 stations, no pycnocline was observed (Fig. 6-9b).

By means of the video system, the very patchy distribution of green/brown ice at the underside of the floes, which indicated the abundance of ice algae, was demonstrated on a small scale. Chlorophyll-*a* values in the lowermost 2 cm of the ice ranged from 0.1 to 37.8 µg/l between stations.

With the exception of some stations on the East Siberian Transekt, under-ice amphipods were found at all stations, however, in lower numbers than expected. *Onisimus* spp. were the most abundant, followed by *Apherusa glacialis*. *Gammarus wilkitzkii* was quite scarce. No signs of reproduction were observed in any species, only some very small *Onisimus* were found.

At some stations, even big specimens of all 3 species were found in brine channels up to 40 cm high in the ice, still alive. Specimens of *Onisimus* and *A. glacialis* were also caught in Bongo-nets in the upper 100 m water layer between ice-floes. These animals probably fall through the water column after they have lost contact to their habitat.

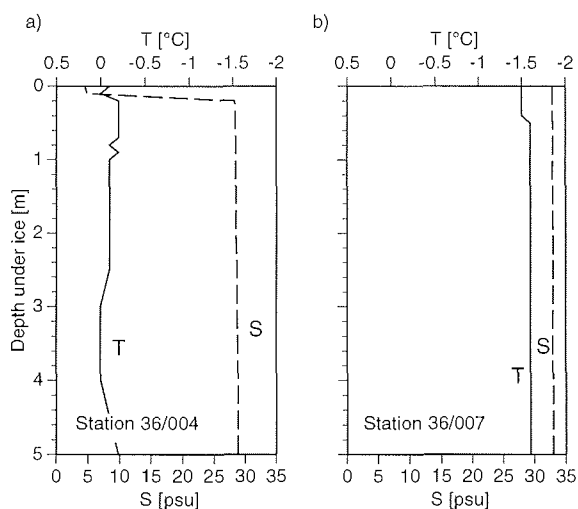


Fig. 6-9: Temperature and salinity profiles under ice floes at 2 different stations during ARK XI/1.

There was very little makrozooplankton (> 200 µm) in the water layer below the ice. Only *Pseudocalanus* species were found regularly and in significant numbers. In contrast, a very diverse and abundant community of smaller zooplankton



(> 50  $\mu\text{m}$ ) seemed to dominate this habitat, e.g. naupliar stages, cyclopoid copepods (*Oithona* spp.) and above all, several groups of harpacticoid copepods (*Tisbe* sp., *Halectinosoma* sp., *Microsetella* sp.), which are partly described to live inside the ice.

Further analyses and experimental work on all main members of the under-ice community, which is thought to function as a mediator for the production and transport of organic matter between the ice and the water column, will hopefully throw some light onto the cryopelagic coupling processes.

#### 6.4 Sediment distribution at the under-ice surface (F. Lindemann, I. Werner)

During the "Polarstern" cruise ARK XI/1 an under-ice video system was deployed at 13 stations to get detailed information about the morphology and structure of the under-ice surface. Usually, the floe surface at the locations, where the video system was installed, looked quite flat and homogeneous, although sometimes small hummock features in the vicinity occurred. Surprisingly, there were only 6 locations with level ice at the underside, when scanning the scenery beneath the ice cover. At 3 locations the under-ice morphology seemed to be slightly deformed by weak ice pressure in former times. A total of 4 locations had a very complex under-ice scenery. These floes were extremely rafted, and stacked floe-packages, up to 3 single floes over each other, could be observed. Most of the floes were orientated in different angles to each other so that cavities of different sizes were formed. Also single floes were built in vertically into this under-ice landscape. Therefore, the total ice thickness varied on a metre-scale, even under a restricted surface area.

At 6 locations, significant amounts of diffuse sediment patches could be recorded, independent of the under-ice morphology. The sizes of the patches ranged from a few centimetres up to some tens of centimetres in diameter. The sediment inclusions seemed to be in the lowest part of the ice column. However, sediments also occurred directly at the underside of the ice floe. The observations indicate that these patches have a significant influence on the light penetration, and probably on the distribution of algae.

At 3 of the 4 extremely rafted locations, the former ice surfaces of the now underlying floes exhibited significant contents of sea ice sediments. The sediments were concentrated into small clods of a few millimetres to some centimetres in size. The surfaces of these underlying floes looked similar to the bottom of shallow, sediment loaden melt-ponds or shallow, newly forming cryoconite holes. At 2 of these locations, almost vertically orientated sediment streaks along the sides of the underlying floes occurred. These streaks could be formed due to sediment redistribution across the floe edge by currents and following gravitational sediment release.

The records of this cruise document that sediment release from ice floes does not only occur due to melting and turn-over processes, but also to the described winnowing-like processes. These observations also show that because of its

extremely patchy distribution, a quantification of the sediment load in the pack ice is very difficult.

#### 6.5 Sediments in sea ice (F. Lindemann)

Investigations of sediments in sea ice were carried out during the "Polarstern" expedition ARK XI/1 in the northern part of the Laptev Sea and the adjacent Arctic Ocean. Thus, the studies covers the area where the Transpolar Drift starts. This drift originates on the broad, shallow Siberian shelves, including the Laptev Sea as an important component, considered as a major ice factory for the Arctic Ocean. Sediment particles and other particular substances seem to be incorporated into newly forming ice during freeze up in autumn and winter. This sediment laden ice is transported by the Transpolar Drift through the Fram Strait into the Norwegian-Greenland-Sea, where the sea ice is ultimately melting. Thus, the incorporated sediments and other particulate substances are released.

During the cruise ice sediment work was carried out at 22 ice stations directly from the vessel and 9 helicopter stations. If there were significant amounts of sea ice sediments on the surface of the floe, bulk samples were taken with spatulas and spoons. The samples were stored frozen for investigations in the home laboratory, e.g. for grain size analyses and analyses of the particulate organic matter (POM). Usually four ice cores, each one metre long, were taken, one core for stratigraphic analyses (done by H. Eicken), another for POM-analyses, the third as an archive core and the fourth for vacuum filtration aboard Polarstern. At six sites, cores over the entire floe thickness up to 4.79 m were recovered. For filtration, the cores were usually splitted into 10 cm segments, melted and filtered through pre-weighed 0.4  $\mu\text{m}$  filter papers. The filter papers are stored frozen for freeze-drying in the home laboratory. There, the filter papers will be re-weighed for quantification of the sediment load in sea ice. Aboard the vessel, 297 ice samples from 24 different sites were filtered for quantifying the sediment load (Tab. 1).

Whenever possible, separate sediment samples for trace metal analyses and for studies of anthropogenic pollutants (e.g. PCB's) were taken and stored frozen (see table). Small subsamples were taken for heavy mineral, diatom and flagellate analyses.

Aboard "Polarstern" no sample analyses could be performed, therefore, only general impressions of the samples are given in the following. Usually only the upper 10 to 20 cm of the ice column showed a diffuse sediment distribution, as visible in ice cores. The deeper core sections seemed to be macroscopically clean, sediments were enriched in layers up to 5 to 10 cm thickness. Commonly the sea ice sediments sampled during this cruise are fine grained and could, as a first impression, be classified as silty clays and clayey silts. Sandy sediments are rare.

At ship stations the sea ice sediments were directly studied by visual inspection to get an overview of the floe surface sediment distribution. Usually the distribution of exposed ice sediments was patchy. The sizes of the patches were in the order of tens of metres.

Tab. : Station list of samples for dirty ice investigations;  
 x = sample taken or present; helicopter = helicopter stations

Ice Station	Ship Station (or time)	Filtered samples	Not yet processed cores	Surface samples	PCB's	Trace metals	Notes
201	001	-	-	x	-	-	helicopter
203	003	18	-	-	-	-	
205	004	11	-	x	x	x	
205b	005	36	x	x	x	x	
206	006	6	-	-	-	-	
207	007	6	-	-	-	-	
208	27.9, 17:00h	14	-	x	x	x	helicopter
209	008	13	-	x	-	-	
210	009	3	-	-	-	-	
216	024	4	-	-	-	-	
219	025	5	-	-	-	-	
221	027	7	-	-	-	-	helicopter
223	11.8., 10:00h	-	-	x	-	-	helicopter
225	036	-	x	x	-	x	helicopter
228	042	10	-	x	-	-	helicopter
228b	042	11	-	-	-	-	
229	044	11	-	x	-	-	helicopter
230	045	12	-	-	-	-	
232	047	11	-	x	-	-	helicopter
232b	047	1	-	-	-	-	
233	048	-	-	x	-	-	
234	049	5	-	x	-	-	
235	051	-	-	x	-	-	
236	052	9	-	-	-	-	
237	055	13	-	-	-	-	
239	057	17	-	-	-	-	
240	060	21	-	x	-	-	
241	062	10	-	-	-	-	
242	066	34	-	-	-	-	
246	074	9	-	-	-	-	
252	9.9., 05:00h	-	x	-	-	-	helicopter

In contrast to ship stations, helicopter stations are more selective and provide the chance to get ice samples with higher sediment load. At one station, a hummocky area of ca. 100 square metres was covered by sand and gravel up to 5 cm in thickness. After sieving, the coarse fraction (>63  $\mu\text{m}$ ) was found to consist of angular to subrounded, sometimes coated quartz grains as the dominant component. Opaque minerals are frequent, as well as coal pieces. In the gravel fraction, rock fragments like shists and coal-pieces (up to 2 cm in diameter) dominate.

In the past, only few investigations have been carried out on the processes that incorporate sediments into newly forming sea ice. During the following expedition TRANSDRIFT III into the Laptev Sea, aboard the Russian icebreaker "Kapitan Dranitsyn", we will get the unique opportunity to study the sediment entrainment processes into growing sea ice during freeze-up.

### 6.6 Export of particulate material from sea ice

(M. Gleitz, S. Grossmann, E.-M. Nöthig, V. Shevshenko)

Organic matter which is not remineralized by ice-associated organisms will eventually be released into the water column. In order to elucidate the contribution of ice-derived organic material to particle flux rates, sedimenting material was collected by short-term deployments of sediment traps attached to ice floes. The sediment traps were deployed by hand through open (melted through) puddles, or, when these could not be found, over the edge of ice floes, at a distance of at least 150 m away from the ship (Table X.2.2.2-1). At one occasion (station 60), traps were deployed 2 n.m. away from *Polarstern*. Deployments consisted of two single traps (Ø 12 cm) positioned at 5 and 25 m, and of one double trap (Ø 15 cm) positioned at 75 m beneath the ice under-surface. On two occasions, two additional double traps were deployed at 5 and 20 m (stations 60 and 75). Trap collections will be analyzed for POC/PON, Chl-*a*, and seston content. Light and electron microscopic analyses will also be performed. The trap data, combined with related data from the water column, will allow quantitative and qualitative evaluation of daily vertical flux.

Tab.: AWI/IO sediment trap deployments during ARK XI/1

Stat. No	Date	Position	Duration (hr)
36/008	28.7.95	79°09.0' N / 146°20.7' E	8.5
36/024	04.8.95	79°02.7' N / 131°24.7' E	16
36/025	07.8.95	81°05.9' N / 105°19.6' E	18
36/027	08.8.95	81°12.8' N / 106°33.7' E	25
36/042	16.8.95	78°43.5' N / 134°44.7' E	11
36/044	17.8.95	79°05.6' N / 135°08.7' E	18
36/047	20.8.95	80°53.0' N / 131°03.4' E	24
36/049	22.8.95	81°03.7' N / 136°29.7' E	16
36/057	27.8.95	81°12.1' N / 150°05.5' E	16
36/060	28.8.95	80°18.6' N / 150°10.6' E	18
36/075	04.9.95	80°52.3' N / 123°01.4' E	24

Seasonal particle flux will additionally be investigated by means of two long-term sediment trap deployments on the Lomonosov Ridge at 150 m below the water surface and 150 m above the sea floor, integrated in the oceanographic "LOMO-2" mooring.

## 7 MARINE BIOLOGY

The functioning of the Arctic Ocean ecosystem and the dynamics and stability of Arctic marine communities are insufficiently investigated and understood so far. Crucial open questions are:

- How intensive is the coupling between the main sub-systems (ice - pelagial - benthal);
- to what extent is life in the ice-covered deep basins dependent on the importation (advection) of organic matter from the shelves, among which the Laptev Sea shelf is assumed to be most important; and
- how sensitive or resilient are populations and communities to strong, unusual environmental variations ?

The Arctic Ocean is regarded a system of high climatic sensitivity. Greenhouse warming and changes in precipitation and continental runoff may reduce the pack ice extent and the water stratification substantially, by which the present coupling of production and sedimentation areas of organic matter will be drastically changed. Altogether, the biota of the Arctic will presumably experience dramatic alterations. Scenaria about the expected ecosystem changes can only be set up, when today's biota distribution and energy flux patterns are sufficiently described. The biological work during and after ARK XI/1 is intended to contribute to these scientific challenges (see also chapters 6 and 8).

### Water Column Studies:

#### 7.1 Phyto- and protozooplankton ecology and vertical particle flux (A. Bartel)

Objectives:

The biological properties of the water column were studied in relation to hydrographical, chemical and other environmental conditions. In addition to the area covered during ARK IX/4 in 1993, it was possible to investigate deeper parts north of the Laptev Sea, to cross the Lomonosov Ridge, and to collect samples in the northwestern part of the East Siberian Sea. Thus, the existing data base could be extended substantially during ARK XI/1.

The following major questions were addressed:

- Are there regional differences in the seasonal distribution patterns of the phyto- and protozooplankton ?
- What are the influences of abiotic factors, such as the hydrographical structure of the water column, nutrient availability and ice coverage ?
- How is the relation between algal growth and grazing pressure ?
- How much of the phyto- and protozooplankton biomass as well as fecal material and other organic matter is transported to the deeper waters and, finally, down to the sea floor ?

## Work at sea:

Chlorophyll-*a* (chl-*a*) *in situ* fluorescence was measured continuously by a flow-through fluorometer, which was connected to the ship's seawater pumping system with the intake pipe located approximately 9 m below the sea surface. The data were recorded on the POLDEV/POLDAT (POLarstern-DATen-System). Every day, one litre water was taken and chl-*a* determined fluorometrically for later calibration in the home laboratory.

Water was sampled at 65 stations with the Rosette sampling system attached to the CTD (s. section 4.1.1). Stratified subsamples were obtained from at least 8 different water depths from the surface layer (5 or 10 m) down to 300 m. (At selected stations of each transect and at each sediment trap station additional subsamples were obtained in the upper 300 m and in deeper layers.) The samples will be analysed for the following parameters:

- Species abundance: Samples (ca. 200 ml) were fixed with hexamine-buffered formalin (final concentration 0.5- 1.0 %) and stored in brown glass bottles. Microscopical analyses of the species composition of plankton will be carried out in the home laboratory (AWI).
- Chl-*a* and phaeopigments: Pigment concentrations were measured on board with a Turner fluorometer after filtration of 2 l water on glass-fibre filters, homogenization and cold extraction in 90% acetone.
- Particulate organic carbon/nitrogen and biogenic silica: 3 l of water were filtered on pre-combusted glass-fibre filters (for POC/PON) or on cellulose acetate filters (Si) and stored at -30°C for later analyses in the home laboratory.
- Seston: 2 l of water were filtered on pre-weighed glass-fibre filters and stored at -30°C for later analysis at AWI.

Proto- and microzooplankton as well as fecal pellet samples were collected with a multinet (55 µm mesh width). Hauls were made at the beginning, on two middle stations and at the end of each transect. The samples were fixed with hexamine-buffered formalin (final concentration 2 %) will be analysed under the microscope at AWI.

Particle flux measurements by sediment trap deployments are described in section 6.6 (export of particulate material from sea ice).

## Preliminary Results:

*Laptev Sea:* The ice conditions were extremely different during this cruise when compared to the 1993 cruise: While the western part (transect D) of the Laptev Sea was ice free in 1995, the eastern Laptev Sea (transect B) was ice covered. Fig. 7-1 shows an example of the chl-*a* distribution: Over the shelf, maximum values were generally observed at 20 to 30 m water depth, whereas above the continental slope, the chl-*a* maximum was found at the surface (10 m). Stations deeper than 1100 m also had highest chl-*a* concentrations at 10 m. The highest chl-*a* value (2.33 µg l<sup>-1</sup>) was measured at station 33 on the westernmost transect E near Severnaya Zemlya at a water depth of 20 m (Fig. 7-2 A). Elevated values (> 1 µg l<sup>-1</sup>) were observed in water depth of 20 to 30 m, whereas lower concentrations were

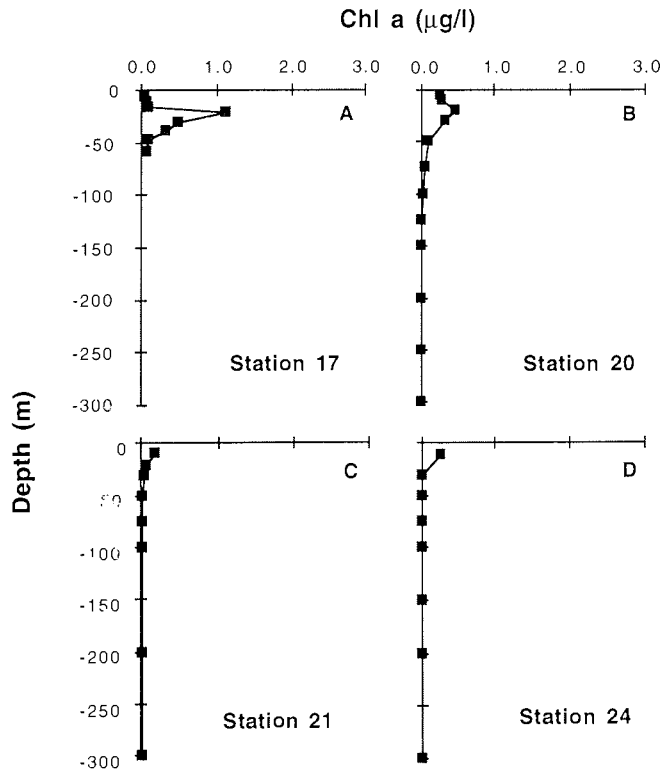


Fig. 7-1: Chl-*a* distribution in the central Laptev Sea (transect C ) on the shelf at 57 m depth (A), over the continental slope at 475 m (B) and 1123 m depth (C) and over the deep sea (3126 m; D).

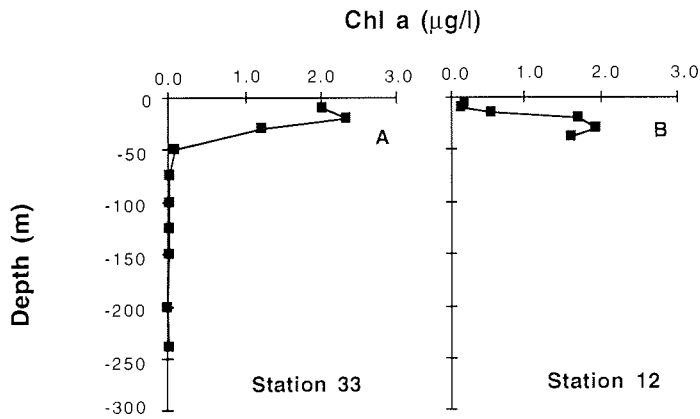


Fig. 7-2: Vertical distribution of chl-*a* at different station depths (A: transect E, 232 m; B: transect B, 45 m).

encountered near the sea surface (10 m). Below 30 m, the chl-*a* concentrations decreased sharply. Exceptions were some shelf stations in the eastern part of the Laptev Sea. These had relatively high chl-*a* values below 15 m down to the bottom (Fig. 7-2 B: Transect B, water depth 45 m).

In order to study the seasonal progression of the plankton community at the same location, one station on the continental slope near Severnaya Zemlya was sampled on the 12th of August (station 33) and 8th of September (station 87). Similar vertical chl-*a* profiles were recorded on the two dates, but, the chl-*a* maximum was slightly lower and also occurred at deeper water depth in September (Figs. 7-2 A, 7-3).

East Siberian Sea: The ice coverage along transect A in the East Siberian Sea varied between 8/10 and 10/10. Chl-*a* values on the shelf, slope and over the deep sea ranged between 0.08 and 0.48  $\mu\text{g l}^{-1}$  with maximum values at 10 m. The highest chl-*a* value was measured at station 64 (509 m) in 10 m water depth (Fig. 7-4).

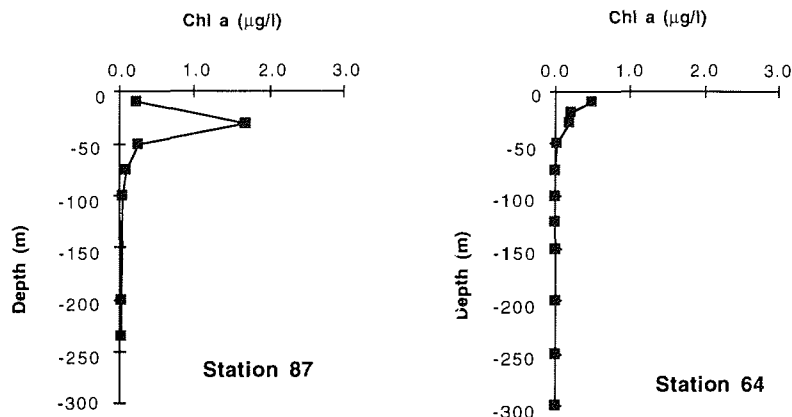


Fig. 7-3 (left): Vertical distribution of chl-*a* at a slope station near Severnaya Zemlya (stat. 87), at the same location as stat. 33 (Fig. 7-2A), but about 4 weeks later.

Fig. 7-4 (right): Distribution of chl-*a* at station 64 in the northwestern East Siberian Sea (transect A, 509 m)

## 7.2 Phytoplankton primary production and bacterial production (M. Gleitz & S. Grossmann)

Objectives:

For the analysis of vertical carbon flux it is essential to quantify the primary production of organic carbon in the upper water column and its subsequent degradation especially by bacteria. Productivity measurements provide an important background to evaluate the channeling of organic matter through the pelagic



microbial food web (carbon turnover), and hence, for the determination of how much of the primary product may eventually be transported into deeper waters.

Work at sea:

Phytoplankton and bacterial production were measured at several stations occupied in open, ice-free waters over the shelf and over the deep ocean. Samples were taken from Niskin bottles at 3 to 5 depths, approximately corresponding to 100, 50, 25, 15, 10, 5 and 1% of light incident on the sea surface. Light depths were calculated prior to sampling by means of Secchi disk measurements according to:

$$\% \text{ light depth (m)} = \ln(\text{light depth [\%]} / 100) * (\text{Secchi depth} / -1.7)$$

For measurement of primary production, subsamples of 40 ml were filled into PC bottles, inoculated with  $\text{NaH}^{14}\text{CO}_3$ , and exposed to quantum fluxes of 2 to 220  $\mu\text{mol photons m}^{-2} \text{s}^{-1}$  for 5 hours at a constant temperature of  $-1^\circ\text{C}$ . Incubations were terminated by filtration onto 0.45 nitrate cellulose filters; and the radioactivity retained on the filters was determined by liquid scintillation counting. Subsamples of 100 ml were allowed to warm to room temperature, and DIC concentrations were determined by acid titration according to Strickland & Parson (1972, Bull. Fish. Res. B. Can. 167, p. 311). Carbon uptake rates were then calculated based on specific radioactivity of the sample and DIC concentration.

Bacterial production was determined by incorporation of  $[^3\text{H}]$ thymidine into cold trichloroacetic acid extractable macromolecules. Incubation of samples and extraction procedure are described in more detail in section X.2.1.2. Thymidine incorporation rates will be converted into units of organic carbon by calibration experiments to be evaluated by microscopy.

Preliminary results:

In order to estimate daily primary production under a square meter of sea surface, carbon assimilation rates of phytoplankton measured in the incubator have to be related to daily downwelling photosynthetically active radiation (PAR). For this purpose, a hemispherical PAR sensor was mounted on the ship's upper deck, and light data were recorded continuously during the cruise as 5 min. mean values. Since light data have only been analyzed for station 12 so far, a production estimate can only be given for this station. Maximum productivity at this station corresponded to the vertical distribution of phytoplankton biomass, and showed a distinct subsurface maximum at 20 m despite the fact that light intensities were reduced at this depth to about 15% of incident irradiance (Fig. 7-5). Integrated primary production at this station amounted to  $338 \text{ mg C m}^{-2} \text{ d}^{-1}$ .

The vertical pattern of bacterial production at station 12 did not correspond to that of algal primary production (Fig. 7-6). Since the conversion factors for calculation of bacterial carbon production have to be evaluated at AWI, relative production rates are plotted, given as nanomoles of thymidine incorporated per  $\text{m}^3$  and day. Maximum productivity of bacteria occurred at the sea surface in a layer of reduced salinity caused by river input. Below this uppermost layer, rates of bacterial production decreased, showing minimal values between 10 and 20 m depth.

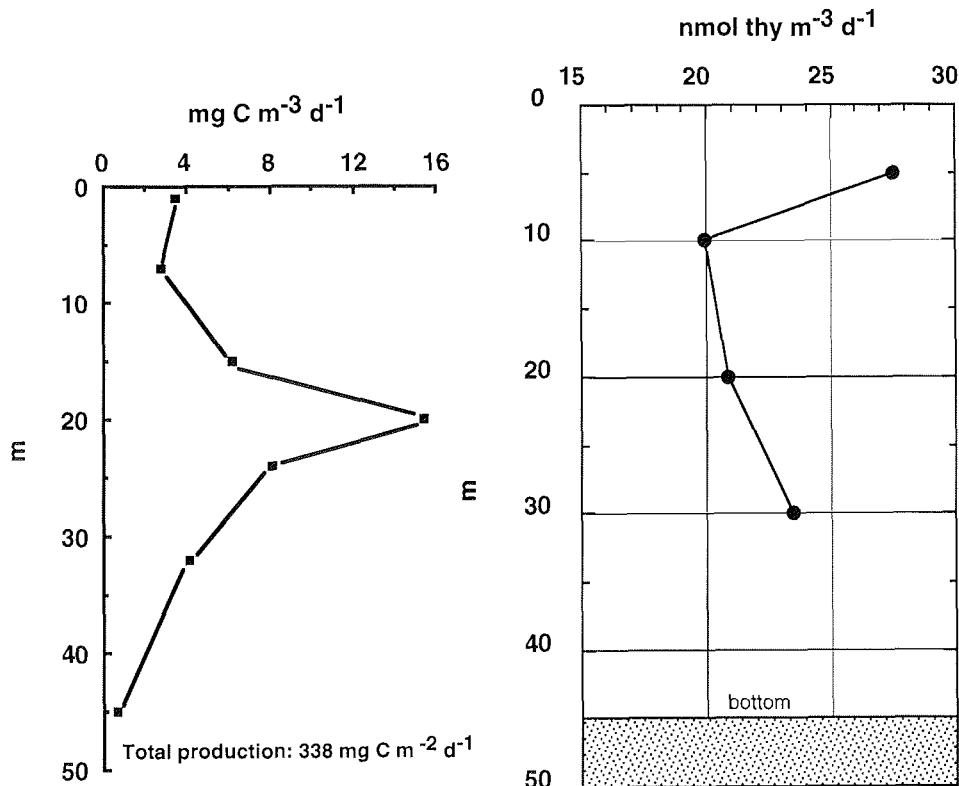


Fig. 7-5 (left): Vertical profile of daily phytoplankton production ( $\text{mg C m}^{-3} \text{ d}^{-1}$ ) at station 12.

Fig. 7-6 (right): Vertical profile of bacterial production at station 12, given as nanomole [ $^3\text{H}$ ]thymidine incorporated per  $\text{m}^3$  and day.

### 7.3 Zooplankton (K. Kosobokova, T. Scherzinger, R. Spielhagen, S. Timofeev)

#### 7.3.1 Copepod ecology (K. Kosobokova & T. Scherzinger)

The results of the ARK IX/4 expedition to the Laptev Sea indicate different reproduction strategies in dominant copepod species. It is yet insufficiently known, whether herbivorous species reproduce under pack-ice in regions with extremely low primary production.

According to our knowledge and results of ARK IX/4, the shallow and deep parts of the Laptev Sea are inhabited by quite different assemblages of zooplankton. The differences in faunal composition, abundance and ecology of zooplankton in shallow and deep regions resulted in different patterns of energy and matter flux in the water column. It is supposed that the particle flux in the water column is heavily influenced by the ice coverage in the Arctic Ocean.

Accordingly, we expect a rather poor, short-pulsed flux of organic matter down to the deep sea with a different nutrient regime for zooplankton living under the ice cover compared with zooplankton in the deep basins. As a consequence we should find different patterns in the transformation of organic matter in both compartments.

In order to understand the biology of the dominant copepod species and the processes of transformation in the pelagic ecosystem, the zooplankton study during the expedition included the following main aspects:

- The faunal composition of zooplankton of the deep basins and the shallow parts of the Laptev Sea. Special attention was paid to the poorly known northern deep region and the marginal ice zone.
- Vertical and horizontal distribution of zooplankton abundance and biomass.
- Reproductive biology, egg production rates and gonadal maturity of dominant copepod species from epi-, meso- and bathypelagic waters.
- Comparisons of lipids, dry weights, carbon contents and carbon/nitrogen ratios of several epi-, meso- and bathypelagic copepod species and their stages as well as investigation for their food.
- Description of the fecal pellets of different copepod species and their copepodit stages.

#### *I. Multinet sampling for the study of the zooplankton community structure*

For the investigation of species composition and distribution, zooplankton was collected by a multiple closing net (multi-net, mesh size 150  $\mu\text{m}$ ), which provided stratified sampling of the entire water column from the bottom to the surface. Multi-net sampling was performed along all the seven cruise transects. Six of them extended seaward from the outer continental shelf over the continental slope into the deep Arctic Ocean basins north of the Laptev and Kara Seas (Transects A - E, G). Transect F followed West - East along latitude 81°16'N across the Lomonosov Ridge. Between three and nine multinet stations were taken on each transect. Two to five layers were sampled at stations situated deeper than 1000 m. In total, 54 multi-net stations were taken, 21 in the shelf region, 21 in the slope region and 12 in the deep sea (seven deeper than 2000 m and five deeper than 3000 m). The samples were preserved in 4% hexamine- buffered formalin for further processing.

#### *II. Egg production (K. Kosobokova)*

##### Methods

Zooplankton for egg production experiments were collected by bongo-net tows (mesh size 310  $\mu\text{m}$  and 500  $\mu\text{m}$ ) from the upper 100 m, from 500-0 m and 1500-0 m. The experiments were carried out with the two interzonal copepod species *Calanus glacialis* and *Metridia longa* and with the meso- and bathypelagic copepods *Scaphocalanus magnus*, *Chiridius obtusifrons*, *Gaidius tenuispinus*, *Aetideopsis rostrata* and *Heterorhabdus norvegicus*.

25 - 30 females of *Calanus glacialis* and *Metridia longa* were sorted from the 0 - 100 m samples immediately after capture and were placed in 2000 ml plexiglas insets having false bottoms of mesh (300 - 500  $\mu\text{m}$ ) to separate eggs from females. These were then suspended in 3000 ml TPX jars containing filtered sea water. Egg production during the first 24 hours was used as a measure of the actual rate in the field (in situ egg production rate). Actual egg production rate was measured at one station in the Wilkitski Strait and at stations in the Laptev Sea. The effect of long-term starvation on egg laying of groups of 25 females and on individual females was studied in *C. glacialis* for 23 and 40 days. Egg production estimates of meso- and bathypelagic copepods were carried out on single females. They were cultivated during 5 - 15 days.

#### First results

The most active spawning of *Calanus glacialis* was observed at stations in the shelf zone with depths between 50 and 200 m. The highest values of egg production rate (58 eggs per female and day) were found at the station 009 in the eastern Laptev Sea in the end of July (Fig. 7-7). On the other stations in the shelf zone of this region egg production rates ranged from 20 to 40 eggs per female and day. Along the Central Laptev Sea Transect (C) reproduction of *C. glacialis* took place in the shelf and slope zones (1 to 27 eggs/female/day), and also at some deep stations situated close to the lowest boundary of the slope edge. On the Severnaya Zemlya Transect (E) *C. glacialis* produced 3,7 - 5,7 eggs/female/day at stations in the outer shelf and upper slope. Further to the north we did not observe any spawning female. No reproduction was observed on all stations investigated after 15th August.

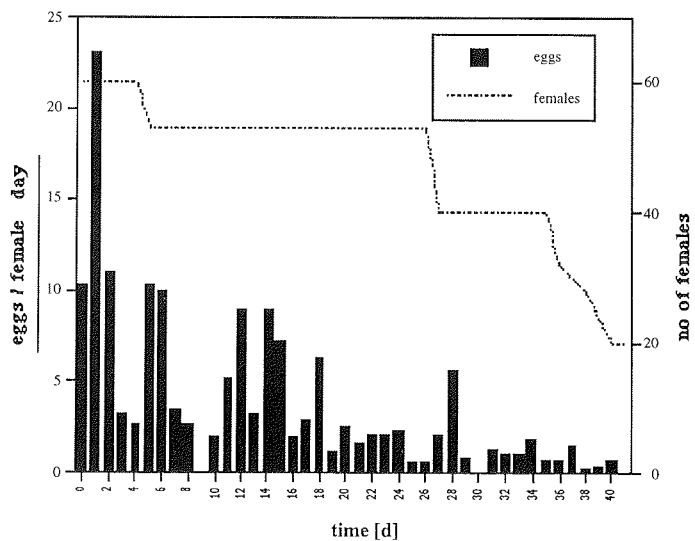
The results indicate that the reproduction of *Calanus glacialis* mostly takes place in the shelf and slope zone and depends to a great extent on phytoplankton availability. Previous investigations on *Calanus glacialis* egg production rates under starvation conditions demonstrated that spawning ceased after 3 - 7 days of starving (Hirche 1989, Kosobokova 1994). The results of two long-term starvation experiments with females from stations 006 and 009 showed that *C. glacialis* with rather high in-situ egg production rates are able to continue spawning for more than one month (Fig. 7-7). This suggests a possibility of transportation of well fed ripe females by currents over long distances.

Next page:

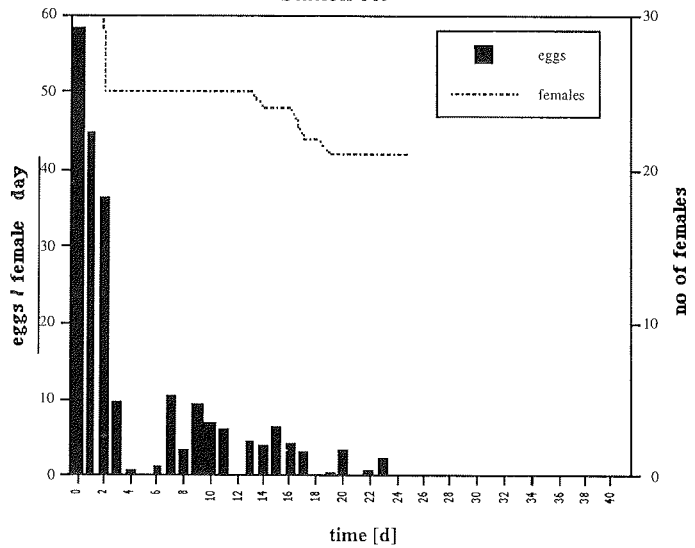
Fig. 7-7: Egg production rate per female per day of *Calanus glacialis* from two shelf stations in the Laptev Sea. Bars indicates the number of eggs per female, the dotted lines show the decreasing quantity of females per day. The experiments were interrupted after 40 (station 006), respectively after 23 days (station 009).

egg production of *Calanus glacialis*

Station 006



Station 009



### III. Transformation of organic matter and particle flux to the deep sea (T. Scherzinger)

#### Material and methods

Bongo-net samples (mesh size 500 and 200  $\mu\text{m}$ , and an additional net with a mesh size of 60  $\mu\text{m}$ ) were collected from surface layers down to 1500 m at stations 23, 24, 27, 40a, 45, 47, 51a, 55, 57, 60, 62, 67, 69, 75, and 89 and down to 500 m at stations 20, 22, 25, 49, 64, 96. Experiments were carried out on different stages of the herbivorous species *Calanus hyperboreus* and *C. glacialis*; the omnivorous *Metridia longa*, *Heterorhabdus norvegicus*, *Scaphocalanus magnus*, *Gaidius tenuispinus*, *Aetideopsis rostrata* and the carnivorous *Pareuchaeta glacialis* and *Pseudochirella spectabilis*.

For determination of carbon contents, carbon/nitrogen ratios and dry weights not less, if possible, than 10 individuals per species and stage with obviously empty guts were sorted out not later than 36 h after each catch. The length of each specimen was measured under the microscope. They were shortly rinsed in aqua dest. and placed in pre-weighed silver caps. For transport to the laboratory in Bremerhaven, the samples were stored at  $-30^{\circ}\text{C}$ .

For lipid composition measurements, 10 - 15 specimens with obviously empty guts were sorted out immediately, transferred to 3 ml dichlormethylene-methanol (2:1), and stored at  $-30^{\circ}\text{C}$ .

Complete bongo-net hauls from different stations were preserved in hexamine-buffered 4% formalin for analyses of gut contents and for morphological studies. Samples for electron microscopy were preserved for 18 h in a mixture of 1.25 % glutaraldehyde and 2.5% paraformaldehyde and thereafter stored at  $+4^{\circ}\text{C}$  in a 0.1 m solution of sodium cacodylate.

For fecal pellet production, 6 - 20 individuals of each species and stage were sorted out immediately at 11 stations and kept separately in cell well plates in filtered sea water. Fecal pellets were collected with a pipette after 2, 8, 12, 24 and 36 hours and preserved for electron microscopy. In the laboratory at AWI Bremerhaven, the sizes of fecal pellets will be measured and their shapes and contents analysed.

20 to 30 females and CV of *Gaidius tenuispinus*, *Scaphocalanus magnus*, *Metridia longa* and *Chiridius obtusifrons* were sorted immediately after capture and kept as individuals in small cell wells<sup>®</sup> with filtered sea water. After one week, when guts were empty, one half of them were fed with detritus from the 60  $\mu\text{m}$  catch, eggs of *Calanus glacialis* from egg production experiments and fecal pellets of *Calanus hyperboreus*. The produced fecal pellets were collected every hour and preserved in glutaraldehyde. They will be investigated for shape features and content by electron microscopy. The results will be compared with the features of fecal pellets from samples of the fecal pellet production experiment.

The effect of starvation on dry weight, carbon and lipid composition was investigated in *Metridia longa*. 20 females were placed in four 3000 ml beakers containing filtered sea water. The water was exchanged once every week.

Immediately after the catch and in weekly intervals, 20 - 25 females were preserved for carbon measurements and lipid analyses.

#### First results

A preliminary comparison of the charges (degrees of filling) of the guts of copepods from the meso- and bathy-pelagial and epipelagic copepods showed pretty full guts in deep layer inhabitants during the whole observation period. Whereas this observation was made independent of oscillations of food in the surface layer, the gut charges of epipelagic copepods were obviously correlated to the varying algal concentrations in the upper water layers.

#### 7.3.2 Chaetognaths: Population biology and ecological significance (especially *Sagitta elegans*). (S. F. Timofeev)

A Bongo net equipped with 200  $\mu\text{m}$  mesh was towed vertically at 0.5  $\text{m s}^{-1}$  for the collection of animals. The whole catch was preserved in 4 % buffered formaline. The catches from other Bongo nets (310 and 500  $\mu\text{m}$  mesh) and from multi-net (150  $\mu\text{m}$  mesh) were used for the species composition analysis only.

In the Laptev Sea chaetognaths have been represented by three species, *Sagitta elegans*, *S. maxima* and *Eukrohnia hamata*. *S. elegans* is the dominant species in the larger part of the area (in biomass terms), while *E. hamata* is dominant at some stations only. *S. maxima* was found at stations 032 (multi-net; 500-200 m), 045 (Bongo net, 200  $\mu\text{m}$ ; 1500-0 m), 052 and 062 (Agassiz trawls). These are the first records of *S. maxima* in the Laptev Sea.

In the shallow waters only immature specimens of *S. elegans* were observed. Ripe *S. elegans* were caught in areas with depth of more than 500-700 m (Fig. 7-8), i.e. in sub-surface Atlantic water layers. We can suggest that in the Laptev Sea, as in the Kara Sea (Timofeev 1991), for normal life cycle should be have possibility to migrating of chaetognaths in the Atlantic water at the winter time.

Morphometric relationships have been investigated in 397 specimens of *S. elegans*: Head width (HW) is closely related to body length (BL). The relationship is described by the equation:

$$\text{HW} = 0.0412\text{BL} + 0.0787 \quad (r^2 = 0.91).$$

Accordingly, it can be suggested that the head width in *S. elegans* (of the same body length) from the Laptev Sea is larger than in the Barents Sea (HW = 0.044BL - 0.032, Falkenhaus 1991).

The relationship between body length (BL) and hook length (HL) is:

$$\text{HL} = 0.0302\text{BL} + 0.0738 \quad (r^2 = 0.90).$$

Individuals of *S. elegans* from the Laptev Sea have a smaller hook length than found in animals from the North Pacific and in the Japan Sea (Terazaki 1993).

Estimates of the predation impact of *S. elegans* on the copepod communities will be carried out after the expedition (after analysis of the body size structure of the copepod communities).

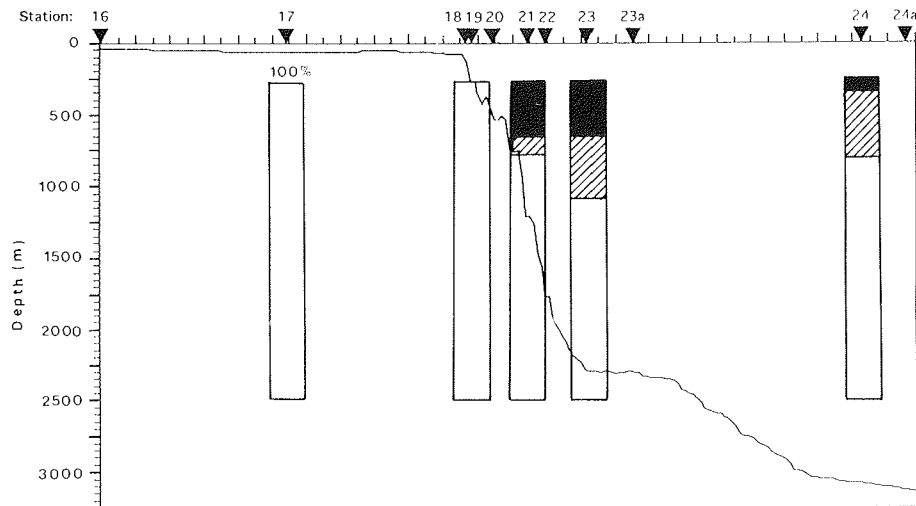


Fig. 7-8: Distribution of developmental stages of *Sagitta elegans* along the transect C (in per cent; I = early stage, II = intermediate, III = mature)

#### 7.3.4 Euphausiids: Distribution and population biology. (S. F. Timofeev)

Catches from all plankton net hauls were used for the analysis of euphausiid species composition. The biomass distribution of euphausiids was investigated in Bongo net (200  $\mu\text{m}$  mesh) samples only.

In the Laptev Sea euphausiids were represented by four species, *Thysanoessa longicaudata*, *T. inermis*, *T. raschi* and *Meganycitiphanes norvegica* (Table 1). *T. longicaudata* is the more widely distributed species, and *M. norvegica* is the more rare (only at one station, 045). The finding of *M. norvegica* is the first in the Laptev Sea.

Table 2 summarizes the results of euphausiid biomass calculations for areas with different depths. The largest biomass values were found at stations with depths between 100 and 200m, 200 and 500m, 1000 and 2000m, and 2000 and 3000m. *T. raschi* is a shallow water species, and in the Laptev Sea these animals inhabit areas with depths between 100 and 500m (the low salinity in the more shallow areas is a limiting factor for the distribution of *T. raschi*). The neritic species, *T. inermis*, occurred in the deeper locations (above the slope), and the oceanic *T. longicaudata* was found at all stations with depths of more than 1000 m.

In the Laptev Sea *T. raschi* were represented by specimens of 19-28 mm body length (21 mm and 24 mm are the modal lengths). In 1993, the length structure of *T. raschi* was the same: 19-28 mm (with modes of 22 mm and 26 mm; Timofeev



1995a). The sex structure of *T. raschi*, however, was different: in 1993 the share of males was 25 %, whereas in 1995 males made up more (50 %).

*T. longicaudata* were represented by specimens of 12.6-17.4 mm length (mean: 15.3 mm), which agrees with the size structure in 1993 (12.2-17.4 mm, mean: 15.3 mm; Timofeev 1995b). The sex structure in 1995 is different from 1993, when specimens with un-developed secondary genital features (thelycum and petasma), predominated. In 1993, males contributed 29 % to all the animals caught (Timofeev 1995b), whereas in 1995 the portion of males was greater (61.4 %).

Table 1: *Euphausiid records in the Laptev Sea in 1995*

Stations	<i>T. longicaudata</i>	<i>T. inermis</i>	<i>T. raschi</i>	<i>M. norvegica</i>
36/003	+	+	-	-
36/007	+	+	-	-
36/008	-	+	-	-
36/019	+	-	-	-
36/020	+	-	-	-
36/021	+	-	-	-
36/022	-	+	-	-
36/023	+	-	-	-
36/024	+	-	-	-
36/025	+	+	-	-
36/040a	+	-	-	-
36/044	+	-	-	-
36/045	+	-	-	+
36/049	+	+	-	-
36/052	+	-	-	-
36/055	+	-	-	-
36/057	+	-	-	-
36/060	+	-	-	-
36/062	+	+	-	-
36/064	+	+	-	-
36/065	+	-	-	-
36/066	+	-	-	-
36/067	+	-	-	-
36/069	+	-	+	-
36/071	+	-	-	-
36/072	-	-	+	-
36/075	+	-	-	-
36/080	+	-	-	-
36/083	+	-	-	-
36/084	-	-	+	-

Table 2: Biomass of euphausiids in the Laptev Sea 1995

Depth (m)	Quantity of Stations	Biomass, mg 1000 m <sup>-3</sup> mean (min/max)	Dominant species
< 100	9	0.0	
101- 200	3	1831.8 (0.0 / 3960.7)	<i>T. raschi</i>
201- 500	8	2088.3 (0.0 / 7810.7)	<i>T. raschi</i>
501- 1000	4	441.1 (0.0 / 1764.3)	
1001-2000	14	1285.4 (0.0 / 6996.4)	<i>T. inermis</i> <i>T. longicaudata</i>
2001-3000	7	1004.3 (0.0 / 3908.6)	<i>T. longicaudata</i>
> 3001	5	115.4 (0.0 / 576.9)	

### 7.3.5 Planktic foraminifers (R. Spielhagen)

Multinet tows (mesh size 55 µm) were collected along transects B (stations 40a, 44, 45, 47), C (stations 19, 21-24, 24a) and E (stations 25, 31-33) for sampling the upper water column. Regular sampling intervals were 500-300 m, 300-200 m, 200-100 m, 100-50 m, 50-0 m; at stations 19 and 33, sampling intervals were 50 m. The catch was preserved with hexamine-buffered 2% formalin and later transferred into ethanol.

After the cruise, planktic foraminifers will be extracted from the samples. Their species distribution will be determined for different water depths and size fractions. Finally, the stable oxygen and carbon isotope composition will be measured using the mass spectrometer of the C-14 Laboratory of Kiel University. The results will be compared with the isotope composition of water samples from the same stations and depths and of dead planktic foraminifers in sediment samples from the surface of the sea floor.

## Sea Floor Investigations:

### 7.4 Zoobenthos (N. Anisimova, H. Deubel, S. Potin, E. Rachor)

#### Introduction

The zoobenthos studies during ARK XI/1 are a contribution to the general ecological work about the carbon fluxes between the marine sub-systems, i.e. to the features and intensities of the ice-pelago-benthic couplings. Together with the microbiological and bio-geochemical investigations, the zoobenthos work is intended to provide quantitative figures about the intensity of biological processes at the sea floor and, thus, on the availability and transformation of decomposable organic matter (food). Of special interest are the areas (transects) from the continental slope to the deep central Arctic Ocean basins, and the transect crossing the Lomonosov Ridge.

The larger, as a rule long-lived, macrofauna is regarded an integrating indicator of environmental conditions; it mirrors longer-term food as well as temperature, salinity, oxygen, sedimentary and other conditions. The occurrences of different communities and dominances of feeding guilds (e.g. suspension versus deposit feeders), therefore, are other main foci of our work.

Moreover, by the transportation of their pelagic larvae by specific water masses, the study of zoobenthos distribution even allows tracing back of relationships under variable water circulation regimes. Accordingly, the zoobenthos work during and after the cruise will contribute also the biogeographical research, especially to a better description of the distribution patterns (gradients) in the continental slope areas between the Kara, Laptev and East Siberian Seas. The knowledge of these patterns are pre-requisite for the understanding of the environmental history of the Eurasian Arctic seas and may serve as baselines for predictions and observations (incl. monitoring) of future changes, especially induced by global and regional climatic and circulation changes.

Some additional studies are devoted on specific population aspects (e.g. on the growth and longevity patterns of brittle stars).

Altogether, the benthos work in 1995 is also to be considered a continuation of the investigations initiated during ARK IX/4 in 1993 (s. RACHOR et al., 1994), substantially extending the areas covered (to the North, Northwest and Northeast of the Laptev Sea).

#### Material and methods:

Zoobenthos were obtained from large box samplers (GKG, quantitative and qualitative, for macrofauna), small multi-corers (MUC; quantitative, for meiofauna), and Agassiz trawls (AGT, qualitative, especially for larger epi- and near-surface living endofauna).

Most of the macrofauna was separated from the sediments by sieving with 250 to 500  $\mu\text{m}$  screens and preserved in 4-5% formaldehyde, buffered with borax. A part of the animals, especially from the AGTs, were pre-sorted, and calcareous

material were transferred to 70% ethanole after fixation with formaldehyde. MUC material was preserved *in toto* with buffered formaldehyde. Species identification, taxonomic and population studies, and quantitative evaluations will be done in the home laboratories (Bremerhaven, Murmansk and St. Petersburg).

For further details about sampling, see the following Table:

Station-No.	Date	Depth	GKG	MUC	AGT
36/002	19.07.1995	150m	1	1	0
36/003	22.07.1995	2080m	1	1	0
36/004	24.07.1995	50m	2	1	1
36/006	25.07.1995	100m	1	0	0
36/007	26.07.1995	220m	1	0	0
36/008	28.07.1995	100m	2	1	0
36/009	29.07.1995	75m	2	0	0
36/010	30.07.1995	50m	1	1	1
36/011	30.07.1995	40m	1	1	0
36/012	31.07.1995	45m	1	0	0
36/016	31.07.1995	50m	1	1	0
36/017	01.08.1995	60m	1	0	1
36/018	01.08.1995	90m	1	1	0
36/019	01.08.1995	270m	1	0	1
36/020	02.08.1995	510m	1	1	0
36/021	02.08.1995	1100m	1	1	2
36/022	03.08.1995	1700m	1	1	0
36/023	03.08.1995	2320m	1	1	1
36/024	05.08.1995	3150m	2	1	0
36/025	07.08.1995	2750m	2	1	0
36/027	08.08.1995	3250m	2	1	1
36/030	10.08.1995	1950m	1	0	1
36/031	11.08.1995	1100m	2	1	0
36/032	11.08.1995	500m	2	1	0
36/033	12.08.1995	250m	2	1	1
36/036	13.08.1995	100m	2	1	0
36/040	15.08.1995	1850m	2	1	1
36/042	16.08.1995	2100m	2	1	0
36/044	17.08.1995	2750m	2	1	0
36/045	18.08.1995	3350m	2	1	0
36/046	18.08.1995	3500m	2	0	0
36/047	20.08.1995	3820m	2	1	0
36/048	21.08.1995	3620m	1	0	0
36/049	22.08.1995	2800m	3	1	0
36/050	23.08.1995	2020m	2	0	0
36/051	23.08.1995	1800m	2	1	1
36/052	24.08.1995	1270m	2	1	0
36/053	25.08.1995	940m	0	0	1
36/055	25.08.1995	1600m	2	1	0

36/056	26.08.1995	2040m	2	1	1
36/057	27.08.1995	2600m	3	1	0
36/059	28.08.1995	2000m	1	1	0
36/060	28.08.1995	1600m	2	1	1
36/062	29.08.1995	1000m	2	1	1
36/064	30.08.1995	570m	2	1	1
36/065	30.08.1995	230m	2	1	0
36/066	31.08.1995	570m	1	0	0
36/067	31.08.1995	980m	1	0	0
36/069	01.09.1995	980m	2	1	1
36/071	01.09.1995	530m	2	1	1
36/072	02.09.1995	215m	2	1	0
36/073	02.09.1995	100m	2	1	0
36/075	04.09.1995	3570m	2	0	0
36/077	06.09.1995	3300m	0	0	1
36/079	06.09.1995	1650m	1	0	0
36/080	06.09.1995	1150m	2	1	1
36/081	06.09.1995	530m	1	0	0
36/083	07.09.1995	250m	1	0	1
36/084	07.09.1995	100m	1	0	0
36/087	06.09.1995	250m	0	1	0
36/088	08.09.1995	1650m	1	0	0
36/089	09.09.1995	2650m	2	1	0
36/090	09.09.1995	1770m	2	0	0
36/091	10.09.1995	1100m	3	0	1
36/092	10.09.1995	540m	3	0	0
36/093	10.09.1995	240m	2	0	0
36/094	10.09.1995	90m	3	0	0
36/095	11.09.1995	320m	2	0	1
36/096	11.09.1995	250m	2	0	0
Station No.	Date	Depth	GKG	MUC	AGT
Sum			112	42	24

GKG (Großkastengreifer) = large box sampler (rectangular corer) of 0.25 m<sup>2</sup> surface area  
MUC (Multicorer) = core tube of the multi-corer, each core covering a circle area of 78.5 cm<sup>2</sup>  
AGT (Agassiztrawl) = Agassiz trawl (POLARSTERN type) of 3 m x 1.1 m frame opening, equipped with a net of 1cm meshes; controlled bottom trawling as a rule for 15-20 min. at a ship speed of 1-2 knots; in the upper frame part of the AGT a small suprabenthic net was fixed to obtain smaller swimming animals (s. SIRENKO et al., 1996).

For specific population analyses, ophiurids were collected from AGT hauls (at the stations 19, 21, 33a, 60b, 62a, 64a, 83 and 95): 3 selections of *Ophiacantha bidentata*, 2 selections of *Ophiocten sericeum*, 2 selections of *Ophioscolex glacialis*, and 7 selections of *Ophiopleura borealis*.

All these four species dominante in different bottom communities. The most remarkable object is *Ophiopleura borealis*, which is large and suitable for investigations of vertebrae ossicles. The material of this species obviously allows to analyse not only size-frequency structures of its populations, but also individual growth rates after growth rings studies (in the arm ossicles). O.

*borealis* is an Arctic species, the distribution of which is completely controlled by Atlantic waters in the Arctic Ocean. The close connection of core Atlantic waters with the densities of populations as well as growth rates can be seen in 3 histogrammes (Fig. 7-9). These show distinguished reductions of modes of disks diameters with increasing depths within the core of Atlantic waters.

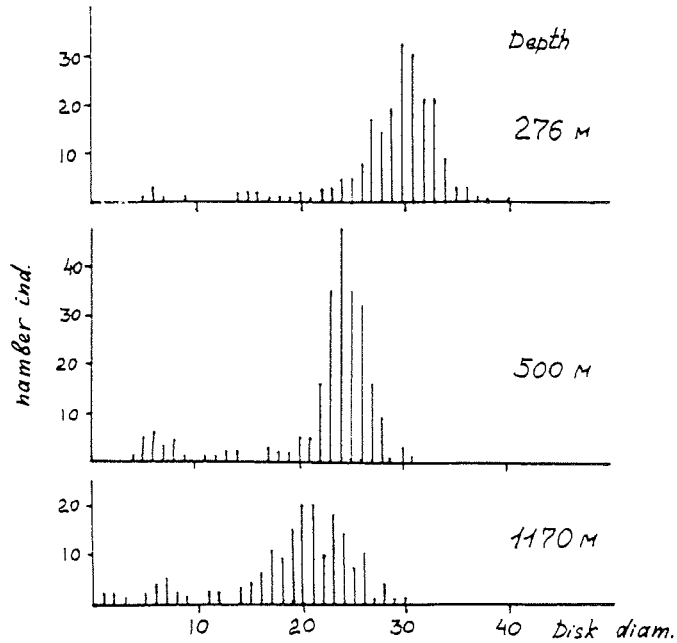


Fig. 7-9: Size-frequency histograms of disk diameters (mm), obtained from 3 populations of *Ophiopleura borealis* found at different depths

#### First results:

Data obtained during this cruise show more complicated distribution patterns of bottom communities than could be anticipated according to the results of the 1993 cruise.

- A main factor influencing the distribution of benthos communities in the central part of the Laptev Sea (see transect C, Fig. 7-10) is the occurrence of different water masses (Arctic surface waters, Atlantic waters, and Arctic Ocean deep sea waters).

Species that indicate the main water masses are:

Arctic surface water: *Arctinula groenlandica*, *Ophiocten sericeum*, *Gorgonocephalus arcticus*.

Atlantic water: *Ophiopleura borealis*, *Pontaster tenuispinus*, *Gorgonocephalus eucnemis*, *Heliometra glacialis*, *Ophioscolex glacialis*.

Deep sea water: *Kolgia hyalina*, *Elpidia glacialis*, *Hyalopecten frigidus*, *Pourtalesia jeffreysi*, and *Ophiopyren striatum*.

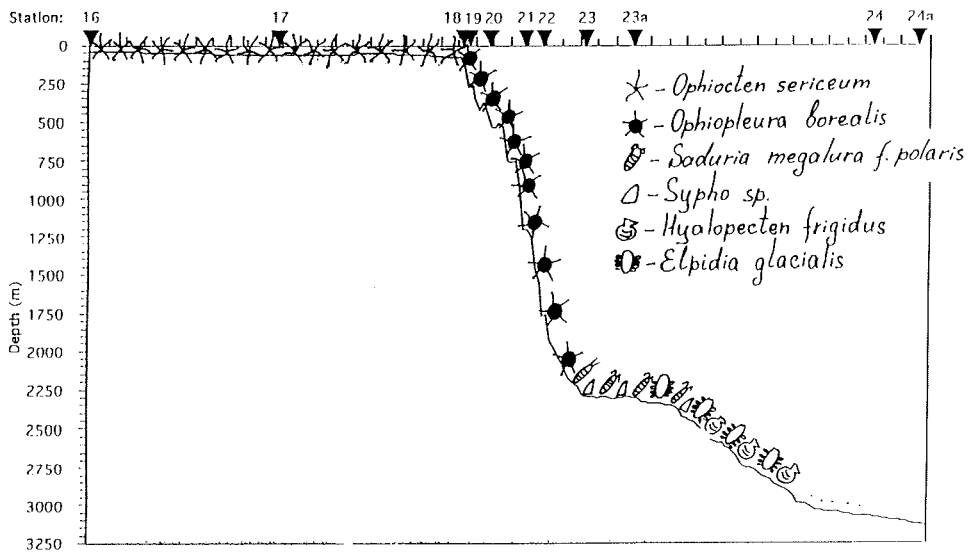


Fig. 7-10: Sketch of the macro-zoobenthos assemblages along transect C (central northern Laptev Sea)

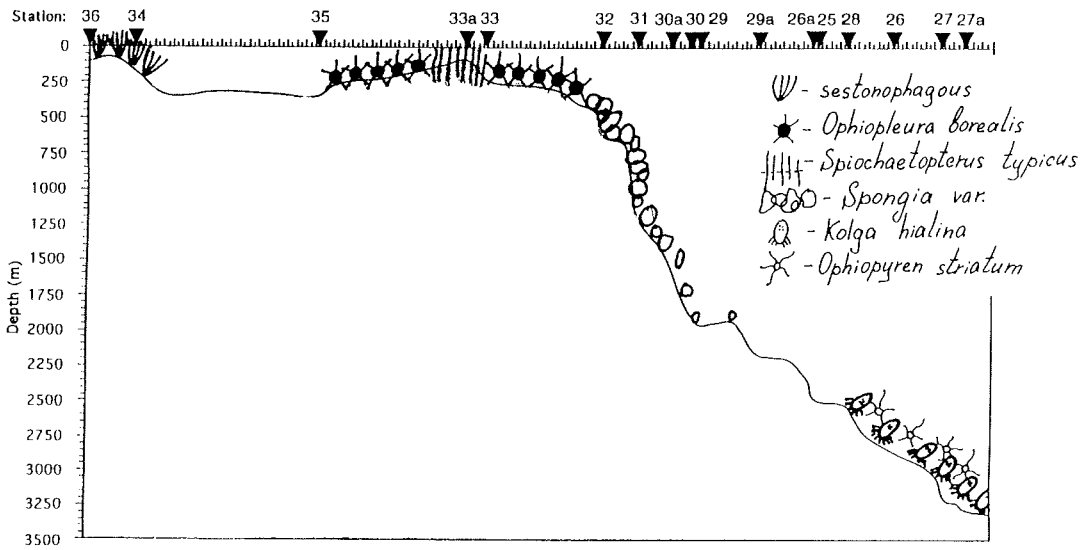


Fig. 7-11: Sketch of the macro-zoobenthos assemblages along transect E (east of Severnaya Zemlya)

- The assemblages of the continental rise are rather variable:

In the shallower parts of the western Laptev Sea continental slope (eastwards from the Severnaya Zemlya archipelago) different bottom deposit types as well as increased current velocities change the distribution of bottom communities (see transect E, Fig. 7-11), in comparison with the central part of the Laptev Sea continental slope (see transect C, Fig. 7-10). Communities of passive suspension feeders (sestonophages: *Gorgonocephalus eucnemis*, *Heliometra glacialis*) appear in shallow waters. In the upper part of the continental slope, dense communities of sponges are developed, while they are absent in the central part of the Laptev Sea at the same depths.

The deeper continental rise in the western part of the sea (see transect E, Fig. 7-11) is occupied by bottom communities, which are dominated by *Kolgia hyalina* and *Ophiopyren striatum*. In the central and eastern parts of the sea, however, communities dominated by *Elpidia glacialis*, *Hyalopecten frigidus* and *Pourtalesia jeffreysi* are common in the same depths (Figs. 7-10 and 7-11).

The communities in the slope area of the northwestern East Siberian Sea (Fig. 7-13, transect A) are again distinguished from those of the Laptev Sea; but, generally, the species in the deeper waters are the same in the Amundsen and Makorov Basins.

- The character of benthos communities in the southern part of the Lomonosov Ridge shows several remarkable features with principally the same communities as in the area of Severnaya Zemlya archipelago. These features are the presence of dense communities of suspension feeders (*Umbellula incrinus*, *Polyometra pro-lyxa*) as well as a belt of sponges at depth of about 1500m - 2000m (Fig. 7-14, transect F; see also Fig. 7-12).

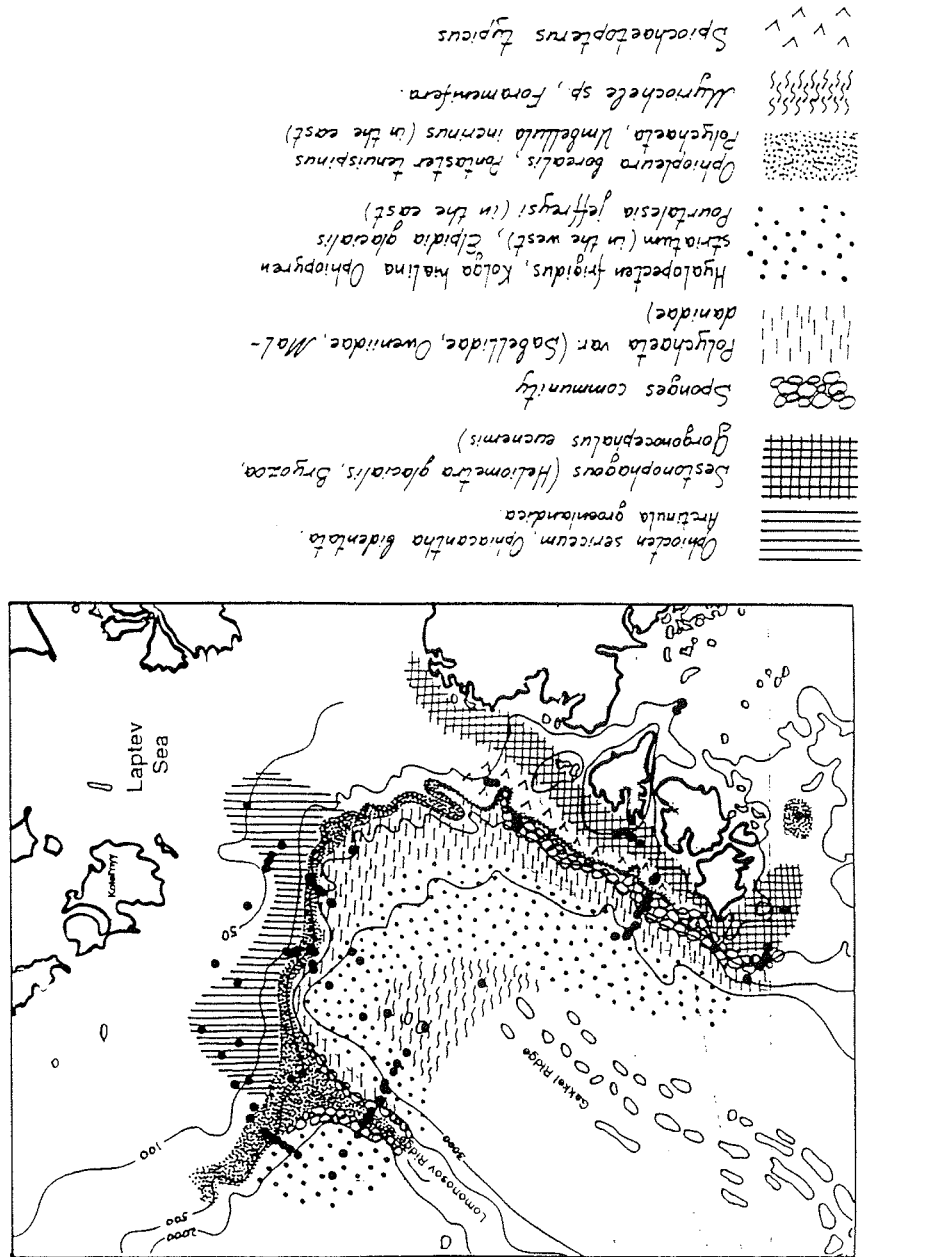
- A quantitative and qualitative poverty of benthos populations of the eastern slope of the Lomonosov Ridge in comparison with its western slope could be noticed even without detailed analyses of our quantitative samples.

- The brittle star *Ophiopleura borealis*, the population size structure of which will be analysed in detail later, is an Arctic species. Its distribution is controlled by Atlantic waters in the Arctic Ocean. We found a close connection of the occurrence and the densities of the *O. borealis* populations with core Atlantic waters. The ophiurids' growth rates seem also to be dependent on these water masses, but, in addition, on depth: The 3 size frequency histograms of the Fig. 7-9 show distinguished reductions of modes of disk diameters with increasing depths within the core of Atlantic waters.

- In the 1993 POLARSTERN expedition, sediment conglomerates with bivalves from a sub-fossil hydrothermal vent fauna had been found at a 2000 m deep slope station in the center of the northern Laptev Sea (where the Gakkel "Ridge" meets the continental slope; s. SIRENKO et al., 1995). During our 1995 cruise, the location was re-visited (station 3) and re-sampled for bottom fauna. So far, no new elements indicating again a former vent fauna have been found in the surface sediments obtained. However, within deeper layers of a long geological core (265-291 cm deep), again rich assemblages of specific mollusc shells were found this year (see chapter 9.4.2., Geology).



Fig. 7-12: Distribution of apparent and dominant macro-zoobenthos assemblages in the North of the Laptev Sea and adjacent waters (combined from AGT and GKG samples)



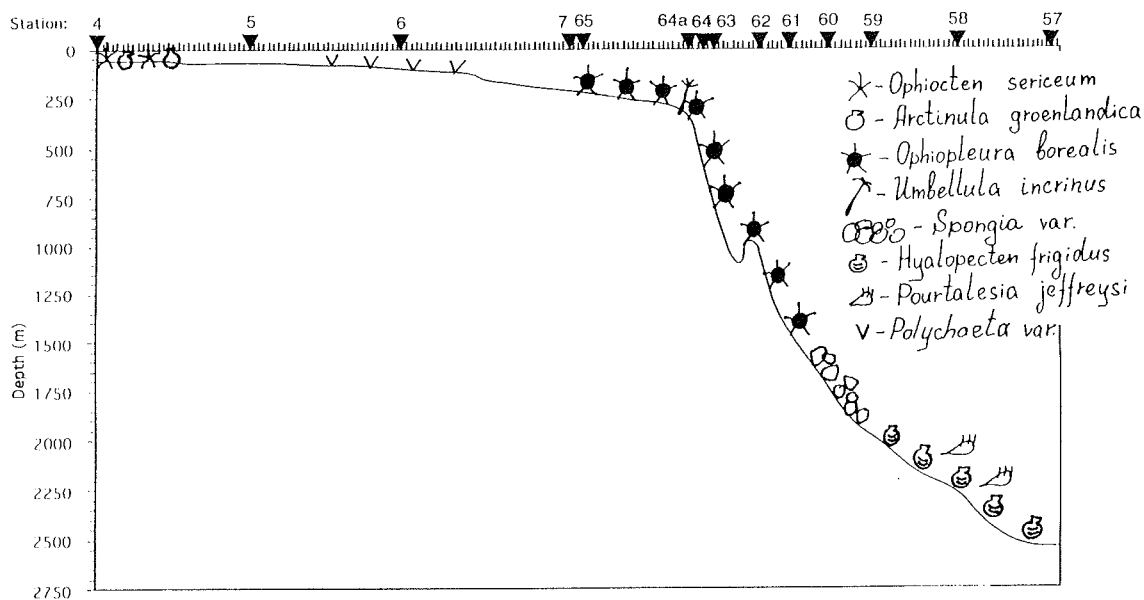


Fig. 7-13: Sketch of the macro-zoobenthos assemblages along transect A (northwesternmost East Siberian Sea)

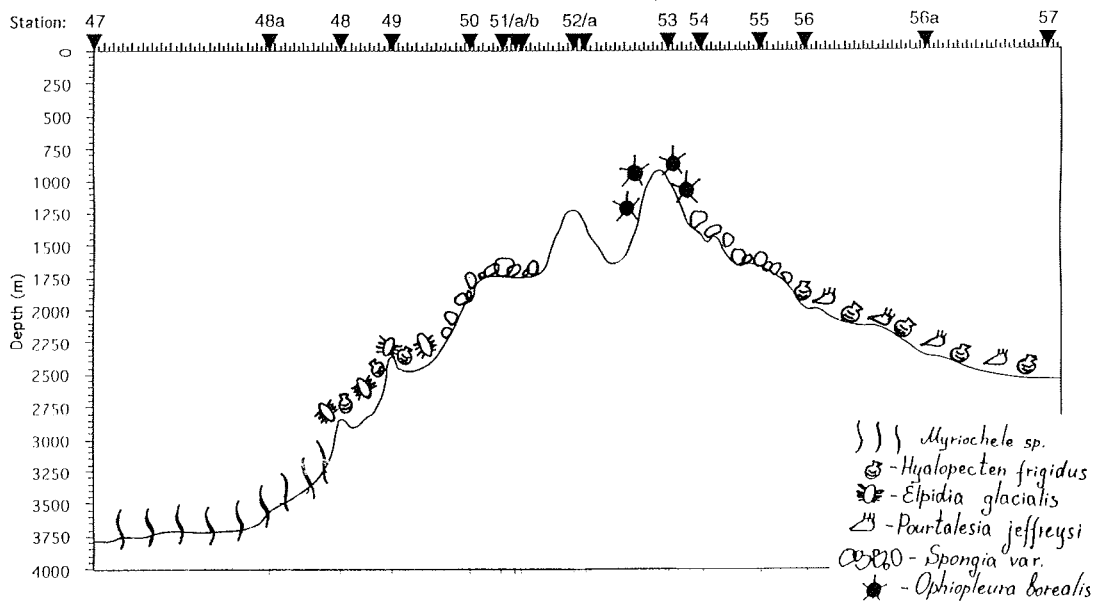


Fig. 7-14: Sketch of the macro-zoobenthos assemblages along transect F (crossing the Lomonosov Ridge from the Amundsen Basin, station 47, to the Makarov Basin, station 57)

## 8 BENTHIC BIO-GEOCHEMISTRY

(E. Damm, C. Grahl & G. Hulthe)

Marine organic matter will either be mineralized to CO<sub>2</sub> in the uppermost sediments or preserved in the sedimentary record. However, the ratio of recycled and buried marine organic carbon is influenced by environmental conditions and varies widely. During the cruise benthic fluxes of oxygen and carbon as well as microbiological activity were measured. Additional physico-chemical analyses of pore water and sediments were performed in order to understand the interaction with other processes of early diagenesis. Together with the investigations of the (zoo-)benthologists and geologists this will contribute to an estimation of the fluxes, sedimentation and transformation of organic matter from the shelf area into the deep-sea regions of the Arctic Ocean.

### 8.1 Sediment sampling and measurements

Sediment samples were obtained by a multiple corer (MUC) built by Buwers & Connelly (UK), which takes eight cores. The samples were taken at 54 stations on the transects A, B, C, D, E, F and G in water depths ranging from 39 m to 3882 m. Immediately after the recovery of the MUC on deck, the sediment cores with a diameter of 10 cm and lengths of 20 to 40 cm, were used for the following measurements and subsampling: At first bottom water samples were taken for oxygen (Winkler titration), total carbonate, alkalinity, dissolved organic carbon (DOC), total and specific sugars and nutrient measurements. One core was frozen at -30° C for later determination of accumulation/bioturbation rate. Two cores for microbiological investigations, two cores for incubation procedure and four cores for measurements of oxygen by microelectrodes and pore water sampling were brought to the laboratory as quickly as possible and kept at 0° C. If additional cores were available, they were preserved for meiofauna studies by the zoo-benthologists. As a rule, the incubated cores were preserved after use for the same purpose.

*Cores for microbiological investigations* in sediments were sampled at 40 stations. They were sliced into one-cm layers between 0-5 cm and 9-10 cm sediment depth. After mixing, 3-5 replicates were taken for the following measurements: Chloroplastic pigment concentration was determined with a Turner fluorometer. ATP was measured with bioluminescence. Potential heterotrophic activity was investigated with fluorescent model substrates (MUF-N-acetylglucosamine, MUF-a- and MUF-b-glucosides, MUF-butyrate, MCA-leucine, MUF-phosphate, MUF-stearate, MUF-sulfate, MUF-xylosite) at saturation level. Furthermore, samples were taken for the following analyses which will be done in the home laboratory: Bacterial biomass will be determined by epifluorescence microscopy; and biomass of the total sediment infauna will be estimated by phospholipid measurements.

*The cores for incubation* were closed with a lid under which 8-15 cm of ambient overlying bottom water was stirred at 30 r.p.m. in an attempt to obtain the

original diffusive boundary layer thickness. They were kept in the dark and at in situ temperature (in the range of  $-1^{\circ}$  to  $+1^{\circ}\text{C}$ ). When a sample was taken, filtered Atlantic water, aerated at  $0^{\circ}\text{C}$ , replaced the sample volume (ca 140ml), helping to keep the oxygen concentration on a reasonable level. Depending on the water depth, samples were taken every day or up to four times per day so that the oxygen content never dropped below 95-75% of the original concentration. 7-9 samples were taken per core. At every sampling occasion a duplicate of the refill water was also taken. Studied parameters were: oxygen, total carbonate, alkalinity, DOC, saccharides and nutrients. The fluxes of these were calculated in two cores at a time from 41 stations.

Alkalinity was determined by titrating a 1-ml sample with 10 mM HCl using Gran evaluation on the acid side of the second equilibrium point (pH ca. 3.5-3.6). Total carbonate was measured coulometrically with a sample volume of ca 7 ml. For DOC measurements a Shimadzu 5000 with autosampler was used. Determinations of total sugar were made by the MBTH method.

*Sediment cores for pore water sampling*, (beginning at the water sediment interface) were split into slices from 1 cm at the top to 2-3 cm thickness at the bottom of the cores. These sediment slices were cooled to  $0^{\circ}\text{C}$  and centrifuged (50 min/3000 r.p.m.). Pore water was collected, combined and filtered (Satorius filters with  $0.45\ \mu\text{m}$  pore diameter) from equivalent levels of three or four cores.

Total carbonate, alkalinity and DOC were measured on the pore water samples by the methods mentioned above. The inorganic nutrients were analyzed with an auto-analyzer by Y. Nalbandov. Oxygen measurements were carried out by using a commercial microelectrode (type 737 Clark style micro-oxygen-electrode, Diamond General, Ann Arbor, USA). The analyses of sediment porosity and of the pore water concentrations of saccharides, dissolved manganese and iron will be carried out in the home laboratory. Estimations of accumulation rates will be carried out by  $^{210}\text{Pb}$  and  $^{14}\text{C}$  measurements at the University of Lund.

## 8.2 Preliminary results

### 8.2.1 Benthic microbiology (C. Grahl)

A good correlation of plant pigment concentrations and the activity of  $\beta$ -glucosidase was found. Both decreased with sediment depth and with increasing water depth. The potential hydrolytic activity of all measured enzymes in the sediment surface decreased down the slope besides the activity of aminopeptidase, which was found to be increasing. These results are in agreement with those of the cruise ARK IX/4 in 1993, obtained by A. Boetius.

An interannual comparison was possible on the western Laptev Sea transect. Compared with the data of 1993, the measured values were between two and five times higher in 1995. This may be due to the influence of ice cover. The region was ice covered in 1993, while open water was met during this cruise. Ice cover could also be the main factor influencing the results along the transect across the Lomonosov Ridge: The content of plant pigments decreased from west to east while the ice cover increased (Fig. 8-1).

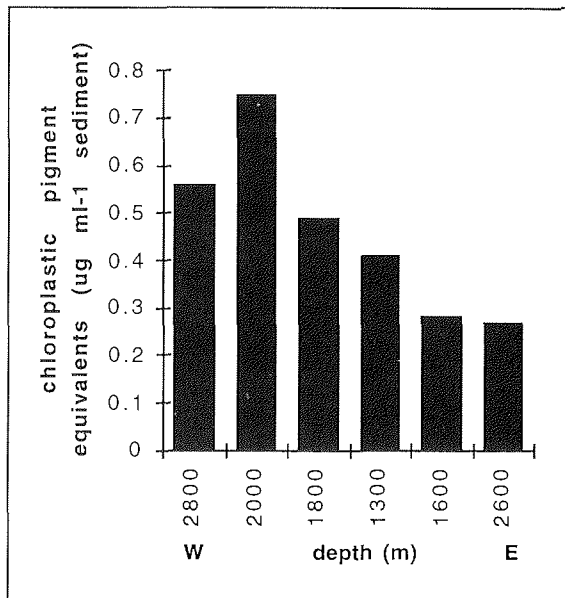


Fig. 8-1: Distribution of sedimented plant pigments along the transect across the Lomonosov Ridge. Mean values of five replicates from the top sediment layer (0-1 cm).

Comparing data from the East Siberian Sea (transect A), the eastern Laptev Sea (B), the central Laptev Sea (C) and across the Lomonosov Ridge (transect F), a high variability was found at deep stations (Fig. 8-2).

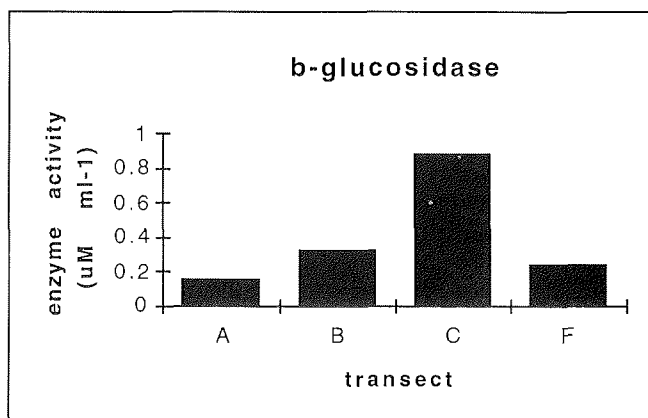


Fig. 8-2: Comparison of enzymatic activity of b-glucosidase, measured in the top sediment layer of different transects at 2000 m water depth.

Also, different dependences of pigment contents with water depth along the transects were measured (Fig. 8-3). At the East Siberian Sea transect (A) a steep decrease from higher values at the shelf stations was found. Along the central Laptev Sea transect (C) the values decreased in a slower and more uniform way. At greater water depth, chloroplastic pigment contents were higher here than in the other transects (at comparable water depth).

Besides ice cover, other factors might influence particle flux to the sediments, such as lateral transport and input from rivers.

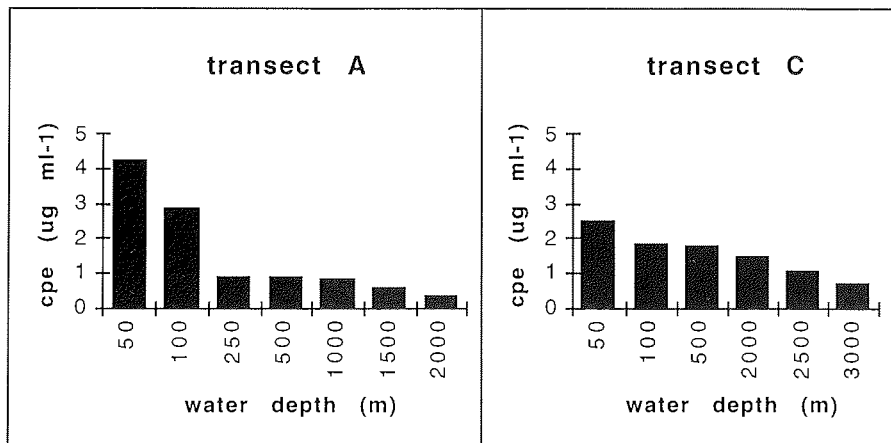


Fig. 8-3: Distribution of plant pigments in the sediments at different water depth.

### 8.2.2 Oxygen concentration profiles (E. Damm)

In general oxygen gradients at the sediment-water interface were steepest at the shallow stations and weakest at the deep stations. At stations beyond 2000 m water depth oxygen depletion was not reached by microelectrode measurements. These oxygen profiles are in accordance with the measurements two years ago.

Oxygen fluxes at the sediment-water interface are a measure of the supply rate of organic matter to the sediment. A comparison of the gradient and penetration depth of oxygen shows that this supply rate is strongly dependent on ice cover in shelf and upper slope areas. This is clearly noticeable by a comparison of the transect D (this cruise) in the ice-free western Laptev Sea with the ice-covered transect F of the cruise in 1993 in the same area.

For the first time oxygen profiles are available from the deeper parts of the eastern Arctic Ocean (130° E - 150° E). In addition to existing profiles (100° E - 130° E), measured two years ago, it can be shown that this areas are not homogeneous, but are rather characterized by large variation in oxygen fluxes and, consequently, in organic matter flux, related to differences observed in benthic activity and biomass. Perhaps, that may be caused by different lateral advection of organic-rich particles via the slope areas.

### 8.2.3 Benthic carbon fluxes - DOC versus $\Sigma\text{CO}_2$ in shelf, slope and deep-sea environments, and relation to oxygen fluxes (G. Hulthe & P. Hall, together with E. Damm)

A fraction of the particulate organic carbon (POC) flux to the sea-floor undergoes burial and constitutes a sink in the oceanic carbon cycle. The remaining fraction is degraded in the sediment. It is generally accepted that the microbial degradation processes in sediments work with an initial hydrolytic step catalyzed by exo-enzymes. Subsequently the hydrolysis products can be taken up by the organisms and undergo oxidation to water and carbon dioxide. The rate of organic carbon oxidation can be measured as the flux of total carbonate ( $\Sigma\text{CO}_2$ ) from the sediment. A portion of the dissolved organic carbon (DOC), released during hydrolysis to the pore water, diffuses through the sediment and escapes to the overlying water.

It has been discussed how important such DOC escape is compared to the organic carbon oxidation, but these processes have very rarely been measured in parallel. Our simultaneous measurements on 41 stations of benthic DOC,  $\Sigma\text{CO}_2$  and  $\text{O}_2$  fluxes from / to shelf, slope and deep-sea sediments in the Kara, Laptev and East Siberian Seas as well as the Amundsen and Makarov Basins during the summer of 1995 show that there was a positive correlation between  $\Sigma\text{CO}_2$  effluxes and total  $\text{O}_2$  uptake rates. The ratios between these two fluxes were in general between 0.7 and 0.8 with a mean ratio close to 0.75. The  $\Sigma\text{CO}_2$  fluxes ranged from ca 0.4 to 4.3 mmol m<sup>-2</sup> d<sup>-1</sup>.

The DOC fluxes ranged from close to zero to 3.6 mmol m<sup>-2</sup> d<sup>-1</sup> with the highest fluxes on the shelves and the lowest in the deep basins and on the slopes. There was a positive correlation between  $\Sigma\text{CO}_2$  and DOC fluxes. Also, the fraction of the total benthic carbon flux (the  $\Sigma\text{CO}_2$  plus the DOC flux) that was made up of DOC, increased with increasing  $\Sigma\text{CO}_2$  fluxes. The DOC flux constituted 30-50 % of the total benthic carbon flux on stations with high (ca 4 mmol m<sup>-2</sup> d<sup>-1</sup>)  $\Sigma\text{CO}_2$  fluxes and in general 10-30 % of the total benthic carbon flux on stations with low (ca 0.5 mmol m<sup>-2</sup> d<sup>-1</sup>)  $\Sigma\text{CO}_2$  fluxes.

These results suggest that DOC release is an important component of carbon cycling in Arctic sediments regardless of water depth (40 to 3900 m). Our findings may also have implications for the estimations of POC rain rates to the sea-floor from measurements of carbon oxidation rates in sediments (from e.g. oxygen consumption rate measurements), because a DOC release requires an additional POC input.

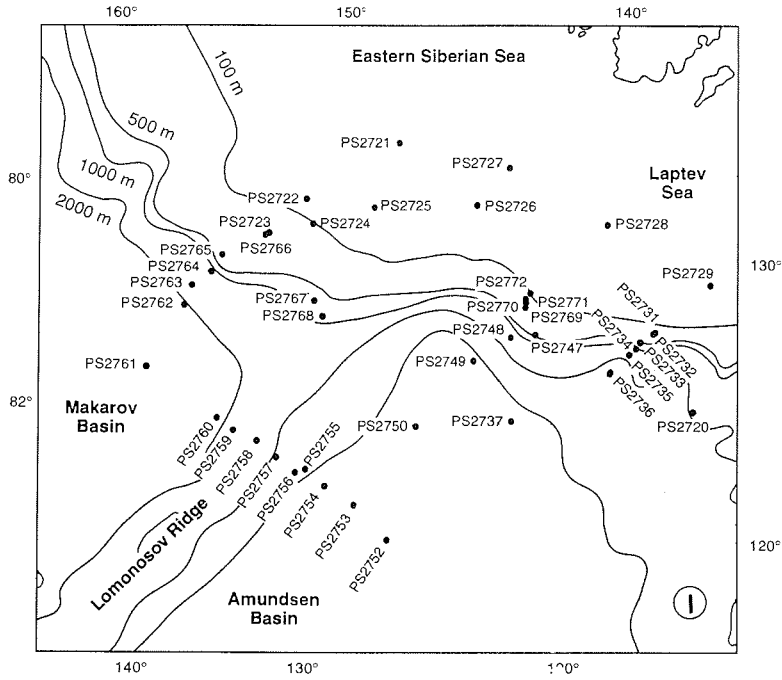


Fig. 9-1: a) Geological station map (eastern part)

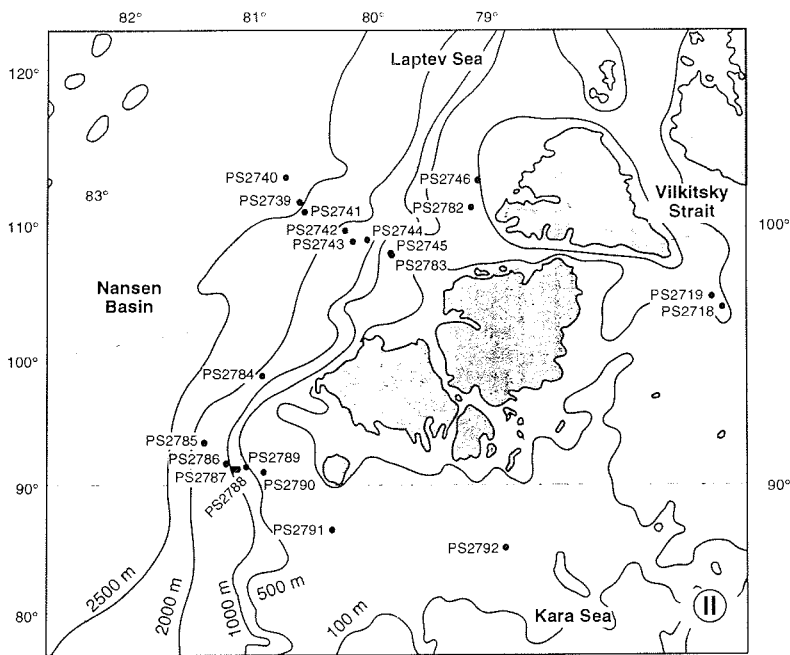


Fig. 9-1: b) Geological station map (western part)



## 9 MARINE GEOLOGICAL INVESTIGATIONS

(R. Stein, M. Behrends, M. Bourtman, K. Fahl, M. Mitjajev, E. Musatov, F. Niessen, N. Nørgaard-Petersen, V. Shevchenko, and R. Spielhagen)

The overall main goal of the marine geological program is to perform high-resolution studies of changes in paleoclimate, paleoceanic circulation, paleo-productivity, and former sea-ice distribution along the Siberian continental margin and its adjacent deep-sea area. Of major interest are the significance of the Arctic Ocean for the global climate system, the correlation of paleo-environmental data from different depositional environments (i.e. shelf-slope-deep sea), and the correlation of marine and terrestrial climatic records. To reach these objectives, detailed sedimentological, geochemical, mineralogical, and micro-paleontological investigations are performed. Research objectives concentrate on:

- high-resolution stratigraphic analyses of the sediment sequences (isotopic stratigraphy, AMS-<sup>14</sup>C-datings, amino-acids, magnetic susceptibility);
- studies of river run-off from the Asian continent and corresponding surface-water salinity changes in space and time (stable isotopes);
- studies of terrigenous sediment supply (grain size; clay; light and heavy minerals; organic compounds; geochemical tracers);
- studies of the fluxes of terrigenous and marine organic carbon (total organic carbon, C/N ratios, hydrogen and oxygen indices, carbon stable isotopes, maceral composition, biomarkers);
- reconstruction of paleo-productivity by tracer analyses: biomarkers (e.g. n-alkanes, fatty acids, alkenones, chlorophyll-a and degradation products), barium, biogenic opal;
- studies of reactions of marine biota to environmental changes;
- studies of physical properties (magnetic susceptibility, wet bulk density, porosity, shear strength);
- studies of specific sedimentary environments with detailed Parasound surveys.

The research program includes investigations of aerosols, particles sampled within the water column using sediment traps and in-situ pumps, sea floor surface sediments, and long sediment cores.

During this *Polarstern*-expedition ARK-XI/1, geological sampling stations were carried out in the northwestern East Siberian Sea, Laptev Sea, and eastern Kara Sea and their adjacent continental slope and deep-sea areas (Figs. 9-1a and b, see also Fig. 2-3). If possible, coring positions were carefully selected using PARASOUND to avoid areas of sediment re-deposition and erosion.

### 9.1 Marine sediment echosounding using PARASOUND

(F. Niessen & E. Musatov)

Bottom and sub-bottom reflection pattern obtained by PARASOUND characterise the uppermost sediments in terms of their acoustic behavior. This can be used to interpret the sedimentary environments and their changes in space and time. During ARK XI/1 the aims of PARASOUND profiling were

- (i) to select coring locations for gravity and box cores,
- (ii) to further investigate and map ice erosional features on the Laptev Sea shelf,
- (iii) to identify lateral differences in sedimentary facies from the shelves of the Kara and Laptev Seas to the deep sea areas of the Nansen, Amundsen and Makarov Basins.

The hull-mounted PARASOUND sediment echosounder was in 24-hour operation along all cruise tracks from the 19.07.1995 (77°00' N, 94°20' E) until the 11.09.1995 (78°50' N, 87°00' E). A total of 4675 naut. miles of high resolution profiles were recorded. The PARASOUND system (Krupp Atlas Electronics, Bremen, Germany) generates two primary frequencies between 18 and 23.5 kHz transmitting in a narrow beam of 4°. As a result of the interaction of the primary frequencies within the water column, a secondary frequency is created based on the parametric effect (difference frequency of the two primary waves transmitted). During the expedition the parametric frequency was set to 4 kHz. This allowed subbottom penetration up to 100 m with a vertical resolution of ca. 30 cm. The recorded shallow seismograms were independently digitized by two different systems: (i) by the PARASOUND system for simultaneous printing on a chart recorder (Atlas Deso 25) and (ii) by the PARADIGMA system (SPIESS 1992) for tape storage and post-processing. The settings of the PARADIGMA system were as follows: sampling rate 25  $\mu$ s, trace length 66.5, 133 or 266 ms, block size 10640 byte, format "SEG-Y packed" (SPIESS 1992). All Parasound data were copied by the post-processing software DISCO and saved on DAT-tapes. Also, DISCO was used to process key examples from different regions for further interpretation.

On the Laptev Sea shelf and slope as well as in the Vilkitsky Strait the investigations of the 1993 cruise (ARK-IX/4) were continued. In addition, PARASOUND profiles of good data quality were obtained from previously uninvestigated areas. These include

- the eastern Kara Sea,
- the Lomonosov Ridge (from the Amundsen to Makarov Basin, transect F),
- the Gakkel Ridge (Amundsen to Nansen Basin, transect D),
- the area east of the Severnaya Zemlya archipelago (transect E).

Some typical examples of PARASOUND profiles are presented and discussed below.

#### *The eastern Kara Sea*

The eastern Kara Sea is characterized by typical shelf deposits. The relief is flat, and the sound penetration is limited to only a few metres. Locally, PARASOUND was able to penetrate into the top few metres of steeply dipping or folded sub-surface strata which are interpreted as sedimentary bedrock. In these locations the

truncated surface is overlain by a few metre thin cover of probably Holocene sediments. Such areas were found in both the southern and the northern parts of the eastern Kara Sea which were studied in the beginning and the end of the cruise, respectively. West of the Vilkitsky Strait, between ca. 94° and 99° E, there are a number of small shelf basins which have water depths of up to 130 m. These basins comprise well-stratified sediments of up to 20 m thickness (Fig. 9-2). The fill is characterized by an alternation of acoustically more transparent strata with sediments causing higher backscatter. Generally, the beds tend to lens out toward the edges of the basins. The top is seen as a 1 to 2 m thick drape which, in places, is overlying the lower fill unconformably. Whether only the top part or the entire sequence is of Holocene age, remains open until datings become available from the sediment cores. An additional shelf basin was investigated at the end of the cruise at ca. 79°33'N / 87°00'E. The geometry and acoustic behaviour of the sediment fill is quite similar to that described above.

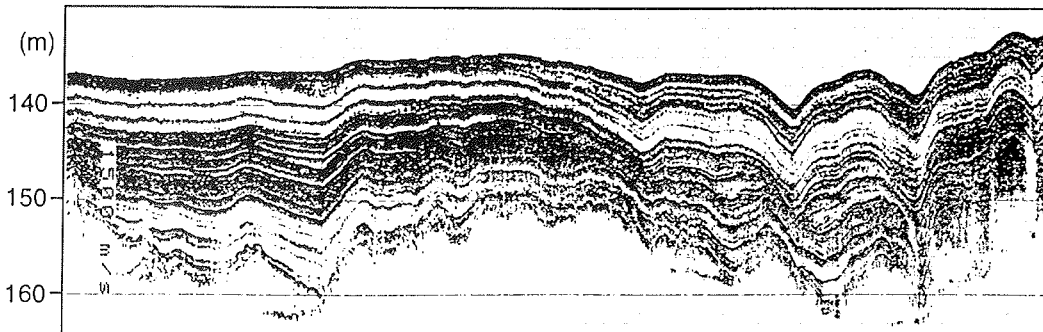


Fig. 9-2: Parasound record near 77°37'N, 97°37'E; section length 7 km

#### *The Vilkitsky Strait and the Khatanga-Vilkitsky Channel*

The Vilkitsky Strait and its eastern extension into the deep sea (Khatanga-Vilkitsky Channel) were already intensively studied using PARASOUND during the cruise ARK-IX/4 in 1993 (FÜTTERER 1994). The area is characterized by up to 100 m thick, well-stratified sediments which are intercalated with (or underlain by) thick, acoustically transparent debris-flow deposits. During ARK-XI/1 some additional profiles were recorded which completed the discoveries of the 1993 expedition as outlined below.

A continuous west to east profile from the Vilkitsky Strait to the Khatanga-Vilkitsky Channel (up to ca 78°N, 112°E) can be used to link individual reflectors of the 1993 and 1995 PARASOUND seismograms over much larger distances in order to construct a better spatial/temporal interpretation of the complex sediment sequences of the area.

There is additional indication for a major source of sediments from the Laptev Sea shelf east of the Taymyr Peninsula. This is indicated by a north-to-south thickening of well-stratified strata by about one order of magnitude and the occurrence of downlaps on the shelf slope between 111° and 115°E. A typical

PARASOUND profile from this area is already shown in the ARK-IX/4 cruise report (Fig. 8.1-7 in FÜTTERER 1994). It has to be tested whether the shelf-proximal accumulation is of Holocene age, represents part of a glacial (low sea level) fan of the Khatanga river, and/or can be explained by local sediment release during deglaciation of the Taymyr region at the termination of one of the last Pleistocene glacial periods.

In addition, there were numerous diapiric features found in well-stratified sediments from both the Vilkitsky Strait and the Khatanga-Vilkitsky Channel. The diapirs form mud mounts on the sea surface (Fig. 9-3). The internal structure of the diapirs is characterized by acoustic voids or by uplifting of stratified sediments. Some of the mounts/diapirs are overlain by younger un-deformed sediments (Fig. 9-3). This may indicate that the upward motion within the diapirs has ceased and/or that the diapirs are buried by rapidly accumulating sediments. In high resolution seismic profiles the occurrence of acoustic voids in association with mud mounts are usually explained by the upward migration of sedimentary gas (BRYANT & ROEMER 1983). Mud diapirs as a result of a density inversion in the sedimentary sequence may also provide a possible explanation.

In general, the origin the post-depositional alteration and the age of the thick sediment fill from the area remains obscure. Three sediment cores which were taken during the cruise along a PARASOUND profile across the Khatanga-Vilkitsky Channel (PS 2779 to PS 2781) may help to date the sequence.

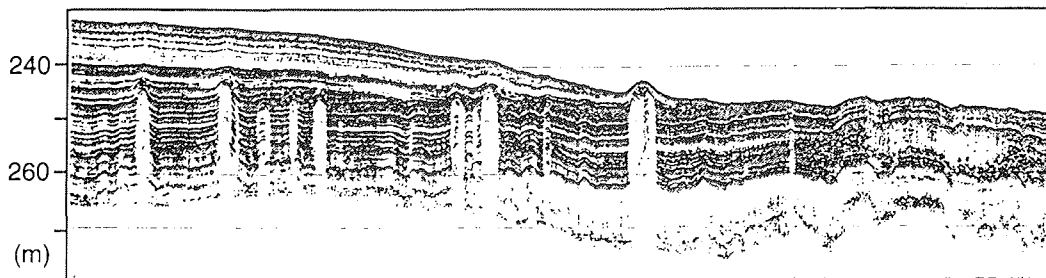


Fig. 9-3: Parasound record near 77°57'N, 104°22'E; section length 7 km

#### *The Shelf areas of the Laptev Sea*

One of the major PARASOUND observations during ARK-IX/4 was the occurrence of a large number of ice gouges (order of magnitude  $10^3$ ) in the western and eastern parts of the Laptev Sea shelf (FÜTTERER 1994). In order to investigate how rapidly such gouges are formed and filled, one section of a PARASOUND profile from the 1993 cruise was repeated between 77°24' N, 133°30' E and 77°30' N, 133°40' E. The total number of 19 gouges recorded in 1993 (see Fig. 8.1-3 in FÜTTERER 1994) were also found during ARK-XI/1. Apparently, no gouges were added and none filled. Moreover, distinct morphological features within the individual gouges were repeated in detail. The comparison shows that the ice gouges in the Laptev Sea can survive for years without any alteration.

This may suggest that the widespread occurring of plough marks on the Laptev Sea shelf is the result of a numerical accumulation from individual ploughing events over longer time periods during the Holocene.

In addition to the shelf areas already explored for ice gouges using PARASOUND during ARK-IX/4, a new area could be examined off the northern islands of the Severnaya Zemlya archipelago. This was of major interest because the shelf is close to the ablation areas of the ice caps of Severnaya Zemlya, where a large number of grounded icebergs were observed (see chapter 5.1). Indeed, the topmost shelf sediments appear to be completely ploughed so that individual gouges can hardly be distinguished (Fig. 9-4a). Ploughing depth into sediments is up to 10 m and ploughing intensity decreases rapidly below 140 m water depth. A few gouges were found down to water depth of 210 m. The pattern is typical for areas affected by major iceberg ploughing such as the East Greenland shelf and fjords (DOWDESWELL et al. 1993).

A strongly ploughed sediment surface was also recorded on the shelf east of the Taymyr Peninsula (Fig. 9-4b), where some grounded icebergs were observed. In contrast, a profile recorded at about similar water depth north of the New Siberian Islands shows some individual ice gouges not more than 2 m deep (Fig. 9-4c). This indicates minor ploughing activity in the latter area. Grounding of icebergs may be the major process for ice-gouge formation in the Laptev Sea and the adjacent areas to the east. The major trajectories of icebergs derived from Severnaya Zemlya are north to south-east (see chapter 5.1). There is no source for icebergs on the New Siberian Islands.

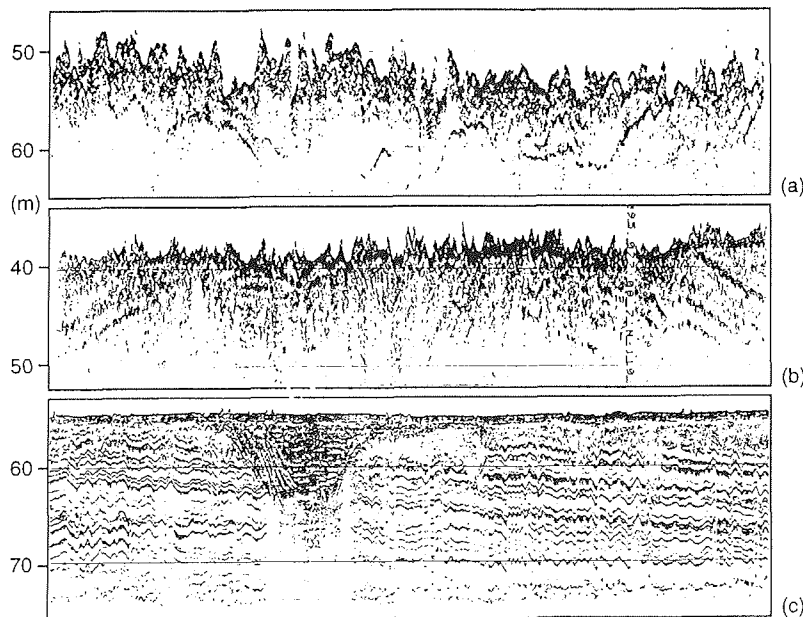


Fig. 9-4: a) Parasound record near 79°26'N, 104°21'E; section length 2.2 km  
 b) Parasound record near 77°09'N, 110°54'E; section length 2.9 km  
 c) Parasound record near 77°57'N, 144°05'E; section length 4.5 km

There is evidence for post-depositional formation of reflectors in the sub-bottom of the Laptev Sea shelf which are not associated with gouge formation. During the 1993 cruise it was shown that PARASOUND penetration of the Laptev Sea shelf sediments can reach 20 m. Profiles often show well-stratified sediments of probably Pleistocene age which commonly dip in easterly directions (Fig. 9-4c). In places, strong reflectors cut these stratified units at about 10 to 20 m sediment depth, thus indicating their post-sedimentary origin. (Fig. 9-5a). The top of the reflectors are flat or hummocky (Fig. 9-5a). One possible explanation for the significant contrast in acoustic impedance at these horizons is the onset of sub-surface permafrost which is commonly observed in Arctic shelf regions (e.g. ROGERS & MORAK 1983). A second possibility is a higher concentration of sedimentary gas. More intensive seismic processing is necessary in order to test the above hypotheses. In some PARASOUND profiles from the Laptev Sea, there is evidence for local release of subbottom gas. Figure 9-5b shows two examples of acoustic voids overlain by mud-mounds, which can be explained by near surface sedimentary gas pockets. Adjacent to these features a small depression is seen which may represent a pock mark (Fig. 9-5b). Pock marks are commonly associated with the release of gas from sediments into the water column (MAX et al. 1992).

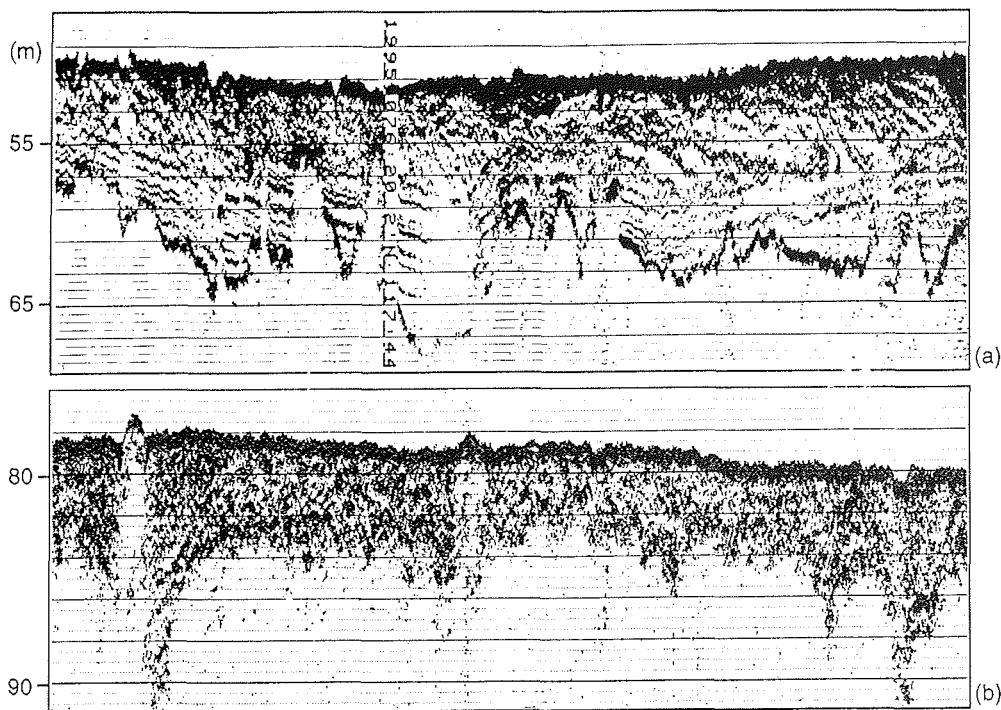


Fig. 9-5: a) Parasound record near  $76^{\circ}20'N$ ,  $117^{\circ}45'E$ ; section length 1.5 km  
 b) Parasound record near  $76^{\circ}49'N$ ,  $121^{\circ}22'E$ ; section length 1.3 km

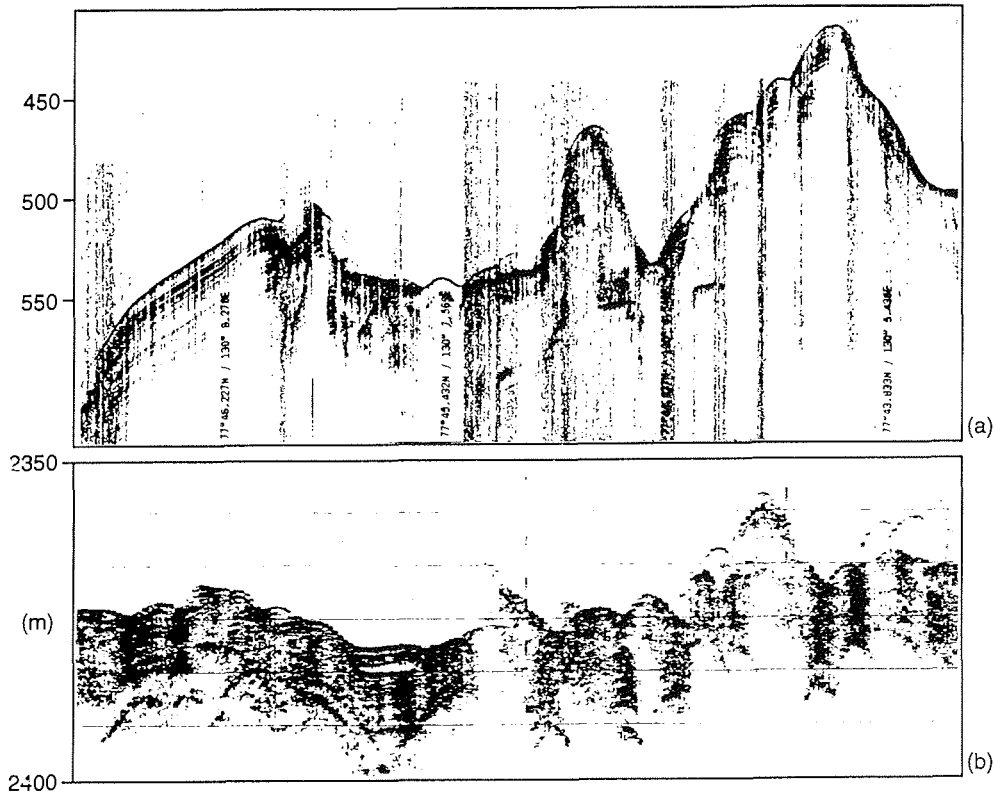


Fig. 9-6: a) Parasound record near  $77^{\circ}45'N$ ,  $130^{\circ}07'E$ ; section length 3.2 km  
 b) Parasound record near  $78^{\circ}11'N$ ,  $129^{\circ}59'E$ ; section length 3.4 km

#### *Continental slope and deep sea areas*

Along the transects across the Lomonosov Ridge and the continental slope of the western Makarov Basin (A and E), the PARASOUND profiles are mostly characterized by well-stratified sediments which drape sub-surface morphologies. Penetration is generally up to about 50 m. For most of the area an upper seismic unit (A) of stronger backscatter can be distinguished from a lower unit (B) which shows a higher degree of acoustic transparency (Fig. 9-6). This subdivision is more pronounced near the crest of the Lomonosov Ridge and in the Makarov Basin and is less distinct towards the Amundsen Basin. The thickness of unit A varies between 4 and more than 30 m. A plot of the variation of thickness versus water depth indicates that the smallest thickness of unit A is observed on and near the crest of the ridge. Also, there is a significant higher thickness of unit A toward the Amundsen Basin compared to the Makarov side of the slope (Fig. 9-7). This implies relatively low sedimentation rates on the eastern (Makarov) part of the transects, which is consistent with the correlation of both lithology and physical property data. Some debris flows are found on the eastern slope of the Lomonosov Ridge which are stratigraphically located near or at the boundary

between the seismic units *A* and *B*. This suggests major changes in sediment supply and/or re-deposition associated with the change in acoustic behaviour at the onset of unit *A*.

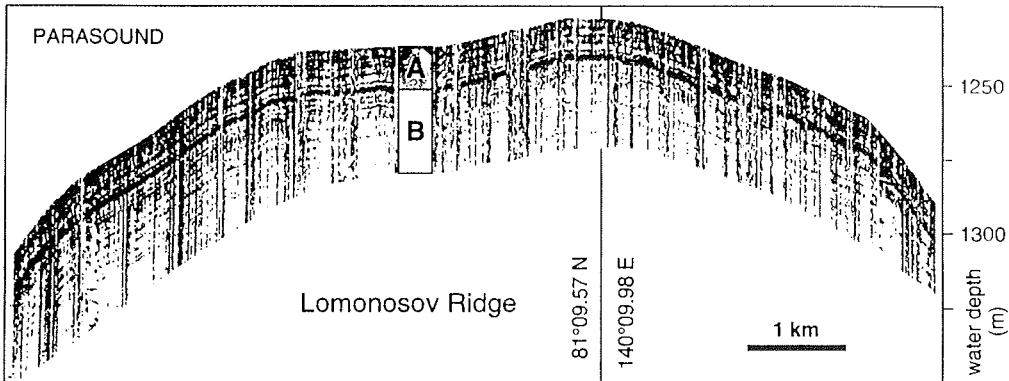


Fig. 9-7: Parasound record across the crest of the Lomonosov Ridge

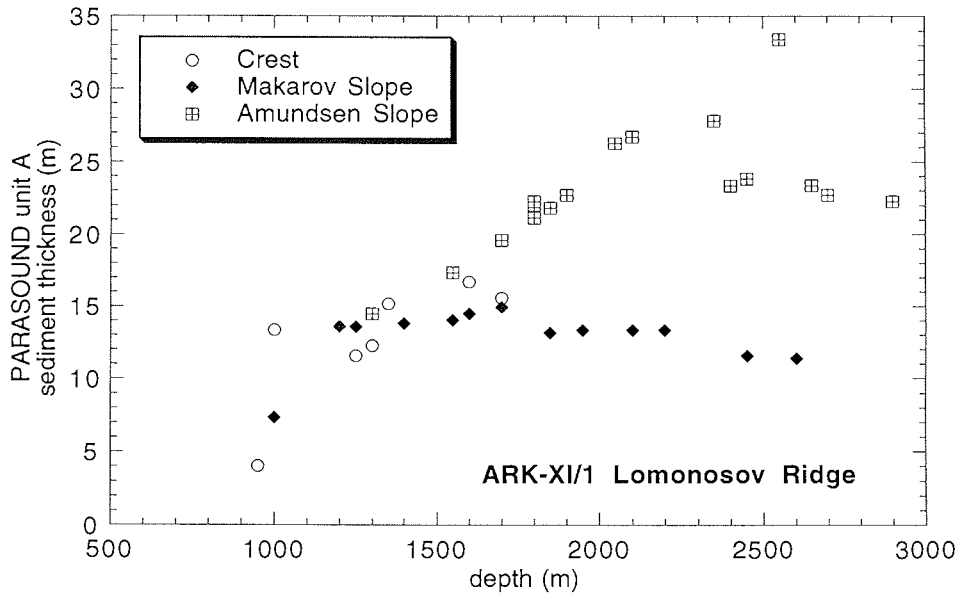


Fig. 9-8: Thickness of Parasound unit "A" (see Fig. 9-7) versus water depth. Note the increase of unit thickness on the slope of the Amundsen Basin and constant values on the Makarov slope



Due to the relatively favourable ice conditions, the PARASOUND profiles are of reasonable quality along transect E. On transect A, however, most of the recording was strongly affected by noise caused by ice-breaking of the vessel.

The PARASOUND records of the eastern Laptev Sea continental slope and the investigated parts of the Amundsen Basin (transects B and C) are largely affected by lateral sediment transport. This was already evident from both high resolution seismic- and sediment-core information of the ARK-IX/4 expedition. The new discoveries along transect B confirmed the previous results from the ARK-IX/4 transect H (Figs. 8.1-5 and 8.1-6 in FÜTTERER 1994). Therefore, they are not described and documented in further detail in this report. Generally, the PARASOUND profiles along transect B are characterized by well-stratified sediments which increase in thickness towards the upper continental slope. Only some small areas above 1800 m of water depth are disturbed by slumps and debris flows. Below 3000 m water depth sound penetration decreases and backscatter increases, which indicates higher reflection coefficients in the sediments. This gradient can be explained by the transition into the turbidite facies of the Amundsen Basin.

Transect C is located near transect G of the 1993 cruise. Different to the situation in 1993, when heavy ice conditions prevailed recording of good quality PARASOUND seismograms in this area, profiling during ARK-XI/1 was commonly in open water. Thus, acoustic disturbances were minor or absent. As a result, the entire slope down into the deep-sea basin to 3200 m water depth can now be described as deep sea fan facies. On the upper fan, down to approximately 1200 m water depth, a distinct relief is formed by channel and levee deposits (Fig. 9-8). Several channels, up to 100 m deep, are observed, which cause high acoustic backscatter, probably as a result of coarser grain size of the channel fill. In contrast, levee deposits are well-stratified. Sound penetration down to 50 m sediment depth is common. The slope of the middle-fan area was too steep to allow suitable PARASOUND records (inclination more than 4°).

The beginning of the lower fan at about 2300 m is characterized by diffraction hyperbolae. This can be explained by small scale morphological features, such as numerous small channels, which form the transition to the morphologically flat turbidite deposits of the Amundsen Basin. This is confirmed by the sediment cores retrieved from stations PS 2736-6 and PS 2737-4, which are dominated by turbidites.

In general, the facies found along transect C have been seen in conjunction with incised channels found on the Laptev Sea shelf during the ARK-IX/4 cruise in 1993 (Fig. 8.1-4 in FÜTTERER 1994). These channels were interpreted as river channels of the Lena (for example), which were eroded during glacial times when the sea level was lower and the shelf area exposed. The marine channel and levee facies as described above is probably part of the low stand fan of the Lena formed at times when the river mouth was close to the present-day shelf edge. This would imply that sediment transport to the Arctic Ocean continued during glacial times in such a way that it was strongly channelized into deep-sea areas. It is too early to interpret whether the observed fan deposits are mostly of

glacial age (e.g. marine oxygen isotope stages 2-4) and whether the channels became inactive after the Holocene transgression into the Laptev Sea.

There are major differences in sedimentary facies on the western transects D, E and G compared to the eastern transects A, B and C. The deep sea area of transect D seems to be dominated by the geology of the Gakkel Ridge. There are two crests seen along profile D (at  $80^{\circ}50.5' N$ ,  $122^{\circ}05' E$  and at  $80^{\circ}36.8' N$ ,  $121^{\circ}01' E$ ). West of about  $122^{\circ}E$  there is evidence for several faulted blocks, more or less vertically displaced by up to 200 m (Fig. 9-9). The blocks are probably related to oceanic crust which is expected to be strongly sheered and faulted due to ocean floor spreading. The blocks are draped by well-stratified sediments which allow sound penetration to about 20 m sediment depth. The topmost parts of these sediments were cored at station PS 2774-1. West of about  $120^{\circ}45'$  there is an increase of thicknesses of stratified sediments observed. This may indicate more abundant distal turbidites along the transition into the Nansen Basin.

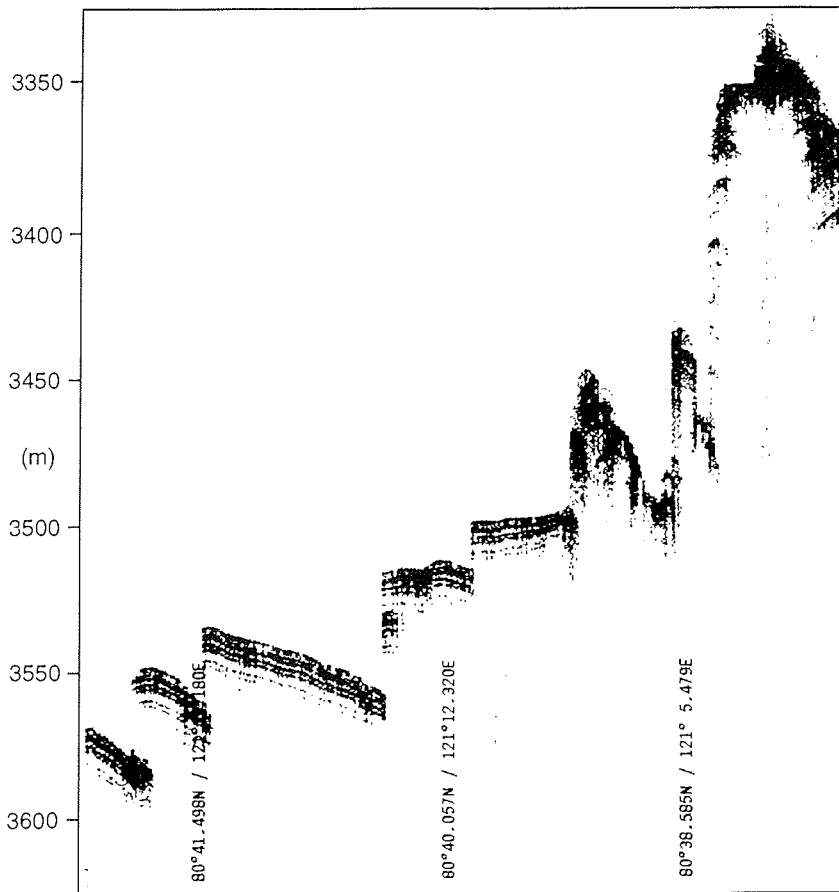


Fig. 9-9: Parasound record near  $80^{\circ}40'N$ ,  $121^{\circ}12'E$ ; section length 8 km

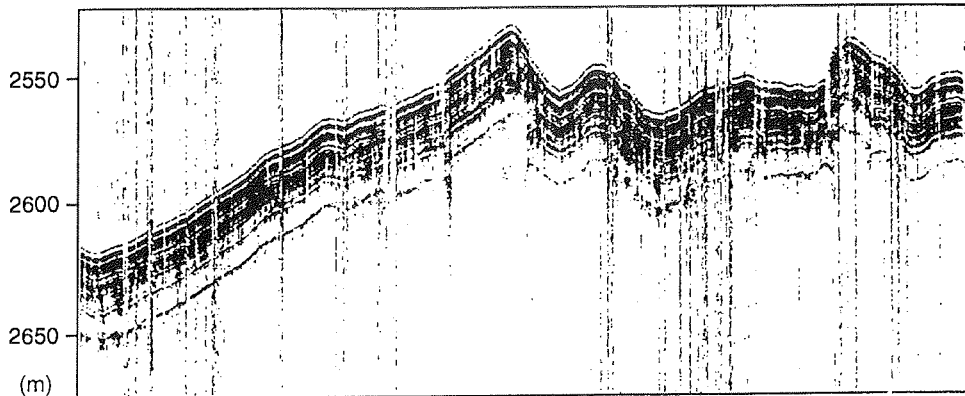


Fig. 9-10: Parasound record near 81°03'N, 105°25'E; section length 7 km

The middle part of the slope of transect D (west of about 116°30'E between 3250m and 2000m water depth) is characterized by a large number of debris flow deposits. Typically, they appear in PARASOUND profiles as lenticular-shape bodies which are acoustically transparent. The thickness of individual flow deposits is about 30 m. A similar sequence of thick debris-flow deposits was observed on a transit profile along the continental slope north-east of the Taymyr Peninsula (between 78°41'N / 120°10'E and 79°33' / 114°20', 2800 to 3200 m water depth, respectively). In both areas there is a thin (few metre thick) drape of stratified sediments on top of the flow deposits. Debris flows imply that there was a strong downslope movement of sediments over a large area of the western continental slope of the Laptev Sea. This differs from the eastern slope, where the Lena fan is indicative for sediment input to the Arctic Ocean from point sources (e.g. river mouths as described above). It has to be tested whether the formation of debris flows along the Taymyr - Severnaya Zemlya slope were related to lateral sediment bulldozing by ice over the western shelf areas of the Laptev Sea during times of stronger glaciation of the area (e.g. marine oxygen isotope stages 2 or 6).

The upper part of transect D cuts across the Khatanga-Vilkitsky Channel, of which the PARASOUND results are described in a separate paragraph above.

The profiles recorded along transect E suggest a lateral distinction of three different types of facies: (i) In deeper water below 2300 m, there are relatively thick packages of well-stratified sediments which drape sub-bottom topographies (Fig. 9-10). Mud penetration of PARASOUND is about 30 m. The top of this sequence was cored at station PS 2741-1. Both the reflection pattern and the lithology of the core suggest mostly fine-grained marine deposits and relatively slow sedimentation rates. (ii) The middle part of the slope (between 2300 and about 1800 m water depth) is characterized by debris-flow deposits. Their thicknesses, regional distribution and acoustic characters are less distinct compared to the more southerly parts of the slope (near the Vilkitsky Channel as described above). (iii) In water depth of less than 1800 m the sound penetration is limited to

only a few metres. This is caused by a strong sub-bottom reflector which is draped by acoustically transparent sediments.

Over most of the upper slope area the drape is about 2 m thick and reaches about 10 m in the deeper part of the Shokalsky Strait at the upper end of transect E. The strong backscatter from the sub-bottom reflector suggests a high acoustic impedance contrast. This can be caused by muds which were over-consolidated by ice load and/or diamicton overlain by non-glacial marine deposits. In deed, sediment cores from stations PS 2742-5 (slope, 1890 m water depth) and station PS 2782-1 (Shokalsky Strait, 340 m water depth) show a few metres of non consolidated muds overlying diamicton (see chapters 9.3 and 9.4.2). Thus, both the high resolution seismic profiles and the sedimentary record give consistent evidence of a larger ice cover and/or more intensive ice rafting towards the east of the present ice edge of Severnaya Zemlya. It is, however, too early for an interpretation of the chrono-stratigraphy of such glacial deposits.

The PARASOUND data of the most westerly transect (G) are very similar to those recorded along transect E, except that chaotic slump deposits dominate the entire slope down to the onset of transect G at about 2700 m water depth. Thus, no suitable deep sea coring stations could be selected. It remains open whether these findings are only of local character or may be characteristic for the entire slope area in the transition between the Laptev and Kara Seas.

## **9.2 Geological sampling, description, and methods applied aboard RV Polarstern**

During the Polarstern-Expedition ARK XI/1, a total of 72 geological coring and sampling stations were carried out. The main study areas were (1) the western East Siberian continental margin (transect A), (2) the Laptev Sea continental margin (transects B, C, and D), (3) the continental margin east and north to west of Severnaya Zemlya (transects E and G), and (4) the Amundsen Basin - Lomonosov Ridge - Makarov Basin area (transect F) (Fig. 9-1a, and b; Station list Table, Annex 11.1). In addition, two cores were taken in the southeasternmost Kara Sea, i.e., west of the Vilkitsky Strait. At 24 of these stations, particles within the water columns were filtrated using in-situ pumps. In addition, aerosol samples were taken during transit times (Annex tables 11.4-1 and 11.4-2).

### **9.2.1 Aerosol sampling and size-distribution measurements (V. Shevchenko)**

Sampling of aerosols for chemical analyses and scanning electron microscopy was carried out aboard RV Polarstern approximately 20 m above sea level. For the chemical analyses, 100-150 cubic metres of air were pumped through AFA-HA filters (about 15 cubic metres per hour).

During the expedition 12 samples for chemical analyses were collected (Annex table 11.4-1). Elemental composition will be studied by instrumental neutron-activation analysis (INAA). For scanning electron microscopy 20-50 m<sup>3</sup> of air were pumped through AFA-HA filters (about 3 m<sup>3</sup> per hour); 4 samples were collected. 2 samples of large (>1 µm) non-sea-salt aerosols were collected by nylon mesh method.

Measurements of aerosol size distribution were carried out at 63 stations (Annex table 11.4-2) using a Royco-218 photoelectrical particle counter (USA). In each series, 3 parallel measurements of particle concentrations in the ranges of 0.5-1; 1-2; 2-3; 3-5; 5-10  $\mu\text{m}$  were done.

### 9.2.2 Sampling in the water column (K. Fahl, V. Shevchenko)

#### *In-situ pumps*

The sampling in the water column was carried out with *in-situ* pumps (Challenger Oceanic Systems and Services -COSS-, UK) at 24 stations (table below). The *in-situ* particulate sampler is designed to filter more than one cubic metre of water in one hour at midwater depth in the open ocean. The aim is to provide sufficient quantities of particulate material for subsequent analyses of chemical moieties (in this case biomarkers). In general, the volume sampled depends on the concentration of the suspended matter, the duration of pumping, and the porosity and matrix of the filters. For the investigations of biomarkers, precombusted large Whatman GF/C filters were used.

In general, the sampling was carried out at 3 stations per transect (shelf, slope, and deep sea; see following table). The pumping depth was selected according to the CTD profile.

*Table: In-situ pumping stations*

Transect	Station	AWI-No.	Depth (m)	Pumping depth (m)
n o	36/003	2720-1	2054	600/2000
n o	36/007	2723-2	220	40/150
n o	36/008	2724-2	101	50
A	36/065	2766-2	234	150/220
A	36/062	2764-2	1054	400/1030
A	36/060	2763-2	1638	700/1620
B	36/069	2769-2	1248	800/1190
B	36/040a	2747-2	1893	600/1700
B	36/044	2749-2	2875	600/2800
B	36/024a	2738-2	3280	600/3000
B	36/047	2752-2	3915	800/3000
C	36/019	2732-2	248	30/200
C	36/022	2735-2	1820	700/1500
D	36/083	2779-2	243	100/220
D	36/080	2776-2	1094	600/1050
D	36/075	2773-2	3650	1500/3580
E	36/033	2745-1	262	60/200
E	36/031	2743-2	1180	600/1100
E	36/027	2740-2	3289	600/3000
F	36/049	2754-2	2420	600/2380
F	36/051	2756-3	1730	600/1700
F	36/052	2757-2	1258	600/1200
F	36/055	2759-2	1654	700/1600
F	36/057	2761-2	2586	500/2500

*Rosette water sampling*

To study the quantitative distribution of total suspended matter, 2-5 l of water taken by the Rosette water sampler from different depth were filtrated through lavsan filters (analog of Nucleopore filters) with a pore size of 0.45  $\mu\text{m}$  and a diameter of 47 mm. 236 samples of TSM were collected.

182 water samples (20 ml) for determination of proteolytic and amylolytic enzymatic activities were taken from the Rosette bottles. These samples are stored at 4°C and will be analyzed by G.A. Korneeva (P.P. Shirshov Institute of Oceanology, Moscow).

126 water samples (100 ml) for bacteria distribution studies in the water column were taken from Rosette bottles and are stored at -30°C. They will be analyzed by D.I. Nikitin (Institute of Microbiology, Moscow).

To study the suspended matter lipid composition off the northern part of Severnaya Zemlya Archipelago, 26 samples were collected by filtration of 7-10 l of water through GF/F Watman filters (diameter of 47 mm) and stored at -30°C for organic geochemical analysis by O.A. Alexandrova (P.P. Shirshov Institute of Oceanology, Moscow).

**9.2.3 Sea floor sediment sampling and description**

(M. Behrends, M. Bourtman, K. Fahl, M. Mitjajev, E. Musatov,  
N. Nørgaard-Petersen, V. Shevchenko, R. Spielhagen, and R. Stein)

*Sampling of near-surface sediments*

In order to get undisturbed surface and near-surface sediments, the giant box corer (GKG) and the multi-corer (MUC) were used. Sampling with the giant box corer (50x50x60 cm) was carried out routinely on almost all geological stations. Two types of multi-corer were used. At all stations but one, cores were taken by the "Göteborg" multi-corer (see chapter Biogeochemistry). At one station, the AWI multi-corer (Fa. Wuttke, Henstedt-Ulzburg, Germany) with eight tubes of 10 cm in diameter was used. The penetration weight of this MUC was 250 kg.

The surface sediments of the GKG were sampled for stable isotopes in foraminifers, sedimentological, micro-paleontological, and geochemical investigations. In addition, three plastic tubes (12 cm in diameter) and one plastic box (cross section of 7.5 x 15 cm) covering the entire sediment column gained by the GKG were taken (for sedimentological, geochemical, and stable isotope investigations, and for archiving at AWI).

Multicorers were sampled as follows, depending on the numbers of cores filled with sediment:

- 2 tubes for investigation of benthic foraminifers and stable isotopes. Sediment samples were taken at 0-1, 1-2, 2-3, 3-4, 4-5, 7-8, 10-11, and 14-15 cm and subsequently mixed with bengal-rosa-ethanol-solution to stain living organisms;
- 2 tubes for sedimentological, geochemical, and stable isotope investigations.

*Coring and sampling of long sediment cores*

The gravity corer (SL) and the Kastenlot corer (KAL) were used to obtain long sediment cores. The gravity corer has a penetration weight of 1.5 t, and a core barrel segment length of 5 m with a diameter of 120 mm. The core barrels used during ARK XI/1 had lengths of 5 and 10 m. At 40 stations, the gravity corer (SL) was used. The lengths of SL cores range from about 70 to 800 cm (Fig. 9-11).

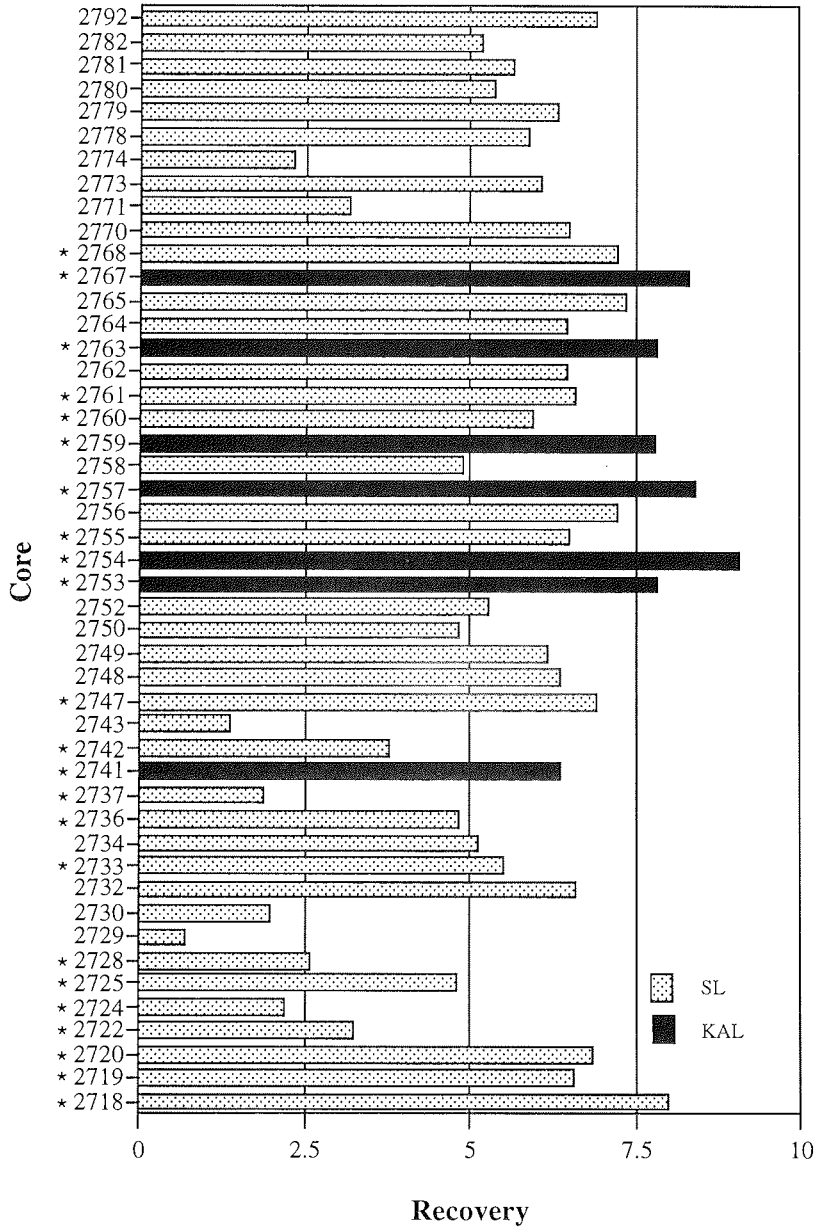
The Kastenlot (Kögler, 1963), a gravity corer with a rectangular cross section of 30x30 cm, has a penetration weight of 3.5 t and a core-box segment sized 30x30x575 cm (manufactured by Hydrowerkstätten Kiel). The length of the core boxes used was 11.75 m plus about 30 cm for the core catcher. The great advantage of this Kastenlot is the wall-thickness of only 0.2 cm. Because of the great cross-sectional area (900 cm<sup>2</sup>) and the small thickness of the walls, the quality of the cores was generally excellent. At 7 stations, the Kastenlot corer was used. The lengths of the obtained cores range from 635 to 905 cm (Fig. 9-11).

23 of the sediment cores (i.e. all KAL cores and 16 of the SL-gravity cores) were opened, described, and sampled onboard Polarstern. Before opening of the SL cores, core logging was performed (see chapter 9.3). Sampling of SL cores was performed for shorebased stratigraphical, sedimentological, geochemical, and micro-paleontological studies (AMS<sup>14</sup>C dating, water content, wet-bulk density, stable isotopes, XRD, heavy minerals, grain size, carbonate, organic carbon, microfossil assemblages, etc.). Sampling of the KAL cores for the same investigations was performed as follows: 3 plastic boxes (100x16x7.5 cm) covering the entire core (AWI Archive; AWI geochemistry, sedimentology, mineralogy, and stable isotopes; GEOMAR sedimentology and stable isotopes). One of the boxes taken for organic-geochemical investigations was immediately deep-frozen at -18°C; 1 plastic box (100x9x7.5 cm) covering the entire core for core logging (see chapter 9.3). In addition, single samples were taken from the entire core for specific mineralogical and micro-paleontological studies (MMBI, Shirshov Institute, VNIIO).

Next page:

Fig. 9-11: Recovery of gravity (SL) and Kastenlot (KAL) cores

GravityCores.ARK-XI/1



\* opened, described, and sampled



*Sediment description and characterization*

## (a) Visual core description

The sediment cores were routinely photographed and described, and are graphically displayed within the Appendix. Sediment colors were identified according to the "Munsell Soil Color Chart". Smear-slide investigations were performed to obtain estimates of the grain size and sediment composition (i.e. biogenic and terrigenous components) and for the classification of the sediment type (e.g. silty clay, sandy silt, etc.; see Annex 11.4).

(b) Coarse fraction (> 63  $\mu\text{m}$ ) analysis

Bulk sediment samples were washed through a 63  $\mu\text{m}$  sieve and dried. On a selected set of samples, the coarse-fraction composition was analysed using a binocular microscope.

## (c) Radiographs

Sediment slabs of 0.5 cm thickness were taken continuously from all SL cores. X-ray images were produced from these in order to elucidate sedimentary and biogenic structures and to determine the number of coarse-grained detritus >2 mm for evaluation of the contents of ice-rafted debris (IRD) (for method, see GROBE, 1987).

**9.3 Physical properties in marine sediments**

(F. Niessen, N. Nørgaard-Pedersen and E. Musatov)

During ARK XI/1 physical properties were determined on whole cores by logging (P-wave velocity, wet bulk density and magnetic susceptibility) and on discrete samples after core opening (wet bulk density and shear strength). Physical properties of marine sediments are important parameters for the interpretation of the sedimentary record.

Magnetic susceptibility is commonly used as an indicator of lithological changes (e.g. NOWACZYK 1991). It is defined as the dimension-less proportional factor of an applied magnetic field in relation to the magnetization in the sample (here expressed in SI units). In marine sediments changes in susceptibility are normally controlled by variations in the content of magnetite. Magnetite has a significant higher susceptibility ( $k = +10^{-2}$ ) than most common minerals ( $-10^{-6}$  to  $+10^{-6}$ ). In marine environments of high latitude areas, magnetite is mostly derived from terrigenous input and/or volcanic ashes. The share of magnetite depends on its dilution by marine components such as carbonates and opal. Hence, the magnetic susceptibility may be used as an indicator for marine versus terrestrial origin of the sediments. Magnetic susceptibility records are also ideal for lateral core correlation.

P-wave velocity and wet bulk density can be used for the calculation of synthetic seismograms in order to compare the cored sedimentary record with high resolution seismic profiles obtained with the PARASOUND system. The aim is a better understanding of the sound reflection behavior of marine sediments. This is controlled by the contrasts of acoustic impedances in the sediment sequence. Acoustic impedance is defined as the product of density and P-wave velocity.

Wet bulk density (WBD) is the density of the total sample, including pore fluid or:

$$\text{WBD} = M_t/V_t$$

Units are reported in  $\text{Mg m}^{-3}$  which is numerically equivalent to  $\text{g cm}^{-3}$ .

Porosity and dry bulk density are two variables required for calculation of sediment accumulation rates ( $\text{g cm}^{-2} \text{ky}^{-1}$ ).

Also, down core logs of wet bulk density are useful to test and confirm lateral core correlation based on magnetic susceptibility. In addition, the wet bulk density and shear strength of marine sediments can be used to interpret their consolidation. For the climate history of the area under investigation it was of major importance to determine whether the sediments underwent consolidation due to ice load or not.

### 9.3.1 Continuous whole-core logging of wet bulk density, P-wave velocity and magnetic susceptibility

Wet bulk density, P-wave velocity and magnetic susceptibility were measured in 1-cm intervals on all gravity and Kastenlot cores taken during the cruise. We have used the "Multi Sensor Core Logger (MSCL)", manufactured by Geotek (UK), which allows the determination of core diameter, P-wave travel time, Gamma-ray attenuation and magnetic susceptibility. The system is automated (PC based) and designed for non-destructive logging of up to 1.3 m long whole-core sections.

<b>P-wave Velocity and Core Diameter</b>	
Transducer diameter	5 cm
Transmitter pulse frequency	500 kHz
Transmitted pulse repetition rate:	1 kHz
Received pulse resolution	50 ns
P-wave travel-time offset	8.47 $\mu\text{s}$ (KAL, 2*3 mm box wall thickness) 7.79 $\mu\text{s}$ (SL, 2*2.5 cm liner wall thickness)
<b>Density</b>	
Gamma ray source	Cs-137
Source activity	356 MBq
Source energy	0.662 MeV
Collimator diameter	5 mm
Gamma detector	Scintillation Counter (John Count Scientific Ltd.)
<b>Magnetic Susceptibility</b>	
Loop sensor type	MS-2B (Bartington Ltd.)
Loop sensor diameter	14 cm
Alternating field frequency	0.565 kHz
Magnetic field intensity	approx. 80 A/m RMS
Loop sensor correction coefficient SL	1 (113 $\text{cm}^2$ core cross section)
Loop sensor correction coefficient KAL	2.324 (59.4 $\text{cm}^2$ core cross section)

Table 9-1: Multi Sensor Core Logger (MSCL) specifications used during ARK-X/2

In case of Kastenlot cores polystyrene boxes (size inside 82.5 x 72 x 1000 mm) were logged, which were previously filled with sediments by pushing the boxes into the cores shortly after the Kastenlot was opened. Because the loop sensor used has a different response to varying core diameter, all magnetic susceptibility values determined for Kastenlot boxes are multiplied by 2.324 (Table 9-1) according to the manufacturer's correction instructions.

A detailed description of the MSCL system is given by KUHN (1994), its calibration described by NIESSEN (1996) and WEBER et. al (submitted). The characteristics are summarized in Table 9-1. During the cruise the  $\gamma$ -ray attenuation was calibrated to density using aluminum, graphite and water. A computer program (KUHN 1995) is used to link the different sensor data according to their actual depth in the core. It also provides the susceptibility correction for the ends of the individual liner sections.

#### *General observations*

Preliminary results demonstrate that the densities calculated from MSCL measurements correlate with those determined in discrete samples (Fig. 9-12). There is a similar trend in both data sets, although, on average, the MSCL densities are slightly higher than those of discrete samples. For the entire area under investigation, there is a positive correlation of MSCL wet bulk density and P-wave velocity (see Annex 11.4). Wet bulk densities and P-wave velocities range from 1.3 g cm<sup>-3</sup> and 1480 m s<sup>-1</sup> to 2.3 g cm<sup>-3</sup> and 1900 m s<sup>-1</sup>, respectively. Densities above 2.0 g cm<sup>-3</sup> and P-wave velocities above 1600 m s<sup>-1</sup> are only found in diamicton (transect E) and in sediments consolidated by diagenesis (transect F, see below). Generally, magnetic susceptibility ranges between 10 and 70 (10<sup>-5</sup> SI). A few distinct peaks of up to 100 (10<sup>-5</sup> SI) are observed in the lower parts of the cores from the Lomonosov Ridge. Exceptionally high susceptibility values of up to 400 (10<sup>-5</sup> SI) were only determined in cores from the Vilkitsky Channel and the adjacent shelf edge.

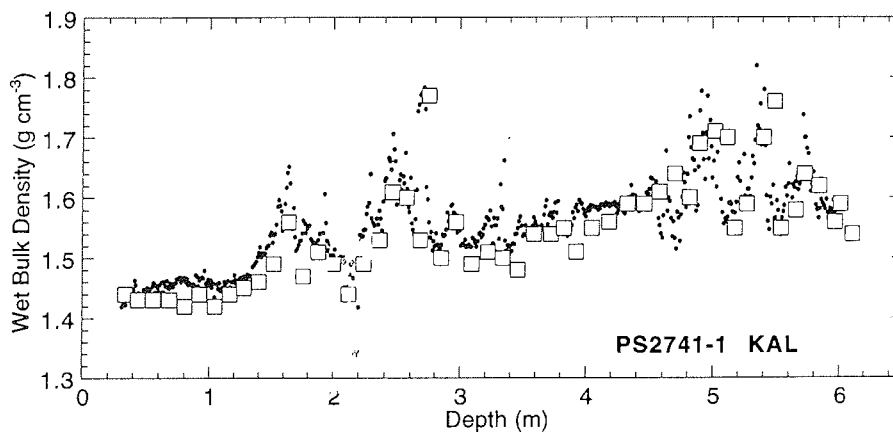


Fig. 9-12: Physical property data of core PS2741-1  
(dots: whole-core logging by MSCL, squares: discrete samples).

*Lomonosov Ridge (transect F)*

Lateral core correlation across the Lomonosov Ridge (transect F) using both, magnetic susceptibility and wet bulk density (Fig. 9-13), suggest a general decrease in unit thicknesses from the Amundsen Basin toward the crest of the ridge (PS 2757-8) and the Makarov Basin. This is in agreement with lithological correlations and the lateral variation of seismic units as described from PARASOUND profiles (chapters 9.1 and 9.4). There is, however, some uncertainty in the correlation toward the westerly end of the profile in the Amundsen Basin (Figs. 9-1 and 9-13, cores PS 2753-2 and PS 2754-8).

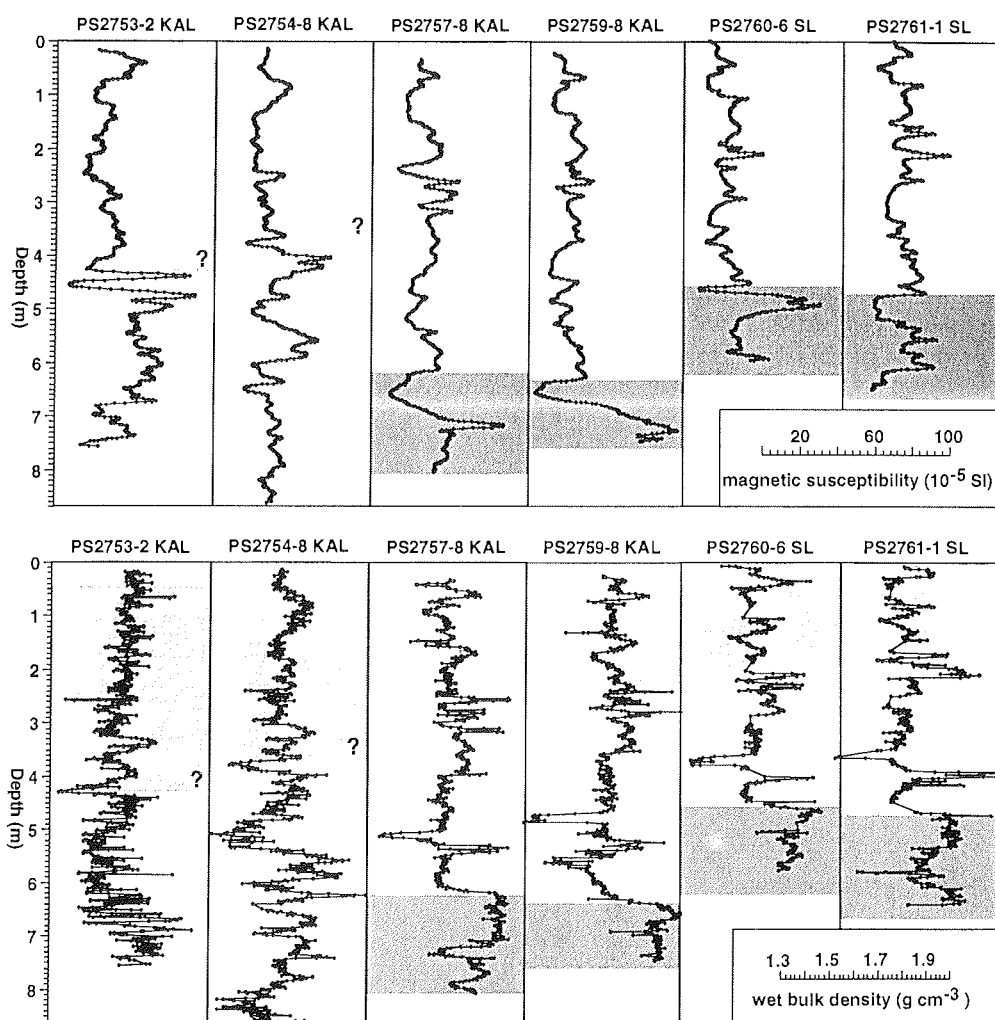


Fig. 9-13: Lateral correlation of whole-core logging results from transect F, Amundsen Basin - Lomonosov Ridge - Makarov Basin

In addition, the density data are characterized by a decrease of "scatter noise" from the west to the east (Fig. 9-13). Generally, density records from the crest and the Makarov Basin appear to be more "smooth". In contrast, strong "noise" is observed in cores retrieved from the Amundsen Basin (PS 2753-2, PS 2754-8). This effect can be caused by thin turbidites which are often characterized by large density variations on small vertical scales due to grain-size grading (e.g. NIESSEN 1996). It implies significantly higher sedimentation rates in the Amundsen Basin compared to the other areas of transect F.

In the susceptibility records, strong fluctuations and high amplitudes of up to  $100 \times 10^{-5}$  SI (Fig. 9-13) coincide with the occurrence of dark gray and very dark gray sediments. These units are also indicated by increased wet bulk densities (up to  $1.9 \text{ g cm}^{-3}$ ).

#### *Makarov Basin - Continental slope (transect A)*

Lateral core correlation from the Makarov Basin (PS 2761-1) towards the continental shelves suggest a strong increase of unit thicknesses and thus sedimentation rates towards the East Siberian/Laptev Seas (Fig. 9-14). This confirms similar observations made along the continental slopes of the Amundsen and Nansen Basins during the Polarstern cruise ARK IX/4 in 1993 (FÜTTERER 1994). The down-core pattern of changes in both the magnetic susceptibility and the density records are less distinct in locations near the shelf (PS 2764-8, PS 2765-8). This may be caused by higher sedimentation rates on the upper continental slope. Therefore, the correlation in Figure 9-14 is preliminary and must be confirmed by further analyses of sediment samples. There is no obvious lateral correlation of down-core physical property patterns between the cores from the slope and the shelf areas.

#### *Severnaya Zemlya slope (transect E)*

Core correlation along the Severnaya Zemlya slope revealed large differences for both lateral variation of unit thicknesses and vertical variation of amplitudes (Fig. 9-15). In particular, densities show high values of up to  $2.2 \text{ g cm}^{-3}$  (diamicton, see chapter 9.4.2) in the lower parts of those cores which were taken from less than 1900 m water depth. It is suggested that these sediments correlate laterally with layers of increased density in PS 2741-1 (Fig. 9-15, eastern end of transect E, 2530 m water depth). The lateral correlation is also seen in the records of magnetic susceptibility (Fig. 9-15). The topmost unit which is overlying diamicton appears extremely thin in upper slope areas (PS 2743). This may be related to winnowing of fine grained sediments by currents. The entire pattern is typical for sediments which underwent stronger influence of ice rafting by icebergs in the past followed by a period of decreased supply of ice rafted debris during and after deglaciation.

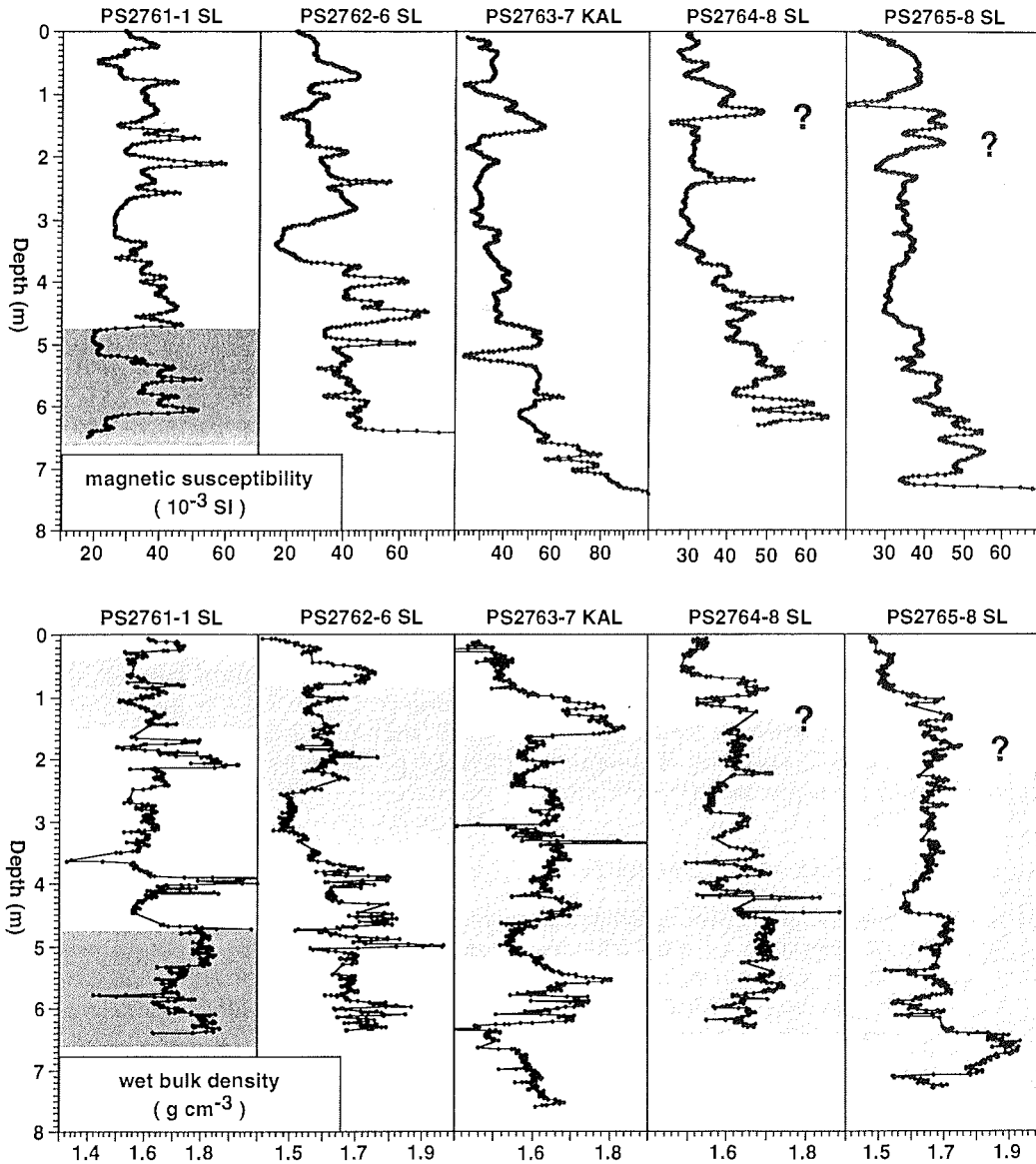


Fig. 9-14: Lateral correlation of whole-core logging results from transect A, Makarov Basin - continental slope

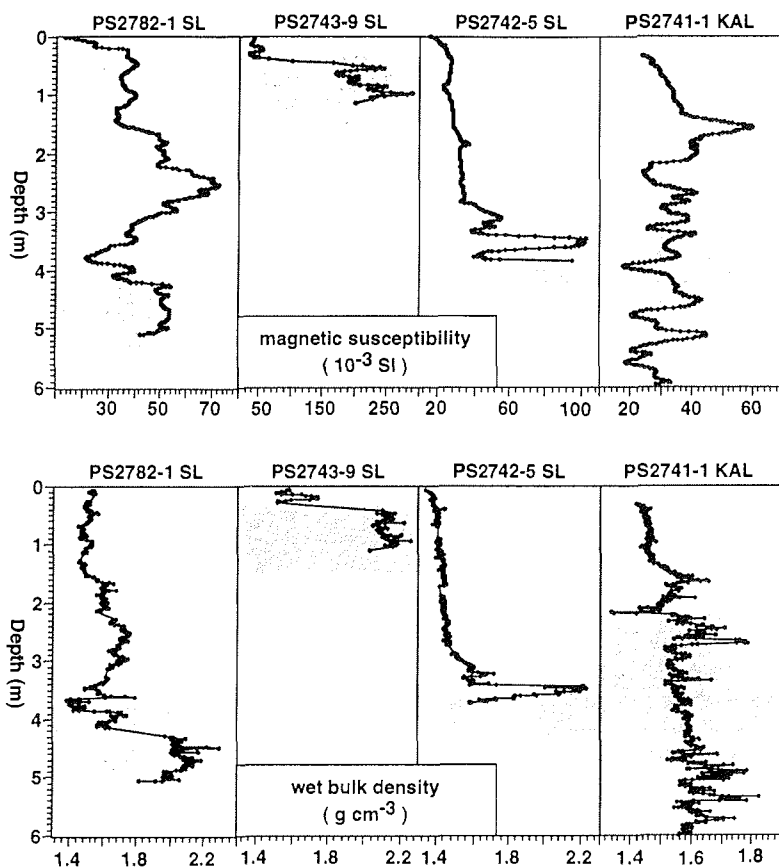


Fig. 9-15: Lateral correlation of whole-core logging results from transect E, Severnaya Zemlya slope.

### 9.3.2 Shear strength measurements and density determination of discrete samples

Shear strength and undrained wet bulk density were measured on all Kastenlot cores and selected gravity cores opened on board. Connected box core sections representing the undisturbed uppermost sediment layers, were measured, too, and are included in the graphic presentations of the long cores. The measurement interval ranged from 2.5 to 15 cm depending on the downcore variability of sediments.

A vane shear instrument (Haake viscometer, RV 3) was used to measure undrained shear strength. A 20 mm × 8.8 mm vane was used with this instrument, inserted 1 cm deep into the sediment and rotated at a speed of 4 rotations per minute ( $24^\circ \text{ sec}^{-1}$ ). At each depth interval 2-4 measurements were made in order to determine the scatter associated with sediment inhomogeneities, such as by bioturbation. Shear strength was measured at peak failure. All values are reported in kPa.

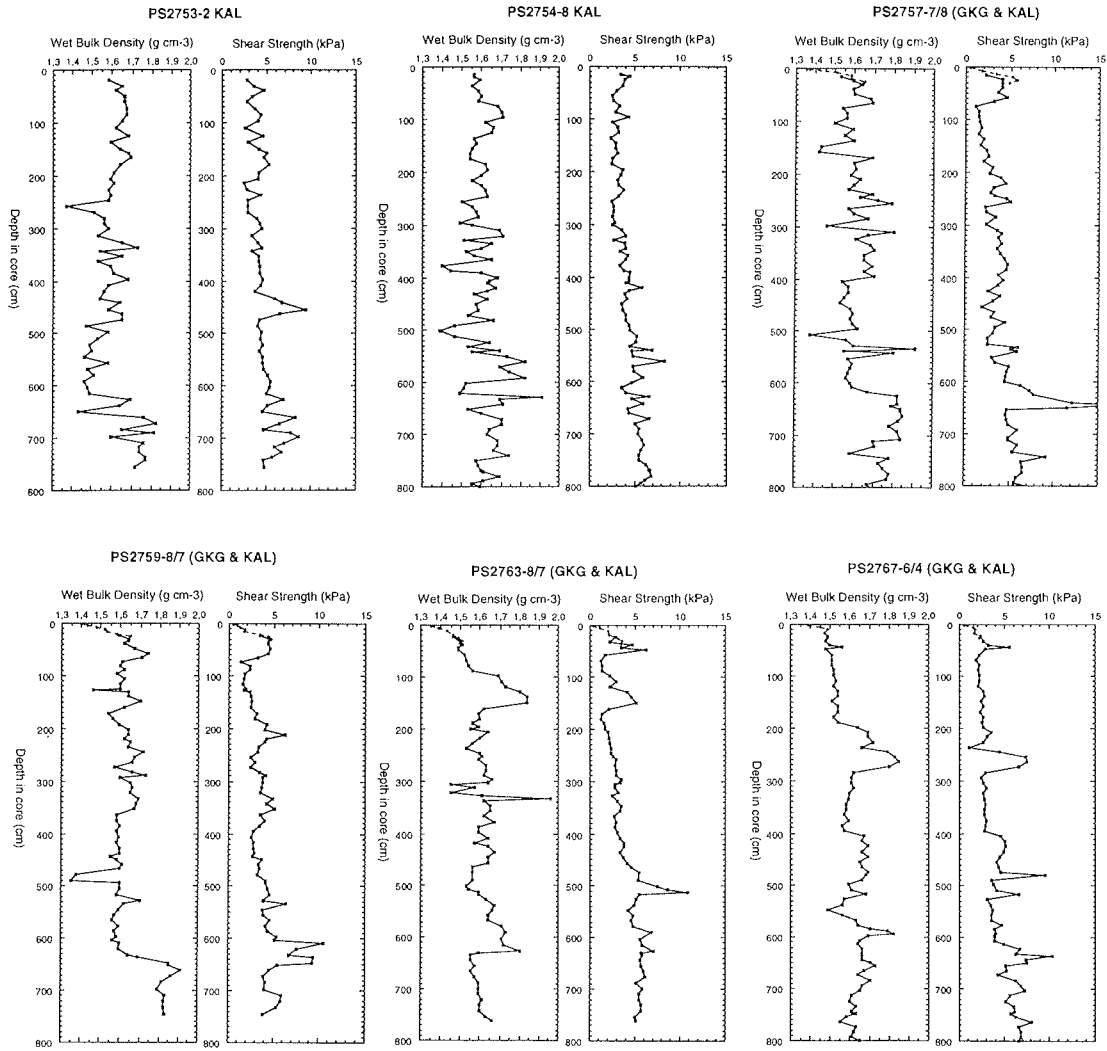


Fig. 9-16: Wet bulk density (discrete samples) and sheer strength of sediments from the Lomonosov Ridge (transect F)



A constant volume tube of 10 cm<sup>3</sup> was used to sample sediments for density determination. The tube was carefully pushed into the sediment, then cut out, trimmed and weighed. To compensate for ship's motion, mass was determined using a technique of differential counter-balancing on twin top loading electronic balances (CHILDRESS & MICKEL, 1980). The computerized precision electronic balance system used during this cruise was kindly provided by GEOMAR Technologie GmbH, Kiel. After determination of the total (wet) mass and volume, samples were stored for later freeze drying and determination of dry mass in the home laboratory. From the index properties, water content and bulk density, sediment phase relationships as dry density, porosity and void ratio can be derived. The index properties can be determined from the direct measurement of the total mass of the sample ( $M_t$ ), the dry mass of the sample ( $M_d$ ) and the total volume of the saturated sample ( $V_t$ ).

*Lomonosov Ridge and the adjacent continental margin*

The six Kastenlot cores retrieved from the Lomonosov Ridge and the adjacent continental margin show physical properties reflecting downcore variation in grain size and diagenetic imprint. The sediment sequence which can be correlated across the ridge (cf. Fig. 9-13) show also well-correlatable downcore profiles of wet bulk density and shear strength (Fig. 9-16). This is especially evident for cores PS 2757-8 and PS 2759-7 located near the crest of the Lomonosov Ridge (Fig. 9-1). In general, wet bulk density is between 1.5-1.7 g cm<sup>-3</sup>. Very low values of 1.35-1.40 g cm<sup>-3</sup> were found in characteristic clayey layers. High wet bulk density values of about 1.8-1.9 g cm<sup>-3</sup> are obtained in cm-thin sand layers. The shear strength curves indicate normal consolidation of the sediment sequence with moderate low shear-strength values increasing from about 2-3 kPa in the upper part of the cores to about 5-7 kPa in the lower part.

*Laptev Sea outer shelf and slope region - transects A & C*

At three closely located coring stations on the outer shelf north of the New Siberian Islands (75-100 m water depth) deformed and firm, silty clay units (folding, slumps?) were found intercalated with undeformed, normal consolidated fine-grained sediments (gravity cores PS 2722-4, PS 2724-10 and PS 2725-5 (lowermost part). The wet bulk density of the deformed units is relatively high (1.8-1.9 g cm<sup>-3</sup>), and shear strength values are between 20 and 30 kPa (Fig. 9-17) suggesting over-consolidation. Comparable high shear strength values of more sandy shelf sediments have been reported north of Kotelny Island by BENTHIEN (1994), who interpreted the degree of consolidation as due to iceberg gouging. According to PARASOUND observations (cf. chapter 9.1) characteristic iceberg plow marks are common surface relief features on the shelf north of the New Siberian Islands. It thus seems probable that the shelf sediments are locally deformed and firmly consolidated due to gouging by stranded icebergs.

From transect C across the Laptev Sea slope, shear strength and WBD were measured on three gravity cores and connected box cores (PS 2733-3/6, PS 2736-3/6 and PS2 737-4/7, Figs. 9-1a, 9-6). The lithologically very homogeneous core PS

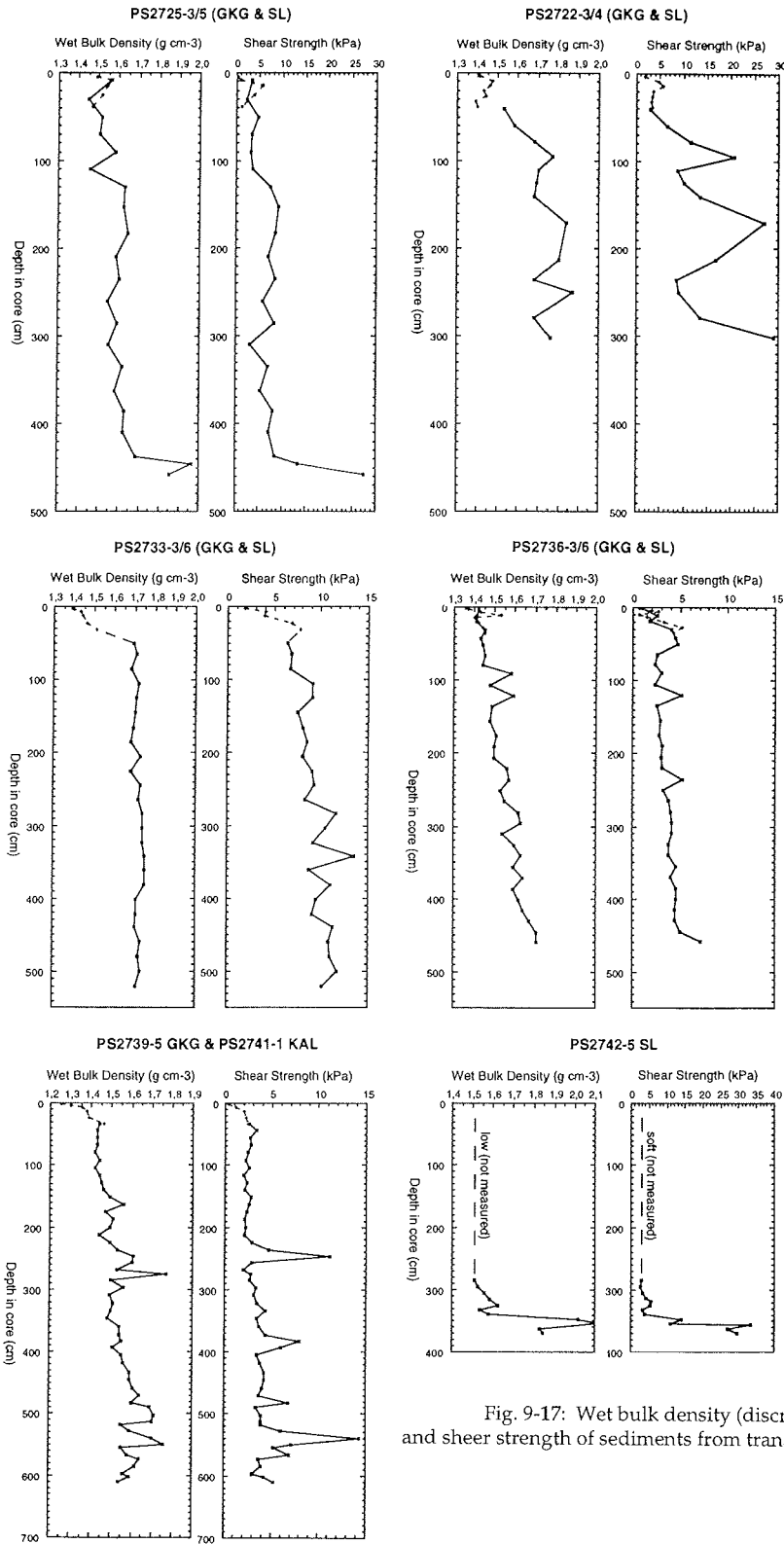


Fig. 9-17: Wet bulk density (discrete samples) and shear strength of sediments from transects A, C, E

2733-3/6 from the upper slope shows relatively high densities of about  $1.7 \text{ g cm}^{-3}$  and shear strength values in the range of 7-10 kPa below the water-rich near-surface sediments. Core 2736-3/6 from the surface of the slope apron has relatively low densities ( $1.4\text{-}1.7 \text{ g cm}^{-3}$ ) and low shear strength values 3-5 kPa. Intervals with higher density in the core correspond to more sandy, dark-colored turbidite deposits.

#### *Severnaya Zemlya slope - transect E*

Across the Severnaya Zemlya slope shear strength and wet bulk density were measured on Kastenlot core PS 2741-1 and gravity core PS 2742-5 (Fig. 9-17). Core PS 2741-1 shows weakly increasing density with depth. Shear-strength values are superimposed by peak values reflecting more silty and sandy sediment units (high wet bulk density) or diagenetic alteration (typically higher shear strength). Wet bulk density is between 1.4 and  $1.7 \text{ g cm}^{-3}$ . The higher densities in the lower part of the core can be ascribed to horizons with thin silty layers (distal turbidites?). These are overlain by less dense, olive-green, banded silty clay units having characteristic high shear strength values (7-15 kPa).

Gravity core PS 2742-5 contains in its lowermost part (3.5 m) a firm pebbly diamict showing shear strength values up to 35 kPa (Fig. 9-17). This over-consolidated sediment may represent ice-loaded moraine material from the Severnaya Zemlya continental margin, probably transported to the core location by a mass-flow event or by iceberg rafting.

## **9.4 Lithostratigraphy and sediment characteristics**

(R. Stein, M. Behrends, R.F. Spielhagen)

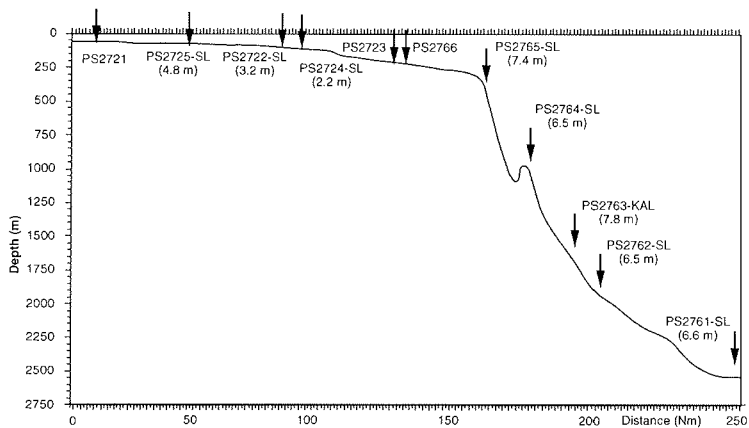
### **9.4.1 Sediment surfaces**

All sediment surfaces of box cores obtained during the cruise were of brown color, indicating well-oxygenated surface layers. The sediment color often had a grayish or olive-grayish touch. On the shelf and on the upper slope down to 500-1000 m water depth, sediments were often described as ranging from sandy-silty clay to silty sand, while on the lower slope and in the deep sea, silty clays were predominant. One exception was the area of the eastern flank of the Lomonosov Ridge (transect F) and the adjacent Makarov Basin (transect A), where surface sediments contained significant amounts of sand even in water depths >1000 m. This may indicate winnowing of fine material by current activities across the Lomonosov Ridge.

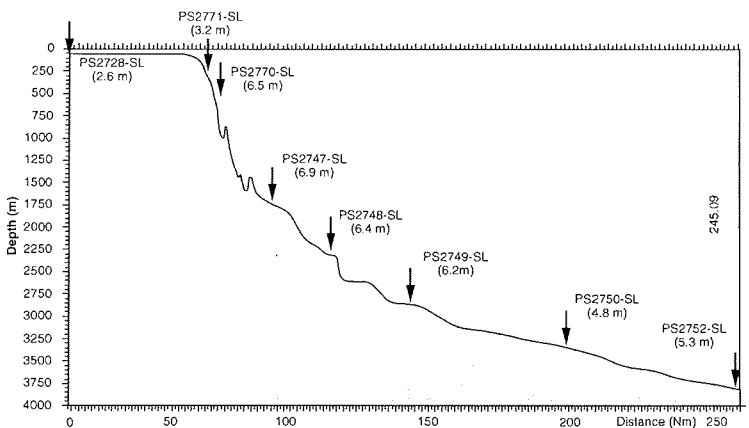
Ice-rafted gravel was generally rare. While one pebble on the surface of PS 2752-8 from the deep Amunsen Basin (3823 m) was an occasional exception, common gravel of up to 5 cm in diameter in the cores taken north and northeast of Severnaya Zemlya from water depths between 200 and 1000 m, however, obviously reflect current rafting by icebergs.

One exceptional feature was the finding of five flat manganese nodules (4-7 cm diameter, 1-2 cm thick) on the surface of PS 2726-5 from the shallow eastern Laptev Sea (48 m water depths). Such nodules were also found in several Agassiz trawl samples from this area and prove a significant regional distribution.

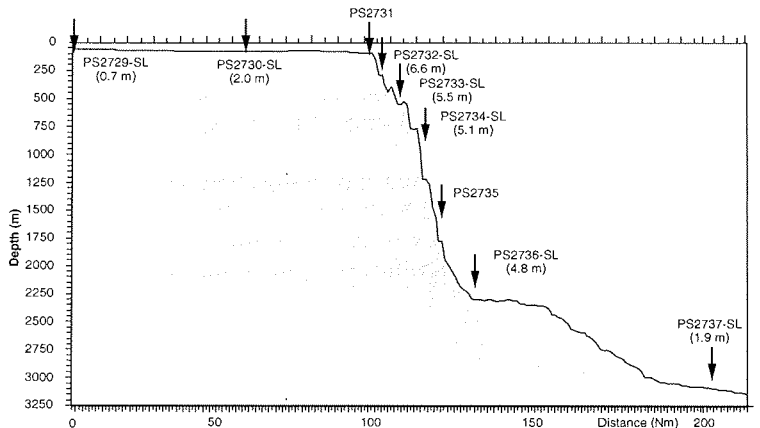
East Siberian Transect (A), Polarstern Cruise ARK-XI/1, 1995

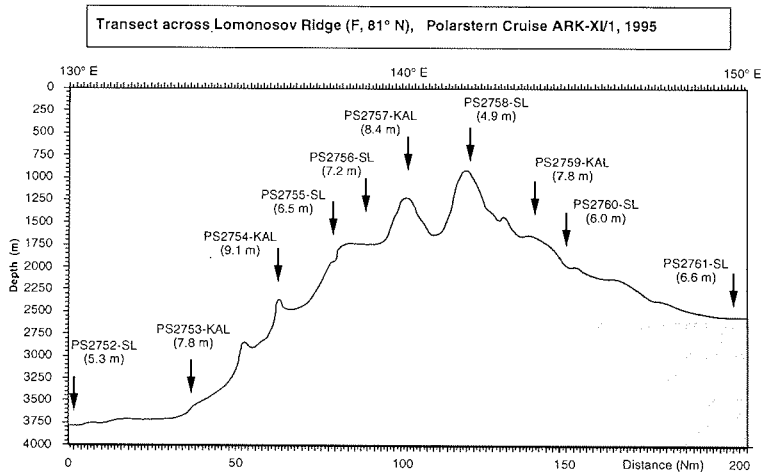
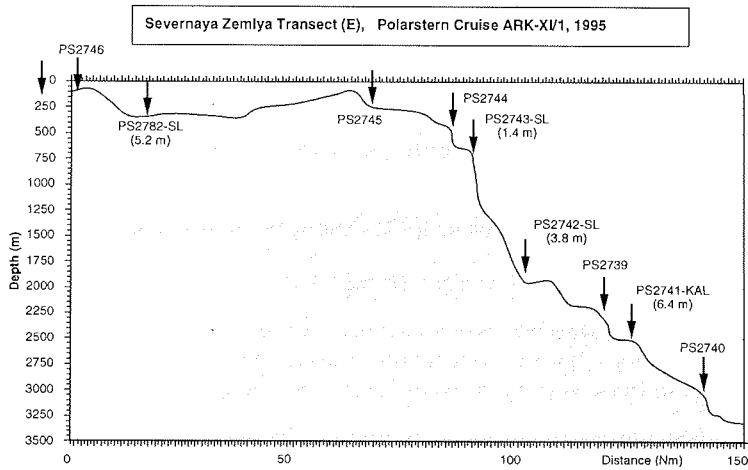
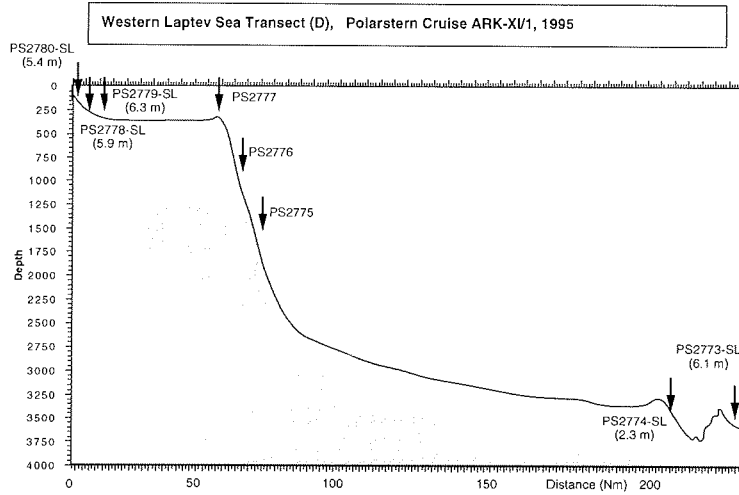


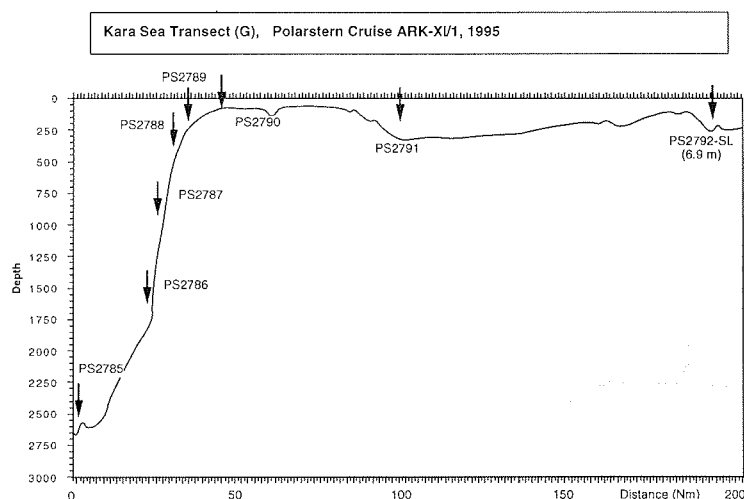
Eastern Laptev Sea Transect (B), Polarstern Cruise ARK-XI/1, 1995



Central Laptev Sea Transect (C), Polarstern Cruise ARK-XI/1, 1995







Ahead:

Figs. 9-18 a-g: Transects with geological stations. Numbers in brackets indicate lengths of Kastenlot (KAL) and gravity (SL) cores (no number: only GKG)

#### 9.4.2 Long sediment cores (see graphic descriptions in Annex 11.4)

##### *The East Siberian continental margin (transect A)*

Thirteen geological stations were carried out in the northwestern-most East Siberian Sea and its adjacent continental margin (Figs. 9-1, 9-18a; transect A). At eight of these stations, gravity cores of 2.2 to 7.8 m length were obtained.

The long sedimentary sequences recovered on the shelf (cores PS 2722-4, PS 2724-10, and PS 2725-5) consist of two lithologic units. Unit 1 is composed of brown-coloured, slightly bioturbated silty clay with a thickness of this uppermost interval ranging between 4 and 15 cm. The underlying Unit 2 consists of dark olive gray and very dark gray to black silty clay with common to abundant black spots throughout in most parts of the unit. In the lowermost part of core PS 2725-5, the silty clay contains a significant amount of sand; thin sandy intervals were recorded in core PS 2722-4 at depth intervals of 171-190, 206-216, and 273-274 cm. Traces of bioturbation are rare and only observed in the lower half of core PS 2725-5. At the closely neighbored cores PS 2722-4 and PS 2724-10 from a water depth of about 100 m, sediments are disturbed in depth intervals between 77 and 200 cm and 118 and 200 cm, respectively, probably by slumping processes. At several depths, well-preserved tests of bivalves (*Hiatella arctica*) and shell debris were found in all three cores. In core PS 2724-10, a large-sized drop-stone of 7 cm diameter occurs in a depth of 149-151 cm.

Five cores were obtained from the continental slope and deep sea in water depths between 550 and 2640 m. Two of them, Kastenlot core PS 2763-7 and gravity core PS 2761-10, were opened and described. At both cores, the uppermost interval (0-55 cm in core PS 2763-7 and 0-14 cm in core PS 2761-10) is composed of dark brown to dark yellowish brown silty clay. Bioturbation is common in core PS 2761-10, whereas in core PS 2763-7 laminated, partly cemented sediments occur in the lower part of this uppermost unit. The underlying sediments are composed of two major types of lithologies. One is characterized by alternations of (dark) brown to grayish brown to olive brown to light olive brown silty clays. Bioturbation is common in core PS 2763-7, and moderate to strong in core PS 2761-10 in these sediments. The other lithology consists of olive gray to dark olive gray and dark gray to very dark gray silty clay. Thin, more sandy intervals occasionally occur. At core PS 2763-7, some disturbance (slumping structures ?) is obvious between 520 and 630 cm.

All sediments from the East Siberian continental margin are absolutely dominated by fine-grained terrigenous material. Most of the sediment is probably transported in suspension by currents and by sea ice. The very rare occurrence of coarse-grained material (i.e. sand and gravel) suggests that sediment transport by icebergs has been only of very minor importance during the time span covered by the sediment cores. The dark olive gray and very dark gray sediment colors and the abundance of black spots (i.e. high amounts of iron-manganese sulphides) indicate reducing conditions, probably caused by the decomposition of marine organic matter by sulphate-reducing bacteria. High sedimentation rates and somewhat increased surface-water productivity may explain the increased flux and preservation of (marine) organic matter in these sediments (e.g. STEIN 1991).

*The Laptev Sea continental margin (transects B, C, and D)*

On three transects perpendicular to the Laptev Sea continental margin (transects B, C, and D; Figs. 9-1, 9-18b, c, and d), 25 geological stations were carried out. At 19 of these stations, gravity cores of 0.7 to 6.9 m lengths were taken. In addition, one gravity core (PS 2720-7) was taken at the central Laptev Sea continental margin near its junction to the Gakkel Ridge, where remainders of a *hydrothermal vent fauna* had been found during the "Polarstern" 1993 cruise (Rachor et al., in Fütterer (ed.) 1994). Along transect D, only a reduced coring program was performed, since on this transect several lower slope and deep-sea sediments were already successfully cored during the 1993 expedition (Fütterer et al., 1994).

Shelf core PS 2728-3 (water depth 46 m) consists of one lithological unit characterized by dark olive gray, very dark gray, and black, partly bioturbated silty clay. Black spots are common. Well-preserved bivalves and shell debris occasionally occur throughout the entire core. Between 213 and 232 cm, core disturbance (by slumping processes ?) is obvious. At the giant box corer (GKG PS 2728-2; see Annex) obtained at the same location, the near-surface upper 3 cm are composed of dark brown silty clay indicating that the uppermost cm of the sedimentary column are not recovered in the gravity column. In general, the sedimentary

sequence is very similar to those obtained on the western East Siberian shelf (see above).

Except for the uppermost 5 to 12 cm of brownish silty clay, the upper slope core PS 2733-6 (transect C, water depth of 525 m) and the middle slope core PS 2747-9 (transect B, water depth of 1771 m) consist of dark olive gray and very dark gray silty clay with common black spots. At core PS 2747-9, sediments are partly bioturbated, and thin olive-brown laminae frequently occur throughout the entire sedimentary sequence. A couple of these laminae are more coarse-grained.

In the lower slope cores PS 2749-4 and PS 2736-6 and the deep-sea core PS 2737-7, three different types of lithology can be distinguished. The uppermost 15 cm are composed of dark brown and very dark grayish brown silty clay. The underlying sediments are dominated by dark gray, very dark gray, and dark olive gray silty clay. Intervals of more sandy-silty material with fining-upward structures (i.e. turbidites) are frequently intercalated.

Based on smear-slide estimates (Fig. 9-19a), the dark gray silty clay to clay at core PS 2737-7 contain about 5 to 30 % silt and 70 to 95 % of clay; sand is absent. Dominant minerals are clay minerals and quartz (Fig. 9-19b). Rough estimates of heavy-mineral assemblages suggest a dominance of pyroxenes and hornblendes (Fig. 9-19c). Concerning grain size and mineralogy, the turbidites display totally different characteristics (Fig. 9-19). They are composed of about 5 to 60 % sand, 25 to 60 % silt, and 10 to 50 % clay. Quartz is the most dominant mineral (50 to 80 %); feldspars, mica, and clay minerals are the next important minerals. In the heavy-mineral spectrum, granate, epidote, hypersthene, and turmaline are determined which are totally absent in the non-turbidites. Based on the mineralogical composition, the source area of the terrigenous material found in the turbidites must be different from that of the normal pelagic sediments. Further detailed sedimentological and mineralogical studies will follow to identify the different source areas.

In core PS 2720-7 taken at the central Laptev Sea slope near its intersection to the Gakkel Ridge, dark yellowish brown silty clay (0-31 cm) is underlain by very dark gray silty clay with common black spots. Thin sandy layers (turbidites) are frequently intercalated. At depths of 265-267 cm and 288-291 cm, large-sized (up to 7 cm in diameter) bivalves were found. Underneath, in depths of 350, 360, 375, 379-381, and 398-402 cm, lithified horizons (concretions) occur. The bivalves and the lithified horizons may again indicate hydrothermal activities in this area (s. above). This hypothesis, however, has to be proved by further geochemical analyses.

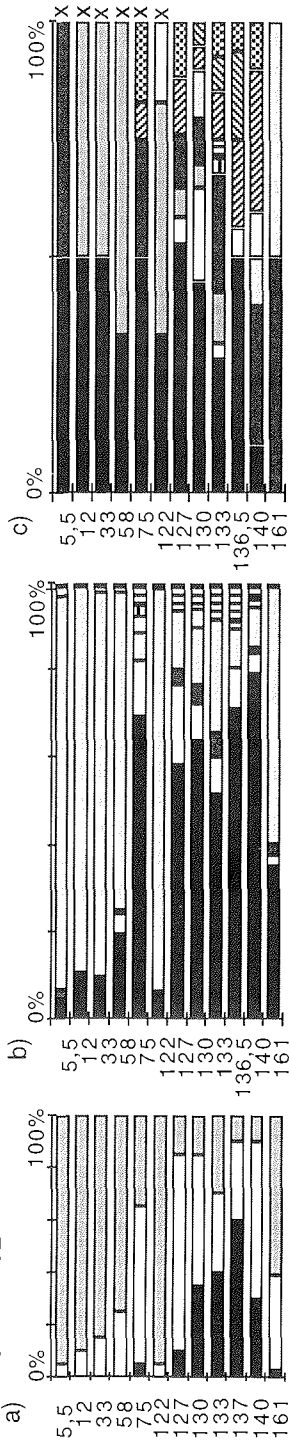
Next page:

Fig. 9-19: Smear slide estimates at cores PS2737-7 (SL) and PS2757-8 (KAL)

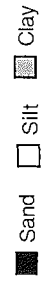
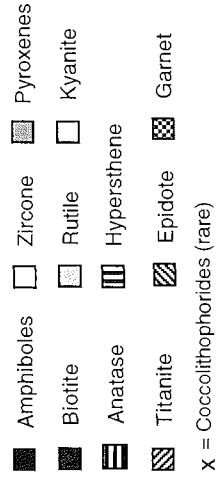
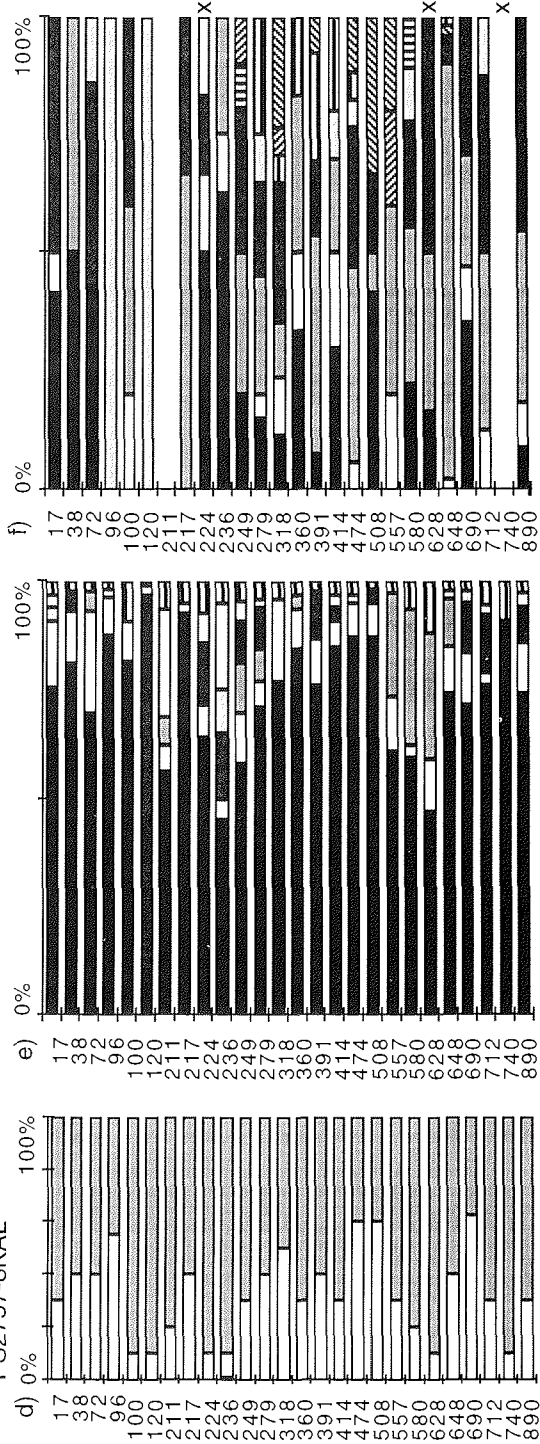
- a) grain size (sand-silt-clay) at core PS2737-7
- b) bulk mineralogy at core PS2737-7
- c) heavy minerals at core PS2737-7
- d) grain size (sand-silt-clay) at core PS2757-8
- e) bulk mineralogy at core PS2757-8
- f) heavy minerals at core PS2757-8



PS2737-7SL



PS2757-8KAL



*The continental margin off Severnaya Zemlya (transects E and G)*

Along the two transects E and G from the continental margin off Severnaya Zemlya (Figs. 9-1, 9-18e and g), seventeen geological stations were carried out. On the eastern transect E, three gravity cores (1.4, 3.8, and 5.2 m long) and one Kastenlot core (6.4 m long) were obtained. On the western profile G, only one gravity core (PS 2792-5, 6.9 m length) was taken in a small depression in the southern Voronin Trough. Based on Parasound records it was decided only to use the giant box corer and the multicorer at all other stations of this transect.

At cores PS 2742-5 and PS 2741-1 (transect E), the uppermost 13 and 40 cm, respectively, are composed of dark brown, olive brown, and grayish brown silty clay. The underlying sedimentary sequence is characterized by alternations of olive gray to dark gray to very dark gray and dark brown to olive brown silty clays, suggesting changes in depositional environment through time. Occasionally, intervals with more silty layers occur throughout.

In core PS 2742-5, a very dark grayish brown to dark brown diamicton with large-sized dropstones (diameters of up to 5 cm) and a silty sand layer on top occurs at 343-360 cm bsf. This diamicton which also can be identified in the physical property data (cf. Fig. 9-17), was probably caused by a major supply of ice-rafted debris during times of an extended ice cap on Severnaya Zemlya. The age of this glacial advance might be the Last Glacial Maximum, which has, however, to be proved by future absolute AMS-<sup>14</sup>C datings.

*Amundsen Basin - Lomonosov Ridge - Makarov Basin (transect F)*

From the Amundsen Basin across the Lomonosov Ridge into the Makarov Basin, a transect at 81°N was sampled with ten geological stations (Figs. 9-1, 9-18f) using giant box corer, multicorer, and gravity/Kastenlot corers. The long cores have lengths between 4.9 and 9.1 m. In addition, two geological stations with all coring gears were carried out on the continental margin in water depths of 584 and 1009 m (core lengths 8.3 and 7.2 m), where the Lomonosov Ridge intercepts the continental margin.

The uppermost 20 to 60 cm of the sedimentary sequence of all cores are composed of dark brown silty clay. The underlying sediments are generally characterized by alternations of olive brown to grayish brown, dark brown, and dark gray to very dark gray silty clays. The dark gray lithologies contain significant amounts of sand. The brownish lithologies are partly laminated, partly bioturbated. Bioturbation is especially strong in the middle part of the sedimentary sequences from the Lomonosov Ridge crest and the Makarov Basin flank. A correlation across the ridge is possible between the cores using the degree of bioturbation, specific silty-sandy layers, and the very prominent and thick dark gray interval in the lower part of the cores (Fig. 9-20). An exception is Kastenlot core PS 2754-8 where the lower dark gray interval was not reached. This correlation suggests that the sedimentation rates are generally higher in the Amundsen Basin compared to the Makarov Basin, which is also supported by magnetic susceptibility and wet bulk density data (cf. Fig. 9-13).

Based on smear-slide estimates performed on sediment samples from Kastenlot core PS 2757-8, the silt (clay) contents of the sediments vary between 10 and 55 % (45 to 90 %); sand is more or less scarce or absent (Fig. 9-19d). Quartz (10-70 %) and clay minerals (30 - 90 %) are the major silici-clastic components (Fig. 9-19e). Feldspars, mica, and rock fragments occur in minor, but significant amounts. In the heavy mineral fraction (which as a total is only of minor importance), hornblendes, pyroxenes, and biotite are the most abundant minerals (Fig. 9-19f). In the interval between about 240 and 600 cm, a very different heavy-mineral assemblage, characterized by granate, epidote, titanite, hypersthen, and anatas, occurs, suggesting a different sediment source area in comparison to the underlying and overlying sediments. Biogenic components (foraminifers and coccoliths) are only observed occasionally in trace amounts.

Based on the core description and smear-slide data, preliminary informations about sedimentary processes, paleo-environment, and their changes through time and space can be obtained. The distinct variations in silici-clastic sediment composition and grain-size distribution of the samples from the Lomonosov Ridge area suggest major changes in the depositional environment related to climate change. The very prominent interval of dark gray to very dark gray, partly more sandy silty clays may represent glacial oxygen isotope stage 6 when glaciation was much more extended than during the Last Glacial Maximum (Stage 2). If this very preliminary shipboard interpretation is correct, the deeper very dark gray lithologies at core PS 2761-10 (Fig. 9-20) may represent older glaciations. In the sediments younger than stage 6 (?), sediment supply by icebergs is of only minor importance as suggested from the very rare occurrence of coarse-grained material.

Further detailed studies, especially the development of a stratigraphic framework, micro-paleontological, sedimentological, and geochemical data have to be produced before a more precise interpretation of the shipboard data is possible.

#### *Southeastern-most Kara Sea*

In the southeastern-most Kara Sea, west of the Strait of Vilkitsky, two gravity cores of 8.0 m (core PS 2718-6) and 6.6 m (PS 2719-1) length were obtained from water depth of 153 and 135 m, respectively (Fig. 9-1). The upper about 15 cm are composed of dark brown to olive silty clay (GKG PS 2718-4; see Annex). The underlying sediments are characterized by dark gray to very dark gray silty clay with common to abundant black spots. The black spots, probably representing iron-manganese sulphides, may be attributed to the decay of organic matter by sulphate-reducing bacteria. Bivalves are found occasionally. At core PS 2719-1, sandy intervals were recorded in the lowermost part of the sedimentary sequence (below 5.4 m). At 323-327 cm, a large-sized dropstone (5 cm in diameter) occurs, indicating occasional, but minor sediment supply by icebergs.

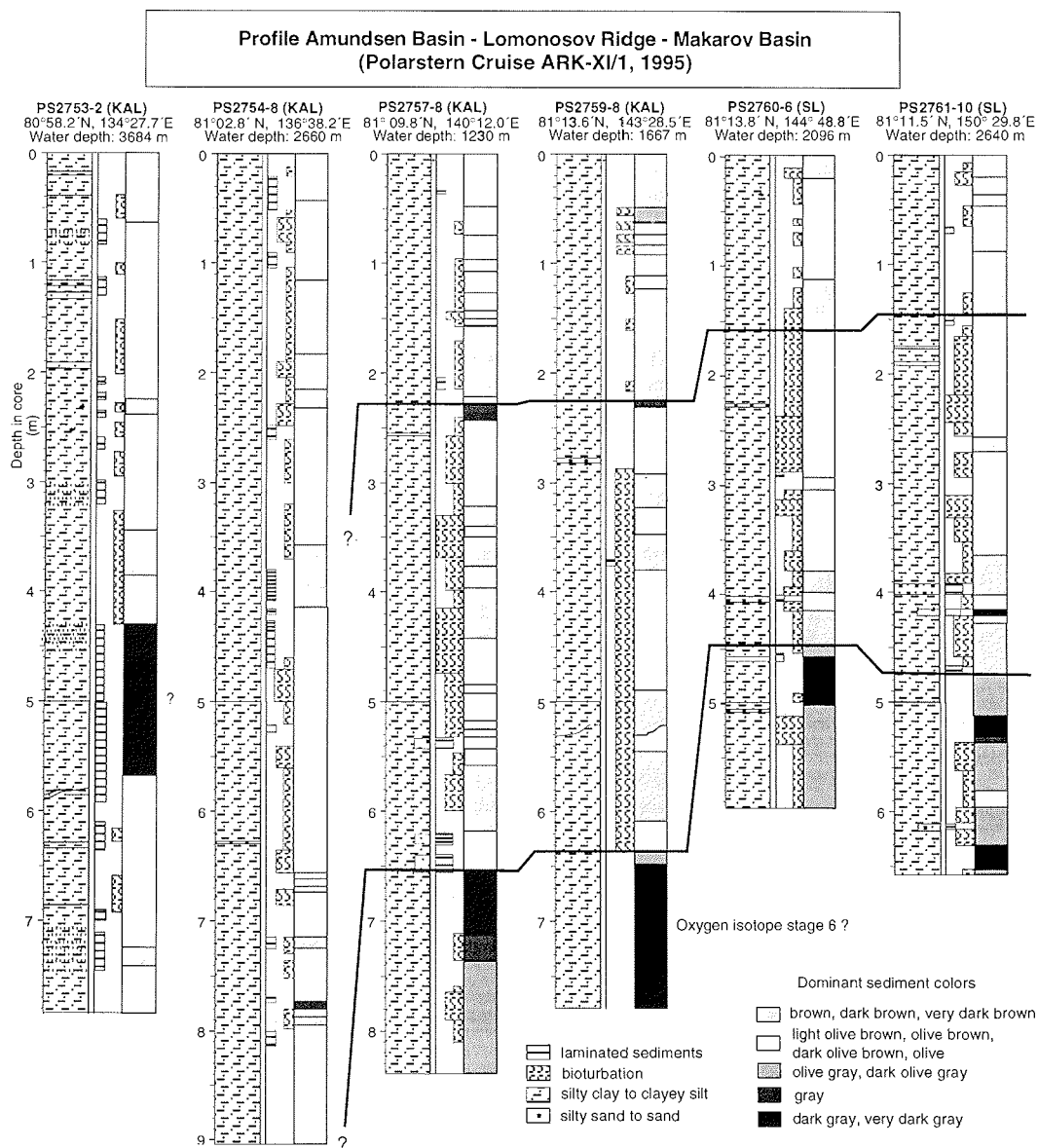


Fig. 9-20: Major lithologies of selected sediment cores from transect F

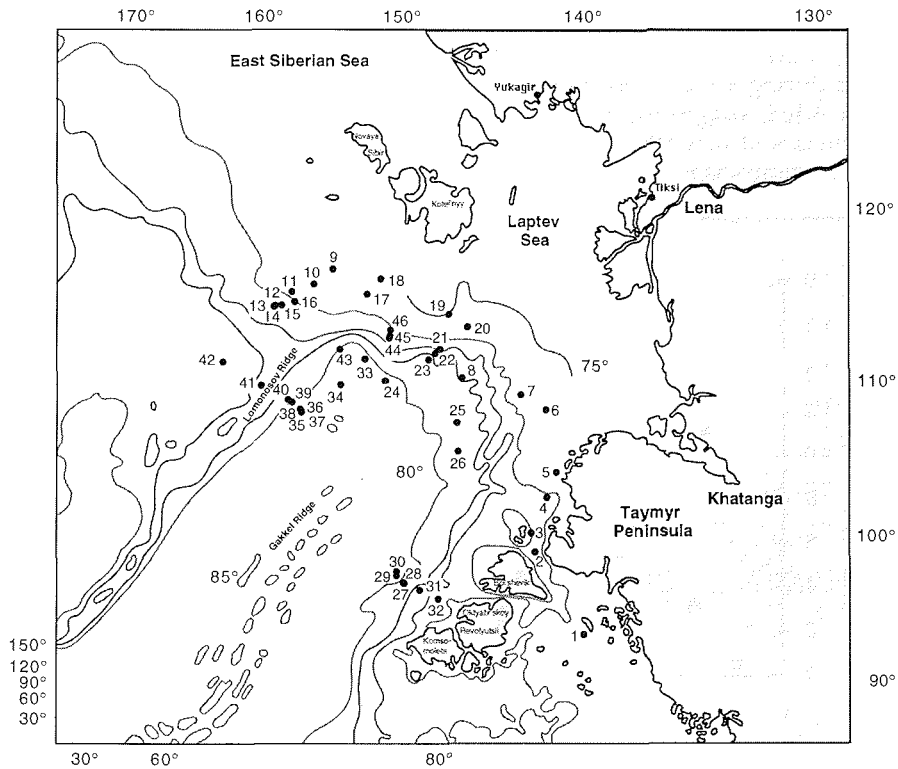


Fig. 9-21: Stations of aerosol sampling during transit

### 9.5. Aerosols (V. Shevchenko)

It is important to know the aerosol size distribution because the sizes of atmospheric particles play an important role in both their chemistry and physics in the atmosphere. Here, preliminary results of the studies of aerosol size distribution over the Laptev Sea are presented. 63 measurements were carried out during the ARK-XI/1 Expedition (Fig. 9-21; table Annex 11.4-2). In general, there is a much greater number of small particles (with sizes from  $0.5 \mu\text{m}$  to  $1 \mu\text{m}$ ) in comparison to large particles. For areas where open water occupies more than 30-50%, there is a positive correlation between wind velocity and the concentration of particles larger than  $0.5 \mu\text{m}$  (Fig. 9-22). This may indicate input of sea salt particles from sea surface microlayer by wind into the atmosphere and the importance of sea salt in the formation of the chemical composition of marine aerosols.

In the northeastern part of the study area, when wind velocity was more than 8 m/s, the concentration of aerosol particles was  $1.05 - 11.23 \text{ particles}\cdot\text{cm}^{-3}$  (on average -  $6.52 \text{ particles}\cdot\text{cm}^{-3}$ ;  $n=10$  samples); but, in the measurement N17 (when wind velocity was 3.3 m/s) we found only  $0.09 \text{ particles}\cdot\text{cm}^{-3}$  (Fig. 9-22).

A typical particle size distribution spectrum for wind velocities  $>8 \text{ m/s}$  in the northeastern area (average of measurements NN24, 35-37, 39-41, 44-46) is presented in the Fig. 9-23. A fast decrease of aerosol particle concentrations with

increasing particle size is obvious. In this figure, the aerosol size distribution measured during a fog is also presented. An increase of particles with sizes of 2-5  $\mu\text{m}$  is recorded, suggesting formation of fog droplets. A more detailed study of the parameters of aerosol size distribution and controlling factors will be carried out later in comparison with others areas (e.g. the Barents and Kara Seas).

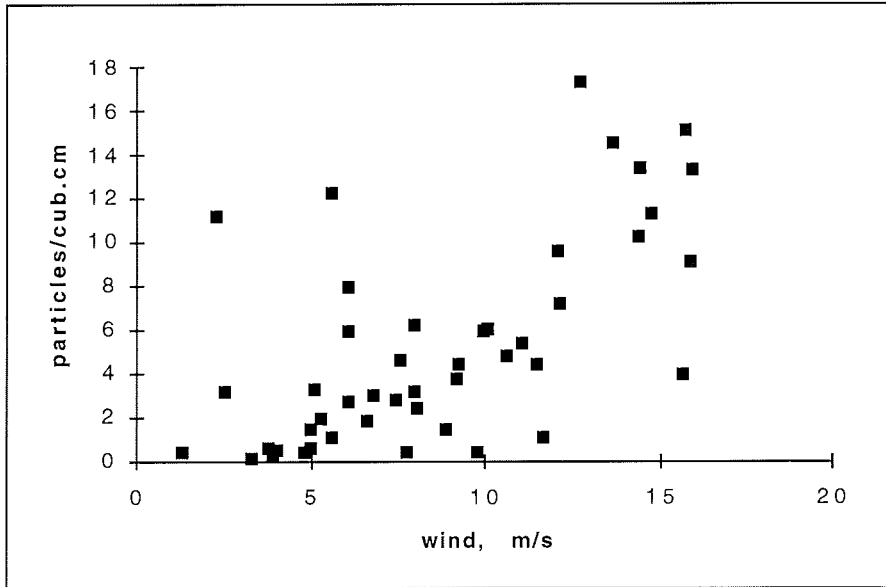


Fig. 9-22: Correlation between wind velocity and concentration of aerosol particles > 0.5  $\mu\text{m}$

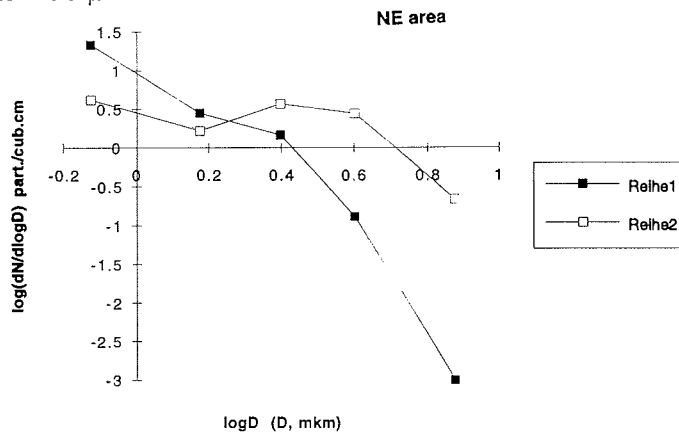


Fig. 9-23: Typical particle size distribution spectrum for wind velocity > 8 m/s in the northeastern part of the study area. Series 1: during winds > 8 m/s; series 2: during fog

## 10. REFERENCES

### CHAPTER 5:

- DORONIN, Yu P., and D. E. KHEISIN (1977): *Sea ice*. Amerind, New Delhi, India.
- EICKEN, H., M. LENSU, M. LEPPÄRANTA, W. B. TUCKER III, A. J. GOW, O. SALMELA (1995): Thickness, structure and properties of level summer multi-year ice in the Eurasian sector of the Arctic Ocean. -J. Geophys. Res. 100, 22697-22710.
- REIMNITZ E., M. McCORMICK, K. McDOUGALL, E. BROUWERS (1993): Sediment export by ice rafting from a coastal polynya, Arctic Alaska, U.S.A. - *Arctic Alpine Res.* 25, 83-98.
- WEISSENBERGER, J., G. DIECKMANN, R. GRADINGER, M. SPINDLER (1992): Sea ice: a cast technique to examine and analyze brine pockets and channel structure. -*Limnol. Oceanogr.*, 37, 179-183.

### CHAPTER 6:

- KOTTMEIER & SULLIVAN (1990): -*Deep-Sea Res.* 37, 1311-1330

### CHAPTER 7:

- FALKENHAUG, T. (1991): Prey composition and feeding rate of *Sagitta elegans* var. *arctica* (Chaetognatha) in the Barents Sea in early summer. - *Polar Res.* 10, 487-506.
- HIRCHE, H.-J. (1989): Egg production of the Arctic copepod *Calanus glacialis*: Laboratory experiments. - *Marine Biology* 103, 311-318
- KOSOBOKOVA, K.N. (1994): Egg production of the dominant copepod species. - *Ber. Polarforsch.* 149, 90-94
- RACHOR, E., HINZ, K., MARTINEZ, P. & B.I. SIRENKO (1994): Zoobenthos (Meiofauna, Macrofauna) in: D.K. Fütterer (ed.): The expedition ARCTIC '93, leg ARK-IX/4 of RV "Polarstern" 1993. - *Ber. Polarforsch.* 149, 94-106.
- SIRENKO, B.I., PETRYASHOV, V.V., RACHOR, E. & K. HINZ (1995): Bottom biocoenoses of the Laptev Sea and adjacent areas. - *Ber. Polarforsch.* 176, 211-221.
- SIRENKO, B.I. et al. (1996): Preliminary data on suprabenthic invertebrates collected during the RV *Polarstern* cruise in the Laptev Sea. - *Polar Biol.* 16, 345-352.
- TERAZAKI, M. (1993): Deep-sea adaptation of the epipelagic chaetognath *Sagitta elegans* in the Japan Sea. - *Mar. Ecol. Prog. Ser.* 98, 79-88.
- TIMOFEEV, S.F. (1991): Distribution and life cycle peculiarities of *Parasagitta elegans* Verrill (*Chaetognatha*) in the south-west part of the Kara Sea. - *Pol. Arch. Hydrobiol.* 37, 461-468.
- TIMOFEEV, S.F. (1995a): Euphausiids in the Laptev Sea. - *Oceanology* (in press; in Russian).

TIMOFEEV, S.F. (1995b): Distribution, biomass and production of *Thysanoessa longicaudata* Kroyer, 1846 (Crustacea, Euphausiacea) in the Arctic. In: Kassens, H. et al. (eds.): Laptev Sea System (Workshop, St. Peterburg, 1994). - Ber. Polarforsch. 176, 200-205.

## CHAPTER 9

- BENTHIEU, A. (1994): Echographiekartierung und physikalische Eigenschaften der oberflächennahen Sedimente in der Laptevsee. - Unpubl. thesis, Univ. Kiel, 80 pp.
- BRYANT, R.W. & ROEMER, B.L. (1983): Structure of the Continental Shelf and Slope of the Northern Gulf of Mexico and its Geohazards and Engineering Constraints. - In: GEYER, R.A. (eds.): Handbook of Geophysical Exploration at Sea, - CRC Mar. Science Ser: 123-185.
- CHILDRESS, J.J. & MICKEL, T.J. (1980): A motion compensated shipboard precision balance system. - Deep Sea Res. 27, 965-970.
- DOWDESWELL, J.A., VILLINGER, H., WHITTINGTON, R.J. & MARIENFELD, P. (1993): Iceberg scouring in Scoresby Sund and on the East Greenland continental shelf. - Mar. Geol. 111, 37-53.
- FÜTTERER, D. K. (ed.; 1994): Die Expedition ARCTIC '93. Der Fahrtabschnitt ARK-IX/4 mit FS "Polarstern" 1993. - Ber. Polarforsch. 149, 244 pp.
- GROBE, H. (1987): A simple method for the determination of ice-rafted debris in sediment cores. - Polarforschung 57, 123-126.
- KUHN, G. (1995): Sedimentphysikalische Untersuchungen. In: GERSONDE, R. (Ed.): Die Expedition ANTARKTIS-XI/2 mit FS "Polarstern" 1993/94. - Ber. Polarforsch. 163, 66-74.
- MAX, M.D., SCHREIBER, R. & CHERKIS, N.Z. (1992): Geological Control of Shallow Gas and Pockmarks in the Norwegian Channel; High Resolution Shallow Subbottom Profiling of Small Scale Features. - Mar. Geophys. Res. 14, 77-85
- NIESSEN, F. (1996): Physical Properties in Marine Sediments. In: KUHN, G. (ed.): Die Expedition ANTARKTIS-XI/4 mit FS "Polarstern" 1994. - Ber. Polarforsch. (in press).
- NOWACZYK, N.R. (1991): Hochauflösende Magnetostratigraphie spätquartärer Sedimente arktischer Meeresgebiete. - Ber. Polarforsch. 78, 187pp.
- RACHOR, E., HINZ, K. & B. SIRENKO (1994): Macrofauna. In: FÜTTERER, D.K. (ed.): The Expedition ARCTIC '93, Leg ARK-IX/4 of RV "Polarstern" 1993. - Ber. Polarforsch. 149, 97-106.
- ROGERS, J.C. & MORACK (1983): Geophysical Detection of Subsea Permafrost. - In: GEYER, R.A. (ed.): Handbook of Geophysical Exploration at Sea, - CRC Mar. Science Ser., 187-210
- SPIESS, V. (1992): Digitale Sedimentechographie - Neue Wege zu einer hochauflösenden Akustostratigraphie. - Ber. Fachb. Geowiss. Univ. Bremen, Nr. 35, 199 pp.
- STEIN, R. (1991): Accumulation of organic carbon in marine sediments. - Lect. Notes Earth Sci., Springer Verlag Heidelberg, Vol. 34, 217 pp.
- WEBER, M.E., NIESSEN, F., KUHN, G. & WIEDICKE, M. (subm.): Multi-Sensor Core Logger - a high resolution tool for estimating geotechnical properties of marine sediments. - J. Geophys. Res.



## ADDITIONAL MATERIAL:

E. RACHOR: POLARSTERN-Expedition ARK XI/1, 7. July - 20. September 1995.  
 Preliminary Cruise Report. - AWI Bremerhaven, November 1995.  
 8 pp. + Annexes 1-6

HSVA-Report (compiled by K.-U. EVERS & P. JOCHMANN):  
 Determination of the Topography of Pressure Ridges in the Laptev Sea.  
 HSVA-Bericht E 258 / 95 (1995), with Appendix (Data and Figures)

Theses, unpublished:

C. HAAS (1996): Bestimmung der Meereisdicke mit seismischen und  
 elektromagnetisch-induktiven Verfahren. - Ph.D.-thesis Univ. Bremen  
 (submitted to: Ber. Polarforsch.)

C. GRAHL (1996): Mikrobielle Aktivität und Biomasse in den Sedimenten der  
 Laptevsee (Arktis). - Diploma thesis Univ. Oldenburg; 77 pp. + 5 tables

Publications:

FAHL, K. & R.STEIN (in press): Modern organic-carbon-deposition in the  
 Laptev Sea and the adjacent continental slope: Surface-water  
 productivity vs. terrigenous input. - Organic Geochemistry

SCHAUER U., R.D. MUENCH, B. RUDELS, L. TIMOKHOV (in press):  
 The impact of eastern Arctic shelf waters on the Nansen Basin  
 intermediate layers. - J. Geophys. Res.



<b>11.</b>	<b>ANNEXES</b>	Page
<b>11.1</b>	<b>Station List</b>	A2
<b>11.2</b>	<b>Weather Data</b>	A18
<b>11.3</b>	<b>Hydrochemistry Data</b>	A28
<b>11.4</b>	<b>Geological Tables and Core Descriptions</b>	A39
<b>11.5</b>	<b>Guidelines</b>	A158
<b>11.6</b>	<b>Participants</b>	A171

## Annex 11.1: Station List

### Explanations:

CTD - Conductivity-temperature-depth probe for oceanography  
 ISP - *In-situ*-pumps  
 HN - Hand net  
 MN - Multi net  
 BN - Bongo net  
 GKG - Großkastengreifer (large box sampler)  
 MUC - Multi-corer  
 SL - Schwerelot (gravity corer)  
 KAL - Kastenlot (long box gravity corer)  
 AGT - Agassiz trawl  
 SD - Secchi disk  
 Handsonde, Lichtsonde - hand-operated small probes  
 (CTD or for light measurements)

### The time (and depth) data in the station list represent:

for ice stations:		beginn and end of work on ice
for oceanographic sampling:	(CTD)	at maximal CTD depth
for geological ssampling:	(MUC, GKG, SL, KAL)	bottom contact
biological stations:	(GKG, MUC, AGT)	bottom contact
	(BN, MN)	at maximal net depth
	(AGT)	at the end of bottom trawling

## A 3

Station	AWI-No.	Date	Time (GMT)	Latitude N	Longitude E	Depth	Activity
Norwegian Sea 36/001	PS2717-1	11.7.95	4:35	70° 00,8'	16° 36,7'	984m	CTD
	PS2717-2	11.7.95	5:28	70° 01,52'	16° 40,03'	1560m	GKG (0cm)
	PS2717-3	11.7.95	6:24	70° 01,65'	16° 41,1'	1488m	MUC
	PS2717-4	11.7.95	7:51	70° 01,65'	16° 42,0'	1458m	SL (0cm)
	PS2717-5	11.7.95	8:28	70° 01,6'	16° 42,57'	1415m	SL (0cm)
South Eastern Kara Sea 36/002	PS2718-1	19.7.95		77° 31,4'	97° 03,9'	129m	CTD
		19.7.95	15:45	77° 31,4'	97° 03,8'		SD
		19.7.95	15:50	77° 31,4'	97° 03,7'		HN
		19.7.95	15:52	77° 31,4'	97° 03,7'		HN
		19.7.95	15:56	77° 31,4'	97° 03,6'		HN
	PS2718-2	19.7.95	16:17	77° 31,3'	97° 03,2'	130m	MN 150 µm
	PS2718-3	19.7.95	16:34	77° 31,4'	97° 03,3'	100m	BN I
	PS2718-4	19.7.95	16:49	77° 31,41'	97° 03,3'	151m	GKG (46cm)
	PS2718-5	19.7.95	17:05	77° 31,45'	97° 03,32'	151m	MUC (32cm)
	PS2718-7	19.7.95	17:32	77° 31,4'	97° 03,6'	153m	MUC (35cm)
	PS2718-6	19.7.95	18:03	77° 31,4'	97° 03,6'	153m	SL (8m)
Western Vilkitsky Strait 36/002a	PS2719-1	19.7.95	19:22	77° 36,48'	97° 32,3'	135m	SL (6,55m)
Central Laptev Sea 36/003		22.7.95	3:03	77° 42,3'	125° 54,6'	1921m	CTD
		22.7.95	3:10	77° 42,4'	125° 55,5'		SD
	PS2720-1	22.7.95	4:26	77° 43,3'	125° 58,8'	2005m	ISP
		22.7.95	6:51	77° 44,0'	126° 04,1'	495m	CTD
		22.7.95	8:28	77° 44,0'	126° 06,1'	2000m	MN 150 µm
		22.7.95	9:48	77° 43,8'	126° 07,9'	500m	MN 150 µm
		22.7.95	10:35	77° 43,8'	126° 07,2'	100m	BN I
	PS2720-2	22.7.95	11:10	77° 43,85'	126° 06,6'	2084m	GKG (0cm)
	PS2720-3	22.7.95	12:09	77° 43,9'	126° 05,8'	2078m	GKG (0cm)
	PS2720-4	22.7.95	13:21	77° 44,3'	126° 05,0'	2086m	MUC (38cm)
	PS2720-5	22.7.95	14:23	77° 44,7'	126° 04,9'	2088m	GKG (47cm)
	PS2720-6	22.7.95	15:25	77° 45,2'	126° 04,7'	2106m	MUC (35cm)
	PS2720-7	22.7.95	16:25	77° 46,1'	126° 07,3'	2054m	SL (6,83m)
East Siberian Sea 36/004	PS2721-1	24.7.95	2:56	78° 00,6'	144° 53,4'	54m	CTD
		24.7.95	2:19	78° 00,6'	144° 53,3'		SD
		24.7.95	2:30	78° 00,5'	144° 53,6'		Lichtmessung
		24.7.95	2:40	78° 00,5'	144° 53,6'	45m	MN 150 µm
		24.7.95	2:57	78° 00,5'	144° 53,7'	45m	MN 55 µm (bio+geo)
		24.7.95	3:11	78° 00,5'	144° 53,1'	30m	BN I
	PS2721-2	24.7.95	3:26	78° 00,5'	144° 52,9'	54m	GKG (bio)
	PS2721-3	24.7.95	3:37	78° 00,5'	144° 52,9'	54m	MUC (24cm)
	PS2721-4	24.7.95	3:51	78° 00,5'	144° 53,3'	54m	GKG (15cm)
	PS2721-5	24.7.95	4:09	78° 00,5'	144° 53,3'	54m	GKG (bio)
	PS2721-6	24.7.95	4:25	78° 00,5'	144° 53,5'	54m	MUC
		24.7.95	5:26	78° 00,6'	144° 54,2'	54m	AGT
	36/005		24.7.95	17:00	78° 31,8'	145° 44,3'	
		24.7.95	19:37	78° 32,1'	145° 43,6'		Eisgruppe a. Bord
36/006	PS2722-1	25.7.95	16:01	78° 58,6'	147° 20,8'	85m	CTD
		25.7.95	15:58	78° 58,6'	147° 20,8'		Eisgruppe v. Bord
		25.7.95	16:30	78° 58,7'	147° 20,7'	75m	BN I
	PS2722-2	25.7.95	16:42	78° 58,73'	147° 20,74'	97m	GKG (bio)
	PS2722-3	25.7.95	17:00	78° 58,7'	147° 20,8'	97m	GKG (43cm)
	PS2722-4	25.7.95	17:20	78° 58,8'	147° 20,9'	97m	SL (3,21m)
		25.7.95	17:27	78° 58,8'	147° 20,9'		SD
		25.7.95	18:17	78° 58,8'	147° 20,9'		Eisgruppe a. Bord
36/007		26.7.95	16:51	79° 27,0'	148° 05,9'		Eisgruppe v. Bord
		26.7.95	23:05	79° 27,6'	148° 06,7'		Eisgruppe a. Bord

Station	AWI-No.	Date	Time (GMT)	Latitude N	Longitude E	Depth	Activity	
36/007	PS2723-1	26.7.95	17:37	79° 27.1'	148° 06.1'	197m	CTD	
	PS2723-2	26.7.95	18:35	79° 27.2'	148° 06.2'	224m	ISP	
		26.7.95	19:25	79° 27.3'	148° 06.5'	197m	CTD	
	PS2723-3	26.7.95	20:21	79° 27.3'	148° 06.6'	200m	MN 150 µm	
		26.7.95	20:47	79° 27.4'	148° 06.7'	100m	BN 1	
		26.7.95	21:03	79° 27.4'	148° 06.7'	224m	GKG (bio)	
		26.7.95	21:47	79° 27.48'	148° 06.75'	224m	GKG (44cm)	
	36/008		28.7.95	2:36	79° 09.0'	146° 20.7'		Eisgruppe v. Bord
		28.7.95	3:48	79° 09.0'	146° 20.7'		Eisgruppe a. Bord	
PS2724-1		28.7.95	2:51	79° 09.0'	146° 20.7'	91m	CTD	
PS2724-2		28.7.95	3:17	79° 09.0'	146° 20.8'	80m	ISP	
		28.7.95	4:31	79° 08.9'	146° 21.1'	75m	MN 150 µm	
		28.7.95	4:46	79° 08.9'	146° 21.1'	80m	BN 1	
PS2724-3		28.7.95	5:04	79° 08.91'	146° 21.18'	102m	GKG (bio)	
PS2724-4		28.7.95	5:24	79° 08.89'	146° 21.26'	100m	GKG (45cm)	
PS2724-5		28.7.95	5:45	79° 08.88'	146° 21.31'	100m	GKG (bio)	
PS2724-6		28.7.95	5:57	79° 08.87'	146° 21.35'	100m	MUC	
PS2724-7		28.7.95	6:36	79° 08.85'	146° 21.47'	99m	MUC	
PS2724-8		28.7.95	7:08	79° 08.83'	146° 21.6'	100m	MUC	
PS2724-9		28.7.95	7:27	79° 08.82'	146° 21.63'	100m	SL(1,78m)	
PS2724-10		28.7.95	8:40	79° 08.8'	146° 21.8'	99m	SL(2,18m)	
		28.7.95	7:27	79° 08.8'	146° 21.8'		SD	
		28.7.95	11:50	79° 08.9'	146° 22.2'		Eisgruppe v. Bord	
		28.7.95	11:50	79° 08.9'	146° 22.2'		Eisgruppe a. Bord	
36/009		PS2725-1	29.7.95	2:17	78° 39.3'	144° 07.3'	67m	CTD
			29.7.95	2:17	78° 39.3'	144° 07.3'		Eisgruppe v. Bord
			29.7.95	6:29	78° 39.3'	144° 07.3'		Eisgruppe a. Bord
		29.7.95	2:45	78° 39.3'	144° 07.4'	65m	MN 150 µm	
		29.7.95	2:58	78° 39.4'	144° 07.6'	65m	BN 1	
	PS2725-2	29.7.95	3:18	78° 39.36'	144° 07.74'	77m	GKG (bio)	
	PS2725-3	29.7.95	3:39	78° 39.37'	144° 07.85'	77m	GKG (43cm)	
	PS2725-4	29.7.95	3:59	78° 39.36'	144° 08.01'	76m	GKG (bio)	
	PS2725-5	29.7.95	4:17	78° 39.36'	144° 08.1'	77m	SL(4,8m)	
	36/010	PS2726-1	30.7.95	2:14	77° 59.9'	140° 01.1'	44m	CTD
		30.7.95	2:32	77° 59.9'	140° 02.4'	40m	MN 150 µm	
		30.7.95	2:44	77° 59.9'	140° 03.1'	40m	BN 1	
		30.7.95	3:02	77° 59.8'	140° 04.2'	40m	MN 55 µm (bio)	
PS2726-2		30.7.95	3:13	77° 59.9'	140° 04.9'	48m	GKG (bio)	
PS2726-3		30.7.95	3:23	77° 59.7'	140° 05.1'	49m	MUC	
PS2726-4		30.7.95	3:35	77° 59.9'	140° 05.3'	48m	GKG	
PS2726-5		30.7.95	3:51	77° 59.7'	140° 05.4'	48m	GKG(30cm)	
PS2726-6		30.7.95	4:02	77° 59.6'	140° 05.7'	50m	MUC	
		30.7.95	4:18	77° 59.4'	140° 06.1'		SD	
PS2726-7		30.7.95	4:28	77° 59.31'	140° 05.94'	51m	MUC	
PS2726-8		30.7.95	4:35	77° 59.19'	140° 05.11'	59m	SL (0cm)	
PS2726-9		30.7.95	5:01	77° 59.19'	140° 04.74'	52m	SL (0cm)	
		30.7.95	5:49	77° 58.9'	140° 04.3'	54m	AGT	
36/011		PS2727-1	30.7.95	10:37	77° 29.9'	140° 00.0'	36m	CTD
		30.7.95	10:56	77° 30.2'	139° 59.7'	25m	MN 150 µm	
		30.7.95	11:07	77° 30.4'	139° 59.7'	31m	BN 1	
	PS2727-2	30.7.95	11:19	77° 30.6'	139° 59.7'	39m	GKG (bio)	
		30.7.95	11:29	77° 30.7'	139° 59.8'		SD	
	PS2727-3	30.7.95	11:38	77° 30.9'	139° 59.8'	39m	GKG (10cm)	
	PS2727-4	30.7.95	11:49	77° 31.1'	140° 00.0'	39m	MUC	
	PS2727-5	30.7.95	12:08	77° 29.9'	140° 00.5'	39m	MUC	
	PS2727-6	30.7.95	12:44	77° 29.9'	140° 00.5'	41m	SL (0cm)	
	PS2727-7	30.7.95	12:55	77° 29.8'	140° 02.1'	40m	SL (0cm)	
	30.7.95	13:08	77° 29.9'	140° 03.5'		Handsonde		
Easrtern Laptev Sea								
36/012	PS2728-1	31.7.95	2:06	77° 14.9'	135° 00.2'	39m	CTD	



Station	AWI-No.	Date	Time (GMT)	Latitude N	Longitude E	Depth	Activity		
36/020	PS2733-4	2.8.95	5:26	77° 42,23'	130° 02,59'	512m	MUC (geo+bio)		
	PS2733-5	2.8.95	6:06	77° 42,20'	130° 02,39'	514m	MUC (geo+bio)		
	PS2733-6	2.8.95	7:13	77° 46,31'	130° 08,24'	527m	SL (5,50m)		
		2.8.95	7:39	77° 46,4'	130° 08,2'	200m	2 Strömungsmesser		
36/021	PS2734-1	2.8.95	10:03	77° 51,0'	130° 02,5'	1089m	CTD		
		2.8.95	9:40	77° 51,0'	130° 02,5'		SD		
		2.8.95	11:26	77° 51,2'	130° 02,3'	1100m	MN 150 µm		
		2.8.95	12:18	77° 51,2'	130° 03,0'	300m	MN 150 µm		
		2.8.95	13:00	77° 51,2'	130° 03,3'	891m	CTD		
		2.8.95	13:55	77° 51,0'	130° 03,6'	500m	MN 55 µm (bio+geo)		
	PS2734-2	2.8.95	14:23	77° 51,0'	130° 03,8'	101m	BN 1		
		2.8.95	14:51	77° 51,0'	130° 03,8'	1139m	GKG (bio)		
		PS2734-3	2.8.95	15:35	77° 51,0'	130° 03,0'	1106m	GKG (13cm)	
		PS2734-4	2.8.95	16:16	77° 50,94'	130° 02,55'	1126m	MUC (geo+bio)	
		PS2734-5	2.8.95	17:06	77° 50,49'	130° 02,31'	1021m	SL (5,13m)	
		2.8.95	17:53	77° 50,4'	130° 04,4'	1242m	AGT		
		2.8.95	19:10	77° 49,7'	130° 14,9'	1330m	AGT		
		36/022	PS2735-1	2.8.95	22:21	77° 55,9'	130° 02,4'	1756m	CTD
				3.8.95	23:08	77° 56,5'	130° 01,1'	1500m	JSP
			PS2735-2	3.8.95	3:27	77° 55,8'	130° 02,5'	500m	BN 2
3.8.95	3:55			77° 55,8'	130° 02,7'	100m	BN 1		
3.8.95	4:22			77° 55,8'	130° 02,7'	500m	MN 55 µm (geo)		
PS2735-3	3.8.95			5:12	77° 55,78'	130° 02,47'	1695m	GKG (bio)	
PS2735-4	3.8.95	6:14	77° 55,87'	130° 02,60'	1719m	GKG (30cm)			
PS2735-5	3.8.95	7:07	77° 55,92'	130° 02,44'	1736m	MUC (geo)			
PS2735-6	3.8.95	8:35	77° 56,1'	130° 02,3'	1787m	MUC (geo+bio)			
36/023	PS2736-4	3.8.95	13:48	78° 09,6'	129° 59'	2289m	CTD		
		3.8.95	13:04	78° 09,6'	129° 58,8'		SD		
		3.8.95	16:11	78° 09,6'	129° 58,7'	2200m	MN 150 µm		
		3.8.95	17:38	78° 09,5'	129° 58,5'	300m	MN 150 µm		
		3.8.95	18:41	78° 09,5'	129° 58,5'	2291m	CTD		
		3.8.95	19:45	78° 09,6'	129° 58,7'	500m	MN 55 µm (geo)		
		3.8.95	21:01	78° 09,6'	129° 58,7'	1486m	BN 2		
		3.8.95	22:04	78° 10,1'	129° 58,8'	100m	BN 1		
	PS2736-1	3.8.95	22:26	78° 10,2'	129° 58,7'	297m	CTD		
		3.8.95	23:58	78° 10,7'	129° 59,2'	2428m	GKG (bio)		
		PS2736-2	4.8.95	1:13	78° 10,8'	129° 59,5'	2324m	MUC (bio+geo)	
		PS2736-3	4.8.95	2:27	78° 10,8'	129° 59,6'	2321m	GKG (41cm)	
		PS2736-5	4.8.95	3:34	78° 10,8'	129° 59,5'	2326m	MUC (bio+geo)	
36/023a	PS2736-6	4.8.95	4:53	78° 11,7'	129° 58,6'	2330m	SL (4,83m)		
		4.8.95	5:26	78° 12,2'	129° 58,7'	2340m	AGT		
		4.8.95	10:10	78° 36,9'	130° 45,7'		Beginn Eisfischen		
		4.8.95	10:18	78° 36,9'	130° 45,2'		Ende Eisfischen		
		4.8.95	10:52	78° 42,1'	130° 57,2'		Beginn Eisfischen		
36/024	PS2737-1	4.8.95	11:46	78° 43,3'	130° 55,9'		Ende Eisfischen		
		PS2737-2	4.8.95	16:11	79° 02,6'	131° 24,8'	3061m	CTD	
			4.8.95	15:25	79° 02,7'	131° 24,7'		Eisgruppe v. Bord	
			4.8.95	21:38	79° 06,9'	131° 26,5'		Eisgruppe a. Bord	
			4.8.95	19:11	79° 04,1'	131° 25,0'	3000m	MN 150 µm	
			4.8.95	21:01	79° 06,2'	131° 26,6'	300m	MN 150 µm	
			4.8.95	22:17	79° 06,5'	131° 26,7'	3145m	CTD	
			4.8.95	23:37	79° 07,8'	131° 26,5'	500m	MN 55 µm (geo)	
		5.8.95	0:05	79° 08,3'	131° 26,1'	100m	BN 1		
		5.8.95	1:10	79° 08,5'	131° 25,9'	1500m	BN 2		
	PS2737-2	5.8.95	2:56	79° 10,4'	131° 25,4'	3171m	GKG(bio)		
	PS2737-3	5.8.95	4:24	79° 12,92'	131° 30,13'	3147m	MUC		
	PS2737-4	5.8.95	5:49	79° 12,92'	131° 28,89'	3155m	GKG (43cm)		
	PS2737-5	5.8.95	7:12	79° 13,58'	131° 30,13'	3151m	MUC (bio+geo)		
	PS2737-6	5.8.95	8:33	79° 13,9'	131° 30,7'	3155m	GKG (bio)		
	PS2737-7	5.8.95	9:41	79° 14,4'	131° 31,0'	3169m	SL (1,85m)		



## A 7

Station	AWI-No.	Date	Time (GMT)	Latitude N	Longitude E	Depth	Activity	
36/024a	PS2738-1	5.8.95	12:11	79° 15,5'	131° 27,9'	3102m	ISP	
	PS2738-2	5.8.95	18:00	79° 18,6'	131° 30,4'	3189m	CTD	
		5.8.95	19:20	79° 19,2'	131° 33,4'	500m	MN 55 µm (geo)	
Western Laptev Sea, Severnaya Zemlya								
36/025		7.8.95	10:54	81° 05,9'	105° 19,6'		Eisgruppe v. Bord	
		7.8.95	12:46	81° 05,9'	105° 21,7'	2507m	CTD	
		7.8.95	15:07	81° 06,2'	105° 23,7'	2500m	MN 150 µm	
		7.8.95	15:49	81° 07,2'	105° 27,0'		SD	
		7.8.95	16:35	81° 07,6'	105° 28,8'	300m	MN 150 µm	
		7.8.95	17:51	81° 07,8'	105° 30,6'	2673m	CTD	
		7.8.95	19:02	81° 08,5'	105° 38,9'	500m	MN 55 µm	
		7.8.95	19:30	81° 05,9'	105° 19,6'		Eisgruppe a. Bord	
		7.8.95	19:52	81° 08,6'	105° 41,7'	500m	BN 2	
		7.8.95	20:18	81° 08,7'	105° 46,9'	100m	BN 1	
		7.8.95	20:42	81° 08,6'	105° 47,4'	487m	CTD	
		PS2739-1	7.8.95	21:42	81° 08,6'	105° 50,6'	2746m	GKG (bio)
		PS2739-2	7.8.95	23:07	81° 08,3'	105° 56,1'	2743m	MUC (geo)
		PS2739-3	8.8.95	0:21	81° 08,2'	105° 59,3'	2769m	GKG (bio)
		PS2739-4	8.8.95	1:34	81° 08,2'	106° 00,1'	2775m	MUC (bio)
		PS2739-5	8.8.95	2:46	81° 07,9'	106° 01,7'	2787m	GKG (40cm)
		PS2739-6	8.8.95	5:03	81° 09,19'	106° 07,4'	2875m	MUC (geo)
36/026		8.8.95	6:49	81° 09,6'	106° 10,3'	2906m	CTD	
36/027		8.8.95	15:49	81° 12,8'	106° 33,7'		Eisgruppe v. Bord	
	PS2740-1	8.8.95	17:38	81° 13,3'	106° 34,6'	3129m	CTD	
		8.8.95	19:20	81° 14,2'	106° 44,3'		Eisgruppe a. Bord	
		8.8.95	21:10	81° 14,3'	106° 45,4'	3000m	MN 150 µm	
		8.8.95	22:50	81° 13,6'	106° 56,4'	300m	MN 150 µm	
		9.8.95	0:03	81° 13,4'	106° 57,2'	3180m	CTD	
		9.8.95	1:16	81° 13,0'	106° 58,7'	500m	MN 55 µm	
		9.8.95	1:45	81° 12,9'	106° 58,7'	100m	BN 1	
		9.8.95	4:29	81° 13,1'	107° 00,4'	1500m	BN 2	
		9.8.95	2:30	81° 12,9'	106° 58,8'		Eisgruppe v. Bord	
		9.8.95	4:47	81° 13,4'	107° 02,5'		SD	
	PS2740-2	9.8.95	6:17	81° 13,6'	107° 04,3'	1040m	ISP	
	PS2740-3	9.8.95	12:12	81° 12,3'	107° 24,1'	3268m	GKG (bio)	
		9.8.95	13:07	81° 11,7'	107° 24,9'		Eisgruppe a. Bord	
	PS2740-4	9.8.95	13:40	81° 11,8'	107° 24,7'	3319m	MUC (bio+geo)	
	PS2740-5	9.8.95	15:21	81° 11,5'	107° 23,9'	3260m	MUC (bio+geo)	
		9.8.95	15:26	81° 11,5'	107° 23,9'		Eisgruppe v. Bord	
	PS2740-6	9.8.95	16:48	81° 11,4'	107° 24,6'	3267m	GKG (bio)	
	PS2740-7	9.8.95	18:20	81° 11,32'	107° 28,28'	3277m	MUC (geo)	
		9.8.95	20:08	81° 11,6'	107° 34,7'		Eisgruppe a. Bord	
	PS2740-8	9.8.95	21:00	81° 11,5'	107° 35,1'	3210m	GKG (41cm)	
	PS2740-9	9.8.95	22:26	81° 10,9'	107° 41,2'	3333m	KAL (0cm)	
36/027a		9.8.95	23:27	81° 10,2'	107° 47,7'	3310m	AGT	
36/028	PS2741-1	10.8.95	6:18	81° 06,34'	105° 23,66'	2530m	KAL (6.30m)	
36/029		10.8.95	9:43	80° 50,1'	104° 10,1'	2059m	CTD	
36/029a		10.8.95	13:02	80° 54,6'	104° 45,3'	2173m	CTD	
		10.8.95	12:49	80° 54,4'	104° 44,8'		Hand-CTD	
36/030	PS2742-1	10.8.95	16:37	80° 47,3'	103° 48,5'	1825m	CTD	
		10.8.95	16:31	80° 47,3'	103° 48,3'		SD	
	PS2742-2	10.8.95	18:05	80° 47,88'	103° 51,10'	1935m	GKG (bio)	
	PS2742-3	10.8.95	19:02	80° 48,26'	103° 54,04'	1956m	GKG (40cm)	
	PS2742-4	10.8.95	19:59	80° 48,47'	103° 57,48'	1994m	MUC (geo)	
	PS2742-5	10.8.95	21:09	80° 47,3'	103° 48,9'	1890m	SL (3.81m)	

## A 8

Station	AWI-No.	Date	Time (GMT)	Latitude N	Longitude E	Depth	Activity
36/030a		10.8.95	22:10	80° 50,4'	103° 36,9'	1850m	AGT
36/031	PS2743-1	11.8.95	2:57	80° 43,6'	103° 18,1'	1177m	CTD
	PS2743-2	11.8.95	3:56	80° 43,9'	103° 17,6'	1149m	ISP
		11.8.95	7:52	80° 45,9'	103° 20,3'	896m	CTD
		11.8.95	8:35	80° 46,2'	103° 21,6'	500m	MN 55 µm (bio+geo)
		11.8.95	9:47	80° 46,4'	103° 23,1'	1435m	MN 150 µm
		11.8.95	10:52	80° 46,8'	103° 26,0'	300m	MN 150 µm
		11.8.95	11:13	80° 46,8'	103° 26,5'	100m	MN 55 µm (bio+geo)
		11.8.95	11:55	80° 46,8'	103° 26,4'	1530m	CTD
		11.8.95	13:11	80° 43,7'	103° 18,1'		HN
		11.8.95	13:13	80° 43,7'	103° 18,1'	100m	BN 1
		11.8.95	13:16	80° 43,7'	103° 18,0'		HN
	PS2743-3	11.8.95	13:39	80° 43,7'	103° 17,1'	1175m	GKG (bio)
	PS2743-4	11.8.95	14:20	80° 43,8'	103° 16,2'	1142m	MUC (bio)
	PS2743-5	11.8.95	14:54	80° 43,9'	103° 14,7'	1107m	GKG (bio)
	PS2743-6	11.8.95	15:28	80° 44,0'	103° 13,2'	1077m	MUC (bio+geo)
	PS2743-7	11.8.95	15:58	80° 44,1'	103° 11,7'	1060m	GKG (19cm)
	PS2743-8	11.8.95	16:30	80° 44,3'	103° 09,84'	1029m	MUC (geo)
	PS2743-9	11.8.95	17:04	80° 44,5'	103° 09,12'	1020m	SL (1.40m)
36/032	PS2744-1	11.8.95	18:49	80° 39,4'	103° 03,3'	546m	CTD
		11.8.95	19:53	80° 39,0'	103° 03,0'	500m	MN 150 µm
		11.8.95	20:15	80° 38,5'	103° 03,2'	500m	MN 55 µm (geo)
		11.8.95	20:41	80° 38,0'	103° 02,9'	100m	BN 1
	PS2744-2	11.8.95	21:00	80° 37,8'	103° 02,7'	532m	GKG(bio)
	PS2744-3	11.8.95	21:22	80° 37,5'	103° 02,9'	507m	MUC (bio+geo)
	PS2744-4	11.8.95	21:48	80° 37,1'	103° 02,8'	459m	GKG (bio)
	PS2744-5	11.8.95	22:09	80° 36,4'	103° 03,0'	459m	MUC (geo)
	PS2744-6	11.8.95	22:32	80° 36,4'	103° 03,2'	455m	GKG (36cm)
	PS2744-7	11.8.95	22:56	80° 36,2'	103° 03,3'	458m	MUC (0cm)
36/033a		12.8.95	1:58	80° 21,9'	101° 52,2'	230m	AGT
36/033		12.8.95	3:09	80° 21,9'	102° 02,1'	Abbruch	CTD
	PS2745-1	12.8.95	3:26	80° 25,1'	102° 01,5'	240m	ISP
		12.8.95	4:52	80° 25,5'	101° 59,9'		SD
		12.8.95	5:24	80° 25,5'	101° 58,4'	245m	MN 150 µm
		12.8.95	6:06	80° 25,9'	101° 58,7'	245m	MN 55 µm (bio+geo)
	PS2745-2	12.8.95	6:35	80° 25,8'	101° 59,4'	237m	CTD
		12.8.95	7:04	80° 25,6'	102° 00,1'	100m	BN 1
		12.8.95	8:25	80° 25,5'	102° 01,3'	228m	CTD
	PS2745-3	12.8.95	8:49	80° 25,4'	102° 02,1'	255m	GKG (bio)
	PS2745-4	12.8.95	9:06	80° 25,4'	102° 02,7'	264m	MUC (bio)
	PS2745-5	12.8.95	9:22	80° 25,2'	102° 03,9'	256m	GKG (bio)
	PS2745-6	12.8.95	9:43	80° 25,0'	102° 05,0'	265m	MUC (bio+geo)
	PS2745-7	12.8.95	9:58	80° 24,9'	102° 05,4'	255m	GKG (33cm)
36/034		12.8.95	16:35	79° 29,3'	103° 49,3'		Parasound Profiling
		12.8.95	19:35	79° 22,4'	104° 51,3'		PP End
36/035		13.8.95	4:17	79° 45,0'	102° 44,6'	316m	CTD
36/036	PS2746-1	13.8.95	7:02	79° 29,3'	104° 28,3'	89m	CTD
		13.8.95	7:08	79° 29,3'	104° 28,2'		SD
		13.8.95	7:19	79° 29,3'	104° 28,5'	92m	BN 1
	PS2746-2	13.8.95	7:34	79° 29,3'	104° 29,0'	106m	MUC (bio+geo)
	PS2746-3	13.8.95	7:49	79° 29,3'	104° 29,2'	106m	GKG (bio)
	PS2746-4	13.8.95	8:00	79° 29,3'	104° 29,7'	101m	GKG (bio)
	PS2746-5	13.8.95	8:11	79° 29,4'	104° 30,4'	104m	MUC (geo)
36/037		14.8.95	2:53	77° 41,2'	115° 06,4'	171m	CTD

## A 9

Station	AWI-No.	Date	Time (GMT)	Latitude N	Longitude E	Depth	Activity
36/038		14.8.95	8:37	77° 17,0'	119° 56,3'	248m	CTD
36/039		14.8.95	16:17	77° 06,9'	126° 39,3'	241m	CTD
36/040		15.8.95	4:46	78° 32,1'	133° 57,4'	1762m	CTD
		15.8.95	6:24	78° 33,3'	133° 55,4'		Verankerung LOMO 1'95
		15.8.95	8:27	78° 30,8'	133° 57,7'		ausgesetzt
Eastern Laptev Sea							
36/040a		15.8.95	9:16	78° 29,9'	133° 56,6'		SD
	PS2747-1	15.8.95	9:26	78° 30,2'	133° 57,3'	1738m	CTD
	PS2747-2	15.8.95	11:05	78° 31,9'	133° 51,9'	1800m	ISP
		15.8.95	15:33	78° 31,0'	133° 49,5'	1700m	MN 150 µm
		15.8.95	16:42	78° 30,7'	133° 49,5'	300m	MN 150 µm
		15.8.95	17:20	78° 30,5'	133° 49,7'	500m	MN 55 µm (bio+geo)
		15.8.95	18:30	78° 30,4'	133° 50,0'	1500m	BN 2
		15.8.95	19:27	78° 30,0'	133° 49,5'	100m	BN 1
	PS2747-3	15.8.95	20:00	78° 29,9'	133° 49,0'	1733m	GKG (bio)
	PS2747-4	15.8.95	20:50	78° 30,1'	133° 48,6'	1773m	MUC (bio+geo) (0cm)
	PS2747-5	15.8.95	21:44	78° 30,4'	133° 46,9'	1818m	MUC (bio+geo)
	PS2747-6	15.8.95	22:34	78° 30,6'	133° 45,3'	1840m	GKG (bio)
	PS2747-7	15.8.95	23:25	78° 30,7'	133° 43,9'	1970m	MUC (bio)
	PS2747-8	16.8.95	0:16	78° 30,8'	133° 42,9'	1995m	GKG (34cm)
	PS2747-9	16.8.95	1:15	78° 30,1'	133° 49,3'	1756m	SL (6,90m)
36/040b		16.8.95	1:45	78° 30,3'	133° 48,1'	2300m	AGT
36/041		16.8.95	5:20	78° 36,9'	133° 52,5'	1912m	CTD
36/042		16.8.95	8:49	78° 43,5'	134° 44,7'		Eisgruppe v. Bord
	PS2748-1	16.8.95	10:31	78° 43,1'	134° 44,3'	2074m	CTD
		16.8.95	12:06	78° 42,2'	134° 40,8'		Pütz
		16.8.95	12:39	78° 42,3'	134° 41,8'	2000m	MN 150 µm
		16.8.95	14:33	78° 41,9'	134° 37,1'	300m	MN 150 µm
		16.8.95	15:29	78° 41,9'	134° 36,7'	2104m	CTD
		16.8.95	16:25	78° 41,9'	134° 36,2'	100m	BN 1
	PS2748-2	16.8.95	16:55	78° 41,87'	134° 36,45'	2122m	GKG (38cm)
	PS2748-3	16.8.95	17:42	78° 41,82'	134° 37,12'	2121m	SL (6,35m)
	PS2748-4	16.8.95	18:33	78° 41,73'	134° 37,97'	2104m	GKG (bio+geo)
		16.8.95	18:40	78° 41,6'	134° 38,5'		Eisgruppe a. Bord
	PS2748-5	16.8.95	19:27	78° 41,56'	134° 39,11'	2099m	MUC (bio+geo)
	PS2748-6	16.8.95	20:21	78° 41,46'	134° 39,9'	2086m	GKG (bio)
		16.8.95	20:35	78° 41,1'	134° 41,0'		Eisgruppe v. Bord
		16.8.95	21:35	78° 40,7'	134° 41,7'		Eisgruppe a. Bord
36/043		17.8.95	0:29	78° 48,6'	135° 00,0'	2478m	CTD
36/044		17.8.95	8:08	79° 10,9'	135° 03,04'		Eisgruppe v. Bord
	PS2749-1	17.8.95	9:43	79° 10,6'	135° 03,04'	2850m	CTD
	PS2749-2	17.8.95	11:25	79° 09,2'	135° 04,9'	2801m	ISP
		17.8.95	13:15	79° 08,3'	135° 02,8'		Eisgruppe a. Bord
		17.8.95	15:20	79° 08,2'	135° 00,5'		Eisgruppe v. Bord
		17.8.95	17:09	79° 08,2'	135° 00,5'	563m	CTD
		17.8.95	18:10	79° 08,3'	135° 01,2'		Eisgruppe a. Bord
		17.8.95	20:35	79° 07,9'	135° 05,3'	100m	BN 1
		17.8.95	20:58	79° 07,9'	135° 05,7'	500m	MN 55 µm (geo)
	PS2749-3	17.8.95	21:44	79° 07,6'	135° 06,8'	2783m	GKG (36cm)
	PS2749-4	17.8.95	22:41	79° 07,2'	135° 08,3'	2769m	SL (6,20m)
	PS2749-5	17.8.95	23:53	79° 06,8'	135° 09,4'	2778m	MUC (bio+geo)
	PS2749-6	18.8.95	0:54	79° 06,02'	135° 09,5'	2769m	GKG (bio)
	PS2749-7	18.8.95	2:00	79° 05,9'	135° 09,2'	2758m	MUC (bio+geo)
	PS2749-8	18.8.95	3:00	79° 05,6'	135° 08,4'	2757m	GKG (bio)
		18.8.95	4:07	79° 05,5'	135° 08,5'		Eisgruppe v. Bord
		18.8.95	5:33	79° 05,6'	135° 08,7'		Eisgruppe a. Bord

## A10

Station	AWI-No.	Date	Time (GMT)	Latitude N	Longitude E	Depth	Activity
36/045	PS2750-1	18.8.95	14:10	79° 59,3'	134° 54,3'		Eisgruppe v. Bord
		18.8.95	14:57	79° 59,3'	134° 54,8'	3353m	CTD
		18.8.95	17:50	79° 59,6'	134° 52,7'	3200m	MN 150 µm
		18.8.95	19:26	80° 00,0'	134° 55,6'	300m	MN 150 µm
		18.8.95	20:30	80° 00,0'	134° 56,9'		Eisgruppe a. Bord
		18.8.95	20:41	80° 00,0'	134° 56,4'	3352m	CTD
		18.8.95	22:07	79° 59,7'	134° 59,9'	500m	MN 55µm (bio+geo)
		18.8.95	23:12	79° 59,5'	135° 00,3'	1500m	BN 2
		18.8.95	0:17	79° 59,0'	135° 00,4'	100m	BN 1
		18.8.95	1:13	79° 58,9'	135° 00,1'	3358m	GKG (43cm)
		18.8.95	2:30	79° 58,8'	134° 59,2'	3366m	SL (4,80)
		18.8.95	4:02	79° 59,0'	134° 58,72'	3358m	MUC (bio+geo)
		18.8.95	5:17	79° 59,19'	134° 59,82'	3344m	GKG (bio)
		18.8.95	6:43	79° 59,32'	135° 02,35'	3353m	MUC (bio+geo)
18.8.95	7:54	79° 59,28'	135° 04,51'	3337m	GKG (bio)		
36/046	PS2751-1	19.8.95	12:44	80° 14,6'	133° 46,0'	3485m	CTD
	PS2751-2	19.8.95	14:42	80° 14,3'	133° 46,2'	3510m	GKG (bio)
	PS2751-3	19.8.95	16:03	80° 14,53'	133° 45,4'	3509m	GKG (bio+geo) (36cm)
Lomonosov Ridge 36/047							
36/047	PS2752-1	20.8.95	4:50	80° 53,0'	131° 03,4'		Eisgruppe v. Bord
		20.8.95	5:58	80° 53,0'	131° 03,4'	3846m	CTD
		20.8.95	7:40	80° 54,0'	131° 04,8'		Eisgruppe a. Bord
		20.8.95	8:15	80° 54,1'	131° 05,2'		Eisgruppe v. Bord
		20.8.95	8:18	80° 54,1'	131° 05,3'	3800m	ISP
		20.8.95	14:27	80° 54,8'	131° 09,0'	3837m	CTD
		20.8.95	17:19	80° 55,1'	132° 00,0'	3500m	MN 150 µm
		20.8.95	18:47	80° 55,5'	131° 12,8'		SD
		20.8.95	19:07	80° 55,5'	131° 12,8'	300m	MN 150 µm
		20.8.95	19:25	80° 55,5'	131° 13,4'	100m	BN 1
		20.8.95	20:22	80° 55,6'	131° 13,8'	1500m	BN 2
		20.8.95	21:32	80° 55,6'	131° 16,6'	500m	MN 55 µm (geo)
		20.8.95	22:32	80° 55,5'	131° 16,6'	3833m	GKG (bio)
		21.8.95	0:17	80° 55,4'	131° 19,1'	3831m	MUC (bio+geo)
		21.8.95	1:43	80° 55,4'	131° 19,5'	3824m	GKG (bio)
		21.8.95	3:14	80° 55,4'	131° 19,5'	3827m	MUC (bio+geo)
		21.8.95	4:36	80° 55,79'	131° 20,33'	3827m	GKG (geo)
		21.8.95	5:20	80° 55,9'	131° 20,8'		Eisgruppe v. Bord
		21.8.95	5:53	80° 56,08'	131° 21,84'	3823m	GKG (29cm)
		21.8.95	7:08	80° 56,37'	131° 24,00'	3825m	SL (5,30)
		21.8.95	7:57	80° 56,5'	131° 25,6'		Eisgruppe a. Bord
36/048a	PS2753-1	21.8.95	13:07	80° 58,0'	134° 26,9'		Eisgruppe v. Bord
		21.8.95	13:51	80° 58,0'	134° 27,3'	3628m	GKG (38cm)
		21.8.95	15:00	80° 58,1'	134° 27,5'		Eisgruppe a. Bord
		21.8.95	15:12	80° 58,2'	134° 27,7'	3644m	KAL (7,84m)
21.8.95	16:42	80° 58,43'	134° 28,60'	3628m	GKG (bio)		
36/048		21.8.95	20:25	80° 58,7'	135° 56,9'	2850m	CTD
36/049	PS2754-1	21.8.95	0:09	81° 01,7'	136° 55,1'	2343m	CTD
		22.8.95	1:38	81° 01,9'	136° 47,4'	2450m	ISP
		22.8.95	6:48	81° 03,1'	136° 34,5'	974m	CTD
		22.8.95	8:56	81° 03,4'	136° 32,4'	2600m	MN 150 µm
		22.8.95	8:58	81° 03,7'	136° 29,7'		Eisgruppe v. Bord
		22.8.95	9:15	81° 03,7'	136° 29,0'		SD
		22.8.95	10:33	81° 03,8'	136° 26,6'	300m	MN 150 µm
		22.8.95	11:07	81° 03,9'	136° 25,5'	500m	BN 2
		22.8.95	11:33	81° 04,0'	136° 24,0'	100m	BN 1
		22.8.95	12:19	81° 04,1'	136° 21,6'	2806m	GKG (bio)
		22.8.95	13:26	81° 04,2'	136° 20,2'	2784m	GKG (bio)
		22.8.95	14:43	81° 04,6'	136° 15,9'	2861m	MUC (bio+geo)
		22.8.95	15:51	81° 04,9'	136° 13,2'	2887m	GKG (bio)
		22.8.95	17:08	81° 05,29'	136° 10,45'	2905m	MUC (bio+geo)
22.8.95	17:50	81° 03,7'	136° 09,6'		Eisgruppe a. Bord		
22.8.95	19:32	81° 02,85'	136° 38,22'	2619m	KAL (9,05m)		
22.8.95	20:42	81° 03,0'	136° 37,5'	2590m	GKG (geo) (0cm)		

## A11

Station	AWI-No.	Date	Time (GMT)	Latitude N	Longitude E	Depth	Activity
36/049	PS2754-10	22.8.95	21:54	81° 03,0'	136° 36,2'	2650m	GKG (geo) (0cm)
36/050	PS2755-1	23.8.95	1:35	81° 02,2'	138° 24,6'	1987m	CTD
	PS2755-2	23.8.95	2:52	81° 02,5'	138° 20,2'	2019m	GKG (bio)
	PS2755-3	23.8.95	3:50	81° 02,8'	138° 18,0'	2026m	MUC (bio+geo)
	PS2755-4	23.8.95	4:41	81° 03,03'	138° 16,49'	2027m	GKG (bio)
	PS2755-5	23.8.95	5:31	81° 03,31'	138° 15,06'	2033m	GKG (38cm)
	PS2755-6	23.8.95	6:18	81° 03,56'	138° 14,25'	2046m	SL (6,50m)
36/051		23.8.95	8:20	81° 04,1'	138° 56,1'	1703m	CTD
	PS2756-1	23.8.95	9:08	81° 04,3'	138° 55,2'		Verankerung LOMO 2 ausgesetzt
36/051a		23.8.95	12:10	81° 06,4'	138° 56,5'		Eisgruppe v. Bord
	PS2756-2	23.8.95	12:31	81° 06,4'	138° 57,0'	1755m	CTD
	PS2756-3	23.8.95	13:56	81° 06,6'	138° 53,6'	1750m	ISP
		23.8.95	13:57	81° 06,6'	138° 53,6'		Eisgruppe a. Bord
		23.8.95	14:57	81° 06,7'	138° 51,7'		Eisgruppe v. Bord
		23.8.95	18:31	81° 07,3'	138° 47,3'	1750m	MN 150 µm
		23.8.95	19:42	81° 07,8'	138° 44,9'	300m	MN 150 µm
		23.8.95	20:04	81° 07,9'	138° 44,6'	100m	BN 1
		23.8.95	20:20	81° 07,9'	138° 44,3'		Eisgruppe a. Bord
		23.8.95	21:02	81° 07,9'	138° 44,3'	1500m	BN 2
	PS2756-4	23.8.95	22:12	81° 08,3'	138° 43,2'	1800m	GKG (bio)
	PS2756-5	23.8.95	22:56	81° 08,4'	138° 42,8'	1810m	MUC (bio+geo)
	PS2756-6	23.8.95	23:38	81° 08,5'	138° 42,1'	1802m	GKG (bio)
	PS2756-7	24.8.95	0:22	81° 08,65'	138° 41,1'	1802m	MUC (bio+geo)
	PS2756-8	24.8.95	1:02	81° 08,7'	138° 40,1'	1797m	GKG (geo) (0cm)
		24.8.95	1:08	81° 08,7'	138° 39,8'		Eisgruppe v. Bord
		24.8.95	1:26	81° 08,7'	138° 39,4'		Eisgruppe a. Bord
	PS2756-9	24.8.95	1:45	81° 08,7'	138° 38,9'	1793m	GKG (39cm)
	PS2756-10	24.8.95	2:27	81° 08,9'	138° 37,7'	1805m	SL (7,20m)
36/051b		24.8.95	3:46	81° 08,9'	138° 54,6'	1838m	AGT
36/052		24.8.95	8:50	81° 09,6'	140° 09,4'		Eisgruppe v. Bord
	PS2757-1	24.8.95	9:45	81° 09,6'	140° 09,3'	1190m	CTD
	PS2757-2	24.8.95	11:08	81° 10,0'	140° 08,3'	1200m	ISP
		24.8.95	12:24	81° 09,6'	140° 09,4'		Eisgruppe a. Bord
		24.8.95	15:17	81° 10,6'	140° 06,3'	1200m	MN 150 µm
		24.8.95	16:08	81° 10,8'	140° 04,7'	300m	MN 150 µm
		24.8.95	16:26	81° 10,9'	140° 04,6'	100m	BN 1
	PS2757-3	24.8.95	16:49	81° 10,96'	140° 04,17'	1278m	GKG (bio)
	PS2757-4	24.8.95	17:25	81° 11,07'	140° 03,59'	1276m	MUC (bio+geo)
	PS2757-5	24.8.95	17:59	81° 11,2'	140° 02,97'	1276m	GKG (bio)
	PS2757-6	24.8.95	18:40	81° 11,37'	140° 02,67'	1290m	MUC (bio+geo)
	PS2757-7	24.8.95	19:47	81° 09,64'	140° 12,07'	1223m	GKG (32cm)
	PS2757-8	24.8.95	20:27	81° 09,8'	140° 12,0'	1241m	KAL (8,40m)
36/052a		24.8.95	1:56	81° 09,9'	140° 27,0'	1340m	CTD
36/053	PS2758-1	25.8.95	2:07	81° 09,5'	141° 52,1'	920m	CTD
	PS2758-2	25.8.95	3:00	81° 09,8'	141° 51,3'	937m	GKG (31cm)
		25.8.95	3:31	81° 10,0'	141° 51,3'		Pütz
	PS2758-3	25.8.95	3:34	81° 09,9'	141° 51,4'	924m	SL (4,90m)
		25.8.95	4:22	81° 10,8'	141° 47,1'	940m	AGT
36/054		25.8.95	7:48	81° 09,7'	142° 35,5'	1361m	CTD
36/055	PS2759-1	25.8.95	10:49	81° 09,1'	143° 25,5'	1650m	CTD
		25.8.95	10:26	81° 09,2'	143° 25,5'		Eisgruppe v. Bord
	PS2759-2	25.8.95	12:07	81° 09,5'	143° 25,4'	1600m	ISP
		25.8.95	12:30	81° 09,7'	143° 25,2'		Pütz
		25.8.95	12:54	81° 09,8'	143° 25,1'		SD

Station	AWI-No.	Date	Time (GMT)	Latitude N	Longitude E	Depth	Activity
36/055		25.8.95	13:41	81° 10,0'	143° 25,5'		Eisgruppe a. Bord
		25.8.95	15:07	81° 10,4'	143° 24,4'		Eisgruppe v. Bord
		25.8.95	16:39	81° 10,6'	143° 24,2'	1600m	MN 150µm
		25.8.95	17:45	81° 11,3'	143° 24,0'	300m	MN 150 µm
		25.8.95	18:04	81° 11,5'	143° 23,9'	100m	BN 1
		25.8.95	18:58	81° 11,5'	143° 24,0'	1500m	BN 2
		25.8.95	19:35	81° 12,1'	143° 24,3'		Eisgruppe a. Bord
	PS2759-3	25.8.95	20:06	81° 12,2'	143° 24,5'	1590m	GKG (bio)
	PS2759-4	25.8.95	20:49	81° 12,4'	143° 24,7'	1588m	MUC (bio+geo)
	PS2759-5	25.8.95	21:30	81° 12,8'	143° 25,5'	1582m	GKG (bio)
PS2759-6	25.8.95	22:13	81° 13,0'	143° 26,0'	1600m	MUC (bio+geo)	
PS2759-7	25.8.95	22:55	81° 13,3'	143° 27,0'	1610m	GKG (39cm)	
PS2759-8	25.8.95	23:38	81° 13,6'	143° 28,1'	1625m	KAL (7,80m)	
36/056	PS2760-1	26.8.95	3:31	81° 12,1'	144° 43,6'	1993m	CTD
	PS2760-2	26.8.95	4:52	81° 12,7'	144° 45,66'	2027m	GKG (bio)
		26.8.95	4:43	81° 12,7'	144° 45,7'		PÜTZ
	PS2760-3	26.8.95	5:48	81° 12,89'	144° 46,56'	2036m	MUC (bio+geo)
	PS2760-4	26.8.95	6:38	81° 13,12'	144° 47,77'	2039m	GKG (bio)
	PS2760-5	26.8.95	7:30	81° 13,63'	144° 47,97'	2044m	GKG (37cm)
	PS2760-6	26.8.95	8:21	81° 13,7'	144° 48,2'	2050m	SL (6,00m)
		26.8.95	9:19	81° 15,1'	144° 57,6'	2090m	AGT
36/056a		26.8.95	16:09	81° 10,6'	147° 23,7'	2386m	CTD
East Siberian Sea							
36/057	PS2761-1	26.8.95	22:18	81° 12,1'	150° 05,5'	2569m	CTD
		26.8.95	21:52	81° 12,1'	150° 05,5'		Eisgruppe v. Bord
		26.8.95	23:51	81° 12,4'	150° 07,1'		Eisgruppe a. Bord
	PS2761-2	26.8.95	23:57	81° 12,4'	150° 07,1'	2520m	ISP
		27.8.95	4:51	81° 12,6'	150° 14,0'	300m	CTD
		27.8.95	6:19	81° 12,5'	150° 14,8'	2500m	MN 150 µm
		27.8.95	7:41	81° 12,0'	150° 18,0'	300m	MN 150 µm
		27.8.95	8:48	81° 11,9'	150° 18,3'	1500m	BN 2
		27.8.95	9:47	81° 11,5'	150° 19,3'	100m	BN 1
	PS2761-3	27.8.95	10:18	81° 11,5'	150° 19,3'	2538m	GKG (bio)
	PS2761-4	27.8.95	11:21	81° 11,4'	150° 19,7'	2586m	MUC (bio+geo)
	PS2761-5	27.8.95	12:18	81° 11,5'	150° 20,7'	2590m	GKG (bio)
		27.8.95	12:20	81° 11,5'	150° 21,1'		Eisgruppe a. Bord
	PS2761-6	27.8.95	13:26	81° 11,5'	150° 21,7'	2592m	MUC (bio+geo)
		27.8.95	13:40	81° 11,6'	150° 23,0'		Eisgruppe v. Bord
	PS2761-7	27.8.95	14:26	81° 11,6'	150° 23,6'	2591m	GKG (geo) (0cm)
	PS2761-8	27.8.95	15:25	81° 11,6'	150° 25,3'	2590m	GKG (bio)
	27.8.95	15:34	81° 11,6'	150° 26,4'		Eisgruppe a. Bord	
PS2761-9	27.8.95	16:27	81° 11,6'	150° 27,2'	2587m	GKG (32cm)	
PS2761-10	27.8.95	17:27	81° 11,5'	150° 29,0'	2590m	SL (6,60m)	
36/058		27.8.95	22:23	80° 50,6'	150° 01,0'	2282m	CTD
36/059	PS2762-1	28.8.95	3:28	80° 30,5'	150° 08,2'	1993m	CTD
		28.8.95	4:20	80° 30,2'	150° 11,9'		Pütz
		28.8.95	4:27	80° 30,2'	150° 11,9'	100m	BN 1
	PS2762-2	28.8.95	4:59	80° 30,06'	150° 13,26'	2010m	GKG (bio)
	PS2762-3	28.8.95	5:55	80° 29,79'	150° 14,64'	2009m	MUC (bio+geo)
	PS2762-4	28.8.95	6:42	80° 29,55'	150° 15,69'	1997m	GKG (38cm)
	PS2762-5	28.8.95	7:36	80° 29,37'	150° 16,38'	1995m	MUC (bio+geo)
PS2762-6	28.8.95	8:28	80° 29,3'	150° 16,8'	1965m	SL (6,50m)	
36/060		28.8.95	11:14	80° 20,4'	149° 58,4'	1710m	CTD
		28.8.95	13:37	80° 19,25'	150° 03,45'		Verankerung LOMO 3 ausgesetzt
	PS2763-1	28.8.95	14:57	80° 18,7'	150° 08,6'	1643m	CTD
		28.8.95	15:18	80° 18,6'	150° 10,6'		Eisgruppe v. Bord
	PS2763-2	28.8.95	16:14	80° 18,5'	150° 12,6'	1620m	ISP
		28.8.95	20:36	80° 17,5'	150° 17,5'	1500m	MN 150 µm
		28.8.95	21:00	80° 17,3'	150° 18,2'		Eisgruppe a. Bord
		28.8.95	21:12	80° 17,3'	150° 18,2'		SD
	28.8.95	21:46	80° 17,3'	150° 18,3'	300m	MN 150 µm	

## A 13

Station	AWI-No.	Date	Time (GMT)	Latitude N	Longitude E	Depth	Activity
36/060		28.8.95	22:22	80° 17,23'	150° 18,4'	500m	MN 55 µm (bio)
		28.8.95	22:50	80° 17,2'	150° 18,7'	100m	BN 1
		28.8.95	23:46	80° 17,2'	150° 18,8'	1500m	BN 2
	PS2763-3	29.8.95	1:00	80° 17,2'	150° 20,6'	1602m	GKG (bio)
	PS2763-4	29.8.95	1:47	80° 17,7'	150° 21,7'	1625m	MUC (bio+geo)
	PS2763-5	29.8.95	2:32	80° 17,1'	150° 22,9'	1609m	GKG (bio)
	PS2763-6	29.8.95	3:20	80° 17,0'	150° 24,5'	1614m	MUC (bio+geo)
	PS2763-7	29.8.95	4:09	80° 16,85'	150° 26,14'	1606m	KAL (7,84m)
	PS2763-8	29.8.95	4:54	80° 16,83'	150° 27,35'	1588m	GKG (41cm)
		29.8.95	6:54	80° 16,0'	150° 19,5'	1580m	AGT
36/061		29.8.95	9:04	80° 12,3'	149° 52,4'	1421m	CTD
36/062		29.8.95	11:20	80° 05,0'	149° 46,9'		Eisgruppe v. Bord
	PS2764-1	29.8.95	11:44	80° 05,0'	149° 46,4'	1035m	CTD
	PS2764-2	29.8.95	13:13	80° 05,0'	149° 47,7'	1030m	ISP
		29.8.95	13:31	80° 05,1'	149° 48,0'		Eisgruppe a. Bord
		29.8.95	14:36	80° 05,1'	149° 49,0'		SD
		29.8.95	16:35	80° 04,8'	149° 50,5'	300m	CTD
		29.8.95	17:49	80° 04,8'	149° 50,7'	1000m	MN 150 µm
		29.8.95	18:43	80° 04,5'	149° 49,8'	300m	MN 150 µm
		29.8.95	19:20	80° 04,5'	149° 50,0'	500m	MN 55 µm (bio)
		29.8.95	20:15	80° 04,1'	149° 49,7'	930m	BN 2
		29.8.95	20:51	80° 04,0'	149° 49,0'	100m	BN 1
	PS2764-3	29.8.95	21:12	80° 04,0'	149° 49,2'	991m	GKG (bio)
	PS2764-4	29.8.95	21:43	80° 04,0'	149° 49,1'	997m	MUC (bio+geo)
	PS2764-5	29.8.95	22:08	80° 04,0'	149° 49,0'	988m	GKG (bio)
	PS2764-6	29.8.95	22:37	80° 04,1'	149° 48,8'	1000m	MUC (bio+geo)
	PS2764-7	29.8.95	23:03	80° 04,1'	149° 48,6'	1001m	GKG (23cm)
	PS2764-8	29.8.95	23:31	80° 04,3'	149° 48,7'	1010m	SL (6,50m)
		30.8.95	0:33	80° 03,2'	149° 46,3'	940m	AGT
36/063		30.8.95	3:08	79° 55,2'	149° 47,3'	704m	CTD
36/064	PS2765-1	30.8.95	4:17	79° 53,0'	149° 48,5'	509m	CTD
		30.8.95	5:01	79° 52,9'	149° 49,1'	500m	MN 150 µm
		30.8.95	5:06	79° 52,7'	149° 49,2'		Pütz
		30.8.95	5:40	79° 52,7'	149° 49,2'	450m	MN 55 µm (bio)
		30.8.95	6:12	79° 52,4'	149° 48,8'	231m	BN 1
		30.8.95	6:38	79° 52,3'	149° 48,6'	400m	BN 2
	PS2765-2	30.8.95	7:21	79° 53,32'	149° 48,49'	580m	GKG (bio)
	PS2765-3	30.8.95	7:45	79° 53,17'	149° 47,94'	584m	MUC (bio+geo)
	PS2765-4	30.8.95	8:07	79° 53,1'	149° 47,7'	563m	GKG (bio)
	PS2765-5	30.8.95	8:29	79° 53,0'	149° 47,2'	570m	MUC (bio+geo)
	PS2765-6	30.8.95	8:53	79° 52,8'	149° 46,9'	557m	GKG (32cm)
	PS2765-7	30.8.95	9:18	79° 52,8'	149° 46,4'	570m	MUC (bio+geo)
PS2765-8	30.8.95	9:46	79° 52,7'	149° 45,7'	559m	SL (7,35m)	
36/064a		30.8.95	10:49	79° 49,1'	149° 38,1'	320m	AGT
36/065	PS2766-1	30.8.95	15:06	79° 30,3'	149° 14,4'	214m	CTD
		30.8.95	15:06	79° 30,3'	149° 14,4'		Eisgruppe v. Bord
	PS2766-2	30.8.95	15:36	79° 30,3'	148° 14,6'	220m	ISP
		30.8.95	17:22	79° 30,1'	148° 14,4'	213m	CTD
		30.8.95	17:40	79° 30,0'	148° 14,2'	225m	MN 150 µm
		30.8.95	17:58	79° 29,9'	148° 13,9'	225m	MN 55 µm (bio)
		30.8.95	18:13	79° 29,8'	148° 13,7'	100m	BN 1
	PS2766-3	30.8.95	18:24	79° 29,8'	148° 13,5'	232m	GKG (bio)
	PS2766-4	30.8.95	18:35	79° 29,7'	148° 13,23'	232m	MUC (bio+geo)
	PS2766-5	30.8.95	18:46	79° 29,66'	148° 13,07'	231m	GKG (bio)
		30.8.95	18:59	79° 29,6'	148° 12,9'		Eisgruppe a. Bord
PS2766-6	30.8.95	19:01	79° 29,61'	148° 12,83'	231m	MUC (bio+geo)	
Lomonosov Ridge 36/066	PS2767-1	31.8.95	2:16	79° 44,9'	144° 02,5'	545m	CTD
		31.8.95	2:51	79° 44,8'	144° 01,8'	100m	BN 1

## A14

Station	AWI-No.	Date	Time (GMT)	Latitude N	Longitude E	Depth	Activity	
36/066	PS2767-2	31.8.95	3:09	79° 44.8'	144° 01.2'	577m	GKG(bio)	
	PS2767-3	31.8.95	3:37	79° 44.7'	144° 01.1'	580m	MUC (bio+geo)	
	PS2767-4	31.8.95	4:08	79° 44.59'	144° 00.37'	572m	KAL (8.30m)	
	PS2767-5	31.8.95	4:35	79° 44.49'	143° 59.76'	557m	GKG (geo) (0cm)	
	PS2767-6	31.8.95	4:56	79° 44.41'	143° 59.38'	557m	GKG (37cm)	
36/067		31.8.95	7:13	79° 49.0'	143° 05.2'		Eisgruppe v. Bord	
	PS2768-1	31.8.95	7:38	79° 49.0'	143° 05.2'	971m	CTD	
		31.8.95	8:19	79° 49.0'	143° 05.0'	100m	BN 1	
		31.8.95	8:54	79° 49.0'	143° 04.9'	965m	BN 2	
		31.8.95	9:15	79° 49.0'	143° 05.1'		Eisgruppe a. Bord	
	PS2768-2	31.8.95	9:44	79° 49.0'	143° 05.2'	986m	GKG (bio)	
	PS2768-3	31.8.95	10:22	79° 49.0'	143° 05.5'	984m	GKG (45cm)	
	PS2768-4	31.8.95	10:58	79° 49.0'	143° 05.9'	990m	SL (7.23m)	
36/068		1.9.95	5:43	78° 31.3'	134° 05.9'	1682m	CTD	
Eastern Laptev Sea								
36/069	PS2769-1	1.9.95	8:17	78° 22.8'	134° 49.2'	1161m	CTD	
		1.9.95	9:21	78° 22.7'	134° 49.2'	1210m	ISP	
		1.9.95	14:15	78° 23.3'	134° 48.9'	1000m	MN 150 µm	
		1.9.95	14:59	78° 23.3'	134° 53.9'	300m	MN 150 µm	
		1.9.95	15:28	78° 23.3'	134° 55.4'	500m	MN 55 µm (bio)	
		1.9.95	16:20	78° 23.3'	134° 57.8'	950m	BN 2	
		1.9.95	16:56	78° 23.1'	135° 01.3'	100m	BN 1	
	PS2769-3	1.9.95	17:16	78° 23.01'	135° 02.44'	984m	GKG (bio)	
	PS2769-4	1.9.95	17:47	78° 23.03'	135° 03.63'	978m	MUC (bio+geo)	
	PS2769-5	1.9.95	18:16	78° 23.07'	135° 04.59'	970m	GKG (bio)	
	PS2769-6	1.9.95	18:49	78° 23.2'	135° 05.37'	998m	MUC (bio+geo)	
	36/069a		1.9.95	19:42	78° 21.7'	135° 04.5'	700m	AGT
36/070		1.9.95	21:18	78° 21.5'	135° 04.5'	792m	CTD	
36/071	PS2770-1	1.9.95	22:24	78° 20.3'	135° 04.4'	580m	CTD	
		1.9.95	23:14	78° 20.9'	135° 05.8'	600m	MN 150 µm	
		1.9.95	23:57	78° 20.4'	135° 09.9'	100m	BN 1	
	PS2770-2	2.9.95	0:16	78° 20.9'	135° 10.8'	534m	GKG (bio)	
		2.9.95	0:27	78° 21.1'	135° 11.8'		Püttz	
	PS2770-3	2.9.95	0:49	78° 21.2'	135° 13.5'	550m	MUC	
	PS2770-4	2.9.95	1:13	78° 21.3'	135° 14.8'	515m	GKG (bio)	
	PS2770-5	2.9.95	2:11	78° 21.0'	135° 13.4'	500m	GKG (Abbruch)	
	PS2770-6	2.9.95	2:49	78° 21.0'	135° 11.7'	531m	GKG (36cm)	
	PS2770-7	2.9.95	3:18	78° 21.2'	135° 13.8'	551m	SL (6.51m)	
36/071a		2.9.95	4:04	78° 19.2'	135° 20.4'	230m	AGT	
36/072	PS2771-1	2.9.95	5:08	78° 19.5'	135° 20.9'	228m	CTD	
		2.9.95	5:42	78° 19.6'	135° 21.7'	220m	MN 150 µm	
		2.9.95	6:03	78° 22.0'	135° 21.7'	220m	MN 55 µm (bio)	
		2.9.95	6:22	78° 19.6'	135° 22.5'	100m	BN 1	
	PS2771-2	2.9.95	6:40	78° 19.57'	135° 23.14'	214m	GKG (bio)	
	PS2771-3	2.9.95	6:52	78° 19.57'	135° 23.34'	214m	MUC (bio+geo)	
	PS2771-4	2.9.95	7:05	78° 19.57'	135° 23.0'	213m	GKG (bio)	
	PS2771-5	2.9.95	7:22	78° 19.62'	135° 23.56'	214m	GKG (32cm)	
	PS2771-6	2.9.95	7:40	78° 19.71'	135° 23.23'	219m	SL (3.18m)	
	36/073	PS2772-1	2.9.95	8:49	78° 14.9'	135° 23.5'	86m	CTD
2.9.95			9:12	78° 15.0'	135° 23.4'	100m	MN 150 µm	
2.9.95			9:27	78° 15.1'	135° 23.3'	100m	BN 1	
PS2772-2		2.9.95	9:40	78° 15.2'	135° 23.3'	104m	GKG (bio)	
PS2772-3		2.9.95	9:54	78° 15.3'	135° 23.4'	109m	MUC	
PS2772-4		2.9.95	10:05	78° 15.4'	135° 23.5'	104m	GKG (bio+geo)	
PS2772-5		2.9.95	10:17	78° 15.5'	135° 23.5'	115m	MUC (bio+geo)	



## A15

Station	AWI-No.	Date	Time (GMT)	Latitude N	Longitude E	Depth	Activity
36/074		3.9.95	13:03	80° 50,1'	122° 23,2'		Eisgruppe v. Bord
		3.9.95	17:19	80° 52,1'	122° 23,2'		Eisgruppe a. Bord
Western Laptev Sea							
36/075		4.9.95	4:20	80° 55,1'	122° 41,4'		Eisgruppe v. Bord
		4.9.95	5:05	80° 55,1'	122° 41,4'	1500m	BN 2
		4.9.95	6:01	80° 55,8'	122° 44,5'	100m	BN 1
	PS2773-1	4.9.95	6:37	80° 55,9'	122° 45,6'	500m	CTD
	PS2773-2	4.9.95	7:48	80° 55,8'	122° 48,0'	3580m	ISP
		4.9.95	13:12	80° 55,7'	122° 38,9'		Eisgruppe a. Bord
		4.9.95	14:34	80° 55,6'	122° 39,8'	3566m	MN 150 µm
		4.9.95	17:16	80° 57,4'	122° 38,9'	300m	MN 150 µm
	PS2773-3	4.9.95	18:08	80° 57,55'	122° 40,7'	3578m	GKG(bio)
		4.9.95	18:45	80° 57,5'	122° 41,6'		Sed.-Fallen-Gr. v. Bord
	PS2773-4	4.9.95	19:37	80° 57,4'	122° 42,54'	3596m	MUC (bio+geo)
	PS2773-5	4.9.95	20:55	80° 57,1'	122° 42,4'	3582m	GKG (bio)
		4.9.95	21:10	80° 57,8'	122° 42,2'		Sed.-Fallen-Gr. a. Bord
	PS2773-6	4.9.95	22:18	80° 56,9'	122° 41,8'	3571m	MUC (bio+geo)
	PS2773-7	4.9.95	23:33	80° 56,8'	122° 38,7'	3561m	GKG (36cm)
	PS2773-8	5.9.95	0:42	80° 57,1'	122° 34,4'	3547m	SL (6,10m)
	36/076						
	PS2774-1	5.9.95	5:40	80° 40,69'	121° 17,0'	3497m	SL (2,30m)
	PS2774-2	5.9.95	7:02	80° 40,87'	121° 17,63'	3489m	GKG (40cm)
36/077							
		5.9.95	11:31	80° 11,9'	119° 01,0'	3315m	CTD
		5.9.95	14:10	80° 11,5'	119° 24,2'	3320m	AGT
36/078							
		5.9.95	20:59	79° 29,9'	115° 53,7'	1617m	CTD
Western Laptev Sea, Severnaya Zemlya							
36/079	PS2775-1	6.9.95	2:59	78° 48,9'	112° 55,9'	1617m	CTD
		6.9.95	3:51	78° 48,9'	112° 58,4'	100m	BN 1
	PS2775-2	6.9.95	4:18	78° 48,73'	112° 58,89'	1658m	GKG (bio)
	PS2775-3	6.9.95	5:14	78° 48,45'	113° 00,01'	1645m	MUC (bio+geo)
	PS2775-4	6.9.95	5:58	78° 48,14'	113° 00,08'	1600m	GKG (35cm)
36/080	PS2776-1	6.9.95	7:46	78° 45,1'	112° 41,0'	1085m	CTD
	PS2776-2	6.9.95	8:46	78° 45,3'	112° 41,8'	1111m	ISP
		6.9.95	12:49	78° 46,1'	112° 43,8'	1189m	CTD
		6.9.95	14:00	78° 45,6'	112° 43,3'	1150m	MN 150 µm
		6.9.95	14:19	78° 45,4'	112° 42,6'		Hand-CTD
		6.9.95	15:33	78° 45,4'	112° 42,7'	300m	MN 150 µm
		6.9.95	15:51	78° 45,5'	112° 43,2'	100m	BN 1
	PS2776-3	6.9.95	16:14	78° 45,61'	112° 43,97'	1204m	GKG (bio)
	PS2776-4	6.9.95	16:51	78° 45,38'	112° 43,13'	1183m	MUC (bio+geo)
	PS2776-5	6.9.95	17:24	78° 45,18'	112° 42,66'	1150m	GKG (bio)
	PS2776-6	6.9.95	17:59	78° 45,0'	112° 42,46'	1124m	MUC (bio+geo)
	36/080a						
		6.9.95	19:00	78° 42,8'	112° 43,4'	750m	AGT
36/081							
	PS2777-1	6.9.95	20:39	78° 40,6'	112° 41,7'	494m	CTD
		6.9.95	21:13	78° 40,6'	112° 40,6'	100m	BN 1
	PS2777-2	6.9.95	21:29	78° 40,7'	112° 40,2'	535m	GKG (bio)
	PS2777-3	6.9.95	21:49	78° 40,7'	112° 39,6'	559m	MUC (bio+geo)
36/082							
	PS2778-1	7.9.95	1:36	77° 58,8'	113° 03,5'	330m	GKG (33cm)
	PS2778-2	7.9.95	1:55	77° 58,7'	113° 03,9'	341m	SL (5,90m)
36/083							
	PS2779-1	7.9.95	3:06	77° 55,7'	113° 31,3'	214m	CTD
	PS2779-2	7.9.95	3:34	77° 55,7'	113° 31,9'	220m	ISP
		7.9.95	5:26	77° 55,6'	113° 32,7'	220m	MN 150 µm
		7.9.95	5:47	77° 55,6'	113° 33,1'	200m	BN 1
	PS2779-3	7.9.95	6:20	77° 55,74'	113° 30,07'	243m	GKG (bio)

## A16

Station	AWI-No.	Date	Time (GMT)	Latitude N	Longitude E	Depth	Activity	
36/083	PS2779-4	7.9.95	6:36	77° 55,78'	113° 30,51'	255m	MUC (bio+geo)	
	PS2779-5	7.9.95	6:54	77° 55,79'	113° 30,93'	248m	GKG (32cm)	
	PS2779-6	7.9.95	7:12	77° 55,77'	113° 31,47'	247m	SL (6,32m)	
36/083a		7.9.95	7:45	77° 56,9'	113° 34,7'	300m	AGT	
36/084	PS2780-1	7.9.95	8:51	77° 53,7'	113° 43,3'	87m	CTD	
		7.9.95	9:11	77° 53,6'	113° 44,1'	95m	MN 150 µm	
		7.9.95	9:25	77° 53,6'	113° 44,9'	90m	BN 1	
	PS2780-2	7.9.95	9:38	77° 53,5'	113° 45,4'	101m	GKG (bio)	
	PS2780-3	7.9.95	9:53	77° 53,5'	113° 46,2'	107m	MUC (bio+geo)	
	PS2780-4	7.9.95	10:25	77° 54,3'	113° 43,9'	140m	MUC (bio+geo)	
	PS2780-5	7.9.95	10:40	77° 54,3'	113° 44,6'	135m	GKG (30cm)	
PS2780-6	7.9.95	11:06	77° 54,3'	113° 43,7'	136m	SL (5,35m)		
36/085	PS2781-1	7.9.95	13:50	78° 07,4'	111° 55,0'	325m	GKG (37cm)	
	PS2781-2	7.9.95	14:14	78° 07,5'	111° 54,6'	330m	SL (5,70m)	
36/086	PS2782-1	8.9.95	2:20	79° 36,6'	103° 21,3'	340m	SL (5,20m)	
	PS2782-2	8.9.95	2:43	79° 36,7'	103° 21,1'	340m	MUC (bio+geo)	
36/087		8.9.95	7:48	80° 25,0'	101° 58,9'	229m	CTD	
		8.9.95	7:49	80° 25,0'	101° 58,7'		SD	
		8.9.95	8:19	80° 24,9'	101° 58,0'	235m	MN 150 µm	
	PS2783-1	8.9.95	8:36	80° 24,9'	101° 58,1'	260m	MUC (bio+geo)	
	PS2783-2	8.9.95	8:52	80° 24,7'	101° 58,7'	254m	MUC (bio+geo)	
North of Sev. Zemlya - Kara Sea								
36/088	PS2784-1	8.9.95	19:27	81° 46,0'	96° 37,0'	1930m	CTD	
	PS2784-2	8.9.95	20:30	81° 45,7'	96° 35,9'	1656m	GKG (bio)	
36/089	PS2785-1	9.9.95	3:32	82° 21,1'	92° 59,8'	2700m	CTD	
		9.9.95	4:43	82° 21,2'	92° 55,1'	100m	BN 1	
		9.9.95	4:48	82° 21,2'	92° 54,9'		Pütz	
		9.9.95	5:52	82° 21,2'	92° 54,9'	2000m	BN 2	
		9.9.95	7:51	82° 20,7'	92° 51,6'	2656m	CTD	
	9.9.95	8:46	82° 20,3'	92° 48,9'		SD		
	PS2785-2	9.9.95	9:11	82° 20,3'	92° 48,8'	2655m	GKG (bio)	
	PS2785-3	9.9.95	10:15	82° 20,4'	92° 45,6'	2646m	MUC (bio+geo)	
	PS2785-4	9.9.95	11:18	82° 20,3'	92° 43,8'	2632m	GKG (bio)	
	PS2785-5	9.9.95	12:23	82° 20,1'	92° 44,1'	2643m	MUC (bio+geo)	
9.9.95	13:40	82° 19,8'	92° 44,5'	300m	CTD			
36/090	PS2786-1	9.9.95	17:37	82° 08,3'	91° 24,4'	1726m	CTD	
		9.9.95	18:21	82° 07,9'	91° 22,7'	100m	BN 1	
	PS2786-2	9.9.95	18:59	82° 08,49'	91° 22,34'	1776m	GKG (bio)	
	PS2786-3	9.9.95	19:43	82° 08,41'	91° 20,76'	1766m	GKG (bio)	
	PS2786-4	9.9.95	20:42	82° 08,6'	91° 19,5'	1806m	GKG (geo) (0cm)	
36/091	PS2787-1	9.9.95	22:18	82° 04,6'	91° 58,2'	998m	CTD	
		9.9.95	23:06	82° 04,2'	91° 00,0'	988m	ISP	
		10.9.95	2:15	82° 04,3'	91° 02,4'	1099m	CTD	
		10.9.95	3:18	82° 04,2'	91° 02,4'	1000m	MN 150 µm	
		10.9.95	4:12	82° 04,2'	91° 01,6'	300m	MN 150 µm	
	PS2787-3	10.9.95	4:32	82° 04,1'	91° 01,5'	100m	BN 1	
		10.9.95	5:08	82° 04,60'	91° 01,91'	1138m	GKG (bio)	
		PS2787-4	10.9.95	5:41	82° 04,49'	91° 01,99'	1150m	MUC (bio+geo)
		PS2787-5	10.9.95	6:14	82° 04,51'	91° 01,26'	1136m	GKG (bio) (0cm)
		PS2787-6	10.9.95	6:40	82° 04,55'	91° 00,62'	1096m	GKG (bio)
		PS2787-7	10.9.95	7:08	82° 04,54'	90° 59,73'	1029m	GKG (38cm)
36/091a			10.9.95	7:54	82° 03,9'	90° 56,3'	1580m	AGT

## A17

Station	AWI-No.	Date	Time (GMT)	Latitude N	Longitude E	Depth	Activity
36/092	PS2788-1	10.9.95	10:23	82° 02,1'	90° 55,8'	514m	CTD
			11:06	82° 02,2'	90° 56,1'	525m	MN 150 µm
			11:31	82° 02,3'	90° 57,2'	100m	BN 1
	PS2788-2	10.9.95	11:47	82° 02,2'	90° 57,8'	526m	GKG (bio)
			12:06	82° 02,3'	90° 58,1'	544m	GKG (bio)
PS2788-4	10.9.95	12:35	82° 02,3'	90° 59,1'	540m	GKG (bio)	
36/093	PS2789-1	10.9.95	14:08	81° 58,0'	90° 58,0'	228m	CTD
			14:38	81° 57,9'	91° 01,2'	240m	MN 150 µm
			14:58	81° 57,8'	91° 01,8'	100m	BN 1
			15:05	81° 57,7'	91° 03,7'		Pütz
			15:13	81° 57,7'	91° 04,1'	240m	GKG (bio)
	PS2789-2	10.9.95	15:31	81° 57,6'	91° 04,9'	240m	MUC (0cm)
			15:51	81° 57,6'	91° 05,1'	238m	GKG (bio)
	PS2789-4	10.9.95	15:51	81° 57,6'	91° 05,1'	238m	GKG (bio)
	PS2789-5	10.9.95	16:14	81° 57,54'	91° 05,97'	235m	GKG (geo)
	36/094	PS2790-1	10.9.95	17:34	81° 49,2'	90° 46,1'	79m
17:56				81° 49,0'	90° 46,6'	75m	MN 150 µm
17:58				81° 48,9'	90° 46,7'		Pütz
18:08				81° 48,9'	90° 46,8'	75 m	BN 1
18:17				81° 48,8'	90° 46,9'	75 m	BN 100/100 µm
PS2790-2		10.9.95	18:26	81° 48,7'	90° 46,8'		SD
			18:31	81° 48,7'	90° 46,81'	90m	GKG (bio)
			18:56	81° 48,57'	90° 46,54'	85m	GKG (bio)
PS2790-4	10.9.95	19:36	81° 48,22'	90° 45,66'	83m	GKG (bio)	
36/095a		11.9.95	0:43	81° 09,7'	88° 48,8'	150m	AGT
36/095	PS2791-1	11.9.95	2:58	81° 09,9'	88° 27,9'	304m	CTD
			3:26	81° 10,2'	87° 29,2'	314m	GKG (bio)
			3:44	81° 10,3'	87° 29,4'	315m	GKG (bio)
			4:00	81° 10,42'	87° 29,92'	328m	MUC (bio+geo)
			4:18	81° 10,43'	87° 30,16'	320m	GKG (36cm)
Kara Sea 36/096	PS2792-1	11.9.95	13:27	79° 33,4'	87° 02,0'	225m	CTD
			13:56	79° 33,4'	87° 00,0'	230m	BN 2
			14:12	79° 33,5'	86° 59,6'	248m	GKG (bio)
			14:31	79° 33,5'	86° 58,5'	247m	GKG (bio)
			14:43	79° 33,5'	86° 57,9'	245m	MUC (bio+geo)
			15:11	79° 33,5'	87° 01,1'	255m	SL (7.10m)
			15:30	79° 33,5'	87° 00,1'	245m	GKG (43cm)

A18  
Annex 11.2: Weather Data

Expedition ARK XI/I RV "Polarstern", Weather Data  
(Bordwetterwarte)  
7.7.95 - 17.9.95

DD.MM.Year	UTC	Lat	Lon	DDD/FF	Bft	Visib.	WX	Weather	Press.	Ta	Td	rH	Tw	Sea	Max.Sea	Ice	Speed
07.07.1995	09	53.6N	8.6E	230/ 8kt	3	10.0km	0 /		1019.5	20.7	13.9	65	17.9	/ m /	/ m /	/ m /	Station
07.07.1995	12	53.6N	8.6E	220/11kt	4	10.0km	0 /		1019.6	20.7	13.2	62	17.9	/ m /	/ m /	/ m /	Station
07.07.1995	15	53.6N	8.6E	300/ 9kt	3	10.0km	0 fair, Ci		1019.3	22.3	14.0	59	18.8	/ m /	/ m /	/ m /	?kt
07.07.1995	18	53.6N	8.5E	340/10kt	3	20.0km	0 no cloud		1019.6	17.8	13.6	76	18.0	/ m /	/ m /	/ m /	W 3kt
07.07.1995	21	53.8N	7.9E	320/ 8kt	3	10.0km	0 no cloud		1021.0	14.5	12.5	88	15.0	/ m /	/ m /	/ m /	SE 8kt
08.07.1995	00	54.0N	7.8E	160/ 2kt	1	10.0km	0 /		1021.3	14.1	12.4	89	16.0	/ m /	/ m /	/ m /	N 3kt
08.07.1995	03	54.2N	7.3E	210/ 5kt	2	10.0km	0 /		1021.2	14.1	12.4	89	14.6	/ m /	/ m /	/ m /	?kt
08.07.1995	06	54.9N	6.9E	230/ 8kt	3	10.0km	0 /		1021.8	14.2	12.6	90	14.4	/ m /	/ m /	/ m /	?kt
08.07.1995	09	55.4N	6.3E	330/10kt	3	10.0km	0 /		1022.7	13.6	11.9	89	0.0	/ m /	/ m /	/ m /	?kt
08.07.1995	12	56.2N	6.0E	280/12kt	4	10.0km	0 /		1023.6	13.6	9.6	77	13.7	/ m /	/ m /	/ m /	N 13kt
08.07.1995	15	57.8N	5.7E	350/17kt	5	10.0km	0 /		1024.4	12.6	99.0	999	14.7	/ m /	/ m /	/ m /	N 28kt
08.07.1995	18	57.6N	5.4E	340/17kt	5	20.0km	0 no cloud		1025.8	11.4	7.5	77	13.1	1.5m	340	1.5m	N 13kt
08.07.1995	21	58.3N	5.0E	330/13kt	4	10.0km	0 /		1027.5	10.1	7.1	82	11.1	/ m /	/ m /	/ m /	N 13kt
09.07.1995	00	59.0N	4.7E	350/11kt	4	10.0km	0 /		1028.2	10.6	99.0	999	11.0	/ m /	/ m /	/ m /	N 13kt
09.07.1995	03	59.7N	4.4E	360/ 7kt	3	20.0km	0 cloudy		1028.9	10.1	5.5	73	12.4	1.0m	280	1.5m	N 13kt
09.07.1995	06	60.5N	4.2E	40/ 8kt	3	20.0km	0 fair		1029.5	9.6	5.3	74	11.9	0.5m	300	2.0m	N 18kt
09.07.1995	09	61.2N	4.0E	30/10kt	3	20.0km	0 fair		1029.9	9.1	5.8	80	11.8	0.5m	290	2.0m	N 13kt
09.07.1995	12	61.9N	4.3E	30/11kt	4	20.0km	0 fair, Ci		1029.7	9.6	5.4	75	11.4	0.5m	310	2.0m	N 13kt
09.07.1995	15	62.5N	5.0E	40/17kt	5	20.0km	0 fair, Ci		1029.5	8.5	4.7	77	10.8	1.5m	340	2.0m	NE 13kt
09.07.1995	18	63.2N	5.8E	60/16kt	5	10.0km	0 /		1029.4	8.3	99.0	999	10.5	/ m /	/ m /	/ m /	NE 18kt
09.07.1995	21	63.9N	6.5E	80/14kt	4	10.0km	0 /		1029.7	7.8	99.0	999	10.0	/ m /	/ m /	/ m /	NE 13kt
10.07.1995	00	64.5N	7.2E	90/ 7kt	3	10.0km	0 /		1029.8	7.4	99.0	999	9.5	/ m /	/ m /	/ m /	NE 13kt
10.07.1995	03	65.1N	7.9E	10/ 1kt	1	10.0km	0 /		1029.3	7.0	99.0	999	9.4	/ m /	/ m /	/ m /	NE 13kt
10.07.1995	06	65.7N	8.7E	260/ 7kt	3	20.0km	0 fair		1028.6	7.5	3.7	77	8.7	0.5m	320	1.5m	NE 13kt
10.07.1995	09	66.3N	9.4E	240/13kt	4	20.0km	0 overcast		1027.8	8.0	3.3	72	8.4	1.0m	300	1.5m	NE 13kt
10.07.1995	12	66.9N	10.2E	220/19kt	5	20.0km	0 overcast		1026.7	8.2	4.8	79	8.6	1.5m	220	1.5m	NE 13kt
10.07.1995	15	67.6N	11.1E	240/19kt	5	4.0km	10 misty		1024.9	7.4	6.1	91	8.0	1.5m	240	1.5m	NE 18kt
10.07.1995	18	68.2N	12.3E	330/10kt	3	4.0km	10 misty		1023.3	6.8	5.7	93	7.7	0.5m	280	1.5m	NE 13kt
10.07.1995	21	68.7N	13.3E	340/17kt	5	10.0km	0 /		1023.0	5.8	99.0	999	7.8	/ m /	/ m /	/ m /	NE 13kt
11.07.1995	00	69.3N	14.9E	280/14kt	4	10.0km	0 /		1021.5	5.2	99.0	999	7.5	/ m /	/ m /	/ m /	NE 13kt
11.07.1995	03	69.9N	16.3E	300/17kt	5	20.0km	0 overcast		1020.0	6.1	4.0	86	7.8	1.5m	300	1.5m	NE 13kt
11.07.1995	06	70.0N	16.7E	320/18kt	5	10.0km	25 r.Shower		1019.8	5.4	5.0	97	7.4	1.5m	320	1.5m	NE 3kt
11.07.1995	09	70.0N	16.7E	300/19kt	5	20.0km	2 overcast		1019.8	6.4	4.7	89	7.7	1.5m	300	1.5m	Station
11.07.1995	12	70.3N	17.9E	280/20kt	5	20.0km	2 overcast		1019.0	6.3	5.7	96	7.5	1.5m	350	2.0m	NE 8kt
11.07.1995	15	70.5N	19.0E	300/23kt	6	4.0km	60 Rain		1017.6	4.0	3.7	98	7.0	2.0m	20	2.5m	NE 8kt
11.07.1995	18	70.6N	19.2E	290/22kt	6	20.0km	2 overcast		1016.7	4.9	3.9	93	7.7	1.5m	290	1.5m	NE 3kt
11.07.1995	21	70.8N	20.7E	300/20kt	5	10.0km	0 /		1014.3	5.8	99.0	999	7.0	/ m /	/ m /	/ m /	E 13kt
12.07.1995	00	71.1N	22.5E	320/33kt	7	10.0km	0 /		1010.5	5.2	99.0	999	6.9	/ m /	/ m /	/ m /	NE 13kt
12.07.1995	03	71.3N	24.3E	310/34kt	8	10.0km	15 (Rain)		1007.1	4.5	4.0	97	6.9	3.5m	310	3.5m	E 13kt
12.07.1995	06	71.3N	26.1E	320/33kt	7	10.0km	15 (Rain)		1003.8	4.4	3.9	97	6.4	4.0m	320	4.0m	E 13kt
12.07.1995	09	71.3N	27.8E	300/26kt	6	4.0km	60 Rain		1002.6	4.2	3.9	98	6.9	3.5m	300	3.5m	E 13kt
12.07.1995	12	71.0N	29.6E	300/27kt	6	10.0km	21 r.Rain		1001.8	4.8	4.6	99	6.3	2.5m	20	3.0m	SE 13kt
12.07.1995	15	70.6N	31.1E	310/29kt	7	4.0km	60 Rain		1001.1	4.6	4.3	98	6.9	3.0m	310	3.0m	SE 13kt
12.07.1995	18	70.2N	32.1E	320/23kt	6	10.0km	0 /		1000.4	5.1	99.0	999	6.4	/ m /	/ m /	/ m /	SE 8kt
12.07.1995	21	69.9N	33.1E	310/24kt	6	10.0km	0 /		999.6	5.5	99.0	999	6.2	/ m /	/ m /	/ m /	SE 8kt
13.07.1995	00	69.5N	33.6E	300/31kt	7	4.0km	60 Rain		998.3	4.7	4.4	98	6.3	2.5m	300	2.5m	SE 8kt
13.07.1995	03	69.0N	33.0E	300/20kt	5	10.0km	0 /		998.4	4.4	3.6	95	6.7	/ m /	/ m /	/ m /	SW 13kt
13.07.1995	06	69.0N	33.1E	310/14kt	4	10.0km	25 r.Shower		996.4	5.3	4.4	94	6.7	/ m /	/ m /	/ m /	E 3kt
13.07.1995	09	69.0N	33.1E	360/14kt	4	10.0km	0 /		996.1	5.9	5.4	97	6.9	/ m /	/ m /	/ m /	Station
13.07.1995	12	69.0N	33.1E	360/10kt	3	10.0km	0 overcast		998.1	6.0	5.4	96	6.8	/ m /	/ m /	/ m /	Station
13.07.1995	15	69.0N	33.1E	10/ 9kt	3	10.0km	0 /		1000.3	5.9	5.3	96	7.3	/ m /	/ m /	/ m /	Station
13.07.1995	18	69.0N	33.1E	360/ 7kt	3	10.0km	0 /		1002.7	5.1	99.0	999	7.2	/ m /	/ m /	/ m /	Station
13.07.1995	21	69.0N	33.1E	350/ 8kt	3	10.0km	0 /		1005.4	5.5	99.0	999	7.0	/ m /	/ m /	/ m /	Station

## A19

DD.MM.Year	UTC	Lat	Lon	DDD/FF	Bft	Visib.	WX	Weather	Press.	Ta	Td	rH	Tw	Sea	Max.Sea	Ice	Speed
14.07.1995	00	69.0N	33.1E	60/10kt	3	10.0km	0	/	1008.6	5.6	99.0	999	7.0	/m	/	/m	Station
14.07.1995	03	69.0N	33.1E	30/6kt	2	10.0km	0	overcast	1010.8	6.2	4.5	89	7.3	/m	/	/m	Station
14.07.1995	06	69.0N	33.1E	20/9kt	3	10.0km	0	overcast	1012.5	7.4	5.6	88	7.7	/m	/	/m	Station
14.07.1995	09	69.0N	33.1E	360/8kt	3	10.0km	0	overcast	1015.2	8.0	6.2	88	7.5	/m	/	/m	Station
14.07.1995	12	69.3N	33.6E	100/14kt	4	10.0km	0	overcast	1017.5	5.0	4.6	97	7.4	/m	/	/m	?kt
14.07.1995	15	69.5N	34.7E	350/20kt	5	10.0km	0	overcast	1017.3	5.0	4.7	98	7.0	/m	/	/m	?kt
14.07.1995	18	69.6N	36.2E	350/18kt	5	10.0km	0	overcast	1016.5	4.9	4.6	98	5.8	/m	/	/m	?kt
14.07.1995	21	69.6N	37.5E	360/17kt	5	10.0km	0	/	1016.8	5.1	99.0	999	5.8	/m	/	/m	E 33kt
DD.MM.Year	UTC	Lat	Lon	DDD/FF	Bft	Visib.	WX	Weather	Press.	Ta	Td	rH	Tw	Sea	Max.Sea	Ice	Speed
15.07.1995	00	69.7N	38.8E	360/18kt	5	10.0km	0	fair	1017.1	5.2	4.2	93	6.0	1.0m	50	1.5m	E 8kt
15.07.1995	03	69.7N	40.1E	350/15kt	4	10.0km	0	/	1017.1	5.2	4.5	95	5.7	/m	/	/m	E 8kt
15.07.1995	06	69.7N	41.4E	340/17kt	5	10.0km	0	overcast	1017.1	5.1	4.3	95	6.5	1.5m	340	1.5m	E 8kt
15.07.1995	09	69.8N	42.8E	350/18kt	5	4.0km	0	misty	1016.7	4.4	4.3	99	5.7	/m	/	/m	E 8kt
15.07.1995	12	69.8N	44.1E	360/17kt	5	10.0km	2	overcast	1016.7	4.4	4.1	98	6.5	1.0m	50	2.0m	E 8kt
15.07.1995	15	69.9N	45.5E	360/20kt	5	4.0km	50	Drizzle	1016.2	3.6	2.9	95	5.5	1.5m	360	1.5m	E 8kt
15.07.1995	18	69.9N	46.8E	10/18kt	5	10.0km	0	overcast	1015.3	3.1	2.8	98	5.7	/m	/	/m	E 8kt
15.07.1995	21	70.0N	48.1E	350/18kt	5	10.0km	0	/	1014.9	2.7	99.0	999	4.9	/m	/	/m	E 8kt
DD.MM.Year	UTC	Lat	Lon	DDD/FF	Bft	Visib.	WX	Weather	Press.	Ta	Td	rH	Tw	Sea	Max.Sea	Ice	Speed
16.07.1995	00	70.0N	49.6E	340/18kt	5	10.0km	0	/	1014.2	2.1	99.0	999	5.0	/m	/	/m	E 8kt
16.07.1995	03	70.0N	51.0E	320/20kt	5	4.0km	10	misty	1012.9	2.7	2.4	98	5.0	1.5m	320	1.5m	E 8kt
16.07.1995	06	70.1N	52.3E	310/20kt	5	10.0km	0	/	1011.7	3.2	99.0	999	5.4	/m	/	/m	E 8kt
16.07.1995	09	70.1N	53.7E	320/19kt	5	10.0km	0	overcast	1010.5	3.9	3.5	97	5.5	1.5m	320	1.5m	E 8kt
16.07.1995	12	70.2N	55.2E	300/21kt	5	20.0km	0	overcast	1008.4	4.5	3.9	96	5.4	1.5m	300	1.5m	E 8kt
16.07.1995	15	70.2N	56.8E	290/21kt	5	20.0km	0	cloudy	1006.4	6.1	5.2	94	6.0	1.5m	290	1.5m	E 13kt
16.07.1995	18	70.3N	58.1E	20/9kt	3	10.0km	0	/	1006.1	6.1	99.0	999	7.5	/m	/	/m	E 8kt
16.07.1995	21	70.7N	59.0E	290/11kt	4	10.0km	0	fair, Ci	1004.3	4.9	99.0	999	5.1	/m	/	/m	NE 8kt
DD.MM.Year	UTC	Lat	Lon	DDD/FF	Bft	Visib.	WX	Weather	Press.	Ta	Td	rH	Tw	Sea	Max.Sea	Ice	Speed
17.07.1995	00	71.1N	60.0E	300/8kt	3	20.0km	0	fair, Ci	1002.8	5.4	4.5	94	6.2	0.0m	300	0.0m	NE 8kt
17.07.1995	03	71.5N	61.1E	260/7kt	3	20.0km	0	cloudy	1001.4	4.1	3.8	98	3.8	0.5m	990	1.0m	NE 13kt
17.07.1995	06	71.8N	62.2E	310/7kt	3	20.0km	0	overcast	1000.8	3.8	2.9	94	3.9	0.5m	310	0.5m	NE 8kt
17.07.1995	09	72.2N	63.3E	310/7kt	3	20.0km	2	overcast	1001.0	2.5	2.1	97	2.7	0.5m	310	0.5m	NE 8kt
17.07.1995	12	72.6N	64.4E	310/7kt	3	20.0km	2	overcast	1001.4	1.9	1.6	98	2.8	0.5m	310	0.5m	NE 8kt
17.07.1995	15	73.0N	65.4E	300/7kt	3	10.0km	0	/	1000.9	2.4	2.0	97	3.7	/m	/	/m	?kt
17.07.1995	18	73.4N	66.3E	270/9kt	3	10.0km	0	/	1000.2	2.8	0.5	85	4.8	/m	/	/m	?kt
17.07.1995	21	73.8N	67.4E	250/11kt	4	10.0km	0	/	999.3	2.9	0.6	85	4.9	/m	/	/m	NE 8kt
DD.MM.Year	UTC	Lat	Lon	DDD/FF	Bft	Visib.	WX	Weather	Press.	Ta	Td	rH	Tw	Sea	Max.Sea	Ice	Speed
18.07.1995	00	74.2N	68.4E	230/12kt	4	20.0km	14	Virga	998.8	3.3	0.8	84	4.7	0.5m	230	0.5m	NE 8kt
18.07.1995	03	74.6N	69.4E	200/10kt	3	20.0km	15	(Rain)	999.0	3.2	0.9	85	5.3	0.5m	200	0.5m	NE 8kt
18.07.1995	06	74.6N	71.0E	120/4kt	2	20.0km	2	overcast	1000.3	2.5	0.6	87	5.9	0.0m	120	0.0m	E 8kt
18.07.1995	09	74.5N	73.2E	210/11kt	4	50.0km	0	fair	1001.4	3.6	1.1	84	6.0	0.5m	210	0.5m	E 13kt
18.07.1995	12	74.3N	75.6E	170/17kt	5	20.0km	0	overcast	1002.6	3.1	2.7	97	6.0	1.0m	170	1.0m	E 13kt
18.07.1995	15	74.2N	78.1E	150/20kt	5	20.0km	0	overcast	1003.7	3.2	2.1	92	4.8	1.0m	150	1.0m	E 13kt
18.07.1995	18	74.3N	80.6E	120/18kt	5	10.0km	0	/	1004.0	2.7	1.0	89	5.2	/m	/	/m	E 13kt
18.07.1995	21	74.8N	82.7E	120/16kt	5	10.0km	0	/	1004.6	1.0	0.6	97	3.7	/m	/	/m	NE 13kt
DD.MM.Year	UTC	Lat	Lon	DDD/FF	Bft	Visib.	WX	Weather	Press.	Ta	Td	rH	Tw	Sea	Max.Sea	Ice	Speed
19.07.1995	00	75.3N	84.8E	130/13kt	4	20.0km	0	overcast	1005.0	1.0	-0.1	92	4.1	0.5m	130	0.5m	NE 13kt
19.07.1995	03	75.8N	86.7E	110/5kt	2	20.0km	0	fair, Ci	1005.0	1.3	1.0	98	4.2	0.0m	110	0.0m	NE 13kt
19.07.1995	06	76.3N	89.2E	60/3kt	1	4.0km	10	misty	1004.5	0.0	-0.3	98	2.4	0.0m	60	0.0m	NE 18kt
19.07.1995	09	76.6N	91.9E	60/10kt	3	0.2km	44	Fog	1003.9	-1.6	-1.9	98	0.8	0.0m	60	0.0m	NE 13kt
19.07.1995	12	77.0N	94.3E	50/10kt	3	1.0km	44	Fog	1003.8	-2.9	-3.2	98	-0.3	0.0m	50	0.0m	NE 13kt
19.07.1995	15	77.4N	96.7E	40/15kt	4	0.2km	45	Fog	1002.1	-2.3	-2.6	98	-1.1	0.0m	40	0.0m	NE 13kt
19.07.1995	18	77.5N	97.1E	20/17kt	5	2.0km	0	/	1000.2	-2.0	-2.3	98	-1.3	/m	/	/m	NE 3kt
19.07.1995	21	77.7N	98.5E	360/20kt	5	10.0km	0	/	996.9	-1.2	-1.5	98	-1.7	/m	/	/m	NE 8kt
DD.MM.Year	UTC	Lat	Lon	DDD/FF	Bft	Visib.	WX	Weather	Press.	Ta	Td	rH	Tw	Sea	Max.Sea	Ice	Speed
20.07.1995	00	77.7N	100.4E	40/25kt	6	10.0km	0	overcast	994.3	0.0	-0.3	98	-0.7	0.0m	40	0.0m	SE 8kt
20.07.1995	03	77.9N	102.5E	50/19kt	5	10.0km	0	/	993.8	-0.4	-0.7	98	-0.1	/m	/	/m	NE 8kt
20.07.1995	06	78.0N	104.8E	50/15kt	4	1.0km	46	Fog	994.4	-0.2	-0.5	98	-0.4	0.5m	50	0.5m	E 8kt
20.07.1995	09	77.9N	106.7E	10/13kt	4	10.0km	2	overcast	996.4	1.4	1.1	98	0.4	0.0m	10	0.0m	E 8kt
20.07.1995	12	77.8N	107.5E	30/15kt	4	20.0km	0	cloudy	997.4	0.3	0.0	98	-1.3	0.0m	30	0.0m	SE 3kt
20.07.1995	15	77.6N	108.7E	40/16kt	5	20.0km	0	no cloud	997.5	0.4	0.1	98	0.2	0.0m	40	0.0m	SE 8kt
20.07.1995	18	77.2N	110.8E	130/28kt	7	10.0km	0	/	997.0	2.9	1.6	91	-0.2	/m	/	/m	SE 13kt
20.07.1995	21	76.7N	112.9E	140/29kt	7	10.0km	0	/	999.0	2.6	2.0	96	-0.6	/m	/	/m	SE 13kt
DD.MM.Year	UTC	Lat	Lon	DDD/FF	Bft	Visib.	WX	Weather	Press.	Ta	Td	rH	Tw	Sea	Max.Sea	Ice	Speed
21.07.1995	00	76.3N	114.4E	150/31kt	7	20.0km	0	fair, Ci	1001.2	2.1	1.8	98	-1.4	0.0m	150	0.0m	SE 13kt
21.07.1995	03	76.2N	116.3E	180/23kt	6	20.0km	0	fair, Ci	1005.2	2.4	2.1	98	-1.4	0.0m	180	0.0m	E 8kt
21.07.1995	06	76.4N	118.2E	150/32kt	7	4.0km	10	misty	1006.9	2.9	2.5	97	-0.2	1.5m	150	1.5m	NE 8kt
21.07.1995	09	76.6N	119.9E	150/31kt	7	0.2km	47	Fog	1009.5	1.5	1.1	97	-0.8	1.5m	150	1.5m	NE 8kt
21.07.1995	12	76.9N	121.6E	150/29kt	7	20.0km	0	fair, Ci	1012.8	1.2	0.8	97	-0.5	1.5m	150	1.5m	NE 8kt
21.07.1995	15	77.1N	123.5E	160/22kt	6	0.2km	0	/	1016.8	-0.1	-0.4	98	-1.2	/m	/	/m	NE 8kt
21.07.1995	18	77.4N	125.3E	140/24kt	6	4.0km	0	misty	1018.5	-0.5	-0.8	98	-1.9	/m	/	/m	NE 8kt
21.07.1995	21	77.6N	125.9E	150/20kt	5	10.0km	0	fair, Ci	1020.5	0.5	0.0	96	-1.9	/m	/	/m	NE 3kt

## A20

DD.MM.Year	UTC	Lat	Lon	DDD/FF	Bft	Visib.	WX	Weather	Press.	Ta	Td	rH	Tw	Sea	Max.Sea	Ice	Speed	
22.07.1995	00	77.7N	125.9E	150/16kt	5	20.0km	0	fair, Ci	1022.0	-0.1	-0.7	96	-1.7	0.0m	150	0.0m	4 N 3kt	
22.07.1995	03	77.7N	125.9E	150/16kt	5	10.0km	0	fair, Ci	1023.3	-0.1	-0.4	98	-1.9	/ m /	/ m /	/ m /	Station	
22.07.1995	06	77.7N	126.0E	140/17kt	5	10.0km	0	fair, Ci	1024.7	0.1	-0.2	98	-1.9	0.0m	140	0.0m	4 Station	
22.07.1995	09	77.7N	126.1E	150/17kt	5	20.0km	0	overcast	1026.6	0.1	-0.2	98	-1.9	0.0m	150	0.0m	4 Station	
22.07.1995	12	77.7N	126.1E	140/17kt	5	20.0km	0	fair, Ci	1027.6	0.2	-0.2	97	-1.9	0.0m	140	0.0m	4 Station	
22.07.1995	15	77.8N	126.1E	130/15kt	4	20.0km	0	cloudy	1028.4	-0.4	-0.7	98	-1.9	0.0m	130	0.0m	4 N 3kt	
22.07.1995	18	77.7N	126.7E	130/10kt	3	0.2km	0	/	1029.3	-1.4	-1.7	98	-1.8	/ m /	/ m /	/ SE	3kt	
22.07.1995	21	77.6N	128.8E	90/10kt	3	0.2km	0	/	1030.0	-2.1	-2.4	98	-0.8	/ m /	/ m /	/ E	8kt	
23.07.1995	00	77.6N	130.5E	90/14kt	4	20.0km	0	fair, Ci	1030.1	-0.8	-1.0	99	-1.1	0.0m	90	0.0m	4 E 8kt	
23.07.1995	03	77.5N	132.5E	50/10kt	3	20.0km	0	fair, Ci	1030.4	0.1	-0.2	98	0.1	0.0m	50	0.0m	2 E 8kt	
23.07.1995	06	77.5N	133.6E	60/10kt	3	20.0km	0	fair, Ci	1030.2	-0.4	-0.7	98	-1.6	0.0m	60	0.0m	4 E 3kt	
23.07.1995	09	77.5N	135.0E	70/13kt	4	10.0km	0	fair, Ci	1029.9	1.7	1.4	98	2.1	/ m /	/ m /	/ E	8kt	
23.07.1995	12	77.6N	137.4E	70/17kt	5	0.5km	44	Fog	1029.5	-0.3	-0.5	99	2.2	1.0m	70	1.0m	/ E	13kt
23.07.1995	15	77.7N	139.4E	90/18kt	5	1.0km	10	misty	1028.9	-2.0	-2.3	98	2.3	1.0m	90	1.0m	/ E	8kt
23.07.1995	18	77.8N	140.7E	90/16kt	5	0.5km	0	/	1028.4	-1.7	-2.0	98	1.3	/ m /	/ m /	/ E	8kt	
23.07.1995	21	77.9N	143.3E	100/14kt	4	10.0km	0	/	1028.2	-1.9	-2.1	99	0.7	/ m /	/ m /	/ E	13kt	
24.07.1995	00	78.0N	144.4E	100/13kt	4	2.0km	44	Fog	1027.9	-2.1	-2.4	98	2.0	1.0m	100	1.0m	/ NE	3kt
24.07.1995	03	78.0N	144.9E	100/16kt	5	1.0km	48	Fog	1027.1	-2.2	-2.5	98	0.2	1.0m	100	1.0m	2 E 3kt	
24.07.1995	06	78.0N	145.0E	100/12kt	4	4.0km	10	misty	1026.3	-1.5	-1.8	98	0.2	0.5m	100	0.5m	/ Station	
24.07.1995	09	78.1N	145.0E	90/13kt	4	4.0km	10	misty	1025.6	-0.9	-1.2	98	-1.3	0.0m	90	0.0m	3 N 3kt	
24.07.1995	12	78.4N	145.3E	110/13kt	4	10.0km	2	overcast	1025.2	-1.0	-1.3	98	-1.3	0.0m	110	0.0m	4 N 8kt	
24.07.1995	15	78.5N	145.7E	120/10kt	3	10.0km	2	overcast	1024.8	-1.3	-1.6	98	-1.3	0.0m	120	0.0m	4 NE	3kt
24.07.1995	18	78.5N	145.7E	110/ 9kt	3	10.0km	0	/	1023.9	-1.3	-1.6	98	-1.4	/ m /	/ m /	/ Station		
24.07.1995	21	78.5N	145.7E	130/ 9kt	3	10.0km	0	/	1023.3	-1.6	-1.9	98	-1.3	/ m /	/ m /	/ Station		
25.07.1995	00	78.5N	145.7E	120/ 9kt	3	20.0km	2	cloudy	1022.9	-1.5	-1.8	98	-0.8	0.0m	120	0.0m	4 Station	
25.07.1995	03	78.6N	145.7E	120/10kt	3	20.0km	0	overcast	1022.2	-1.4	-1.7	98	-0.7	0.0m	120	0.0m	4 N 3kt	
25.07.1995	06	78.6N	145.8E	130/11kt	4	10.0km	0	overcast	1021.9	-1.3	-1.6	98	-0.7	0.0m	130	0.0m	5 Station	
25.07.1995	09	78.7N	146.2E	130/10kt	3	4.0km	10	misty	1021.9	-1.7	-2.0	98	-0.8	0.0m	130	0.0m	5 NE	3kt
25.07.1995	12	78.9N	146.8E	130/17kt	5	20.0km	0	overcast	1021.5	-1.6	-1.9	98	-0.8	0.0m	130	0.0m	5 SE	3kt
25.07.1995	15	79.0N	147.3E	140/17kt	5	20.0km	0	cloudy	1021.6	-0.8	-1.1	98	-0.7	0.0m	140	0.0m	5 NE	3kt
25.07.1995	18	79.0N	147.3E	140/16kt	5	10.0km	0	/	1020.7	-0.2	-0.5	98	-0.5	/ m /	/ m /	/ Station		
25.07.1995	21	79.1N	147.3E	140/10kt	3	10.0km	0	/	1021.0	-0.3	-0.7	97	-0.7	/ m /	/ m /	/ N	3kt	
26.07.1995	00	79.1N	147.4E	140/12kt	4	20.0km	0	overcast	1020.3	-0.6	-0.9	98	-0.7	0.0m	140	0.0m	5 Station	
26.07.1995	03	79.1N	147.4E	150/10kt	3	20.0km	0	cloudy	1019.7	-0.4	-0.7	98	-1.6	0.0m	150	0.0m	5 Station	
26.07.1995	06	79.2N	147.5E	140/11kt	4	20.0km	0	fair, Ci	1019.9	-0.3	-0.6	98	-1.3	0.0m	140	0.0m	5 N 3kt	
26.07.1995	09	79.4N	147.7E	150/11kt	4	20.0km	0	overcast	1018.8	-0.7	-1.0	98	-1.3	0.0m	150	0.0m	5 N 3kt	
26.07.1995	12	79.4N	148.0E	150/10kt	3	20.0km	0	overcast	1018.7	-0.9	-1.2	98	-1.3	0.0m	150	0.0m	5 E 3kt	
26.07.1995	15	79.4N	148.1E	150/ 9kt	3	10.0km	0	fair, Ci	1017.1	-0.9	-1.2	98	-1.2	/ m /	/ m /	/ Station		
26.07.1995	18	79.5N	148.7E	140/ 9kt	3	10.0km	0	fair, Ci	1016.2	-1.2	-1.5	98	-1.2	/ m /	/ m /	/ Station		
26.07.1995	21	79.5N	148.1E	160/10kt	3	10.0km	0	/	1015.0	-1.4	-1.7	98	-1.1	/ m /	/ m /	? ?kt		
27.07.1995	00	79.5N	148.1E	170/ 9kt	3	20.0km	0	fair, Ci	1014.4	-0.9	-1.8	94	-1.1	0.0m	170	0.0m	5 Station	
27.07.1995	03	79.5N	148.2E	190/ 8kt	3	2.0km	10	misty	1014.0	-1.9	-2.5	96	-1.0	0.0m	190	0.0m	5 Station	
27.07.1995	06	79.5N	148.2E	190/ 9kt	3	0.5km	45	Fog	1013.4	-1.4	-1.7	98	-1.0	0.0m	190	0.0m	5 Station	
27.07.1995	09	79.5N	148.2E	250/ 8kt	3	1.0km	10	misty	1013.7	-0.8	-1.0	99	-0.4	0.0m	250	0.0m	5 Station	
27.07.1995	12	79.5N	148.2E	270/ 9kt	3	0.5km	45	Fog	1013.9	-1.0	-1.3	98	-0.4	0.0m	270	0.0m	5 Station	
27.07.1995	15	79.5N	148.2E	280/ 8kt	3	10.0km	28	r.Fog	1014.0	-1.7	-2.0	98	-1.5	0.0m	280	0.0m	5 Station	
27.07.1995	18	79.4N	147.7E	300/ 8kt	3	10.0km	0	/	1014.9	-1.3	-1.6	98	-1.3	/ m /	/ m /	/ SW	3kt	
27.07.1995	21	79.3N	147.2E	290/ 5kt	2	0.2km	0	/	1015.6	-1.1	-1.4	98	-1.2	/ m /	/ m /	/ SW	3kt	
28.07.1995	00	79.2N	146.5E	260/ 2kt	1	0.2km	45	Fog	1016.3	-0.8	-1.1	98	-1.1	0.0m	260	0.0m	5 SW	3kt
28.07.1995	03	79.1N	146.3E	230/ 6kt	2	0.5km	44	Fog	1016.1	-0.8	-1.1	98	-1.1	0.0m	230	0.0m	5 S 3kt	
28.07.1995	06	79.1N	146.3E	240/ 6kt	2	0.2km	42	Fog	1016.2	-0.8	-1.1	98	-1.0	0.0m	240	0.0m	5 E 3kt	
28.07.1995	09	79.1N	146.4E	230/ 6kt	2	1.0km	10	misty	1016.3	-0.7	-1.0	98	-1.0	0.0m	230	0.0m	5 Station	
28.07.1995	12	79.1N	146.4E	220/ 5kt	2	0.2km	47	Fog	1016.6	-0.8	-1.1	98	-1.0	0.0m	220	0.0m	5 Station	
28.07.1995	15	79.1N	146.0E	220/11kt	4	0.5km	44	Fog	1016.4	0.0	-0.3	98	-0.4	0.0m	220	0.0m	5 W 3kt	
28.07.1995	18	79.0N	145.4E	220/ 9kt	3	0.2km	0	/	1016.2	-0.5	-0.8	98	-1.0	/ m /	/ m /	/ SW	3kt	
28.07.1995	21	78.9N	145.2E	190/10kt	3	0.2km	0	/	1016.0	0.2	-0.1	98	-1.0	/ m /	/ m /	/ S	3kt	
29.07.1995	00	78.8N	144.5E	200/ 8kt	3	0.5km	44	Fog	1015.8	0.4	0.1	98	-0.4	0.0m	200	0.0m	5 SW	3kt
29.07.1995	03	78.7N	144.1E	190/10kt	3	0.2km	44	Fog	1015.3	0.2	-0.1	98	-0.9	0.0m	190	0.0m	5 SW	3kt
29.07.1995	06	78.7N	144.1E	170/11kt	4	0.5km	44	Fog	1014.9	0.3	-0.1	97	-0.9	0.0m	170	0.0m	5 Station	
29.07.1995	09	78.5N	143.4E	160/11kt	4	1.0km	10	misty	1014.3	0.5	0.2	98	-0.3	0.0m	160	0.0m	5 SW	3kt
29.07.1995	12	78.3N	142.0E	180/10kt	3	0.5km	44	Fog	1013.8	1.2	0.8	97	-0.4	0.0m	180	0.0m	4 SW	8kt
29.07.1995	15	78.1N	141.2E	160/ 7kt	3	0.5km	45	Fog	1013.0	1.7	1.4	98	1.2	0.0m	160	0.0m	/ SW	3kt
29.07.1995	18	78.0N	140.0E	140/ 4kt	2	0.2km	0	/	1012.4	2.1	1.8	98	2.3	/ m /	/ m /	/ W	3kt	
29.07.1995	21	78.0N	139.8E	200/ 2kt	1	4.0km	0	misty	1011.4	1.2	0.9	98	2.6	/ m /	/ m /	/ W	3kt	

## A21

DD.MM.Year	UTC	Lat	Lon	DDD/FF	Bft	Visib.	WX	Weather	Press.	Ta	Td	rH	Tw	Sea	Max.Sea	Sea Ice	Speed
30.07.1995	00	78.0N	139.8E	60/1kt	1	4.0km	10	misty	1011.3	3.4	3.1	98	2.8	0.0m	60	0.0m	/ Station
30.07.1995	03	78.0N	140.1E	140/5kt	2	4.0km	10	misty	1010.7	1.4	1.0	97	2.3	0.0m	140	0.0m	/ E 3kt
30.07.1995	06	78.0N	140.1E	150/10kt	3	10.0km	15	(Rain)	1010.1	2.6	2.2	97	3.2	0.0m	150	0.0m	/ Station
30.07.1995	09	77.6N	139.9E	170/14kt	4	20.0km	2	overcast	1009.5	3.7	3.1	96	3.8	0.5m	170	0.5m	/ S 8kt
30.07.1995	12	77.5N	140.0E	140/12kt	4	10.0km	0	overcast	1009.0	3.9	2.2	89	3.8	0.5m	140	0.5m	2 S 3kt
30.07.1995	15	77.5N	139.8E	110/11kt	4	20.0km	0	no cloud	1007.6	3.1	2.3	94	3.0	0.5m	110	0.5m	2 W 3kt
30.07.1995	18	77.4N	138.2E	120/13kt	4	10.0km	0	/	1005.9	2.3	2.0	98	4.3	/ m /	/ m /	W 8kt	
30.07.1995	21	77.3N	136.7E	110/13kt	4	10.0km	0	/	1004.0	3.4	3.0	97	4.1	/ m /	/ m /	?kt	

DD.MM.Year	UTC	Lat	Lon	DDD/FF	Bft	Visib.	WX	Weather	Press.	Ta	Td	rH	Tw	Sea	Max.Sea	Sea Ice	Speed
31.07.1995	00	77.3N	135.2E	100/12kt	4	20.0km	0	cloudy	1002.2	4.6	3.1	90	4.1	0.5m	100	0.5m	/ W 8kt
31.07.1995	03	77.2N	135.0E	110/12kt	4	20.0km	0	overcast	1001.1	2.9	1.5	90	4.2	0.5m	110	0.5m	/ SW 3kt
31.07.1995	06	77.1N	133.4E	110/11kt	4	0.1km	47	Fog	999.9	2.3	2.0	98	5.2	0.5m	110	0.5m	/ W 8kt
31.07.1995	09	77.0N	131.9E	120/7kt	3	4.0km	10	misty	999.2	2.8	2.4	97	5.3	0.5m	120	0.5m	/ W 8kt
31.07.1995	12	76.9N	131.3E	60/5kt	2	0.2km	45	Fog	998.7	1.5	1.1	97	4.1	0.0m	90	0.5m	/ SW 3kt
31.07.1995	15	76.7N	130.8E	30/3kt	1	1.0km	10	misty	997.9	1.8	1.5	98	6.3	0.0m	30	0.0m	/ SW 3kt
31.07.1995	18	76.2N	130.2E	360/5kt	2	0.5km	0	/	997.9	1.9	1.6	98	6.9	/ m /	/ m /	S 8kt	
31.07.1995	21	76.0N	130.0E	340/9kt	3	4.0km	0	misty	997.9	1.4	1.0	97	9.2	/ m /	/ m /	S 3kt	

DD.MM.Year	UTC	Lat	Lon	DDD/FF	Bft	Visib.	WX	Weather	Press.	Ta	Td	rH	Tw	Sea	Max.Sea	Sea Ice	Speed
01.08.1995	00	76.5N	130.0E	330/9kt	3	10.0km	2	overcast	998.6	1.7	1.3	97	6.3	0.5m	330	0.5m	/ N 8kt
01.08.1995	03	76.9N	130.0E	340/10kt	3	10.0km	0	/	999.0	1.6	1.3	98	3.8	/ m /	/ m /	N 8kt	
01.08.1995	06	76.9N	130.0E	330/17kt	5	10.0km	2	overcast	999.9	0.8	0.5	98	3.6	1.0m	330	1.0m	/ N 3kt
01.08.1995	09	77.3N	130.0E	350/22kt	6	10.0km	2	overcast	1001.2	-0.1	-0.4	98	2.9	1.5m	350	1.5m	/ N 8kt
01.08.1995	12	77.6N	130.0E	330/16kt	5	10.0km	2	overcast	1003.1	-0.8	-1.0	99	2.0	1.5m	330	1.5m	/ N 8kt
01.08.1995	15	77.6N	130.1E	330/14kt	4	10.0km	0	overcast	1003.8	-1.6	-2.1	96	1.8	/ m /	/ m /	Station	
01.08.1995	18	77.6N	130.0E	340/11kt	4	10.0km	0	/	1004.5	-1.8	-2.1	98	2.2	/ m /	/ m /	Station	
01.08.1995	21	77.7N	130.0E	320/10kt	3	10.0km	0	/	1005.2	-2.1	-2.7	96	2.4	/ m /	/ m /	N 3kt	

DD.MM.Year	UTC	Lat	Lon	DDD/FF	Bft	Visib.	WX	Weather	Press.	Ta	Td	rH	Tw	Sea	Max.Sea	Sea Ice	Speed
02.08.1995	00	77.9N	130.1E	30/4kt	2	4.0km	10	misty	1005.6	-1.8	-2.7	94	1.6	0.0m	30	0.0m	0 N 3kt
02.08.1995	03	77.7N	130.0E	30/2kt	1	4.0km	11	ShallFog	1005.9	-2.3	-3.0	95	2.1	0.0m	30	0.0m	/ S 3kt
02.08.1995	06	77.7N	130.0E	100/1kt	1	10.0km	2	overcast	1006.3	-2.1	-2.9	94	1.9	0.0m	100	0.0m	/ Station
02.08.1995	09	77.8N	130.0E	30/7kt	3	10.0km	0	overcast	1006.3	-2.4	-2.7	98	2.3	0.0m	30	0.0m	/ Station
02.08.1995	12	77.8N	130.0E	50/8kt	3	10.0km	0	overcast	1006.0	-1.6	-1.9	98	2.3	0.5m	50	0.5m	/ Station
02.08.1995	15	77.8N	130.1E	80/10kt	3	10.0km	0	overcast	1005.7	-1.1	-1.4	98	2.2	0.5m	80	0.5m	/ Station
02.08.1995	18	77.8N	130.2E	70/12kt	4	10.0km	0	/	1005.3	-0.7	-1.0	98	2.1	/ m /	/ m /	Station	
02.08.1995	21	77.9N	130.2E	70/15kt	4	10.0km	0	/	1004.9	-0.7	-1.0	98	1.9	/ m /	/ m /	?kt	

DD.MM.Year	UTC	Lat	Lon	DDD/FF	Bft	Visib.	WX	Weather	Press.	Ta	Td	rH	Tw	Sea	Max.Sea	Sea Ice	Speed
03.08.1995	00	77.9N	130.0E	90/16kt	5	0.5km	45	Fog	1005.4	-0.2	-0.5	98	2.3	1.0m	90	1.0m	/ W 3kt
03.08.1995	03	77.9N	130.0E	70/12kt	4	10.0km	0	overcast	1005.2	0.0	-0.3	98	2.4	1.0m	70	1.0m	/ Station
03.08.1995	06	77.9N	130.0E	70/14kt	4	10.0km	2	overcast	1005.5	-1.1	-1.4	98	2.2	1.0m	70	1.0m	/ Station
03.08.1995	09	77.9N	130.0E	80/14kt	4	4.0km	11	ShallFog	1006.2	-2.3	-2.6	98	1.9	1.0m	80	1.0m	/ Station
03.08.1995	12	78.3N	130.0E	70/12kt	4	10.0km	11	ShallFog	1006.9	-2.5	-2.8	98	1.1	0.5m	70	0.5m	/ N 8kt
03.08.1995	15	78.2N	130.0E	60/13kt	4	0.5km	45	Fog	1006.7	-1.0	-1.3	98	0.8	1.0m	60	1.0m	/ S 3kt
03.08.1995	18	78.2N	130.0E	70/17kt	5	10.0km	0	/	1006.6	-0.9	-1.2	98	0.6	/ m /	/ m /	Station	
03.08.1995	21	78.2N	130.0E	100/18kt	5	0.2km	0	/	1006.5	-0.2	-0.5	98	0.3	/ m /	/ m /	Station	

DD.MM.Year	UTC	Lat	Lon	DDD/FF	Bft	Visib.	WX	Weather	Press.	Ta	Td	rH	Tw	Sea	Max.Sea	Sea Ice	Speed
04.08.1995	00	78.2N	130.0E	110/21kt	5	0.2km	45	Fog	1006.5	0.0	-0.3	98	0.4	1.5m	110	1.5m	/ Station
04.08.1995	03	78.2N	130.0E	110/21kt	5	1.0km	10	misty	1006.4	0.7	0.4	98	0.7	1.0m	110	1.0m	/ Station
04.08.1995	06	78.2N	130.0E	120/24kt	6	2.0km	10	misty	1006.7	0.1	-0.2	98	0.6	1.5m	120	1.5m	/ Station
04.08.1995	09	78.4N	130.3E	120/27kt	6	0.5km	44	Fog	1006.1	0.0	-0.3	98	0.6	1.5m	120	1.5m	/ N 3kt
04.08.1995	12	78.7N	130.9E	120/25kt	6	1.0km	10	misty	1007.1	-0.9	-1.2	98	0.0	0.0m	120	0.0m	2 N 8kt
04.08.1995	15	79.0N	131.4E	110/28kt	7	4.0km	10	misty	1006.7	-0.9	-1.2	98	-1.2	0.0m	110	0.0m	4 N 8kt
04.08.1995	18	79.1N	131.4E	120/26kt	6	4.0km	0	misty	1005.8	-0.7	-1.0	98	-1.1	/ m /	/ m /	N 3kt	
04.08.1995	21	79.1N	131.4E	120/27kt	6	4.0km	0	misty	1005.4	-0.6	-0.9	98	-1.0	/ m /	/ m /	Station	

DD.MM.Year	UTC	Lat	Lon	DDD/FF	Bft	Visib.	WX	Weather	Press.	Ta	Td	rH	Tw	Sea	Max.Sea	Sea Ice	Speed
05.08.1995	00	79.1N	131.4E	120/30kt	7	4.0km	2	misty	1005.4	-0.8	-1.1	98	-0.9	0.0m	120	0.0m	5 Station
05.08.1995	03	79.2N	131.4E	130/27kt	6	0.2km	45	Fog	1005.7	-0.8	-1.1	98	-0.9	0.0m	130	0.0m	5 Station
05.08.1995	06	79.2N	131.5E	130/26kt	6	2.0km	10	misty	1005.1	-0.6	-0.9	98	-0.9	0.0m	130	0.0m	5 Station
05.08.1995	09	79.2N	131.5E	130/25kt	6	4.0km	10	misty	1004.9	-0.7	-1.0	98	-0.9	0.0m	130	0.0m	5 Station
05.08.1995	12	79.3N	131.5E	130/23kt	6	4.0km	51	Drizzle	1004.9	-0.4	-0.7	98	-1.3	0.0m	130	0.0m	5 N 3kt
05.08.1995	15	79.3N	131.5E	150/20kt	5	4.0km	60	Rain	1004.9	-0.3	-0.6	98	-1.2	/ m /	/ m /	5 Station	
05.08.1995	18	79.3N	131.5E	160/17kt	5	10.0km	0	/	1005.2	-0.6	-0.9	98	-1.1	/ m /	/ m /	Station	
05.08.1995	21	79.2N	131.0E	160/14kt	4	0.5km	0	/	1004.9	-0.7	-1.0	98	-1.3	/ m /	/ m /	SW 3kt	

DD.MM.Year	UTC	Lat	Lon	DDD/FF	Bft	Visib.	WX	Weather	Press.	Ta	Td	rH	Tw	Sea	Max.Sea	Sea Ice	Speed
06.08.1995	00	78.7N	129.3E	300/11kt	4	10.0km	2	overcast	1006.1	-2.3	-2.6	98	-0.3	0.5m	160	1.5m	/ SW 13kt
06.08.1995	03	78.2N	127.5E	340/13kt	4	0.2km	47	Fog	1006.4	-1.7	-2.0	98	-1.5	0.0m	340	0.0m	6 SW 13kt
06.08.1995	06	77.7N	125.0E	350/10kt	3	20.0km	2	overcast	1007.9	-1.4	-1.7	98	-0.7	0.5m	350	0.5m	/ SW 13kt
06.08.1995	09	78.0N	122.6E	310/6kt	2	20.0km	2	fair	1008.6	0.3	0.0	98	-0.3	0.0m	310	0.0m	4 NW 13kt
06.08.1995	12																

## A22

DD.MM.Year	UTC	Lat	Lon	DDD/FF	Bft	Visib.	WX	Weather	Press.	Ta	Td	rH	Tw	Sea	Max.Sea	Sea Ice	Speed
07.08.1995	00	79.9N	112.3E	150/41kt	9	10.0km	60	Rain	989.1	0.9	0.5	97	0.2	2.5m	150	2.5m	NW 13kt
07.08.1995	03	80.4N	109.7E	160/43kt	9	4.0km	10	misty	980.6	1.3	0.9	97	-1.0	4.0m	160	4.0m	NW 13kt
07.08.1995	06	80.8N	107.2E	170/37kt	8	10.0km	2	overcast	977.4	0.1	-1.1	92	-1.6	3.5m	170	3.5m	NW 13kt
07.08.1995	09	81.1N	105.3E	200/35kt	8	20.0km	0	fair	981.8	0.3	-1.3	89	-1.7	0.0m	200	0.0m	NW 8kt
07.08.1995	12	81.1N	105.4E	190/31kt	7	20.0km	0	cloudy	984.8	-0.6	-1.7	92	-1.8	0.0m	190	0.0m	5 Station
07.08.1995	15	81.1N	105.4E	190/29kt	7	20.0km	0	cloudy	986.5	-1.0	-1.6	96	-1.8	0.0m	190	0.0m	5 Station
07.08.1995	18	81.1N	105.6E	200/26kt	6	10.0km	0	/	987.6	-0.9	-1.5	96	-1.8	/ m /	/ m /	E 3kt	
07.08.1995	21	81.1N	105.8E	200/23kt	6	10.0km	0	fair, Ci	988.8	-1.1	-1.8	95	-1.8	/ m /	/ m /	E 3kt	
08.08.1995	00	81.1N	106.0E	210/25kt	6	20.0km	0	fair, Ci	990.3	-0.6	-1.5	94	-1.8	0.0m	210	0.0m	5 E 3kt
08.08.1995	03	81.1N	106.0E	200/25kt	6	20.0km	2	cloudy	991.5	-0.4	-1.2	94	-1.4	0.0m	200	0.0m	5 Station
08.08.1995	06	81.2N	106.2E	200/26kt	6	4.0km	85	Shower	992.5	-1.5	-1.8	98	-1.8	0.0m	200	0.0m	5 N 3kt
08.08.1995	09	81.2N	106.4E	220/25kt	6	20.0km	2	overcast	993.4	-0.5	-1.1	96	-1.2	0.0m	220	0.0m	5 E 3kt
08.08.1995	12	81.1N	105.3E	220/24kt	6	20.0km	2	cloudy	994.2	-0.9	-1.2	98	-1.4	0.0m	220	0.0m	5 SW 3kt
08.08.1995	15	81.2N	106.6E	230/21kt	5	20.0km	0	cloudy	994.7	-0.4	-0.9	96	-1.7	0.0m	230	0.0m	5 NE 3kt
08.08.1995	18	81.2N	106.6E	190/17kt	5	10.0km	0	/	995.0	-1.7	-2.0	98	-1.5	/ m /	/ m /	Station	
08.08.1995	21	81.2N	106.8E	230/20kt	5	10.0km	0	/	995.0	-1.5	-1.8	98	-1.4	/ m /	/ m /	E 3kt	
09.08.1995	00	81.2N	107.0E	220/18kt	5	20.0km	0	overcast	995.6	-1.3	-1.6	98	-1.4	0.0m	220	0.0m	5 E 3kt
09.08.1995	03	81.2N	107.0E	230/14kt	4	20.0km	0	overcast	996.6	-1.8	-2.3	96	-1.4	0.0m	230	0.0m	5 Station
09.08.1995	06	81.2N	107.1E	240/20kt	5	20.0km	0	overcast	997.4	-1.9	-2.2	98	-1.3	0.0m	240	0.0m	5 Station
09.08.1995	09	81.2N	107.3E	250/16kt	5	2.0km	70	Snow	999.9	-1.8	-2.1	98	-1.2	0.0m	250	0.0m	5 E 3kt
09.08.1995	12	81.2N	107.4E	270/17kt	5	10.0km	2	overcast	1001.8	-2.1	-2.4	98	-1.3	0.0m	270	0.0m	5 Station
09.08.1995	15	81.2N	107.4E	270/20kt	5	4.0km	0	misty	1004.2	-2.5	-2.8	98	-1.2	0.0m	270	0.0m	5 Station
09.08.1995	18	81.2N	107.5E	270/20kt	5	4.0km	0	misty	1005.6	-2.2	-2.5	98	-1.3	/ m /	/ m /	Station	
09.08.1995	21	81.2N	107.6E	270/19kt	5	10.0km	0	/	1007.3	-2.1	-2.4	98	-1.4	/ m /	/ m /	Station	
10.08.1995	00	81.2N	107.8E	280/19kt	5	10.0km	0	overcast	1008.9	-2.2	-2.5	98	-1.7	0.0m	280	0.0m	5 E 3kt
10.08.1995	03	81.2N	107.1E	280/21kt	5	10.0km	2	overcast	1011.1	-2.1	-2.4	98	-1.6	0.0m	280	0.0m	3 W 3kt
10.08.1995	06	81.1N	105.4E	290/17kt	5	4.0km	10	misty	1013.5	-2.0	-2.3	98	-1.7	0.0m	290	0.0m	4 W 8kt
10.08.1995	09	80.8N	104.2E	280/19kt	5	10.0km	0	overcast	1016.3	-2.4	-2.7	98	-1.7	0.0m	280	0.0m	7 SW 8kt
10.08.1995	12	80.9N	104.6E	280/15kt	4	0.5km	47	Fog	1017.9	-2.4	-2.7	98	-1.8	0.0m	280	0.0m	6 NE 3kt
10.08.1995	15	80.8N	104.5E	250/14kt	4	0.2km	0	/	1018.5	-3.0	-3.2	99	-1.7	/ m /	/ m /	S 3kt	
10.08.1995	18	80.8N	103.8E	220/11kt	4	10.0km	0	fair, Ci	1018.3	-2.8	-3.1	98	-1.4	/ m /	/ m /	W 3kt	
10.08.1995	21	80.8N	103.8E	170/10kt	3	10.0km	0	fair, Ci	1017.3	-2.6	-2.9	98	-1.5	/ m /	/ m /	Station	
11.08.1995	00	80.8N	103.3E	170/10kt	3	10.0km	2	overcast	1015.3	-1.6	-1.9	98	-1.3	0.0m	170	0.0m	6 Station
11.08.1995	03	80.7N	103.3E	150/13kt	4	10.0km	61	Rain	1012.2	-1.6	-1.9	98	-1.3	0.0m	150	0.0m	6 S 3kt
11.08.1995	06	80.8N	103.3E	130/14kt	4	10.0km	61	Rain	1008.7	-1.1	-1.4	98	-1.7	0.0m	130	0.0m	7 N 3kt
11.08.1995	09	80.8N	103.4E	110/10kt	3	10.0km	61	Rain	1005.3	-1.1	-1.4	98	-1.6	0.0m	110	0.0m	7 Station
11.08.1995	12	80.8N	103.4E	70/15kt	4	2.0km	61	Rain	1002.2	-1.3	-1.5	99	-1.3	0.0m	70	0.0m	6 Station
11.08.1995	15	80.7N	103.2E	30/16kt	5	10.0km	60	Rain	1001.2	-2.0	-2.3	98	-1.1	0.0m	30	0.0m	6 S 3kt
11.08.1995	18	80.7N	103.1E	360/19kt	5	2.0km	0	/	1002.5	-2.1	-2.4	98	-1.6	/ m /	/ m /	Station	
11.08.1995	21	80.6N	103.0E	330/19kt	5	1.0km	0	/	1004.8	-3.7	-4.0	98	-1.2	/ m /	/ m /	S 3kt	
12.08.1995	00	80.5N	102.7E	340/27kt	6	4.0km	77	Snow	1007.1	-3.6	-3.8	99	-1.5	0.5m	340	0.5m	7 SW 3kt
12.08.1995	03	80.4N	101.9E	330/20kt	5	4.0km	77	Snow	1009.2	-2.7	-3.0	98	-1.3	0.0m	330	0.0m	7 SW 3kt
12.08.1995	06	80.4N	102.0E	310/20kt	5	10.0km	2	overcast	1009.5	-2.4	-2.7	98	-1.1	0.0m	310	1.0m	7 Station
12.08.1995	09	80.4N	102.0E	280/13kt	4	20.0km	77	Snow	1010.1	-1.5	-1.8	98	-1.0	0.0m	280	0.0m	7 Station
12.08.1995	12	80.2N	102.5E	220/21kt	5	10.0km	11	ShallFog	1008.7	-2.6	-2.9	98	-1.3	0.0m	220	0.0m	6 SE 3kt
12.08.1995	15	79.8N	103.3E	250/21kt	5	20.0km	0	fair, Ci	1007.8	1.0	-1.2	85	0.5	0.5m	250	0.5m	2 S 8kt
12.08.1995	18	79.5N	104.5E	260/23kt	6	10.0km	0	fair, Ci	1006.7	0.6	-0.8	90	-1.3	/ m /	/ m /	SE 8kt	
12.08.1995	21	79.4N	104.5E	260/31kt	7	10.0km	0	/	1005.3	2.1	-1.0	80	-1.3	/ m /	/ m /	S 3kt	
13.08.1995	00	79.6N	103.6E	250/29kt	7	10.0km	60	Rain	1004.6	0.1	-0.6	95	-0.5	0.5m	250	0.5m	2 NW 3kt
13.08.1995	03	79.7N	103.0E	270/12kt	4	10.0km	21	r.Rain	1004.5	0.6	0.2	97	0.3	0.0m	270	0.0m	2 NW 3kt
13.08.1995	06	79.6N	104.1E	260/20kt	5	2.0km	68	Rain	1004.5	-1.2	-1.5	98	0.5	0.5m	260	0.5m	/ SE 3kt
13.08.1995	09	79.4N	105.0E	270/22kt	6	10.0km	2	overcast	1004.5	-0.8	-1.1	98	-1.3	0.5m	270	0.5m	2 SE 3kt
13.08.1995	12	79.0N	106.7E	300/11kt	4	10.0km	2	overcast	1004.5	0.2	-0.1	98	-0.9	0.0m	300	0.0m	4 SE 8kt
13.08.1995	15	78.5N	108.8E	300/9kt	3	4.0km	50	Drizzle	1004.3	-0.7	-1.0	98	-0.1	0.0m	300	0.0m	/ SE 13kt
13.08.1995	18	78.2N	111.0E	280/11kt	4	4.0km	0	misty	1003.5	-0.5	-0.8	98	1.3	/ m /	/ m /	SE 13kt	
13.08.1995	21	78.0N	113.1E	320/16kt	5	10.0km	0	/	1003.1	0.6	0.2	97	1.9	/ m /	/ m /	SE 8kt	
14.08.1995	00	77.8N	114.7E	320/19kt	5	20.0km	0	overcast	1003.2	0.2	-0.3	96	1.6	0.5m	320	0.5m	/ SE 8kt
14.08.1995	03	77.7N	115.1E	320/18kt	5	10.0km	0	/	1003.7	-1.2	-1.5	98	1.7	/ m /	/ m /	SE 3kt	
14.08.1995	06	77.5N	117.7E	330/21kt	5	10.0km	0	/	1004.0	-1.2	-3.0	87	1.5	/ m /	/ m /	E 13kt	
14.08.1995	09	77.3N	119.9E	330/22kt	6	20.0km	2	overcast	1004.6	-2.4	-3.9	89	1.8	1.5m	330	1.5m	/ SE 8kt
14.08.1995	12	77.2N	122.8E	300/18kt	5	20.0km	15	(Rain)	1004.4	-1.6	-3.7	85	0.4	1.5m	300	1.5m	/ E 13kt
14.08.1995	15	77.0N	125.7E	300/23kt	6	20.0km	2	overcast	1002.9	-1.3	-2.8	89	0.7	1.5m	300	1.5m	/ E 13kt
14.08.1995	18	77.3N	127.5E	310/28kt	7	10.0km	0	/	1000.8	-1.4	-1.6	99	1.7	/ m /	/ m /	NE 8kt	
14.08.1995	21	77.7N	129.8E	300/23kt	6	10.0km	0	/	999.5	-1.8	-2.1	98	0.8	/ m /	/ m /	NE 13kt	



DD.MM.Year	UTC	Lat	Lon	DDD/FF	Bft	Visib.	WX	Weather	Press.	Ta	Td	rH	Tw	Sea	Max.Sea	Ice	Speed	
15.08.1995	00	78.1N	132.3E	320/25kt	6	20.0km	0	overcast	998.5	-1.3	-1.7	97	1.6	1.5m	320	1.5m	NE 13kt	
15.08.1995	03	78.4N	134.5E	320/24kt	6	20.0km	0	overcast	997.8	-2.4	-2.7	98	-1.4	0.0m	320	0.0m	3 NE 13kt	
15.08.1995	06	78.5N	134.0E	310/27kt	6	4.0km	10	misty	997.2	-1.8	-2.1	98	-1.0	0.0m	310	0.0m	4 N 3kt	
15.08.1995	09	78.5N	134.0E	300/27kt	6	1.0km	70	Snow	997.1	-2.9	-3.2	98	-0.5	1.0m	300	1.0m	7 Station	
15.08.1995	12	78.5N	133.9E	300/29kt	7	1.0km	71	Snow	996.5	-2.9	-3.2	98	-0.9	1.0m	300	1.0m	7 Station	
15.08.1995	15	78.5N	133.8E	310/28kt	7	4.0km	10	misty	996.5	-2.8	-3.1	98	0.6	1.0m	310	1.0m	7 Station	
15.08.1995	18	78.5N	133.8E	320/23kt	6	2.0km	0	/	996.3	-2.1	-2.4	98	1.0	/	/	/	/	Station
15.08.1995	21	78.5N	133.8E	320/27kt	6	1.0km	0	/	995.8	-2.1	-2.4	98	0.8	/	/	/	/	Station

DD.MM.Year	UTC	Lat	Lon	DDD/FF	Bft	Visib.	WX	Weather	Press.	Ta	Td	rH	Tw	Sea	Max.Sea	Ice	Speed	
16.08.1995	00	78.5N	133.7E	330/22kt	6	4.0km	10	misty	996.4	-2.5	-2.8	98	0.8	0.0m	330	0.0m	7 Station	
16.08.1995	03	78.5N	133.6E	330/18kt	5	4.0km	10	misty	997.1	-2.3	-2.6	98	0.7	0.0m	330	0.0m	7 Station	
16.08.1995	06	78.6N	133.9E	340/22kt	6	20.0km	2	overcast	998.1	-2.8	-3.1	98	-0.5	0.0m	340	0.0m	3 NE 3kt	
16.08.1995	09	78.7N	134.7E	340/22kt	6	20.0km	2	overcast	999.6	-3.3	-3.6	98	-1.5	0.0m	340	0.0m	4 NE 3kt	
16.08.1995	12	78.7N	134.7E	350/23kt	6	20.0km	2	overcast	1001.4	-2.8	-3.1	98	-1.4	0.0m	350	0.0m	4 Station	
16.08.1995	15	78.7N	134.6E	350/24kt	6	20.0km	26	r.Shower	1003.2	-3.7	-3.9	99	-1.5	0.0m	350	0.0m	4 Station	
16.08.1995	18	78.7N	134.6E	350/17kt	5	10.0km	0	/	1004.4	-4.5	-5.0	96	-1.5	/	/	/	/	Station
16.08.1995	21	78.7N	134.7E	330/20kt	5	10.0km	0	/	1005.1	-4.1	-4.4	98	-1.5	/	/	/	/	Station

DD.MM.Year	UTC	Lat	Lon	DDD/FF	Bft	Visib.	WX	Weather	Press.	Ta	Td	rH	Tw	Sea	Max.Sea	Ice	Speed	
17.08.1995	00	78.8N	135.0E	330/23kt	6	20.0km	77	Snow	1004.7	-4.4	-4.7	98	-1.3	0.0m	330	0.0m	5 NE 3kt	
17.08.1995	03	78.8N	135.1E	300/24kt	6	20.0km	2	overcast	1004.2	-4.0	-4.4	97	-1.0	0.0m	300	0.0m	5 Station	
17.08.1995	06	79.1N	135.0E	300/20kt	5	20.0km	2	overcast	1003.2	-2.7	-3.0	98	-1.4	0.0m	300	0.0m	5 N 8kt	
17.08.1995	09	79.2N	135.1E	290/21kt	5	20.0km	2	overcast	1003.3	-3.1	-3.4	98	-1.2	0.0m	290	0.0m	5 N 3kt	
17.08.1995	12	79.1N	135.1E	280/16kt	5	10.0km	2	overcast	1003.1	-2.6	-2.9	98	-1.2	0.0m	280	0.0m	5 S 3kt	
17.08.1995	15	79.1N	135.0E	290/16kt	5	20.0km	2	overcast	1002.6	-2.8	-3.1	98	-1.3	0.0m	290	0.0m	5 Station	
17.08.1995	18	79.1N	135.0E	290/13kt	4	10.0km	0	/	1002.4	-2.6	-2.9	98	-1.2	/	/	/	/	Station
17.08.1995	21	79.1N	135.1E	270/15kt	4	10.0km	0	/	1002.2	-2.1	-2.4	98	-1.2	/	/	/	/	Station

DD.MM.Year	UTC	Lat	Lon	DDD/FF	Bft	Visib.	WX	Weather	Press.	Ta	Td	rH	Tw	Sea	Max.Sea	Ice	Speed	
18.08.1995	00	79.1N	135.2E	270/17kt	5	4.0km	70	Snow	1002.2	-2.4	-2.7	98	-1.3	0.0m	270	0.0m	5 Station	
18.08.1995	03	79.1N	135.1E	280/17kt	5	2.0km	70	Snow	1002.2	-2.0	-2.3	98	-1.3	0.0m	280	0.0m	5 Station	
18.08.1995	06	79.1N	135.1E	280/15kt	4	20.0km	2	overcast	1002.4	-1.3	-1.5	99	-1.2	0.0m	280	0.0m	5 Station	
18.08.1995	09	79.5N	135.0E	290/13kt	4	2.0km	10	misty	1003.3	-1.3	-1.6	98	-1.3	0.0m	290	0.0m	5 N 8kt	
18.08.1995	12	79.9N	134.9E	260/7kt	3	2.0km	77	Snow	1004.3	-1.5	-1.8	98	-1.2	0.0m	260	0.0m	5 N 8kt	
18.08.1995	15	80.0N	134.9E	270/7kt	3	0.2km	47	Fog	1005.2	-1.5	-1.8	98	-1.3	0.0m	270	0.0m	5 N 3kt	
18.08.1995	18	80.0N	134.9E	250/7kt	3	0.2km	0	/	1005.2	-1.6	-1.9	98	-1.4	/	/	/	/	Station
18.08.1995	21	80.0N	135.0E	230/6kt	2	10.0km	0	/	1005.9	-1.9	-2.2	98	-1.4	/	/	/	/	Station

DD.MM.Year	UTC	Lat	Lon	DDD/FF	Bft	Visib.	WX	Weather	Press.	Ta	Td	rH	Tw	Sea	Max.Sea	Ice	Speed	
19.08.1995	00	80.0N	135.0E	220/7kt	3	0.2km	45	Fog	1006.2	-2.1	-2.4	98	-1.4	0.0m	220	0.0m	5 Station	
19.08.1995	03	80.0N	135.0E	220/8kt	3	0.2km	44	Fog	1006.6	-2.9	-3.2	98	-1.4	0.0m	220	0.0m	5 Station	
19.08.1995	06	80.0N	135.0E	250/8kt	3	0.5km	42	Fog	1007.4	-2.4	-2.7	98	-1.4	0.0m	250	0.0m	5 Station	
19.08.1995	09	80.0N	135.0E	230/7kt	3	2.0km	10	misty	1007.7	-1.6	-1.9	98	-1.5	0.0m	230	0.0m	5 Station	
19.08.1995	12	80.2N	133.8E	240/6kt	2	0.2km	77	Snow	1007.9	-1.3	-1.6	98	-1.5	0.0m	240	0.0m	5 NW 8kt	
19.08.1995	15	80.2N	133.8E	240/5kt	2	0.5km	42	Fog	1008.1	-1.9	-2.1	99	-1.4	0.0m	240	0.0m	5 Station	
19.08.1995	18	80.3N	133.3E	170/5kt	2	0.2km	0	/	1007.9	-1.4	-1.7	98	-1.3	/	/	/	/	NW 3kt
19.08.1995	21	80.6N	131.9E	140/8kt	3	0.5km	0	/	1007.8	-2.3	-2.6	98	-1.3	/	/	/	/	NW 8kt

DD.MM.Year	UTC	Lat	Lon	DDD/FF	Bft	Visib.	WX	Weather	Press.	Ta	Td	rH	Tw	Sea	Max.Sea	Ice	Speed	
20.08.1995	00	80.5N	131.0E	120/12kt	4	20.0km	2	cloudy	1006.6	-2.1	-2.4	98	-1.1	0.0m	120	0.0m	5 SW 3kt	
20.08.1995	03	80.8N	131.0E	130/13kt	4	20.0km	0	overcast	1005.7	-2.1	-2.4	98	-1.2	0.0m	130	0.0m	5 N 8kt	
20.08.1995	06	80.9N	131.1E	120/14kt	4	20.0km	0	overcast	1004.9	-1.6	-1.9	98	-1.4	0.0m	120	0.0m	5 N 3kt	
20.08.1995	09	80.9N	131.1E	150/13kt	4	0.5km	45	Fog	1004.5	-1.6	-1.8	99	-1.5	0.0m	150	0.0m	5 Station	
20.08.1995	12	80.9N	131.1E	160/10kt	3	0.5km	45	Fog	1004.0	-1.7	-2.0	98	-1.5	0.0m	160	0.0m	5 Station	
20.08.1995	15	80.9N	131.2E	190/9kt	3	20.0km	2	overcast	1003.5	-1.7	-2.0	98	-1.5	0.0m	190	0.0m	5 Station	
20.08.1995	18	80.9N	131.2E	210/9kt	3	0.2km	0	/	1003.4	-0.8	-1.0	99	-1.4	/	/	/	/	Station
20.08.1995	21	80.9N	131.3E	240/11kt	4	0.2km	0	/	1003.9	-0.4	-0.6	99	-1.4	/	/	/	/	Station

DD.MM.Year	UTC	Lat	Lon	DDD/FF	Bft	Visib.	WX	Weather	Press.	Ta	Td	rH	Tw	Sea	Max.Sea	Ice	Speed	
21.08.1995	00	80.9N	131.3E	210/10kt	3	0.1km	45	Fog	1004.1	-0.3	-0.5	99	-1.4	0.0m	210	0.0m	5 Station	
21.08.1995	03	80.9N	131.3E	200/11kt	4	0.2km	45	Fog	1003.6	1.2	0.9	98	-1.4	0.0m	200	0.0m	5 Station	
21.08.1995	06	80.9N	131.4E	200/15kt	4	0.1km	45	Fog	1002.0	0.6	0.5	99	-1.4	0.0m	200	0.0m	5 Station	
21.08.1995	09	80.9N	132.0E	200/16kt	5	0.1km	45	Fog	1001.3	-0.7	-1.0	98	-1.7	0.0m	200	0.0m	5 E 3kt	
21.08.1995	12	81.0N	134.2E	210/13kt	4	0.2km	45	Fog	1001.7	-0.6	-0.9	98	-1.6	0.0m	210	0.0m	5 E 8kt	
21.08.1995	15	81.0N	134.5E	180/9kt	3	0.2km	45	Fog	1000.4	-0.1	-0.4	98	-1.4	0.0m	180	0.0m	5 E 3kt	
21.08.1995	18	81.0N	134.8E	330/1kt	1	0.5km	0	/	1001.1	-0.5	-0.8	98	-1.4	/	/	/	/	E 3kt
21.08.1995	21	81.0N	135.9E	60/17kt	5	0.2km	0	/	1002.3	-1.4	-1.7	98	-1.4	/	/	/	/	E 3kt

DD.MM.Year	UTC	Lat	Lon	DDD/FF	Bft	Visib.	WX	Weather	Press.	Ta	Td	rH	Tw	Sea	Max.Sea	Ice	Speed	
22.08.1995	00	81.0N	136.9E	60/23kt	6	2.0km	10	misty	1004.6	-1.6	-1.9	98	-1.4	0.0m	60	0.0m	5 E 3kt	
22.08.1995	03	81.0N	136.7E	70/25kt	6	10.0km	2	overcast	1006.7	-2.2	-2.5	98	-1.4	0.0m	70	0.0m	5 W 3kt	
22.08.1995	06	81.1N	136.6E	70/22kt	6	10.0km	0	/	1010.0	-2.8	-3.1	98	-1.5	/	/	/	/	N 3kt
22.08.1995	09	81.1N	136.5E	70/22kt	6	20.0km	0	overcast	1010.9	-2.7	-3.0	98	-1.4	0.0m	70	0.0m	5 Station	
22.08.1995	12	81.1N	136.4E	70/24kt	6	10.0km	2	overcast	1012.0	-3.1	-3.3	99	-1.5	0.0m	70	0.0m	5 Station	
22.08.1995	15	81.1N	136.3E	80/22kt	6	20.0km	0	overcast	1012.6	-3.6	-3.9	98	-1.4	0.0m	80	0.0m	5 Station	
22.08.1995	18	81.1N	136.1E	90/20kt	5	10.0km	0	/	1012.6	-4.1	-4.4	98	-1.5	/	/	/	/	W 3kt
22.08.1995	21	81.1N	136.6E	90/17kt	5	10.0km	0	/	1012.7	-3.0	-3.3	98	-1.2	/	/	/	/	E 3kt

## A24

DD.MM.Year	UTC	Lat	Lon	DDD/FF	Bft	Visib.	WX	Weather	Press.	Ta	Td	rH	Tw	Sea	Max.Sea	Ice	Speed
23.08.1995	00	81.0N	137.8E	80/22kt	6	2.0km	10	misty	1012.8	-3.4	-3.7	98	-1.5	0.0m	80	0.0m	5 SE 3kt
23.08.1995	03	81.0N	138.3E	80/20kt	5	1.0km	10	misty	1012.7	-3.2	-3.5	98	-1.4	0.0m	80	0.0m	5 E 3kt
23.08.1995	06	81.1N	138.3E	80/20kt	5	4.0km	10	misty	1012.6	-3.1	-3.4	98	-1.4	0.0m	80	0.0m	5 N 3kt
23.08.1995	09	81.1N	138.9E	90/18kt	5	4.0km	10	misty	1012.7	-2.9	-3.2	98	-1.2	0.0m	90	0.0m	5 E 3kt
23.08.1995	12	81.1N	138.9E	90/16kt	5	4.0km	10	misty	1012.9	-3.1	-3.4	98	-1.4	0.0m	90	0.0m	5 Station
23.08.1995	15	81.1N	138.9E	80/17kt	5	10.0km	0	overcast	1012.7	-3.1	-3.4	98	-1.5	0.0m	80	0.0m	5 Station
23.08.1995	18	81.1N	138.8E	90/20kt	5	10.0km	0	/	1012.7	-2.9	-3.2	98	-1.5	/ m /	/ m /	/ m / Station	
23.08.1995	21	81.1N	138.7E	100/18kt	5	10.0km	0	/	1012.6	-2.3	-2.6	98	-1.5	/ m /	/ m /	/ m / Station	
24.08.1995	00	81.1N	138.7E	90/17kt	5	10.0km	0	overcast	1012.4	-2.0	-2.2	99	-1.5	0.0m	90	0.0m	5 Station
24.08.1995	03	81.1N	138.7E	90/18kt	5	1.0km	10	misty	1012.3	-1.2	-1.5	98	-1.4	0.0m	90	0.0m	5 Station
24.08.1995	06	81.2N	138.7E	80/18kt	5	0.2km	45	Fog	1011.8	-1.6	-1.9	98	-1.5	0.0m	80	0.0m	5 N 3kt
24.08.1995	09	81.2N	140.2E	100/17kt	5	0.5km	45	Fog	1012.2	-1.1	-1.4	98	-1.2	0.0m	100	0.0m	5 E 3kt
24.08.1995	12	81.2N	140.1E	100/14kt	4	0.2km	45	Fog	1012.4	-1.9	-2.1	99	-1.4	0.0m	100	0.0m	5 Station
24.08.1995	15	81.2N	140.1E	100/16kt	5	0.2km	45	Fog	1012.2	-2.7	-3.0	98	-1.5	0.0m	100	0.0m	5 Station
24.08.1995	18	81.2N	140.0E	110/15kt	4	0.2km	0	/	1012.3	-3.1	-3.4	98	-1.5	/ m /	/ m /	/ m / Station	
24.08.1995	21	81.2N	140.2E	120/18kt	5	0.5km	0	/	1012.4	-3.1	-3.4	98	-1.4	/ m /	/ m /	/ m / E 3kt	
25.08.1995	00	81.2N	141.1E	120/19kt	5	0.5km	48	Fog	1012.6	-2.0	-2.3	98	-1.3	0.0m	120	0.0m	5 E 3kt
25.08.1995	03	81.2N	141.9E	120/20kt	5	0.2km	0	/	1012.9	-2.1	-2.4	98	-1.4	/ m /	/ m /	/ m / E 3kt	
25.08.1995	06	81.2N	141.9E	120/21kt	5	0.2km	48	Fog	1012.6	-2.2	-2.4	99	-1.5	0.0m	120	0.0m	5 Station
25.08.1995	09	81.2N	142.9E	120/19kt	5	0.2km	48	Fog	1013.0	-2.1	-2.3	99	-1.3	0.0m	120	0.0m	5 E 3kt
25.08.1995	12	81.2N	143.4E	130/20kt	5	0.2km	48	Fog	1013.2	-2.1	-2.4	98	-1.4	0.0m	130	0.0m	5 E 3kt
25.08.1995	15	81.2N	143.4E	140/20kt	5	10.0km	25	r.Shower	1012.6	-1.5	-1.8	98	-1.5	0.0m	140	0.0m	5 Station
25.08.1995	18	81.2N	143.4E	140/24kt	6	10.0km	0	/	1011.7	-0.9	-1.2	98	-1.5	/ m /	/ m /	/ m / Station	
25.08.1995	21	81.2N	143.4E	160/26kt	6	10.0km	0	/	1010.9	0.0	-0.3	98	-1.5	/ m /	/ m /	/ m / Station	
26.08.1995	00	81.2N	143.5E	170/23kt	6	20.0km	2	overcast	1010.8	0.0	-0.3	98	-1.5	0.0m	170	0.0m	5 Station
26.08.1995	03	81.2N	144.7E	170/24kt	6	10.0km	60	Rain	1011.6	0.3	0.0	98	-0.9	0.0m	170	0.0m	5 E 3kt
26.08.1995	06	81.2N	144.8E	160/27kt	6	10.0km	60	Rain	1010.4	0.6	0.2	97	-1.5	0.0m	160	0.0m	4 Station
26.08.1995	09	81.2N	144.8E	150/29kt	7	10.0km	25	r.Shower	1009.4	0.4	0.1	98	-1.6	0.0m	150	0.0m	4 Station
26.08.1995	12	81.2N	145.0E	160/26kt	6	10.0km	2	overcast	1007.3	-0.2	-0.5	98	-1.6	0.0m	160	0.0m	5 E 3kt
26.08.1995	15	81.2N	147.2E	170/24kt	6	10.0km	60	Rain	1006.9	-0.7	-1.0	98	-1.4	0.0m	170	0.0m	5 E 8kt
26.08.1995	18	81.2N	148.0E	180/23kt	6	10.0km	0	/	1005.1	-0.4	-0.7	98	-1.3	/ m /	/ m /	/ m / E 3kt	
26.08.1995	21	81.2N	150.0E	170/20kt	5	4.0km	0	misty	1003.3	-0.8	-1.1	98	-1.2	/ m /	/ m /	/ m / E 8kt	
27.08.1995	00	81.2N	150.1E	200/18kt	5	2.0km	63	Rain	1000.3	-0.9	-1.2	98	-1.3	0.0m	200	0.0m	5 Station
27.08.1995	03	81.2N	150.2E	240/12kt	4	10.0km	2	overcast	999.3	-1.0	-1.3	98	-1.3	0.0m	240	0.0m	5 Station
27.08.1995	06	81.2N	150.3E	260/12kt	4	0.2km	45	Fog	1000.6	-1.0	-1.3	98	-1.3	0.0m	260	0.0m	5 Station
27.08.1995	09	81.2N	150.3E	260/13kt	4	0.2km	45	Fog	1002.1	-0.9	-1.2	98	-1.3	0.0m	260	0.0m	5 Station
27.08.1995	12	81.2N	150.3E	250/15kt	4	0.1km	45	Fog	1002.7	-1.1	-1.4	98	-1.4	0.0m	250	0.0m	5 Station
27.08.1995	15	81.2N	150.4E	230/15kt	4	0.2km	44	Fog	1002.7	-0.8	-1.1	98	-1.4	0.0m	230	0.0m	5 Station
27.08.1995	18	81.2N	150.5E	220/17kt	5	10.0km	0	/	1001.4	-0.3	-0.5	99	-1.4	/ m /	/ m /	/ m / Station	
27.08.1995	21	80.8N	150.0E	220/19kt	5	2.0km	0	/	1001.0	-0.5	-0.8	98	-1.0	/ m /	/ m /	/ m / S 3kt	
28.08.1995	00	80.8N	150.0E	230/20kt	5	0.2km	45	Fog	1001.4	-0.6	-0.9	98	-1.2	0.0m	230	0.0m	5 Station
28.08.1995	03	80.5N	150.1E	240/19kt	5	1.0km	10	misty	1002.5	-1.0	-1.3	98	-1.3	0.0m	240	0.0m	5 S 8kt
28.08.1995	06	80.5N	150.2E	250/14kt	4	0.2km	45	Fog	1003.2	-1.3	-1.6	98	-1.4	0.0m	250	0.0m	5 Station
28.08.1995	09	80.5N	150.3E	260/13kt	4	0.2km	45	Fog	1004.0	-1.1	-1.4	98	-1.4	0.0m	260	0.0m	5 Station
28.08.1995	12	80.3N	150.0E	260/14kt	4	0.5km	44	Fog	1005.0	-1.4	-1.7	98	-1.3	0.0m	260	0.0m	4 S 3kt
28.08.1995	15	80.3N	150.2E	270/13kt	4	0.5km	45	Fog	1005.4	-1.6	-1.9	98	-1.4	0.0m	270	0.0m	5 E 3kt
28.08.1995	18	80.3N	150.3E	270/14kt	4	4.0km	0	misty	1005.7	-1.9	-2.2	98	-1.4	/ m /	/ m /	/ m / Station	
28.08.1995	21	80.3N	150.3E	270/13kt	4	1.0km	0	/	1006.0	-1.8	-2.1	98	-1.5	/ m /	/ m /	/ m / Station	
29.08.1995	00	80.3N	150.3E	280/12kt	4	1.0km	44	Fog	1006.6	-1.4	-1.7	98	-1.5	0.0m	280	0.0m	5 Station
29.08.1995	03	80.3N	150.4E	280/15kt	4	4.0km	44	Fog	1007.0	-1.8	-2.1	98	-1.5	0.0m	280	0.0m	5 Station
29.08.1995	06	80.3N	150.5E	280/12kt	4	4.0km	10	misty	1008.3	-2.1	-2.4	98	-1.5	0.0m	280	0.0m	5 Station
29.08.1995	09	80.2N	149.9E	280/9kt	3	2.0km	10	misty	1008.9	-1.7	-2.0	98	-1.6	0.0m	280	0.0m	3 SW 3kt
29.08.1995	12	80.1N	149.8E	270/8kt	3	4.0km	78	Snow	1009.7	-1.6	-1.9	98	-1.4	0.0m	270	0.0m	4 S 3kt
29.08.1995	15	80.1N	149.8E	270/6kt	2	10.0km	71	Snow	1009.6	-1.8	-2.1	98	-1.3	0.0m	270	0.0m	5 Station
29.08.1995	18	80.1N	149.8E	270/3kt	1	2.0km	0	/	1010.2	-1.9	-2.2	98	-1.4	/ m /	/ m /	/ m / Station	
29.08.1995	21	80.1N	149.8E	340/3kt	1	10.0km	0	/	1010.7	-1.9	-2.2	98	-1.5	/ m /	/ m /	/ m / Station	
30.08.1995	00	80.1N	149.8E	30/2kt	1	10.0km	70	Snow	1011.5	-1.8	-2.1	98	-1.5	0.0m	30	0.0m	3 Station
30.08.1995	03	79.9N	149.8E	10/4kt	2	10.0km	78	Snow	1012.2	-2.0	-2.3	98	-1.2	0.0m	10	0.0m	4 S 3kt
30.08.1995	06	79.9N	149.8E	10/5kt	2	10.0km	70	Snow	1013.0	-2.2	-2.4	99	-1.1	0.0m	10	0.0m	4 Station
30.08.1995	09	79.9N	149.8E	10/9kt	3	0.5km	46	Fog	1014.1	-1.8	-2.1	98	-1.1	0.0m	10	0.0m	4 Station
30.08.1995	12	79.7N	149.3E	30/14kt	4	2.0km	10	misty	1015.0	-1.3	-1.6	98	-1.2	0.0m	30	0.0m	4 Station
30.08.1995	15	79.5N	148.2E	40/16kt	5	1.0km	10	misty	1015.7	-1.9	-2.2	98	-1.2	0.0m	40	0.0m	4 SW 8kt
30.08.1995	18	79.5N	148.2E	30/16kt	5	10.0km	0	/	1016.8	-3.0	-3.3	98	-1.3	/ m /	/ m /	/ m / Station	
30.08.1995	21	79.6N	147.2E	30/16kt	5	2.0km	0	/	1018.3	-4.9	-5.2	98	-1.1	/ m /	/ m /	/ m / NW 3kt	

## A25

DD.MM.Year	UTC	Lat	Lon	DDD/FF	Bft	Visib.	WX	Weather	Press.	Ta	Td	rH	Tw	Sea	Max.Sea	Sea Ice	Speed
31.08.1995	00	79.7N	144.7E	20/12kt	4	10.0km	2	overcast	1019.7	-5.7	-6.0	98	-1.4	0.0m	20	0.0m	5 W 8kt
31.08.1995	03	79.7N	144.0E	340/13kt	4	0.2km	47	Fog	1020.0	-6.2	-6.5	98	-1.4	0.0m	340	0.0m	4 W 3kt
31.08.1995	06	79.8N	143.5E	330/14kt	4	0.5km	49	Fog	1019.5	-6.5	-6.8	98	-1.0	0.0m	330	0.0m	4 NW 3kt
31.08.1995	09	79.8N	143.1E	320/11kt	4	4.0km	78	Snow	1019.5	-6.1	-6.4	98	-1.3	0.0m	320	0.0m	4 W 3kt
31.08.1995	12	79.8N	142.8E	320/13kt	4	10.0km	77	Snow	1019.2	-6.2	-6.4	98	-1.1	0.0m	320	0.0m	5 W 3kt
31.08.1995	15	79.7N	141.4E	320/11kt	4	4.0km	78	Snow	1019.0	-7.0	-7.3	98	-0.9	0.0m	320	0.0m	5 W 3kt
31.08.1995	18	79.5N	139.2E	280/7kt	3	0.2km	0	/	1018.7	-8.1	-8.4	98	-1.3	/m	/	/m	/ SW 8kt
31.08.1995	21	79.4N	138.2E	250/4kt	2	0.2km	0	/	1018.2	-7.4	-7.7	98	-1.2	/m	/	/m	/ SW 3kt
DD.MM.Year	UTC	Lat	Lon	DDD/FF	Bft	Visib.	WX	Weather	Press.	Ta	Td	rH	Tw	Sea	Max.Sea	Sea Ice	Speed
01.09.1995	00	79.1N	137.3E	210/5kt	2	20.0km	2	fair, Ci	1017.3	-4.3	-4.6	98	-1.3	0.0m	210	0.0m	4 SW 8kt
01.09.1995	03	78.7N	135.6E	200/15kt	4	0.2km	45	Fog	1015.5	-2.9	-3.2	98	0.6	0.0m	200	0.0m	2 SW 8kt
01.09.1995	06	78.5N	134.1E	190/20kt	5	10.0km	2	overcast	1014.6	-0.8	-1.1	98	1.6	0.5m	190	0.5m	/ SW 8kt
01.09.1995	09	78.4N	134.8E	180/21kt	5	4.0km	10	misty	1012.4	0.1	-0.2	98	1.5	1.0m	180	1.0m	/ SE 3kt
01.09.1995	12	78.4N	134.8E	180/21kt	5	20.0km	2	overcast	1010.3	1.0	0.7	98	1.7	1.0m	230	1.5m	/ Station
10.09.1995	15	78.4N	134.9E	170/21kt	5	20.0km	0	overcast	1008.7	0.8	0.5	98	1.5	1.0m	170	1.0m	/ Station
01.09.1995	18	78.4N	135.1E	170/27kt	6	4.0km	0	misty	1006.3	1.0	0.7	98	1.3	/m	/	/m	/ E 3kt
01.09.1995	21	78.4N	135.1E	150/25kt	6	10.0km	0	/	1004.4	0.7	0.4	98	1.1	/m	/	/m	/ Station
DD.MM.Year	UTC	Lat	Lon	DDD/FF	Bft	Visib.	WX	Weather	Press.	Ta	Td	rH	Tw	Sea	Max.Sea	Sea Ice	Speed
02.09.1995	00	78.3N	135.2E	150/28kt	7	10.0km	0	overcast	1003.3	1.0	0.7	98	0.5	1.5m	150	1.5m	/ S 3kt
02.09.1995	03	78.4N	135.2E	150/30kt	7	20.0km	0	overcast	1002.2	1.5	1.2	98	0.6	1.5m	150	1.5m	/ N 3kt
02.09.1995	06	78.3N	135.4E	140/31kt	7	20.0km	0	overcast	1001.7	1.4	1.0	97	0.7	2.0m	200	2.5m	/ S 3kt
02.09.1995	09	78.2N	135.4E	150/31kt	7	20.0km	0	overcast	1001.8	1.9	1.4	96	0.5	2.0m	200	2.5m	/ S 3kt
02.09.1995	12	78.3N	134.8E	150/30kt	7	10.0km	0	overcast	1001.3	1.9	1.5	97	1.2	2.5m	200	3.0m	/ NW 3kt
02.09.1995	15	78.6N	132.8E	140/28kt	7	2.0km	52	Drizzle	999.6	1.1	0.8	98	1.1	2.5m	200	3.0m	/ NW 8kt
02.09.1995	18	78.8N	130.7E	130/24kt	6	0.5km	0	/	998.3	0.5	0.2	98	-1.0	/m	/	/m	/ NW 8kt
02.09.1995	21	79.1N	128.5E	140/15kt	4	0.2km	0	/	998.1	-0.5	-0.8	98	-0.7	/m	/	/m	/ NW 8kt
DD.MM.Year	UTC	Lat	Lon	DDD/FF	Bft	Visib.	WX	Weather	Press.	Ta	Td	rH	Tw	Sea	Max.Sea	Sea Ice	Speed
03.09.1995	00	79.3N	126.6E	110/11kt	4	1.0km	10	misty	998.0	-1.0	-1.3	98	-0.9	0.0m	110	0.0m	2 NW 8kt
03.09.1995	03	79.5N	124.3E	100/14kt	4	20.0km	28	r.Fog	998.0	-1.1	-1.4	98	-0.1	/m	/	/m	/ NW 8kt
03.09.1995	06	79.9N	123.0E	110/17kt	5	0.5km	46	Fog	998.5	-1.3	-1.6	98	-0.3	0.0m	110	0.0m	/ NW 8kt
03.09.1995	09	80.4N	122.6E	100/18kt	5	4.0km	10	misty	1000.3	-2.0	-2.3	98	-1.0	0.0m	100	0.0m	/ N 8kt
03.09.1995	12	80.8N	122.4E	100/15kt	4	0.2km	47	Fog	1001.5	-1.6	-1.9	98	-1.5	0.0m	100	0.0m	5 N 8kt
03.09.1995	15	80.9N	122.3E	100/17kt	5	0.2km	47	Fog	1002.0	-1.2	-1.5	98	-0.9	0.0m	100	0.0m	5 N 3kt
03.09.1995	18	80.9N	122.7E	80/19kt	5	0.2km	0	/	1002.3	-1.7	-2.0	98	-1.5	/m	/	/m	/ E 3kt
03.09.1995	21	80.9N	123.0E	80/20kt	5	0.5km	0	/	1002.4	-1.6	-1.9	98	-1.4	/m	/	/m	/ E 3kt
DD.MM.Year	UTC	Lat	Lon	DDD/FF	Bft	Visib.	WX	Weather	Press.	Ta	Td	rH	Tw	Sea	Max.Sea	Sea Ice	Speed
04.09.1995	00	80.9N	122.8E	80/21kt	5	2.0km	61	Rain	1002.5	-1.3	-1.6	98	-1.4	0.0m	80	0.0m	5 W 3kt
04.09.1995	03	80.9N	122.7E	100/20kt	5	1.0km	10	misty	1003.0	-1.3	-1.6	98	-1.4	0.0m	100	0.0m	5 Station
04.09.1995	06	80.9N	122.7E	110/16kt	5	0.5km	48	Fog	1004.1	-2.1	-2.4	98	-1.2	0.0m	110	0.0m	5 Station
04.09.1995	09	80.9N	122.8E	110/10kt	3	0.2km	48	Fog	1005.4	-2.8	-3.1	98	-1.3	0.0m	110	0.0m	5 Station
04.09.1995	12	80.9N	122.7E	100/9kt	3	0.2km	48	Fog	1006.4	-3.1	-3.4	98	-0.9	0.0m	100	0.0m	5 Station
04.09.1995	15	80.9N	122.6E	80/8kt	3	1.0km	10	misty	1006.9	-3.3	-3.5	99	-1.2	0.0m	80	0.0m	5 Station
04.09.1995	18	81.0N	122.7E	60/10kt	3	10.0km	0	/	1006.7	-2.3	-2.6	98	-1.1	/m	/	/m	/ N 3kt
04.09.1995	21	81.0N	122.7E	80/11kt	4	0.2km	0	/	1006.6	-1.8	-2.1	98	-1.3	/m	/	/m	/ Station
DD.MM.Year	UTC	Lat	Lon	DDD/FF	Bft	Visib.	WX	Weather	Press.	Ta	Td	rH	Tw	Sea	Max.Sea	Sea Ice	Speed
05.09.1995	00	80.9N	122.6E	110/11kt	4	0.2km	49	Fog	1006.8	-1.7	-2.0	98	-1.3	0.0m	110	0.0m	5 S 3kt
05.09.1995	03	80.9N	122.2E	80/10kt	3	0.2km	48	Fog	1006.4	-1.4	-1.7	98	-1.4	0.0m	80	0.0m	5 W 3kt
05.09.1995	06	80.7N	121.3E	60/14kt	4	0.5km	61	Rain	1004.5	-1.5	-1.8	98	-0.5	0.5m	60	0.5m	/ SE 3kt
05.09.1995	09	80.5N	120.2E	40/21kt	5	0.5km	73	Snow	1002.2	-0.8	-1.1	98	0.7	1.0m	40	1.0m	/ SW 3kt
05.09.1995	12	80.2N	119.0E	90/12kt	4	4.0km	10	misty	1000.1	-1.3	-1.6	98	1.5	1.0m	90	1.0m	/ SW 8kt
05.09.1995	15	80.2N	119.5E	130/12kt	4	0.5km	42	Fog	1000.5	-2.0	-2.3	98	0.3	0.5m	130	0.5m	/ E 3kt
05.09.1995	18	79.8N	117.6E	160/19kt	5	10.0km	0	/	999.9	-0.2	-0.5	98	1.7	/m	/	/m	/ SW 8kt
05.09.1995	21	79.5N	115.9E	160/12kt	4	10.0km	0	/	1000.4	-0.3	-0.6	98	1.9	/m	/	/m	/ SW 8kt
DD.MM.Year	UTC	Lat	Lon	DDD/FF	Bft	Visib.	WX	Weather	Press.	Ta	Td	rH	Tw	Sea	Max.Sea	Sea Ice	Speed
06.09.1995	00	79.2N	114.5E	190/14kt	4	10.0km	28	r.Fog	1000.4	-0.3	-0.6	98	2.0	1.0m	190	1.0m	/ SW 8kt
06.09.1995	03	78.8N	112.9E	210/12kt	4	10.0km	70	Snow	1001.1	-1.2	-1.5	98	2.1	1.0m	210	1.0m	/ SW 8kt
06.09.1995	06	78.8N	113.0E	200/13kt	4	10.0km	2	overcast	1001.4	-1.0	-1.2	99	2.1	1.0m	200	1.0m	/ Station
06.09.1995	09	78.8N	112.7E	200/11kt	4	10.0km	2	overcast	1002.1	-1.3	-1.6	98	2.1	1.0m	200	1.0m	/ W 3kt
06.09.1995	12	78.8N	112.7E	200/10kt	3	2.0km	10	misty	1002.2	-1.3	-1.5	99	2.1	0.5m	200	0.5m	/ Station
06.09.1995	15	78.8N	112.7E	290/3kt	1	10.0km	2	overcast	1002.3	-1.2	-1.5	98	1.8	0.0m	990	0.5m	/ Station
06.09.1995	18	78.8N	112.7E	330/11kt	4	2.0km	0	/	1002.6	-1.0	-1.2	99	1.8	/m	/	/m	/ Station
06.09.1995	21	78.7N	112.7E	320/14kt	4	10.0km	0	/	1003.4	-0.3	-0.6	98	1.9	/m	/	/m	/ S 3kt
DD.MM.Year	UTC	Lat	Lon	DDD/FF	Bft	Visib.	WX	Weather	Press.	Ta	Td	rH	Tw	Sea	Max.Sea	Sea Ice	Speed
07.09.1995	00	78.3N	112.9E	290/20kt	5	2.0km	10	misty	1005.1	-1.0	-1.3	98	1.1	0.0m	290	0.0m	/ S 8kt
07.09.1995	03	77.9N	113.5E	300/20kt	5	10.0km	14	Virga	1006.3	-1.3	-1.5	99	1.2	1.5m	300	1.5m	/ S 8kt
07.09.1995	06	77.9N	113.5E	290/18kt	5	10.0km	70	Snow	1007.8	-1.8	-2.1	98	1.1	1.5m	290	1.5m	/ Station
07.09.1995	09	77.9N	113.7E	280/15kt	4	20.0km	2	overcast	1008.8	-1.5	-2.4	94	1.3	1.0m	280	1.0m	/ E 3kt
07.09.1995	12	78.0N	113.3E	300/19kt	5	10.0km	77	Snow	1008.9	-1.8	-2.3	96	1.1	1.5m	300	1.5m	/ NW 3kt
07.09.1995	15	78.2N	111.6E	300/19kt	5	10.0km	2	overcast	1009.2	-2.0	-2.8	94	0.9	1.5m	300	1.5m	0 NW 8kt
07.09.1995	18	78.6N	109.4E	290/20kt	5	10.0km	0	/	1009.2	-2.6	-2.9	98	0.0	/m	/	/m	/ NW 13kt
07.09.1995	21	79.0N	107.0E	310/19kt	5	10.0km	0	/	1009.5	-2.6	-4.1	89	-0.2	/m	/	/m	/ NW 13kt

## A26

DD.MM.Year UTC	Lat	Lon	DDD/FF	Bft	Visib.	WX	Weather	Press.	Ta	Td	rH	Tw	Sea	Max.Sea	Ice	Speed
08.09.1995 00	79.4N	104.8E	290/15kt	4	20.0km	14	Virga	1009.6	-2.6	-4.2	89	-0.3	0.5m	290	0.5m	6 NW 13kt
08.09.1995 03	79.6N	103.3E	290/11kt	4	20.0km	2	overcast	1009.1	-3.0	-4.1	92	-0.2	0.0m	290	0.0m	/ NW 8kt
08.09.1995 06	80.1N	102.5E	300/15kt	4	10.0km	26	r.Shower	1007.6	-3.3	-3.6	98	-1.0	0.0m	300	0.0m	3 N 8kt
08.09.1995 09	80.4N	102.0E	290/18kt	5	10.0km	2	overcast	1006.8	-4.0	-4.7	95	-1.0	0.0m	290	0.0m	3 N 8kt
08.09.1995 12	80.8N	100.3E	330/21kt	5	2.0km	71	Snow	1005.9	-5.5	-6.1	96	-0.9	1.0m	330	1.0m	6 NW 8kt
08.09.1995 15	81.3N	98.5E	350/20kt	5	20.0km	2	overcast	1005.9	-7.5	-8.2	95	-1.5	0.0m	350	0.0m	4 NW 13kt
08.09.1995 18	81.7N	96.7E	340/24kt	6	10.0km	0	/	1006.0	-7.6	-8.1	96	-1.2	/ m /	/ m /	/ NW 8kt	
08.09.1995 21	81.8N	96.6E	330/22kt	6	10.0km	0	/	1006.0	-7.0	-7.3	98	-1.2	/ m /	/ m /	/ N 3kt	

DD.MM.Year UTC	Lat	Lon	DDD/FF	Bft	Visib.	WX	Weather	Press.	Ta	Td	rH	Tw	Sea	Max.Sea	Ice	Speed
09.09.1995 00	82.1N	94.4E	340/26kt	6	20.0km	0	overcast	1006.2	-6.9	-7.2	98	-1.4	0.0m	340	0.0m	3 NW 8kt
09.09.1995 03	82.4N	93.0E	350/23kt	6	10.0km	0	overcast	1006.6	-7.2	-7.5	98	-1.4	0.0m	350	0.0m	3 NW 8kt
09.09.1995 06	82.3N	92.9E	340/23kt	6	20.0km	0	overcast	1006.9	-9.0	-9.6	95	-1.2	0.5m	340	0.5m	3 S 3kt
09.09.1995 09	82.3N	92.8E	340/19kt	5	20.0km	2	overcast	1006.7	-8.2	-9.0	94	-1.3	0.0m	340	0.0m	3 Station
09.09.1995 12	82.3N	92.7E	340/14kt	4	20.0km	2	overcast	1005.5	-8.3	-9.4	92	-1.2	0.0m	320	0.0m	3 Station
09.09.1995 15	82.3N	92.0E	330/16kt	5	1.0km	71	Snow	1004.2	-10.1	-10.9	94	-1.5	0.0m	330	0.0m	3 W 3kt
09.09.1995 18	82.1N	91.4E	330/13kt	4	4.0km	0	misty	1003.5	-10.1	-11.2	92	-1.2	/ m /	/ m /	/ S 3kt	
09.09.1995 21	82.1N	91.3E	350/16kt	5	10.0km	0	/	1003.9	-10.7	-11.6	93	-1.3	/ m /	/ m /	/ Station	

DD.MM.Year UTC	Lat	Lon	DDD/FF	Bft	Visib.	WX	Weather	Press.	Ta	Td	rH	Tw	Sea	Max.Sea	Ice	Speed
10.09.1995 00	82.1N	91.0E	340/16kt	5	20.0km	2	overcast	1004.8	-11.5	-12.0	96	-1.3	0.0m	340	0.0m	3 W 3kt
10.09.1995 03	82.1N	91.0E	330/14kt	4	10.0km	70	Snow	1004.7	-10.8	-12.4	88	-1.1	0.0m	330	0.0m	3 Station
10.09.1995 06	82.1N	91.0E	330/ 9kt	3	10.0km	70	Snow	1004.7	-10.6	-12.1	89	-1.2	0.0m	330	0.0m	4 Station
10.09.1995 09	82.1N	91.0E	350/ 8kt	3	10.0km	2	overcast	1005.2	-10.1	-11.2	92	-1.4	0.0m	350	0.0m	3 Station
10.09.1995 12	82.0N	91.0E	340/ 7kt	3	20.0km	70	Snow	1005.6	-9.4	-10.6	91	-1.2	0.0m	340	0.0m	3 S 3kt
10.09.1995 15	82.0N	91.0E	20/ 3kt	1	20.0km	70	Snow	1005.7	-8.4	-9.3	93	-1.0	0.0m	20	0.0m	3 Station
10.09.1995 18	81.8N	90.8E	360/ 4kt	2	10.0km	0	/	1005.8	-6.3	-7.1	94	-1.3	/ m /	/ m /	/ S 3kt	
10.09.1995 21	81.6N	90.3E	330/ 9kt	3	10.0km	0	/	1006.4	-7.4	-8.3	93	-1.5	/ m /	/ m /	/ S 3kt	

DD.MM.Year UTC	Lat	Lon	DDD/FF	Bft	Visib.	WX	Weather	Press.	Ta	Td	rH	Tw	Sea	Max.Sea	Ice	Speed
11.09.1995 00	81.2N	89.1E	340/ 7kt	3	20.0km	78	Snow	1006.6	-6.8	-7.9	92	-0.9	0.0m	340	0.0m	2 SW 8kt
11.09.1995 03	81.2N	87.5E	10/ 9kt	3	10.0km	78	Snow	1006.7	-6.3	-6.6	98	-0.1	0.0m	10	0.0m	0 W 3kt
11.09.1995 06	80.9N	87.5E	10/11kt	4	20.0km	2	overcast	1006.2	-5.4	-6.0	96	-0.3	0.0m	10	0.0m	/ S 8kt
11.09.1995 09	80.3N	87.3E	360/16kt	5	10.0km	15	(Rain)	1005.7	-5.3	-6.0	95	0.2	0.5m	360	0.5m	/ S 13kt
11.09.1995 12	79.7N	87.0E	350/19kt	5	10.0km	15	(Rain)	1004.3	-5.8	-6.5	95	-0.1	1.0m	350	1.0m	/ S 13kt
11.09.1995 15	79.6N	87.0E	350/25kt	6	20.0km	0	overcast	1002.8	-4.8	-5.5	95	-0.2	1.5m	350	1.5m	/ S 3kt
11.09.1995 18	79.2N	86.9E	330/25kt	6	10.0km	0	/	1001.5	-4.6	-5.4	94	1.5	/ m /	/ m /	/ S 8kt	
11.09.1995 21	78.7N	87.0E	340/28kt	7	4.0km	0	misty	1000.3	-4.3	-4.8	96	0.4	/ m /	/ m /	/ S 8kt	

DD.MM.Year UTC	Lat	Lon	DDD/FF	Bft	Visib.	WX	Weather	Press.	Ta	Td	rH	Tw	Sea	Max.Sea	Ice	Speed
12.09.1995 00	78.2N	87.0E	330/26kt	6	1.0km	73	Snow	999.2	-3.7	-4.0	98	1.8	2.0m	330	2.0m	/ S 8kt
12.09.1995 03	78.0N	85.6E	340/29kt	7	2.0km	70	Snow	998.7	-3.4	-4.0	96	1.6	2.0m	340	2.0m	/ SW 8kt
12.09.1995 06	77.9N	83.4E	340/27kt	6	20.0km	0	overcast	998.2	-3.9	-4.7	94	1.5	2.5m	340	2.5m	/ W 8kt
12.09.1995 09	77.9N	81.2E	330/25kt	6	20.0km	2	overcast	998.7	-3.6	-4.9	91	1.7	2.5m	330	2.5m	/ W 8kt
12.09.1995 12	77.7N	79.3E	300/27kt	6	2.0km	71	Snow	997.1	-2.7	-3.0	98	1.7	2.5m	300	2.5m	/ SW 8kt
12.09.1995 15	77.3N	77.9E	290/33kt	7	1.0km	73	Snow	994.5	-1.9	-2.2	98	2.1	3.0m	290	3.0m	/ SW 8kt
12.09.1995 18	77.0N	76.5E	310/28kt	7	1.0km	0	/	993.1	-2.2	-2.5	98	1.6	/ m /	/ m /	/ SW 8kt	
12.09.1995 21	76.6N	75.2E	290/24kt	6	10.0km	0	/	991.4	-2.0	-2.3	98	2.1	/ m /	/ m /	/ SW 8kt	

DD.MM.Year UTC	Lat	Lon	DDD/FF	Bft	Visib.	WX	Weather	Press.	Ta	Td	rH	Tw	Sea	Max.Sea	Ice	Speed
13.09.1995 00	76.3N	73.9E	280/22kt	6	10.0km	2	overcast	990.7	-1.1	-1.8	95	2.6	2.5m	330	3.0m	/ SW 8kt
13.09.1995 03	75.9N	72.5E	280/19kt	5	4.0km	86	Shower	990.8	-0.6	-1.8	92	3.2	2.5m	340	3.0m	/ SW 8kt
13.09.1995 06	75.6N	71.2E	330/14kt	4	20.0km	15	(Rain)	991.8	0.0	-2.8	81	4.7	1.5m	340	2.5m	/ SW 8kt
13.09.1995 09	75.2N	69.9E	320/ 7kt	3	20.0km	2	cloudy	992.7	0.3	-3.7	74	5.1	1.0m	340	1.5m	/ SW 8kt
13.09.1995 12	74.9N	68.6E	310/13kt	4	20.0km	15	(Rain)	993.4	-0.1	-4.0	75	4.6	1.0m	290	2.0m	/ SW 8kt
13.09.1995 15	74.5N	67.6E	360/ 8kt	3	10.0km	15	(Rain)	994.1	-0.5	-3.4	81	5.5	0.5m	280	2.0m	/ SW 8kt
13.09.1995 18	74.1N	66.5E	160/ 2kt	1	10.0km	0	/	994.3	-0.7	-1.8	92	5.2	/ m /	/ m /	/ SW 8kt	
13.09.1995 21	73.7N	65.5E	350/ 6kt	2	10.0km	0	fair, Ci	994.6	-0.6	-3.5	81	5.2	/ m /	/ m /	/ SW 8kt	

DD.MM.Year UTC	Lat	Lon	DDD/FF	Bft	Visib.	WX	Weather	Press.	Ta	Td	rH	Tw	Sea	Max.Sea	Ice	Speed
14.09.1995 00	73.3N	64.5E	30/ 7kt	3	20.0km	2	cloudy	995.1	0.3	-4.3	71	5.5	0.5m	990	1.5m	/ SW 8kt
14.09.1995 03	72.9N	63.4E	90/ 8kt	3	1.0km	86	Shower	995.9	-0.8	-2.3	90	5.8	0.5m	340	1.5m	/ SW 8kt
14.09.1995 06	72.5N	62.5E	80/15kt	4	20.0km	15	(Rain)	997.2	-0.1	-0.4	98	6.0	0.5m	340	1.5m	/ SW 8kt
14.09.1995 09	72.1N	61.5E	80/14kt	4	20.0km	26	r.Shower	998.7	1.6	-1.2	82	6.8	0.5m	990	1.5m	/ SW 8kt
14.09.1995 12	71.7N	60.6E	110/16kt	5	20.0km	15	(Rain)	999.6	2.4	-2.8	68	6.6	0.5m	340	1.5m	/ SW 8kt
14.09.1995 15	71.3N	59.7E	110/15kt	4	20.0km	2	cloudy	1000.8	2.1	-1.9	75	6.4	1.0m	340	1.5m	/ SW 8kt
14.09.1995 18	70.9N	58.8E	90/17kt	5	10.0km	0	/	1002.1	2.2	-2.0	74	6.7	/ m /	/ m /	/ SW 8kt	
14.09.1995 21	70.5N	58.0E	60/11kt	4	10.0km	0	/	1003.5	1.4	-0.5	87	6.0	/ m /	/ m /	/ SW 8kt	

DD.MM.Year UTC	Lat	Lon	DDD/FF	Bft	Visib.	WX	Weather	Press.	Ta	Td	rH	Tw	Sea	Max.Sea	Ice	Speed
15.09.1995 00	70.2N	57.0E	60/14kt	4	10.0km	0	/	1004.8	2.0	-2.3	73	5.7	/ m /	/ m /	/ SW 8kt	
15.09.1995 03	70.2N	55.5E	40/19kt	5	20.0km	15	(Rain)	1006.8	2.3	0.2	86	6.9	1.0m	40	1.0m	/ W 8kt
15.09.1995 06	70.1N	54.1E	50/17kt	5	20.0km	2	fair	1009.3	2.8	-1.3	74	7.1	0.5m	50	0.5m	/ W 8kt
15.09.1995 09	70.1N	52.5E	10/14kt	4	20.0km	0	fair	1011.5	2.8	0.5	85	7.4	0.5m	10	0.5m	/ W 8kt
15.09.1995 12	70.1N	51.1E	360/14kt	4	20.0km	0	cloudy	1013.6	3.1	0.0	80	7.0	1.0m	360	1.0m	/ W 8kt
15.09.1995 15	70.0N	49.7E	350/17kt	5	20.0km	14	Virga	1014.3	2.7	1.0						

A27

DD.MM.Year	UTC	Lat	Lon	DDD/FF	Bft	Visib.	WX	Weather	Press.	Ta	Td	rH	Tw	Sea	Max.Sea	Sea Ice	Speed	
16.09.1995	00	69.9N	45.4E	360/19kt	5	10.0km	0	/	1017.7	2.2	1.5	95	7.2	/ m /	/ m /	W	8kt	
16.09.1995	03	69.8N	44.0E	310/18kt	5	20.0km	14	Virga	1018.5	2.4	1.2	92	7.2	1.0m	310	1.0m /	W	8kt
16.09.1995	06	69.8N	42.6E	280/ 9kt	3	20.0km	0	overcast	1019.1	3.2	1.1	86	7.5	0.5m	990	1.0m /	W	8kt
16.09.1995	09	69.8N	41.1E	270/18kt	5	4.0km	16	(Rain)	1018.9	4.7	4.3	97	7.5	1.0m	270	1.0m /	W	8kt
16.09.1995	12	69.7N	39.8E	300/18kt	5	10.0km	0	/	1019.1	5.2	3.7	90	7.8	/ m /	/ m /	W	8kt	
16.09.1995	15	69.7N	38.5E	310/20kt	5	20.0km	14	Virga	1019.8	5.7	4.8	94	7.8	1.5m	310	1.5m /	W	8kt
16.09.1995	18	69.6N	37.3E	290/19kt	5	10.0km	0	/	1020.3	5.3	4.9	97	7.8	/ m /	/ m /	W	8kt	
16.09.1995	21	69.6N	36.0E	300/26kt	6	10.0km	0	/	1020.7	5.8	3.8	87	7.7	/ m /	/ m /	W	8kt	
17.09.1995	00	69.5N	34.7E	310/19kt	5	10.0km	0	/	1021.3	6.1	1.4	72	8.1	/ m /	/ m /	W	8kt	
17.09.1995	03	69.3N	33.5E	280/ 8kt	3	10.0km	0	overcast	1022.5	5.2	1.2	75	7.7	0.0m	280	0.0m /	W	8kt
17.09.1995	06	69.0N	33.1E	210/ 4kt	2	20.0km	0	overcast	1023.4	2.2	1.8	97	8.2	0.0m	210	0.0m /	SW	8kt
17.09.1995	09	69.0N	33.1E	170/ 4kt	2	10.0km	0	overcast	1023.1	4.5	3.6	94	8.4	0.0m	170	0.0m /	Station	
17.09.1995	12	69.0N	33.1E	270/ 9kt	3	10.0km	0	/	1022.8	6.4	3.4	81	8.5	/ m /	/ m /	Station		
17.09.1995	15	69.0N	33.1E	300/ 8kt	3	20.0km	0	overcast	1023.1	7.0	3.0	76	8.5	0.0m	300	0.0m /	Station	
17.09.1995	18	69.0N	33.1E	240/ 3kt	1	10.0km	0	/	1023.2	6.0	2.9	80	8.5	/ m /	/ m /	Station		
17.09.1995	21	69.0N	33.1E	180/ 7kt	3	10.0km	0	/	1022.5	5.7	3.6	86	8.6	/ m /	/ m /	Station		

Abbreviations/Comments

DD.MM.Year	UTC	Lat	Lon	Date, Time and Location
DDD/FF	Bft			Wind direction, speed (knots and Beaufort)
Visib				Measurement based on light backscattering
WX	Weather			WX weather code no. according to SYNOP/FMI2
				Weather and clouds according to SYNOP/FMI2
Press.				Air pressure in hpa
Ta, Tw				Air/water Temperature in deg C
Td				Air dewpoint temperature in deg C
rH				Air relative humidity in %
Sea				Characteristic wave height in m
Max.Sea				Direction and height of swell
ICE				Ci of ICE -code
				0 no sea ice visible
				1 ship is within a lead wider than 1nm or in fast ice
				2 ice cover less than 3/10, open water or loose drift ice
				3 drift ice cover 4...6/10
				4 drift ice cover 7...8/10
				5 drift ice cover 9/10 or more but <10/10
				6 small fields of drift ice with open water
				7 small fields of dense drift ice
				8 fast ice, open water or loose drift ice seaward of ice edge
				9 fast ice, dense drift ice seaward of ice edge
				/ no data because of darkness or bad visibility
Speed				Direction and speed of ship

Attention: The WX and weather information is only available for data from manual observation. As observations are partly fully automatic, a "/" does not necessarily imply that there was no significant weather at this time. The same holds for ICE, sea and swell observation, respectively.

**Annex 11.3 : Hydrochemistry data**

(preliminary results, selected according to standardized water depths)

Y. Nalbandov

<i>Depth</i> <i>m</i>	<i>Temp.</i> <i>°C</i>	<i>Salin.</i> <i>o/oo</i>	<i>Oxygen</i> <i>ml/l</i> %		<i>pH</i> <i>--</i>	<i>Eh</i> <i>mV</i>	<i>Alk</i> <i>mg-eq/l</i>	<i>PO-4</i> <i>μM</i>	<i>NO-2</i> <i>μM</i>	<i>NO-3</i> <i>μM</i>	<i>Si</i> <i>μM</i>
-----											
St. # 002											
10	-1.188	31.377	8.47	99.9	7.93	181	2.19	1.31	0.04	1.44	4.76
20	-1.754	33.438	7.76	91.4	7.63	175	2.28	1.31	0.16	5.60	7.95
31	-1.746	33.568	7.57	89.3	7.63	172	2.28	1.15	0.14	6.45	8.14
138	-1.291	34.257	6.97	83.7	7.63	159	2.29	0.93	0.12	12.40	4.39
St. # 003											
10	-1.478	30.413	9.81	114.0	7.88	147	2.14	0.58	0.02	0.21	4.09
29	-1.621	31.880	7.83	91.6	7.82	147	2.26	0.98	0.01	7.35	7.18
99	-1.482	34.189	7.42	88.6	7.67	150	2.28	1.03	0.01	10.22	6.30
494	0.788	34.873	7.01	89.3	7.70	153	2.31	1.75	0.01	18.00	11.79
989	-0.090	34.884	7.15	89.0	7.65	158	2.28	1.90	0.01	17.76	13.47
1911	-0.801	34.924	6.81	83.2	7.77	170	2.31	1.98	0.06	21.71	20.93
St. # 004											
5	0.425	30.560	7.03	86.2	7.85	123	2.27	1.22	0.07	3.43	18.78
10	-1.747	33.068	7.04	82.8	7.82	128	2.27	1.25	0.08	3.33	18.77
20	-1.748	33.071	7.04	82.7	7.68	133	2.28	1.13	0.07	3.25	18.85
30	-1.750	33.073	6.99	82.1	7.73	135	2.29	1.09	0.07	3.13	19.09
46	-1.751	33.075	7.28	85.6	7.77	107	2.31	1.04	0.06	1.93	17.77
St. # 006											
5	-1.774	33.387	7.55	88.9	7.84	172	2.22	0.94	0.06	5.39	6.04
14	-1.794	33.452	7.45	87.6	7.94	154	2.24	1.07	0.05	6.22	6.59
20	-1.799	33.476	7.35	86.5	7.88	152	2.26	1.06	0.05	5.86	6.45
31	-1.799	33.490	7.34	86.4	7.83	153	2.27	1.21	0.04	5.94	6.35
87	-1.454	33.801	7.03	83.8	7.80	150	2.28	1.50	0.04	8.14	7.18
St. # 007											
17	-1.760	33.231	7.76	91.2	7.92	176	2.22	1.59	0.05	5.59	5.40
30	-1.783	33.304	7.74	91.0	7.85	173	2.26	1.57	0.03	5.53	5.66
99	-1.100	34.132	7.09	85.5	7.77	155	2.28	1.78	0.01	10.18	6.48
203	0.823	34.751	6.92	88.1	7.85	152	2.30	2.00	0.02	13.15	6.69
St. # 008											
5	-1.780	33.400	7.35	86.6	7.85	186	2.22	0.52	0.05	4.70	5.17
10	-1.780	33.404	7.41	87.2	7.80	173	2.21	0.64	0.05	7.15	5.26
20	-1.786	33.421	7.40	87.1	7.78	172	2.25	0.64	0.06	3.94	5.55
30	-1.794	33.446	7.33	86.3	7.80	167	2.26	0.72	0.04	4.97	6.44
90	-1.487	33.757	7.10	84.5	7.76	155	2.28	0.86	0.03	6.13	6.84
St. # 009											
5	-1.706	32.870	7.82	91.8	7.85	166	2.20	0.81	0.07	0.04	7.84
10	-1.721	33.012	7.61	89.5	7.75	162	2.22	0.82	0.09	0.76	8.43
31	-1.793	33.411	7.17	84.3	7.59	163	2.27	0.94	0.06	2.80	9.26
64	-1.794	33.443	7.13	84.0	7.55	158	2.29	0.96	0.06	2.46	8.73

## A29

Depth	Temp.	Salin.	Oxygen	pH	Eh	Alk	PO-4	NO-2	NO-3	Si	
St. # 010											
5	1.605	32.228	8.74	111.7	8.08	182	2.19	0.25	0.01	0.00	1.52
10	-0.096	32.554	8.91	109.1	8.02	178	2.20	0.26	0.02	0.00	2.01
30	-1.648	33.061	7.89	93.0	7.80	173	2.27	0.60	0.06	0.93	7.19
46	-1.664	33.083	7.85	92.5	7.80	172	2.27	0.62	0.06	0.00	5.27
St. # 011											
5	2.916	31.557	7.90	103.9	7.84	206	2.28	0.75	0.02	0.00	3.77
9	2.398	32.380	7.94	103.7	7.82	203	2.28	0.88	0.02	0.00	5.41
33	0.203	32.971	7.85	97.2	7.77	193	2.29	0.90	0.05	0.00	4.83
St. # 012											
5	4.014	29.953	8.20	109.8	7.95	207	2.10	1.07	0.01	2.79	1.80
10	1.874	30.653	8.76	111.5	7.88	202	2.15	1.12	0.03	3.30	1.70
31	-1.688	32.749			7.67	186	2.25	1.32	0.07	9.61	6.35
38	-1.689	32.774	7.62	89.5	7.70	186	2.25	1.44	0.07	13.44	7.85
St. # 016											
5	2.361	28.782	8.30	105.7	7.92	206	2.03	1.20	0.00	7.55	4.50
10	1.629	29.049	8.35	104.5	7.87	202	2.08	1.25	0.00	8.48	5.35
30	-1.487	33.098	6.70	79.4	7.73	197	2.26	1.69	0.04	18.37	10.75
95	-1.347	33.660	6.41	76.5	7.73	196	2.27	1.82	0.08	20.70	12.90
St. # 017											
5	3.001	28.657	8.30	107.4	7.96	212	2.02	1.45	0.01	11.34	3.45
9	1.374	28.793	8.65	107.4	7.91	201	2.03	1.53	0.01	11.87	6.00
30	-1.500	33.008	7.26	85.8	7.77	195	2.26	1.82	0.05	20.81	7.35
47	-1.358	33.889	6.94	82.9	7.76	193	2.28	2.22	0.13	31.29	8.20
57	-0.819	34.160	6.62	80.4	7.76	193	2.28	2.10	0.21	25.07	6.05
St. # 018											
5	2.327	28.709	8.42	107.1	7.88	223	2.03	1.72	0.02	16.58	4.85
10	0.628	29.096	8.71	106.3	7.88	218	2.08	1.76	0.04	17.07	5.70
30	-1.598	32.847	7.59	89.5	7.80	206	2.23	2.03	0.05	25.20	6.70
74	-0.918	34.200	7.35	89.1	7.78	202	2.29	2.28	0.08	31.02	7.65
90	-0.925	34.200	7.13	86.4	7.79	197	2.29	2.19	0.08	28.85	6.55
St. # 019											
4	1.901	28.693	8.78	110.4	7.78	216	2.03	0.35	0.01	0.00	2.77
10	-1.124	30.364	8.85	103.9	7.77	211	2.13	0.35	0.02	0.00	2.76
30	-1.604	33.327	7.56	89.3	7.72	208	2.27	0.49	0.03	5.87	3.83
100	-0.956	34.297	7.31	88.6	7.73	206	2.29	0.53	0.03	8.07	3.53
229	-0.824	34.353	7.28	88.5	7.75	203	2.29	0.62	0.04	8.48	3.83
St. # 020											
5	0.716	29.115	8.64	105.6	7.88	147	2.06	0.33	0.02	0.00	3.45
10	-0.574	29.859	8.67	102.9	7.82	147	2.10	0.33	0.07	0.00	4.19
30	-1.633	32.690	7.71	90.7	7.72	149	2.23	0.51	0.04	5.07	5.12
99	-1.368	34.174	7.42	88.8	7.70	151	2.29	0.60	0.02	6.14	4.17
395	1.538	34.877	7.14	92.8	7.72	162	2.31	0.79	0.02	9.78	4.16
461	1.440	34.878	7.09	91.9	7.77	170	2.31	0.84	0.02	10.52	4.54
St. # 021											
10	-0.978	29.812	8.68	101.9	7.83	274	2.14	0.67	0.07	0.00	7.81
29	-1.649	32.229	8.01	93.8	7.73	267	2.22	0.70	0.04	0.27	7.74

## A30

<i>Depth</i>	<i>Temp.</i>	<i>Salin.</i>	<i>Oxygen</i>		<i>pH</i>	<i>Eh</i>	<i>Alk</i>	<i>PO-4</i>	<i>NO-2</i>	<i>NO-3</i>	<i>Si</i>
St. # 021 ctd.											
98	-1.460	34.159	7.48	89.2	7.74	258	2.28	0.84	0.01	7.62	7.55
493	0.868	34.856	7.18	91.7	7.73	242	2.31	0.93	0.01	9.93	7.21
1033	-0.011	34.876	7.14	89.0	7.74	241	2.31	0.99	0.03	10.97	6.58
1138	-0.112	34.879	7.14	88.8	7.75	239	2.31	1.00	0.00	11.63	8.17
St. # 022											
10	-0.492	29.847	8.55	101.7	7.85	258	2.14	0.59	0.07	0.00	8.34
30	-1.618	32.282	7.89	92.6	7.78	251	2.23	0.73	0.04	3.28	7.52
99	-1.604	34.137	7.60	90.4	7.90	246	2.27	0.83	0.01	6.93	6.03
544	0.491	34.851	7.18	90.7	7.81	237	2.31	1.12	0.00	11.53	7.37
938	0.051	34.873	7.14	89.2	7.76	236	2.31	1.18	0.01	11.83	8.66
1745	-0.642	34.912	6.92	84.9	7.78	235	2.31	1.29	0.01	14.25	11.88
St. # 023											
10	-1.143	30.308	8.67	101.6	7.87	257	2.06	1.60	0.04	2.57	9.33
30	-1.741	32.729	8.24	96.7	7.78	247	2.20	1.75	0.07	6.37	8.60
100	-1.489	34.160	7.59	90.5	7.79	240	2.28	1.99	0.03	14.06	13.62
493	0.817	34.888	7.07	90.1	7.85	222	2.31	2.16	0.02	16.11	14.27
987	-0.199	34.885	7.14	88.6	7.79	224	2.31	2.39	0.01	25.64	19.44
1970	-0.747	34.917	6.93	84.8	7.80	223	2.31	2.33	0.04	18.70	27.26
2288	-0.794	34.928	6.90	84.3	7.83	223	2.32	2.55	0.04	27.62	19.97
St. # 024											
11	-1.410	29.887	8.49	98.5	7.83	244	2.12	0.00	0.06	2.60	2.03
31	-1.670	31.660	8.16	95.2	7.72	234	2.20	0.07	0.02	5.64	3.09
98	-1.421	34.153	7.57	90.5	7.75	223	2.28	0.41	0.01	14.38	3.63
495	0.805	34.884	7.09	90.3	7.75	219	2.31	0.75	0.01	19.98	6.35
992	-0.300	34.889	7.14	88.4	7.76	217	2.31	0.90	0.01	21.29	8.90
1972	-0.751	34.917	6.99	85.5	7.77	212	2.32	1.12	0.02	25.99	14.73
3066	-0.752	34.938	6.88	84.1	7.82	213	2.32	0.97	0.01	16.48	14.05
St. # 025											
9	-1.732	33.389	8.68	102.3	7.96	224	2.12	0.25	0.05	1.88	2.11
31	-1.759	34.152	7.85	93.0	7.82	217	2.23	0.55	0.12	8.40	4.45
99	-1.720	34.455	7.49	88.9	7.78	212	2.30	0.73	0.02	12.26	6.56
492	1.049	34.890	7.12	91.3	7.81	202	2.32	1.07	0.01	20.52	12.47
986	-0.209	34.907	7.02	87.1	7.79	202	2.31	1.11	0.01	21.74	17.24
2504	-0.794	34.932	6.98	85.3	7.77	199	2.32	1.21	0.01	24.09	20.48
St. # 026											
11	-1.707	33.063	8.14	95.7	7.95	218	2.22	0.48	0.07	5.47	5.75
31	-1.602	34.273	7.71	91.8	7.82	212	2.27	0.72	0.06	10.57	8.16
98	-0.343	34.523	7.37	90.9	7.76	206	2.30	0.89	0.01	14.60	10.99
507	1.646	34.944	7.07	92.1	7.70	207	2.32	1.12	0.00	19.57	14.77
989	-0.196	34.908	7.02	87.1	7.64	207	2.32	1.20	0.00	21.55	18.03
1969	-0.771	34.915	6.97	85.1	7.68	208	2.32	1.29	0.00	23.22	15.06
2874	-0.764	34.935	6.95	85.0	7.70	208	2.32	0.31	0.01	22.25	23.48
St. # 027											
11	-1.685	33.051	8.22	96.8	7.91	230	2.23	0.55	0.07	3.52	10.61
31	-1.649	34.323	7.66	91.0	7.86	221	2.25	0.85	0.09	10.32	15.38
99	-1.758	34.441	7.58	89.9	7.76	217	2.29	0.92	0.01	11.36	16.56
495	1.748	34.947	7.14	93.3	7.76	211	2.32	0.98	0.01	13.64	18.34
989	-0.195	34.908	7.00	86.9	7.69	214	2.32	1.00	0.01	14.73	20.74



## A 31

Depth	Temp.	Salin.	Oxygen	pH	Eh	Alk	PO-4	NO-2	NO-3	Si
St. # 027 ctd.										
1969	-0.768	34.916	6.96 85.1	7.70	213	2.31	1.19	0.00	20.58	25.37
2947	-0.771	34.933	6.95 85.0	7.70	213	2.32	1.13	0.00	17.89	25.06
3076	-0.750	34.938	6.90 84.4	7.76	213	2.32	1.37	0.01	23.30	28.19
St. # 029										
11	-1.594	32.293	8.61 101.1	7.90	166	2.15	0.67	0.08	1.48	0.00
31	-1.803	34.212	8.09 95.7	7.87	163	2.22	0.83	0.18	3.69	0.56
122	-0.873	34.563	7.34 89.3	7.85	163	2.30	0.93	0.02	7.55	1.49
594	-0.523	34.819	7.42 91.3	7.85	167	2.32	1.08	0.01	8.51	2.53
986	-0.404	34.871	7.32 90.3	7.82	168	2.32	1.19	0.01	9.49	3.30
1997	-0.800	34.921	7.06 86.3	7.78	173	2.32	1.38	0.01	12.32	5.53
St. # 029A										
11	-1.651	32.541	9.21 108.1	8.06	230	2.20	0.89	0.04	0.00	2.24
31	-1.797	34.280	7.97 94.3	7.85	230	2.28	1.03	0.18	3.55	2.91
100	-1.587	34.471	7.50 89.4	7.83	226	2.30	1.14	0.03	6.22	3.19
492	1.259	34.927	7.05 90.9	7.88	224	2.32	1.43	0.02	10.23	3.85
987	-0.252	34.907	7.04 87.2	7.79	224	2.32	1.44	0.02	10.89	4.52
1969	-0.771	34.916	7.00 85.5	7.88	225	2.32	1.54	0.02	11.94	8.91
2169	-0.805	34.926	6.94 84.8	7.88	224	2.32	1.55	0.05	11.83	9.67
St. # 030										
10	-1.668	32.398	9.03 105.9	8.12	237	2.19	1.06	0.03	0.00	3.28
30	-1.809	34.230	7.77 91.9	7.93	235	2.30	1.31	0.16	8.46	5.00
98	-1.443	34.468	7.51 89.8	7.83	234	2.30	1.30	0.02	5.92	4.78
495	-0.450	34.812	7.40 91.1	7.77	230	2.32	1.46	0.02	8.51	6.80
987	-0.629	34.846	7.44 91.2	7.83	228	2.32	1.57	0.01	8.56	6.94
1822	-0.738	34.914	7.28 89.0	7.86	228	2.32	1.95	0.02	12.09	9.18
St. # 031										
11	-1.567	32.307	8.98 105.5	8.06	175	2.14	1.12	0.01	0.00	5.24
29	-1.692	33.664	8.75 103.5	7.98	174	2.25	1.15	0.07	0.61	5.76
99	-1.202	34.485	7.44 89.7	7.82	176	2.31	1.74	0.08	12.85	11.09
593	-0.544	34.758	7.40 90.9	7.85	178	2.32	1.65	0.02	10.72	12.36
983	-0.579	34.789	7.42 91.1	7.84	179	2.32	1.99	0.02	17.58	16.38
1173	-0.557	34.814	7.36 90.4	7.82	180	2.32	1.83	0.01	13.05	17.39
St. # 032										
10	-1.403	32.518	8.97 106.0	8.00	182	2.22	1.21	0.02	0.00	12.20
30	-1.571	34.141	7.79 92.6	7.74	175	2.27	1.38	0.11	4.63	12.57
95	-0.530	34.478	7.34 90.1	7.72	174	2.30	1.57	0.02	8.40	14.26
493	-0.277	34.740	7.38 91.3	7.68	177	2.32	1.70	0.01	9.79	14.13
559	-0.414	34.738	7.35 90.6	7.67	177	2.31	1.67	0.01	8.96	14.09
St. # 033										
11	-1.519	33.534	8.42 100.0	7.92	213	2.23	1.39	0.09	1.72	12.35
32	-1.589	34.388	7.57 90.1	7.85	211	2.28	1.64	0.12	9.10	13.27
104	0.385	34.743	7.27 91.6	7.85	208	2.31	1.73	0.03	11.88	14.35
235	-0.332	34.754	7.32 90.5	7.84	208	2.31	1.90	0.04	12.55	15.84
St. # 035										
0	0.131	32.723	8.28 102.1	7.80	221	2.19	1.36	0.06	0.00	13.80
11	0.127	32.717	8.29 102.2	7.85	224	2.23	1.39	0.07	0.10	14.41
22	-1.112	33.768	8.15 97.9	7.89	221	2.29	1.54	0.19	5.15	15.22

## A32

Depth	Temp.	Salin.	Oxygen	pH	Eh	Alk	PO-4	NO-2	NO-3	Si	
St. # 035 ctd.											
50	-1.742	34.480	7.52	89.3	7.85	220	2.30	1.82	0.07	11.83	24.13
99	-1.328	34.576	7.44	89.4	7.84	222	2.30	1.92	0.02	12.37	18.60
316	0.018	34.800	7.21	89.9	7.85	218	2.31	1.99	0.04	15.66	17.29
St. # 036											
0	-1.248	31.463	8.46	99.7	7.90	220	2.15	1.44	0.06	0.49	13.75
10	-1.281	32.037	8.39	99.1	7.92	220	2.18	1.44	0.08	0.57	13.96
31	-1.350	33.852	7.91	94.4	7.87	222	2.28	1.58	0.10	3.96	15.48
90	-1.465	34.322	7.63	91.2	7.85	219	2.30	1.84	0.14	9.13	18.91
St. # 037											
12	-1.270	32.695	7.44	88.4	7.77	251	2.23	1.68	0.10	4.95	16.67
26	-1.491	33.187	7.36	87.2	7.78	243	2.25	1.73	0.10	4.25	17.09
101	-1.483	33.824	7.32	87.1	7.76	233	2.28	1.91	0.09	8.63	18.62
177	-0.637	34.486	7.56	92.5	7.80	229	2.23	1.77	0.05	4.84	16.60
St. # 038											
0	1.786	29.588	7.97	100.6	7.85	250	2.07	1.46	0.02	0.00	15.02
30	-1.456	33.391	7.47	88.7	7.72	242	2.26	1.67	0.11	3.71	17.20
49	-1.492	33.734	7.30	86.8	7.68	237	2.27	1.66	0.11	6.15	17.81
98	-1.376	34.018	7.32	87.5	7.70	231	2.28	1.66	0.05	5.50	17.28
249	0.010	34.652	7.12	88.7	7.73	223	2.30	1.80	0.05	8.44	17.58
St. # 039											
4	0.933	29.408	8.33	102.6	7.79	252	2.05	1.45	0.02	0.00	16.89
10	0.695	29.581	8.37	102.6	7.75	249	2.07	1.44	0.03	0.00	16.95
30	-1.544	32.762	7.67	90.5	7.63	243	2.24	1.64	0.08	3.96	18.22
109	-1.288	34.097	7.26	87.0	7.63	228	2.29	1.76	0.06	6.65	18.65
243	-0.642	34.461	7.30	89.3	7.66	225	2.30	1.89	0.05	8.10	18.04
St. # 040											
3	-1.811	33.624	8.36	98.4	7.87	238	1.99	0.42	0.03	0.19	2.65
9	-1.813	33.631	8.71	102.6	7.87	235	2.05	0.49	0.03	0.68	3.63
31	-1.412	34.226	7.93	94.9	7.83	232	2.23	0.47	0.04	3.93	2.53
98	1.933	34.874	7.55	99.0	7.87	232	2.28	0.65	0.02	8.16	1.74
506	0.558	34.859	7.15	90.6	7.83	221	2.31	0.84	0.02	10.71	3.64
977	-0.633	34.910	7.16	87.9	7.84	228	2.31	0.82	0.02	10.33	4.17
1698	-0.634	34.909	6.98	85.6	7.83	227	2.31	0.87	0.01	11.21	7.18
St. # 042											
0	-1.578	30.306	8.64	100.1	7.85	241	2.11	0.48	0.10	1.20	4.52
10	-1.562	30.876	8.41	97.8	7.76	238	2.11	0.57	0.11	4.33	8.19
30	-1.678	31.760	8.26	96.4	7.74	234	2.16	0.74	0.03	6.88	8.35
99	-1.608	34.109	7.71	91.6	7.81	233	2.26	0.65	0.02	6.89	2.84
499	0.667	34.875	7.11	90.3	7.87		2.31	0.79	0.01	10.49	4.63
987	-0.189	34.756	7.17	88.9	7.84		2.31	0.85	0.01	11.10	5.44
2075	-0.747	34.902	6.94	84.9	7.78		2.31	0.84	0.01	12.64	9.43
St. # 044											
0	-1.608	30.862	8.65	100.5	7.85	297	2.09	0.38	0.09	1.56	4.62
10	-1.616	30.762	8.61	99.9	7.74	288	2.12	0.38	0.08	1.63	4.56
30	-1.676	32.034	8.31	97.1	7.72	281	2.20	0.35	0.10	2.77	4.12
99	-1.467	34.115	7.57	90.3	7.64	272	2.28	0.47	0.02	6.86	2.51
499	0.752	34.874	7.14	90.9	7.71	258	2.31	0.67	0.01	10.12	4.29

## A33

<i>Depth</i>	<i>Temp.</i>	<i>Salin.</i>	<i>Oxygen</i>		<i>pH</i>	<i>Eh</i>	<i>Alk</i>	<i>PO-4</i>	<i>NO-2</i>	<i>NO-3</i>	<i>Si</i>
St. # 044 ctd.											
986	-0.316	34.876	7.19	89.0	7.61	257	2.31	0.61	0.01	9.79	4.89
1970	-0.734	34.913	7.00	85.6	7.60	255	2.31	0.81	0.00	11.95	8.72
2815	-0.765	34.932	6.88	84.1	7.65	248	2.32	0.75	0.01	11.44	9.32
St. # 045											
0	-1.603	30.400	8.72	101.0	7.75	228	2.06	0.42	0.11	1.14	4.95
8	-1.602	30.416	8.72	101.1	7.86	230	2.07	0.33	0.07	1.20	4.78
31	-1.725	32.301	8.45	98.9	7.68	235	2.20	0.36	0.04	2.19	4.33
100	-1.448	34.122	7.61	90.8	7.72	241	2.28	0.42	0.02	6.42	2.51
495	0.779	34.878	7.13	90.8	7.70	225	2.32	0.70	0.01	9.97	4.45
982	-0.343	34.885	7.16	88.5	7.68	233	2.31	0.65	0.01	9.74	5.38
1969	-0.748	34.914	7.05	86.2	7.72	242	2.32	0.81	0.01	11.47	8.82
3347	-0.731	34.935	6.91	84.6	7.70	245	2.32	0.80	0.02	11.99	9.69
St. # 046											
0	-1.737	32.550	8.70	102.0	7.79	305	2.07	0.43	0.07	1.29	5.38
11	-1.634	30.837	8.68	100.8	7.88	300	2.10	0.41	0.05	1.63	5.48
30	-1.819	33.366	8.36	98.3	7.85	297	2.24	0.41	0.01	3.49	1.90
93	-1.837	33.583	8.24	96.9	7.82	293	2.26	0.37	0.01	4.11	1.94
494	0.712	34.868	7.13	90.6	7.77	284	2.31	0.65	0.00	8.81	4.73
985	-0.299	34.879	7.17	88.7	7.72	283	2.31	0.70	0.00	8.99	6.04
1970	-0.744	34.915	7.00	85.6	7.76	278	2.31	0.88	0.00	12.07	10.92
3490	-0.723	34.936	7.01	85.8	7.78	276	2.31	0.81	0.01	10.49	10.57
St. # 047											
0	-1.654	31.201	9.01	104.8	7.74	359	2.13	0.40	0.08	0.38	3.02
11	-1.608	31.197	9.03	105.2	7.88	367	2.13	0.34	0.05	0.27	3.07
30	-1.720	32.262	8.63	101.0	7.83	362	2.16	0.37	0.06	1.64	3.89
100	-1.212	34.254	7.59	91.2	7.78	358	2.28	0.53	0.01	5.53	2.99
495	0.809	34.880	7.12	90.7	7.69	346	2.31	0.71	0.00	8.55	5.06
987	-0.190	34.898	7.08	87.9	7.71	345	2.31	0.74	0.01	8.77	6.42
1969	-0.748	34.916	7.00	85.6	7.71	343	2.31	0.81	0.00	9.95	9.49
2948	-0.783	34.930	7.00	85.5	7.68	342	2.32	0.85	0.00	10.55	10.36
3837	-0.692	34.937	6.94	85.0	7.68	340	2.32	0.82	0.00	10.87	11.06
St. # 049											
0	-1.589	30.504	8.84	102.5	7.93	297	2.13	0.38	0.09	0.05	4.77
11	-1.600	30.507	8.78	101.8	7.87	297	2.13	0.36	0.04	0.36	4.88
31	-1.761	32.707	8.37	98.1	7.82	295	2.16	0.44	0.02	2.74	3.77
94	-1.576	34.023	7.66	91.0	7.81	292	2.28	0.53	0.03	5.46	3.38
494	0.649	34.867	7.15	90.8	7.83	289	2.31	0.79	0.01	10.55	5.71
986	-0.279	34.876	7.22	89.5	7.78	288	2.31	0.80	0.01	10.46	6.58
2342	-0.790	34.923	6.94	84.9	7.78	285	2.32	0.97	0.00	14.22	12.66
St. # 051											
0	-1.663	31.352	8.96	104.3	7.97	289	2.10	0.47	0.08	1.84	3.77
11	-1.661	31.122	8.74	101.6	7.90	286	2.12	0.49	0.09	2.96	4.36
30	-1.719	32.276	8.49	99.3	7.82	285	2.23	0.56	0.04	4.25	3.83
99	-1.275	34.192	7.49	89.9	7.75	283	2.28	0.80	0.03	8.29	3.96
494	0.571	34.849	7.17	90.8	7.83	280	2.31	1.17	0.02	12.52	5.66
987	-0.157	34.865	7.18	89.2	7.85	280	2.31	1.17	0.02	11.25	5.81
1774	-0.698	34.917	6.93	84.9	7.85	279	2.25	1.39	0.01	13.50	10.64

## A 34

<i>Depth</i>	<i>Temp.</i>	<i>Salin.</i>	<i>Oxygen</i>	<i>pH</i>	<i>Eh</i>	<i>Alk</i>	<i>PO-4</i>	<i>NO-2</i>	<i>NO-3</i>	<i>Si</i>	
St. # 052											
0	-1.662	31.251	8.93	103.9	7.88	327	2.13	0.91	0.07	2.11	4.40
11	-1.664	31.211	8.82	102.5	7.85	325	2.16	0.92	0.09	2.32	5.31
31	-1.747	32.539	8.32	97.4	7.75	322	2.23	1.01	0.02	4.66	4.96
99	-1.462	34.100	7.56	90.2	7.74	320	2.28	1.12	0.01	7.88	5.05
496	0.603	34.864	7.14	90.5	7.77	314	2.31	1.40	0.02	11.45	6.58
986	-0.242	34.878	7.19	89.1	7.72	313	2.31	1.41	0.01	11.40	7.55
1204	-0.418	34.891	7.12	87.9	7.75	312	2.31	1.46	0.02	12.36	9.81
St. # 053											
0	-1.648	31.035	8.85	102.8	7.88	323	2.13	1.13	0.06	1.70	6.64
10	-1.642	31.034	8.87	103.1	7.80	322	2.16	1.07	0.03	1.60	6.27
37	-1.774	33.120	8.17	95.9	7.78	320	2.23	1.13	0.02	4.66	8.38
99	-1.029	34.274	7.35	88.8	7.77	319	2.28	1.29	0.01	8.34	9.79
494	0.678	34.860	7.11	90.4	7.75	313	2.31	1.47	0.01	10.39	11.07
742	0.066	34.860	7.17	89.6	7.74	312	2.31	1.54	0.01	11.04	11.56
918	-0.194	34.874	7.13	88.5	7.60	312	2.31	1.66	0.05	12.40	12.92
St. # 055											
0	-1.657	31.120	8.81	102.4	7.86	320	2.15	1.26	0.07	1.86	11.18
10	-1.660	31.146	8.80	102.3	7.85	318	2.15	1.19	0.06	2.09	11.56
30	-1.726	32.613	8.38	98.2	7.76	315	2.23	1.25	0.06	4.23	9.92
99	-1.256	34.186	7.40	88.8	7.60	313	2.28	1.41	0.02	8.50	10.51
494	0.464	34.854	7.14	90.2	7.70	308	2.31	1.64	0.02	11.97	11.82
887	-0.162	34.870	7.13	88.6	7.69	308	2.31	1.71	0.02	12.56	13.17
1087	-0.366	34.878	7.15	88.3	7.67	308	2.31	1.76	0.02	12.49	13.26
1646	-0.426	34.940	6.70	82.6	7.75	305	2.32	1.90	0.01	14.35	17.99
St. # 056											
0	-1.663	31.485	8.82	102.8	7.80	315	2.12	1.35	0.05	1.88	10.90
12	-1.776	31.577	8.58	99.8	7.73	314	2.17	1.37	0.09	3.33	11.20
30	-1.766	32.933	8.40	98.6	7.73	310	2.23	1.34	0.03	4.30	10.35
100	-1.146	34.230	7.39	88.9	7.53	308	2.28	1.54	0.03	9.17	11.55
496	0.559	34.856	7.16	90.7	7.63	305	2.31	1.69	0.01	11.79	12.48
988	-0.277	34.868	7.18	88.9	7.65	304	2.31	1.84	0.03	12.09	13.26
1991	-0.404	34.946	6.65	82.2	7.70	301	2.31	2.04	0.01	14.71	20.06
St. # 057											
0	-1.728	32.307	8.71	101.9	7.82	278	2.17	1.56	0.11	2.67	10.60
12	-1.732	32.194	8.65	101.1	7.79	277	2.18	1.52	0.08	2.85	10.70
30	-1.734	32.901	8.42	98.9	7.75	276	2.23	1.56	0.09	4.25	10.95
98	-1.281	34.198	7.41	88.9	7.71	273	2.27	1.73	0.01	8.06	12.04
495	0.686	34.861	7.08	89.9	7.60	272	2.31	1.96	0.00	10.73	13.90
987	-0.180	34.876	7.11	88.3	7.62	271	2.31	2.02	0.01	11.11	14.69
1970	-0.413	34.941	6.76	83.5	7.62	272	2.31	2.22	0.00	13.65	20.57
2566	-0.368	34.946	6.67	82.4	7.64	271	2.31	2.22	0.00	13.10	20.75
St. # 058											
21	-1.731	32.205	8.66	101.2	7.78	323	2.17	1.73	0.08	2.37	11.72
51	-1.743	33.244	8.12	95.6	7.43	321	2.22	1.77	0.02	4.21	12.10
98	-1.353	34.158	7.40	88.6	7.43	319	2.25	1.94	0.01	8.22	12.51
544	0.307	34.849	7.18	90.3	7.25	315	2.30	2.18	0.01	12.34	15.00
985	-0.222	34.874	7.19	89.1	7.40	312	2.31	2.03	0.01	11.37	15.33
2280	-0.386	34.946	6.71	82.9	7.53	309	2.31	2.26	0.02	13.21	21.48

## A35

<i>Depth</i>	<i>Temp.</i>	<i>Salin.</i>	<i>Oxygen</i>	<i>pH</i>	<i>Eh</i>	<i>Alk</i>	<i>PO-4</i>	<i>NO-2</i>	<i>NO-3</i>	<i>Si</i>	
St. # 059											
0	-1.719	32.153	8.59	100.4	7.88	301	2.19	1.88	0.11	2.71	12.63
10	-1.718	32.192	8.56	100.0	7.80	296	2.21	1.83	0.11	2.67	12.54
32	-1.732	32.811	8.46	99.3	7.76	293	2.22	1.84	0.08	3.06	12.44
99	-1.190	34.205	7.37	88.7	7.71	293	2.28	2.03	0.02	8.12	14.21
496	0.679	34.860	7.11	90.4	7.77	288	2.31	2.12	0.02	11.20	15.53
985	-0.191	34.872	7.17	89.0	7.80	287	2.31	2.26	0.02	10.97	16.18
1994	-0.400	34.945	6.63	81.9	7.77	284	2.31	2.55	0.01	13.75	22.65
St. # 060											
0	-1.710	32.196	8.59	100.4	7.93	283	2.16	2.00	0.11	2.48	13.30
9	-1.705	32.116	8.60	100.5	7.93	282	2.17	1.96	0.09	2.59	13.39
31	-1.751	32.905	8.36	98.2	7.90	281	2.23	1.98	0.06	3.70	13.72
100	-1.289	34.140	7.44	89.1	7.83	278	2.27	2.58	0.01	7.70	15.03
494	0.617	34.852	7.16	90.8	7.83	277	2.31	2.75	0.02	10.98	18.32
988	-0.152	34.872	7.15	88.8	7.79	277	2.31	2.94	0.03	10.55	19.65
1646	-0.450	34.939	6.69	82.5	7.83	273	2.31	2.75	0.02	11.69	26.14
St. # 062											
0	-1.697	32.344	8.60	100.7	7.88	328	2.15	2.57	0.09	2.50	14.47
10	-1.684	32.187	8.52	99.6	7.78	327	2.18	2.38	0.08	4.13	16.56
30	-1.749	32.943	8.24	96.8	7.82	321	2.23	2.49	0.06	6.92	18.60
99	-1.154	34.228	7.35	88.5	7.72	318	2.28	2.78	0.02	13.12	20.52
495	0.413	34.841	7.19	90.7	7.78	312	2.31	2.84	0.02	16.60	20.78
741	0.004	34.847	7.19	89.6	7.74	313	2.31	2.81	0.01	16.93	21.30
1035	-0.182	34.876	7.14	88.6	7.73	310	2.31	2.97	0.02	18.68	23.10
St. # 064											
0	-1.626	32.017	8.59	100.5	7.83	249	2.14	2.41	0.07	3.34	17.61
8	-1.637	32.075	8.48	99.2	7.84	250	2.16	2.48	0.07	4.83	19.49
30	-1.714	33.245	7.93	93.3	7.68	252	2.24	2.58	0.04	7.71	20.53
99	-1.041	34.188	7.16	86.5	7.70	252	2.28	2.81	0.01	12.45	23.52
494	0.634	34.839	7.17	91.0	7.71	253	2.31	2.92	0.02	11.15	21.37
508	0.567	34.838	7.19	91.1	7.76	253	2.31	3.09	0.02	17.15	22.42
St. # 065											
0	-1.700	32.092	8.18	95.6	7.77	254	2.18	2.55	0.11	3.10	21.33
9	-1.710	32.337	8.22	96.2	7.75	254	2.19	2.58	0.09	3.97	23.28
30	-1.739	32.867	7.74	90.9	7.70	253	2.24	2.58	0.07	4.71	22.49
98	-1.112	34.142	7.24	87.2	7.69	254	2.28	2.78	0.01	10.73	21.73
227	1.075	34.751	7.01	89.9	7.73	253	2.31	2.89	0.03	11.01	22.67
St. # 069											
0	0.742	29.401	8.24	101.1	7.88	239	1.96	1.10	0.02	0.93	4.66
9	0.963	29.142	8.18	100.6	7.86	240	2.05	1.15	0.05	2.07	4.03
31	-1.597	33.038	7.79	91.9	7.78	241	2.17	1.33	0.04	5.01	3.96
99	-1.337	34.213	7.46	89.4	7.77	243	2.28	1.53	0.02	7.41	3.66
497	0.868	34.862	7.13	91.0	7.79	244	2.31	1.87	0.02	10.39	4.63
791	0.080	34.865	7.17	89.6	7.78	244	2.31	1.95	0.02	10.71	5.34
1161	-0.151	34.877	7.17	89.1	7.79	243	2.31	2.00	0.01	10.68	5.75
St. # 071											
0	-0.424	30.424	8.45	101.1	7.93	235	1.99	1.61	0.03	1.07	4.59
10	0.584	28.897	8.35	101.6	7.86	234	2.02	1.62	0.03	0.56	4.63
30	-1.517	32.489	7.79	91.8	7.76	237	2.23	1.81	0.06	4.00	4.66

## A36

<i>Depth</i>	<i>Temp.</i>	<i>Salin.</i>	<i>Oxygen</i>		<i>pH</i>	<i>Eh</i>	<i>Alk</i>	<i>PO-4</i>	<i>NO-2</i>	<i>NO-3</i>	<i>Si</i>
St. # 071 ctd.											
99	-1.246	34.163	7.21	86.6	7.72	238	2.29	2.04	0.05	6.75	4.78
493	0.852	34.864	7.13	91.0	7.79	239	2.31	2.34	0.02	10.48	5.45
578	0.600	34.861	7.16	90.7	7.79	238	2.31	2.36	0.03	10.30	5.37
St. # 072											
0	-1.221	31.241	8.33	98.0	7.90	241	2.01	1.85	0.06	0.39	5.30
10	-0.350	29.760	8.46	101.0	7.93	241	2.04	1.87	0.03	0.63	5.11
30	-1.505	33.320	7.54	89.4	7.76	242	2.25	2.14	0.06	5.05	5.07
100	-1.297	34.116	7.30	87.5	7.73	243	2.28	2.28	0.03	6.72	4.74
233	-0.746	34.368	7.28	88.7	7.72	238	2.29	2.40	0.04	7.26	4.51
St. # 073											
0	-1.043	30.690	8.34	98.3	7.92	253	2.02	2.13	0.06	0.11	4.51
10	0.160	28.827	8.48	101.9	7.85	252	2.02	2.10	0.02	0.09	4.74
30	-1.490	33.507	7.51	89.2	7.75	254	2.26	2.34	0.06	4.54	4.81
91	-1.297	34.090	7.29	87.3	7.73	253	2.28	2.51	0.04	5.94	5.19
St. # 075											
0	-1.725	32.221	8.78	102.6	7.98	218	2.09	0.97	0.09	1.36	1.55
10	-1.724	32.214	8.84	103.4	7.90	220	2.09	0.95	0.05	2.16	1.66
30	-1.771	33.404	8.52	100.4	7.84	221	2.21	1.15	0.00	3.90	1.90
99	-1.227	34.286	7.55	90.8	7.80	223	2.27	1.29	0.02	5.68	2.14
492	0.872	34.896	7.04	89.9	7.78	225	2.31	1.43	0.00	8.53	4.65
998	-0.279	34.901	7.03	87.1	7.76	227	2.31	1.56	0.01	9.39	6.44
1969	-0.759	34.917	6.99	85.5	7.78	227	2.31	1.62	0.00	9.30	8.47
2947	-0.778	34.930	6.98	85.3	7.80	228	2.31	1.67	0.00	10.22	9.31
3522	-0.721	34.936	6.88	84.2	7.79	228	2.31	1.69	0.00	9.85	9.42
St. # 077											
0	-1.621	32.194	8.03	94.1	7.83	211	2.06	1.21	0.02	0.12	1.76
19	-1.741	33.244	8.31	97.8	7.79	213	2.20	1.31	0.04	1.83	3.44
30	-1.805	33.703	8.19	96.5	7.80	215	2.22	1.32	0.02	2.29	3.20
100	-1.526	34.236	7.76	92.5	7.78	215	2.27	1.34	0.01	3.77	2.60
498	1.219	34.914	7.06	91.0	7.78	216	2.31	1.72	0.00	7.86	3.91
988	-0.278	34.900	7.03	87.1	7.77	218	2.31	1.97	0.00	8.57	5.10
1960	-0.768	34.914	6.99	85.4	7.78	220	2.31	2.24	0.00	9.94	7.73
3295	-0.733	34.934	6.87	84.1	7.80	220	2.31	2.47	0.01	10.16	8.69
St. # 079											
0	-1.141	33.733	7.93	95.2	7.97	212	2.13	2.08	0.02	0.11	0.43
11	0.815	32.610	8.42	105.7	7.97	213	2.19	2.03	0.01	0.23	0.19
30	-1.619	34.260	7.62	90.6	7.83	216	2.28	2.37	0.08	2.01	0.66
100	-1.314	34.529	7.49	90.0	7.76	218	2.30	2.60	0.03	3.37	2.10
496	0.280	34.849	7.18	90.2	7.79	223	2.31	2.99	0.01	5.96	3.53
1615	-0.625	34.907	6.92	85.0	7.78	225	2.31	3.29	0.00	9.12	7.71
St. # 081											
0	0.181	32.796	7.90	97.7	7.98	217	2.16	2.85	0.01	0.06	0.05
10	0.983	32.449	8.50	107.1	7.95	217	2.20	2.74	0.01	0.17	0.05
30	-1.389	34.167	7.64	91.4	7.84	218	2.28	3.08	0.19	3.62	0.16
99	-1.140	34.534	7.43	89.7	7.80	218	2.30	3.20	0.03	4.28	2.67
297	0.648	34.823	7.22	91.6	7.80	220	2.31	3.49	0.01	7.78	3.98

## A37

<i>Depth</i>	<i>Temp.</i>	<i>Salin.</i>	<i>Oxygen</i>		<i>pH</i>	<i>Eh</i>	<i>Alk</i>	<i>PO-4</i>	<i>NO-2</i>	<i>NO-3</i>	<i>Si</i>
St. # 081 ctd.											
394	0.112	34.809	7.21	90.2	7.80	221	2.31	3.52	0.01	7.89	4.46
517	0.060	34.822	7.19	89.8	7.78	219	2.31	3.54	0.02	7.95	4.46
St. # 083											
0	-0.717	31.404	8.22	98.2	7.93	217	2.05	3.20	0.07	0.13	0.03
11	-0.252	30.229	8.13	97.7	7.83	218	2.16	3.19	0.06	0.09	1.22
31	-1.498	33.257	7.51	89.0	7.74	220	2.26	3.37	0.11	4.32	5.17
98	-1.260	34.209	7.21	86.5	7.73	221	2.29	3.49	0.03	5.83	5.52
224	-0.420	34.569	6.98	85.9	7.73	222	2.28	3.62	0.03	9.20	6.48
St. # 084											
0	-0.265	30.570	8.26	99.3	7.95	218	2.01	3.27	0.04	0.04	1.33
9	-0.130	30.155	8.28	99.7	7.87	220	2.11	3.29	0.04	0.40	1.09
31	-1.494	33.244	7.52	89.1	7.76	222	2.26	3.48	0.11	6.07	5.75
90	-1.372	34.036	7.31	87.4	7.75	223	2.28	3.63	0.06	8.03	7.78
St. # 089											
0	-1.684	32.723	8.60	101.0	8.08	213	2.08	0.68	0.03	0.20	0.44
11	-1.638	32.754	8.66	101.8	8.04	215	2.08	0.71	0.01	0.59	2.23
29	-1.452	33.377	8.24	97.8	7.97	217	2.24	0.98	0.08	5.88	2.14
100	2.122	34.801	7.04	92.7	7.87	220	2.31	1.64	0.01	14.23	10.61
495	1.382	34.924	7.15	92.5	7.87	225	2.31	2.15	0.00	15.75	16.79
990	-0.627	34.860	7.39	90.6	7.84	228	2.31	2.06	0.00	11.34	15.81
2684	-0.778	34.931	6.86	83.8	7.88	227	2.31	2.43	0.02	17.56	24.51
St. # 090											
0	-1.586	32.709	8.53	100.5	8.03	217	2.18	1.34	0.03	0.22	2.57
9	-1.591	32.717	8.55	100.7	7.98	215	2.17	1.30	0.00	0.61	2.69
31	-1.435	33.791	8.21	97.9	7.91	218	2.24	1.59	0.08	5.03	6.60
100	0.313	34.623	7.31	91.8	7.79	220	2.30	2.11	0.01	10.84	11.98
528	0.151	34.829	7.40	92.7	7.78	223	2.31	2.28	0.01	11.47	10.70
987	-0.484	34.877	7.38	90.9	7.77	226	2.31	2.48	0.02	12.56	17.17
1715	-0.699	34.906	6.96	85.2	7.77	227	2.31	2.54	0.00	15.54	17.86
St. # 091											
0	-1.625	32.273	8.64	101.3	7.93	217	2.16	1.68	0.02	0.07	3.04
10	-1.630	32.340	8.70	102.0	7.92	218	2.17	1.66	0.01	0.45	3.16
30	-1.524	33.485	8.35	99.1	7.84	218	2.24	1.89	0.09	6.41	5.07
98	-1.131	34.511	7.45	89.9	7.77	223	2.29	2.24	0.07	11.64	9.88
496	-0.291	34.841	7.43	92.0	7.77	223	2.31	2.63	0.06	15.24	16.06
991	-0.624	34.854	7.48	91.7	7.77	225	2.31	2.61	0.05	14.77	14.86
St. # 092											
0	-1.587	32.323	8.60	101.0	8.00	218	2.14	1.80	0.03	2.26	4.15
10	-1.490	32.681	8.78	103.6	7.95	219	2.15	1.83	0.01	2.65	4.05
30	-1.587	33.730	8.13	96.4	7.83	221	2.24	2.17	0.10	10.13	6.07
99	-0.505	34.586	7.48	91.9	7.80	222	2.30	2.51	0.17	18.52	13.54
494	-0.713	34.845	7.49	91.7	7.79	221	2.31	2.81	0.04	17.57	19.49
515	-0.709	34.845	7.50	91.8	7.78	221	2.31	2.56	0.04	15.20	14.05

## A38

<i>Depth</i>	<i>Temp.</i>	<i>Salin.</i>	<i>Oxygen</i>		<i>pH</i>	<i>Eh</i>	<i>Alk</i>	<i>PO-4</i>	<i>NO-2</i>	<i>NO-3</i>	<i>Si</i>
St. # 093											
0	-1.423	32.061	8.55	100.6	7.97	340	2.15	1.97	0.03	5.24	5.67
10	-1.407	32.226	8.64	101.9	7.92	335	2.16	1.98	0.01	5.46	5.79
30	-1.486	34.250	7.96	95.0	7.80	332	2.28	2.21	0.15	11.02	7.93
94	1.402	34.861	7.21	93.3	7.83	328	2.31	2.72	0.02	19.63	13.97
227	-0.930	34.796	7.49	91.1	7.78	325	2.31	2.81	0.03	19.89	17.79
St. # 094											
0	-1.661	32.266	8.59	100.6	7.92	340	2.16	2.11	0.07	8.51	6.74
11	-1.670	32.192	8.47	99.2	7.89	340	2.19	2.08	0.04	10.45	6.97
31	-1.562	34.238	7.68	91.5	7.75	338	2.28	2.47	0.12	17.43	8.88
79	-1.358	34.516	7.16	85.9	7.71	327	2.29	2.77	0.09	20.66	15.94



## ANNEX 11.4: GEOLOGICAL TABLES and CORE DESCRIPTIONS

## 11.4-1: Table with list of samples of aerosols collected by filtration

Samples of aerosols collected by filtration  
through AFA-HA filters

No.	Date - time (UTC)	Coordinates	
		Latitude (N)	Longitude (E)
1	19.07-16.00	77°31.4'	97°03.5'
	20.07-04.45	77°56.5'	103°54.4'
	20.07-10.00	77°54.1'	107°03.5'
	20.07-11.45	77°51.3'	107°31.3'
	20.07-17.10	77°17.7'	110°10.7'
	20.07-20.00	76°52.6'	112°16.2'
	21.07-06.10	76°28.8'	118°34.0'
	21.07-11.00	76°47.9'	121°07.6'
21.07-12.40	76°55.3'	122°07.1'	
2	22.07-03.30	77°42.8'	125°56.6'
	22.07-06.35	77°44.0'	126°04.2'
	22.07-07.30	78°33.3'	126°06.41'
	22.07-14,20	77°45.2'	126°04.8'
22.07-18.00	77°44.4'	126°44.85'	
3	24.07-02.30	78°00.5'	144°53.7'
	24.07-05.00	78°58.7'	147°20.7'
	25.07-16.30	78°58.7'	147°20.7'
	27.07-18.45	79°22.0'	147°28.3'
	28.07-05.30	79°08.9'	146°21.3'
	28.07-15.00	79 05.1'	145 56.6'
4	30.07-02.45	77°59.9'	140°03.3'
	30.07-08.20	77°42.3'	139°57.6'
	30.07-12.20	77°31.1'	140°01.1'
	30.07-13.30	77°30.0'	140°05.6'
	30.07-15.25	77°28.5'	139°34.9'
	30.07-19.30	77°22.4'	137°30.3'
	30.07-22.00	77°19.4'	136°11.3'
	31.07-07.30	77°01.3'	132°15.0'
31.07-09.05	76°59.1'	131°50.0'	
5	31.07-21.55	76°08.4'	129°59.6'
	01.08-00.05	76°29.9'	129°59.0'
	01.08-06.15	76°59.8'	129°59.9'
	01.08-08.50	77°18.2'	129°57.8'
	02.08-03.00	77°42.2'	130°02.8'
	02.08-10.20	77°51.2'	130°02.3'

## A 40

5ctd.	02.08-12.55	77°51.2'	130°03.6'
	03.08-10.10	78°03.9'	130°00.0'
	03.08-12.45	78°09.8'	129°58.4'
6	05.08-01.25	79°09.5'	131°25.3'
	05.08-03.30	79 11.3'	131 26.1'
7	07.08-13.35	81°06.2'	105°23.5'
	07.08-17.35	81°08.1'	105°33.7'
	07.08-22.10	81°08.3'	105°54.9'
	08.08-21.00	81°14.2'	106°51.2'
	09.08-00.40	81°13.0'	106°58.7'
	09.08-18.50	81°11.5'	107°30.7'
8	10.08-17.00	80°47.4'	103°48.8'
	10.08-20.50	80°47.3'	103°48.7'
	12.08-04.20	80°25.3'	102°00.6'
	12.08-07.30	80°25.7'	102°00.1'
	12.08-10.00	80 24.9'	102 05.4'
9	17.08-12.40	79°08.7'	135°03.8'
	19.08-05.00	79°59.1'	134°59.4'
	19.08-08.30	79 59.3'	135 04.5'
10	22.08-09.20	81°03.6'	136°27.0'
	22.08-16.00	81°05.0'	136°12.0'
	22.08-20.30	81°03.2'	136°37.2'
	23.08-04.40	81°03.0'	138°16.5'
	23.08-08.30	81°04.3'	138°55.7'
11	01.09-08.40	78°22.8'	134°49.2'
	01.09-12.40	78°24.5'	134°51.1'
	02.09-09.10	78°15.0'	135°23.4'
	02.09-10.17	78 15.5'	135 23.5'
12	08.09-16.05	81°24.3'	97°32.8'
	08.09-18.25	81°46.2'	96°35.3'
	09.09-00.00	82°04.2'	94°24.4'
	09.09-02.00	82°18.1'	93°21.1'
	09.09-02.30	82°20.6'	93°10.4'
	09.09-03.10	82°21.1'	92°58.3'
	09.09-19.20	82°08.4'	91°21.8'
	09.09-22.40	82°04.2'	90°59.4'
	10.09-00.50	82°04.3'	91°01.7'

Time and locations at the beginning, at intermediate points and at the end of sampling are given.

## 11.4-2: Table with list of samples of aerosols collected by filtration

Sampling times and locations for analyses of particle size distributions in aerosols of the Laptev Sea

Number	Date - Time (UTC)	Coordinates	
		Latitude (N)	Longitude (E)
1	19.07-17.00	77°09.4'	95°06.4'
2	20.07-06.00	77°57.0'	104°53.9'
3	20.07-10.00	77°54.1'	107°03.5'
4	20.07-17.10	77°17.7'	110°10.7'
5	20.07-20.00	76°52.6'	112°16.2'
6	21.07-06.00	76°27.8'	118°34.0'
7	21.07-11.00	76°47.9'	121°07.6'
8	22.07-06.35	77°44.0'	126°04.2'
9	24.07-02.30	78°00.5'	144°53.7'
10	25.07-04.35	78°33.3'	145°40.5'
11	25.07-16.30	78°58.7'	147°20.7'
12	26.07-17.00	79°27.1'	148°06.1'
13	26.07-22.30	79°27.6'	148°06.8'
14	27.07-14.50	79°29.4'	148°13.2'
15	27.07-18.45	79°22.0'	147°28.3'
16	28.07-05.30	79°08.9'	146°21.3'
17	30.07-04.35	77°59.3'	140°05.8'
18	30.07-12.20	77°31.1'	140°01.1'
19	31.07-07.30	77°01.3'	132°15.0'
20	01.08-03.00	76°53.1'	129°59.6'
21	02.08-03.00	77°42.2'	130°02.8'
22	02.08-10.20	77°51.2'	130°02.3'
23	03.08-10.10	78°03.9'	130°00.0'
24	05.08-01.25	79°09.5'	131°25.3'
25	06.08-11.00	78°24.7'	122°11.9'
26	06.08-15.30	78°44.4'	119°11.5'
27	07.08-13.35	81°06.2'	105°23.5'
28	07.08-17.35	81°08.1'	105°33.7'
29	08.08-21.00	81°14.2'	106°51.2'
30	09.08-18.50	81°11.5'	107°30.7'
31	10.08-17.00	80°47.4'	103°48.8'
32	12.08-04.20	80°25.3'	102°00.6'
33	17.08-12.40	79°08.7'	135°03.8'
34	19.08-05.00	79°59.1'	134°59.4'
35	22.08-09.00	81°03.6'	136°30.0'
36	22.08-14.45	81°04.7'	136°15.9'
37	22.08-16.00	81°05.0'	136°12.0'
38	22.08-20.30	81°03.2'	136°37.2'
39	23.08-04.40	81°03.0'	138°16.5'
40	23.08-08.30	81°04.3'	138°55.7'
41	25.08-20.15	81°12.4'	143°24.7'
42	27.08-04.30	81°12.7'	150°13.7'

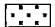
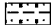


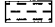
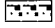
## A42

43	31.08-20.25	79°23.0'	138°13.3'
44	01.09-12.40	78°24.5'	134°51.1'
45	01.09-20.30	78°20.7'	135°00.8'
46	02.09-09.10	78°15.0'	135°23.4'
47	06.09-13.25	78°45.6'	112°43.1'
48	07.09-04.25	77°55.7'	113°31.8'
49	07.09-06.00	77°55.5'	113°32.0'
50	08.09-16.05	81°24.3'	97° 32.8'
51	08.09-19.50	81°45.9'	96° 36.2'
52	08.09-22.05	81°49.3'	95° 40.3'
53	09.09-00.00	82°04.2'	94° 24.4'
54	09.09-02.00	82°18.1'	93° 21.1'
55	09.09-04.20	82°21.2'	92° 55.5'
56	09.09-19.20	82°08.4'	91° 21.8'
57	09.09-22.40	82°04.2'	90° 59.4'
58	10.09-07.20	82°04.6'	90° 59.4'
59	10.09-16.50	81°54.3'	90° 54.5'
60	10.09-22.15	81°26.3'	89° 38.4'
61	11.09-00.10	81°10.3'	89° 00.7'
62	11.09-04.25	81°10.4'	87° 30.2'
63	11.09-13.35	79°33.5'	87° 01.5'

**Annex 11.4-3: Graphical Core Descriptions**

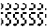
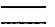
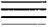





Legend:

**Lithology**

-  sand
-  sandy silt
-  sandy clay
-  sandy mud
-  silt
-  mud
-  clay
-  diamicton

-  foraminiferal ooze
-  nannofossil ooze
-  diatomaceous ooze
-  radiolarian ooze
-  volcanic ash
-  chert / porcellanite
-  pebbles, dropstones
-  sediment clasts

**Structure**

-  bioturbation
-  stratification
-  lamination
-  coarsening upward sequence
-  fining upwards sequence
-  sharp boundary
-  gradational boundary
-  transition zone

A44

PS2718-4 (GKG)

W'Vilkitsky Strait

ARK-XI/1

Recovery: 0.47 m

77° 31.4' N, 97° 03.3' E

Water depth: 151 m

Lithology	Texture	Color	Description	Age
Surface				
10YR 4/2, even surface, silty clay, dark grayish brown, with small mudclasts, common ophiura, one sarduria				
Depth in core (cm) 0 10 20 30 40 50			0-3 cm: silty clay, dark grayish brown, soft, homogeneous	
		10YR 4/2	3-4 cm: silty clay, olive, homogeneous	
		5Y 4/3	4-7 cm: silty clay, olive gray, homogeneous	
		5Y 4/2	7-10 cm: silty clay, olive, homogeneous, mottled with sediment from below	
		10YR 3/3	10-13 cm: silty clay, dark brown, homogeneous, mottled with sediment from below	
		10YR 3/1	13-16 cm: silty clay, very dark gray, homogeneous, mottled with sed. from below	
	10YR 4/2	16-26 cm: silty clay, dark grayish brown, with some darker mottles		
	5Y 3/1	26-47 cm: silty clay, very dark gray, homogeneous at top, dark horizontal streaks at base		
			end of core: 46 cm	

A45

PS2718-6 (SL)

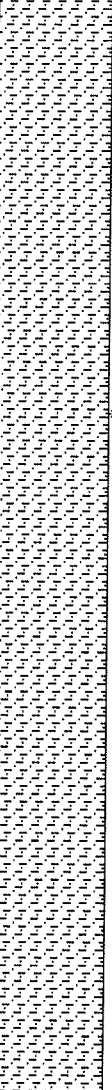
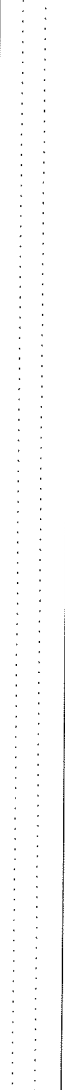
W' Vilkitsky Strait

ARK-XI/1

Recovery: 8.00 m

77° 31.5' N, 97° 04.4' E

Water depth: 153 m

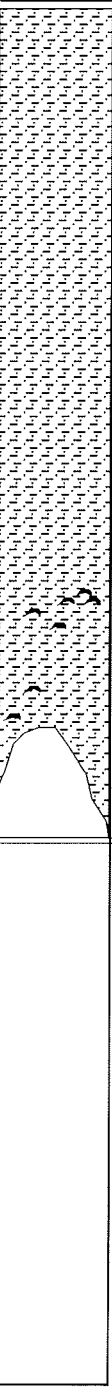
Lithology	Texture	Color	Description	Age
			Section 0-100 cm lost	
		<p>5Y3/1 to 5Y4/1</p> <p>5Y3/1 to 5Y4/1</p>	<p>silty clay and clay, dark gray 5Y4/1, very dark gray (5Y3/1) to black (5Y/2.5.1). Common to abundant black spots throughout (abundant 125-135 cm, 176-200 cm, 253-289 cm, 305-310 cm, 317-340 cm, 350-355, 360-365, 368-500 cm).</p>	

Depth in core (m)

A46

PS2718-6 (SL)

ARK-XI/1

Lithology	Texture	Color	Description	Age
<p>5</p>  <p>6</p> <p>7</p> <p>8</p> <p>9</p> <p>10</p> <p>Depth in core (m)</p>	<p>5Y3/1 to 5Y2.5/1</p>		<p>silty clay and clay, very dark gray (5Y3/1) to black (5Y2.5/1). Common to abundant black spots throughout (abundant between 500-764 cm). Small bivalves (diameter 3 to 10 mm) at 713-715 cm, 717 cm, 726 cm, 747 cm, and 757 cm.</p>	



A47

PS2719-1 (SL)

W' Vilkitsky Strait

ARK-XI/1

Recovery: 6.55 m

77° 36' N, 97° 32' E

Water depth: 135 m

Lithology	Texture Color	Description	Age
	10YR 3/3	0 - 1 cm: silty clay, dark brown (10YR 3/3)	
	5Y4/1	1 - 3 cm: silty clay, olive gray (5Y 4/2)  3 - 10 cm: silty clay, dark brown (10YR 4/3) and olive gray (5Y 4/2), mottled/bioturbated  10 - 51 cm: silty clay, dark gray (5Y 4/1); black (Fe-sulfide?) lenses (1 cm in diameter) at 15-16 cm and 27-28 cm, black layer at 21 cm, 48-51 cm black spots  51 - 500 cm: silty clay, very dark gray (5Y 3/1), common to abundant black spots throughout; black horizons at 59-61 cm, 66-67 cm, 70 cm, 100 cm, 424-426 cm; bivalves at 84 cm, 97 cm, 136 cm, 162 -163 cm, 289 cm, 472-473 cm; horizon with bivalves and gastropodes at 384-386 cm; large dropstone (black sand/siltstone, 5 cm in diameter) at 323-327 cm; coal fragment at 397-398 cm	
	5Y3/1		



A49

PS2720-7 (SL)

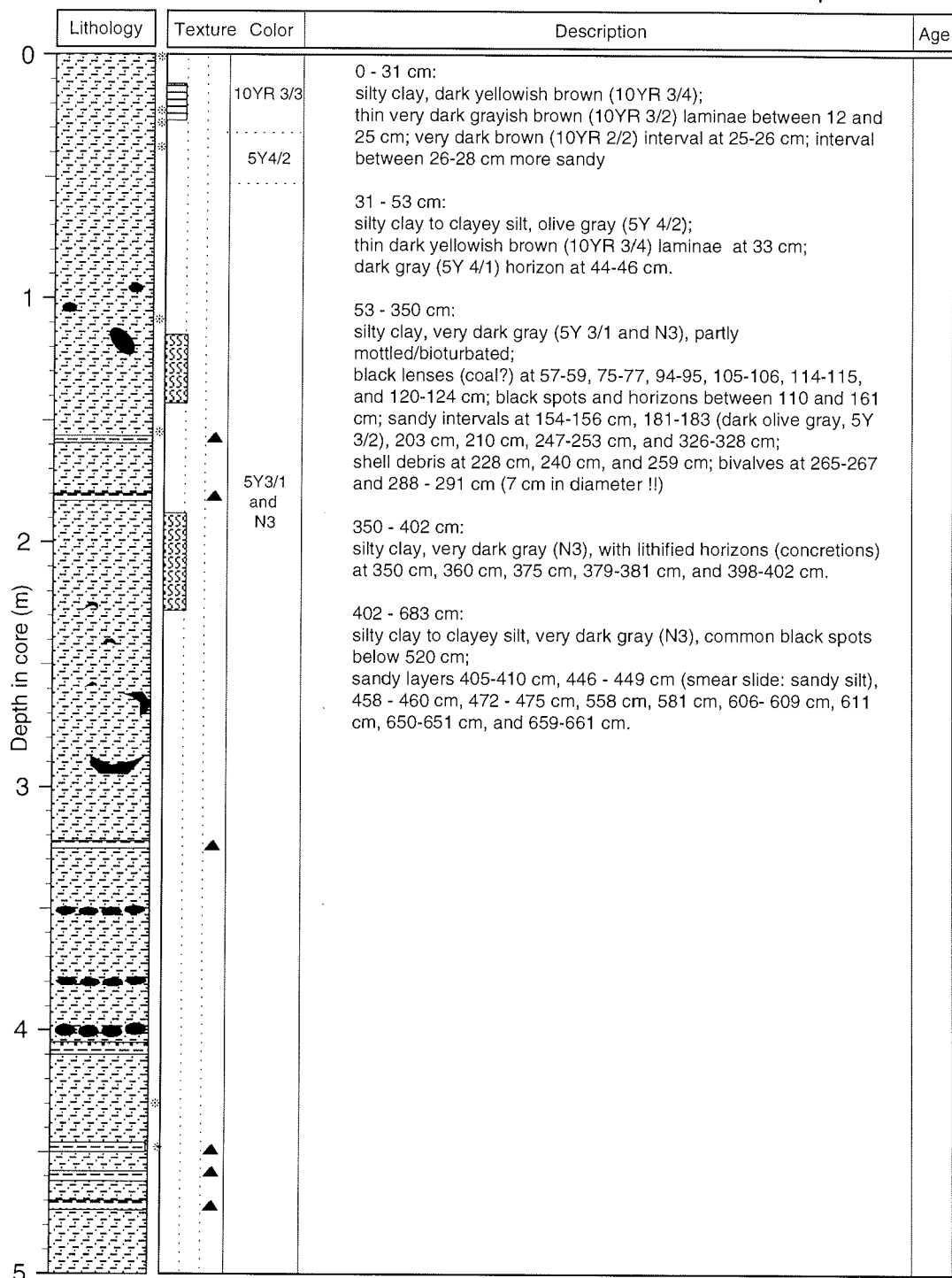
Central Laptev Sea Cont. Margin

ARK-XI/1

Recovery: 6.83 m

77° 46.1' N, 126° 07.4' E

Water depth: 2054 m



A50

PS2720-7 (SL)

ARK-XI/1

	Lithology	Texture	Color	Description	Age
5		A vertical dotted line representing a specific texture, with two small black triangles pointing upwards at approximately 6.2m and 6.6m depth.	N3		
6					
7					
8					
9					
10					

A51

PS2721-4 (GKG)

Western East Siberian Sea

ARK-XI/1

Recovery: 0.15 m

78°00.5'N, 144°53.3'E

Water depth: 54 m

Lithology	Texture	Color	Description	Age
Surface				
7.5YR3/2, uneven surface, clayey sandy silt, dark brown, ophiura, bivalvia, sipunculidae, crustaceans, amphipoda				
		7.5YR3/2	0-4 cm: clayey sandy silt, dark brown, homogeneous	
		5Y3/1	4-15 cm: clayey sandy silt, very dark gray, with brownish burrows and rare black mottles in lower part	
			end of core: 15 cm	

A52

PS2722-3 (GKG)

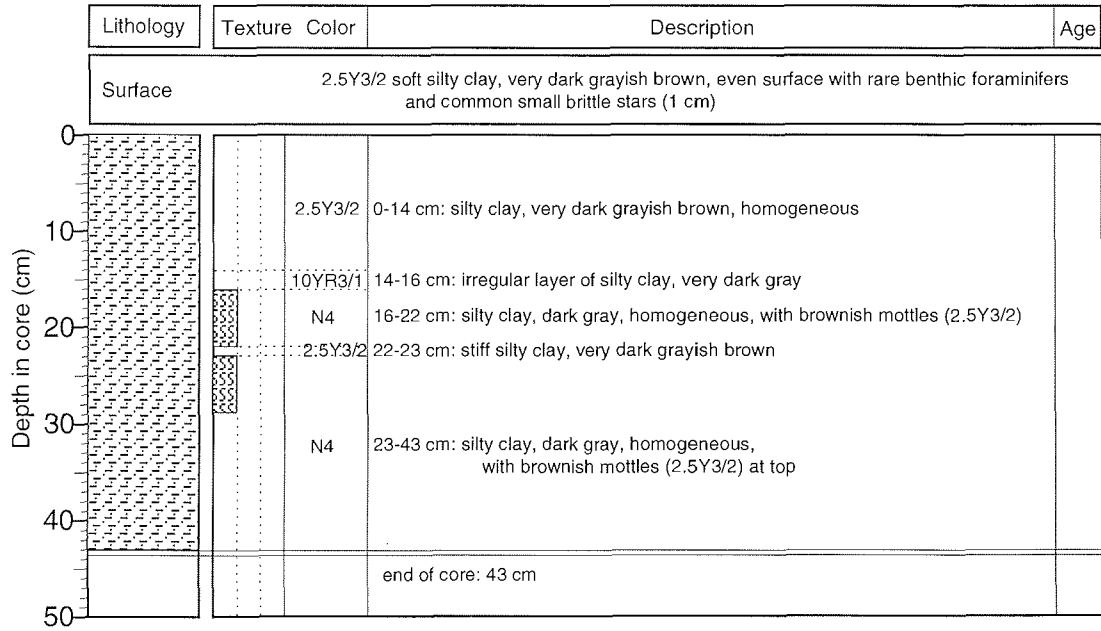
Western East Siberian Sea

ARK-XI/1

Recovery: 0.43 m

78°58.7'N, 147°20.8'E

Water depth: 97 m



A53

PS2722-4 (SL)

Western East Siberian Sea

ARK-XI/1

Recovery: 3.21 m

78° 58.8'N, 147° 20.8'E

Water depth: 97 m

Lithology	Texture Color	Description	Age
0	10YR3/3	0 - 8 cm:	
	5Y 3/2	Silty clay, dark brown (10YR 3/3)	
		8 - 9 cm:	
		Silty clay, very dark grayish brown (10YR 3/2)	
		9 - 11 cm:	
	5Y 3/1	Silty clay, dark yellowish brown (10YR 3/4); mud clasts ?	
		11 - 12 cm:	
		Silty clay, olive gray (5Y 4/2)	
		12 - 40 cm:	
		Silty clay, dark olive gray (5Y 3/2), homogeneous	
		40 - 121 cm:	
	5Y 3/1 to 5Y 3/2	Silty clay, very dark gray (5Y 3/1); common black spots/horizons throughout, black layer at 91-92 cm; shell debris at 87-88 cm and 110-111 cm; rotated sediment blocks (slump) at 77-92 cm; bioturbation at 108-115 cm.	
		121 - 221 cm:	
	5Y 3/2	Silty clay, very dark gray (5Y 3/1) to dark olive gray (5Y 3/2), strongly disturbed by slumping; sandy intervals, about 2 cm in thickness, at 171-190 cm and 206-216 cm;	
		shell debris at 128-130 cm, 131 cm, 141 cm, 167-173 cm, and 209 cm; bilvalve ( <i>Hiatella arctica</i> , 3 cm in diameter) at 166-168 cm	
	5Y 3/2 to 5Y 3/1	221 - 245 cm:	
		Silty clay, dark olive gray (5Y 3/2)	
	5Y 3/2	245 - 305 cm:	
		Silty clay, dark olive gray (5Y 3/2) to very dark gray (5Y 3/1), slump structures (folding); sand lenses at 273-274 cm;	
		bivalves ( <i>Hiatella arctica</i> ) at 232 cm, 251-252 cm, 270-272 cm, and 290-292 cm	
		305 - 321 cm:	
		Silty clay, dark olive gray (5Y 3/2)	

A54

PS2723-4 (GKG)

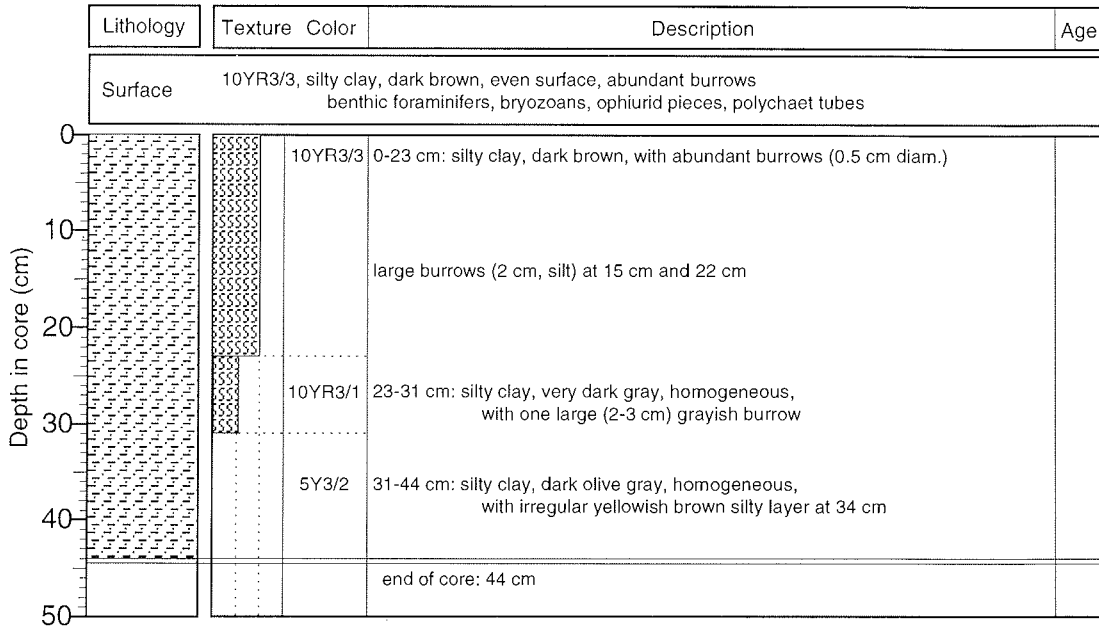
Western East Siberian Sea

ARK-XI/1

Recovery: 0.44 m

79°27.5'N, 148°06.8'E

Water depth: 224 m





A55

PS2724-4 (GKG)

Western East Siberian Sea

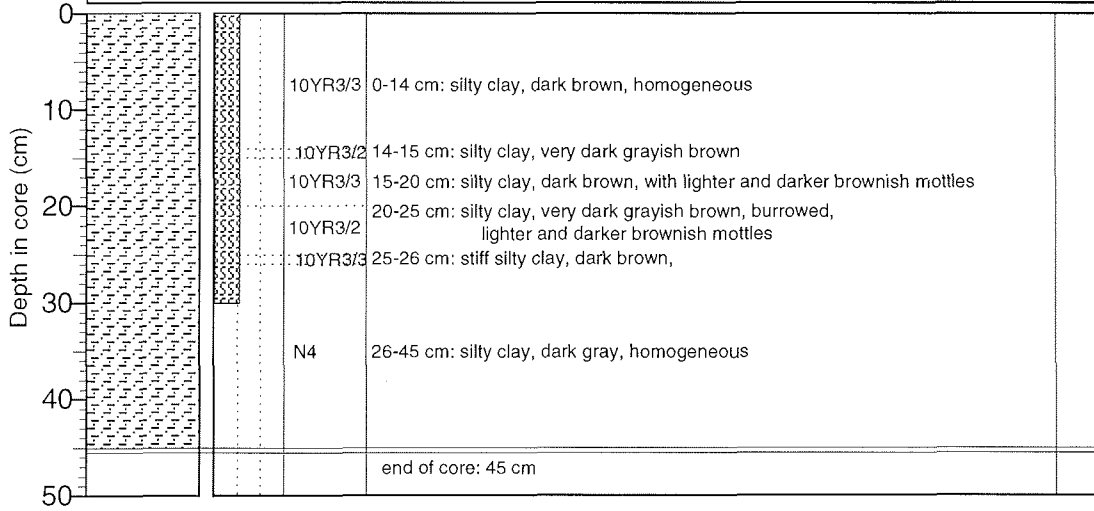
ARK-XI/1

Recovery: 0.45 m

79°08.9'N, 146°21.3'E

Water depth: 100 m

Lithology	Texture Color	Description	Age
Surface	10YR3/3	soft silty clay, dark brown, even surface, common brittle stars, bryozoans, polychaet tubes, etc.	



A56

PS2724-10 (SL)

Western East Siberian Sea

ARK-XI/1

Recovery: 2.18 m

79° 08.8'N, 146° 21.7'E

\* Water depth: 99 m

Lithology	Texture Color	Description	Age
	<p>10YR3/2</p> <p>2.5Y 4/2</p> <p>5Y 3/2</p> <p>5Y 3/1 to 5Y 3/2</p>	<p>0 - 9 cm: Silty clay, very dark grayish brown (10YR 3/2)</p> <p>9 - 11 cm: Silty clay, dark yellowish brown (10YR 3/4); mud clasts ?</p> <p>11 - 15 cm: Silty clay, olive brown (2.5Y 4/4); mud clasts ?</p> <p>15 - 17 cm: Silty clay, olive gray (5Y 4/2)</p> <p>17 - 29 cm: Clay, gray (2.5Y 5/1) to darkgray (2.5Y 4/2), homogeneous</p> <p>29 - 118 cm: Silty clay, dark olive gray (5Y 3/2); occasionally black spots between 45 and 75 cm, lower part slightly mottled/bioturbated; few shell debris at 33 cm, 48 cm, 57 cm, and 74 cm;</p> <p>118 - 218 cm: Silty clay, very dark gray (5Y 3/1) to dark olive gray (5Y 3/2), partly mottled/disturbed (slump structures ?); large dropstone (7 cm in diameter) at 149-151 cm</p>	



A58

PS2725-5 (SL)

Western East Siberian Sea

ARK-XI/1

Recovery: 4.78 m

78° 39.4'N, 144° 08.1'E

Water depth: 77 m

Lithology	Texture Color	Description	Age
	2.5Y 4/2	0 - 4 cm:	
	5Y 3/1	Silty clay, dark grayish brown (2.5Y 4/2)	
	5Y 3/1	4 - 178 cm: Silty clay, very dark gray (5Y 3/1); common to abundant black spots below 30 cm, black horizons at 117-118 cm and 127 cm; dark grayish brown (2.5Y 4/2) horizon at 24-25 cm; bivalves at 93-94 cm, 110-111 cm, 112-113 cm, and 115-116 cm	
	5Y 3/1	178 - 307 cm: Silty clay, black (5Y 2.5/1) to very dark gray (5Y 3/1), partly mottled/bioturbated; bivalves at 204-205 cm, 207-208 cm, 236-237 cm, 255-256 cm, 280-281 cm, 290-291 cm, and 339-340 cm	
	5Y 2.5/1 to 5Y 3/1	307 - 440 cm: Alternation of silty clay, black (5Y 2.5/1), and silty clay, very dark gray (5Y 3/1), slightly mottled throughout; thin sand layer at 412-413 cm; bivalves at 339-340 cm, 353-354 cm, 356-357 cm, 359-360 cm, 392-393 cm, 421-422 cm, and 430-431 cm	
	5Y 2.5/1	440 - 478 cm:	
	5Y 3/1	Silty clay (with significant amount of sand), dark olive (5Y 3/2);	
	5Y 2.5/1	black horizon at 444-445 cm	
	5Y 3/1		
	5Y 2.5/1		
5Y 3/1			
5Y 2.5/1			
5Y 3/1			
5Y 2.5/1			
5Y 3/1			
5Y 3/2			

A59

PS2726-5 (GKG)

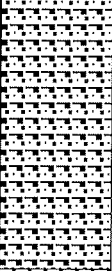
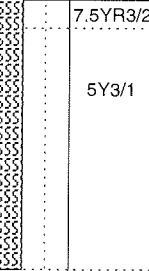
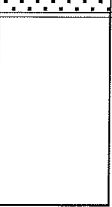
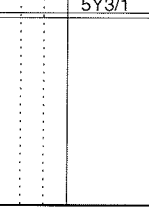
Western East Siberian Sea

ARK-XI/1

Recovery: 0.30 m

77°59.7'N, 140°05.4'E

Water depth: 48 m

Lithology	Texture Color	Description	Age
Surface 7.5Y3/2, sandy silty clay, dark brown, disturbed, five manganese nodules (diam. 5 cm), brittle stars, polychaets, bivalves, brachiopods, amphipods, hydrozoans			
		7.5Y3/2 0-3 cm: sandy silty clay, dark brown, homogeneous	
		5Y3/1 3-28 cm: sandy silty clay, very dark gray, homogeneous, few mottles few bivalves (e.g., <i>Maeoma caleacea</i> ), few polychaets	
		5Y3/1 28-30 cm: fine sand, very dark gray	
		end of core: 30 cm	

A60

PS2727-3 (GKG)

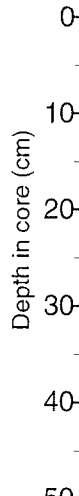
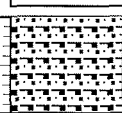
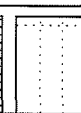
Western East Siberian Sea

ARK-XI/1

Recovery: 0.10 m

77°30.9'N, 139°59.8'E

Water depth: 39 m

Lithology	Texture	Color	Description	Age
Surface				
2.5Y3/2, sandy silty clay, even surface, extremely rich benthic life: abundant brittle stars, common hydrozoans, worms, etc.				
			0-1 cm: as surface	
			5Y3/1	1-10 cm: sandy silty clay, very dark gray, homogeneous
			end of core: 10 cm	

A61

PS2728-2 (GKG)

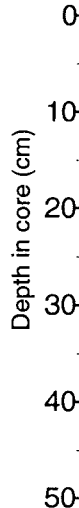
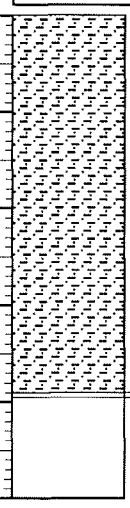
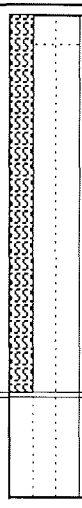
Eastern Laptev Sea

ARK-XI/1

Recovery: 0.39 m

77°15.0'N, 135°00.5'E

Water depth: 44 m

Lithology	Texture	Color	Description	Age
Surface				
10YR3/3, silty clay, dark brown, even surface, common polychaet tubes				
			10YR3/3 0-3 cm: silty clay, dark brown, homogeneous	
			5Y3/1 3-39 cm: silty clay, very dark gray, with faint lamination and thin (several mm) black lenses	
			end of core: 39 cm	

A62

PS2728-3 (SL)

Eastern Laptev Sea

ARK-XI/1

Recovery: 2.56 m

77° 15.0'N, 135° 00.2'E

Water depth: 46 m

Lithology	Texture Color	Description	Age
	2.5Y2/0	0 - 9 cm:	
	5Y 3/2	Silty clay, black (2.5Y2/0) and dark olive gray (5Y 3/2), mottled	
	5Y 3/1	9 - 22 cm:	
		Silty clay, dark olive gray (5Y 3/2)	
	5Y 3/1 to 5Y 3/2	22 - 55 cm:	
		Silty clay, very dark gray (5Y 3/1); black spots between 24 and 47 cm; thin light olive brown (2.5Y 5/4) laminae; bivalve at 27-28 cm, gastropode at 38 cm	
		55 - 155 cm:	
	Silty clay, very dark gray (5Y 3/1) to dark olive gray (5Y 3/2); common black spots throughout; bivalves at 67-68 cm (3 cm in diameter, both tests preserved), 73 cm, and 140 cm		
5Y 3/2 and 2.5Y2/0	155-207 cm:		
	Silty clay, dark olive gray (5Y 3/2) and black (2.5Y 2/0), mottled; wet soft interval at 200-201 cm; bivalve at 181 cm		
2.5Y2/0	207 - 241 cm:		
	Silty clay, black (2.5Y 2/0); 213-232 disturbed (slumping?); bivalves at 213-215 cm and 238 cm		
2.5Y2/0 and 5Y 3/2	241 - 256 cm:		
	Silty clay, dark olive gray (5Y 3/2) and black (2.5Y 2/0), mottled		



A63

PS2729-3 (GKG)

Central Laptev Sea

ARK-XI/1

Recovery: 0.33 m

75°59.9'N, 129°58.8'E

Water depth: 53 m

Lithology	Texture	Color	Description	Age
Surface				
2.5Y3/3 sandy silty clay, dark olive brown, even surface, abundant brittle stars, holothurians, polychaets, bivalvia				
0-2	2.5Y3/3		0-2 cm: sandy silty clay, dark olive brown	
2-33	N3		2-33 cm: sandy silty clay, very dark gray, with dark spots (common at top, abundant at base), common bivalves	
end of core: 33 cm				

A64

PS2730-3 (GKG)

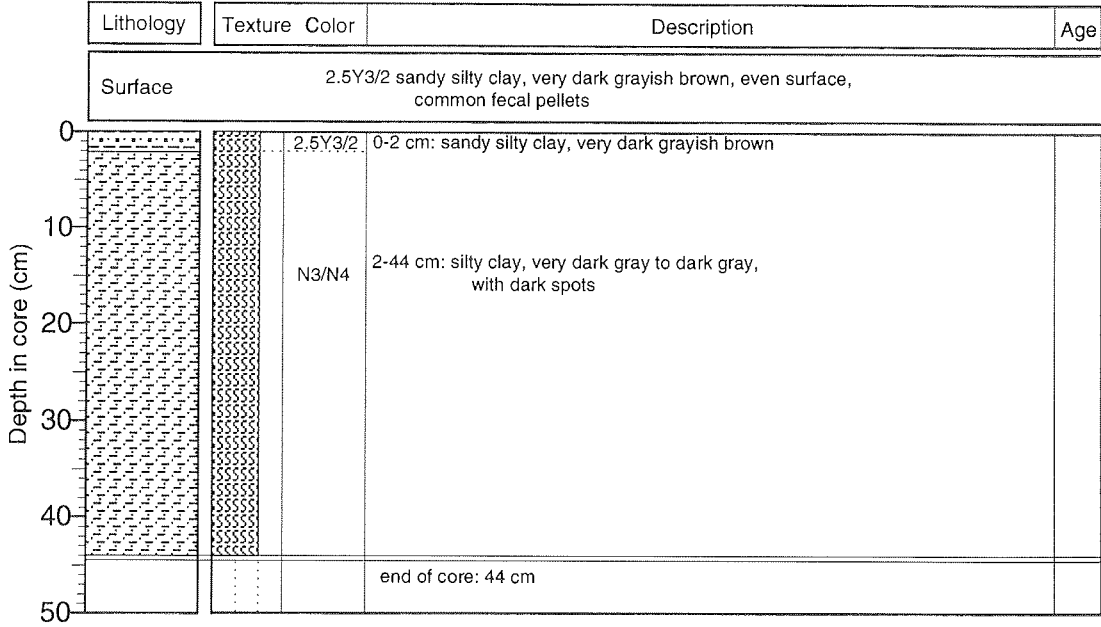
Central Laptev Sea

ARK-XI/1

Recovery: 0.44 m

76°53.1'N, 129°59.7'E

Water depth: 60 m



A65

PS2731-3 (GKG)

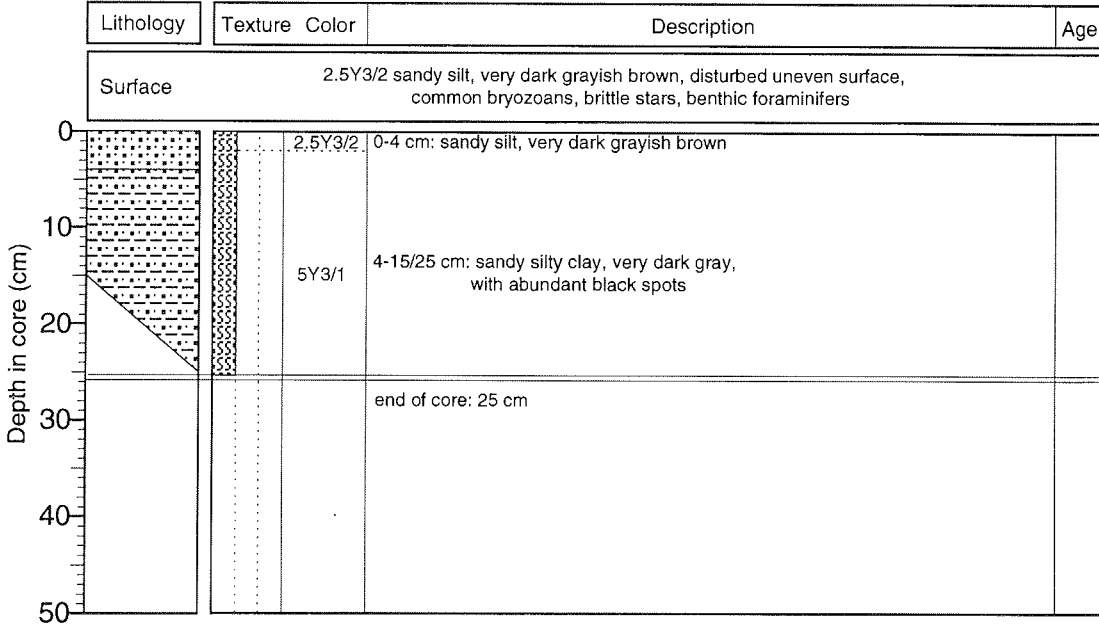
Central Laptev Sea

ARK-XI/1

Recovery: 0.15 m

77°35.9'N, 130°02.2'E

Water depth: 90 m



A66

PS2732-4 (GKG)

Central Laptev Sea

ARK-XI/1

Recovery: 0.43 m

77°37.2'N, 130°02.5'E

Water depth: 272 m

Lithology	Texture	Color	Description	Age
Surface				
2.5Y3/3 silty clay, dark olive brown, uneven surface, common amphipods, benthic foraminifers				
Depth in core (cm) 0 10 20 30 40 50			0-4 cm: silty clay, dark olive brown	
		2.5Y3/3	4-43 cm: silty clay, dark gray, with some dark spots	
		N4		
			end of core: 43 cm	

A67

PS2733-3 (GKG)

Central Laptev Sea Cont. Margin

ARK-XI/1

Recovery: 0.43 m

77°42.2'N, 130°02.4'E

Water depth: 510 m

Lithology	Texture Color	Description	Age
Surface 2.5Y3/2 silty clay, very dark grayish brown, even surface, common polychaets, benthic foraminifers			
	<p>0</p> <p>10</p> <p>20</p> <p>30</p> <p>40</p> <p>50</p>	<p>2.5Y3/2 0-8 cm: sandy silty clay, very dark grayish brown, mottled with olive gray spots</p> <p>10YR2/2 8-9 cm: sandy silty clay, very dark brown, irregular layer</p> <p>2.5Y3/3 9-12 cm: sandy silty clay, dark olive brown, irregular layer</p> <p>5Y4/1 12-43 cm: silty clay, dark gray, homogeneous</p> <p>end of core: 43 cm</p>	

A68

PS2733-6 (SL)

Central Laptev Sea Cont. Margin

ARK-XI/1

Recovery: 5.46 m

77° 46.3'N, 130° 08.3'E

Water depth: 525 m

Lithology	Texture Color	Description	Age
	<p>10YR 3/4 5Y 4/1</p> <p>5Y 3/1</p>	<p>0 - 4 cm: Silty clay, dark yellowish brown (10YR 3/4); mud clasts ?; dropstone (1 cm in diameter) at 0-1 cm</p> <p>4 - 9 cm: Silty clay, dark gray (5Y 4/1), homogeneous</p> <p>9 - 546 cm: Silty clay, very dark gray (5Y 3/1); common to abundant black spots throughout; coal (iron-sulfide-filled worm tube) between 65 and 78 cm</p>	

A69

PS2734-3 (GKG)

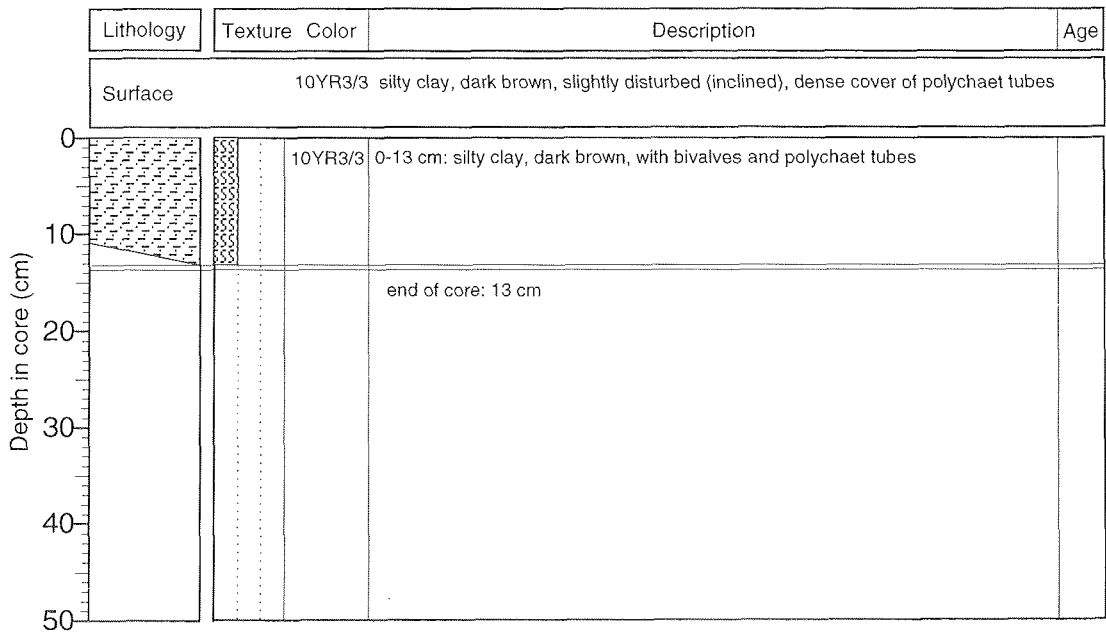
Central Laptev Sea Cont. Margin

ARK-XI/1

Recovery: 0.13 m

77°51.0'N, 130°03.0'E

Water depth: 1106 m



A70

**PS2735-4 (GKG)**

Central Laptev Sea Cont. Margin

**ARK-XI/1**

Recovery: 0.30 m

77°55.9'N, 130°02.6'E

Water depth: 1719 m

Lithology	Texture	Color	Description	Age
Surface				
10YR3/2 silty clay, very dark grayish brown, even surface				
	10YR3/2		0-17 cm: silty clay, very dark grayish brown, fine lamination	
	5Y3/1		17-30 cm: silty clay, very dark gray, with thin dark horizontal lenses	
			end of core: 30 cm	



A71

PS2736-3 (GKG)

Central Laptev Sea Cont. Margin

ARK-XI/1

Recovery: 0.41 m

78°10.8'N, 129°59.6'E

Water depth: 2321 m

Lithology	Texture Color	Description	Age
Surface			
2.5Y3/3 silty clay, dark olive brown			
0		2.5Y3/3 0-9 cm: silty clay, dark olive brown	
10		10YR2/2 9-10 cm: stiff clay, very dark brown	
		5Y3/1 10-12 cm: sandy silty clay (turbidite?), very dark gray, graded bedding	
20		5Y3/1 12-25 cm: silty clay, homogeneous, very dark gray, grading to dark olive brown at base	
30		2.5Y3/3 25-31 cm: silty clay, dark olive brown, with darker layers at 26-28 cm and 30-31 cm	
40		5Y3/1 + 2.5Y3/3 31-41 cm: silty clay, lamination of very dark gray and dark olive brown layers	
50		end of core: 41 cm	

A72

PS2736-6 (SL)

Central Laptev Sea Cont. Margin

ARK-XI/1

Recovery: 4.83 m

78° 11.8'N, 129° 58.6'E

Water depth: 2309 m

Lithology	Texture Color	Description	Age
	10YR4/3	0 - 6 cm:	
	10YR3/3	Silty clay, brown (10YR 4/3) and dark grayish brown (2.5Y 4/2), partly laminated	
	5Y 3/2	6 - 14 cm:	
	2.5Y 4/2	Silty clay, dark brown (10YR 3/3), sharp (erosional?) contact at the base	
	10YR3/2	14 - 15 cm:	
	2.5Y 4/2	Silty clay, very dark gray (5Y 3/1), homogenous	
	5Y 4/2	15 - 19 cm:	
	5Y 4/2	Silty clay, dark olive gray (5Y 3/2)	
	5Y 2.5/1	19 - 27 cm:	
	5Y 3/2	Silty clay, dark grayish brown (2.5Y 4/2), slightly mottled/bioturbated	
	5Y 2.5/1	27 - 43 cm:	
	5Y 4/1	Alternation of very dark grayish brown (10YR 3/2) and dark olive gray (2.5Y 4/2) silty clay (each horizon ca. 1 cm in thickness)	
	5Y 3/2	43 - 55cm:	
	5Y 3/2	Alternation of olive gray (5Y 4/2) and dark grayish brown (10YR 4/2) silty clay; small mud clasts ? in the upper part	
5Y 3/1	55 - 83 cm:		
5Y 3/1	Silty clay, olive gray (5Y 4/2); occasionally thin dark grayish brown layers		
5Y 3/1	83 - 93 cm:		
5Y 3/1	Silty clay to (sandy) clayey silt, black (5y 2.5/1) to dark gray (5Y 4/1), fining-upwards structures (coarse particles small black mud clasts/coal?), sharp contact at the base		
5Y 3/1	93 - 107 cm:		
5Y 3/1	Silty clay, dark olive gray (5Y 3/2), occasionally black spots		
5Y 3/1	107 - 128 cm:		
5Y 3/1	Silty clay to (sandy) clayey silt, black (5Y 2.5/1) to dark gray (5Y 4/1), fining-upwards structures (coarse particles black mud clasts/coal?), sharp contact at the base		
5Y 3/1	128 - 183 cm:		
5Y 3/1	Silty clay, dark olive gray (5Y 3/2), common black spots below 150 cm; sandy interval at 149-150 cm (fining-upwards structure)		
5Y 3/1	183 - 483 cm:		
5Y 3/1	Silty clay, very dark gray (5Y 3/1); common (below 412 cm abundant) black spots throughout; thin horizons of black particles (coal?) between 305 and 380 cm, thicker intervals of black particles (mudclasts/coal?) at 335-342 cm, 348-362 cm (base of turbidite?), and 456-462 cm; black horizons at 391-392 cm, 401 cm, 403 cm, 405 cm, 407 cm, 409 cm, and 419 cm; more silty horizons (fining-upward structures, turbidites) at 327-328 cm, 344-347 cm, 372-374 cm, and 380-381 cm; bivalves at 204 cm, 265 cm, and 349 cm		

A73

PS2737-4 (GKG)

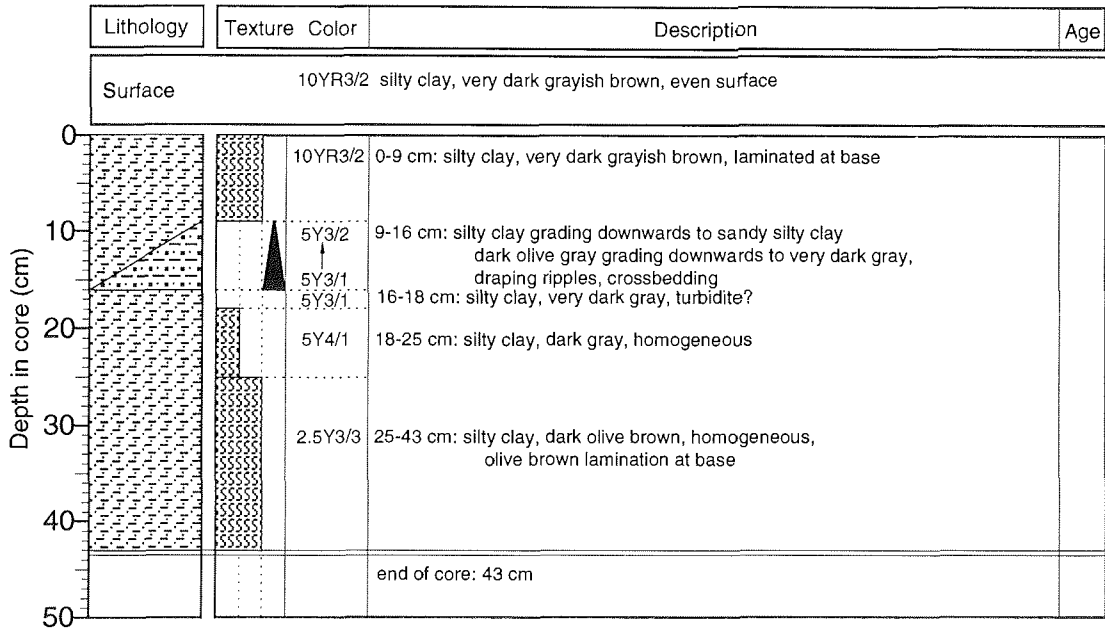
Amundsen Basin

ARK-XI/1

Recovery: 0.43 m

79°12.9'N, 131°28.9'E

Water depth: 3155 m



PS2737-7 (SL)

Amundsen Basin

ARK-XI/1

Recovery: 1.85 m

79° 14.0'N, 131° 30.0'E

Water depth: 3150 m

Lithology	Texture	Color	Description	Age
		<p>10YR 3/3 10YR 3/2 5Y 4/1 5Y 4/1 5Y 4/2 5Y 4/1 5Y 3/1 5Y 3/2 5Y 3/1 5Y 3/2 5Y 3/2 5Y 4/2 5Y 3/1</p>	<p>0 - 14 cm: Silty clay, dark brown (10YR 3/3), brown (10YR 4/3), dark grayish brown (10YR 3/2, 2.5Y 4/2)</p> <p>14 - 19 cm: Silty clay, dark grayish brown (10YR 4/2) to very dark grayish brown (10YR 3/2), slightly laminated; small mud clasts ?</p> <p>19 - 85 cm. Silty clay, olive gray (5Y 4/2) and dark gray (5Y 4/1); dark yellowish brown interval (10YR 3/4) intervals at 29-30 cm and 70-71 cm, slightly laminated; thin sandy layers at 31 cm, 39-41 cm, 44 cm, 63 cm, 70-71 cm, 74-75 cm (fining upwards), 81 cm, and 85 cm; at 20 cm flat MnFe-crust/concretion (1 cm in diameter)</p> <p>85 - 146 cm: Silty clay, very dark gray (5Y 3/1) and dark olive gray (5Y 3/2); common thin sandy layers intercalated, fining-upwards sequences (turbidites) at 85-91 cm, 100-101 cm, 108-110 cm, 125-126 cm, 128-140 cm, and 142-145 cm</p> <p>146 - 185 cm. Silty clay, very dark gray (5Y 3/1), relatively firm, abundant black spots</p>	
<p>2</p> <p>3</p> <p>4</p> <p>5</p>				

A75

PS2739-5 (GKG)

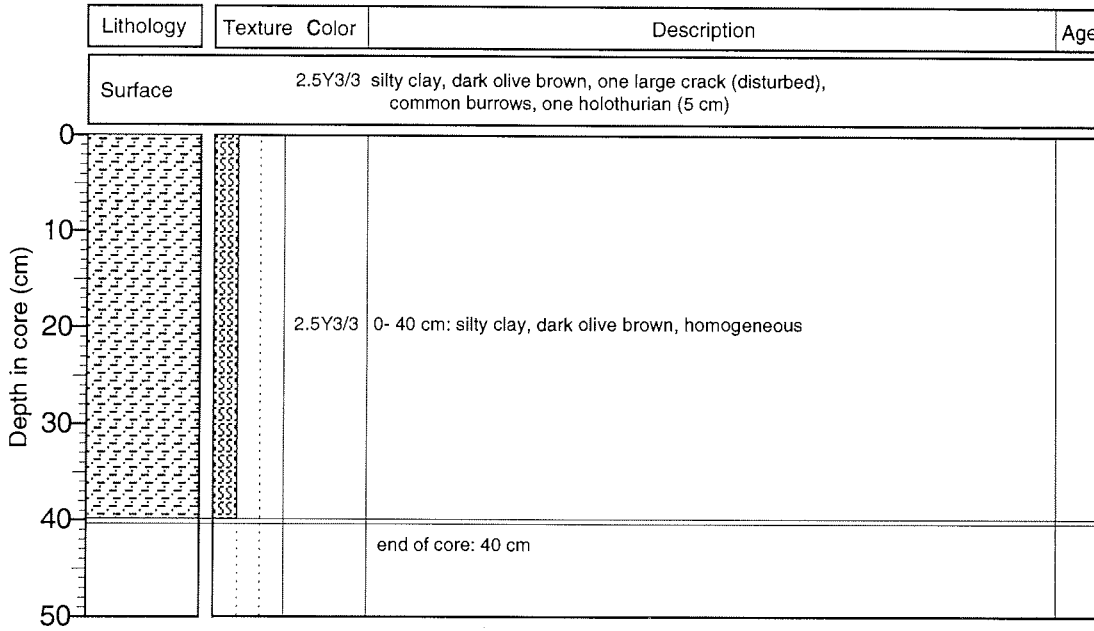
Nansen Basin

ARK-XI/1

Recovery: 0.40 m

81°07.9'N, 106°01.7'E

Water depth: 2787 m



A76

PS2740-8 (GKG)

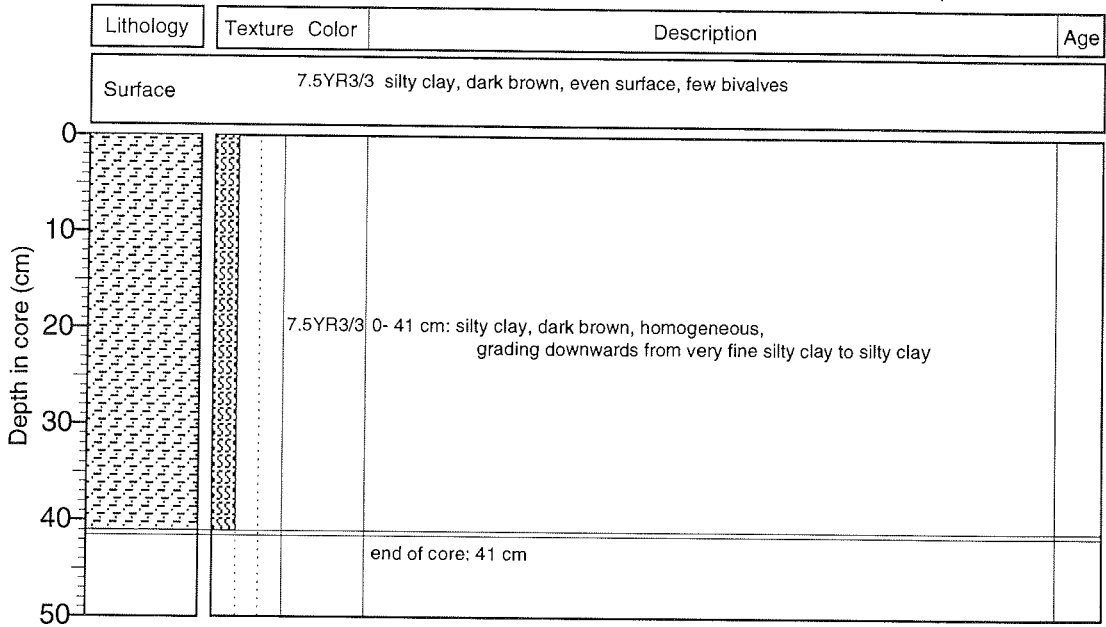
Nansen Basin

ARK-XI/1

Recovery: 0.41 m

81°11.5'N, 107°35.1'E

Water depth: 3210 m





PS2741-1 (KAL)

ARK-XI/1

Lithology	Texture	Color	Description	Age
		<p>5Y 3/1</p> <p>2.5Y 4/2</p> <p>5Y 3/1</p> <p>2.5Y 4/2</p> <p>5Y 3/1</p> <p>5Y 4/2</p> <p>5Y 4/1</p> <p>5Y 4/2</p>	<p>509 - 541 cm:                      silty clay, olive brown (2.5Y 4/2), upper part slightly mottled/                      bioturbated, lower part laminated;                      gray layer 85Y 5/1) at 534 cm</p> <p>541 - 547 cm.                      silty clay, very dark gray (5Y 3/1);                      thin gray silty laminae at 542cm, 543cm, and 545 cm</p> <p>547 - 564 cm.                      silty clay, olive brown (2.5Y 4/2), upper part slightly mottled/                      bioturbated, lower part laminated</p> <p>564 - 594 cm:                      silty clay, very dark gray (5Y 3/1);                      thin gray silty layers at 565 cm, 568 cm, 572 cm, 573 cm, 574 cm,                      575 cm, 576 cm, 577 cm, 579 cm, and 580 cm; 580-594 cm                      homogenous</p> <p>594 - 609 cm:                      silty clay, olive brown (5Y 4/2)</p> <p>609 - 613 cm.                      silty clay, dark gray (5Y 4/1)</p> <p>613 - 635 cm:                      silty clay, olive gray (5Y 4/2)</p> <p>635 - 637 cm:                      silty clay, very dark gray (5Y 3/1)</p>	

Depth in core (m)



A79

PS2742-3 (GKG)

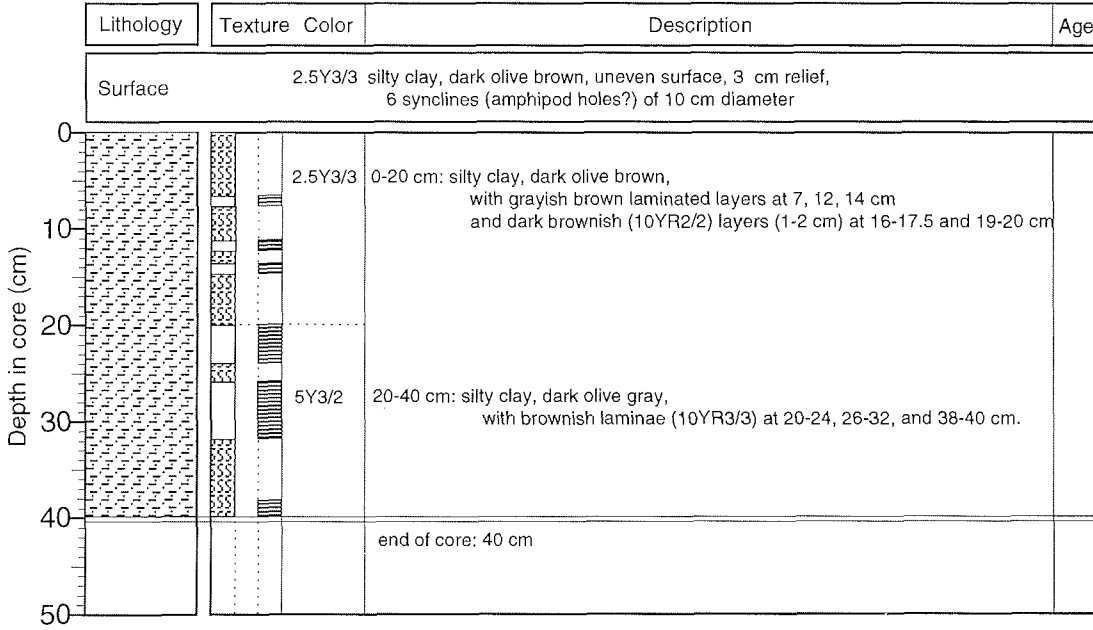
Western Laptev Sea Cont. Margin

ARK-XI/1

Recovery: 0.40 m

80°48.3'N, 103°54.0'E

Water depth: 1956 m



A80

PS2742-5 (SL)

Western Laptev Sea Cont. Margin

ARK-XI/1

Recovery: 3.81 m

80° 47.3'N, 103° 49.6'E

Water depth: 1890 m

Lithology	Texture Color	Description	Age
	10YR 4/3 10YR 2/2	0 - 6 cm: Silty clay, brown (10YR 4/3); very dark brown (10YR 2/2) layers at 2, 4, and 5 cm	
	5Y 4/2	6 - 11 cm: Silty clay, very dark brown (10YR 2/2), thin brown laminae (finely laminated)	
		11 - 13 cm: Silty clay, grayish brown (2.5Y 5/2), with very dark brown silty clay interval	
	5Y 3/2	13 - 81 cm: Silty clay, olive gray (5Y 4/2), with common thin brown (10YR 5/3) laminae throughout (13-25 cm brown intervals more abundant)	
		81 - 195 cm: Silty clay, dark olive gray (5Y 3/2); thin brown laminae at 87, 88, 94, 122, and 144 cm; black spots at 107 cm; 10 cm long tube at 170 - 173 cm	
		195 - 300 cm: Silty clay, very dark gray (5Y 3/1), abundant black spots throughout	
	5Y 3/1	300 - 314 cm: Silty clay, olive gray (5Y 4/2)	
		314 - 326 cm: Silty clay, dark grayish brown (2.5Y 4/2), mottled/bioturbated	
	5Y 4/2	326 - 341 cm: Silty clay, olive brown (2.5Y 4/4)	
	2.5Y 4/2 2.5Y 4/4	341 - 343 cm: Silty sand, olive brown (2.5Y 4/4)	
10YR 3/2 10YR 3/3	343 - 360 cm: Diamicton, very dark grayish brown (10YR 3/2) to dark brown (10YR 3/3), large-sized dropstones of up to 5 cm in diameter; sand lense at 356-358 cm		
5Y 3/2 5Y 3/1	360 - 381 cm: Silty clay, very dark gray (5Y 3/1) and dark olive gray (5Y 3/2)		
5			

A81

PS2743-7 (GKG)

Western Laptev Sea Cont. Margin

ARK-XI/1

Recovery: 0.19 m

80°44.1'N, 103°11.7'E

Water depth: 1060 m

Lithology	Texture	Color	Description	Age
Surface				
10YR3/3 pebbly sandy silt, dark brown, even surface, benthic fauna on pebbles				
	10YR3/3		0-10 cm: pebbly sandy silt, dark brown, homogeneous, grading downwards from very fine silty clay to silty clay	
	2.5Y5/4		10-19 cm: silty clay, light olive brown, homogeneous	
			end of core: 19 cm	

A82

PS2744-6 (GKG)

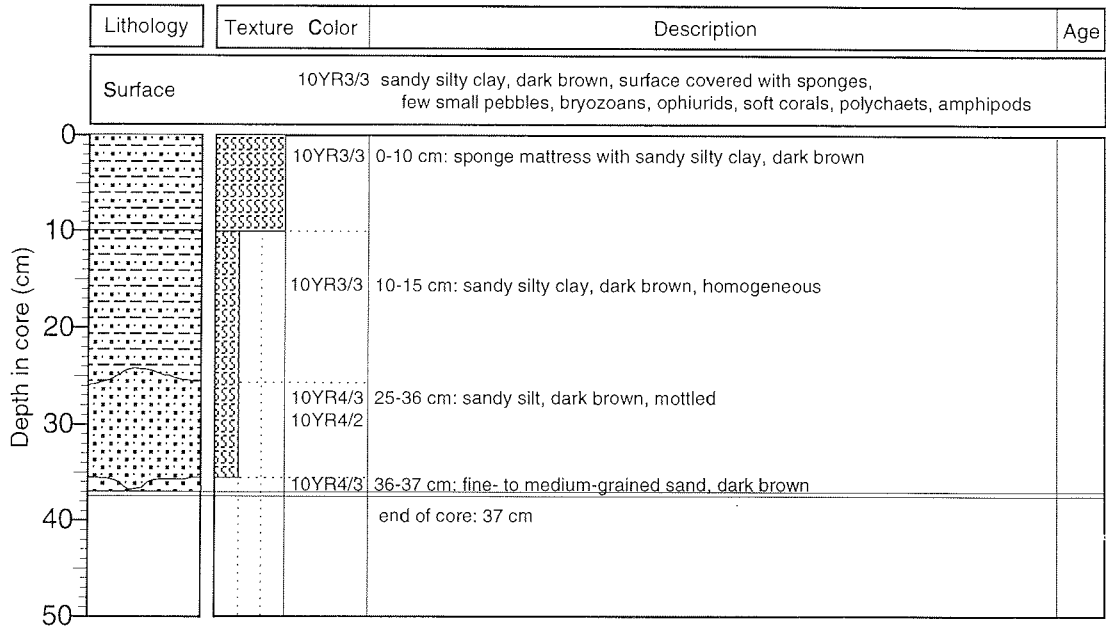
Western Laptev Sea Cont. Margin

ARK-XI/1

Recovery: 0.36 m

80°36.4'N, 103°03.2'E

Water depth: 455 m



A83

PS2745-7 (GKG)

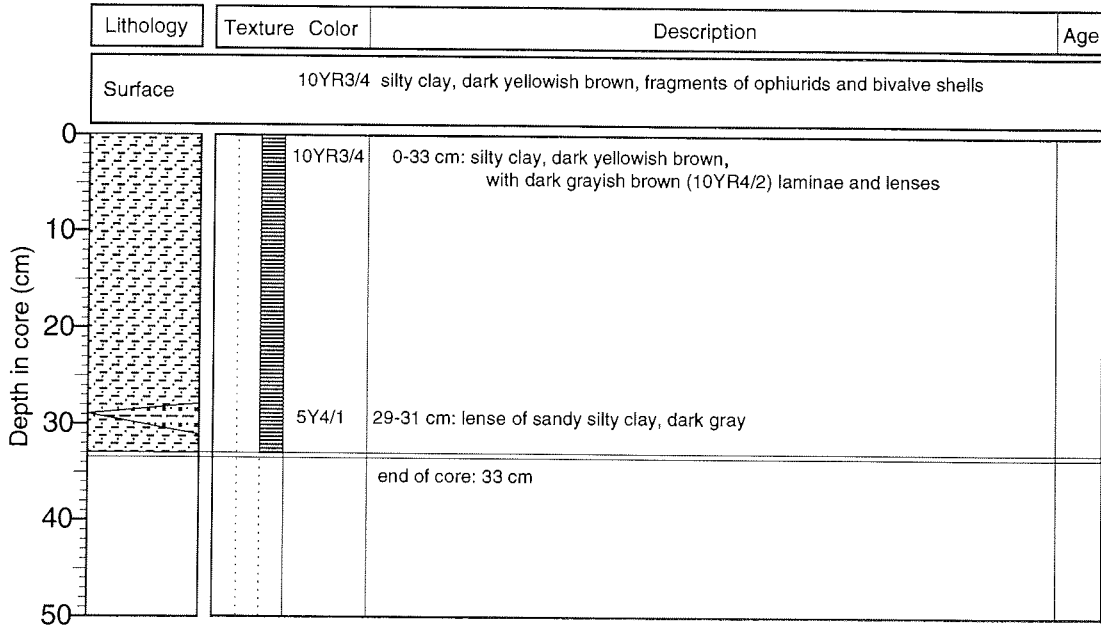
Western Laptev Sea

ARK-XI/1

Recovery: 0.33 m

80°24.9'N, 102°05.4'E

Water depth: 255 m



A84

PS2747-8 (GKG)

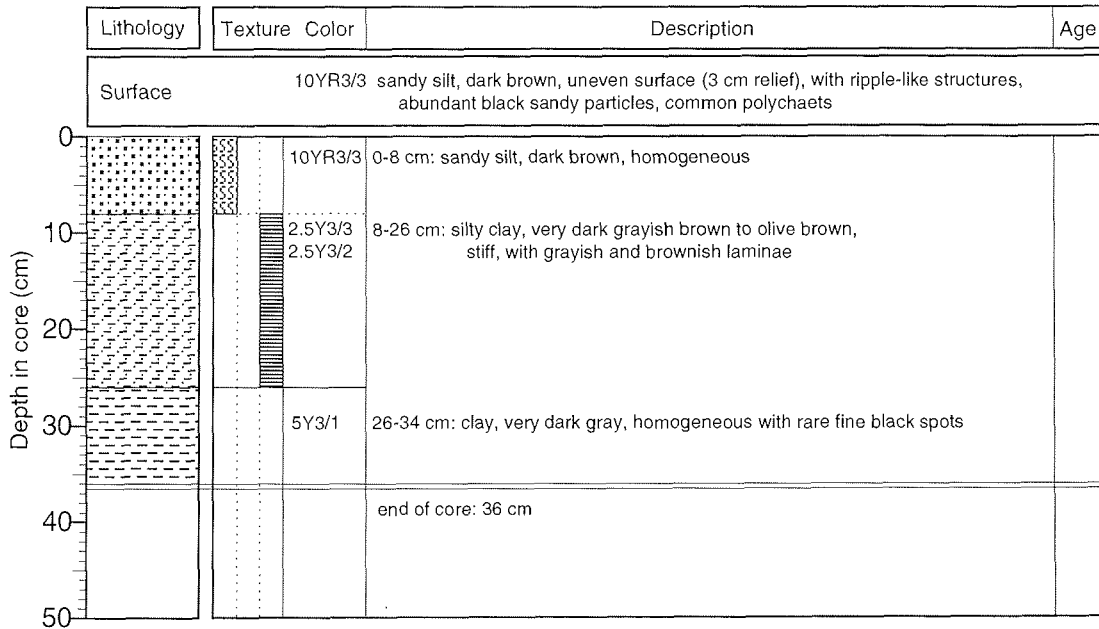
Eastern Laptev Sea Cont. Margin

ARK-XI/1

Recovery: 0.36 m

78°30.8'N, 133°42.9'E

Water depth: 1995 m



A85

PS2747-9 (SL)

Eastern Laptev Sea Cont. Margin

ARK-XI/1

Recovery: 6.91 m

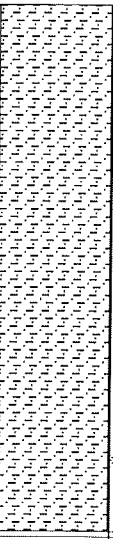

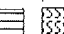
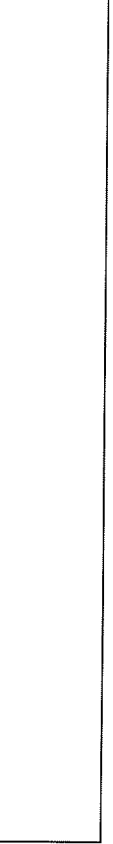
78° 30.0' N, 133° 49.6' E

Water depth: 1771 m

Lithology	Texture Color	Description	Age
	10YR 4/3 5Y 4/1	0 - 1 cm: silty clay, dark brown (10YR 3/3);  1 - 12 cm: alternation of approx. 0.5 cm thick layers of brown (10YR 4/3) and dark gray (5Y 4/1) silty clay	
	5Y3/1	12 - 691 cm: silty clay, very dark gray (5Y 3/1) and dark olive gray (5Y 3/2), partly mottled/bioturbated; thin olive brown (2.5Y 4/4) laminae at 20, 24, 29, 38, 40, 50, 57, 67, 84, 110, 125, 130, 139, 145, 151, 160, 164, 169, 185, 203, 221, 228, 240, 243 (more coarse/silty), 254, 258, 264, 298, 318, 324 (more coarse/silty), 335, 337 (more coarse/silty), 480, 483 (more coarse/silty), 528, 540, 607, 610, 613, 643, and 649 cm: occasionally black spots and/or laminae between 0 and 100 cm, 345 and 456 cm, 530 and 580 cm, and 624 and 691 cm	
	5Y3/2		
	5Y3/1		
	5Y3/2		
	5Y 3/1 to 5Y 3/2		

PS2747-9 (SL)

ARK-XI/1

Lithology	Texture	Color	Description	Age
		5Y3/1		
		5Y3/2		
		5Y3/1		
		5Y3/2		
				

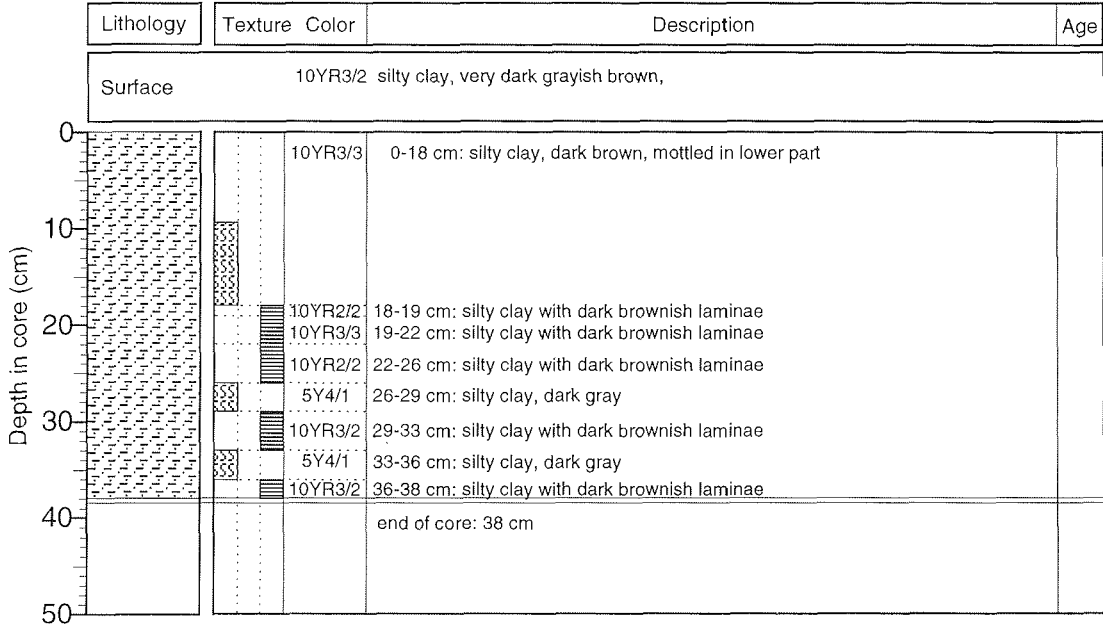
5  
6  
7  
8  
9  
10

Depth in core (m)



A87

PS2748-2 (GKG) Eastern Laptev Sea Cont. Margin ARK-XI/1  
 Recovery: 0.37 m 78°41.9'N, 134°36.5'E Water depth: 2122 m



A88

**PS2749-3 (GKG)**

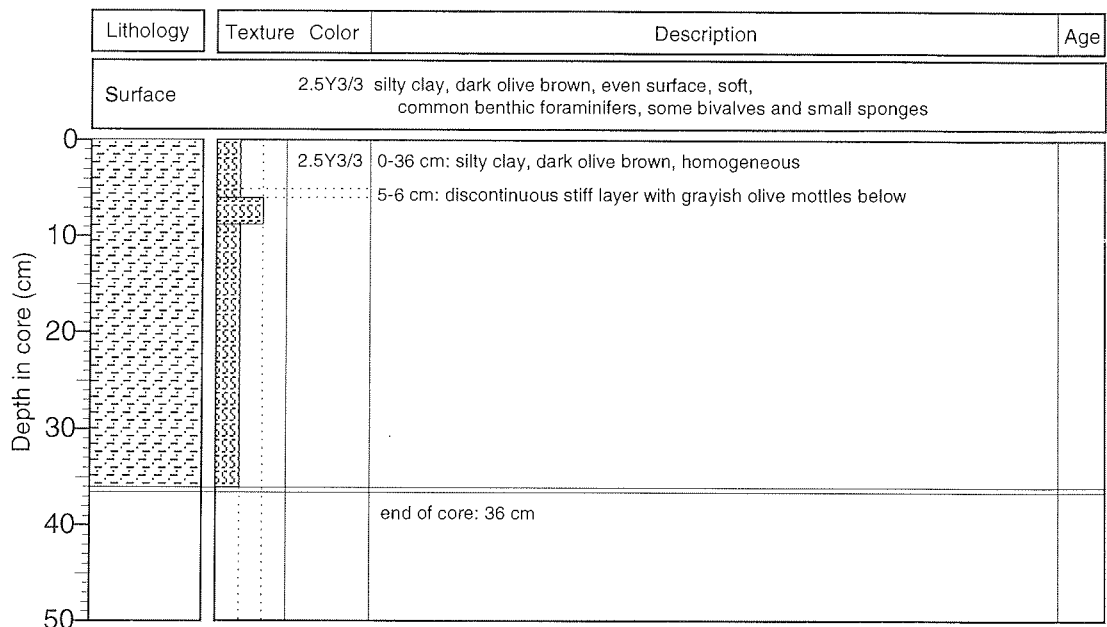
Eastern Laptev Sea Cont. Margin

**ARK-XI/1**

Recovery: 0.36 m

79°07.6'N, 135°06.8'E

Water depth: 2783 m



A89

PS2750-2 (GKG)

Amundsen Basin

ARK-XI/1

Recovery: 0.43 m

79°58.9N, 135°00.1'E

Water depth: 3358 m

Lithology	Texture Color	Description	Age
Surface			
2.5Y3/3 silty clay, dark olive brown, with bivalves up to 1.5 cm			
	2.5Y3/3	0-9 cm: silty clay, dark olive brown, with lenses (several mm) of darker silty clay (10YR3/4)	
	5Y3/1	9-16 cm: sandy silty clay, very dark gray, with dropstones of gray carbonate sandstone	
	5Y4/3	16-21 cm: sandy silty clay, olive, stiff	
	2.5Y4/4	21-37 cm: sandy silty clay, olive brown, homogeneous	
	2.5Y4/4	37-43 cm: sandy silty clay, olive brown, with thin (3-5 mm) lenses and layers of darker (10YR3/4) sandy silty clay	
end of core: 43 cm			

A90

PS2752-8 (GKG)

Amundsen Basin

ARK-XI/1

Recovery: 0.29 m

80°56.1'N, 131°21.8'E

Water depth: 3823 m

Lithology	Texture	Color	Description	Age
Surface				
		2.5Y3/3	clayey sandy silt, dark olive brown, one dropstone of 1 cm in diameter	
Depth in core (cm) 0 10 20 30 40 50		2.5Y3/3	0-9 cm: clayey sandy silt, dark olive brown, homogeneous	
		2.5Y3/4	9-29 cm: clayey sandy silt, olive brown, slightly lighter towards base	
			end of core: 29 cm	

A91

PS2753-1 (GKG)

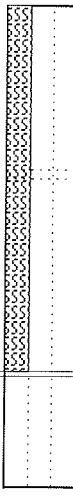
Amundsen Basin

ARK-XI/1

Recovery: 0.38 m

80°58.0'N, 134°27.3'E

Water depth: 3628 m

Lithology	Texture Color	Description	Age
Surface 2.5Y4/2 silty clay, dark grayish brown, soft, even surface, common benthic foraminifers, rare bivalves, sponges, amphipods, polychaets			
Depth in core (cm) 0 10 20 30 40 50		2.5Y4/2 0-38 cm: silty clay, dark grayish brown, homogeneous  17-18 cm: slightly grayish layer  end of core: 38 cm	

PS2753-2 (KAL)

Amundsen Basin

ARK-XI/1

Recovery: 7.84 m

80° 58.2' N, 134° 27.7' E

Water depth: 3684 m

Lithology	Texture Color	Description	Age
0		0-50 cm: silty clay, dark brown (10YR 4/3); coring disturbance in the upper 14 cm; thin gray (2.5Y5/0) layers at 18, 20, and 40-41 cm.	
	10YR 4/3	50-58 cm: silty clay, dark brown (10YR 4/3) and very dark grayish brown (10YR 3/2); mottled/bioturbated	
	10YR 4/3-3/2 10YR 4/4	58-63 cm: silty clay, dark yellowish brown (10YR 4/4), mottled/bioturbated	
1		63-140 cm: silty clay, olive brown (2.5Y4/4); mottled/bioturbated between 100 and 110 cm; very dark brown horizons at 63-65, 68-71, 88-89, 90, 91-92, and between 113 and 133 cm; silty laminae at 71, 73, 76, and 82 cm	
	2.5Y 4/4	140-143 cm: silty clay, gray (2.5Y5/0)	
		143-170 cm: silty clay, olive brown (2.5Y4/4), mottled/bioturbated	
	2.5Y 4/4	170-200 cm: silty clay, dark grayish brown (2.5Y4/2); dark gray (2.5Y4/0) silty layers at 191 and 195 cm	
	2.5Y 4/2 and 2.5Y 4/0	200-203 cm: silty clay, dark yellowish brown (10YR 4/6)	
2		203-210 cm: silty clay, dark yellowish brown (2.5Y4/2)	
	2.5Y 4/2 2.5Y 5/2 2.5Y 4/2	210-215 cm: silty clay, grayish brown (2.5Y5/2)	
	10YR 4/4	215-225 cm: alternation of dark grayish brown (2.5Y4/2) and grayish brown (2.5Y5/2) silty clay	
	2.5Y 5/4	225-238 cm: silty clay, dark yellowish brown (10YR 4/4); dark gray (2.5Y 4/0) layers at 237 and 238 cm; large-sized dropstone (diameter 2.5 cm) at 232-233 cm	
	2.5Y 4/4-4/2 2.5Y 4/4	238-257 cm: silty clay, olive brown (2.5Y5/4); dropstone (diameter 0.5 cm) at 252 cm	
3		257-259 cm: silty clay, yellowish brown (10YR 5/4)	
	2.5Y 4/4 and 4/0	259-270 cm: alternation of olive brown (2.5Y 4/4) and dark grayish brown (2.5Y4/2) silty clay	
	2.5Y 5/4	270-300 cm: silty clay, olive brown (2.5Y4/4), mottled/bioturbated	
	2.5Y 4/2	300-320 cm: alternation of olive brown (2.5Y4/4) silty clay and dark gray (2.5Y4/0) clayey silt	
	10YR 4/3 10YR 3/3 10YR 4/3	320-330 cm: silty clay, light olive brown (2.5Y5/4); dark gray silty layer at 325 cm	
4		330-340 cm: silty clay, dark grayish brown (2.5Y4/2), mottled/bioturbated	
	2.5Y 4/4	340-344 cm: silty clay, light olive brown (2.5Y5/4)	
	2.5Y 4/2	344-355 cm: silty clay, brown (10YR 4/3)	
	2.5Y 5/2		
5			
	2.5Y 4/0		



PS2754-8 (KAL)

Lomonosov Ridge

ARK-XI/1

Recovery: 9.05 m

81° 02.8' N, 136° 38.2' E

Water depth: 2660 m

Lithology	Texture Color	Description	Age
	10YR 3/3	0 - 43 cm: silty clay, dark brown (10YR 3/3); coring disturbance in the upper 12 cm; slightly mottled/bioturbated between 17 and 21 cm; abundant very dark brown (10YR 2/2) layers between 21 and 43 cm (most prominent at 21 and 25 cm)	
	2.5Y 4/4	43 - 59 cm: silty clay, olive brown (2.5Y 4/4); in the upper part dark grayish brown layers, lower part slightly bioturbated	
	2.5Y 4/2		
	2.5Y 5/4		
	2.5Y 4/4		
	2.5Y 4/2		
	2.5Y 4/4		
	2.5Y 5/4		
	2.5Y 4/4		
	2.5Y 4/2		
	2.5Y 4/4		
	2.5Y 5/4		
	2.5Y 5/4		
	2.5Y 5/4		
	2.5Y 5/4		
	2.5Y 5/4		
	2.5Y 5/4		
	2.5Y 5/4		
	2.5Y 5/4		
	2.5Y 5/4		
2.5Y 5/4			
2.5Y 5/4			
2.5Y 5/4			
2.5Y 5/4			
2.5Y 5/4			
2.5Y 5/4			
2.5Y 5/4			
2.5Y 5/4			
2.5Y 5/4			
2.5Y 5/4			
2.5Y 5/4			
2.5Y 5/4			
2.5Y 5/4			
2.5Y 5/4			
2.5Y 5/4			
2.5Y 5/4			
2.5Y 5/4			
2.5Y 5/4			
2.5Y 5/4			
2.5Y 5/4			
2.5Y 5/4			
2.5Y 5/4			
2.5Y 5/4			
2.5Y 5/4			
2.5Y 5/4			
2.5Y 5/4			
2.5Y 5/4			
2.5Y 5/4			
2.5Y 5/4			
2.5Y 5/4			
2.5Y 5/4			
2.5Y 5/4			
2.5Y 5/4			
2.5Y 5/4			
2.5Y 5/4			
2.5Y 5/4			
2.5Y 5/4			
2.5Y 5/4			
2.5Y 5/4			
2.5Y 5/4			
2.5Y 5/4			
2.5Y 5/4			
2.5Y 5/4			
2.5Y 5/4			
2.5Y 5/4			
2.5Y 5/4			
2.5Y 5/4			
2.5Y 5/4			
2.5Y 5/4			
2.5Y 5/4			
2.5Y 5/4			
2.5Y 5/4			
2.5Y 5/4			
2.5Y 5/4			
2.5Y 5/4			
2.5Y 5/4			
2.5Y 5/4			
2.5Y 5/4			
2.5Y 5/4			
2.5Y 5/4			



PS2754-8 (KAL)

ARK-XI/1

	Lithology	Texture	Color	Description	Age
5			2.5Y 4/2	426 - 434 cm:	
			2.5Y 4/4	alternation of light olive brown (2.5Y5/4) and very dark grayish brown (10YR 3/2) silty clay, laminated	
6			2.5Y 4/2	434 - 471 cm:	
			2.5Y 4/4	alternation of light olive brown (2.5Y 5/4) and dark grayish brown (2.5Y 4/2) silty clay, lower part slightly bioturbated	
			2.5Y 4/2	471 - 476 cm:	
			2.5Y 4/2 and 2.5Y 4/4	silty clay, very dark grayish brown (2.5Y 3/2)	
			2.5Y 4/4	476 - 602 cm:	
			2.5Y 4/4	alternation of silty clay, dark grayish brown (2.5Y 4/2), slightly bioturbated (476-516 cm, 521-546 cm, 551-560 cm, and 591-602 cm, and silty clay, olive brown (2.5Y 4/4) (516-521 cm, 546-551 cm, and 586-591 cm); short-term alternation of both lithologies between 560 and 586 cm; dark gray (2.5Y 4/0) silt layer at 559 cm	
			2.5Y 4/2	602 - 623 cm:	
			2.5Y 4/2	silty clay, light olive brown (2.5Y 5/4), slightly bioturbated	
			10YR 5/3	623 - 656 cm:	
			2.5Y 4/4	silty clay, dark grayish brown (2.5Y 4/2); light olive brown (2.5Y 5/4) mottling/bioturbation between 635 and 656 cm; dark olive gray sandy layers at 627 and 629 cm; silt layer at 654 cm	
7			10YR 3/2	656 - 661 cm:	
			2.5Y 4/4	silty clay, brown (10YR 5/3)	
			2.5Y 5/4	661 - 668 cm:	
			10YR 3/2	silty clay, olive brown (2.5Y 4/4)	
			2.5Y 3/2	668 - 673 cm:	
			2.5Y 4/2	silty clay, very dark grayish brown (10YR 3/2) and olive brown (2.5Y 4/4), strongly mottled/bioturbated	
			2.5Y 5/4	673 - 685 cm:	
			2.5Y 5/4	silty clay, olive brown (2.5Y 4/4) and dark grayish brown (2.5Y 4/2), mottled/bioturbated	
			2.5Y 5/0	685 - 715 cm:	
			2.5Y 4/2	silty clay, light olive brown (2.5Y 5/4)	
8			10YR 5/3	715 - 725 cm:	
			2.5Y 5/2 to 2.5Y 4/2	silty clay, very dark grayish brown (10YR 3/2) and light olive brown (2.5Y 5/4) alternations, mottled/bioturbated	
			2.5Y 4/2	725 - 733 cm:	
			2.5Y 4/2	silty clay, very dark grayish brown (2.5Y 3/2)	
			2.5Y 4/2	733 - 746 cm:	
			2.5Y 4/2	silty clay, dark grayish brown (2.5Y 4/2), mottled/bioturbated	
			2.5Y 4/2	746 - 774 cm:	
			2.5Y 4/2	silty clay, light olive brown (2.5Y 5/4); very dark brown (10YR 2/2) silty layers between 770 and 774 cm	
			2.5Y 3/2	774 - 780 cm:	
			2.5Y 3/2	silty clay, gray (2.5Y 5/0)	
9			2.5Y 3/2	780 - 788 cm:	
			2.5Y 3/2	silty clay, dark grayish brown (2.5Y 4/2), mottled/bioturbated	
			2.5Y 3/2	788 - 795 cm:	
			2.5Y 3/2	silty clay, brown (10YR 5/3)	
			2.5Y 3/2	795 - 799 cm:	
			2.5Y 3/2	silty clay, light olive brown (2.5Y 5/4) and olive brown (2.5Y 4/4)	
			2.5Y 3/2	799 - 843 cm:	
			2.5Y 3/2	silty clay, grayish brown (2.5Y 5/2) to dark grayish brown (2.5Y 4/2), very dark brown layers at 799-804, 809, 811 cm; silt layer at 839 cm	
			2.5Y 3/2	843 - 864 cm: silty clay, dark grayish brown (2.5Y 4/2)	
			2.5Y 3/2	864 - 905 cm: silty clay, very dark grayish brown (2.5Y 3/2)	
10					

A96

PS2755-5 (GKG)

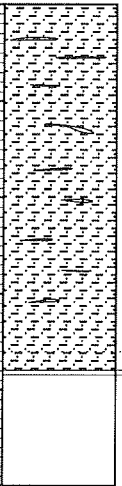
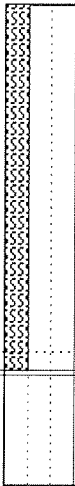
Lomonosov Ridge

ARK-XI/1

Recovery: 0.38 m

81°03.3'N, 138°15.1'E

Water depth: 2033 m

Lithology	Texture	Color	Description	Age
Surface				
10YR3/3 silty clay, dark brown, soft, even surface,				
Depth in core (cm)			10YR3/3 0-36 cm: silty clay, dark brown, thin grayish (10YR3/2) lenses	
			5Y3/2 36-38 cm: silty clay, dark olive gray	
			end of core: 38 cm	

A97

PS2755-6 (SL)

Lomonosov Ridge

ARK-XI/1

Recovery: 6.48 m

81° 03.6' N, 138° 14.3' E

Water depth: 2085 m

	Lithology	Texture Color	Description	Age
0		10YR 4/3 10YR 3/3	0 - 28 cm: silty clay, dark yellowish brown (10YR 3/4); very dark brown (10YR 2/2) laminae/ layers between 18 and 22 cm	
		2.5Y 4/2	28 - 40 cm: silty clay, dark brown (10YR 3/3)	
		2.5Y 4/4	40 - 92 cm: silty clay, dark grayish brown (2.5Y 4/2), moderately to strongly mottled/bioturbated	
1		2.5Y 4/4	92 - 140 cm: silty clay, olive brown (2.5Y 4/4), moderately to strongly mottled/bioturbated (light olive brown, 2.5Y 5/4)	
		2.5Y 5/4	140 - 150 cm: silty clay, light olive brown (2.5Y 5/4), moderately to strongly mottled/bioturbated	
		2.5Y 4/4	150 - 181 cm: silty clay, olive brown (2.5Y 4/4), moderately mottled; light olive brown (2.5Y 5/4) interval between 174 and 178 cm	
		2.5Y 4/4, 4/2, 3/2	181 - 205 cm: silty clay, olive brown (2.5Y 4/4), dark grayish brown (2.5Y 4/2), and very dark grayish brown (2.5Y 3/2), strongly mottled/bioturbated	
2		2.5Y 4/4, 5/4, 3/2	205 - 235 cm: silty clay, dark grayish brown (2.5Y 3/2), olive brown (2.5Y 4/4), and light olive brown (2.5Y 5/4), strongly mottled	
		10YR 4/3 2.5Y 4/4	235 - 248 cm: silty clay, brown (10YR 4/3) to olive brown (2.5Y 4/4), mottled/bioturbated	
		2.5Y 4/4	248 - 306 cm: alternation of olive brown (2.5Y 4/4) and light olive brown (2.5Y 5/4) silty clay intervals, moderately mottled/bioturbated	
		2.5Y 5/4	306 - 315 cm: silty clay, very dark brown (10YR 2/2) and light olive brown (2.5Y 5/4)	
3		2.5Y 4/4	315 - 327 cm: alternation of brown (10YR 4/3) and dark grayish brown (2.5Y 4/2) to olive brown (2.5Y 4/4); thin laminae of mud clasts (?), semi-lithified layers (?)	
		10YR 4/3 2.5Y 4/4 10YR 4/3 2.5Y 4/2 5Y 3/2 10YR 3/2	327 - 345 cm: silty clay, dark olive gray (5Y 3/2) and very dark brown (10YR 3/2)	
		2.5Y 4/4	345 - 364 cm: silty clay, olive brown (2.5Y 4/4), mottled/bioturbated; brown laminae at 359 and 360 cm	
		2.5Y 4/2	364 - 372 cm: sandy silt, dark grayish brown (2.5Y 4/2); sandy layer, dark gray (2.5Y 4/1) at 371-372 cm	
4		5Y 4/2 to 5Y 3/2	372 - 435 cm: silty clay, olive gray (5Y 4/2) to dark olive gray (5Y 3/2), lower part mottled/bioturbated	
		2.5Y 5/4	435 - 448 cm: silty clay, olive brown (2.5Y 4/4), mottled/bioturbated; silty layer at 342 cm	
		2.5Y 4/4 and 5/4	448 - 468 cm: silty clay, olive brown (2.5Y 4/4) and light olive brown (2.5Y 5/4), partly mottled/bioturbated, partly laminated	
		2.5Y 4/2 to 5/4		
		2.5Y 5/4		
5				

PS2755-6 (SL)

ARK-XI/1

Lithology	Texture Color	Description	Age
	2.5Y 4/2 2.5Y 5/4	468 - 486 cm: silty clay, dark grayish brown (2.5Y 4/2) to light olive brown (2.5Y 5/4), mottled/bioturbated; gray (2.5Y 5/0) sandy layer at 473 cm; brown horizon at 485-486 cm	
	2.5Y 4/4	486 - 496 cm: silty clay, light olive brown (2.5Y 5/4)	
	5Y 4/2	496 - 501 cm: silty clay, very dark grayish brown (10YR 3/2) and light olive brown (2.5Y 5/4), laminated	
	2.5Y 4/4	501 - 514 cm: silty clay, light olive brown (2.5Y 5/4)	
	5Y 5/2 5Y 4/2	514 - 518 cm: silty clay, very dark grayish brown (10YR 3/2)	
	5Y 4/2 and 2.5Y 4/4	518 - 528 cm: silty clay, olive brown (2.5Y 4/4); very dark grayish brown layer at the base	
	2.5Y 4/4	528 - 541 cm: silty clay with significant amount of sand, olive gray (5Y 4/2); dark gray (2.5Y 4/0) interval intercalated between 537-540 cm; thin silt layer at 540 cm	
	10YR 3/2 2.5Y 4/4	541 - 552 cm: silty clay, olive brown (2.5Y 4/4), mottled/bioturbated	
	5Y 5/3	552 - 556 cm: silty clay, olive gray (5Y 4/2)	
		556 - 566 cm: silty clay, olive brown (10YR 4/4), lower half very dark grayish brown (10YR 3/2)	
		566 - 578 cm: silty clay, olive gray (5Y 5/2 to 5Y 4/2)	
		578 - 606 cm: silty clay, olive gray (5Y 4/2) and olive brown (2.5Y 4/4), mottled	
		606 - 611 cm: silty clay, olive brown (2.5Y 4/4)	
		611 - 633 cm: silty clay, olive brown (2.5Y 4/4), olive gray (5Y 4/2), and very dark grayish brown (10YR 3/2), mottled/bioturbated; sandy layer at 611-614 cm	
	633 - 648 cm: silty clay, olive (5Y 5/3)		

A99

PS2756-9 (GKG)

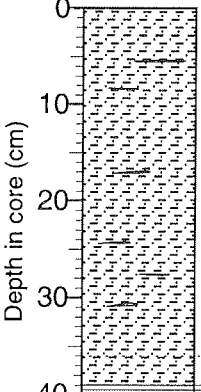
Lomonosov Ridge

ARK-XI/1

Recovery: 0.39 m

81°08.7'N, 138°38.9'E

Water depth: 1793 m

Lithology	Texture Color	Description	Age
Surface 10YR3/3 silty clay, dark brown, soft, even surface,			
	10YR3/3 10YR3/2	0-36 cm: silty clay, dark brown, thin yellowish (10YR3/2) and brownish lenses  36-39 cm: silty clay, dark brown to very dark grayish brown	
		end of core: 39 cm	

Depth in core (cm)

0  
10  
20  
30  
40  
50

A100

PS2757-7 (GKG)

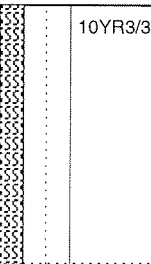
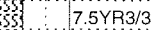
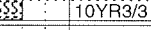
Lomonosov Ridge

ARK-XI/1

Recovery: 0.32 m

81°09.6'N, 140°12.1'E

Water depth: 1223 m

Lithology	Texture Color	Description	Age
Surface 10YR3/3 silty clay, dark grayish brown, even surface, one vertical crack (disturbed), common polychaets, scaphopods, sponges, bivalves			
Depth in core (cm) 0 10 20 30 40 50		10YR3/3 0-27 cm: silty clay, dark grayish brown, homogeneous	
		7.5YR3/3 27-30 cm: silty clay, dark brown, homogeneous	
		10YR3/3 30-32 cm: silty clay, dark grayish brown, homogeneous	
	end of core: 32 cm		

A101

PS2757-8 (KAL)

Lomonosov Ridge

ARK-XI/1

Recovery: 8.40 m

81° 09.8' N, 140° 12.0' E

Water depth: 1230 m

Lithology	Texture Color	Description	Age
		0 - 48 cm: silty clay, dark brown (10YR 3/3); coring disturbance in the upper 14 cm; very dark brown (10YR 2/2) layers at 33-35 cm	
	10YR 3/3	48 - 60 cm and 68 - 74 cm: silty clay, dark grayish brown (2.5Y 4/2)	
		60 - 68 cm: silty clay, olive brown (2.5Y 4/4), mottled/bioturbated	
	2.5Y 4/2		
	2.5Y 4/4		
	2.5Y 4/2	74 - 96 cm: silty clay, brown (10YR 5/3)	
	10YR 5/3		
		96 - 107 cm: silty clay, light olive brown (2.5Y 5/4), mottled/bioturbated	
	2.5Y 5/4		
	10YR 5/3	107 - 126 cm: silty clay, brown (10YR 5/3), mottled/bioturbated	
		126 - 143 cm: silty clay, light olive brown (2.5Y 5/4), mottled/bioturbated	
	2.5Y 5/4		
	10YR 5/3	143 - 150 cm: silty clay, brown (10YR 5/3), mottled/bioturbated	
	2.5Y 5/4		
		150 - 157 cm: silty clay, light olive brown (2.5Y 5/4), mottled/bioturbated	
	10YR 4/3		
		157 - 188 cm: silty clay, brown (10YR 4/3), mottled/bioturbated	
	10YR 3/3		
		188 - 203 cm: silty clay, dark brown (10YR 3/3), bioturbated	
	10YR 2/2		
		203 - 214 cm: alternation of dark brown (10YR 3/3) and very dark brown (10YR 2/2)	
	10YR 4/3		
	2.5Y 5/4	214 - 221 cm: silty clay, slightly mottled/bioturbated	
	2.5Y 5/0		
	2.5Y 6/4	221 - 228 cm: silty clay, brown (10YR 4/3) and light olive brown (2.5Y 5/4), mottled; silty layer at 216 cm	
	2.5Y 4/4		
	2.5Y 6/4	228 - 242 cm: silty clay, grayish brown (2.5Y 5/2)	
	2.5Y 4/4		
to	242 - 250 cm: silty clay, gray (2.5Y 5/0), mottled/bioturbated		
2.5Y 5/4			
	250 - 267 cm: silty clay, light yellowish brown (2.5Y 6/4), mottled/bioturbated		
2.5Y 5/4			
10YR 4/4	267 - 274 cm: silty clay, olive brown (2.5Y 4/4), strongly mottled/bioturbated; sandy layer at 256 cm		
2.5Y 5/4			
	274 - 297 cm: silty clay, light yellowish brown (2.5Y 6/4), mottled/bioturbated		
10YR 5/3			
2.5Y 4/4	297 - 300 cm: silty clay, olive brown (2.5Y 4/4) to light olive brown (2.5Y 5/4), mottled/bioturbated		
2.5Y 5/4			
	300 - 321 cm: silty clay, light yellowish brown (2.5Y 6/4), mottled/bioturbated		
10YR 4/4			
	321 - 340 cm: silty clay, light olive brown (2.5Y 5/4), mottled/bioturbated, black spots; dark brown (10YR 3/3) horizon at 320-321 cm		
10YR 3/2			
	340 - 350 cm: silty clay, dark yellowish brown (10YR 4/4), moderately to strongly mottled/bioturbated		
10YR 4/4 and 2.5Y 4/2 and 2.5Y 5/3			
2.5Y 4/2	350 - 377 cm: silty clay, light olive brown (2.5Y 5/4), strongly bioturbated		
10YR 5/3			

A102

PS2757-8 (KAL)

ARK-XI/1

	Lithology	Texture	Color	Description	Age
5			2.5Y 5/4	377 - 389 cm:	
			2.5Y 6/4	silty clay, olive brown (2.5Y 4/4), moderately bioturbated	
6			10YR4/3-	389 - 396 cm:	
			2.5Y6/6	silty clay, light olive brown (2.5Y 5/4), moderately bioturbated	
			10YR3/2-	396 - 415 cm:	
			2.5Y 5/4	silty clay, dark yellowish brown (10YR 4/4), mottled	
			10YR 5/3	415 - 424 cm:	
			10YR 3/3	silty clay, very dark grayish brown (10YR 3/2) and dark yellowish brown (10YR 4/4), mottled/bioturbated	
			10YR2/2-	424 - 475 cm:	
			10YR 4/4	silty clay, dark yellowish brown (10YR 4/4), dark grayish brown (2.5Y 4/2), and light olive brown (2.5Y 5/3), strongly mottled/bioturbated	
			2.5Y 5/4-	475 - 483 cm:	
			2.5Y 4/4 to 2.5Y 4/2	483 - 493 cm:	
7			2.5Y 4/0	493 - 498 cm:	
			2.5Y 4/0	silty clay, dark grayish brown (2.5Y 4/2) and light olive brown (2.5Y 5/3), mottled/bioturbated	
			2.5Y 4/0	498 - 507 cm:	
			2.5Y 4/0	silty clay, light olive brown (2.5Y 5/4), mottled/bioturbated; dark brown clay lense at 501-502 cm	
			2.5Y 5/0	507 - 517 cm:	
			2.5Y 5/0	silty clay, olive yellow (2.5Y 6/6) and light olive brown (2.5Y 5/4); very dark brown (10YR 2/2) horizons at 508-509 and 516-517 cm	
			5Y 5/3	517 - 532 cm:	
			5Y 5/3 to 5Y 3/2	silty clay, brown (10YR 4/3) and olive yellow (2.5Y 6/6) to light olive brown (2.5Y 5/4), mottled/bioturbated	
			5Y 5/3	532 - 543 cm:	
			5Y 5/3	alternation of silty clay and silty-sandy layers, light olive brown (2.5Y 5/4) and very dark grayish brown (10YR 3/2)	
8			5Y 5/3	543 - 558 cm:	
			5Y 5/3	silty clay, light olive brown (2.5Y 5/4), more dark brown in the middle part	
			5Y 5/3	558 - 562 cm:	
			5Y 5/3	silty clay, brown (10YR 5/3)	
			5Y 5/3	562 - 599 cm:	
			5Y 5/3	silty clay, dark brown (10YR 3/3), moderately bioturbated	
			5Y 5/3	599 - 608 cm:	
			5Y 5/3	silty clay, very dark brown (10YR 2/2) and dark brown (10YR 4/3)	
			5Y 5/3	608 - 618 cm:	
			5Y 5/3	silty clay, dark yellowish brown (10YR 4/4), light olive brown (10YR 5/4) interval at 612-613 cm	
9			5Y 5/3	618 - 629 cm:	
			5Y 5/3	alternation of light olive brown (2.5Y 5/4) and dark gray brown (2.5Y 4/2) silty clay, abundant silt layers	
			5Y 5/3	629 - 654 cm:	
			5Y 5/3	silty clay, olive brown (2.5Y 4/4) to dark grayish brown (2.5Y 4/2), common brown silt layers	
			5Y 5/3	654 - 712 cm:	
			5Y 5/3	silty clay with significant amounts of sand, dark gray (2.5Y 4/0); sharp boundary at top	
			5Y 5/3	712 - 735 cm: silty clay, gray (2.5Y 5/0), mottled	
			5Y 5/3	735 - 840 cm:	
			5Y 5/3	silty clay, olive gray (5Y 5/3); between 764 and 790 cm olive to dark olive gray (5Y 3/2), strongly mottled/bioturbated	
			5Y 5/3		
10					



A103

PS2758-2 (GKG)

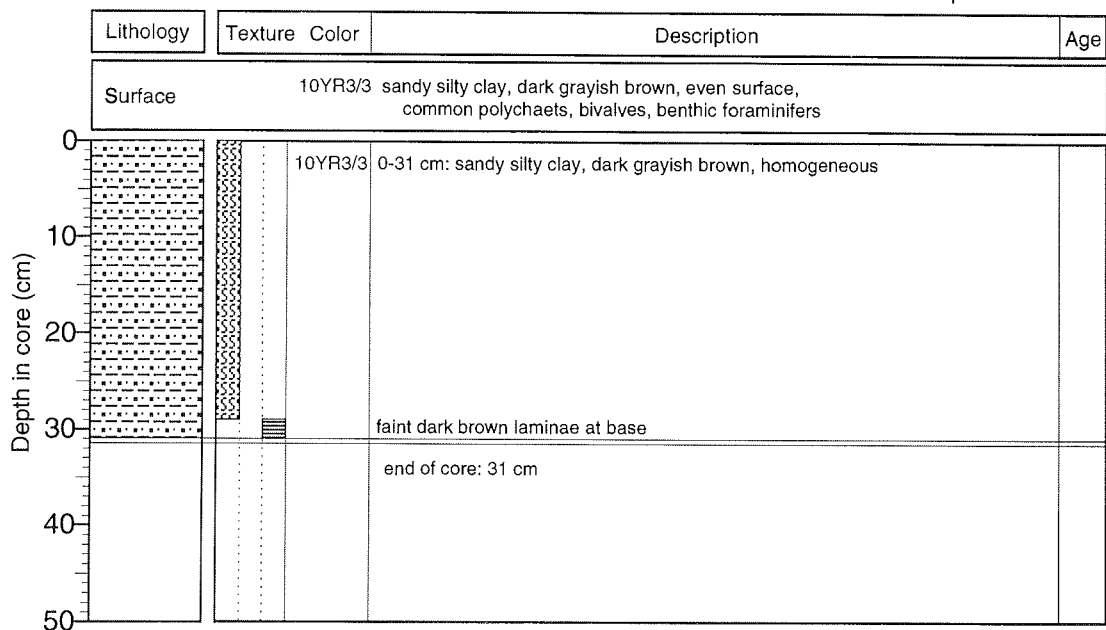
Lomonosov Ridge

ARK-XI/1

Recovery: 0.31 m

81°09.8'N, 141°51.3'E

Water depth: 937 m



A104

PS2759-7 (GKG)

Lomonosov Ridge

ARK-XI/1

Recovery: 0.39 m

81°13.3'N, 143°27.0'E

Water depth: 1610 m

Lithology	Texture	Color	Description	Age
Surface		10YR3/3	sandy silty clay, dark grayish brown, even surface, one sponge, common polychaets and benthic foraminifers	
		10YR3/3	0-22 cm: sandy silty clay, dark grayish brown, homogeneous	
		10YR3/2	22-29 cm: sandy silty clay, very dark grayish brown, homogeneous	
			end of core: 39 cm	

A105

PS2759-8 (KAL)

Lomonosov Ridge

ARK-XI/1

Recovery: 7.80 m

81° 13.6' N, 143° 28.5' E

Water depth: 1667 m

Lithology	Texture Color	Description	Age
		0 - 49 cm: silty clay, very dark grayish brown (10YR 3/2); dark yellowish brown (10YR 3/4) laminae between 36 and 38 cm; coring disturbance in the upper 15 cm	
	10YR 3/2	49 - 62 cm: silty clay, dark olive gray (5Y 3/2)	
	5Y 3/2	62 - 73 cm: silty clay, grayish brown (2.5Y 5/2), partly mottled/bioturbated	
	2.5Y 5/2	73 - 83 cm: silty clay, dark brown (10YR 4/3), partly mottled/bioturbated	
	10YR 4/3	83 - 92 cm: silty clay, light olive brown (2.5Y 5/4), mottled/bioturbated	
	2.5Y 5/4	92 - 135 cm: alternation of yellowish brown (10YR 5/4) silty clay (at 92-111, 115-117, and 123-132 cm) and light olive brown (2.5Y 5/4) silty clay (at 111-115, 117-123, and 132-135 cm), partly bioturbated	
	10YR 5/4	135 - 224 cm: silty clay, dark yellowish brown (10YR 4/4); very dark grayish brown (10YR 3/2) horizons at 209-212 and 213-214 cm, slightly bioturbated	
	10YR 4/4	224 - 230 cm: clay, gray (2.5Y 5/0)	
	10YR 3/2	230 - 291 cm: silty clay, light olive brown (2.5Y 5/4), partly mottled/bioturbated; sandy layers at 278, 280, and 281 cm	
	10YR 4/4	291 - 350 cm: silty clay, dark yellowish brown (10YR 4/4); light yellowish brown (2.5Y 6/4) to olive brown (2.5Y 4/4) mottling, moderately bioturbated	
	2.5Y 5/0	350 - 353 cm: silty clay, light yellowish brown (2.5Y 6/4)	
	2.5Y 5/4	353 - 380 cm: silty clay, dark yellowish brown (10YR 4/4); very dark grayish brown (10YR 3/2) layers between 370 and 375 cm	
	10YR 4/4	380 - 472 cm: silty clay, light olive brown (2.5Y 5/4), mottled/bioturbated; very dark grayish brown (10YR 3/2) interval between 450 and 455 cm	
	10YR 4/4 (+2.5Y 6/4, 2.5Y 4/4)	472 - 490 cm: silty clay, light yellowish brown (2.5Y 6/4), mottled/bioturbated	
	10YR 4/4	490 - 527 cm: silty clay, dark brown (10YR 3/3), mottled/bioturbated	
2.5Y 5/4			
2.5Y 5/4			
2.5Y 6/4			
10YR 3/3			

PS2759-8 (KAL)

ARK-XI/1

Lithology	Texture Color	Description	Age
<p>5</p>	<p>10YR 3/3</p> <p>2.5Y 5/2</p> <p>10YR 4/3</p> <p>10YR 5/4</p> <p>10YR 4/3</p> <p>10YR 3/2</p> <p>10YR 4/3</p> <p>2.5Y 5/2</p> <p>2.5Y 4/4</p> <p>2.5Y 5/2</p> <p>5Y 4/2</p> <p>2.5Y 4/0</p> <p>cc</p>	<p>527 - 545 cm: silty clay, grayish brown (2.5Y 5/2), mottled/bioturbated</p> <p>545 - 550 cm: silty clay, brown (10YR 4/3), mottled/bioturbated</p> <p>550 - 555 cm: silty clay, yellowish brown (10YR 5/4), mottled/bioturbated</p> <p>555 - 599 cm: silty clay, brown (10YR 4/3), mottled/bioturbated</p> <p>599 - 603 cm: silty clay, very dark grayish brown (10YR 3/2)</p> <p>603 - 608 cm: silty clay, brown (10YR 4/3)</p> <p>608 - 613 cm: silty clay, grayish brown (2.5Y 5/2)</p> <p>613 - 625 cm: silty clay, olive brown (2.5Y 4/4), mottled/bioturbated</p> <p>625 - 636 cm: silty clay, olive gray (5Y 5/2), yellowish brown mottling (bioturbation); brown lithified (?) horizon at 635-636 cm</p> <p>636 - 648 cm: silty clay, dark olive gray (5Y 4/2); brown layers at 641 and 647 cm</p> <p>648 - 746 (777) cm: silty clay with significant amount of sand, dark gray (2.5Y 4/0)</p>	
<p>6</p> <p>7</p> <p>8</p> <p>9</p> <p>10</p>			

A107

PS2760-5 (GKG)

Lomonosov Ridge

ARK-XI/1

Recovery: 0.38 m

81°13.6'N, 144°48.0'E

Water depth: 2044 m

Lithology	Texture Color	Description	Age
Surface 10YR3/3 sandy silty clay, dark grayish brown, uneven surface, several large holes (up to 7 cm diam.) with living amphipods			
	10YR3/3	0-38 cm: sandy silty clay, dark grayish brown, homogeneous	
		end of core: 38 cm	

A108

PS2760-6 (SL)

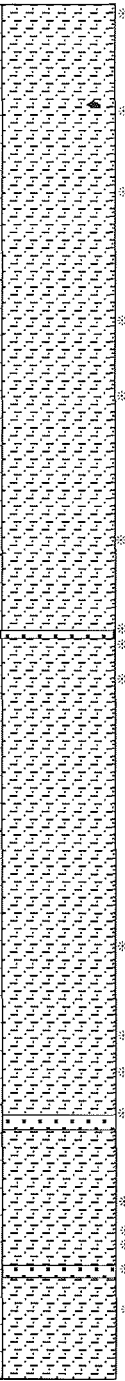
Lomonosov Ridge

ARK-XI/1

Recovery: 5.96 m

81° 13.8' N, 144° 48.8' E

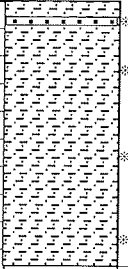
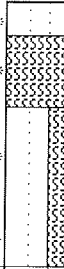
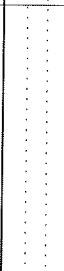
Water depth: 2096 m

Lithology	Texture Color	Description	Age
	10YR 4/3	0 - 12 cm:	
	10YR 3/2	12 - 22 cm:	
	2.5Y 3/2	22 - 45 cm:	
	2.5Y 4/4	45 - 64 cm:	
	2.5Y 6/4	64 - 71 cm:	
	2.5Y 5/4	71 - 103 cm:	
	2.5Y 4/4	103 - 113 cm:	
	10YR 4/4	113 - 140 cm:	
	10YR 4/3	140 - 144 cm:	
	2.5Y 4/2	144 - 160 cm:	
	2.5Y 5/4	160 - 185 cm:	
	2.5Y 4/4	185 - 239 cm:	
	10YR 4/3	239 - 294 cm:	
	2.5Y 4/4	294 - 306 cm:	
	10YR 4/3	306 - 339 cm:	
	2.5Y 4/4	339 - 349 cm:	
	2.5Y 5/2	349 - 351 cm:	
	2.5Y 4/4	351 - 362 cm:	
	2.5Y 5/4	362 - 380 cm:	
	10YR 3/3	380 - 400 cm:	
2.5Y 6/4	400 - 416 cm:		
10YR 4/3	416 - 443 cm:		
5Y 4/4	443 - 447 cm:		
2.5Y 3/0	447 - 456 cm:		
2.5Y 4/0	456 - 500 cm:		

A109

PS2760-6 (SL)

ARK-XI/1

	Lithology	Texture	Color	Description	Age
5			5Y 5/3 to 5Y 4/3 ..... 5Y 3/2  5Y 4/3	456 - 458 cm: silty clay, dark brown (10YR 3/3), mud clasts at the base 458 - 491 cm: silty clay with significant amount of sand, very dark gray 2.5Y 3/0), silty-sandy layers (brown) between 458 and 463 cm 491 - 502 cm: silty clay, dark gray (2.5Y 4/0) 502 - 504 cm: silty clay, gray (2.5Y 5/0) 504 - 538 cm: silty clay, olive (5Y 5/3 - 4/3), strongly mottled; silty-sandy layer (dark gray) at 507 cm 538 - 579 cm: silty clay, dark olive gray (5Y 3/2), mottled/bioturbated 579 - 596 cm: silty clay, olive (5Y 4/3), mottled/bioturbated	
6					
7					
8					
9					
10					

A110

PS2761-9 (GKG)

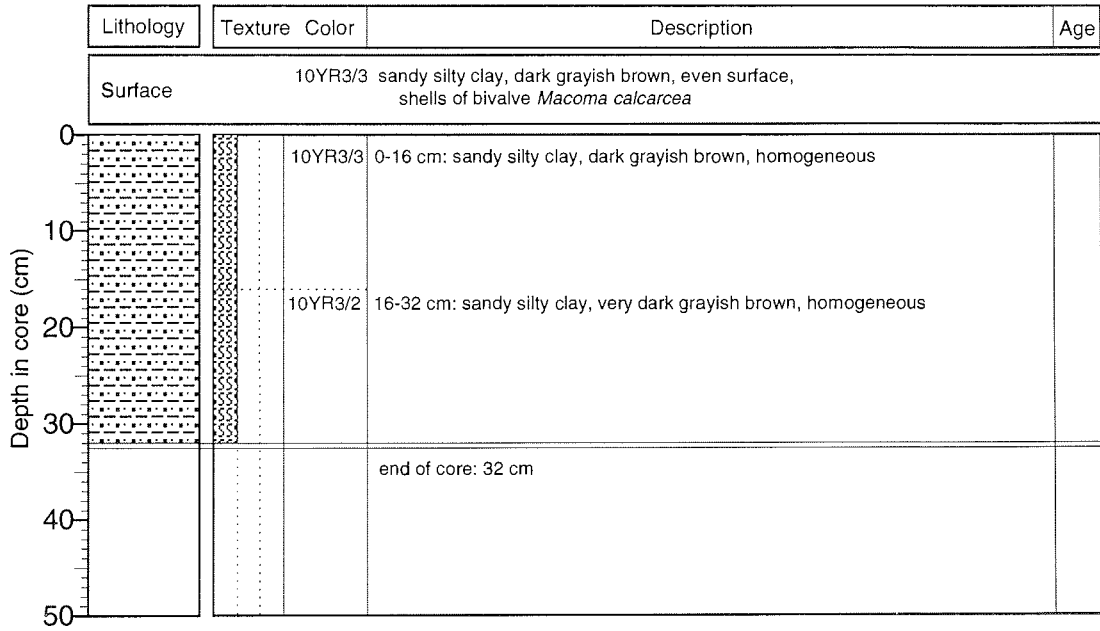
Makarov Basin

ARK-XI/1

Recovery: 0.32 m

81°11.6'N, 150°57.2'E

Water depth: 2587 m





A111

PS2761-10 (SL)

Makarov Basin

ARK-XI/1

Recovery: 6.58 m

81° 11.5' N, 150° 29.8' E

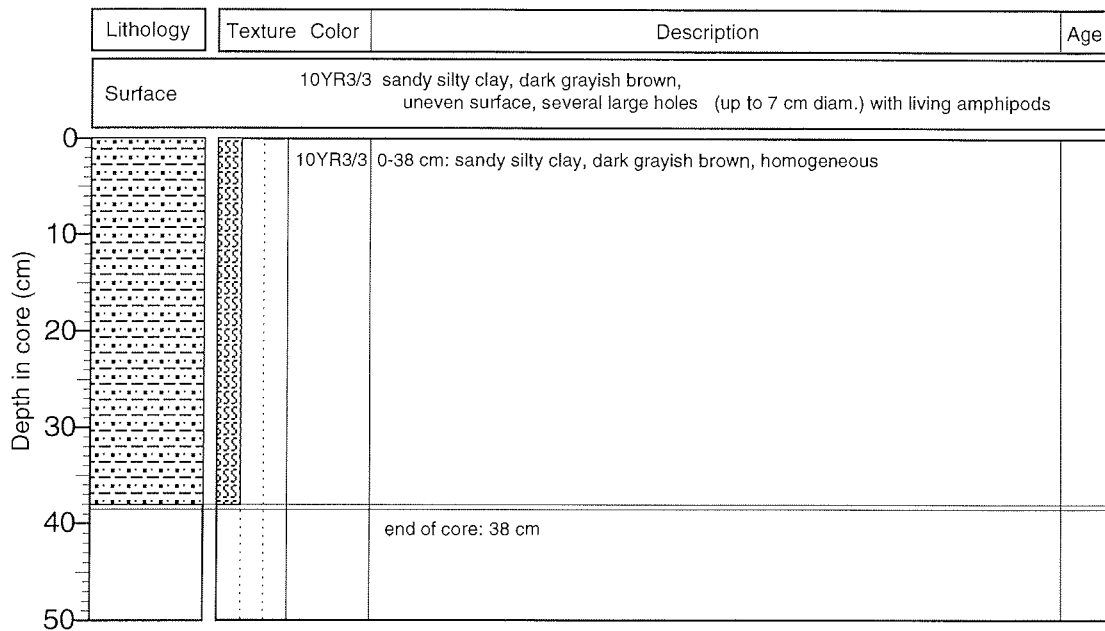
Water depth: 2640 m

Lithology	Texture Color	Description	Age
	10YR 3/4	0 - 6 cm:	
	10YR 3/3 -3/3, 4/0	silty clay, dark yellowish brown (10YR 3/4)	
	2.5Y 3/2	6 - 14 cm:	
	2.5Y 4/4	silty clay, dark brown (10YR 3/3)	
	10YR 4/3	14 - 21 cm:	
	2.5Y 5/4	silty clay (with significant amount of sand), dark brown (10YR 3/3) and dark gray (2.5Y 4/0), mottled/bioturbated	
	2.5Y 5/2	21 - 28 cm:	
	2.5Y 5/4	silty clay, very dark grayish brown (2.5Y 3/2)	
	10YR 5/3	28 - 36 cm:	
	10YR 3/4 and -4/3	36 - 46 cm:	
	10YR 4/3 and -3/2	46 - 71 cm:	
	2.5Y 5/4	silty clay, light olive brown (2.5Y 5/4), lower part dark brown laminae	
	2.5Y 5/4	71 - 81 cm:	
	2.5Y 5/4	silty clay, grayish brown (2.5Y 5/2), at the base light yellowish brown (2.5Y 6/4) layer	
	2.5Y 5/4	81 - 88 cm:	
	2.5Y 4/2 and -4/4	88 - 109 cm:	
	2.5Y 5/4 and -4/4	109 - 125 cm:	
	10YR 3/3 10YR 4/3	125 - 145 cm:	
	2.5Y 4/4	145 - 156 cm:	
	10YR 3/3 10YR 4/3	156 - 195 cm:	
2.5Y 4/4	195 - 215 cm:		
2.5Y 4/4 and -4/2	(sandy) silty clay, dark grayish brown (2.5Y 4/2) and olive brown (2.5Y 4/4), moderately to strongly mottled/bioturbated		
2.5Y 4/4	215 - 258 cm:		
2.5Y 5/4	258 - 271 cm:		
10YR 3/4	271 - 308 cm:		
-3/4, -4/4 -2/2, -4/4	308 - 331 cm:		
2.5Y 5/2 2.5Y 5/4 2.5Y 4/0	331 - 353 cm:		
10YR 3/2	353 - 366 cm:		
10YR 4/3	366 - 382 cm:		
-2/2, -4/3	382 - 392 cm:		
5Y 3/2	392 - 400 cm:		

Lithology	Texture	Color	Description	Age	
5		5Y 3/2	392 - 402 cm:		
		2.5Y 4/0	silty-sandy layers, very dark brown (10YR 2/2) and olive brown (2.5Y 4/4)		
		2.5Y 5/0	402 - 410 cm:		
		5Y 4/2 and 5Y 5/3	silty clay, grayish brown (2.5Y 5/2), mottled/bioturbated		
		5Y 4/2	410 - 415 cm:		
		2.5Y 4/4	silty clay, light olive brown (2.5Y 5/4), mottled/bioturbated		
	6		5Y 4/2	415 - 419 cm:	
			2.5Y 4/4	alternation of silty clay and sandy silt, dark gray (2.5Y 4/0)	
			5Y 4/2, 5Y 5/3	419 - 428 cm:	
			5Y 4/2, 5Y 5/3	silty clay, light olive brown (2.5Y 5/4), mottled/bioturbated	
			5Y 3/2, 5Y 5/3	428 - 434 cm:	
			2.5Y 4/0	silty clay, very dark grayish brown (10YR 3/2), mottled/bioturbated	
			5Y 3/2, 5Y 5/3	434 - 468 cm:	
			2.5Y 4/0	silty clay, brown (10YR 4/3), mottled/bioturbated	
		5Y 4/2	458 - 468 cm:		
		5Y 4/2	silty clay, brown (10YR 4/3), mottled/bioturbated		
7			468 - 474 cm:		
			alternation of brown (10YR 4/3) and very dark brown (10YR 2/2) silty clay; lower part (semi-) lithified		
			474 - 513 cm:		
			silty clay, dark olive gray (5Y 3/2); brown spots and silty layers with small mud clasts		
			513 - 532 cm:		
			silty clay, dark gray (2.5Y 4/0)		
			532 - 536 cm:		
			silty clay, gray (2.5Y 5/0)		
			536 - 563 cm:		
			silty clay, olive gray (5Y 4/2) and olive (5Y 5/3), moderately mottled/bioturbated		
			563 - 580 cm:		
			silty clay, olive gray (5Y 4/2), mottled/bioturbated		
			580 - 584 cm:		
			silty clay, light yellowish brown (2.5Y 6/4), mottled/bioturbated		
8			584 - 591 cm:		
			silty clay, olive brown (2.5Y 4/4), mottled/bioturbated		
			591 - 596 cm:		
			silty clay, olive brown (2.5Y 4/4) and brown (10YR 4/3)		
			596 - 611 cm:		
			silty clay, olive gray (5Y 4/2) and olive (5Y 5/3), moderately mottled/bioturbated		
			611 - 614 cm:		
			alternation of silty clay and sandy silt, brown (10YR 4/3) and olive brown (2.5Y 4/4)		
	9			614 - 631 cm:	
				silty clay, dark olive gray (5Y 3/2) and olive (5Y 5/3), moderately mottled/bioturbated	
			631 - 653 cm:		
			silty clay, dark gray (2.5Y 4/0)		
			563 - 658 cm:		
			silty clay, olive gray (5Y 4/2), mottled/bioturbated		
10					

A113

**PS2762-4 (GKG)** Western East Siberian Cont. Margin **ARK-XI/1**  
Recovery: 0.38 m 80°29.6'N, 150°15.7'E Water depth: 1997 m



A114

PS2763-7 (KAL)

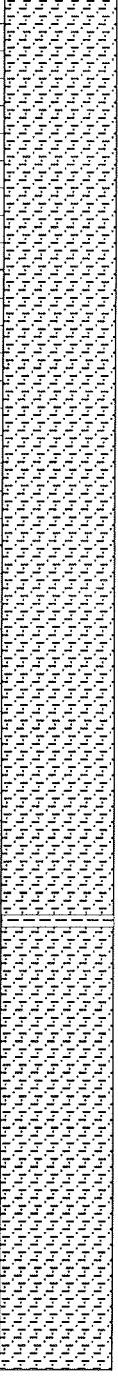
Western East Sib. Cont. Margin

ARK-XI/1

Recovery: 7.84 m

80° 16.9' N, 150° 26.1' E

Water depth: 1591 m

Lithology	Texture Color	Description	Age
		0 - 49 cm: silty clay, dark yellowish brown (10YR 3/4); very dark grayish brown (10YR 3/2) layers between 33 and 45 cm; coring disturbance in the upper 8 cm	
	10YR 3/2	46 - 55 cm: silty clay, brown (10YR 4/3), top cm (semi-) lithified (?) and laminated	
	10YR 4/3	55 - 92 cm: silty clay, dark gray (2.5Y 4/0)	
	2.5Y 4/0	92 - 120 cm: silty clay, olive gray (5Y 4/2)	
	5Y 4/2	120 - 130 cm: silty clay, dark grayish brown (2.5Y 4/2), mottled/bioturbated	
	2.5Y 4/2	130 - 140 cm: silty clay, silty clay, very dark grayish brown (2.5Y 3/2)	
	2.5Y 3/2	140 - 155 cm: silty clay, dark grayish brown (2.5Y 4/2); lowermost part very dark grayish brown (10YR 3/2), mottling/bioturbation	
	2.5Y 4/2	155 - 164 cm: silty clay, olive gray (5Y 4/2), mottled/bioturbated	
	5Y 4/2	164 - 220 cm: silty clay, dark grayish brown (2.5Y 4/2), partly mottled	
	2.5Y 4/2	220 - 248 cm: silty clay, light olive brown (2.5Y 5/4)	
	2.5Y 5/4	248 - 257 cm: silty clay, grayish brown (2.5Y 5/2), mottled/bioturbated	
	2.5Y 5/4	257 - 292 cm: silty clay, light olive brown (2.5Y 5/4), mottled/bioturbated	
	2.5Y 5/2	292 - 300 cm: silty clay, dark grayish brown (2.5Y 4/2)	
	2.5Y 5/4	300 - 308 cm: silty clay, very dark grayish brown (2.5Y 3/2); very dark brown (10YR 2/2) and light yellowish brown (2.5Y 6/4) mottling/bioturbation	
	2.5Y 4/2	308 - 317 cm: silty clay, dark grayish (2.5Y 4/2), mottled/bioturbated	
	2.5Y 3/2	317 - 333 cm: silty clay, olive brown (2.5Y 4/4)	
	2.5Y 4/2	333 - 337 cm: silty sand, olive gray (5Y 4/2)	
	5Y 4/2	337 - 353 cm: silty clay, dark grayish brown (2.5Y 4/2) and olive brown (2.5Y 4/4), mottled/bioturbated	
	2.5Y 4/2	353 - 425 cm: silty clay, dark olive gray (5Y 3/2), occasionally dark brown layers	
	5Y 3/2	425 - 450 cm: silty clay, dark grayish brown (2.5Y 4/2), mottled/bioturbated	
2.5Y 4/2	450 - 464 cm: silty clay, light olive brown (2.5Y 5/6)		
2.5Y 4/2	464 - 467 cm: silty clay, dark grayish brown (2.5Y 4/2), mottled/bioturbated		
2.5Y 5/6	467 - 500 cm: silty clay, olive brown (2.5Y 4/4), upper part mottled		
2.5Y 4/4			

A115

PS2763-7 (KAL)

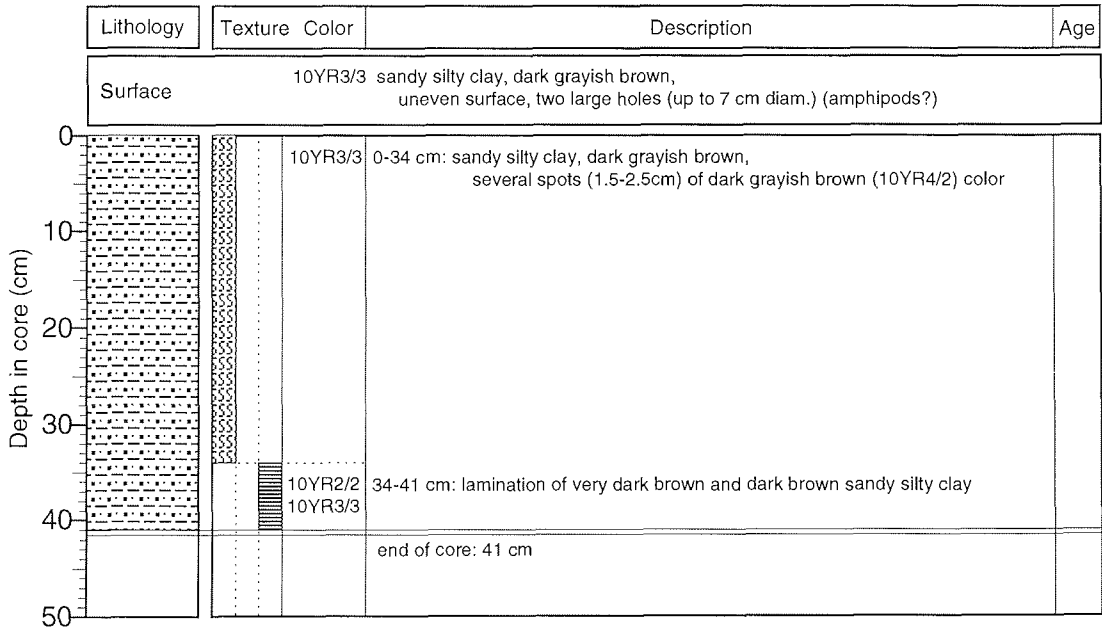
ARK-XI/1

Lithology	Texture	Color	Description	Age
		<p>2.5Y 4/2</p> <p>2.5Y 4/0</p> <p>2.5Y 4/0 to 2.5Y 4/2</p> <p>2.5Y 5/0</p> <p>2.5Y 4/0 to 2.5Y 3/0</p>	<p>500 - 520 cm: silty clay, dark grayish brown (2.5Y 4/2) and olive brown (2.5Y 4/4), partly laminated</p> <p>520 - 630 cm: silty clay, dark gray (2.5Y 4/0), in the lower part also olive gray (5Y 4/2) lenses and layers; slumping structures ?</p> <p>630 - 635 cm: silty clay, gray (2.5Y 5/0)</p> <p>635 - 639 cm: silty clay, olive brown (2.5Y 4/4); on top dark yellowish brown (10YR 4/4) layer</p> <p>639 - 760 (784) cm: silty clay, dark gray (2.5y 4/0) to very dark gray (2.5Y 3/0), below 670 cm common black spots</p> <p>CC</p>	

Depth in core (m)

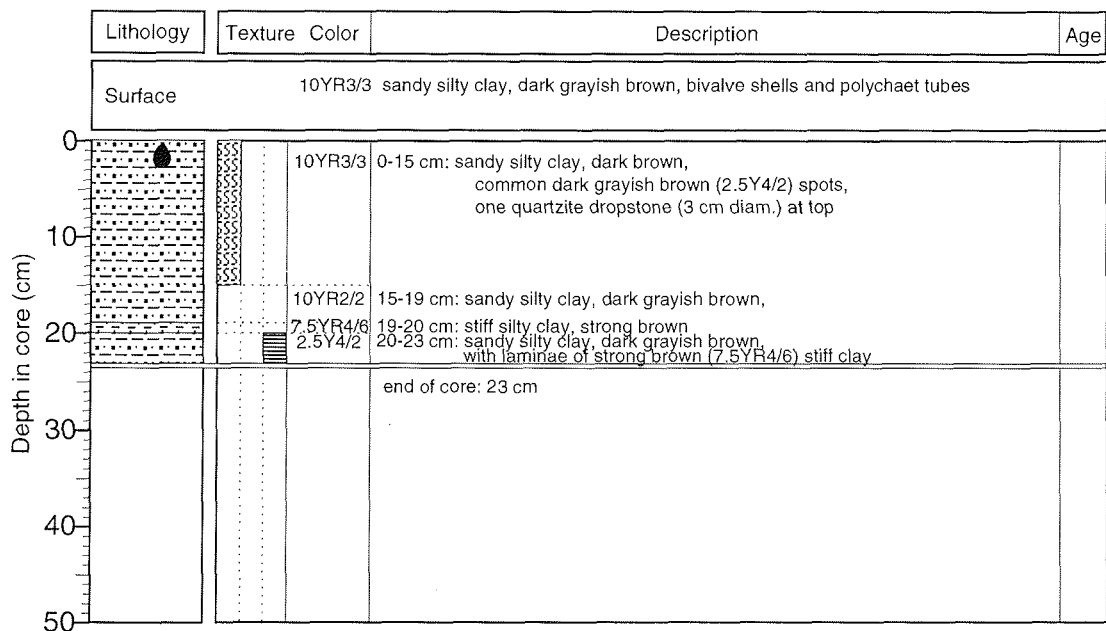
A116

**PS2763-8 (GKG)** Western East Siberian Cont. Margin **ARK-XI/1**  
 Recovery: 0.41 m 80°16.8'N, 150°27.4'E Water depth: 1588 m



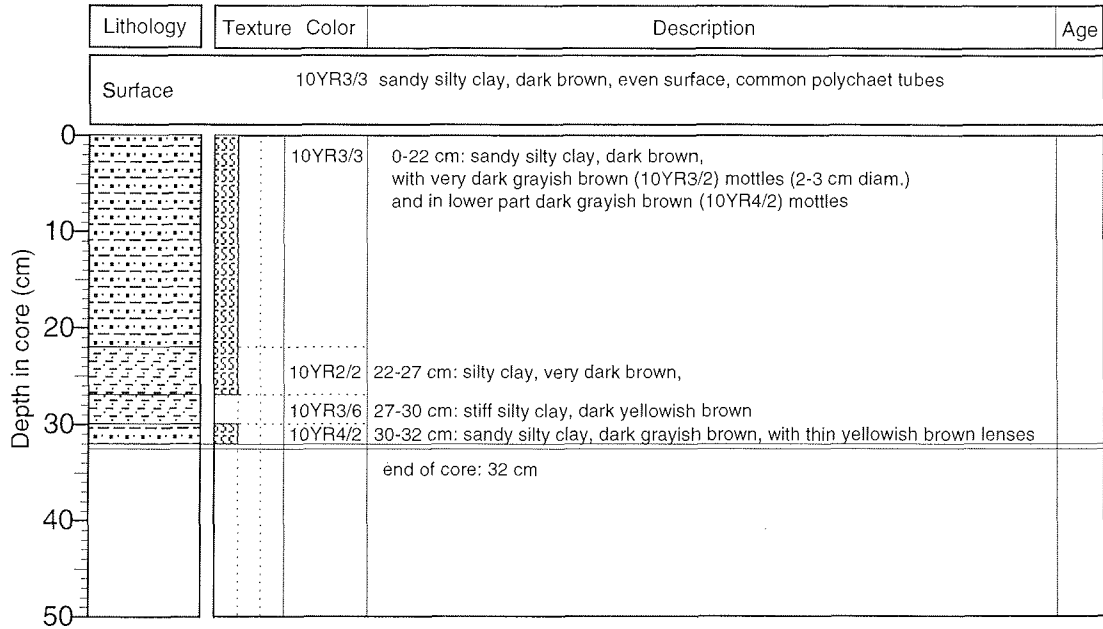
A117

PS2764-7 (GKG) Western East Siberian Cont. Margin ARK-XI/1  
 Recovery: 0.23 m 80°04.1'N, 149°48.6'E Water depth: 1001 m



A118

**PS2765-6 (GKG)** Western East Siberian Cont. Margin **ARK-XI/1**  
 Recovery: 0.32 m 79°52.8'N, 149°46.9'E Water depth: 557 m





A119

PS2767-4 (KAL)

Lomonosov Ridge


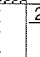
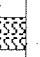

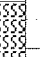

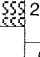
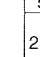
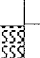
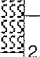

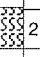
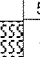

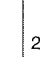

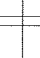

ARK-XI/1

Recovery: 8.30 m

79° 44.6' N, 144° 00.4' E

Water depth: 584 m

Lithology	Texture Color	Description	Age
	10YR 3/4 10YR 3/4 2.5Y 4/4	0 - 37 cm: silty clay, dark yellowish brown (10YR 3/4), lower part more brown (10YR 4/3); thin very dark grayish brown (10YR 3/2) layers between 26 and 29 cm; coring disturbance in the upper 19 cm	
	2.5Y 4/0 2.5Y 4/0	37 - 41 cm: silty clay, very dark brown (10YR 2/2) 41 - 47 cm: silty clay, olive brown (2.5Y 4/4)	
	2.5Y 4/0 2.5Y 3/0	47 - 125 cm: silty clay, dark gray (2.5Y 4/0); mottling/bioturbation (olive brown) between 47 and 56 cm 125 - 190 cm: silty clay, very dark gray (2.5Y 3/0), abundant black spots throughout 190 - 239 cm: silty clay, dark gray (2.5Y 4/0), lowermost part more olive gray (5Y 3/2)	
	2.5Y 4/0 2.5Y 4/0	239 - 315 cm: silty clay, olive brown (2.5Y 4/4), mottling/bioturbation (olive gray) between 239-255 cm and 275-280 cm; dark grayish brown (2.5Y 4/2) horizons at 285-292 cm and 295 cm, very dark brown (10YR 2/2) laminae at 301, 304-306, and 308-310 cm 315 - 355 cm: silty clay, brown (2.5Y 4/2)	
	2.5Y 4/0 2.5Y 4/4	355 - 377 cm: silty clay, olive brown (2.5Y 4/4), mottled/bioturbated 377 - 400 cm: silty clay, light olive brown (2.5Y 5/4), mottled/bioturbated; very dark brown (10YR 2/2) laminae between 394 and 398 cm	
	2.5Y 4/4 2.5Y 4/4	400 - 420 cm: silty clay, dark grayish brown (2.5Y 4/2) and light olive brown (2.5Y 5/4) 420 - 455 cm: silty clay, dark gray (2.5Y 4/0)	
	2.5Y 4/2 2.5Y 4/4	455 - 480 cm: silty clay, dark gray (5Y 4/1) and olive gray (5Y 5/2), mottled/bioturbated; brown layer at 479 cm 480 - 494 cm: silty clay, dark gray (2.5Y 4/0)	
	2.5Y 4/4 2.5Y 5/4	494 - 500 cm: silty clay, dark gray (5Y 4/1) and olive gray (5Y 5/2), mottled/bioturbated	
	2.5Y 4/2 and 5/4 2.5Y 4/0		
	5Y 4/1 and 5/2 2.5Y 4/0		
	2.5Y 4/0 2.5Y 4/0		
	2.5Y 4/0		

Lithology	Texture	Color	Description	Age
5 6 7 8 9 10 Depth in core (m)		5Y 4/2 and 5/2	500 - 520 cm: silty clay, olive gray (5Y 4/2 and 5Y 5/2), mottled/bioturbated;	
		2.5Y 4/0	brown layer at 519 cm	
		5Y 4/2	520 - 525 cm: silty clay, dark gray (2.5Y 4/0)	
		5Y 4/2	525 - 555 cm: silty clay, olive gray (5Y 4/2), lower part mottled/bioturbated	
		5Y 3/2	555 - 587 cm: silty clay, dark olive gray (5Y 3/2)	
		5Y 4/2	587 - 597 cm: silty clay, olive gray (5Y 4/2), mottled/bioturbated	
		5Y 4/3	597 - 610 cm: silty clay, olive (5Y 4/3), mottled/bioturbated	
		2.5Y 5/4	610 - 636 cm: silty clay, light olive brown (2.5Y 5/4), mottled/bioturbated; very dark brown (10YR 2/2) horizon between 631 and 634 cm	
		5Y 4/3	636 - 645 cm: silty clay, olive (5Y 4/3), thin brown laminae throughout	
		2.5Y 4/0	645 - 670 cm: silty clay, dark gray (2.5Y 4/0), lowermost 2 cm gray (2.5Y 5/0); thin brown laminae between 645 and 652 cm	
		5Y 4/3	670 - 687 cm: silty clay, olive (5Y 4/3), mottled/bioturbated	
		2.5Y 5/4	687 - 711 cm: silty clay, light olive gray (2.5Y 5/4)	
		5Y 4/2	711 - 725 cm: silty clay, olive gray (5Y 4/2)	
		2.5Y 4/2	725 - 740 cm: silty clay, dark grayish brown (2.5Y 4/2), mottled/bioturbated	
		5Y 3/2	740 - 749 cm: silty clay, dark olive gray (5Y 3/2), mottled/bioturbated	
	5Y 4/2	749 - 765 cm: silty clay, olive gray (5Y 4/2), mottled/bioturbated		
	2.5Y 4/0	765 - 768 cm: silty clay, olive brown (2.5Y 4/4)		
	CC	768 - 800 (830) cm: silty clay, dark gray (2.5Y 4/0); brown laminae in the uppermost part		

A121

PS2767-6 (GKG)

Lomonosov Ridge

ARK-XI/1

Recovery: 0.37 m

79°44.1'N, 143°59.4'E

Water depth: 557 m

Lithology	Texture Color	Description	Age
Surface			
	10YR3/3	silty clay, dark grayish brown, even surface, soft corals, gastropods	
0			
10			
20			
30			
40			
50			
	10YR3/3	0-23 cm: silty clay, dark grayish brown, homogeneous	
	10YR3/2 10YR3/3	23-29 cm: silty clay, irregular lamination, very dark grayish brown and dark grayish brown	
	10YR3/2 10YR3/2	29-31 cm: silty clay, very dark grayish brown 31-35 cm: silty clay,	
	10YR3/3 5Y4/2	irregular lamination, very dark grayish brown and dark grayish brown 35-37 cm: silty clay, olive gray	
		end of core: 37 cm	

A122

**PS2768-3 (GKG)**

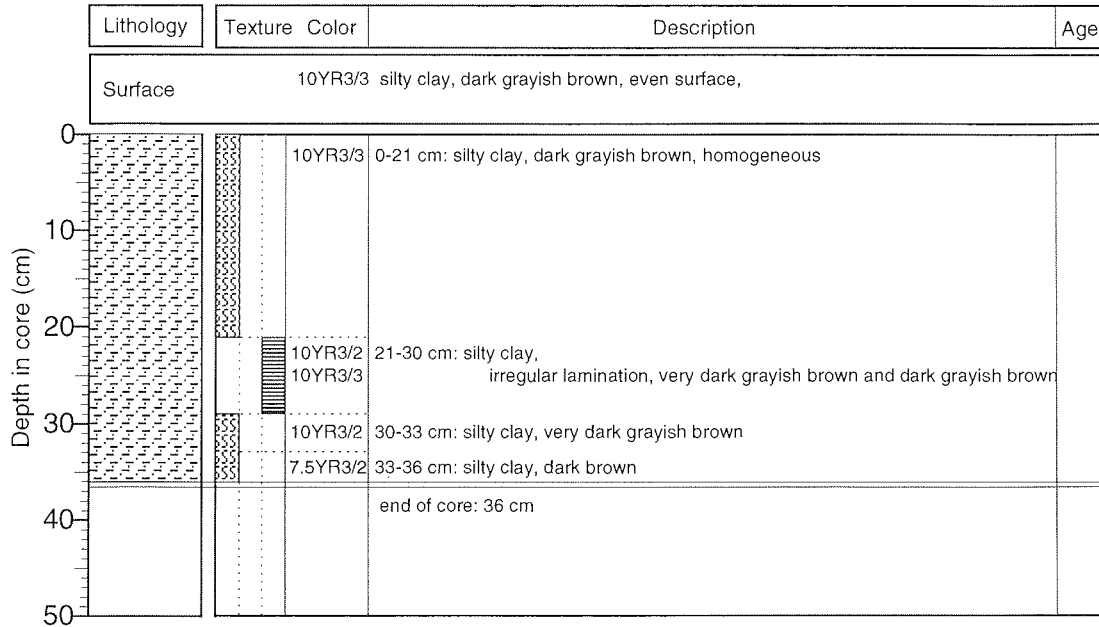
Lomonosov Ridge

**ARK-XI/1**

Recovery: 0.36 m

79°49.0'N, 143°05.5'E

Water depth: 984 m



A123

PS2768-4 (SL)

Lomonosov Ridge

ARK-XI/1

Recovery: 7.23 m

79° 49.0' N, 143° 06.0' E

Water depth: 1009 m

Lithology	Texture Color	Description	Age
0	10YR 3/3	0 - 11 cm: silty clay, dark brown (10YR 3/3)	
	10YR 3/3 and - 2/2	11 - 28 cm: alternation of dark brown (10YR 3/3) and very dark brown (10YR 2/2)	
	10YR 3/3 5Y 4/1	silty clay, partly finely laminated	
	5Y 4/1 to 5Y 3/2	28 - 41 cm: alternation of dark gray (5Y 4/1) and dark brown (10YR 3/3) silty clay, laminated	
	5Y 3/1	41 - 121 cm: silty clay, dark gray (5Y 4/1) to dark olive gray (5Y 3/2), occasionally dark brown laminae	
	5Y 3/1	121 - 240 cm: silty clay, very dark gray (5Y 3/1), below 150 cm abundant black spots throughout	
	5Y 3/1	240 - 259 cm: silty clay, dark olive gray (5Y 3/2), mottled/bioturbated; dark brown silty layer at the base	
	5Y 3/1	259 - 274 cm: silty clay, very dark gray (5Y 3/1)	
	5Y 3/1	274 - 295 cm: silty clay, olive gray (5Y 4/2) and olive (5Y 5/3), moderately to strongly mottled/bioturbated	
	5Y 3/2	295 - 322 cm: silty clay, dark olive gray (5Y 3/2); dark brown laminae at 295, 297, 299, 301, and 304 cm	
	5Y 3/2	322 - 343 cm: silty clay, olive gray (5Y 4/2), mottled/bioturbated	
	5Y 3/1	343 - 402 cm: silty clay, dark grayish brown (2.5Y 4/2), moderately mottled/ bioturbated; very dark brown (10YR 2/2) horizons at 366-367, 388-389, and 398-402 cm	
	5Y 4/2 and -5/3	402 - 433 cm: silty clay, olive gray (5Y 4/2), mottled/bioturbated	
	5Y 3/2	433 - 469 cm: silty clay, light olive brown (2.5Y 5/4) and olive brown (2.5Y 4/4), strongly mottled/bioturbated	
	5Y 4/2	469 - 497 cm: silty clay, olive gray (5Y 4/2) and dark grayish brown (2.5Y 4/2); very dark brown (10YR 2/2) layers at 474, 479, 485-487, 490, and 494-497 cm	
	2.5Y 4/2	497 - 523 cm: silty clay, dark gray (5Y 4/1) to olive gray (5Y 4/2), mottled/ bioturbated	
	5Y 4/2	523 - 537 cm: silty clay, olive gray (5Y 4/2) and dark grayish brown (2.5Y 4/2), moderately mottled/bioturbated	
	5Y 4/2	537 - 548 cm: silty clay, dark gray (2.5Y 4/0), brown horizons at 538-539 and 541-542 cm	
	2.5Y 5/4 and 2.5Y 4/4	548 - 584 cm: silty clay, olive gray (5Y 4/2) and dark grayish brown (2.5Y 4/2), moderately mottled/bioturbated	
	5Y 4/2 to 2.5Y 4/2	584 - 651 cm: silty clay, dark olive gray (5Y 3/2)	
	5		

A124

PS2768-4 (SL)

ARK-XI/1

Lithology	Texture Color	Description	Age
	5Y 4/1 to -4/2	651 - 672 cm: silty clay, dark olive gray (5Y 3/2) to olive gray (5Y 4/2)	
	5Y 4/2 2.5Y 4/2	672 - 695 cm: silty clay, olive brown (2.5Y 4/4) to dark grayish brown (2.5Y 4/2), mottled/bioturbated; very dark grayish brown (10YR 3/2) horizons at 690-691 and 694 cm	
	2.5Y 4/0		
	5Y 4/2 to 2.5Y 4/2	695 - 700 cm: silty clay, olive gray (5Y 4/2)	
	5Y 3/2	700 - 704 cm: silty clay, dark gray (2.5Y 4/0)	
	5Y 3/2 to - 4/2	704 - 714 cm: silty clay, olive (5Y 4/3)	
	5Y 3/2 to - 4/2	note: 714-723 cm gap (core catcher)	
	2.5Y 4/4 to - 4/4		
	5Y 4/2 2.5Y 4/0 5Y 4/3		

Depth in core (m)

5

6

7

8

9

10

A125

**PS2770-6 (GKG)**

Eastern Laptev Sea Cont. Margin

**ARK-XI/1**

Recovery: 0.36 m

78°21.0'N, 135°11.7'E

Water depth: 500 m

Lithology	Texture	Color	Description	Age
Surface				
10YR3/3 sandy silty clay, dark grayish brown, even surface common ophiurids and polychaets				
	10YR3/3		0-8 cm: sandy silty clay, dark grayish brown, homogeneous	
	7.5YR3/4		8-9 cm: stiff silty clay, dark brown	
	10YR4/2		9-14 cm: sandy silty clay, dark grayish brown, with dark brown lenses	
	N3		14-36 cm: sandy silty clay, very dark gray, homogeneous	
			end of core: 36 cm	

A126

PS2771-5 (GKG)

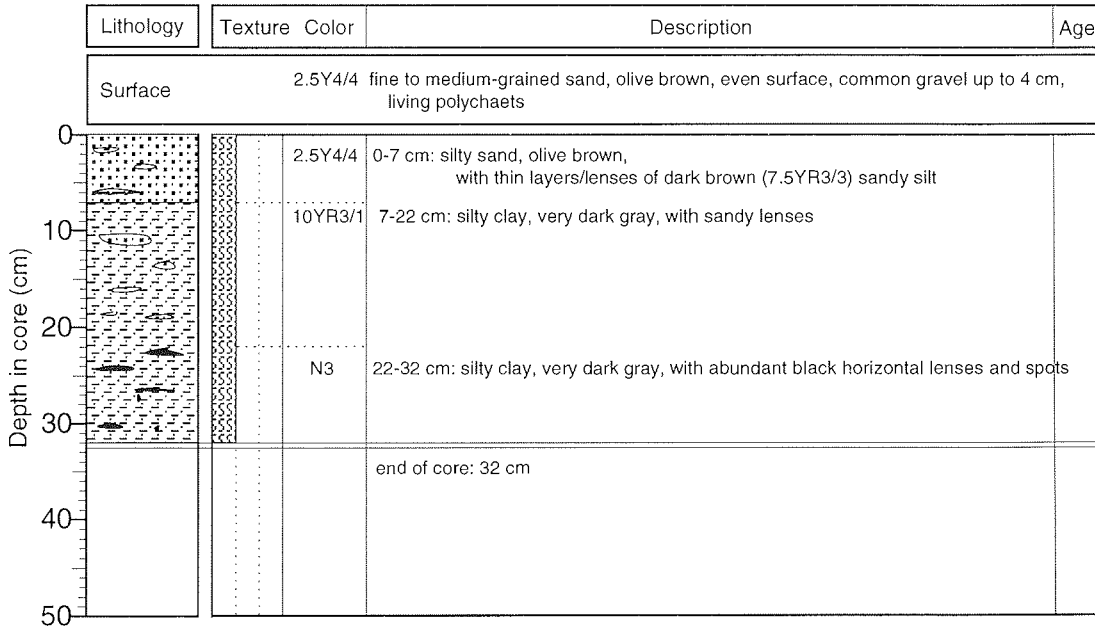
Eastern Laptev Sea Cont. Margin

ARK-XI/1

Recovery: 0.32 m

78°19.6'N, 135°23.6'E

Water depth: 214 m





A127

PS2773-7 (GKG)

Gakkel Ridge

ARK-XI/1

Recovery: 0.36 m

80°56.8'N, 122°38.7'E

Water depth: 3561 m

Lithology	Texture Color	Description	Age
Surface 10YR3/3 sandy silty clay, dark grayish brown, even surface			
		10YR3/3 0-18 cm: sandy silty clay, dark grayish brown, with dark yellowish brown(10YR3/4) mottles (5-6 cm diam.)  10YR3/4 18-22 cm: sandy silty clay, homogeneous 10YR3/3 22-36 cm: sandy silty clay, dark brown, homogeneous	
		end of core: 36 cm	

Depth in core (cm)

0  
10  
20  
30  
40  
50

A128

PS2774-2 (GKG)

Gakkel Ridge

ARK-XI/1

Recovery: 0.40 m

80°40.9'N, 121°17.6'E

Water depth: 3489 m

Lithology	Texture	Color	Description	Age
Surface				
10YR3/3 sandy silty clay, dark brown, even surface, some shell fragments				
Depth in core (cm) 0 10 20 30 40 50			10YR3/3 0-23 cm: silty clay, dark brown, homogeneous	
			10YR3/2 17-22 cm: sandy silty clay, very dark grayish brown, mottled	
			10YR3/3 22-33 cm: silty clay, dark brown, homogeneous	
			10YR4/2 33-40 cm: silty clay, dark grayish brown, mottled	
			end of core: 40 cm	

A129

PS2779-5 (GKG)

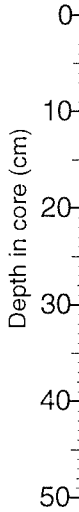
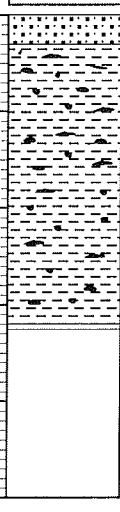
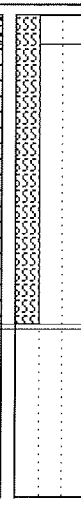
Western Laptev Sea Cont. Margin

ARK-XI/1

Recovery: 0.32 m

77°55.8'N, 113°30.9'E

Water depth: 248 m

Lithology	Texture	Color	Description	Age
Surface				
10YR3/4 silty sand, dark yellowish brown, even surface, bivalve fragments, soft corals, polychaets				
			10YR3/4 0-3 cm: silty sand, dark yellowish brown, homogeneous	
			5Y3/1 3-32 cm: clay, very dark gray, with small black lenses and spots	
			end of core: 32 cm	

A130

PS2780-5 (GKG)

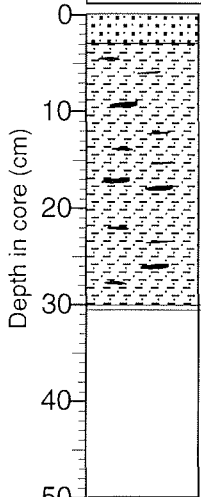
Western Laptev Sea Cont. Margin

ARK-XI/1

Recovery: 0.30 m

77°54.3'N, 113°44.6'E

Water depth: 135 m

Lithology	Texture	Color	Description	Age
Surface				
		10YR3/4	silty sand, dark yellowish brown, even surface, bivalve fragments, soft corals, polychaets	
		10YR3/4	0-3 cm: silty sand, dark yellowish brown, homogeneous	
		5Y3/2	3-30 cm: silty clay, dark olive gray, with thin black horizontal lenses and and rare gravel	
			end of core: 30 cm	

A131

PS2781-1 (GKG)

Western Laptev Sea Cont. Margin

ARK-XI/1

Recovery: 0.37 m

78°07.4'N, 111°55.0'E

Water depth: 325 m

Lithology	Texture	Color	Description	Age
Surface				
10YR3/3 silty clay, dark brown, even surface, some polychaets				
	10YR3/3		0-8 cm: silty clay, dark brown, homogeneous	
	2.5Y4/2		8-37 cm: silty clay, dark grayish brown, with polychaet tubes, few brownish mottles in upper part	
			end of core: 37 cm	

A132

PS2787-7 (GKG)

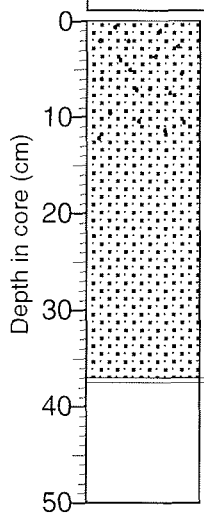
Eastern Kara Sea Cont. Margin

ARK-XI/1

Recovery: 0.38 m

82°04.5'N, 90°59.7'E

Water depth: 1029 m

Lithology	Texture	Color	Description	Age
Surface		10YR3/3	pebbly sandy silt, dark brown, inclined surface with sponge mattress and pebbles, common gastropods,	
		10YR3/3	0-13 cm: pebbly sandy silt, dark brown, abundant sponge spicules at top, vertical dark brown burrows	
		2.5Y3/2	13-29 cm: silty sand, very dark grayish brown, with few reddish concretions (1 cm diam.)	
		N4	29-38 cm: silty sand, dark gray, homogeneous, with few dark brownish concretions (1 cm diam.)	
			end of core: 37 cm	

A133

PS2791-5 (GKG)

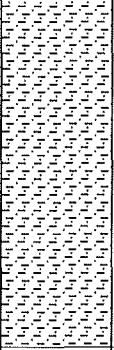
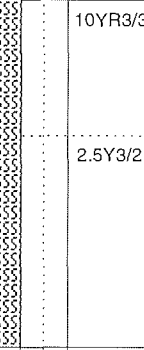

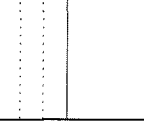
Eastern Kara Sea

ARK-XI/1

Recovery: 0.36 m

81°10.4'N, 87°30.2'E

Water depth: 320 m

Lithology	Texture Color	Description	Age
Surface 10YR3/3 silty sand, dark brown, even surface, abundant small gravel, ophiurids, polychaets			
		10YR3/3 0-14 cm: sandy silt, dark brown, homogeneous  2.5Y3/2 14-36 cm: silty clay, very dark grayish brown, homogeneous	
		end of core: 36 cm	

Depth in core (cm)

0  
10  
20  
30  
40  
50

A134

PS2792-6 (GKG)

Eastern Kara Sea

ARK-XI/1

Recovery: 0.43 m

79°33.5'N, 87°00.1'E

Water depth: 245 m

Lithology	Texture	Color	Description	Age
Surface				
		7.5YR3/4	0-13 cm: silty clay, dark brown, even surface, some polychaets	
		7.5YR3/4	0-13 cm: silty clay, dark brown, homogeneous	
		7.5YR3/2	13-16 cm: silty clay, dark brown, homogeneous	
		5Y3/2	16-33 cm: silty clay, dark olive gray with abundant dark brown (7.5YR3/2) and dark brown (10YR3/3) spots and mottles	
		5Y3/2	33-43 cm: silty clay, dark olive gray, with common dark brown (10YR3/3) spots and mottles	
			end of core: 43 cm	



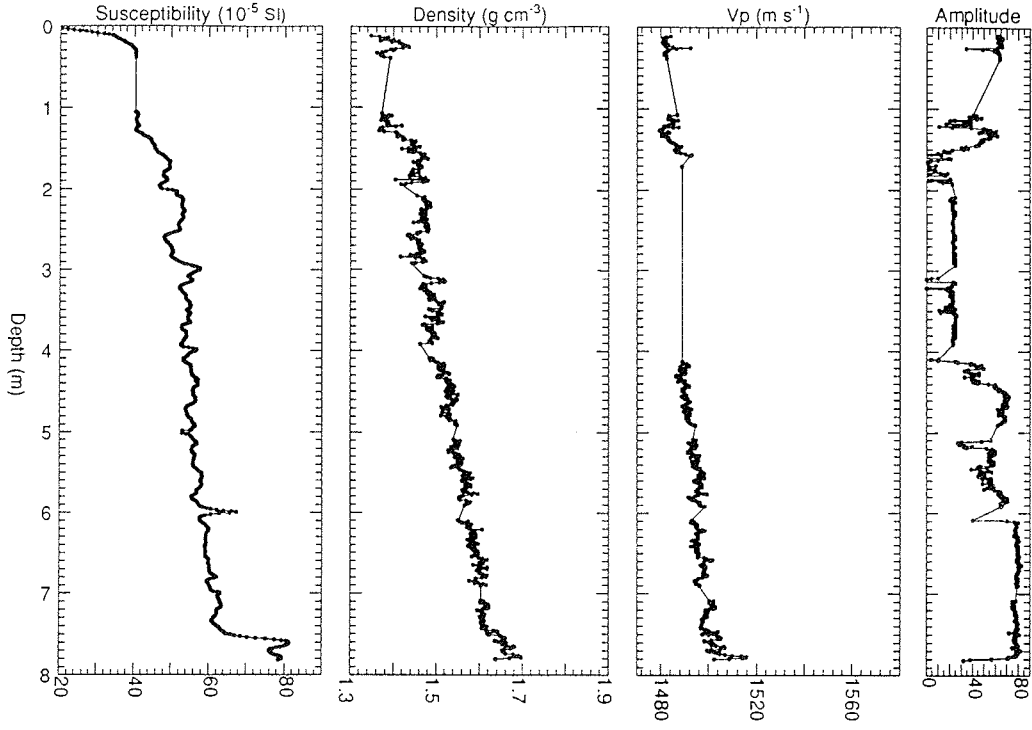
A135

**Annex 11.4-4: Core Logging Graphs**

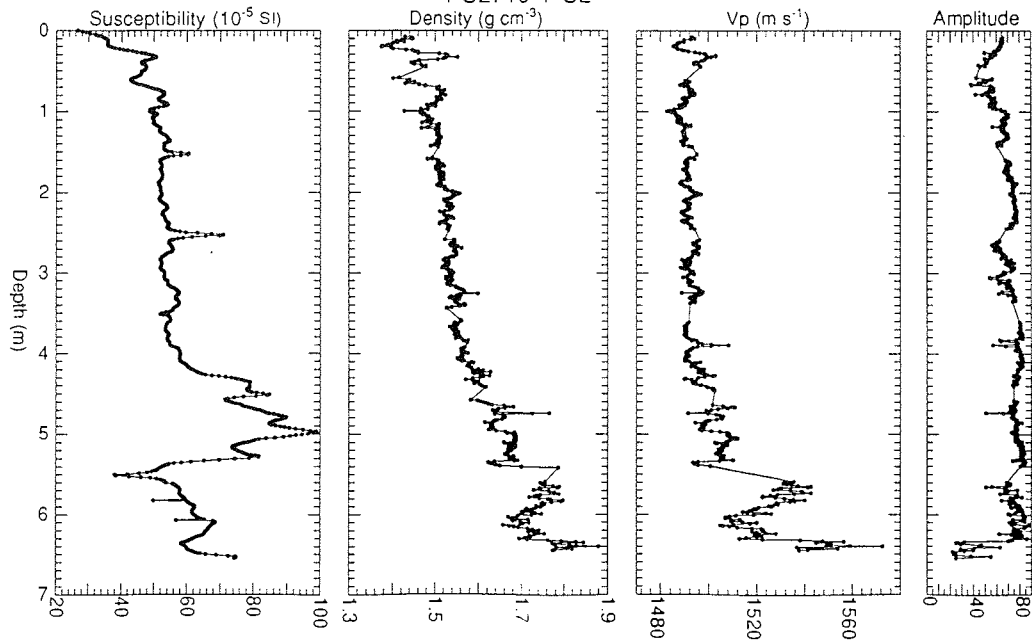
showing  
magnetic susceptibility, wet bulk density,  
p-wave velocity ( $V_p$ ) and its amplitude  
versus  
core length (depth)

A136

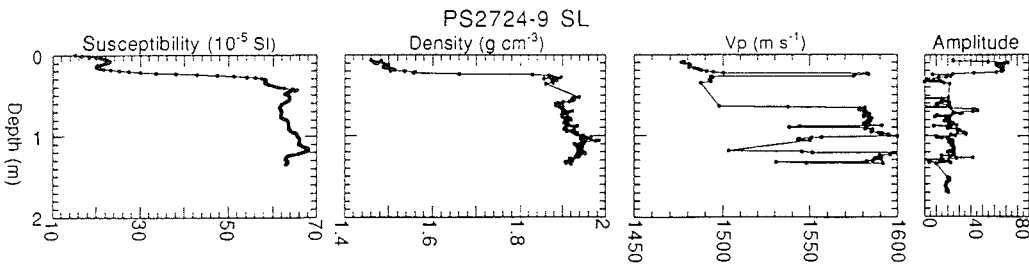
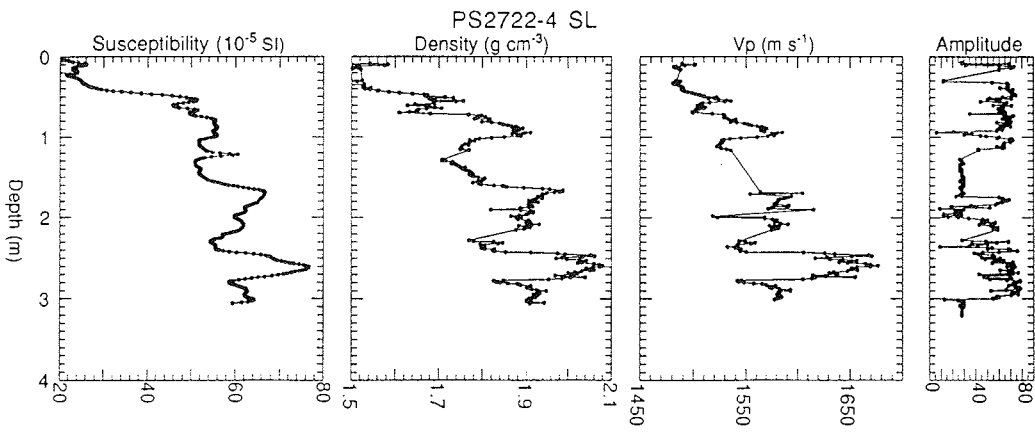
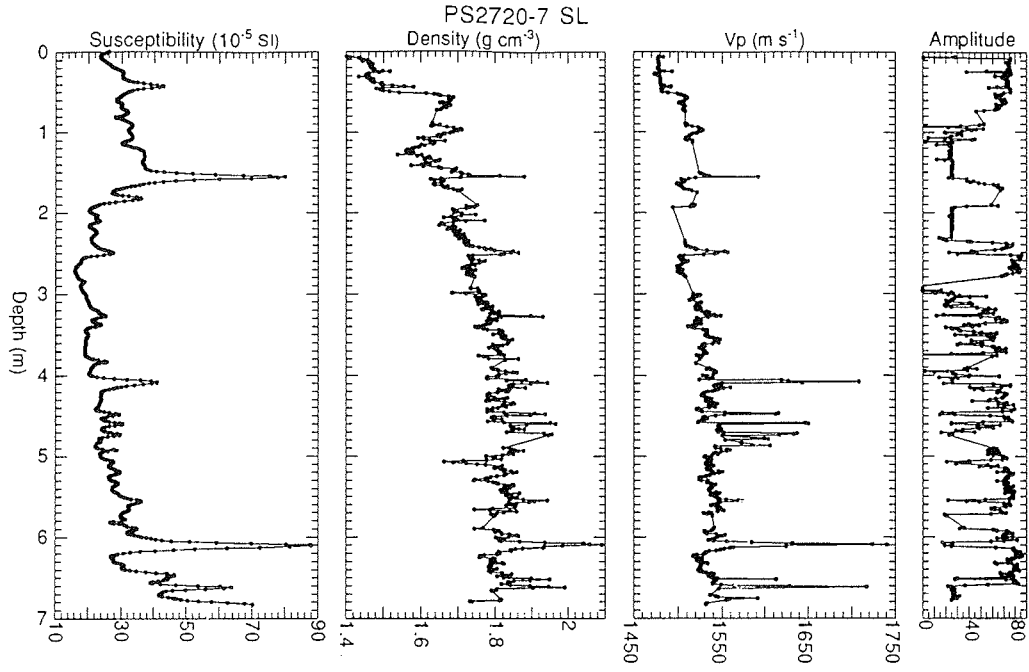
PS2718-6 SL



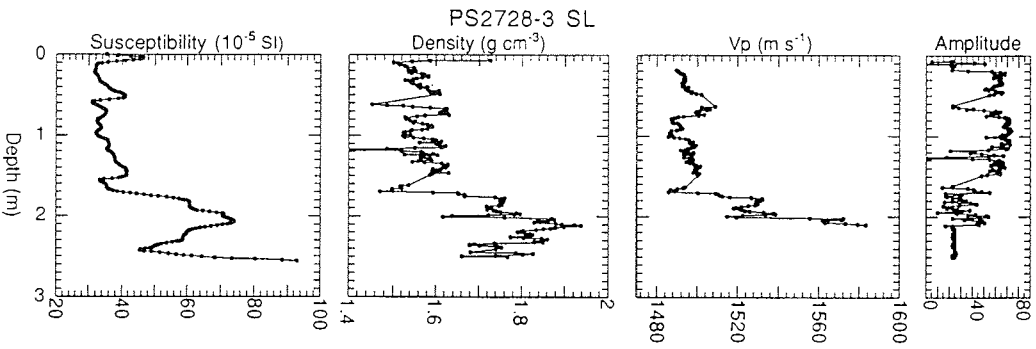
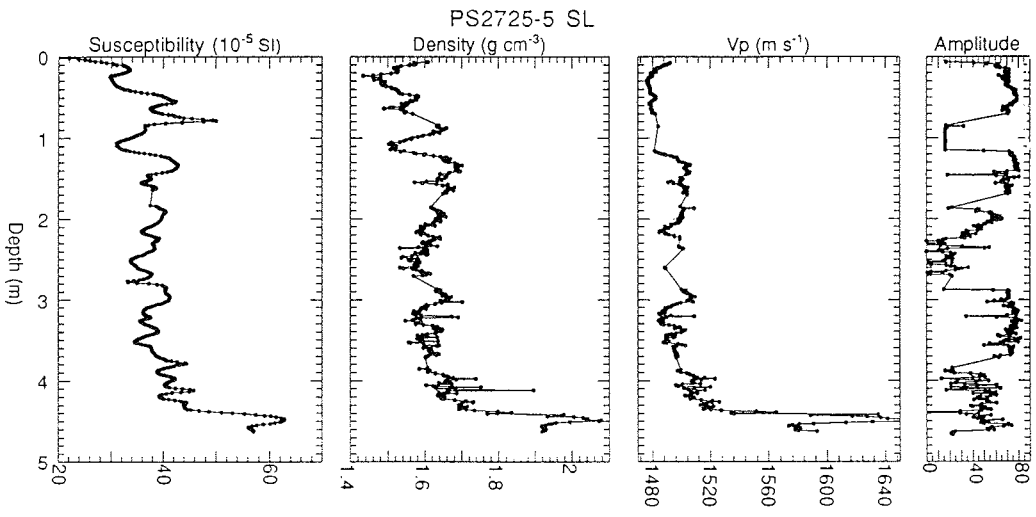
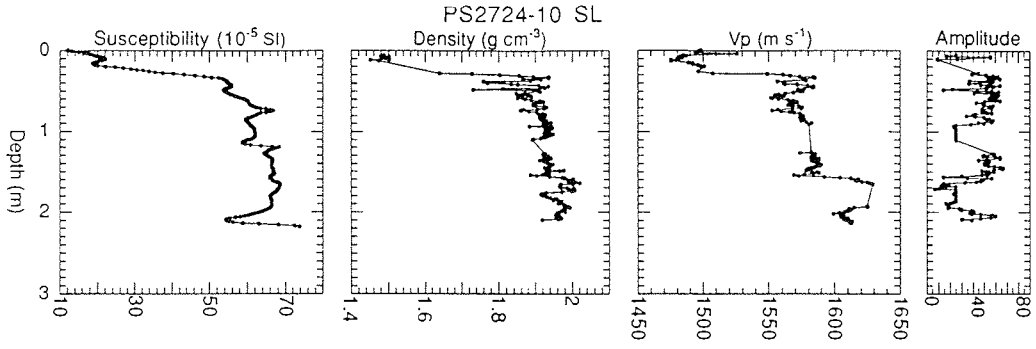
PS2719-1 SL



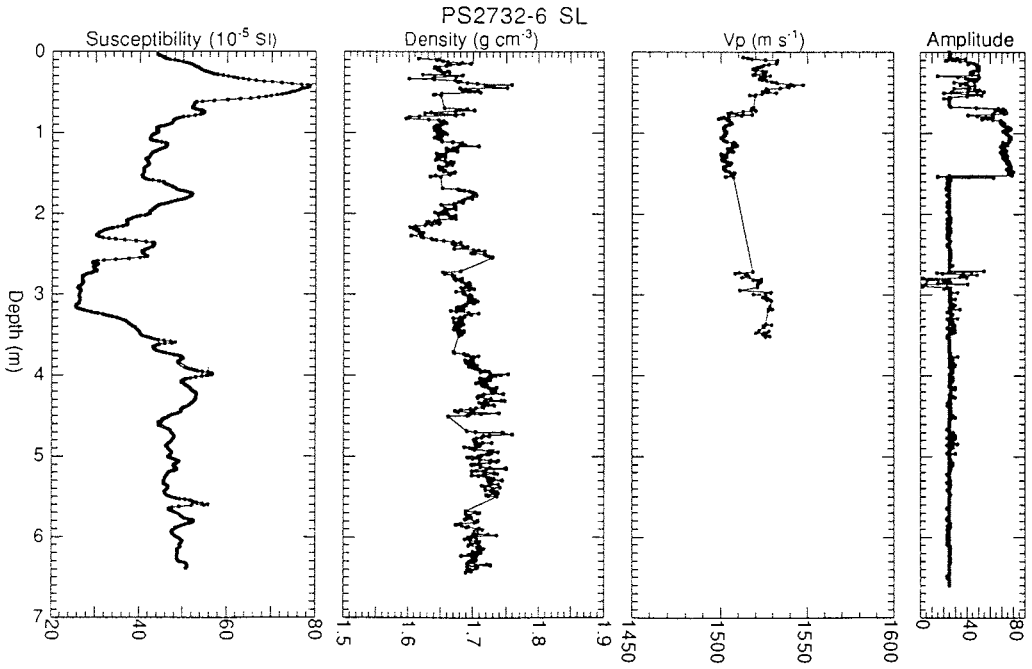
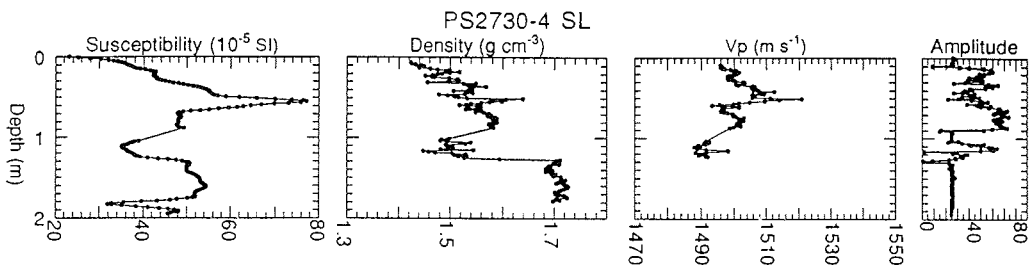
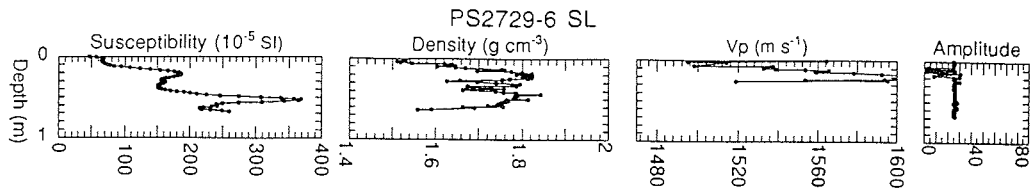
A137



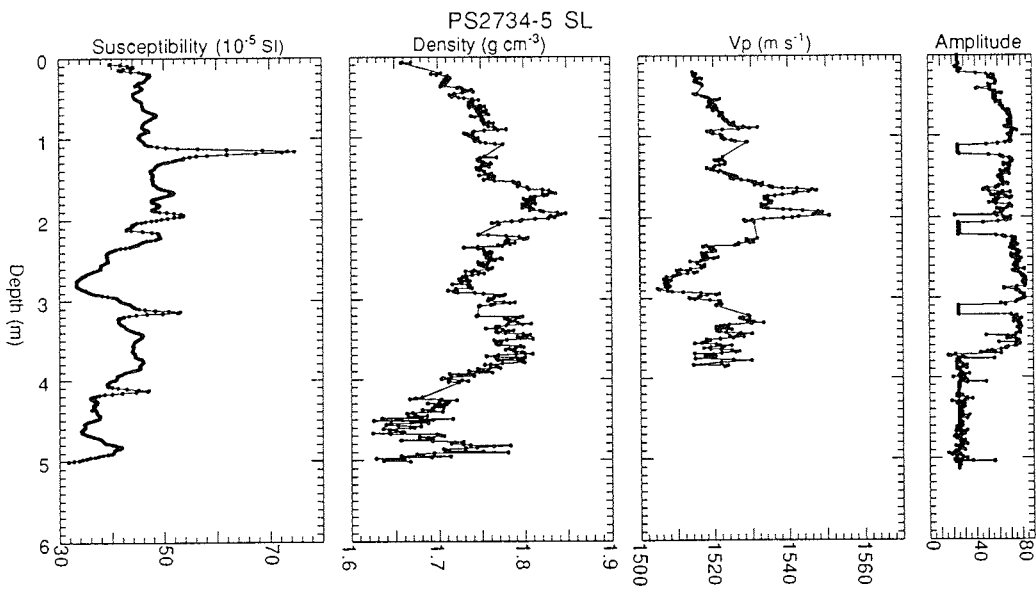
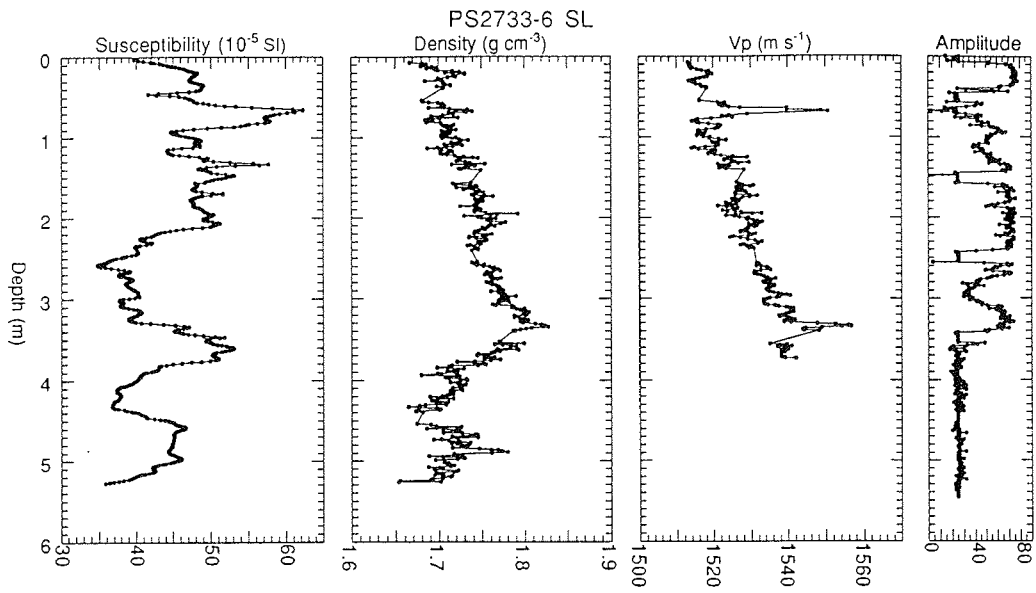
A138



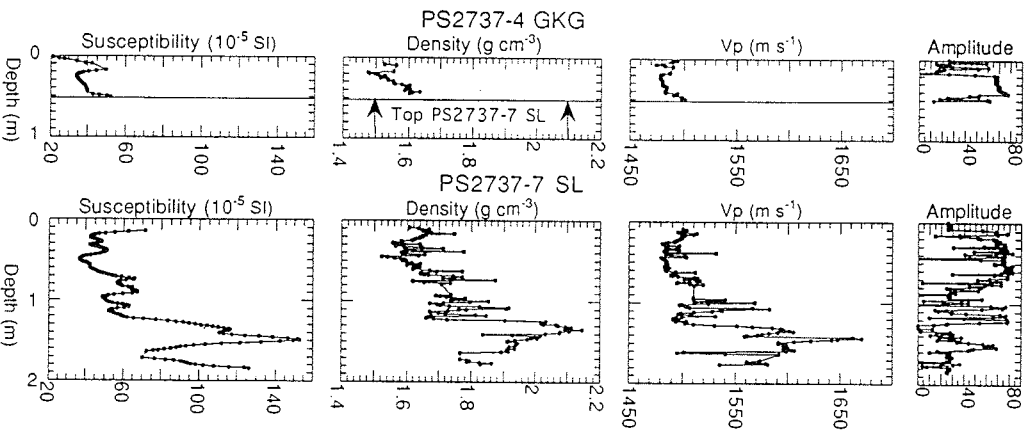
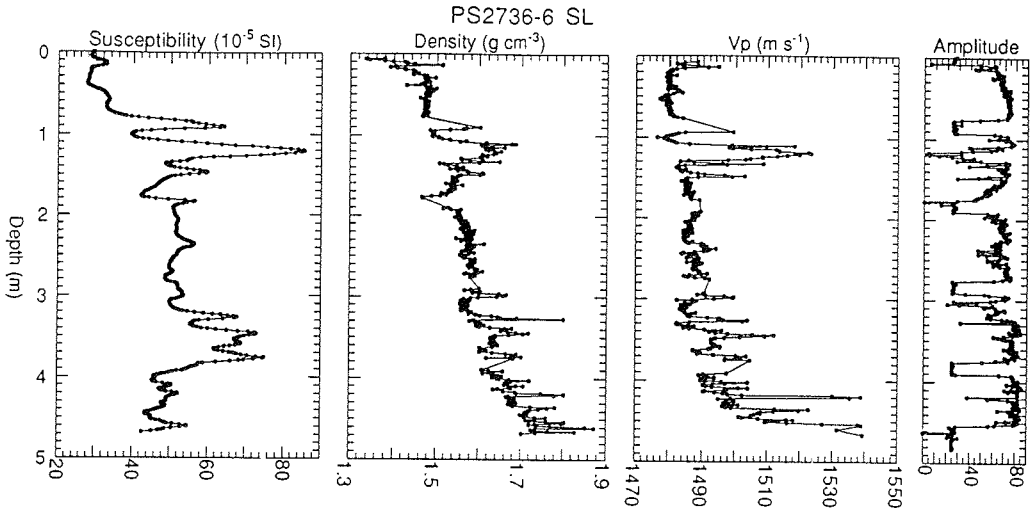
A139



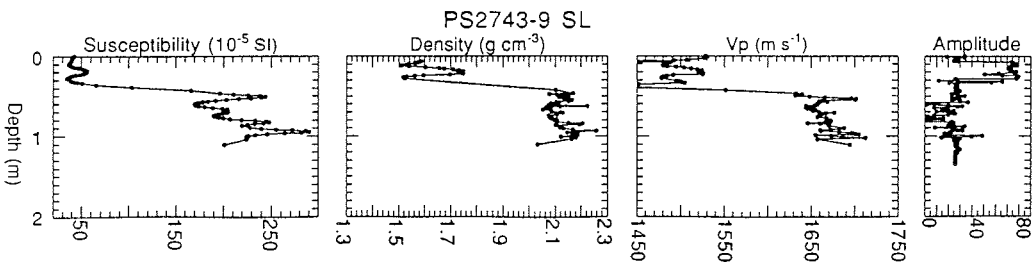
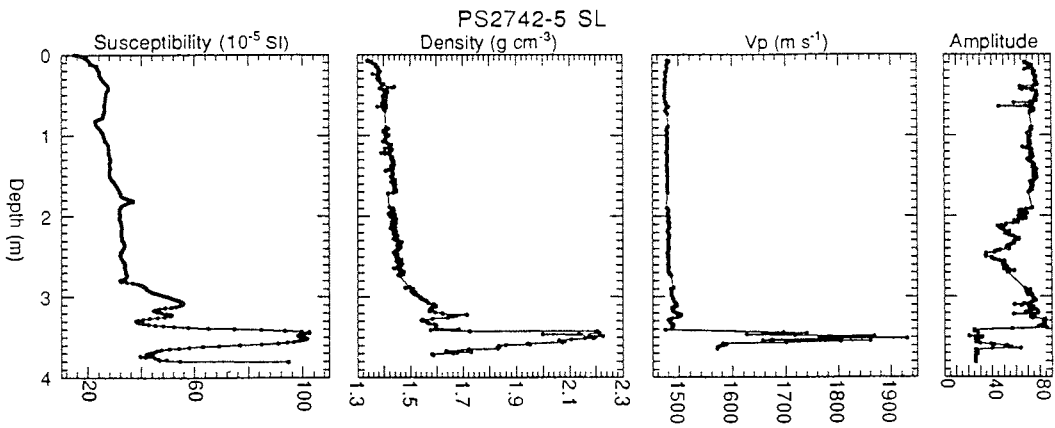
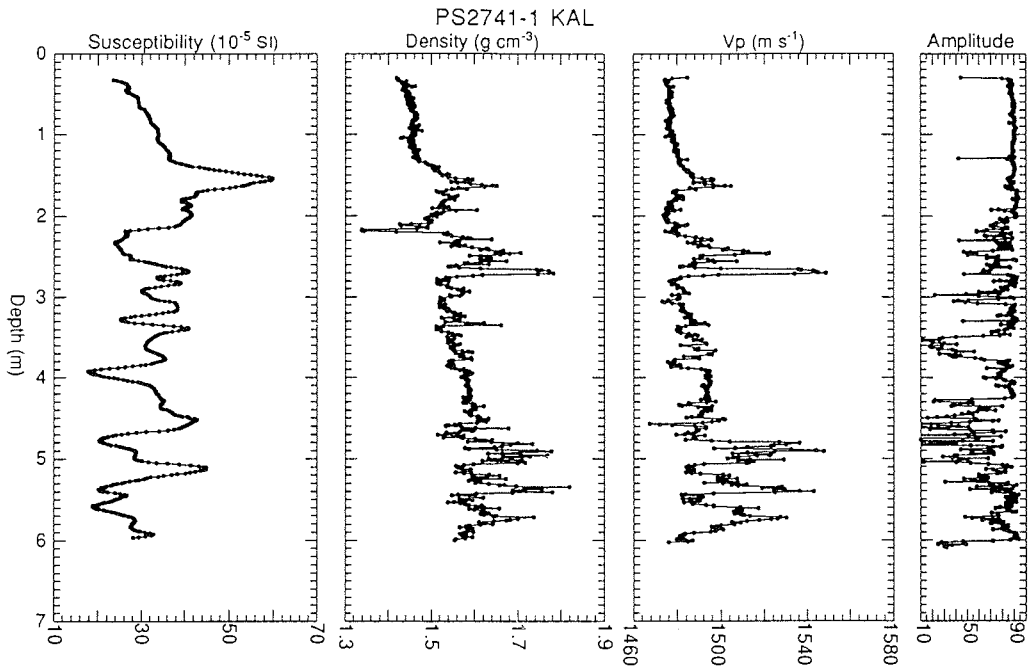
A140



A141



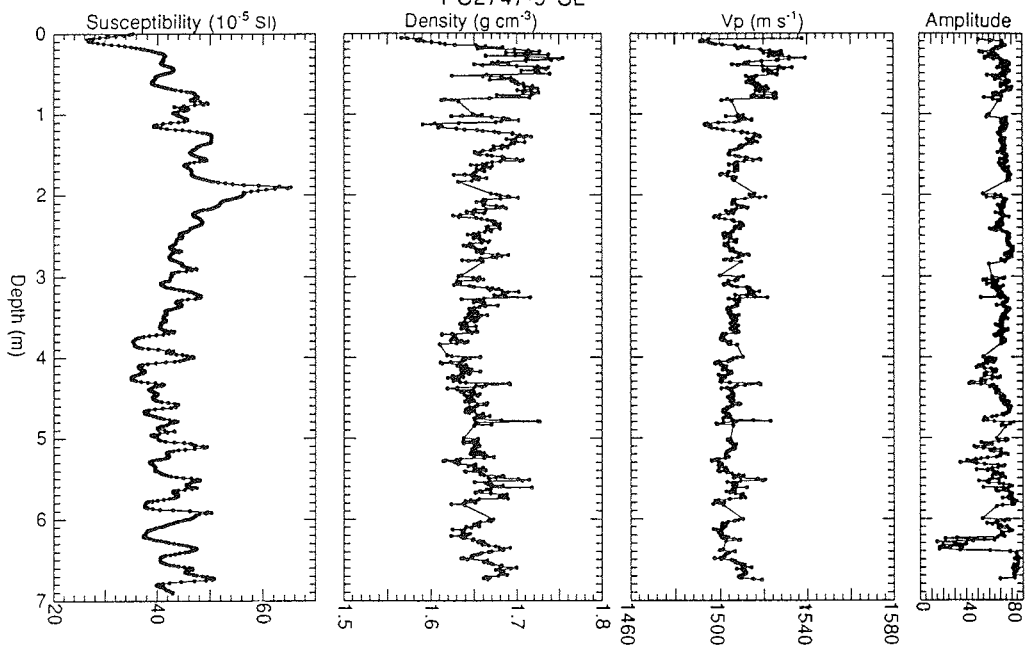
A142



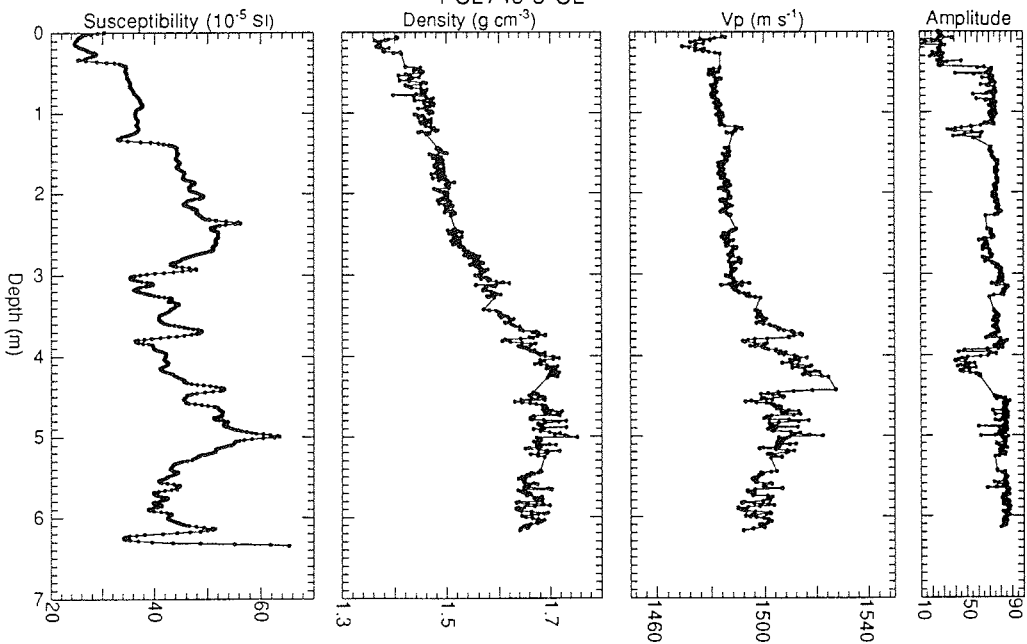


A143

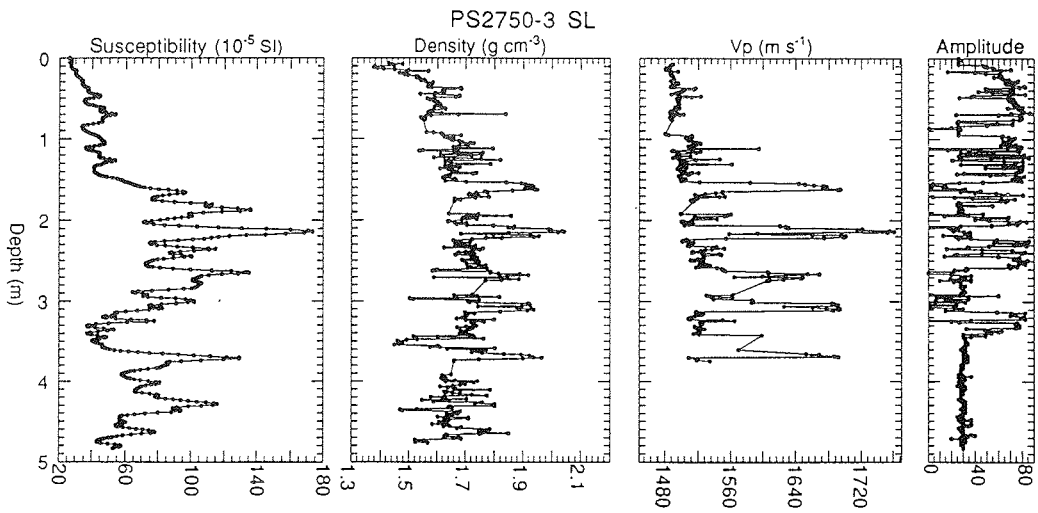
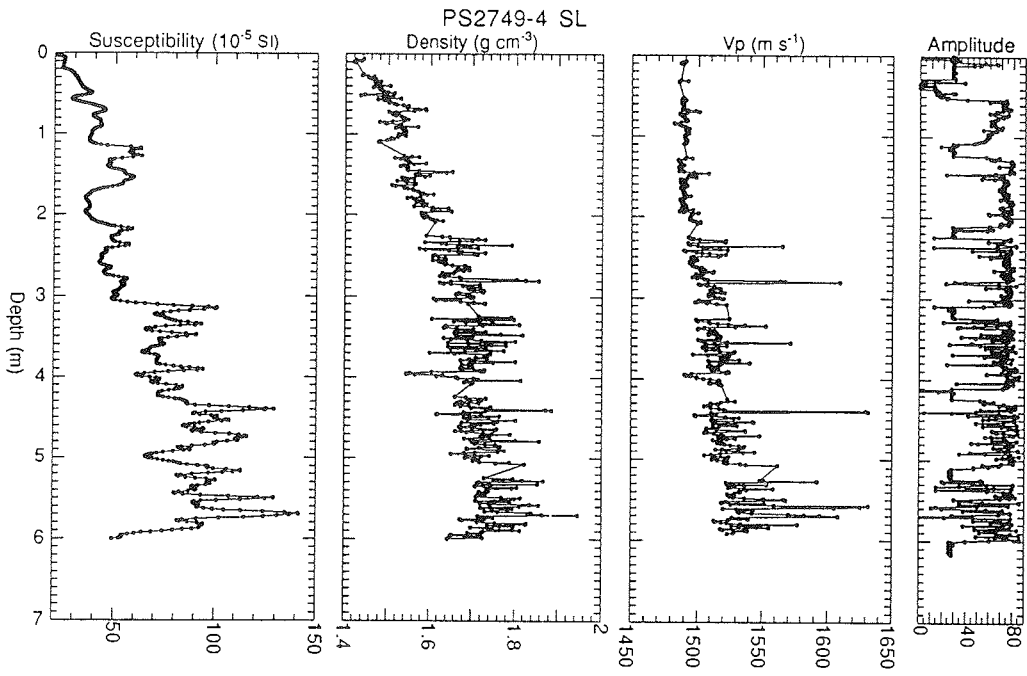
PS2747-9 SL



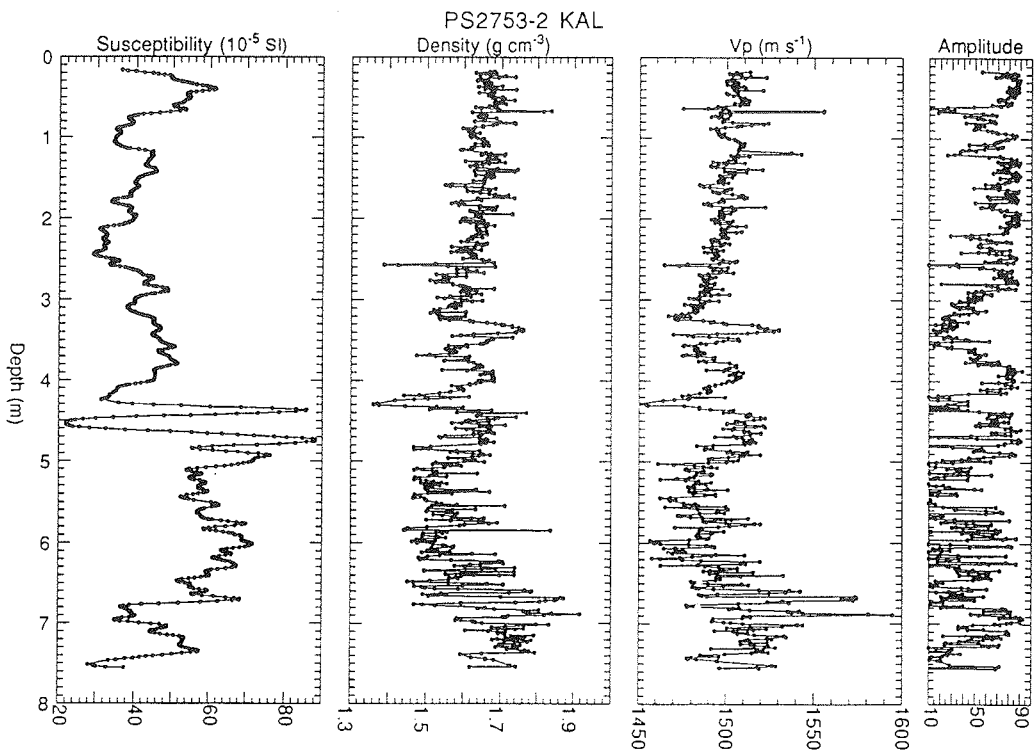
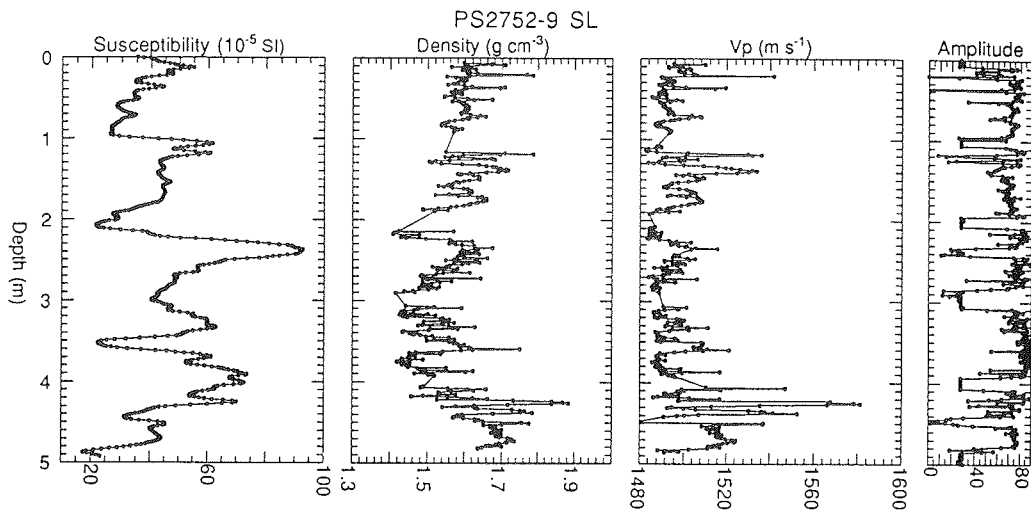
PS2748-3 SL



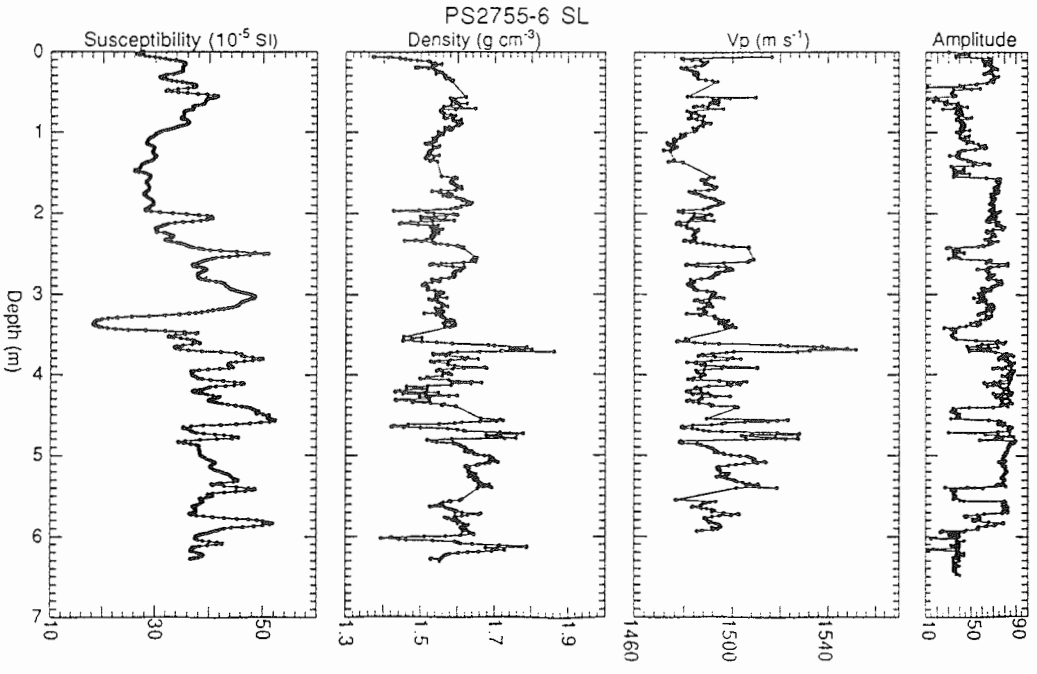
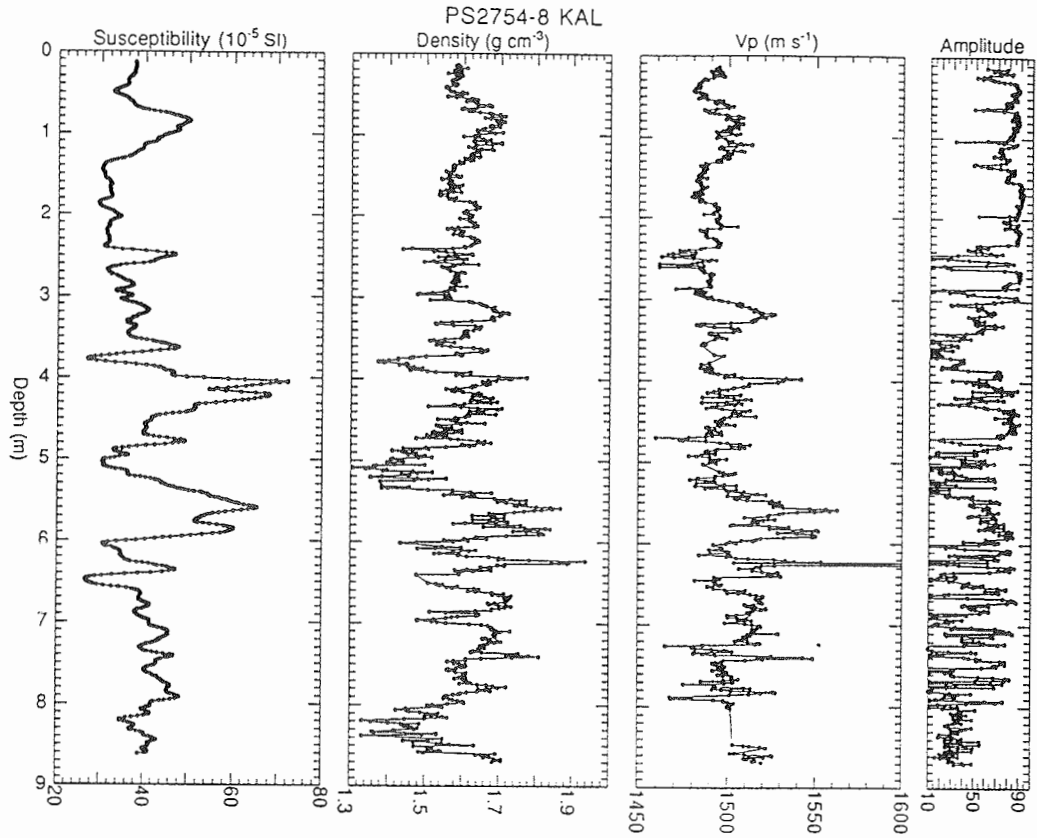
A144



A145

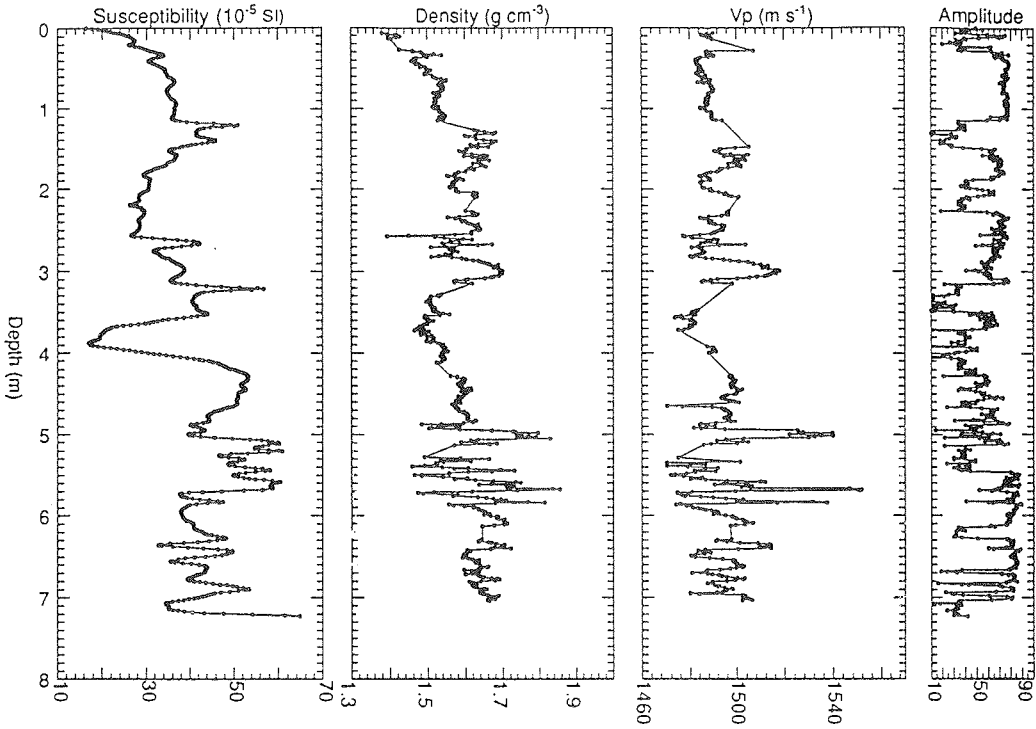


A146

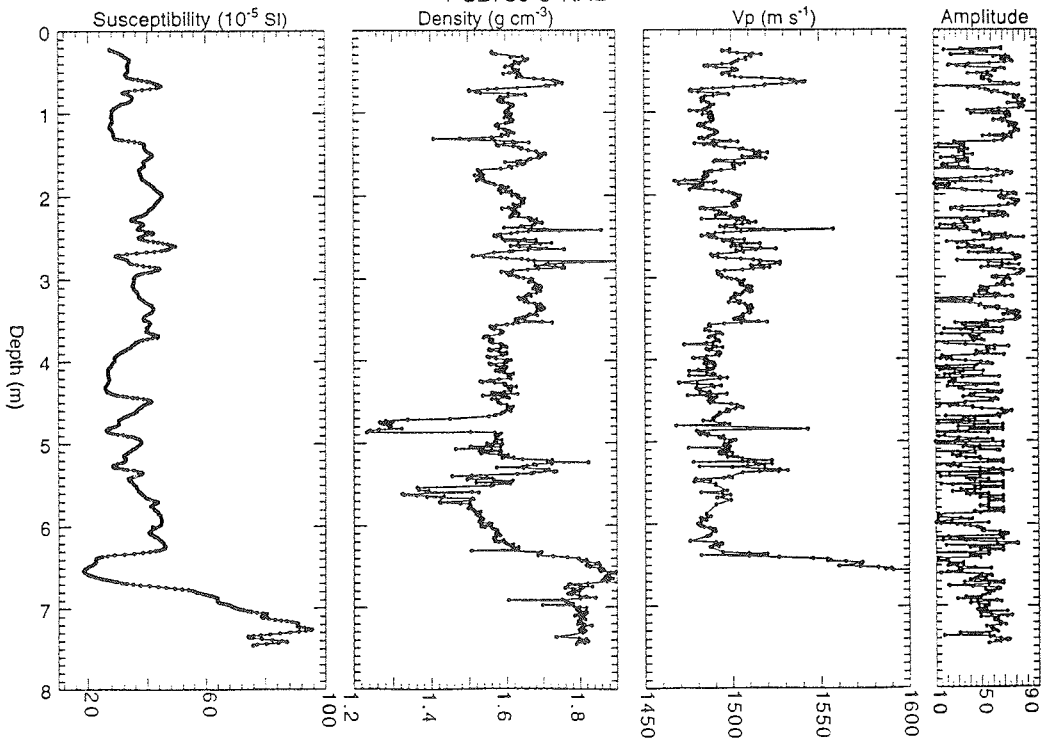


A147

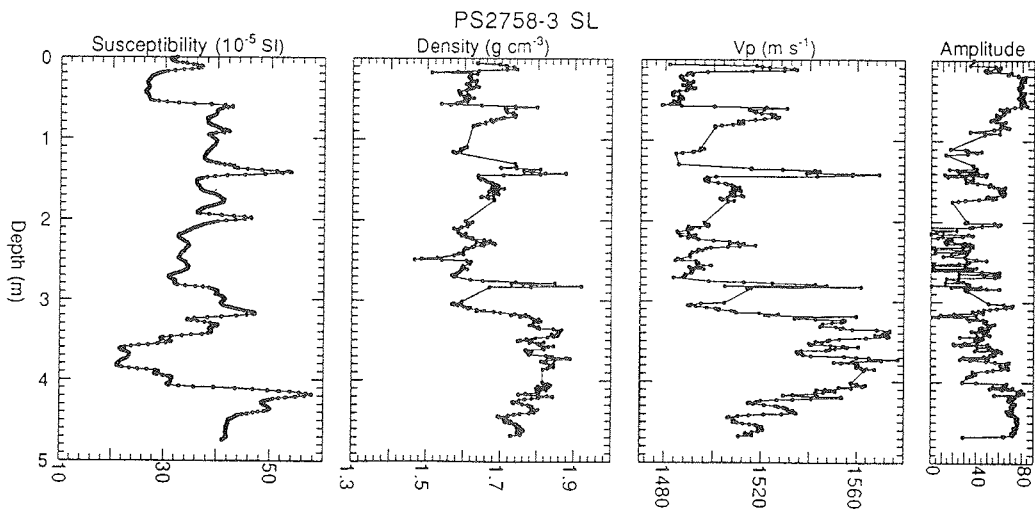
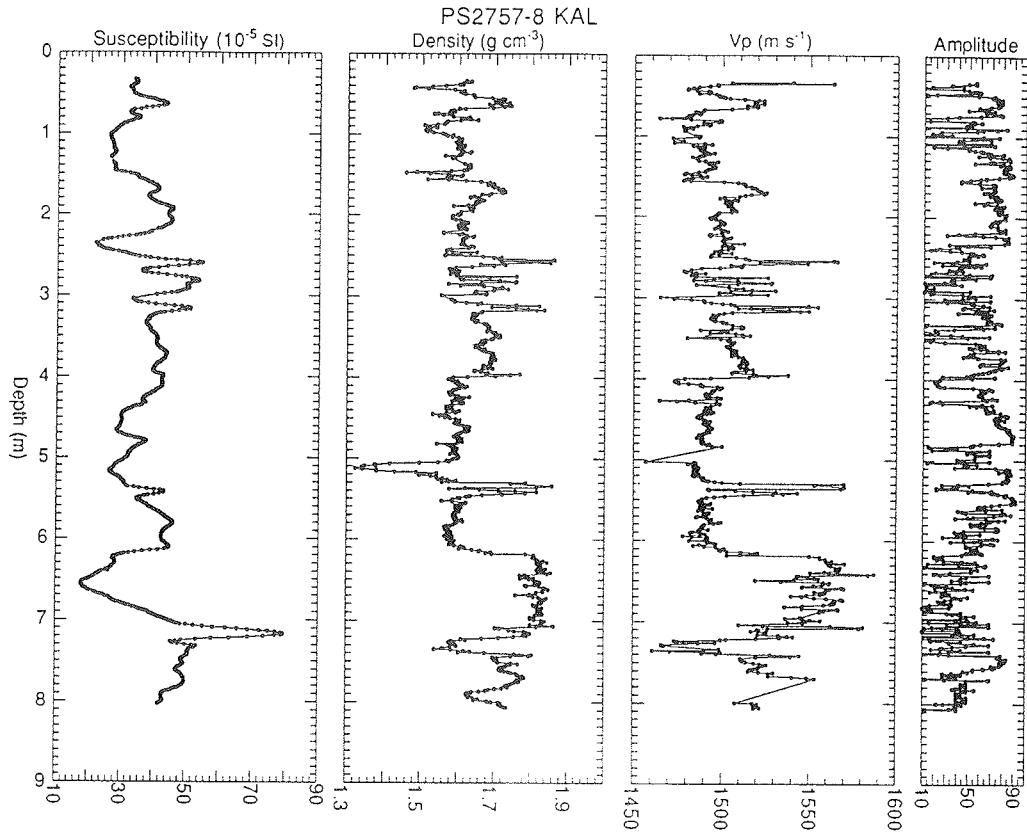
PS2756-10 SL



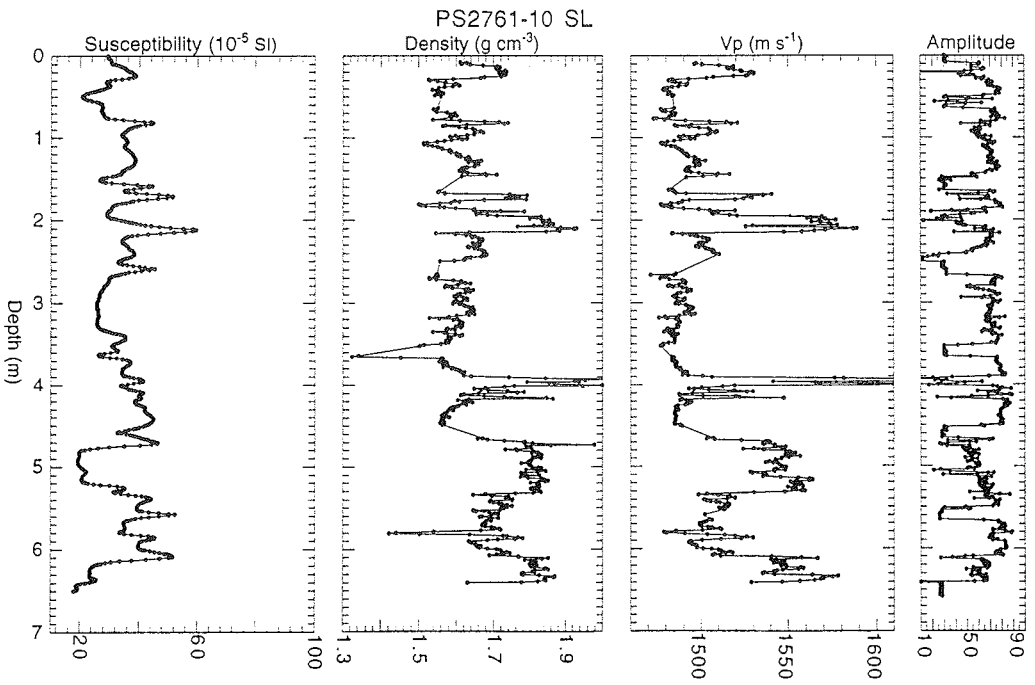
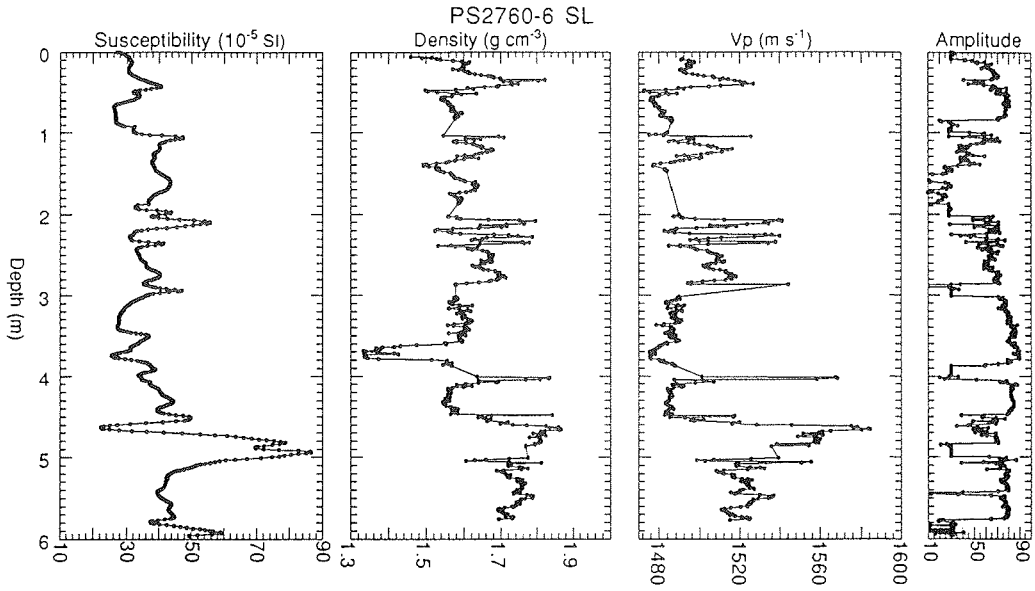
PS2759-8 KAL



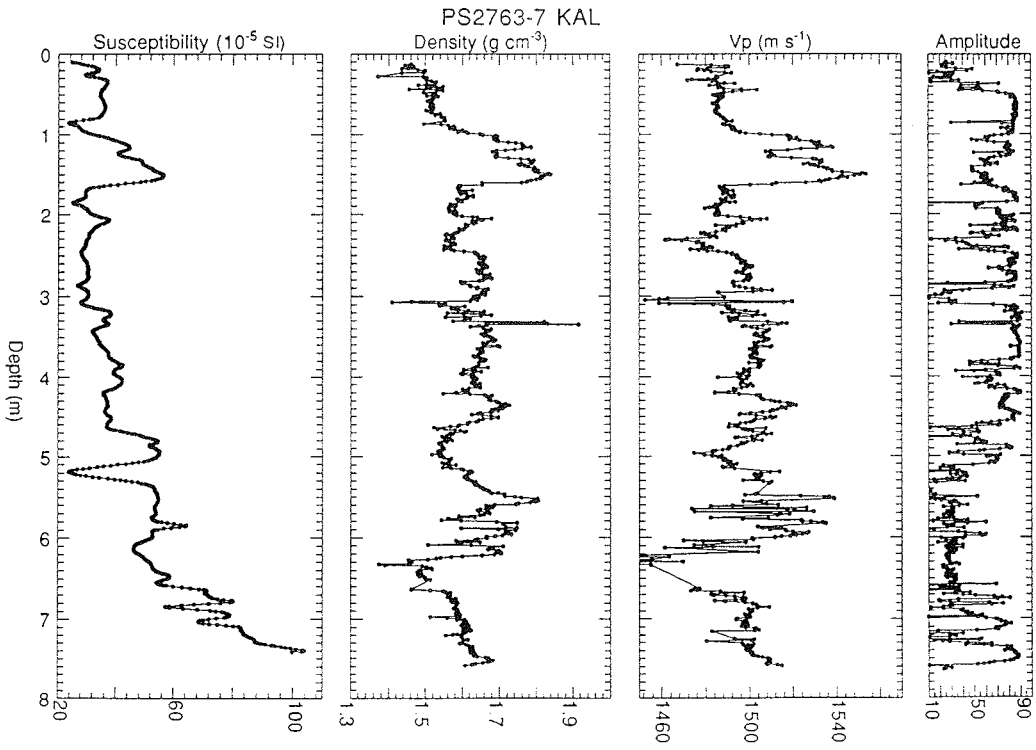
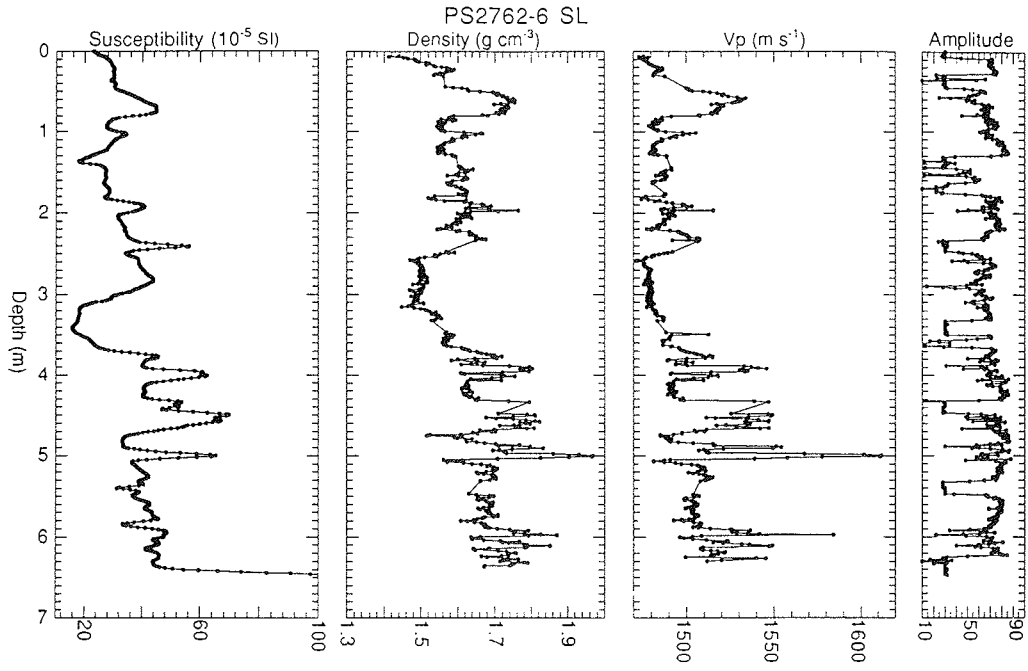
A148



A149

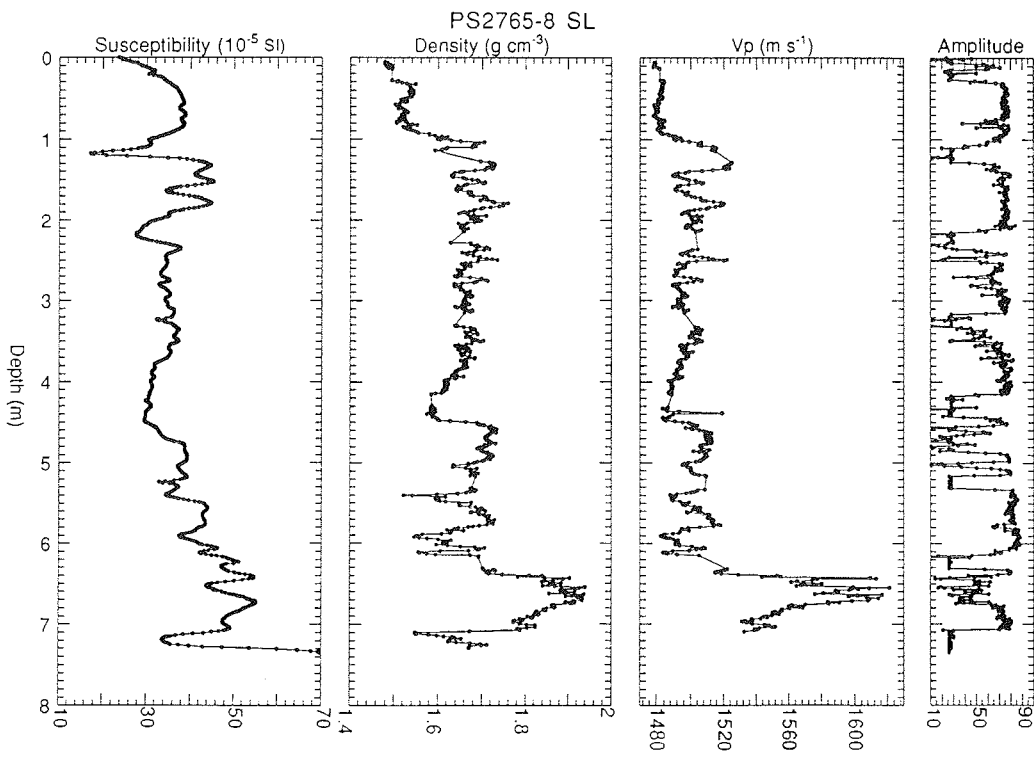
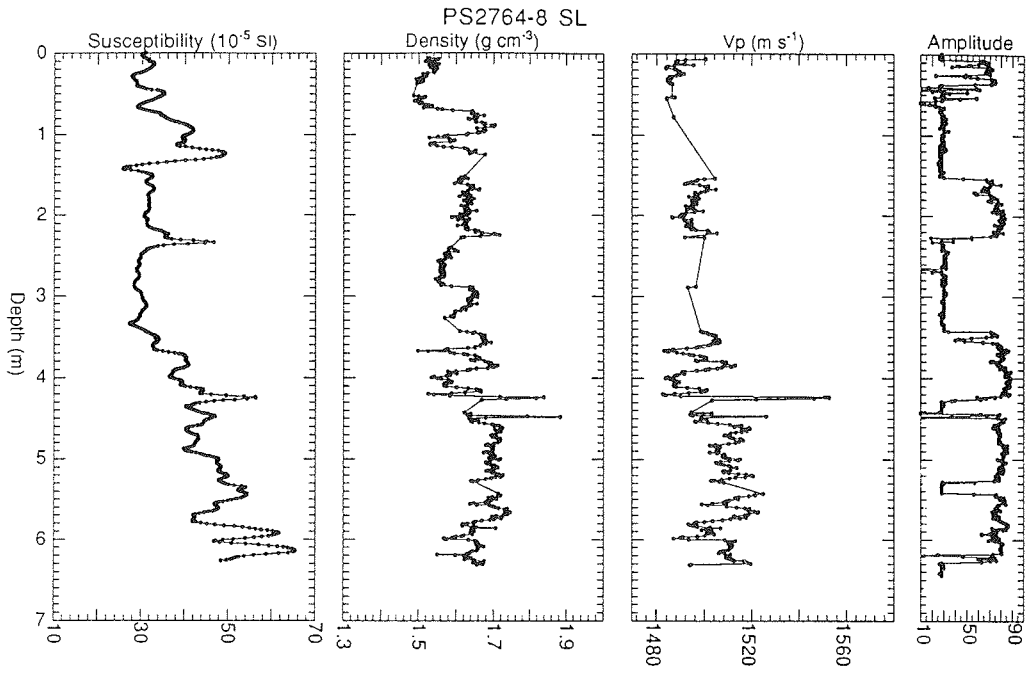


A150

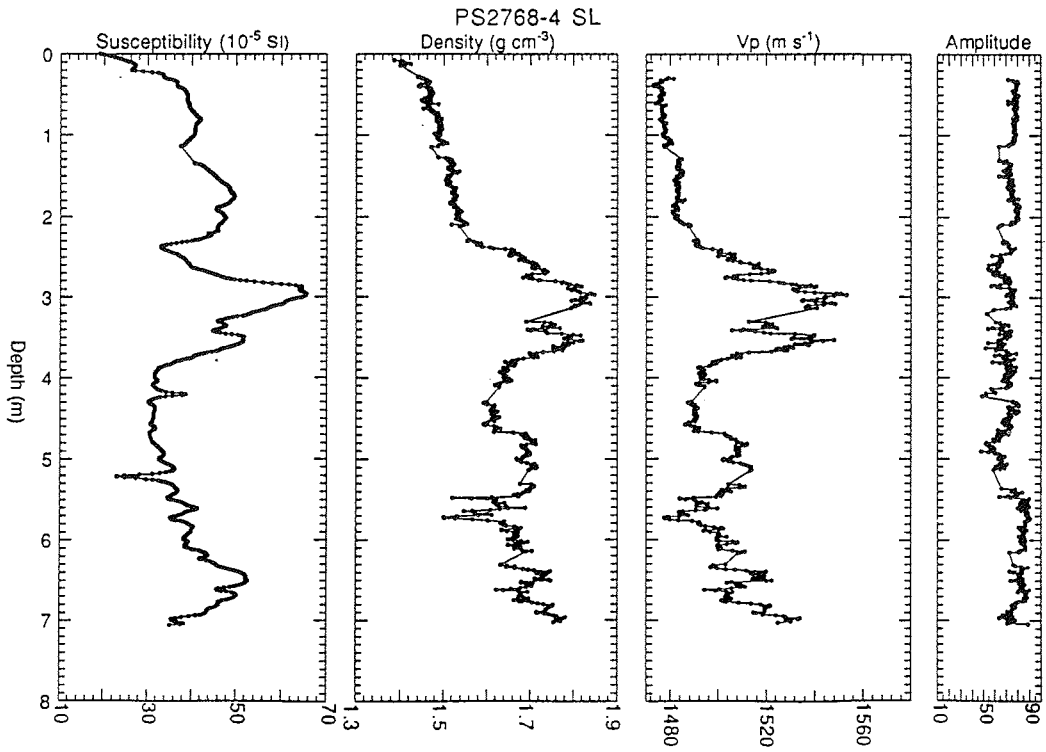
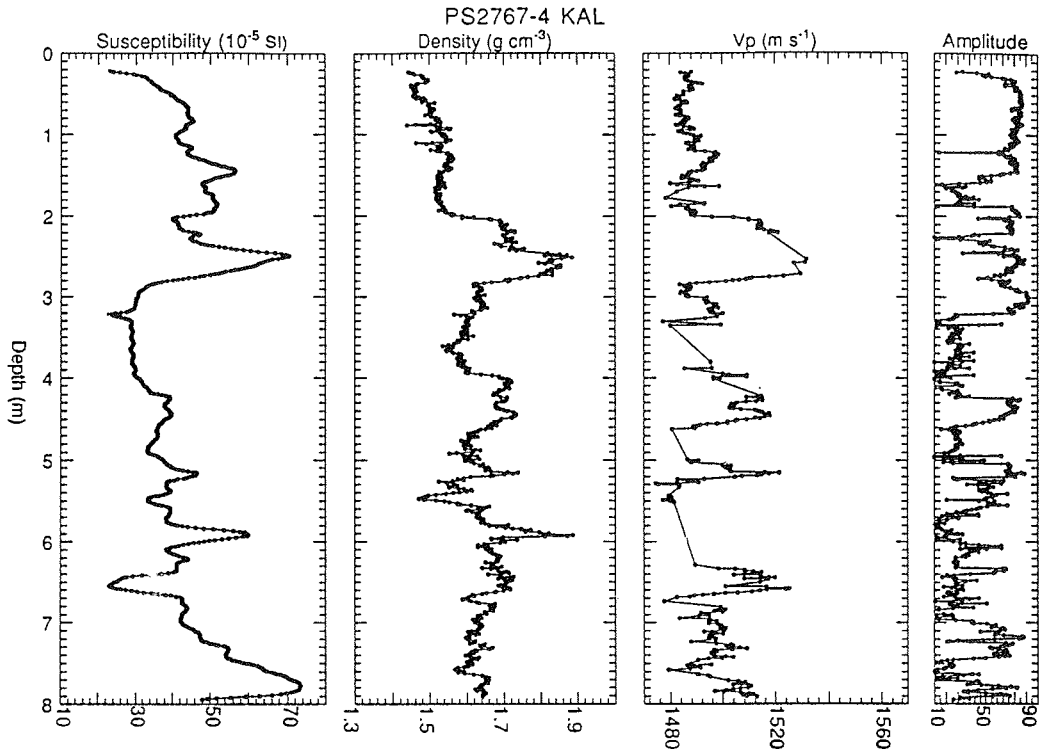




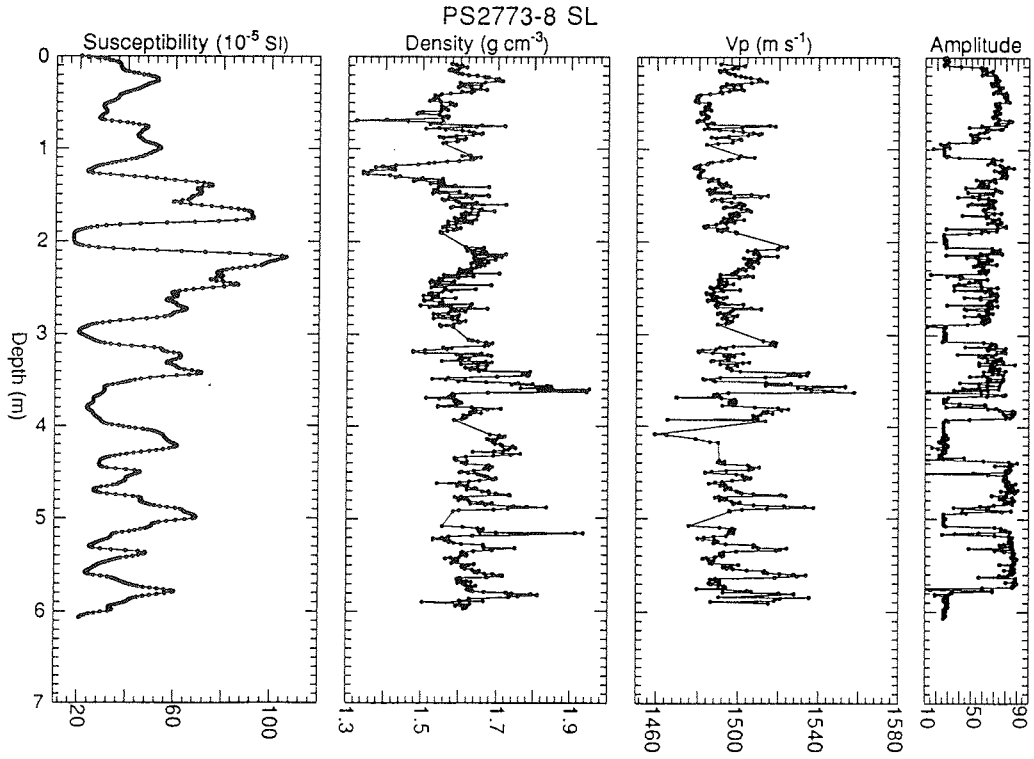
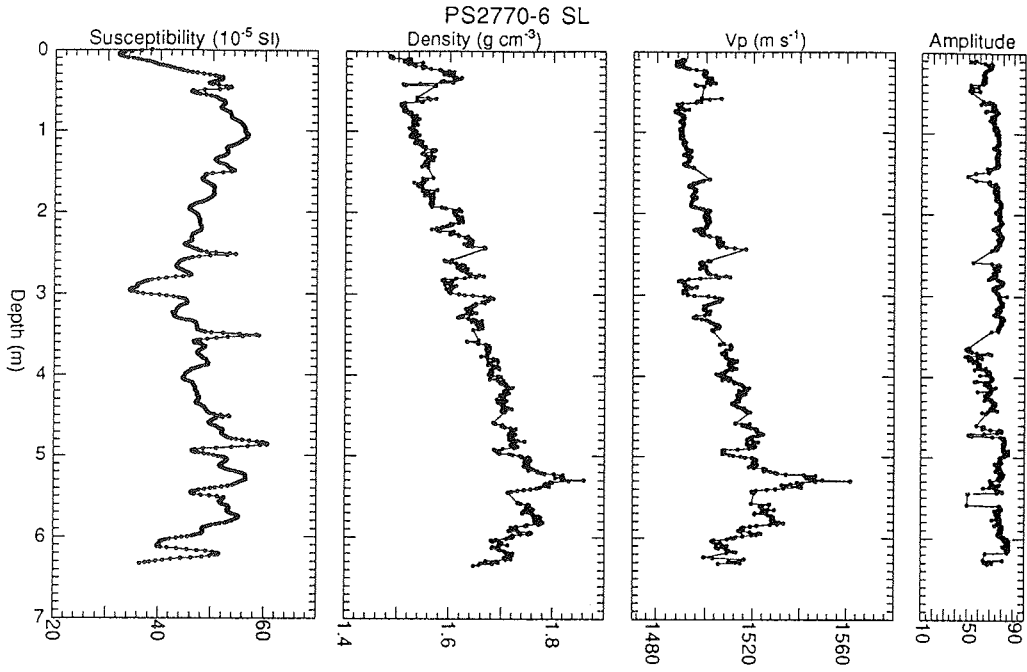
A151



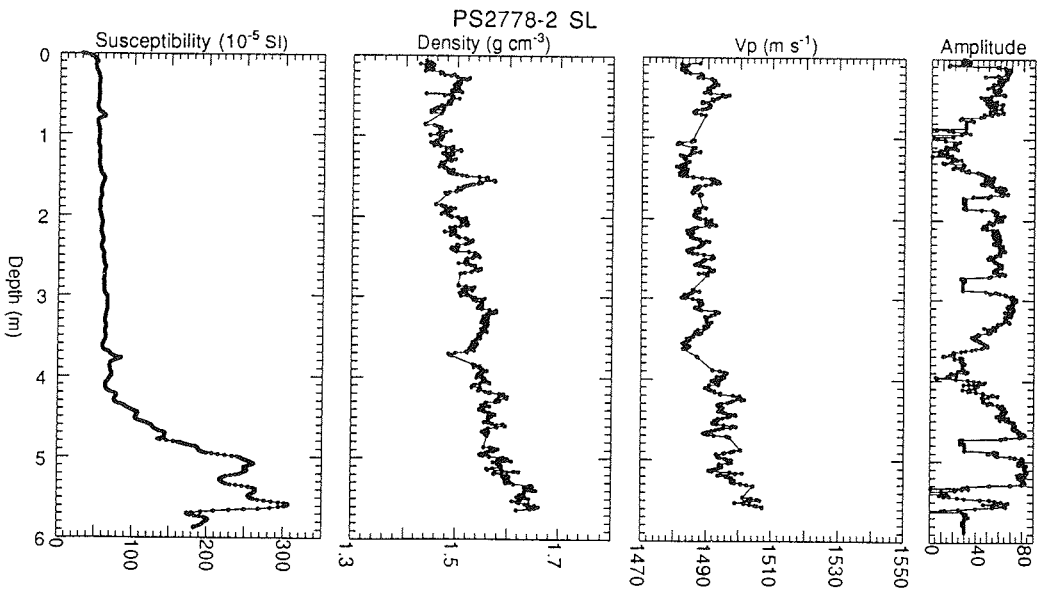
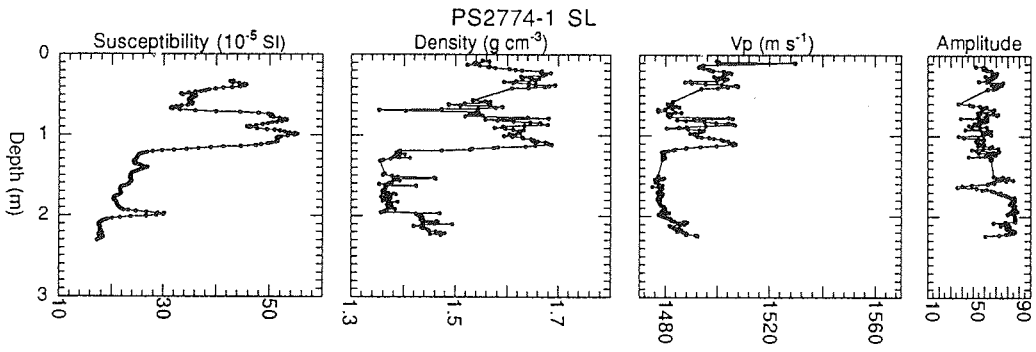
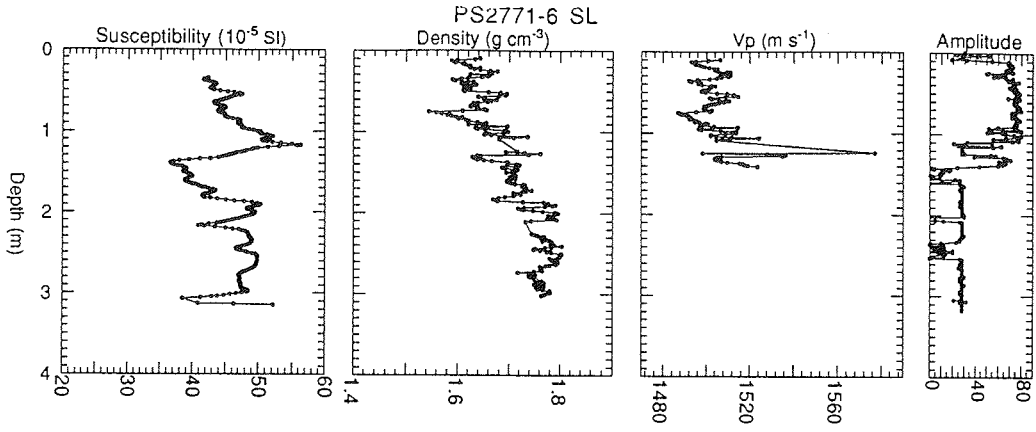
A152



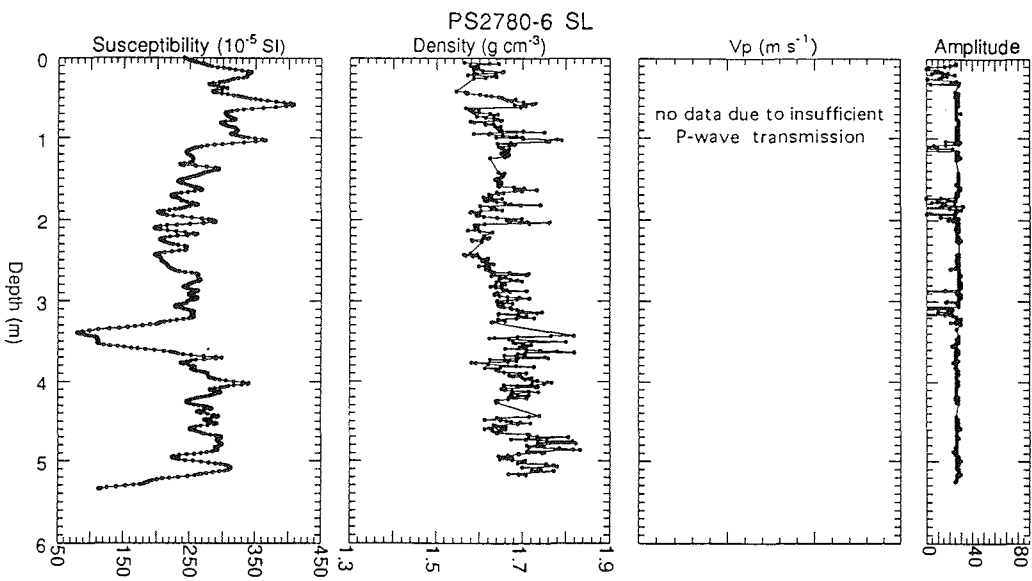
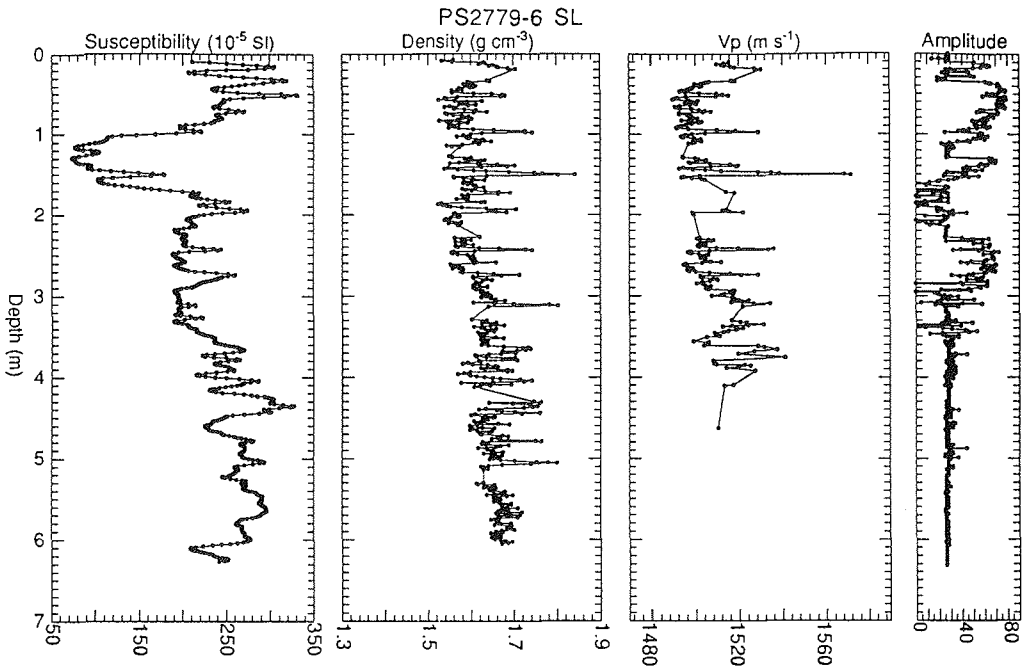
A153



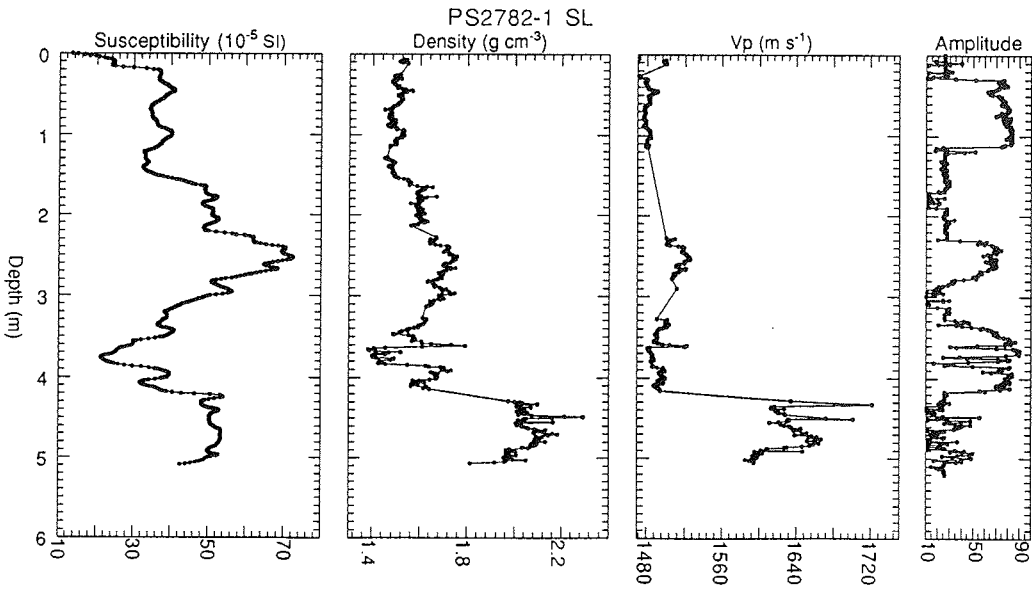
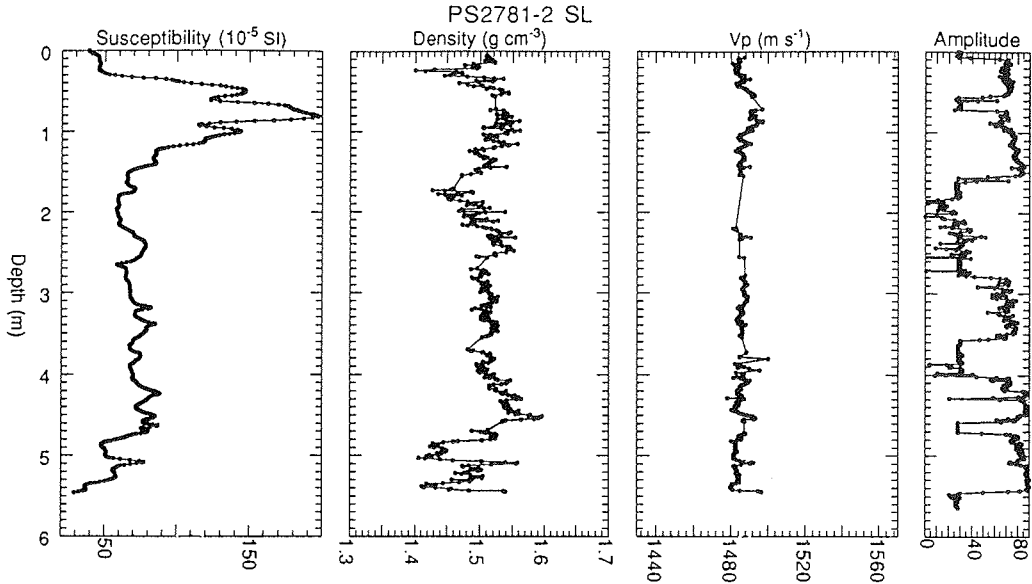
A154



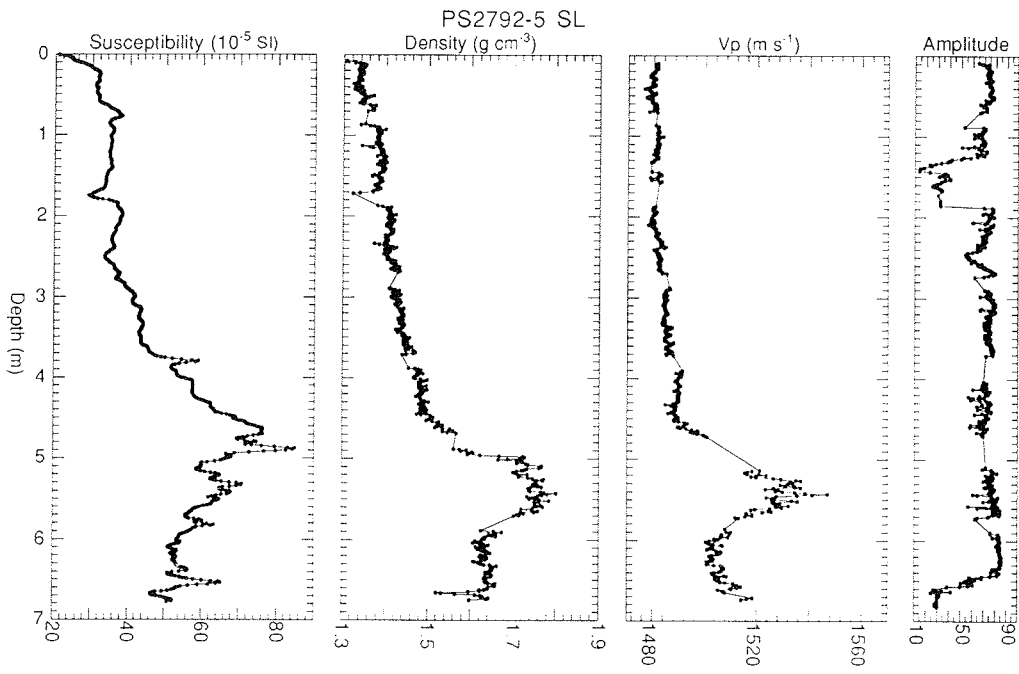
A155



A156



A157



**Annex 11.5:**

**GUIDELINES FOR DATA AND SAMPLE DISTRIBUTION,  
ANALYSES AND PUBLICATIONS**

POLARSTERN-Expedition ARK XI/I ("LADI")

The 1995 expedition ARK XI/1 of the German RV POLARSTERN to the Laptev Sea and adjacent waters including all material and data obtained are to be regarded a main contribution to the project "Ecological-climatological system of the Laptev Sea" of the Agreement about Marine and Polar Research between the Ministry of Science and Technology Policy of the Russian Federation and the Federal Ministry of Education, Science, Research and Technology of the Federal Republic of Germany from 10 February 1995.

Based on the experience of the 1993 German-Russian expedition ARK IX/4, the participating scientists of the POLARSTERN cruise ARK XI/1 (1995) agreed again on general guidelines for the exchange of sample material and data obtained during the expedition. As the different disciplines working on board have their specific demands, the guidelines have been set up by these disciplinary groups to best meet their specific needs.

To optimize information about the further evaluation and treatment of data and results, especially for those not participating in the cruise or who are associated by shorebased studies and analyses, lists of potential working titles (which may result in publications) have been attached. The names of the major contributors and contact persons are given in *italics*.

The use of material and data will be restricted to the participants and their partners indicated in these guidelines for two years, unless no other agreement is made and AWI on the German side has consented after consultation with AARI on the Russian side.

Results of the analyses of data (of observations/measurements) and samples obtained by scientists from other countries having participated in the cruise or the subsequent analyses, are to be presented to the Russian and German sides after publication, including non-published data.

It is proposed to provide interim reports about progress of the work until the end of 1996.

If there is any substantial proposal for a change in the distribution and use of material and data, the scientists responsible have to be contacted and asked. In addition, AWI (Bremerhaven, Chief Scientist) and AARI (St. Petersburg) have to agree.

Regarding publications, the AWI library has to receive two reprints. Abstracts of these publications will appear in the "POLARSTERN ABSTRACTS", edited by AWI.

On board POLARSTERN, 16 September 1995

*(Signed by Chief Scientist, Eike Rachor, AWI,  
and Speaker of Russian Scientists, A. Darovskikh, AARI)*



HINT: As there is a strong relation of the ARK XI/1-expedition to other activities in the Laptev Sea within the German-Russian "**Laptev Sea System Project**" (like the expedition TRANSDRIFT III on board the Russian icebreaker "Kapitan Dranitsyn" in October 1995), its coordinator, *Dr. Heidemarie Kassens*, GEOMAR Kiel, is referred to as contact person.

## 1 PHYSICAL OCEANOGRAPHY

### CTD observations:

Principal Investigators: *B. Rudels* (IfM, Hamburg), *J. Gunn* (SAIC), *U. Schauer* (AWI), *L. Timokhov* (AARI).

Distribution of preliminary data at the end of the cruise:

*B. Rudels* (all data, responsible for final processing)

*L. Timokhov* (all scans in ASCII format)

Members of the CTD group (*C. Darnall*, *J. Gunn*, *E. Zakharchuk*) (1 db mean)

Users of the rosette (bottle data plus standard depth)

The data made available for the users of the rosette are for their personal use to help evaluating their water samples. If any publications or public presentations are being made using and presenting CTD data before a general work on the CTD data and the hydrography has been published and can be referred to, the appropriate principal investigator should be notified and, if he wishes, be included as co-author.

Working titles:

- General hydrography of the eastern Eurasian Basin and the Laptev Sea. - *B. Rudels*, *J. Gunn*, *Y Nalbandov*, *U. Schauer*, et. al.
- Frontal mixing, inversions and interleaving: the importance of double diffusive convection for the merging of water masses in the Arctic Ocean. - *B. Rudels*
- Characteristics of the mixed layer and halocline waters in the eastern Eurasian Basin and their influence on the vertical oceanic heat flux. - *B. Rudels*, et al.
- An estimate of the circulation of the intermediate depth waters in the Eurasian Basin using a variational approach. - *B. Rudels*, *H. Friedrich* (IfM Hamburg)
- Investigations of the space and time structure of internal waves in the Laptev Sea. - *E. Zakharchuk*
- On the influence of breaking internal waves on the vertical heat transfer from the lower layers to the surface. - *E. Zakharchuk*

### ADCP observations:

Principal Investigators: *J. Gunn* (SAIC), *R. Muench* (ERS), *U. Schauer* (AWI).

Working titles:

- Distribution of internal wave energy in the Laptev Sea as measured by an ADCP. - *J. Gunn, R. Muench, U. Schauer & E. Zakharchuck* -
- Summer vertical heat and salt fluxes in the Laptev Sea. - *R. Dewey (SAIC), R. Muench & U. Schauer*

Mooring deployment:

Working title and principal investigators:

- Year long current and ice thickness measurements on the Siberian continental slope and at the Lomonosov Ridge. - *K. Aagaard, G. Björk, E. Fahrbach, J. Meincke, R. Moritz, R. Muench, B. Rudels & U. Schauer*

## 2 CHEMICAL OCEANOGRAPHY

Principal Investigators: *G. Kattner (AWI), Y. Nalbandov (IORAS), R. Bayer (Univ. Heidelberg), W. Smethie (Lamont), M. Rutgers van der Loeff (AWI)*

Natural radioactive tracers:

- Distribution of radium isotopes in the Laptev and adjacent Seas. - *F. Legeleux, M. Rutgers van der Loeff, J.-L. Reyss (1), W. Stein and D. Calmet (2)*
- Distribution of  $^{234}\text{Th}$  in the Laptev and adjacent Seas. - *F. Legeleux and M. Rutgers van der Loeff*

(1) Centre des faibles Radioactivités, Gif-sur-Yvette, France

(2) IPSN, Orsay, France. - This institute may be interested in radionuclide measurements in sediments

Freon and Krypton:

*William Smethie* et al. (Lamont-Doherty Earth Observatory)

The tracer data will be interpreted within the framework of the hydrographic data and in collaboration with the other tracer and physical oceanographic PI's including *R. Bayer, P. Schlosser, B. Rudels, U. Schauer, L. Timokhov* and *R. Muench*.

Tritium-, Helium- and  $^{18}\text{O}$ - Data:

Principal Investigator: *R. Bayer* (Inst. Umweltphysik, Univ. Heidelberg)

Working Titles:

- On the circulation of river-runoff in the Kara and Laptev Sea: Implications from the distribution of  $^{18}\text{O}$  and humic substances. - *W. Stein, J. Lobbes and R. Bayer*:

- On the circulation of the intermediate waters in the Arctic Ocean: Implications from  $^3\text{H}/^3\text{He}$ -data out of the Nansen, Amundsen and Makaron Basin. - W. Stein and R. Bayer:
- A method to detect river-runoff waters in situ in the water column of the Arctic Ocean. - J. Lobbes, W. Stein and G. Kattner
- Correlation of  $^{18}\text{O}$ - and  $^{13}\text{C}$ -values of the surface waters with values of planktic foraminifers from the sediment surface and from plankton tows (s. Geology). - R. F. Spielhagen, H. Erlenkeuser (Univ. Kiel) and W. Stein:

Nutrients and other parameters:

Principal Investigator: *Yuri Nalbandov* (IORAS, Moscow)  
(in cooperation with B. Rudels and AWI biologists)

Data are available from Y. Nalbandov and E. Rachor (AWI)

Working titles:

- Some elements of the carbonate system in the Laptev Sea during summer 1995. - Y. Nalbandov, in cooperation with Göteborg University
- Chemical features of the upper water layer in the Laptev Sea and adjacent areas during summer 1995. - Y. Nalbandov
- Physical, chemical (esp. nutrients and oxygen) and biological features in the Eurasian part of the Arctic Ocean; a comparison of results from 1991, 1993, 1995. - B. Rudels, Y. Nalbandov, A. Luchetta (Trieste), U. Schauer, E. Rachor

Dissolved organic matter:

G. Kattner, R. Lara, J. Lobbes (AWI)

Future work:

- Distribution of Lignin monomers in humic substances, information about the origin and age of dissolved organic matter
- Distribution of Lignin monomers in surface sediments of the Laptev Sea
- Genesis of humic substances in the Arctic Ocean
- Fluorescence characteristics of different water masses in the Arctic Ocean
- Interaction and exchange between dissolved and particular organic matter in the Arctic Ocean
- Bioavailability of humic substances in the ice and the water column
- Combined and free amino acids, dissolved organic carbon (DOC) and nitrogen (DON) distribution in the Laptev Sea
- Diagenesis of proteins and amino acids, epimerization and racemization of amino acids
- Elemental composition of DOM and POM in the Laptev Sea
- $^{13}\text{C}/^{12}\text{C}$ -ratio in concentrated samples of humic substances in the Laptev Sea
- Molecular size and charge variations of humic substances in the Laptev Sea

Cooperation:

W. Stein, R. Bayer (Univ. Heidelberg), R. Stein (AWI), B. Rudels (ZMK)

### 3 SEA-ICE RESEARCH

Contact persons: *H. Eicken* (AWI), *A. Darovskikh* (AARI)

#### a. Data availability and exchange (on request)

- hourly ice-observation data made from the ship's bridge by a team of observers are available from HSVA (K.-H. Evers, P. Jochmann)
- surface and bottom profiles of pressure ridges are available from HSVA (K.-U. Evers, P. Jochmann)
- ice-core and ice-thickness profile data (including puddle depths) obtained at ice stations are available from AWI (H. Eicken, C. Haas)
- remote sensing data (AVHRR) are available from AWI (J. Kolatschek, T. Martin)
- data on the temperature and salinity regime of puddles based on measurements made during the cruise are available from AARI (A. Zachek)
- data of temperatures, salinities and current velocities of the under-ice water layer are available from IPÖ (I. Werner, C. Krembs)
- copies of video tapes of side-looking and nadir-viewing video camera images from helicopter flights will be supplied to AARI (A. Darovskikh) by AWI (H. Eicken)
- helicopter side-looking radar data are available from AARI (A. Darovskikh)

#### b. Collaboration and topics of planned research based on cruise data

- Detection of different ice types, morphometry of sea ice and ice motion derived from side-looking radar overflights in combination with video camera recordings, laser-altimeter data, ice morphology measurements and Okean radar data (Darovskikh, Syrtsov, Eicken, Haas, Kolatschek, Evers, Jochmann)
- Statistical properties of radar images (Darovskikh, Syrtsov)
- Thermal conditions of open and frozen melt puddles (Zachek)
- Advective heat exchange between puddles and the surface layer of sea ice (Freitag, Zachek, Eicken)
- Characterisation and quantification of sediments in sea ice (*Lindemann*)
- Integral and spectral albedos of sediment-laden sea ice in the Laptev Sea (Kolatschek, Zachek, Lindemann, Eicken)
- Detection and mapping of sediment-laden ice masses from satellite data (Kolatschek)
- Small-scale redistribution of sea-ice sediments as a function of absorption of solar radiation and meltwater fluxes (Freitag)
- Entrainment modes and small-scale redistribution of ice-rafted sediments based on ice-core analysis (Eicken, Freitag, Lindemann)
- Transport of sediments by sea ice as a result of a massive entrainment event in the eastern Laptev and western East Siberian Sea (Eicken, Freitag, Kolatschek, Lindemann)
- Roughness characteristics of first-year sea ice (Haas)
- Underwater and surface profiling of ice pressure ridges in the Laptev Sea

(Evers, Jochmann)

- Effects of ablation processes on microstructure and morphology of first-year sea ice (Eicken, Haas, Freitag)
- Three-dimensional reconstruction and analysis of sea-ice pore microstructure as a function of physico-chemical boundary conditions (Eicken, Valero Delgado)

#### 4 SEA ICE ECOLOGY

Principal Investigators / contact persons:

S. Grossmann (AWI) and R. Gradinger (IPOE Kiel)

Working titles of research (and cooperation partners):

- Primary and bacterial productivity of sea ice - and under-ice water microbial assemblages. - M. Gleitz, S. Grossmann, AWI  
(On-board incubations with radiolabelled substrates (bicarbonate - phytoplankton, thymidine - bacteria). Determination of *in situ* photosynthetically active radiation. Determination of phytoplankton and bacterial biomass)
- The role of micro-heterotrophs (bacteria, protozoa) for ice-related microbial food webs. - S. Grossmann, M. Gleitz, E.-M. Nöthig (AWI), C. Krembs (IPOE)  
(Determination of protozoan grazing by serial dilution method.  
Determination of phytoplankton, bacterial and protozoan biomass (Chl *a*, Utermöhl, AODC and DAPI preparations for microscopy at home laboratory).  
Determination of spatial distribution of organisms within sea ice.)
- Interaction and small scale distribution of members of the sympagic food web in comparison with the three dimensional ice microstructure and variability of hydrodynamic properties at the ice water interface (scale 1 m to 10 cm) for different areas of the Laptev sea. - C. Krembs
- Analysis of the spatial distribution (scale 10 cm to 1µm) and abundance of organisms and transparent extracellular mucopolysaccharides (TEP) within the complex three dimensional brine channel system determined with a new cryogenic substitution method, that will be compared with the adjacent underice water column. - C. Krembs
- Colonization experiments and video observation of an artificial brine channel system under simulated *in situ* hydrodynamic conditions to determine factors that lead to small scale distributions of ice inhabiting organisms within brine channels. - C. Krembs, in cooperation with: C. Friedrich (IPOE), A. Juhl (Scripps Institution of Oceanography)
- Further description of the habitat for sympagic organisms, surface, volume and porous parameters in the ice described with three different techniques: Resin cast technique, contrast pore analysis, controlled surface adsorption technique. C. Krembs, in cooperation with: H. Eiken, J. Freitag, J. Weissenberger (AWI)
- First results of new non freeze up *in situ* equipment (current meter probe for longer deployment in the ice & inflatable underice flow tank (30 x 100 x 14 cm) deployed through a 10 cm core hole) to determine the variability of exchange processes across the ice water interface with dye tracers and simulated *in situ* hydrodynamic conditions. - C. Krembs
- Under-ice fauna ecology. - I. Werner, R. Gradinger (in cooperation with AWI)

## 5 PHYTO- / BACTERIO-PLANKTON and PARTICLE FLUX

Principal investigators and contact persons: *E.-M. Nöthig*, *Markus Gleitz* (AWI) in cooperation with *V. Shevshenko* (IORAS)

Working titles of research (and other cooperation partners):

- Biological properties of the water column. -  
A. Bartel, *E.-M. Nöthig*, Y. Nalbandov, IORAS, B. Rudels, ZMK  
(Determination of Chl-*a*, biogenic silicate, POC, PON, seston and phytoplankton species composition in relation to hydrography and nutrient concentrations)
- Primary and bacterial productivity in open (ice-free) waters. -  
*M. Gleitz*, S. Grossmann, A. Bartel, *E.-M. Nöthig*, V. Shevshenko  
(in cooperation with Russian microbiologists), Y. Nalbandov, B. Rudels  
(On-board incubations with radiolabelled substrates).
- Determination of phytoplankton and bacterial biomass (Chl-*a*, AODC, Utermöhl. Determination of microbial enzymatic activity) - AWI biologists.
- Enzymatic activity in the water column of the Laptev Sea. - G.A.Korneeva, V.P.Shevchenko (in cooperation with AWI biologists)
- Distribution of bacteria in the water column of the Laptev Sea. -  
D.I. Nikitin (Institute of Microbiology, Moscow), V. Shevshenko (in cooperation with AWI biologists)
- Vertical matter flux in the water column; export of organic material into the deep sea: long-term sediment trap deployment over the Lomonosov Ridge („LOMO 2“). *E.-M. Nöthig*, C. Darnall, in cooperation with AWI-geologists. (Determination of POC, PON, seston, Chl-*a*, Utermöhl preparations, lipids)
- Vertical matter flux in ice-covered waters: short-term sediment trap deployments from ice floes. - S. Grossmann, *M. Gleitz*, *E.-M. Nöthig*, *V. Shevshenko* (Determination of POC, PON, seston, Chl-*a*, light- and electron microscopy on samples collected at 5, 25 and 75 m water depth)

## 6 ZOOPLANKTON ECOLOGY

Principal Investigators and contact persons: *Ksenia Kosobokova* (IORAS Moscow), *H.-J. Hirche* (AWI), *S.F. Timofeev* (MMBI)

Material:

Zooplankton material is distributed between the Institute of Oceanology Moscow (IORAS; multinet material, especially from deep waters, bongo net material, 0.5 mm), the Murmansk Marine Biological Institute (MMBI; epipelagic bongo net 0.2 mm), and the Alfred-Wegener-Institute Bremerhaven (AWI; parts of the material from multi- and bongo nets).

Intended scientific work:

- Zooplankton assemblages of the shallow and deep parts of the Laptev Sea and adjacent waters. - K.N. Kosobokova (IORAS)
- Lipid composition and carbon content of the dominant zooplankton species

- from the Laptev Sea. - K.N. Kosobokova, H.-J. Hirche (AWI), T. Scherzinger
- On the reproductive biology of mesopelagic and bathypelagic copepods in the Laptev Sea. - K.N. Kosobokova
- Trophodynamic relationships in the Arctic meso- and bathypelagic zooplankton and their impact on the transformation of particular organic substances. - T. Scherzinger (together with H.-J. Hirche)
- Distribution, biomass and population structures of euphausiids and chaetogaths. - S.F. Timofeev
- Distribution of Atlantic species of zooplankton. - S.F. Timofeev, H.-J. Hirche and K.N. Kosobokova
- Larval plankton. - S.F. Timofeev

Cooperation:

AWI biology and Univ. Tromsø for studies of pelago-benthic coupling; IPOE Kiel for Arctic copepods and kryo-pelagic coupling; Inst. of Marine Research, Bergen, for euphausiid studies; Zool. Inst. RAS St. Petersburg for taxonomic studies.

## 7 BENTHIC ECOLOGY

Principal Investigators and contact persons:

*E. Rachor* (AWI) and *B. Sirenko* (ZISP)

Material:

All zoobenthos samples and data obtained during ARK XI/1 are to be labelled with POLARSTERN's station numbers, indicating the gear used.

The material will be distributed as follows:

- Most quantitative (Grosskastengreifer, GKG) macrofauna and all meiofauna (multorerer) samples from the Laptev Sea and adjacent eastern and deep sea waters will be kept and treated at AWI (E. Rachor, H. Deubel, in cooperation with ZISP, MMBI, and IPOE).  
A part of the meiofauna samples will be treated at the University of Oldenburg (Prof. Schmincke, P. Martinez).
- Quantitative macrofauna samples and Agassiz trawl samples from the Kara Sea as well as selected ophiurid material will be kept and treated by MMBI (N. Anisimova, in cooperation with AWI and ZISP).
- Almost all other Agassiz trawl and some GKG material will be kept and treated at ZISP (Invertebrates: B. Sirenko, in cooperation with AWI, MMBI; for shallow waters of less than 250 m depths also with IPOE; Fishes: A. Neyelov, N. Chernova).
- Some selected animals from the Agassiz trawls are kept by AWI (E. Rachor) for analyses of carbon isotopes and trace organic contaminants (together with AWI Chemistry and AWI Potsdam).

Intended work / publications:

- 1.1 Bottom communities and their zonation along the continental slopes and in the adjacent deep sea basins (Nansen, Amundsen, Makarov)

- *B. Sirenko*, V. Potin (ZISP), E. Rachor, M. Klages (AWI), N. Anisimova (MMBI)
- 1.2 Shallow water (shelf) communities of the Laptev Sea. - *B. Sirenko*, V. Petryashev (ZISP), E. Rachor, Hendrik Deubel (AWI), N. Anisimova (MMBI), K. Hinz (IPOE)
  - 1.3 Shallow water (shelf) communities of the transition area to the East Siberian shelf - *B. Sirenko*, V. Potin (ZISP), E. Rachor, H. Deubel, AWI
  - 1.4 Shallow water (shelf) communities of the transition area to the Kara Sea - *N. Anisimova* et al. (MMBI), E. Rachor (AWI)
  2. Taxonomy: - *ZISP* (Fish: N. Chernova and A. Neyelov; Polychaetes: G. Buzchinskaja, V. Potin et al.; Molluscs: B. Sirenko.; Echinoderms: I. and A. Smirnov; Crustaceans: S. Vassilenko et al.); MMBI (Ophiurids: N. Anisimova); AWI (Amphipods: M. Klages; Nematodes: F. Riemann et al.)
  3. Zoogeography: - *B. Sirenko* et al. (ZISP), E. Rachor et al. (AWI), N. Anisimova et al. (MMBI)
  4. Growth/Population dynamics in ophiurids. - *N. Anisimova* (MMBI)
  5. Density and diversity of macro- and meiofauna (abundances and biomass) in relation to the primary productivity and fluxes of organic matter (pelago-benthic coupling): *E. Rachor*, H. Deubel (AWI, in cooperation with AWI biologists and geologists, and in future also with partners of an Arctic Ocean Grand Challenge project)
  6. Density structures of zoobenthos and its requirements of organic matter in the Lomonossov Ridge area, in comparison with selected Laptev Sea continental slope areas (eastern- and westernmost), (1993, 1995, 1996 samples): *H. Deubel*, *E. Rachor* (AWI)
  7. Zoobenthos contribution to sediment oxygen flux budgets (compared with NW Barents Sea and North Sea): *E. Rachor*, M. Klages, E. Damm, C. Grahl (AWI), G. Hulthe (Göteborg), P. Martinez (Oldenburg)
  8. Indicators of a former hydrothermal vent activity in the northern central Laptev Sea: *E. Rachor*, Rüdiger Stein, Monika Wahsner (AWI), *B. Sirenko*, J. Starobogatov et al. (ZISP)
  9. Carbon isotopes ( $\delta$ -C-13) as indicators of the food origin of the benthic fauna in the Laptev and adjacent Seas: *E. Rachor* (AWI), K. Danton (Texas Univ.), *B. Sirenko* (ZISP)
  10. Meiofauna, especially harpacticoids, from the continental slopes of the Laptev Sea: P. Martinez, Schmincke (Univ. Oldenburg)

Cooperation:

Main partners: AWI (including other biologists, geologists and biogeochemists for fluxes of organic matter and pelago-benthic coupling); ZISP, MMBI, IPOE; and several groups of participants of ARK XI/1 (and ARK IX/4), and of the German-Russian Laptev-Sea-System-Project

Associated partners: Univ. Oldenburg (meiofauna), Univ. Gent (meiofauna), Univ. Moscow/Zool. Museum Moscow (taxonomy), Norsk Polarinstitut, Univ. Tromsø (pelago-benthic coupling/fluxes and diversity)

Microbial Benthos: see Sediment Biogeochemistry



## 8 SEDIMENT BIOGEOCHEMISTRY

Contact Persons / Principal Investigators:

*Ellen Damm* (AWI) and *Per Hall* (Univ. Göteborg)

- Contribution to pelago-benthic coupling studies. C. Grahl, E. Damm, A. Boetius (Determination of surface sediment chloroplastic pigment concentrations)
- Enzymatic activity and microbial biomass in sediments at deep sea stations and along the continental slope in the Laptev Sea. - Grahl, C. & Boetius, A.
- Oxygen consumption rates in sediments of different regions of the Arctic ocean by incubation and microelectrodes measurements. - Damm, E., Rutgers van der Loeff, M. & Hulthe, G.
- The flux of dissolved organic matter between sediments and bottom water in the Laptev Sea. - Hulthe, G., Hall, P. & Damm, E.
- Nutrient profiles in sediments of the Laptev Sea. - Damm, E., Nalbandov, Y. & Hulthe, G.
- The fate of carbonates in early diagenesis in the Laptev Sea. - Hulthe, G., Hall, P. & Damm, E.
- Degradation rates of organic matter in relation to diagenetical zones of shelf and slope sediments in the Laptev Sea. - Damm, E. & Hulthe, G.
- Early diagenesis in the Laptev sea by oxygen uptake and total inorganic carbon-release measurements. - Hulthe, G., Damm, E. & Hall, P.

## 9 MARINE GEOLOGY

Contact Persons: *R. Stein* (AWI), *E. Musatov* (VNIIOkeanGeologia)

*Sediment sample distribution guidelines for ARK-XI/1 material:*

The sample distribution guidelines for ARK-XI/1 are designed to guarantee a fair distribution of material, to minimize the duplication of scientific effort and maximize the scientific return from these valuable samples.

The Alfred-Wegener Institute (AWI) shall serve as the core repository for all ARK XI/1 sediment samples. AWI will be responsible for the distribution of samples to shipboard and shorebased investigators. AWI will maintain a record of all samples that have been distributed and the nature of the investigations being undertaken. This information will be available to investigators on request.

All cores collected on the expedition will be labelled and recorded according to the AWI and *Polarstern* standard scheme. Samples distributed from these cores will be labelled with a standard identifier which will include a core identifier and the interval from which the sample was removed. This standard identifier should be associated with all data reported; residues of samples should remain labelled so that they can be related to earlier data.

Any investigator wishing to request samples from the expedition shall submit, in writing, a sample request to AWI. The request should contain a statement of the nature of the proposed research, the size and approximate number of samples

required to complete the study. Costs associated with the taking and/or receiving samples from the AWI repository shall be accounted for by the requesting party.

For two years following the expedition, sampling shall be limited to shipboard participants and shorebased investigators agreed upon by the geoscience participants during the expedition. Recognizing the tremendous investment of time and energy expended by members of the expedition's scientific party, in general preference shall be given to sample requests from shipboard participants.

For further information, please, contact the curator of the AWI Sediment Core & Data Repository, *Dr. Hannes Grobe*.

*Tentative scientific working titles on geological material and data:*

- The Eurasian Arctic Shelf during the last Glaciations: Ice Cap versus local Glaciers. Indication from high resolution seismic cross sections: E-Kara Sea and Laptev Sea (F. Niessen AWI and E. Musatov)
- Sub-marine ice gouges in the Laptev Sea as seen on high resolution seismic (PARASOUND) profiles: distribution and environmental implication: F. Niessen & H. Eicken (AWI), E. Reimnitz (USGeol. Survey) in cooperation with H. Kassens, GEOMAR.
- High resolution seismic facies and stratigraphy of the Laptev Sea continental margin: Late Quaternary sea-level variations and changes in sediment distribution (F. Niessen, R. Stein & D. Weiel, AWI, E. Musatov)
- Postdepositional reflection pattern in near surface sediments of the Laptev Sea - indication for permafrost and the release of sedimentary gas. (F. Niessen)
- Multi Sensor Core Logging of physical properties of sediment cores from the Arctic Ocean - high resolution stratigraphy and depositional implications. (F. Niessen AWI, E. Musatov, in cooperation with GEOMAR).
- Stable oxygen and carbon isotopes in planktonic foraminifers and late Quaternary variability of Arctic Ocean paleoenvironment (R.F. Spielhagen, GEOMAR; R. Stein, AWI)
- Physical properties of sediment cores from the Laptev Sea shelf and continental margin related to depositional processes and glacial history (Niessen, F., AWI; Nørgaard-Pedersen, N. and H. Kassens, GEOMAR)
- Accumulation rates of the Laptev Sea and the adjacent Lomonosov Ridge Quaternary sediment sequence derived from physical properties (Nørgaard-Pedersen, N., and H. Kassens, GEOMAR)
- Depth distribution and stable O and C isotopes of planktic foraminifers in surface waters of the Laptev Sea continental margin (Spielhagen, R. F., GEOMAR, and Erlenkeuser, H., GPI Kiel)
- Stable oxygen and carbon isotopes in planktic foraminifers from sediment surface samples obtained during ARK XI/1 (Spielhagen, R. F., GEOMAR, and Erlenkeuser, H., GPI Kiel)
- Ventilation of water masses at the Laptev Sea continental margin derived from  $^{13}\text{C}/^{12}\text{C}$  data of water samples (Spielhagen, R. F., GEOMAR, and Erlenkeuser, H., GPI Kiel)
- Correlation of  $\text{d}^{18}\text{O}$  and  $\text{d}^{13}\text{C}$  values of the surface waters with values of

- planktic foraminifers from the sediment surface and from plankton tows (Spielhagen, R. F., GEOMAR; Erlenkeuser, H., GPI Kiel; W. Stein)
- Beryllium and Thorium isotopes in sediment cores obtained during ARK XI/1 (Spielhagen, R. F., GEOMAR, and Mangini, A., Univ. Heidelberg)
  - History of Late Quaternary river runoff from Northern Siberia derived from stable O and C isotopes in planktic foraminifers from sediment cores obtained during ARK XI/1 (Spielhagen, R. F. and Nørgaard-Pedersen, N.; GEOMAR)
  - Coarse fraction composition of surface sediments obtained during ARK IX/4 and XI/1 (Spielhagen, R. F. and Nørgaard-Pedersen, N.; GEOMAR)
  - History of Northern Siberian ice sheets during the Late Cenozoic (Nørgaard-Pedersen, N., Spielhagen, R. F., et al.)
  - Establishment of a litho- and chronostratigraphy for sediment cores obtained during ARK XI/1 and correlation to existing Arctic stratigraphies (Behrends, M., Nørgaard-Pedersen, N., Spielhagen, R. F., Stein, R., et al.)
  - Paleoenvironmental history of the Laptev Sea continental margin and adjacent areas during the late Cenozoic (Nørgaard-Pedersen, N., Spielhagen, R. F., Stein, R., et al.)
  - Clay mineral distribution and major and minor elements in sediments from the Eurasian continental margin and adjacent deep-sea area: Implications for paleoenvironment, transport processes, and terrigenous sediment source (R. Stein et al., AWI)
  - Heavy mineral distribution in late Quaternary sediments from the Laptev Sea continental margin and adjacent deep-sea area: Indicator for source areas and transport mechanisms of terrigenous matter (M. Behrends, AWI)
  - Heavy mineral distribution in late Quaternary sediments from the Kara Sea and its adjacent continental margin: Indicator for source areas and transport mechanisms of terrigenous matter (M. Bourtman, IORAS Moscow)
  - Late Neogene variability of flux and composition of terrigenous matter along the Eurasian continental margin and eastern central Arctic Ocean and its paleoenvironmental significance - A synthesis (R. Stein, M. Behrends, F. Niessen, C. Vogt, M. Wahsner, et al.)
  - Barium, biogenic opal, and organic carbon in Arctic shelf, slope, and deep-sea sediments: Indicator for late Quaternary variability in surface-water productivity (D. Nürnberg and R. Stein, AWI)
  - Amino-acid stratigraphy and late Quaternary paleoenvironment in the Arctic Ocean deep sea - R. Stein et al., AWI
  - Organic carbon flux in late Quaternary sediments from the Eurasian continental margin and adjacent deep-sea area: Terrigenous input versus surface-water productivity.- R. Stein and K. Fahl (AWI, in cooperation with AWI biologists)
  - Palynology and biomarker in late Quaternary Arctic Ocean sediments and paleoenvironment. - K. Fahl and R. Stein (AWI)
  - Biomarker composition in the water column and underlying sedimentary sequences in the Laptev Sea and adjacent deep-sea area: Indicator for organic-carbon sources and pathways, and late Quaternary environmental variability. - K. Fahl et al. (AWI)
  - Benthic foraminiferan assemblages and their stable oxygen and carbon isotope signal in late Quaternary sediments from the Laptev Sea continental margin

- and adjacent deep-sea area. - A. Mackensen (AWI)
- Quantitative distribution of total suspended matter in the Laptev Sea /V.P.Shevchenko, A.P.Lisitzin, O.V.Minaeva, N.G.Maierova (IO) /
- Composition of suspended matter lipids off the northern part of the Severnaya Zemlya Archipelago. - O.A.Alexandrova, V.P.Shevchenko (IO)
- Main features of granulometric and mineralogical (light minerals) composition of late Cenozoic deposits of the Laptev Sea /N.Kukina, G.A.Tarasov (MMBI) /
- General character of late Cenozoic sedimentation in the Laptev Sea. - G.A.Tarasov, Mityaev M., M.V.Gerasimova, I.Pogodina (MMBI) (in cooperation with other participants of ARK XI/1)
- Geomorphological structure and history of neotectonic development of the Laptev Sea. - M.V.Gerasimova, G.G.Matishov, M.Mityaev, G.A.Tarasov (MMBI), (in cooperation with AWI, F. Niessen; see also next theme)
- Bathymetry and geomorphology of the Laptev Sea shelf and adjacent continental slope. - E. Musatov (in cooperation with AWI)
- Thicknesses of recent sediments at the Laptev Sea shelf. - E. Musatov
- Paleogeography of the Laptev Sea region through the Late Cenozoic. - E. Musatov.

Explanation: "et. al." - this contribution is open for additional, especially Russian authors.

## 10 AEROSOLS

Contact Persons: *V.P. Shevchenko* (IORAS, Moscow), *R. Stein* (AWI).

The material is kept at IORAS Moscow

Working titles:

- Composition of aerosols over the Laptev Sea in July-September, 1995. - V.P. Shevchenko (IO), A.A. Vinogradova (Institute of the Atmospheric Physics, Moscow), R. Stein (AWI), U. Bergholter (DWD), *A.P. Lisitzin* (IO), G.I. Ivanov (VNIIO)
- Aerosol size distribution over the Laptev Sea in July-September, 1995. - V.V. Smirnov (Institute of Experimental Meteorology, Obninsk), V.P. Shevchenko (IO), A.V. Savchenko (Institute of Experimental Meteorology, Obninsk), R. Stein (AWI), *A.P. Lisitzin* (IO)

## Annex 11.6

**Research Participants ARK XI/1**  
 (part-leg Murmansk-Murmansk)

<u>Name</u>	<u>Institute</u>	<u>Discipline</u>	
Natalya A. Anisimova	MMBI	Murmansk	Biology (zoobenthos)
Anja Bartel	AWI	Bremerhaven	Biology (phytoplankton)
Marion Behrends	AWI	Bremerhaven	Geology
Uwe Bergholter, Met.	DWD/SWA	Hamburg	Meteorology
Vladimir P. Bogdanov	Russ. Fed.	Moscow	Plenipotentiary
Maria V. Bourtman	IO	Moscow	Geology
Dirk Brinkmann	HSW	Hamburg	Helicopter-Service
Jürgen Büchner	HSW	Hamburg	Helicopter-Service
Ellen Damm	AWI	Bremerhaven	Biogeochemistry
Clark Darnall	APL	Seattle	Oceanography
Andrey Darovskikh	AARI	St. Petersburg	Ice Research
Hendrik Deubel	AWI	Bremerhaven	Biology (zoobenthos)
Wolfgang Dinkeldein	HSW	Hamburg	Helicopter-Service
Hajo Eicken	AWI	Bremerhaven	Ice Research
Karl-Ulrich Evers	HSVA	Hamburg	Ice Research
Kirsten Fahl	AWI	Bremerhaven	Geology
Johannes Freitag	AWI	Bremerhaven	Ice Research
Markus Gleitz	AWI	Bremerhaven	Biology (phytoplankton)
Claudia Grahl	AWI	Bremerhaven	Biology (microbiology)
Grossmann, Sönneke	AWI	Bremerhaven	Biology (ice algae)
John Gunn	SAIC	Seattle	Oceanography
Christian Haas	AWI	Bremerhaven	Ice Research
Frank Haubrich	AWI	Bremerhaven	Chemistry (tracers)
Gustaf Hulthe	AMCG	Göteborg	Biogeochemistry
Peter Jochmann	HSVA	Hamburg	Ice Research
Herbert Köhler, Met.	DWD/SWA	Hamburg	Meteorology
Josef Kolatschek	AWI	Bremerhaven	Ice Research (remote sensing)
Ksenia Kosobokova	IO	Moscow	Biology (zooplankton)
Christopher Krembs	IPOE	Kiel	Ice Biology
Françoise Légeleux	AWI	Bremerhaven	Chemistry (tracers)
Frank Lindemann	GEOMAR	Kiel	Ice Research
Jörg Lobbes	AWI	Bremerhaven	Chemistry (tracers)
Volker Lundström	HSW	Hamburg	Helicopter-Service
Maxim Mitjajev	MMBI	Murmansk	Geology
Eugene Musatov	VNIIO	St. Petersburg	Geology
Yuri Nalbandov	IO	Moscow	Chemistry (nutrients)
Frank Niessen	AWI	Bremerhaven	Geology
Niels Nørgaard-Pedersen	GEOMAR	Kiel	Geology
Vladislav Potin	ZISP	St. Petersburg	Biology (zoobenthos)
Eike Racher	AWI	Bremerhaven	Biology (benthos)
Bert Rudels	ZMK	Hamburg	Oceanography
Till Scherzinger	AWI	Bremerhaven	Biology (zooplankton)
Sarah Searson	L-DEO	Palisades	Chemistry (tracers)
Vladimir Shevshenko	IO	Moscow	Aerosols/Geology
Robert Spielhagen	GEOMAR	Kiel	Geology
Ruediger Stein	AWI	Bremerhaven	Geology

<u>Name</u>	<u>Institute</u>	<u>Discipline</u>
Wilhelm Stein	IUH Heidelberg	Chemistry (tracers)
Sergey Syrtsov	INTAARI St. Petersburg	Ice Research (surveying)
Sergey Timofeev	MMBI Murmansk	Biology (zooplankton)
Fernando Valero Delgado	AWI Bremerhaven	Ice Research
Iris Werner	IPOE Kiel	Ice Biology
Andrey Zachek	AARI St. Petersburg	Ice Research
Eugene Zakharchuk	AARI St. Petersburg	Oceanography

#### INSTITUTIONS

AARI	Arctic and Antarctic Research Institute, St. Petersburg, Russia
AMCG	Dept. of Analytical and Marine Chemistry, Univ. Göteborg, Sweden
APL	Applied Physics Laboratory, Univ. Washington, Seattle, USA
AWI	Alfred-Wegener-Institut für Polar- und Meeresforschung, Bremerhaven, D
DWD/SWA	Deutscher Wetterdienst, Seewetteramt Hamburg, Germany (D)
GEOMAR	GEOMAR Kiel, Germany
HSVA	Hamburgische Schiffbau-Versuchsanstalt, Germany
HSW	Helicopter Service Wasserthal, Hamburg, Germany
INTAARI	St. Petersburg
IUH	Institut für Umweltp Physik, Univ. Heidelberg, Germany
IO	P.P. Shirshov Institute of Oceanology, Moscow, Russia
IPOE	Institut für Polarökologie, Kiel, Germany
L-DEO	Lamont-Doherty Observatory, Columbia Univ., Palisades, N.Y, USA
MMBI	Murmansk Marine Biological Institute RAS, Russia
SAIC	Science Applications International Corp., Seattle, W.A., USA
VNIIO	All-Russian Research Institute for Geology and Mineral Resources of the World Ocean, VNIIOkeangeologia, St. Petersburg, Russia
ZISP	Zoological Institute RAS, St. Petersburg, Russia
ZMK	Zentrum für Meeres- und Klimaforschung, Univ. Hamburg, Germany

#### Ship's Crew:

Function	Name
Kapitän	Heinz G.W. Jonas
1. Offizier	Ingo Varding
Naut. Offizier	Stefan Schwarze
Naut. Offizier	Steffen Spielke
Naut. Offizier	Michael Block

A 173

Ship's Crew ctd.:

Function	Name
Arzt/Physician	Uwe Kapiéske
Ltd. Ingenieur	Klaus Müller
1. Ingenieur	Wolfgang Delff
2. Ingenieur	Henryk Folta
2. Ingenieur	Wolfgang Simon
Funkoffizier	Johann Butz
Funkoffizier	Werner Thonhauser
Elektroniker	Klaus-Jürgen Hoops
Elektroniker	Andreas Piskorzynski
Elektroniker	Helmar E. Pabst
Elektroniker	Martin Froeb
Elektriker	Reinhard Erdmann
Koch	Hans-Jürgen Schaefer
Kochsmaat	Thomas H.G. Voelske
Kochsmaat	Mustafa Vavuz
1. Stewardess	Agnes Hopp
Stewardess	Claudia Lehmbecker
Stewardess	Bärbel Hildebrandt
Stewardess	Regine Klemet
Steward	Busro Amran
2. Steward	Chi Lung Wu
2. Steward	Chung-Leung Yu
Wäscher	Chih Cheung Ching
Bootsmann	Reiner Robert Loidl
Zimmermann	Peter Kassubeck
Matrosen:	Siegfried Moser Lukas R. Klesper Stefan Claußen Herbert Thillmann Hasim Avcilar Jose Novo Loveira Antonio Suarez Paisal Ev Dominguez-Quintas
Lagerhalter	Bernhard Barth
Maschinen-Warte	Ernst-Uwe Hartmann Helmut Bloedorn Achim H.F. Schade Tassilo Rosenthal Marius Hirsekorn
Russian Ice Pilot	N. Krylov

